Mediterranean sea surface temperatures and planktonic foraminifera palaeoecology during short-term climate oscillations of the Late Pleistocene

by

Margaret Ann Browne

Thesis submitted for the degree of

Doctor of Philosophy

Supervisor: **Dr Angela Cloke-Hayes**

Department of Geography

Mary Immaculate College

(Coláiste Mhuire Gan Smál)

University of Limerick

Submitted to the University of Limerick, September 2020

Abstract

Mediterranean sea surface temperatures and planktonic foraminifera palaeoecology during short-term climate oscillations of the Late Pleistocene

Margaret Ann Browne

The Mediterranean is a semi-enclosed sea, ideally located for recording and amplifying global climate signals. Heinrich Stadial 1 (HS1), the Bølling-Allerød (BA) and Younger Dryas (YD) are periods of extreme climatic change that occurred during the last deglacial. Planktonic foraminifera were utilised to address the extent the Mediterranean Sea responded to these events, and how they impacted sea surface temperatures (SSTs), hydrology and distribution of planktonic foraminifera on a basin-wide scale. This was further expanded upon in the Gulf of Lion, in order to determine the palaeoenvironmental impacts and main drivers in this region during the deglacial.

A database of planktonic foraminiferal counts from 67 cores located across the Mediterranean Sea were compiled. SSTs were reconstructed using Artificial Neural Networks (ANN) and mapped for each chronozone, along with key planktonic foraminifera and palaeoenvironmental proxies. Mean annual SSTs ranged from 13.57°C and 14.19°C during HS1 and the YD, both cooler than the Last Glacial Maximum (LGM). SSTs during the BA increased to 15.03°C. The western basin, Adriatic and Aegean Seas remained cool and strongly eutrophic, dominated by Neogloboquadrina species, *G. bulloides*, *T. quinqueloba* and *G. inflata* since the BA. The eastern basin was more productive than today, with a mix of eutrophic species and *G. ruber* plexus, though it became increasingly seasonal, oligotrophic and stratified as SSTs warmed during the BA and YD. These reconstructions highlight the complexity of these chronozones across the Mediterranean Sea. They also illustrated how global drivers such as the southerly position of the polar front, North Atlantic atmospheric circulation, precipitation and wind strength, sea level, summer insolation and position of the ITCZ governed these signals. River discharge and meltwater pulses were regionally important along northern margins.

Analysis of the high-resolution Gulf of Lion core M40/4 82-2SL focused the late HS1 to mid Holocene (~15.5 to 7.4 kyr). SSTs were predicted using ANN, and a combination of faunal abundance, multivariate statistics (PCA) and palaeoenvironmental proxies were utilised to reconstruct the palaeoenvironment. Predicted SSTs showed strong correlation with Greenland $\delta^{18}O$ ice cores, especially during the BA (15.19°C). SSTs during the late HS1 (10.18°C) and YD (8.3°C) were cooler than the LGM. The assemblage was strongly eutrophic throughout, with a more diverse, seasonal assemblage restricted to the early Bølling and Holocene. Holocene SSTs were cooler than expected (15.06 to 15.76°C), as the early Holocene was overprinted by a strong cyclical river/meltwater signal. This freshening of surface waters impacted the depth of the pycnocline, which had significant impacts on *N. incompta*. Variations in wind-strength, precipitation, river discharge and Alpine meltwaters were the main factors governing the Gulf of Lion during the Late Pleistocene to mid Holocene transition.

Declaration

I hereby declare that this thesis represents my work and has not been submitted in whole or in part, by me or another person, for the purpose of obtaining any other qualification.

Signed: _____
           Margaret A. Browne

Date: _____

Acknowledgements

Dedicated to my father

John Browne

(1942 – 2009)

Wish you were here…

and

Izzy

(2005 – 2017)

🐾🐾

My girl

x

Table of Contents

List of Figures

List of Tables

Abbreviations

Abbreviation	Explanation
AABW	Antarctic Bottom Waters
AAIW	Antarctic Intermediate Waters
AC	Algerian Current
AdDW	Adriatic Deep Water
AeDW	Aegean Deep Water
AeIW	Aegean Intermediate Water
AHP	African Humid Period
AIS	Atlantic-Ionian Stream
ALD	Average Living Depths
AMC	Asia Minor Current
AMOC	Atlantic Meridional Overturning Circulation
ANN	Artificial Neural Networks
AQ	Age Quality
BA	Bølling-Allerød
BSW	Black Sea Water
CCD	Carbonate Compensation Depth
DCM	Deep Chlorophyll Maximum
DO	Dansgaard-Oeschger
DWF	Deep Water Formation
EA	Eastern Atlantic
EAG	Eastern Alboran Gyre
EAM	East African Monsoon
EMDW	Eastern Mediterranean Deep Water
ENSO	El Niño-Southern Oscillation
GI	Greenland Interstadial
GISP	Greenland Ice Sheet Project
GL	Greenlandian
GS	Greenland Stadial
HE	Heinrich Events
HS1	Heinrich Stadial 1
IACP	Intra-Allerød Cold Period
IRD	Ice Rafted Debris
ITCZ	Intertropical Convergence Zone
kyr	Thousand years
LGM	Last Glacial Maximum
LIW	Levantine Intermediate Water
LSW	Levantine Surface Water
Ma	Million Years
MAT	Modern Analog Technique
MAW	Modified Atlantic Water
MIS	Marine Isotope Stages
MIW	Mediterranean Intermediate Waters
MMJ	Mid-Mediterranean Jet
MOW	Mediterranean Outflow Water
MWP-1A	Meltwater Pulse 1A

Abbreviation	Explanation
MWP-1B	Meltwater Pulse 1B
NAC	North Atlantic Current
NAdDW	North Adriatic Deep Water
NADW	North Atlantic Deep Waters
NAO	North Atlantic Oscillation
NASW	North Atlantic Surface Waters
NG	Northgrippian
NGRIP	North Greenland Ice Core Project
OD	Older Dryas
ORL1	Organic Rich Layer 1
PCA	Principal Component Analysis
Pre-ORL1	Pre-Organic Rich Layer 1
psu	Practical Salinity Units
RAM	Revised Analog Method
S1	Sapropel 1
SAM	South Asian Monsoon
SLP	Sea Level Pressure
SO	Southern Oscillation
SST	Sea Surface Temperature
TDW	Tyrrhenian Dense Water
WAG	Western Alboran Gyre
WIW	Winter Intermediate Water
WMDW	Western Mediterranean Deep Water
WOA	World Ocean Atlas
YD	Younger Dryas
yr(s)	Year(s)

Chapter 1.

1   Introduction

The Quaternary Period spans the last ~2.6 million years and is comprised of the Pleistocene (2.58 - 0.0117 Ma) and Holocene (0.0117 Ma – Present) Epochs. During this time, vast ice sheets expanded and retreated across the northern hemisphere in a series of glacial and interglacial cycles. The most recent glaciation culminated in the Last Glacial Maximum (LGM) which ended around 19 kyr (Monnin *et al.*, 2001; Marcott *et al.*, 2014; McCarroll, 2015; Paillard, 2015). The subsequent deglaciation was interrupted by a series of rapid, short-term climatic events occurring between ~17.5 and 11.7 kyr. Heinrich Stadial 1 (HS1) was a brief cool period (~17.5 to 14.7 kyr BP), where the release of iceberg armadas into the North Atlantic deposited layers of ice-rafted debris layers as far south as 50 to 40°N (Ruddiman, 1977; Heinrich, 1988). This inflow of freshwater weakened the strength of the Atlantic Meridional Overturning Circulation (AMOC) and North Atlantic Deep Water (NADW) formation, cooling SSTs and impacting on atmospheric and oceanic circulation patterns in the northern hemisphere. This was followed by the warmer Bølling-Allerød (BA), when the recovery of the AMOC and an increase of CO_2 rapidly increased atmospheric temperatures (Bond *et al.*, 1993; Dansgaard *et al.*, 1993). The final Younger Dryas period was brief return to very cold conditions where, once again, a potential freshwater influx into the North Atlantic slowed the AMOC and NADW formation (Broecker *et al.*, 1988). Evidence of these extreme events have been recorded in ice-cores, marine sediments and a range of terrestrial proxies across the northern hemisphere.

The Mediterranean Sea is an ideal location in which to study short term climatic events as the low signal to noise ratio amplifies the signals associated with climatically induced environmental change (Cacho *et al.*, 2001; Cacho *et al.*, 2002; Moreno *et al.*, 2005). For this reason, the Mediterranean Sea has been the target of numerous studies focusing on these Late Pleistocene abrupt climatic events. Specifically, fluctuations in sea surface temperatures (SSTs) have been recorded using alkenones (Emeis *et al.*, 2000; Cacho *et al.*, 2001; Essallami *et al.*, 2007; Castañeda *et al.*, 2010; Mojtahid *et al.*, 2015; Bazzicalupo *et al.*, 2018) and transfer functions (Kallel *et al.*, 1997b; Sicre *et al.*, 2013; Dubois-Dauphin *et al.*, 2017) providing much needed palaeoenvironmental data during these late glacial events. However, these studies are constrained to specific locations

(e.g. the Alboran Sea, the Tyrrhenian Sea and the Levantine Basin) and are generally based on a small number of cores prohibiting a basin-wide analysis of these climatic events.

As known reliable indicators of palaeoceanographic and palaeoclimatic change, planktonic foraminiferal assemblages have been the focus of research for many years to better understand the prevailing hydrological systems associated with these short-term climatic events (Cacho *et al.*, 1999; Buccheri *et al.*, 2002; Sbaffi *et al.*, 2004; Geraga *et al.*, 2005; Frigola *et al.*, 2008; Kontakiotis, 2016; Giamali *et al.*, 2020). Again, while providing an extensive local palaeoceanographic history, they cannot be confidently extrapolated and applied over a basin-wide scale (Hayes *et al.*, 1999). Some basin-wide studies have been undertaken in the Mediterranean Sea, for example Hayes *et al.* (2005) reconstructed SSTs during the LGM, whilst Thomopoulos *et al.* (2010) mapped the distribution of some planktonic foraminifera at 1000-year intervals during the last 18 kyr. Both studies provide significant palaeoenvironmental analysis across the entire Mediterranean Sea, but do not focus specifically on the aforementioned short-term climatic events that characterise the deglacial period.

The modern north-western Mediterranean Sea is a key location for seasonal Western Mediterranean Deep Water (WMDW) and is characterised by cool, highly productive waters (Wüst, 1961; Medoc, 1970; Estrada, 1996). The region is strongly influenced by cold katabatic winds and winter storms that originate in the North Atlantic, as well as outflow from the River Rhône that drive this WMDW and high productivity (Estrada, 1996; Millot and Taupier-Letage, 2005; Palanques *et al.*, 2006; Papadopoulos *et al.*, 2012). As a consequence, the modern planktonic foraminifera assemblage is primarily composed of cool water eutrophic species that peak during the winter-spring bloom, which is unusual for the generally warm oligotrophic Mediterranean Sea (Rigual-Hernández *et al.*, 2012). Numerous studies in the eastern basin, Alboran and Tyrrhenian Seas utilise planktonic foraminifera as a palaeoenvironmental proxy for reconstructing the Late Pleistocene/early Holocene (Kallel *et al.*, 1997b; Cacho *et al.*, 1999; Cacho *et al.*, 2001; Sbaffi *et al.*, 2004; Di Donato *et al.*, 2008; Melki *et al.*, 2009; Martrat *et al.*, 2014; Rodrigo-Gámiz *et al.*, 2014a; Dubois-Dauphin *et al.*, 2017; Bazzicalupo *et al.*, 2018). From these studies, it is evident that the response of planktonic foraminifera to rapid climate change was varied and asynchronous across the western basin. Given the strong connectivity of the north-western Mediterranean to the North Atlantic atmospheric circulation systems, as demonstrated by speleothem and palaeobotany

proxy records in the surrounding hinterlands, it is an ideal location to test the timing and impact of global drivers of these rapid climate changes (Frisia *et al.*, 2005; Genty *et al.*, 2006; Fletcher *et al.*, 2010; Moreno *et al.*, 2010; Belli *et al.*, 2013; Morales-Molino and García-Antón, 2014; Naughton *et al.*, 2016). Unfortunately, the north-western basin is poorly serviced by palaeoenvironmental studies using planktonic foraminifera (Rohling *et al.*, 1998; Melki *et al.*, 2009). Therefore, our understanding of how planktonic foraminifera responded to the most recent deglacial in this key location is limited.

To this end, this work addresses several important research questions:

1. To what extent are HS1, the BA and the YD recorded in the Mediterranean Sea and what was the basin-wide significance of these short-term events?
2. What was the impact of these climatic events on the prevailing hydrological systems?
3. How did these climatic events affect the basin-wide distribution of planktonic foraminifera and to what degree?
4. Specifically, to what extent was the north-western Mediterranean Sea impacted by the deglacial, and how can planktonic foraminifera inform our understanding of the associated changes in surface water hydrology?

Acknowledging these research questions, the following aims and objectives formulate the basis of this thesis:

Aims:

1. To provide a detailed and comprehensive basin-wide palaeoclimatic and palaeoecological reconstruction of HS1, the BA and the YD climatic events in the Mediterranean Sea.
2. To reconstruct SSTs and palaeoenvironment of the deglacial and early Holocene periods in the north-western Mediterranean Sea, to test the timing and impact of rapid climate change in the region.

Objectives:

1. To construct a chronologically constrained dataset for each chronozone comprising of planktonic foraminiferal census counts.
2. To reconstruct SSTs using the artificial neural networks (ANN) transfer function for each chronozone.

3. To map the distribution of individual planktonic foraminiferal species for each chronozone.
4. Provide a detailed planktonic foraminifera assemblage for the late HS1 to early Holocene period in the Gulf of Lion.
5. To reconstruct SSTs and provide a palaeoecological interpretation for the Gulf of Lion during the deglacial/Holocene transition.

To achieve these aims and objectives it was necessary to obtain faunal count data from a plethora of sediment cores covering as large a spatial area as possible. The collation of this data comprised of existing published data and the addition of new unpublished data. All data had to meet specific criteria, e.g. chronological control points and >150µm size fraction. This sampling strategy would ensure that all the requirements for a comprehensive dataset would be met. SSTs were reconstructed using the ANN transfer function. This technique was chosen as it has a low prediction error rate (±1°C), thereby producing reliable SST estimates. In addition, using the ANN also enabled direct comparisons with results obtained in the LGM study undertaken by Hayes *et al.* (2005).

Core M40/4 82-2SL was chosen for this study as it was a known high-resolution core from the Gulf of Lion, which extended through the deglacial and early Holocene time series (Broggy, 2011). Detailed sampling provides a sub-centennial record of planktonic foraminifera counts and SST predictions using ANN, to accurately test the timing and degree of palaeoenvironmental change was experienced in the Gulf of Lion.

It is anticipated that having completed the aims and objectives, this research will enhance our understanding of the late glacial palaeoenvironments in the Mediterranean Sea. In addition, the provision of palaeotemperatures can be used to assess the quality of numerical models. The high-resolution record in the Gulf of Lion will test the degree that global and/or regional controls had on palaeoenvironmental change in north-western Mediterranean Sea during the deglacial and early Holocene period.

Chapter 2.

2 Climatology and physical oceanography of the Mediterranean region

The Mediterranean Sea is a semi-enclosed basin located between the subtropics of northern Africa and the more temperate north-western Europe. Due to the complex land distribution, the Mediterranean Sea is composed of two deep basins (the western and eastern basin), which are separated by the shallower Strait of Sicily (Figure 2.1). The western basin connects to the North Atlantic through the Strait of Gibraltar and contains a number of distinct sub-basins, i.e. the Alboran, Balearic and Tyrrhenian Seas and the Gulf of Lion. Once through the Strait of Sicily, the eastern basin is comprised of the Ionian and Levantine Seas, with the Adriatic and Aegean sub-basins to the north.
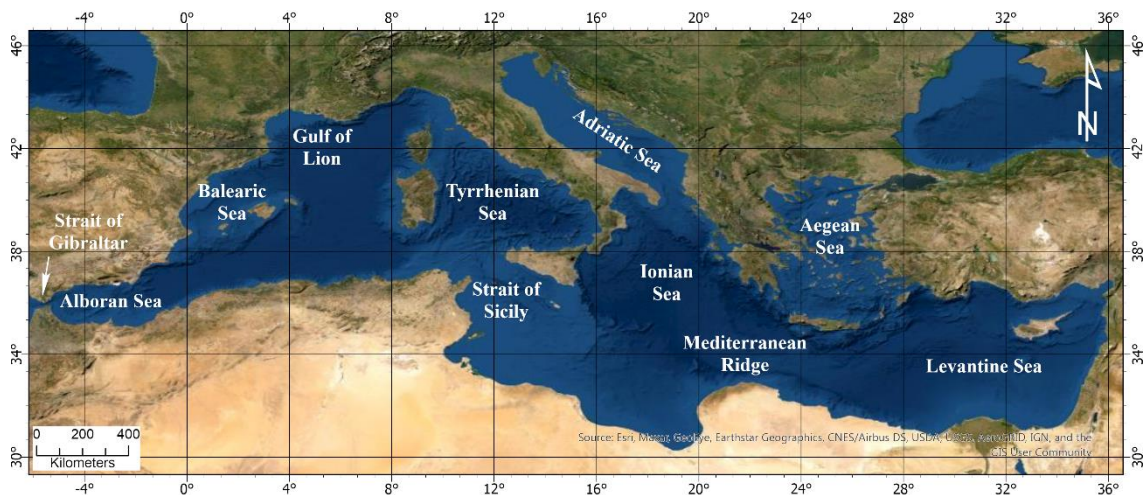
Figure 2.1: Map of the Mediterranean region, encompassing the sea and surrounding topography.

Given its transitional location, both the climate and oceanography of the Mediterranean Sea are strongly influenced by seasonal changes in atmospheric circulation and oceanography of the North Atlantic, as well as from the subtropical high-pressure systems from further south. To determine the processes that influenced the Mediterranean region in the Late Pleistocene, we need to understand the climate and oceanography of the present-day Mediterranean, as well as potential factors that may have operated in the region in the past. Therefore, this chapter will introduce and review the global and regional atmospheric patterns that impact the modern Mediterranean region, as well as outline the hydrographic structure of the sea, as well as the processes that influence it.

2.1 Climate

2.1.1 Atmospheric variability

Global atmospheric variability is characterised by the complex interaction of latitudinal variations in insolation, albedo, land-sea distribution and ocean circulation, and the effect of the rotation of the earth on these factors. Variations in latitudinal net radiation mean that warm, less dense equatorial air rises, moves poleward, sinks as colder denser polar air and moves back towards the equator, in what is called a Hadley Cell. However, as these air masses are subject to the Coriolis force, they are subdivided into three separate cells, the low latitude Hadley Cell (between 0-30° N/S), the Ferrel Cell in the mid latitudes (30-60° N/S) and the high latitudes Polar Cell (60-90° N/S) (Figure 2.2) (Lockwood, 1985). Each of these cells are separated by different pressure regimes. Between the ascending branches of the high-pressure Hadley Cells at the equator, the convergence of warm, moist buoyant air by the Trade Winds forms a low-pressure belt called the Intertropical Convergence Zone (ITCZ) (O'Hare *et al.*, 2013). The ITCZ is characterised by heavy precipitation, cloudiness, and intense latent-heat release.
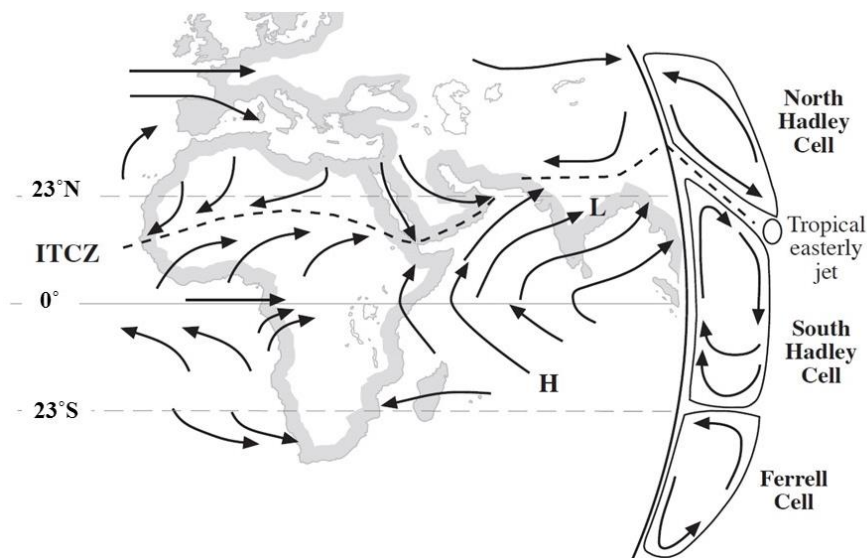
Figure 2.2: Northern Hemisphere atmospheric circulation patterns during the summer. Arrows illustrate the movement of the dominant winds: H=areas of high sea level pressure; L = areas of low sea level pressure. Taken from Rohling et al. (2009).

Between the Hadley Cell and the Ferrel Cell, cold dry air descends giving an area of high pressure known as the Subtropical High-Pressure Belt (i.e. the Azores high-pressure cell in the North Atlantic) (Lionello *et al.*, 2006b; Seager *et al.*, 2019). Circulation changes within the Hadley cell causes the location of the ITCZ and the Azores High to migrate with the changing seasons (Alpert *et al.*, 2006). In particular,

the position of the ITCZ migrates, following the annual cycle of surface solar heating, i.e. it moves towards the equator during winter months and poleward in the summer. In addition, the mean location of the ITCZ is to the north of the equator. This is linked to the oceanic heat transfer from the southern hemisphere into the North Atlantic by the Atlantic Meridional Overturning Circulation (AMOC), which is balanced somewhat by the southern transport of atmospheric energy by the northerly location of the ascending branch of the Hadley Cell and ITCZ (Marshall *et al.*, 2013; Schneider *et al.*, 2014). This interconnection between the AMOC and the ITCZ was important for the Mediterranean region during the abrupt climate changes of the Late Pleistocene and will be discussed in Chapter 4.

These atmospheric cells and their associated pressure regimes dictate the global wind patterns located at different latitudes. Within the Hadley Cells, convergence of warm air towards the equator generates the Trade winds. Between 30-60° (N/S), as warmer tropical air moves poleward, it is deflected to the east by Coriolis force, creating the Westerlies, which are intrinsic to the Mediterranean climate, especially during the winter (Lionello *et al.*, 2006a). Towards the poles, the high-pressure Polar Cell is characterised by cold dense dry air. The winds from the Polar cell are deflected, forming the weak Polar Easterlies. There is a significant pressure and thermal gradient between the northern flowing milder low latitude air and the cold polar air, and they do not readily mix (O'Hare *et al.*, 2013). Where this convergence occurs is known as the Polar Front Zone. The polar front has a significant influence on the development of cyclogenesis in the Northern Hemisphere, which directly impacts on regional weather systems in the Mediterranean region. The pressure differences create the high-altitude, fast moving circumpolar Upper Westerly winds, which meander in long waves, known as Rossby Waves. In winter months, when the temperature gradient is greater, the meanders become shallower and low-pressure systems (depressions) can form. Within these Upper Westerlies, strong, narrow currents (i.e. jet streams) occur and are instrumental in the formation and flow direction of these storm tracks (O'Hare *et al.*, 2013). For example, depressions can travel rapidly cross the North Atlantic Sea, bringing wet and windy conditions to western Europe and the north western Mediterranean.

Changes in the pressure and acceleration of the jet stream along the poleward limbs of the Rossby Waves, help initiate depression formation and enhanced cyclogenesis. The Polar Front Theory was developed by the Bergen school over a century ago, and

describes the six stages of the development of these mid-latitude cyclones (depression) that track from west to east along the atmospheric polar front (Figure 2.3) (O'Hare *et al.*, 2013). During the initial Stage A, a front is formed, dividing cold and warm air masses. During Stage B, a wave develops along the front, and a low-pressure centre becomes established along the crest of this wave. As the cyclone develops into Stage C, the wave becomes more pronounced due to the cyclonic movement of the air masses. The eastern edge of the wave is characterised by a warm front that is followed by the westerly flowing warm air mass, with the cold front and cold air mass moving in from behind. As the depression deepens (Stages D-E), the cold front moves faster, and the fronts start to become occluded. Warmer air from the contracting warm sector is pushed upwards, cooling and condensing to form zones of rainfall that precede the fronts. The cyclone reaches maturity (Stage E) when the fronts are fully occluded, and rainfall is firmly established along this occluded front. The occluded front lengthens and moves away from the centre of the depression (Stage F). Mid-latitude cyclones last 3-5 days from initiation and once it dissipates, the polar front is re-established. However, depressions usually occur in families, which progressively form further south, as they trail the previous depression (O'Hare *et al.*, 2013).
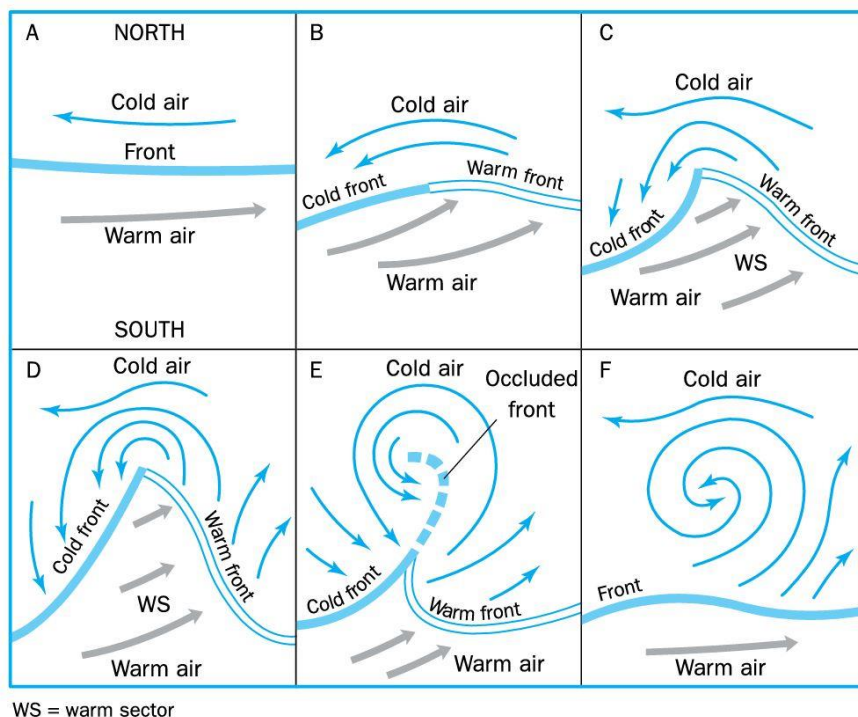
Figure 2.3: Six stages of the formation of mid-latitude depressions. Taken from O'Hare et al. (2013).

In the northern hemisphere, these mid-latitude cyclones dominate winter weather patterns in north-west Europe. However, there is also a strong positive correlation of

winter precipitation in the Mediterranean, especially the western basin, and these North Atlantic depression systems, which are tracked into the region by the more southerly location of the polar front jet and associated strong Westerly winds (Trigo *et al.*, 2006; Baldi *et al.*, 2008). In contrast, when Westerly winds and jet streams are weakened during the summer, the Mediterranean region is dominated by the high pressure ridge extending from the subtropical Azores High, leading to warm, dry conditions (Xoplaki *et al.*, 2003).

2.1.2 Mediterranean climate

The Mediterranean climate can be broadly described as having warm to hot summers with low precipitation, and mild wet winters (Lionello *et al.*, 2006b; Lionello *et al.*, 2012a). Due to its transitional location, there are two main Köppen-Geiger climate types, the Arid (B) desert and steppe climates to the south and the Temperate (C) Mediterranean and Humid Subtropical climates to the north. Arid regions along the north African coastline are characterised as dry, with near unbroken sunshine throughout the year and are directly linked to the presence of global high-pressure cells (Hess and Tasa, 2010). Precipitation rates in the Sahara region are <30cm/year (with or without a defined wet season), with air temperatures ranging from mid-teens in winter to >30°C during the summer (Hess and Tasa, 2010).

In the more temperate northern regions, annual rainfall is 38-64cm, though with variable seasonal precipitation rates. Summers are virtually rainless (<40 mm rain in the driest month) and winter rates are approximately 8-13cm per month (Hess and Tasa, 2010). Summers are dominated by stable high-pressure systems linked to subtropical highs which, in combination with cool ocean water, lead to a dry stable atmosphere, clear skies and significant sunshine (Hess and Tasa, 2010). Air temperatures range from 16-21°C in the north-western margins of the western basin, to 24-27°C in the eastern basin (Hess and Tasa, 2010). In winter, these high-pressure systems move south, allowing for more influence by the Westerlies and midlatitude cyclones and associated rain-dominant fronts. Winter air temperatures are mild and can vary from 7-13°C (Hess and Tasa, 2010).

2.1.3 Prevailing winds

Due to the complex topography and land distribution of the Mediterranean region, and its location in a transitional area between the Westerlies to the north and the Azores

High pressure system to the south, winds are complex and seasonally variable (Ruti *et al.*, 2016). More than 45 different winds have been described from the region (MEDEX, 1996). In winter, the winds are strongly influenced by pressure ridges and troughs at 500mb level in the atmosphere, mainly from the north, which cause more active weather in the Mediterranean region (Quantic, 2008). In the summer the weather is usually more settled, both on the surface and at 500mb level (Quantic, 2008).

The Mediterranean region is strongly influenced by several katabatic air flows, which are characterised by the sinking of dense cold air, generated in higher ground, which is then funnelled downslope through the surrounding valleys (Quantic, 2008). These winds are not as influenced by atmospheric pressure gradients, though can be strengthened by passing lows. These winds can reach gale force, especially if the mountainous source is snow covered, flowing down through long and steep valleys. In the western, northern and eastern rim of the Mediterranean, regional winds are influenced by the surrounding topography. The Mistral and Tramontane winds are funnelled into the Gulf of Lion, while the Bora and Etesian winds extend into both the Adriatic and Aegean seas (Figure 2.4).
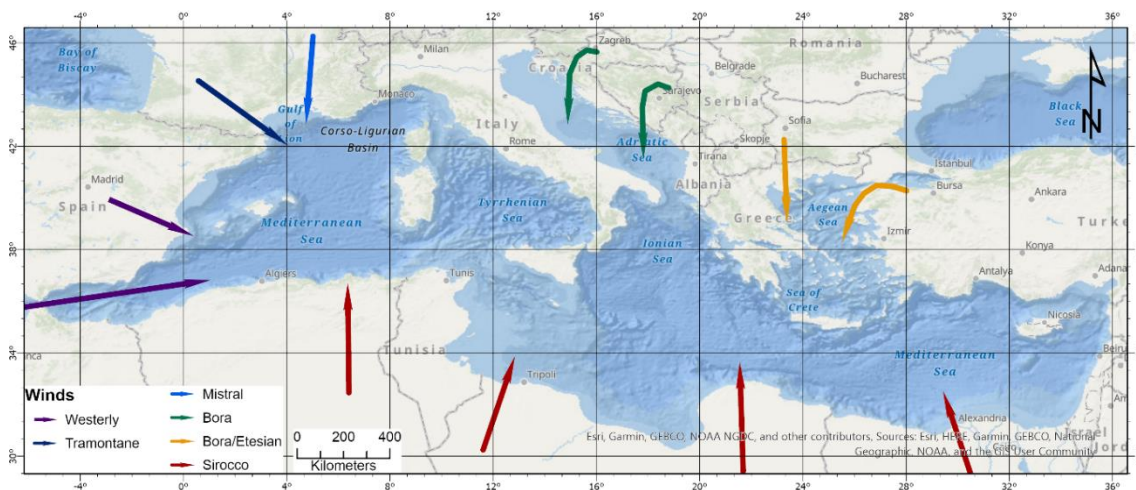
Figure 2.4: Topography of Mediterranean region, with associated winds (MEDEX, 1996).

The Mistrals are cold northerly katabatic winds that flow south from central southern France through both the Garonne and Rhone Valleys to the west and east of Massif Central to the Gulf of Lion (MEDEX, 1996). The Tramontane winds form part of the Mistral system, but flow into the Gulf of Lion from a more north-westerly direction through the Naurouze Gap between the Pyrenees and the Massif Central (Lionello *et al.*, 2006a). The Mistral and Tramontane winds are most common in the winter, though they can occur year-round (Givon *et al.*, 2021). Gale force Mistrals often develop when

cyclogenesis occurs over the Gulf of Genoa with the passage of the 500mb trough through eastern France (MEDEX, 1996) (see section: Cyclogenesis). These ~100 knot winds can extend through the western and central Mediterranean. In the eastern basin, Bora winds are generated when cold winter polar air builds in the Balkans and are katabatically funnelled through gaps in the surrounding mountain ranges towards both the Adriatic and Aegean Seas (MEDEX, 1996; Quantic, 2008). East of the Adriatic, these cold Bora winds flow in a south-west direction through the Dinaric Alps across the sea; whereas in the Aegean Sea region, north/north-east Bora winds flow from the Balkan Peninsula through the Rhodope and Boz Dağlar mountains in western Turkey, and the Pindus Mountains in Greece (MEDEX, 1996; Quantic, 2008). Following a similar track of the winter Bora winds, the north-eastern Etesian winds are generated by northerly monsoonal winds that flow into the Aegean Sea and eastern Mediterranean (see section: Monsoons). These winds are affected by low-pressure systems over Turkey and high pressure in eastern Europe (MEDEX, 1996).

In addition, there are several non-katabatic winds of note, including the cold Westerly winds, and warm Levante and Sirocco winds. Westerly winds flow in from the North Atlantic through the Straits of Gibraltar from autumn through to spring, either coming before cold fronts (from the south-west) or after passing cold fronts (from the south-east) (Quantic, 2008). They are concentrated in the Alboran Sea and south of the Balearic Islands, and are associated with 500mb low-pressure troughs passing through the straits (MEDEX, 1996). In contrast, during the summer, the warm Levante winds are channelled westward from the Alboran Channel through the Straits of Gibraltar and when gale-force, they can extend out as far as the Gulf of Cadiz (MEDEX, 1996; Quantic, 2008). Along the east coast of Spain, the more north-easterly Levante winds occur throughout the year, though more commonly during the spring and autumn (Quantic, 2008). These winds are generated when there are high-pressure systems over Central Europe, with relatively low pressure in the western Mediterranean; if there is a high-pressure system over the Balearic Islands, or if there is an approaching cold front coming in from the west. Finally, Sirocco is the name for all hot, dry, dust-laden winds that flow north from the hot deserts of Northern Africa into the central and eastern Mediterranean region (Quantic, 2008). The warm Sirocco winds are unique in the Mediterranean region, as they are not generated or channelled by mountainous topography; they occur when surface or upper level depressions travel eastward along the southern Mediterranean/north Africa coast. They can occur throughout the year but

reach gale force mainly during the spring (MEDEX, 1996). As the wind travels north over the sea, it brings warm moist air and clouds to the northern margins of the Mediterranean (MEDEX, 1996; Quantic, 2008).

2.1.4   Cyclogenesis

One of the dominant features of the Mediterranean climate is the occurrence of frequent intense cyclones, especially during the winter and spring. During the Northern Hemisphere winter, the Mediterranean is one of the most cyclogenetic regions in the world and cyclones are one of the influential factors determining weather patterns in the region (Pettersen, 1956; HMSO, 1962). There are several factors that contribute to the frequency, intensity and duration of cyclones in the region, such as its location between the subtropics and the mid latitudes, the complex land-sea distribution, the steep orography of the northern coast and the thermal differences between the Mediterranean Sea and the incoming atmospheric winds (Harding *et al.*, 2009; Lionello *et al.*, 2012a). The enclosed sea is a significant source of moisture and energy for the generation of cyclones, and the surrounding mountain ranges and steep-sided valleys are instrumental in focussing and directing cyclonic systems, especially south of the Alps towards the Gulf of Genoa (Lionello *et al.*, 2006a). Most significant cyclogenesis occurs in the western basin, with cyclolysis occurring in central and eastern Mediterranean (Lionello *et al.*, 2012a). Although not as deep, extensive or long lasting as North Atlantic systems, cyclones in the Mediterranean region form a separate branch of the northern hemisphere storm track and are characterised by increased precipitation, wind, storm surges, waves and landslides (Lionello *et al.*, 2006a).

The highest rate of cyclogenesis occurs mainly during winter months, peaking in January (HMSO, 1962; Lionello *et al.*, 2006a; Almazroui *et al.*, 2017). In the western basin, orographic cyclogenesis is concentrated mainly in the Gulf of Genoa into the Ligurian Sea, as well as the Gulf of Lion and south of both the Pyrenees and Apennines. The Gulf of Genoa is the main centre for cyclogenesis within the Mediterranean throughout the year (Trigo *et al.*, 2002; Ulbrich *et al.*, 2012). Most cyclones do not develop into extreme weather events and not all severe weather events are associated with cyclones (Jansa *et al.*, 2014). However, in some instances deep cyclones are associated with intense and persistent rainfall and strong winds, and it is estimated that 80% of all heavy rainfall in the western basin is associated with a nearby cyclone, which channels and forces upward low-level warm moist air, leading to heavy precipitation

(Jansa *et al.*, 2001; Jansa *et al.*, 2014; Ruti *et al.*, 2016). This association between heavy precipitation and strong winds with cyclonic activity is also observed in the eastern basin, where heavy rain and snow in Greece is associated with fast moving cold orographic cyclones (Jansa *et al.*, 2014).

2.1.5 Monsoons

The South Asian Monsoon (SAM) is a substantial pattern of winds and precipitation centred over southern Asia and the Indian Ocean. As a result of the seasonal northward migration of the ITCZ during the summer, in addition to rapid warming over the Indian continent, strong westerly winds trigger large scale cyclones, bringing with them the characteristic intense summer monsoonal rains (Rodwell and Hoskins, 1996; Goswami, 2012). The SAM has been demonstrated to be critical in influencing the eastern Mediterranean (Reddaway and Bigg, 1996; Rodwell and Hoskins, 1996; Rodwell and Hoskins, 2001; Kothe *et al.*, 2014). The Rossby wave response to the increase in temperature and westerly winds of the SAM, causes an area of adiabatically descending air to form to the west of the SAM (Rodwell and Hoskins, 1996). This descent forms the Persian trough from the Persian Gulf into the Aegean Sea; its flow and direction governed by the eastern Mediterranean mountain ranges (Tyrlis *et al.*, 2012). Intensification of the SAM enhances the Persian trough, which combined with the subtropical Azores high to the west, causes an atmospheric pressure difference between the two basins. This is positively correlated to increasing the east-west SLP gradient, strengthening Etesian winds over the Ionian Sea, decreasing winds in the central western basin, the hydrostatic decline in SST across the Mediterranean and is characterised by the dry arid conditions experienced in the eastern basin (Reddaway and Bigg, 1996; Xoplaki, 2002; Ziv *et al.*, 2004; Tyrlis *et al.*, 2012).

Finally, the East African Monsoon (EAM) had an indirect impact on the Mediterranean climate through fluvial discharge from the Blue Nile/Atbara, which drains the spring/autumn monsoonal rains from the Ethiopian Highlands into the Levantine Basin (prior to the opening of the Aswan High Dam in 1964) (Weldeab *et al.*, 2014). The two monsoon events (i.e. spring "long-rains" and autumn "short rains") are associated with the south-north and then returning north-south migration of the ITCZ (Camberlin and Philippon, 2002). During the spring, the direction of the trade winds reverse, bringing moist oceanic air and monsoonal rains inland from the Indian Ocean. In the summer, the south-westerly Somali Jet is strengthened with a region of subsidence forming along its

western side, shutting down the monsoons for the summer months; then in the autumn, the Somali jet weakens bringing less intense rains into the eastern Horn of Africa (Funk *et al.*, 2016). Prior to the mid-1960s, 70% of the average discharge from the Nile came from the monsoon-related Blue Nile/Atbara discharge (Rohling *et al.*, 2009). The impact of this Nile discharge on the Levantine Basin will be discussed in the following section.

2.2 Oceanography

The Mediterranean Sea is distinct in that it is a semi-enclosed sea, subdivided into two deep basins (>4000m in places) by the Strait of Sicily (~330m average depth), with inflow of Atlantic waters through the Straits of Gibraltar (Wüst, 1961). Mean annual sea surface temperatures (SSTs) are warm (19.7°C), ranging from cooler (~17°C) along the northern margins (i.e. north-west Mediterranean, northern Adriatic and Aegean Seas), increasing towards the south-eastern basin (~23°C) (Figure 2.5; Table 2.1) (Locarnini, 2018). It is an evaporitic basin (i.e. evaporation (E) exceeds input from precipitation (P) and rivers (R)), with a mean salinity value is 38.2 practical salinity units (psu), which has a direct influence on the circulation and biogeochemistry of the sea (Table 2.1) (Tanhua *et al.*, 2013; Locarnini, 2018).
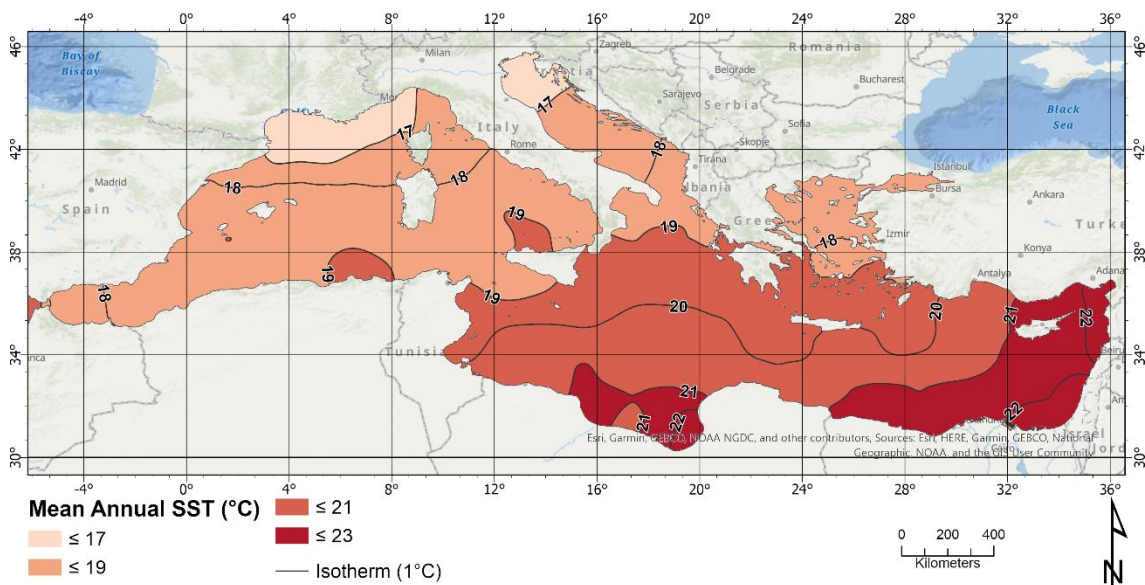
Figure 2.5: Mean annual SSTs in the Mediterranean Sea (at 10m depth). Data from the World Ocean Atlas (2018) (Locarnini, 2018).

In its most simplistic form, fresher cooler Atlantic waters enter through the Straits of Gibraltar, flow eastward along the north African coast into the eastern basin, increasing in temperature (T) and salinity (S), until they sink and form intermediate waters that

flow back towards the western basin (Figure 2.6). This deeper water then exits the Straits of Gibraltar into the North Atlantic as the Mediterranean Outflow Water (MOW). However, the circulation of Mediterranean waters is more complex due to the presence of the Adriatic and Aegean sub-basins, net evaporation during the summer and deep-water formation initiated by winter cooling of surface waters by katabatic winter winds.

	Mediterranean Sea	Western Basin	Eastern Basin
SST (°C)	19.70	18.61	20.34
Salinity (psu)	38.20	37.62	38.54

Table 2.1: Mean annual SST (°C) and salinity (psu) for the Mediterranean Sea and western and eastern basins derived from the World Ocean Atlas (WOA) (2018) (Locarnini, 2018). psu = practical salinity units.
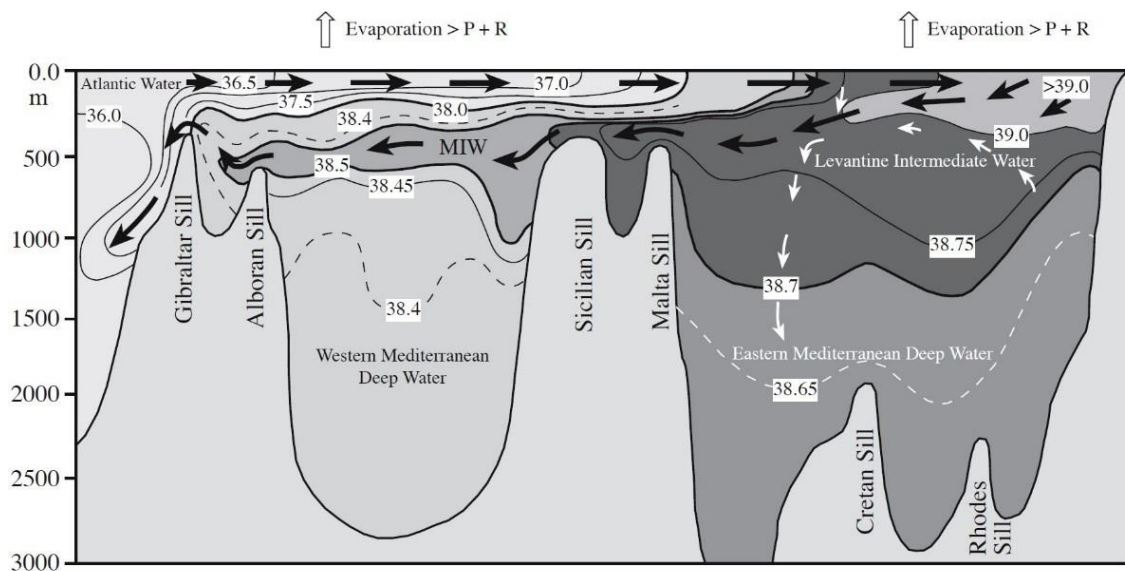
Figure 2.6: Longitudinal cross section of Mediterranean Sea Water masses, with modern winter current direction and salinity (psu). Taken from Rohling et al. (2009).

Therefore, this section will outline the main present-day surface, intermediate and deep circulation patterns, areas of deep-water formation, as well as the influences of freshwater discharge into this warm hypersaline sea. This review of oceanic processes is essential to understand the hydrographic systems in the Mediterranean Sea. These systems ultimately control parameters which determine the distribution of foraminifera. In addition, understanding modern oceanic process will allow us to identify potential differences during the deglacial period since the LGM. For example, to what extent did sea surface temperatures (SSTs) vary during the Late Pleistocene and were these changes homogenous across the Mediterranean Sea? Also, is there evidence of extensive changes or restructuring of the ocean circulation, or hydrological structure during these periods and what are the potential drivers of these changes?

2.2.1 Surface circulation

Incoming North Atlantic Surface Waters (NASW) that flow through the Straits of
Gibraltar into the Alboran Sea (S: 36.1-36.2 psu; T:15-16°C) are quickly entrained and
mixed during periods of upwelling with the Mediterranean Intermediate Waters (MIW)
to form the warmer (T: 16°C), slightly more saline (S: 36.5 psu) Modified Atlantic
Water (MAW) (Figure 2.6; Figure 2.7) (Millot and Taupier-Letage, 2005). This fast-
moving 100-200m deep MAW jet is instrumental in the formation of two highly
productive, semi-permanent anti-cyclonic gyres; namely the Western and Eastern
Alboran Gyres (WAG and EAG) (Figure 2.7) (Millot, 1999). As a result of the
incoming NASW, upwelling of the MIW, the presence of the gyres and intense winter
Westerlies, the Alboran Sea is rich in nutrients and highly productive, especially during
the winter bloom (Nov-Mar) (Bárcena *et al.*, 2004; Hernández-Almeida *et al.*, 2011)
(Figure 2.7).
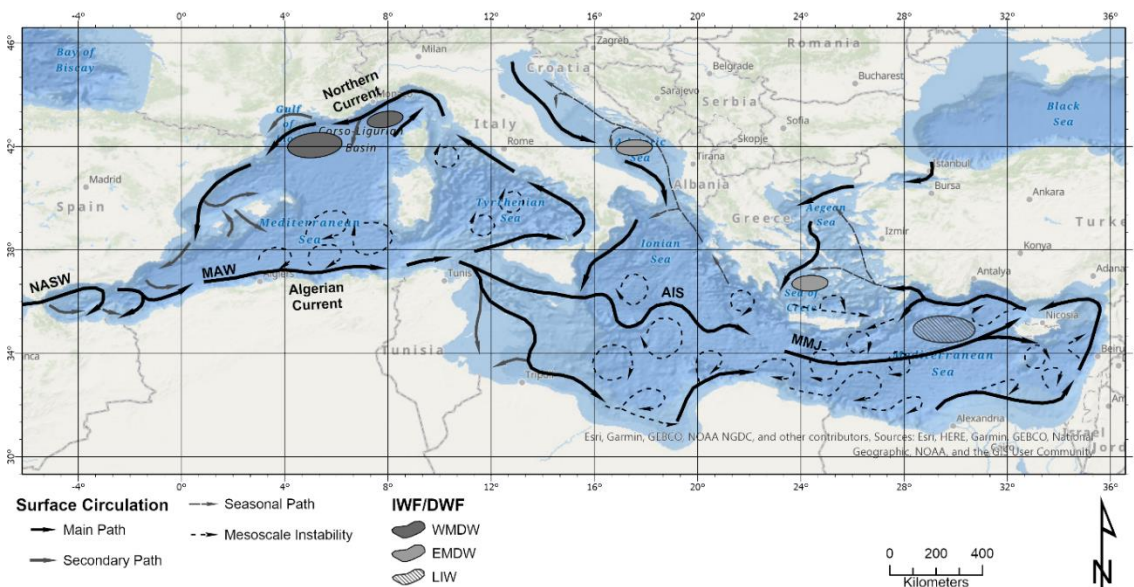
Figure 2.7: Surface water circulation in the Mediterranean Sea. Modified from Millot (1999), Millot and Taupier-
Letage (2005) and Rohling et al. (2009).

On the eastern edge of the EAG, the MAW is deflected south towards Oran where it
meets the dense and more saline (S: >37.6 psu) resident Mediterranean waters, forming
the semi-permanent Almeria-Oran Front (Tintore *et al.*, 1988; Arnone *et al.*, 1990;
Millot, 1999). From here, the MAW bifurcates, flowing west to complete the gyre and
east as the cool nutrient rich Algerian Current, lying approximately 30km off the
Algerian coast (Figure 2.7). The Algerian Current begins as a narrow (30-50km) and
deep (200-400m) current, but as it extends eastward towards the Channel of Sardinia, it
thins, widens and becomes increasingly unstable (Millot, 1999; Robinson *et al.*, 2001).

It is characterised by large scale meanders (~10kms) and "coastal eddies" (~10s-100kms in diameter) that can be subdivided into i) smaller short lived cyclonic eddies and ii) longer-term and larger anticyclonic eddies (associated with upwelling) that migrate and expand (30-100km) both northward as "open sea eddies" and towards the east (Arnone *et al.*, 1990; Millot, 1999).

The instability of the Algerian Current to the south of Sardinia causes the MAW to split, with one branch flowing to the north of Sicily towards the Tyrrhenian Sea; the other to the east towards the Straits of Sicily into the eastern basin (Figure 2.7). In the western basin, the MAW forms the Western Basin Gyre as it flows northward along the continental slope off the coast of Italy into the Ligurian-Provençal Basin, where it becomes known as the Northern Current, then south through the Catalan Basin, and finally returning to the Alboran Sea where it is entrained and mixed with the incoming NASW (Millot, 1999; Millot and Taupier-Letage, 2005). Once the greatly modified MAW returns to the Alboran Sea, its distinct salinity, density and SST gradients are instrumental in the formation of the Almeria-Oran Front. Within the central and northern Tyrrhenian Sea, seasonal cyclonic eddies can occur, triggered by winter wind upwelling events, especially east of the Strait of Bonifacia; this is in contrast to the southwestern Tyrrhenian Sea where the orography of the islands protect it from such events (Millot, 1999).

At the Straits of Sicily, it has been estimated that two-thirds of the MAW (winter SST: ~15°C; S: 37-37.5 psu) flow into the eastern basin (Garzoli and Maillard, 1979; Tsimplis *et al.*, 2006; El-Geziry and Bryden, 2014). Due to the complex topography, width of the strait and the number of islands, on first leaving the Strait of Sicily the MAW splits i) as a branch that flows to the north-east; ii) as mesoscale eddies that move towards the central Ionian Sea; iii) south as branches towards Tunisia and Libya (Millot and Taupier-Letage, 2005). As the northern branch, known as the Atlantic-Ionian Stream (AIS), meanders eastward through the Ionian Sea, it feeds the Mid Ionic Jet and fast-flowing Mid-Mediterranean Jet (MMJ). By the time the MMJ reaches the Ligurian Sea, temperature, evaporation and salinity have increased (T$_{(winter)}$: ~17°C; S: <38.8 psu), and it has become increasingly unstable, forming a series of cyclonic and anticyclonic gyres and eddies, including the Rhodes, Mersa Matruh, Cretan and West Cyprus gyres (Figure 2.7) (Malanotte-Rizzoli *et al.*, 1997; Robinson *et al.*, 2001). At Cyprus, the MMJ splits again i) to the north to form the Asia Minor Current (AMC); ii) south towards the Shikmona eddy (Robinson *et al.*, 2001).

2.2.2 Intermediate water formation

During winter storm events in the Levant, cold Bora/Etesian winds track across the sea, cooling surface waters (T: 16-17°C) and increasing rates of evaporation which, when combined with the high salinities (S: ~39.2 psu), cause this dense water to sink to form the Levantine Intermediate Water (LIW) (Figure 2.6) (Robinson *et al.*, 1992; Malanotte-Rizzoli *et al.*, 1997). The main areas of LIW formation are within the Rhodes Gyre, though it may extend across the whole north Levantine basin, as well as the Aegean Sea and south Levantine Sea (Figure 2.8) (Malanotte-Rizzoli *et al.*, 1997; Tsimplis *et al.*, 2006).
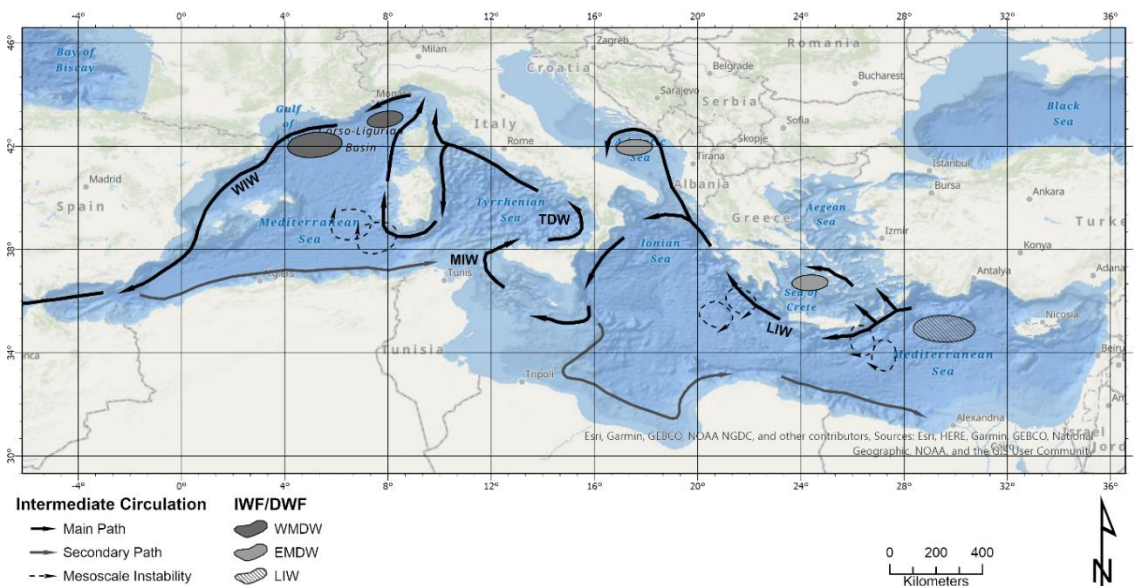
Figure 2.8: Intermediate water circulation in the Mediterranean Sea. Modified from Millot and Taupier-Letage (2005).

The LIW can be identified by a distinct halocline (salinity maximum) that lies between 150-600 m depth (Wüst, 1961). It spreads out across the eastern basin, where it is entrained and recirculated by the many gyres and eddies, deflected north into the Adriatic and southern Aegean Seas, and west towards the Straits of Sicily where it is partially deflected back into the Ionian Sea, as well as exiting into the western basin as Mediterranean Intermediate Water (MIW) (T: 14°C; S: ~38.5 psu) (Garzoli and Maillard, 1979; Malanotte-Rizzoli *et al.*, 1997). West of the Straits of Sicily the LIW splits with i) one branch deflected to the north by the Coriolis force into the Tyrrhenian Sea (forming the Tyrrhenian Dense Water (TDW) at 200-2000m) and to the west around Sardinia; ii) the other branch flows west along the north African coast to the Alboran Sea (T: 13.2°C; S: 38.5 psu), through the Straits of Gibraltar into the North Atlantic as the MOW (Malanotte-Rizzoli *et al.*, 1997; Millot, 1999; Tsimplis *et al.*,

2006). In the North Atlantic, the MOW can be identified as a rotating lenses of warm salty water (36.5 to 37.5 psu and T: 10.5 to 14.0°C) that sits at ~1000m depth and flows northward along the north-western European coast (van Dijk *et al.*, 2018).

In the north-western basin, Winter Intermediate Water (WIW) forms when the winter Mistral winds track across the Gulf of Lion and the Ligurian Sea, cooling the surface Northern Current enough to cause the cooler dense saline water (T: 12.5-13°C; S: 38.1-38.3 psu) to sink beneath the MAW, but not enough to trigger deep mixing (Millot, 1999). Millot (1999) also noted that the degree of winter storminess can directly influence the depth of vertical mixing; therefore, during milder winters WIW formation can exceed that of deep water formation in this region. WIW form during colder winters, though they may be easily mixed with the upper boundary of deeper waters, meaning they can be harder to differentiate. WIW can be differentiated from the slightly warmer LIW, and both flow in a similar southerly direction as the Northern Current to join the LIW as it enters the Alboran Sea and out the Straits of Gibraltar (Figure 2.8) (Millot, 1999; Robinson *et al.*, 2001; Tsimplis *et al.*, 2006).

2.2.3 Deep water formation

Within the Mediterranean, deep water formation (DWF) is crucial for the thermohaline circulation of the Mediterranean Sea. During winter months, well oxygenated deep waters are formed in the northern regions of both the west and east basins, though through slightly different mechanisms (Tanhua *et al.*, 2013).
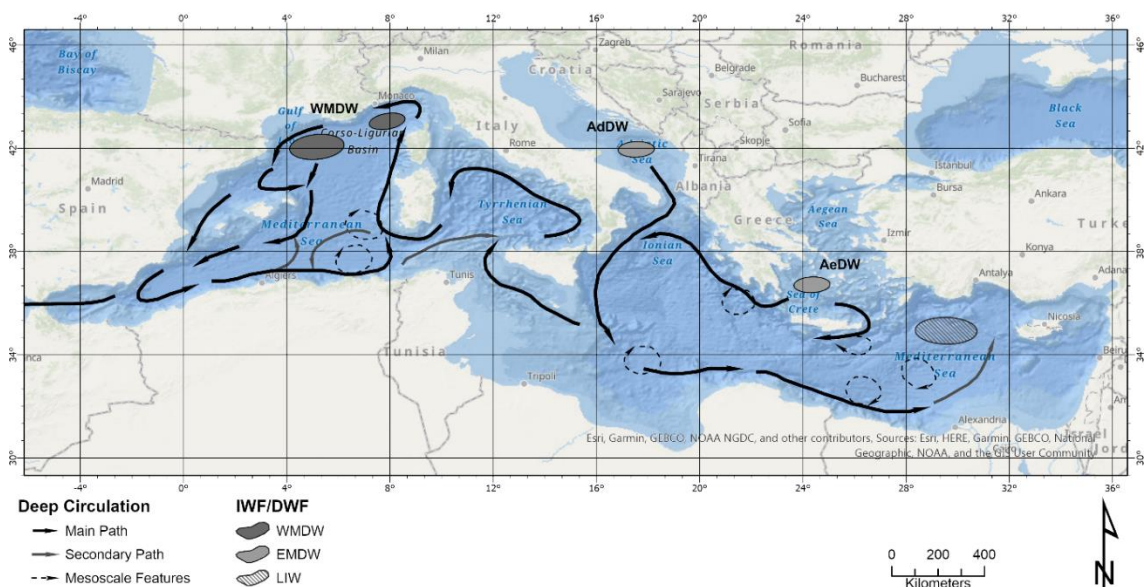
Figure 2.9: Areas of intermediate (IWF) and deep water formation (DWF) and deep water circulation in the Mediterranean Sea. Modified from Millot and Taupier-Letage (2005).

2.2.3.1 *Western Mediterranean Deep Water*

The Gulf of Lion, Ligurian and Provençal sub-basins are the key areas for DWF in the western basin (Figure 2.9). There is strong seasonality in the structure of the water column. From April to early autumn, the stratified oligotrophic waters develop a strong thermocline (10-20m thick) that deepens through the summer (10-50m deep), separating the cold bottom waters (~13.5°C) and the warmer fresh buoyant surface waters (20-25°C) (Millot, 1979). During these periods a deep chlorophyll maximum (DCM) develops within the pycnocline located at the base of the nutrient-depleted euphotic zone (where light levels are approximately 1% of the surface), in close association with the nutricline (Estrada, 1985; Estrada *et al.*, 1993; Estrada, 1996).
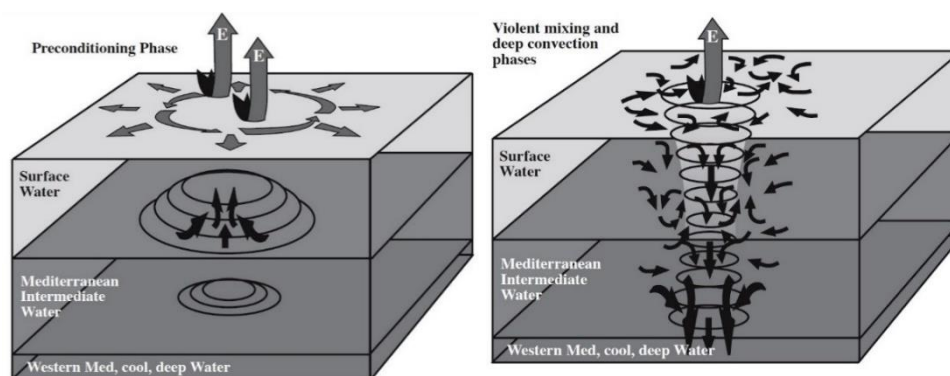
Figure 2.10: The preconditioning and violent mixing phases of deep-water formation in the Gulf of Lion. Taken from Rohling et al. (2009).

During winter months however, the combination of intense storms, winter SST cooling, high salinities and increasing water density trigger violent mixing of the water column, to form the Western Mediterranean Deep Water (WMDW). It is a three-phase process: i) the preconditioning phase; ii) violent mixing phase, and iii) sinking and spreading of the deep water (Figure 2.10) (Medoc, 1970). The preconditioning phase begins during winter months when the saline surface waters begin to cool (T: 10-12°C; S: 38.4 psu) causing the density of the waters to increase (Wüst, 1961). There is some mixing of the water column at this stage, but it retains its three distinct layers, i.e. the cold fresher surface waters overlying the warm saline WIW, with cold medium saline deep waters below. With the onset of winter storms, increased cyclogenesis and strong Mistral winds, intense cooling and evaporation of surface waters increase and the pycnocline shallows from 200-250m to <100m (Petrenko, 2003; Papadopoulos *et al.*, 2012). By February, the density rapidly increases causing the water column to become unstable, triggering deep vertical mixing that extends vertically as columns to depths >2000m,

thus eliminating surface and intermediate waters (Medoc, 1970).

This deep mixing upwells nutrient rich deep waters up to the photic zone increasing productivity, leading to strong winter-spring blooms (Rigual-Hernández *et al.*, 2012). It is also noted that productivity of north-western Mediterranean waters is closely linked to atmospheric patterns, i.e. colder stormier years leads to deeper vertical mixing and increased entrainment of nutrients, thus higher productivity (Estrada *et al.*, 1985). When the winter storms abate, this cold saline (T: 12.8-13°C; S: 38.4 psu) nutrient rich, well oxygenated mixed water spreads out and sinks to 1500-3000m; the densest water is trapped in the deepest parts of the basin in the Algero-Provençal Basin (2700-2900m), with the less dense waters redistributed by the western basin anticyclonic gyre and mesoscale eddies (Millot, 1999; Millot and Taupier-Letage, 2005). From the Algerian Basin, the least dense WMDW can flow northeast into the deep Tyrrhenian Sea where it sinks to below the TDW (~3900m), or west into the Alboran Sea (Millot, 1999). WMDW in the Alboran Sea, though residing at depths of >1000m can form part of the outgoing MOW, through seasonal mixing with MIW (Bergamasco and Malanotte-Rizzoli, 2010).

2.2.3.2   *Eastern Mediterranean Deep Water*

Eastern Mediterranean Deep Water (EMDW) is formed in the southern Adriatic and Aegean Seas (Figure 2.9). When compared to WMDW, the EMDW is warmer, has a higher salinity and is denser. As with the western basin, deep mixing is influenced by winter cooling of highly saline waters by orographic winds such as the Bora and Etesian winds. Prior to the mid-1990s the Adriatic Sea was regarded as the main source of deep-water formation in the eastern basin and the role and importance of the Aegean Sea as a major contributor to EMDW was debated (Klein *et al.*, 1999; Roether *et al.*, 2007). In the late 1980s to late 1990s, during a period of increased salinity followed by cold climatic forcing, the density of the Aegean Deep Water (AeDW) increased so that the outflow of AeDW superseded the Adriatic Deep Water (AdDW) as the primary source of DWF in the Eastern Mediterranean. This oscillation is known as the "Eastern Mediterranean Transient" (EMT) (Figure 2.11) (Klein *et al.*, 1999; Roether *et al.*, 2007).
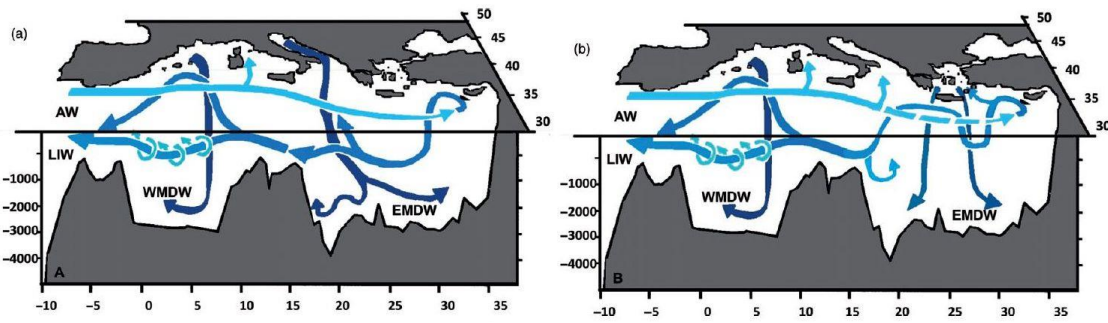
Figure 2.11: Thermohaline Circulation of the western and eastern basins a) before and b) after the Eastern Mediterranean Transient. Taken from Bergamasco and Malanotte-Rizzoli (2010).

The structure within the Adriatic Sea is comprised of: i) relatively fresh surface waters that are fed by rivers such as the River Po into the northern basin; ii) the incoming warm salty LIW; iii) the locally formed AdDW that also exits through the Strait of Otranto (Gačić *et al.*, 2001). Deep water within the Adriatic forms through two different processes, i.e. shelf convection in the northern Adriatic and open ocean convection in the southern Adriatic (Amitai *et al.*, 2018). In the northern Adriatic, the shallow topography (<100m depth) and significant wind-driven winter cooling of surface waters are key in forming North Adriatic Deep Water (NAdDW) (Manca *et al.*, 2002; Tsimplis *et al.*, 2006). As the cold winter winds significantly cool the shallow fresh waters, the density increases triggering deep vertical mixing, ventilation and homogenisation of the water column (T: ~9°C; S: 38.11 psu) (Mantziafou and Lascaratos, 2004). This cold high-density water then flows south along the western side of the basin, where it splits to sink down into the Middle Adriatic pit (250m, where additional wind-driven DWF occurs), or continues further south into the southern Adriatic (Mantziafou and Lascaratos, 2004; Chiggiato *et al.*, 2016). During the height of winter cooling (Feb-Mar), the south flowing NAdDW reaches the Bari region of the ~1200m deep Southern Adriatic Pit where it destabilises, mixes with incoming LIW and sinks down with the existing deep-waters of the southern Adriatic. In addition, there is a shallower (<700m) locally produced deep-water that forms through open ocean convection within the ~150m wide southern Adriatic gyre at the Southern Adriatic Pit (Mantziafou and Lascaratos, 2004). The processes here reflect those of the Gulf of Lion, where stratification of surface waters above the warm dense saline LIW occurs during in the summer/autumn preconditioning phase, followed by the violent mixing phase caused by winter wind-driven cooling, and finally the sinking and spreading phase (Mantziafou and Lascaratos, 2004). Although salinities of the AdDW (S: <38.7 psu) are less than the MIW (S: >39 psu), due to their cooler temperature (13-13.6°C) the dense AdDW sinks below the MIW and exits the Adriatic through the Otranto Strait into the Ionian Sea

(Robinson *et al.*, 1992; Tanhua *et al.*, 2013).

In the Aegean Sea, the situation is a little more complicated by the identification of the EMT in the mid-1990s. In general, the Aegean is characterised by significant temperature and salinity fluctuations (T: <13°C to >24°C; S: <31 to >39 psu) (Poulos *et al.*, 1997). Salinity varies with the varying sources of surface water inflow, including substantial summer inflow from the Marmara Sea of the brackish Black Sea Water (BSW) (S: ~18 psu), winter fluvial discharge and fresher MAW surface waters (S: ~38.5-38.9 psu), which are in contrast to the inflow of the high salinity Levantine Surface Water (LSW) (S: >39.3 psu) (Poulos *et al.*, 1997; Millot and Taupier-Letage, 2005; Velaoras *et al.*, 2014; Herrle *et al.*, 2018). Aegean Intermediate Water (AeIW) which is colder than LIW (T: 14.39°C; S: 38.93 psu), is formed during winter convection events to depths of 200-300m and can be identified throughout the Aegean (Gertman *et al.*, 1990). To the south in the Cretan Sea, intense winter cooling by Bora/Etesian winds within the Cretan Cyclonic Gyre can trigger deep mixing to depths of 400-700m forming the colder, denser Cretan Intermediate Water, which exits into the Ionian Sea usually settling below the LIW, at depths between 500-1200m (Klein *et al.*, 1999; Roether *et al.*, 2007; Velaoras *et al.*, 2014).

However, during the extreme winter of 1987 densities below 1000m began to increase to their peak in 1992-1993 when there was a significant outflow of warm dense AeDW (T: 13.6 °C; S: >38.8 psu) over the Cretan Sills into the eastern Mediterranean. The cause of this AeDW has been attributed to a sustained cold period with low precipitation; increase in the salinity of the LSW, which blocked the inflow of the MAW; a redistribution of the internal salt budget and a decrease in BSW (Klein *et al.*, 1999; Velaoras *et al.*, 2014). This outflow of AeDW accounted for 65% of EMDW during that period (Roether *et al.*, 1996). It has been suggested that these AeDW formation events have occurred in other periods of the recent past, where there is a salinity preconditioning phase within the Cretan Sea, that increases the density of the CIW and the amplitude of the DWF is governed by the degree of atmospheric forcing during the event (Velaoras *et al.*, 2014).

The outflow of both the AdDW and AeDW cascade down into the northern Levantine, Cretan and Ionian Seas, where they mix with the upper layers of the resident deep EMDW (>800m). These newly formed EMDW circulate in a basin-wide counter-clockwise gyre, where branches of the least dense waters exit through the deeper

channel at the Tunisian side of the Strait of Sicily (Millot and Taupier-Letage, 2005). Renewal time of for EMDW formed mainly from AdDW is estimated to be ~126 years at depths >1200m (Robinson *et al.*, 2001).

2.2.4 Freshwater input

The water budget of the Mediterranean Sea is composed of the inflow of lower salinity and brackish waters from the Atlantic and Black Sea, freshwater from rivers and precipitation, and evaporation. Of the net contributors to the annual water budget, input from rivers accounts for <20% (modern estimates from direct observations: ~8.1 x $10^3 m^3$ s^{-1}; when including unaccounted rivers: 10.4 x $10^3 m^3$ s^{-1}) (Struglia *et al.*, 2004). Variations in the rates of freshwater discharge have an important influence on coastal SST, the buoyancy of surface waters, the formation of LIW and WMDW/EMDW, as well as being an important source of sediment and nutrients, which has a direct impact on the
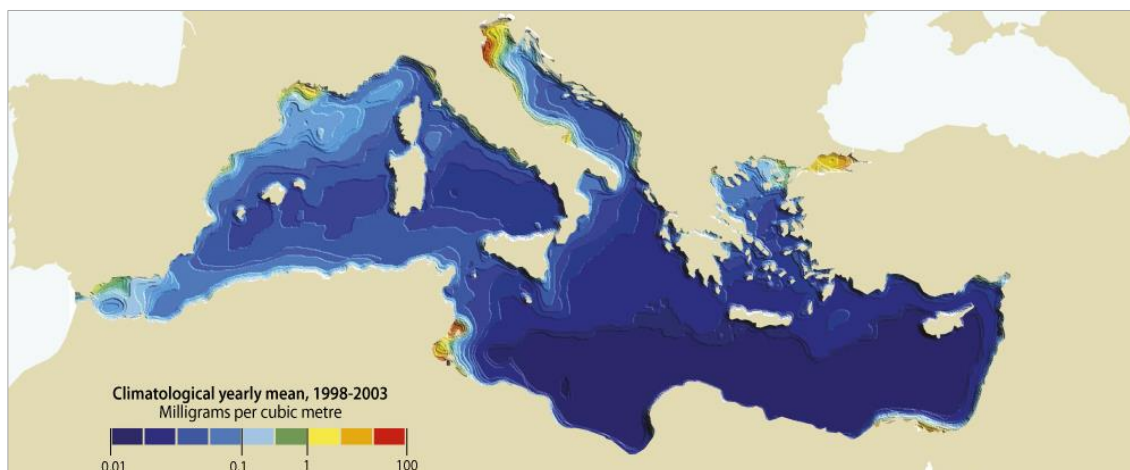
Figure 2.12: Schematic illustration of chlorophyll-α concentration in the Mediterranean Sea. Taken from GRID-Arendal (2013a); data source Barale et al. (2008).

primary productivity of coastal regions (Figure 2.12) (Struglia *et al.*, 2004; Ludwig *et al.*, 2009). In addition, the rates of E - (P + R) are not consistent throughout the region or annually; E rates are reduced in the northern Mediterranean due to the location of major rivers (62% of annual discharge is located in the Gulf of Lion, Adriatic and Aegean Seas) and during the winter/spring, E - (P + R) rates are broadly comparable (Robinson *et al.*, 1992; Struglia *et al.*, 2004). Annual rates of fluvial discharge are naturally linked to rates of precipitation, as well as the North Atlantic depression systems tracked into the Mediterranean (Struglia *et al.*, 2004) (see sections: Atmospheric variability and Cyclogenesis).
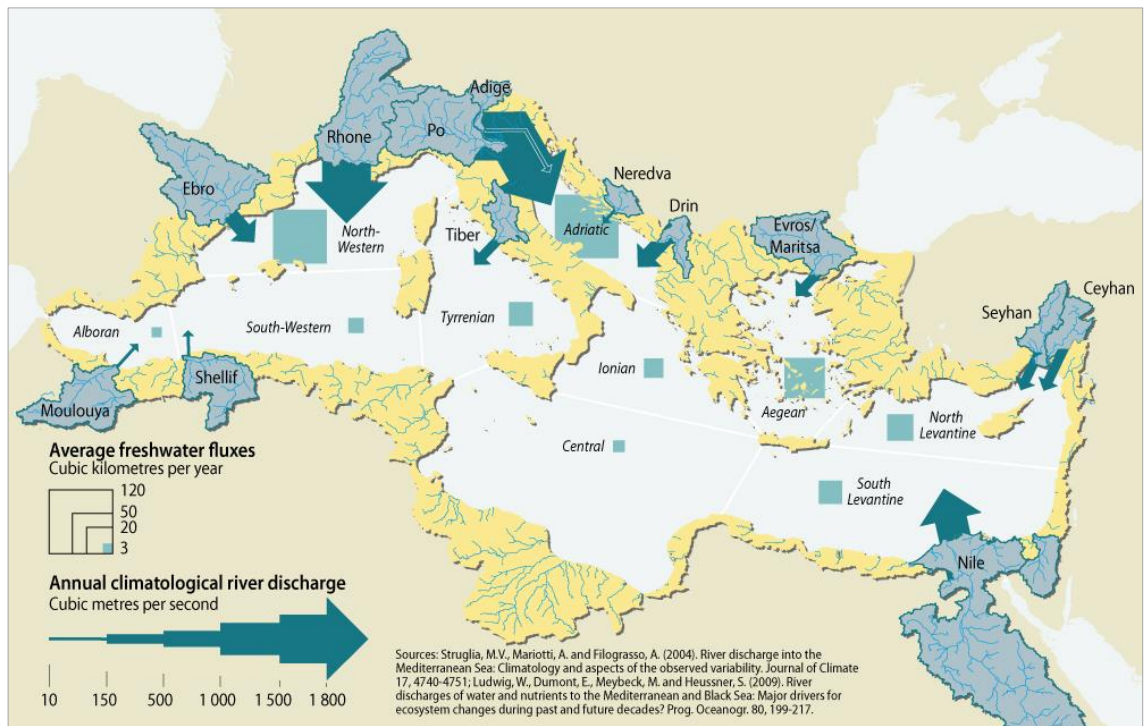
Figure 2.13: Schematic illustration of the main rivers and volume of freshwater discharge into the Mediterranean Sea. Taken from GRID-Arendal (2013b); Data source Struglia et al. (2004); Ludwig et al. (2009).

In the western basin, the main rivers are the Rhône River and deltaic system in the Gulf of Lion and the Ebro into the Balearic Sea, with contributions from the Tiber into the Tyrrhenian Sea and the Moulouya and Shellif into the Alboran Sea and Algerian Basin, respectively (Figure 2.13). In the eastern basin, the alpine River Po and the outflow of the Black Sea are significant sources of fresh/hyposaline water for the Adriatic and Aegean, while the Nile dominants the southern Levantine Sea (Figure 2.13). The Po and other alpine rivers that discharge into the Adriatic contribute the greatest volume of freshwater (annual mean $2500m^3$ s^{-1}), followed by the Rhône (annual mean $1700m^3$ s^{-1}) and rivers of the northern Aegean ($\sim500m^3$ s^{-1}) (Struglia *et al.*, 2004). Peak flow is in early spring (spring melt), followed by the dry season in August, and second peak in the autumn due to enhanced rainfall (Struglia *et al.*, 2004).

Outflow from rivers and their associated sediment plumes are normally deflected to the right by Coriolis force, then entrained by surface currents, e.g. the Northern Current in the Gulf of Lion, which redistributes suspended sediments and nutrients to the south-southwest along the coast (Millot and Taupier-Letage, 2005). In addition, local hydrography, submarine physiography and climatic patterns can play a part in the dispersal of suspended particulates, i.e. winds and mesoscale gyres can deflect waters from the river plumes to be transported 10-100km out in the basins over the subsequent days and months (Arnau *et al.*, 2004). Nitrogen (N), phosphorous (P) and silica (Si) are

main nutrients transported by rivers; the form in which these nutrients are transported (i.e. dissolved, particulate, organic and inorganic) has a bearing on how available the nutrient is for biological activity (Ludwig *et al.*, 2009). Chlorophyll-α concentration, which is a good indirect indicator of phytoplankton biomass, is concentrated in coastal waters, usually in proximity of river outflow (Figure 2.12) (Colella *et al.*, 2016).

Deposition of terrestrial sediments by rivers and deltaic systems are also key in areas such as the Gulf of Lion, where ~80% of sediment deposited on the continental shelf is supplied by the Rhône (Jallet and Giresse, 2005; Jalali *et al.*, 2018). It has been estimated that the total suspended solids discharged from the large Rhône catchment ($95600 km^2$) is on average $60\text{-}100\ 10^5$ t/yr^{-1}, with Holocene sediment rates estimated as ~80cm (1000yr)$^{-1}$ (Roussiez *et al.*, 2005; Jalali *et al.*, 2016).

Chapter 3.

3   Planktonic foraminifera as palaeoenvironmental proxy

3.1   Introduction to foraminifera

Foraminifera (Kingdom: Protozoa; Subkingdom: Biciliata; Infrakingdom Rhizaria; Phylum: Sarcomastigophora; Subphylum: Sarcodina; Superclass: Rhizopodea; Class: Granuloreticulosa; Order: Foraminiferida) are complex unicellular organisms composed of soft-tissue (cytoplasm) enclosed within a small calcareous ($CaCO_3$) chambered shell or test (usually <1mm) (Armstrong and Brasier, 2009; Schiebel and Hemleben, 2017). It has been estimated globally that there are over 6,000 distinct species and another 1,500 thus far unknown, and it is estimated that this abundant group account for 55 to 90% of deep sea biomass (Armstrong and Brasier, 2009; Appeltans *et al.*, 2012).

Foraminifera can be further subdivided into benthic and planktonic forms. Benthic foraminifera are the oldest and most diverse group, with the most primitive forms dating back to the Precambrian (1150-690 Ma) and the first fossils recorded in the Early Cambrian (ca. 520 Ma) (Culver, 1991; Pawlowski *et al.*, 2003). They live on or within sediment or attached to harder substrates such as rock or plant material and inhabit a wide range of aquatic environments, from intertidal marshes to distal deep-sea sediments. Depending on their life mode, the morphology of their tests is quite diverse (e.g. trochospiral, milioline, planispiral or spherical) and can be composed of secreted organic matter (tectin), secreted minerals such as calcite, aragonite or in rare cases silica, or formed by the entrainment and cementation of external particulates to form an agglutinated test (Gupta, 1999; Armstrong and Brasier, 2009). They range in size from the ubiquitous smaller benthic (<1mm), to larger symbiotic-bearing benthic species (>1mm) found mainly in oligotrophic surface waters (Armstrong and Brasier, 2009).

Planktonic foraminifera are the main proxy used in this research and will be discussed in detail in the following sections. Planktonic foraminifera are exclusively marine protists that float within the water column, from shallow surface waters to the deep sea and inhabit all latitudes in the global oceans and marginal seas. The planktonic mode of life has evolved many times since the mid-Jurassic from benthic groups; however following the Cretaceous-Palaeogene (K/Pg) extinction event that decimated the early planktonic communities, modern planktonic foraminifera emerged, evolved and

diversified during the early Paleogene (Darling *et al.*, 2009; Schiebel and Hemleben, 2017). Although there are only an estimated 45-50 extant planktonic morphospecies in modern oceans, the contribution of planktonic foraminifera to the deposition of global biogenic carbonate has been estimated to be 32-80% of the total deep-marine $CaCO_3$ budget (Schiebel, 2002). Their abundance, test geochemistry and excellent preservation has enabled them to be the one of the most utilised proxies for palaeoceanographic research (Kučera, 2007).

Classification of planktonic foraminifera genera was traditionally governed by test wall texture, i.e. pore size and presence/absence of spines. Based on work by Loeblich and Tappan (1987), the systematic study of extant morphospecies has placed planktonic foraminifera in the Suborder Globigerinina, then further subdivided them into three Superfamilies: Globigerinoidea (spinose), Globorotaliacea (macroperforate, non-spinose) and Heterohelicoidea (microperforate, non-spinose) (Schiebel and Hemleben, 2005; Darling and Wade, 2008). Defining characteristics of species included wall texture (e.g. spinose, cancellate, smooth, microperforate); test shape (e.g. globigeriniform, spherical, spiro-convex or umbilico-convex trochospiral); coiling mode (e.g. streptospiral, planispiral, trochospiral); chamber shapes (e.g. spherical, angular conical, clavate); aperture type and position (e.g. umbilical, extra-umbilical), modification of the aperture (e.g. teeth, bulla) and the shape of spines.

However, pioneering work with gene sequencing by Wade *et al.* (1996), Darling *et al.* (1996), de Vargas *et al.* (1997) and Darling *et al.* (1999) through to more recent work (André *et al.*, 2014; Weiner, 2014; Morard *et al.*, 2018) on the small ribosomal subunit RNA gene (SSU rDNA) has revealed the true complexity of the diversity of planktonic foraminifera. The discovery of over 250 genotypes has broadly corroborated the taxonomic grouping of morphospecies, with some exceptions, e.g. *Globigerinella siphonifera*, and has enabled greater understanding of the seemingly broad ecological ranges and patterns seen in modern morphospecies (Darling and Wade, 2008; de Vargas *et al.*, 2015). There are suggestions that variations of reproductive periodicity or distribution patterns of species may be due in part to different reproduction and ecological preferences of genotypes (Schiebel and Hemleben, 2017).

Family	Group	Species	Sub-species	Geno-types	Mediterranean Sea & adjacent regions		Faunal province
					Sub-types	Distribution	
Candeinidae	Micro-perforate non-spinose	*Candeina nitida*		I	I	West Atlantic	T
		Globigerinita glutinata		4	I; III	North Atlantic	ST / TL
		Tenuitella iota		ND			
Globorotalidae	Macro-perforate non-spinose	*Globoconella inflata*		2	I	Cosmopolitan	TL / ST
		Globorotalia scitula		1	I		
		Globorotalia truncatulinoides	Dextral	4*	II	Mediterranean, South Atlantic	T / ST
			Sinistral				
		Neogloboquadrina incompta		2	I	Atlantic	SP / TL
		Neogloboquadrina pachyderma		4*	IIa; IIb	North Atlantic	P / SP
Globigerinidae	Spinose	*Beella digitata*		I	I		ST
		Globigerina bulloides		3	Ib	Mediterranean, Red Sea	ST
						Southern North Atlantic Current, Canary Current	TL / ST
		Globigerinella calida		2-3	IIIb; IIIc	Red Sea, Atlantic	
		Globigerinella siphonifera		4	IIa Complex	Arabian Sea, Cosmopolitan	ST / TL
						Off Canary Is, Azores Current, Cosmopolitan	T / TL

29

Family	Group	Species	Sub-species	Geno-types	Mediterranean Sea & adjacent regions		Faunal province
					Sub-types	Distribution	
					IIb	North Atlantic Current, Canary Is, Azores Current	ST / TL
Globigerinidae	Spinose	*Globigerinoides ruber* plexus (+ *Globigerinoides elongatus*)	Pink	6	Pink	Off Canary Is, Mediterranean	T / ST
			White		Ia1	Mediterranean	T to TL
					IIa1	W. Mediterranean	T to TL
					IIa2	E. Mediterranean	
					IIb	E. Atlantic, Mediterranean	
		Trilobatus sacculifer plexus	With sac	1	I		ST / T
			Without sac				
			T. quadrilobatus				
		Globoturborotalita rubescens		ND			
		Globoturborotalita tenella		ND			
		Orbulina universa		3	III	Mediterranean, Atlantic, Red Sea	T, ST & TL
		Turborotalita humilis		ND			
		Turborotalita quinqueloba		2	IIb?	North Atlantic	P/SP

*Table 3.1: List of all morphospecies, including their genotypes and subtypes recorded in this study. * Molecular genetics are not fully resolved. ND is No Data. Faunal province: T = Tropical; ST = Subtropical; TL = Transitional; SP = Subpolar; P = Polar. Based on Kennett and Srinivasan (1983); Chaisson and Pearson (1997); Darling and Wade (2008); Aurahs et al. (2009); Ujiié et al. (2010); Aurahs et al. (2011); Morard et al. (2011); André et al. (2013); André et al. (2014); Spezzaferri et al. (2015); Schiebel and Hemleben (2017); Spezzaferri et al. (2017).*

Fluctuations in the quality or abundance of prey over spatial or temporal timescales in similar habitats or regions may lead to niche partitioning and ecological adaption by different genotypes (Darling and Wade, 2008; Schiebel and Hemleben, 2017). The specific morphospecies, with their genotypes and subtypes that are found in the modern Mediterranean Sea and surrounding waters are listed in Table 3.1

3.1.1   Morphology

The calcareous ($CaCO_3$) planktonic foraminiferal test (usually <600µm) is divided by a number of successive interconnected globular chambers that are continually added in increasing size throughout the life cycle of the organism (Hemleben *et al.*, 1989; BouDagher-Fadel, 2015). The test is composed mainly of bilamellar calcite or aragonite walls, with additional carbonates ($MgCO_3$, $FeCO_3$), SiO_2, Sr and amino acids (Sadekov *et al.*, 2005; Boltovskoy and Correa, 2014). The globular nature of the chambers is an adaption to aid buoyancy as they float within the water column. Chambers are typically trochospirally coiled and depending on the species, they may have external thin spines. The internal cytoplasm (or endoplasm) of the organisms' single cell incorporates the nucleus, mitochondria, chloroplasts, Golgi body and food vacuoles, and all biological activity of the organism is controlled from here (Armstrong and Brasier, 2009). This endoplasm interconnects with the spiral chambers and the outside environment through pores and an aperture in the test surface. Pores in the test walls range in size and density, from small (<1µm) and sparsely spaced pores in microperforate forms, to larger (>1µm) and more densely spaced pores in macroperforate species (BouDagher-Fadel, 2015; Schiebel and Hemleben, 2017).

In the final chamber and outside of the test, the cytoplasm changes to a frothy ectoplasm that can form pseudopodia, which allow the transport of nutrients into the endoplasm. Pseudopodia can occur as networks of sticky net-like rhizopodia, filopodia or reticulopodia that stream out into the surrounding waters supported by spines, if present, or radiate out from the test in non-spinose species and enable the foraminifera to trap food and transport particles into the test (BouDagher-Fadel, 2015; Schiebel and Hemleben, 2017). Each species has specific food requirements, such as bacteria, diatoms, chrysophytes and other small protozoa (Schiebel and Hemleben, 2017).

Globigerinid spinose species are more likely to be symbiont-bearing and inhabit shallow warmer waters (Fairbanks *et al.*, 1982; Hemleben *et al.*, 1989). The spine distribution, base type and shape in cross-section (e.g. round, triradiate, triangular) can vary between

species. There have been a number of suggested benefits for the evolution of spines, such as to allow the foraminifera to control and maintain their depth in higher energy shallower waters; to increase the surface area of their rhizopodial network for food capture, and for the wide distribution of endosymbionts along the spines to more efficiently diffuse CO_2 and O_2 (Hemleben *et al.*, 1989; BouDagher-Fadel, 2015).

The test surfaces of most extant Heterohelicoidea and Globorotaliacea non-spinose species are coated in conical calcite pustules that occur in greater density and size near the aperture and reduce in size and abundance near the periphery of the test. It has been suggested from observations of *Globorotalia menardii*, that these pustules form an anchor point for rhizopodia in non-spinose species (Hemleben *et al.*, 1989). Non-spinose species generally do not contain symbionts, though there are some exceptions to this such as facultative symbionts observed in *G. glutinata* and *G. inflata* (see below). Therefore, non-spinose species have wider depth habits than symbiont-bearing species, which are restricted to the photic zone.

3.1.2   Symbionts

Symbionts are a key component of many planktonic foraminifera, especially spinose species (Table 3.2). Symbionts are usually dinoflagellate or chrysophyte algae that can be found within the rhizopodial system and internal cytoplasm of their host. Symbionts are not transferred through sexual reproduction from parent to the gamete, therefore shortly after fertilisation offspring must acquire their symbionts independently. This has been suggested to occur at the Deep Chlorophyll Maximum (DCM), where there are sufficient numbers of algae and food to allow for the juveniles to successfully acquire symbionts (Hemleben *et al.*, 1989). Once they acquire their photosynthesising symbionts, compounds such as oxygen, carbon and nitrogen are transferred to the foraminifera (Uhle *et al.*, 1997; Schiebel and Hemleben, 2017). These compounds are intrinsic for supporting the metabolism, stable isotope ratios of the test, calcite and organic products, respiration rates, and the calcification and chamber formation of the hosts (Schiebel and Hemleben, 2017). It has been observed that *T. sacculifer*, *O. universa* and *G. ruber* have the same algal endosymbiont and display very similar growth rates, indicating that the thermal preference of their endosymbionts may influence their growth patterns (Table 3.2) (Lombard *et al.*, 2009; Schiebel and Hemleben, 2017).

Availability of algal symbionts in the water column is dependent on variations in

seasonal or regional temperature, salinity and trophic conditions, as well as changes in turbidity or water depth. Changes in these conditions can therefore affect the abundance, growth and development of symbiont-bearing species. The presence of symbionts has been suggested as a catalyst for increased diversification of species during the Paleogene. This enabled such species to expand their habitat niche into environments such as warm, oligotrophic surface waters where food and nutrients are scarce, but light is abundant. This gives these species a distinct advantage to symbiont-barren species in such low-nutrient waters (Norris, 1996). Ortiz *et al.* (1995) noted that abundance and size of symbiont-bearing species in the northern Californian Current system increased further offshore as biomass and turbidity levels decreased, indicating that ambient light levels were one of the main controlling factors for the distribution of symbiont-bearing species within their optimum sea surface temperature (SST) range. In turbid eutrophic waters, these symbiont-bearing species have smaller shell sizes and are rare as they are outcompeted by generalist or opportunistic species, such as *G. bulloides* or *G. glutinata* (Ortiz *et al.*, 1995; Kučera, 2007). It is also assumed that higher productivity, thus increased turbidity within the mixed layer forces symbiont bearing species to shoal for optimum light levels (Rebotim *et al.*, 2017).

Algal symbionts		Facultative algal symbionts	
G. ruber white *G. ruber* pink *T. sacculifer* *O. universa* *G. rubescens* *G. tenella*	Dinoflagellates	*C. nitida* *G. glutinata* *G. inflata* *T. quinqueloba*	Chrysophytes
G. siphonifera	Chrysophytes		
G. falconensis	Yes (no details)	**Bacterial symbionts**	
G. calida	Yes (Uncharacterised)	*G. bulloides*	Cyanobacterial
Symbiont-barren		**Unknown**	
G. scitula *G. truncatulinoides* *N. incompta* *N. pachyderma*		*B. digitata*	

Table 3.2: Symbionts-bearing and symbiont-barren planktonic foraminifera (Kučera, 2007; Schiebel and Hemleben, 2017; Takagi et al., 2019)

Most non-spinose species do not contain algal symbionts, though some such as *G. inflata* and *G. glutinata* are found to contain facultative chrysophytes, which may mean these foraminifera periodically utilise the algal photosynthate products, then digest the algae at a later date (Schiebel and Hemleben, 2017).

3.1.3 Reproduction

It is believed that planktonic foraminifera reproduce primarily sexually to promote greater genetic diversity, allowing species to adapt to a wider range of habits (Armstrong and Brasier, 2009). However, planktonic foraminifera are now thought to have retained the ability to reproduce asexually, and has been observed in both *G. uvula* and *N. pachyderma* (Davis *et al.*, 2020; Takagi *et al.*, 2020). To assist successful reproduction of such small organisms, planktonic foraminifera have evolved a range of strategies to narrow the time and location for synchronised reproduction (Weinkauf *et al.*, 2020). Such strategies include releasing a large number ($\geq 10^5$) of motile gametes that contain sufficient food for a prolonged period of locomotion, and species-specific preferences for the periodicity and water depth that trigger gametogenesis (Schiebel and Hemleben, 2017). There are a series of stages for gametogenesis, e.g. shallow dwelling spinose species sink, shorten then discard their spines; a sack-like chamber develops and symbiont-bearing species ingest or expel their symbionts; their cytoplasm becomes granular, changes colour then withdraws within the test; a bulging mass of cytoplasm appears at the aperture, then ruptures to expel the many flagellated gametes and finally the empty parental test sinks to the sea floor (Schiebel and Hemleben, 2017). Variations to this generalised cycle occur between spinose vs non-spinose, and symbiont-bearing vs barren species. In addition, during ontogeny and the process of gametogenesis, morphological changes can occur to the foraminifer test. Such changes include the late growth of a coarse crystalline calcite crust (e.g. *G. truncatulinoides*); the addition of layers of calcite before gametogenesis (i.e. gametogenic calcification) (e.g. *G. bulloides*, *N. pachyderma*); formation of sac-like final chambers (e.g. *T. sacculifer*), a bulla (e.g. *G. glutinata*) or the final chamber may be smaller or disfigured, i.e. a kummerform chamber (e.g. *G. ruber*), and *O. universa* may add a "Biorbulina" sphere over its final chamber (Hemleben *et al.*, 1989).

The patterns, rates and periodicity of reproduction are different for each species, and potentially within morphospecies, i.e. specific for each genotype (Figure 3.1). Reproduction in many shallow dwelling species is triggered by a synodic lunar cycle, such as once per month e.g. *T. sacculifer*, *G. calida*, *G. glutinata*, *G. bulloides, O. universa*, or twice per month, e.g. *G. ruber* white, *G. ruber* pink and *G. siphonifera* (Bijma *et al.*, 1990; Jonkers *et al.*, 2015). Recent models suggest that if planktonic foraminifera reproduce purely sexually, some form of temporal synchronisation and spatial concentration must occur, such as migrating to a physical boundary layer, such

as the halocline or pycnocline (Weinkauf *et al.*, 2020). It is inferred that the productive DCM layer represents the best trophic conditions to support juvenile foraminifera (Hemleben *et al.*, 1989; Schiebel and Hemleben, 2005). Intermediate or deeper water species have different reproductive patterns, e.g. *G. truncatulinoides* has an annual cycle, where is ascends to shallow waters in productive regions or gyres during the early spring and undergoes gametogenesis (Hemleben *et al.*, 1989).
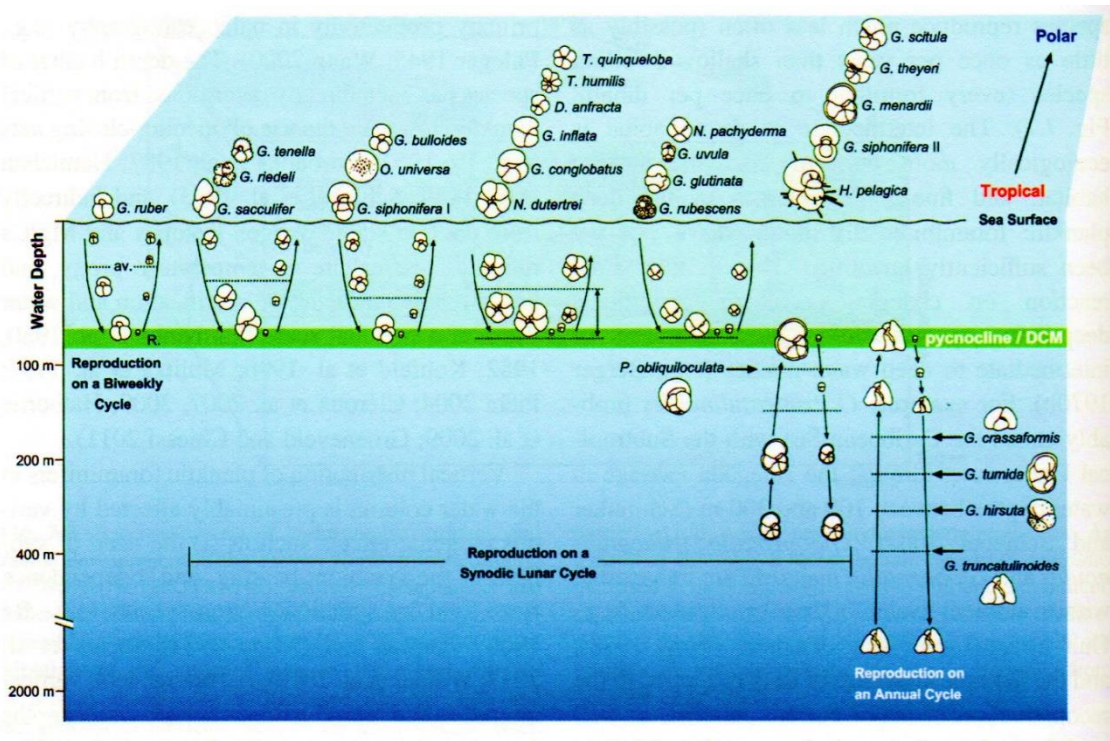
Figure 3.1: Schematic diagram illustrating the depth habitats and reproduction cycles of planktonic foraminifera from tropical to polar waters. The average living depth habitat is represented by a stippled horizontal line. Taken from Schiebel and Hemleben (2017).

3.2   Faunal Distribution

Globally, the geographic distribution of planktonic foraminifera morphotypes is seen to adhere to the following five broad latitudinal faunal provinces: i) the extensive warm tropical and ii) subtropical waters roughly between 40˚N to 40˚S; iii) a narrow transitional zone characterised by a mix of "warm" and "cold" species, the upper boundary of which is marked by an annual isotherm of 18°C; iv) subpolar and v) polar waters (Figure 3.2) (Bé and Tolderlund, 1971; Kučera, 2007). These faunal provinces correspond to the broad requirements of planktonic foraminiferal species, such as temperature, salinity, turbidity, radiance requirements for symbiont-bearing species, trophic demands and prey availability (Schiebel and Hemleben, 2017). Upwelling regions, characterised by eutrophic waters, high availability of algal prey, increased

turbidity and dominance of *G. bulloides*, have been proposed as a 6th faunal province (Thiede, 1975).

Although the geographic distribution of individual species can extend across these faunal provinces (e.g. *G. glutinata* has the broadest distribution and optimum mean SST (6.9 – 27°C) of all morphospecies (Hilbrecht, 1996)), each zone is typified by a
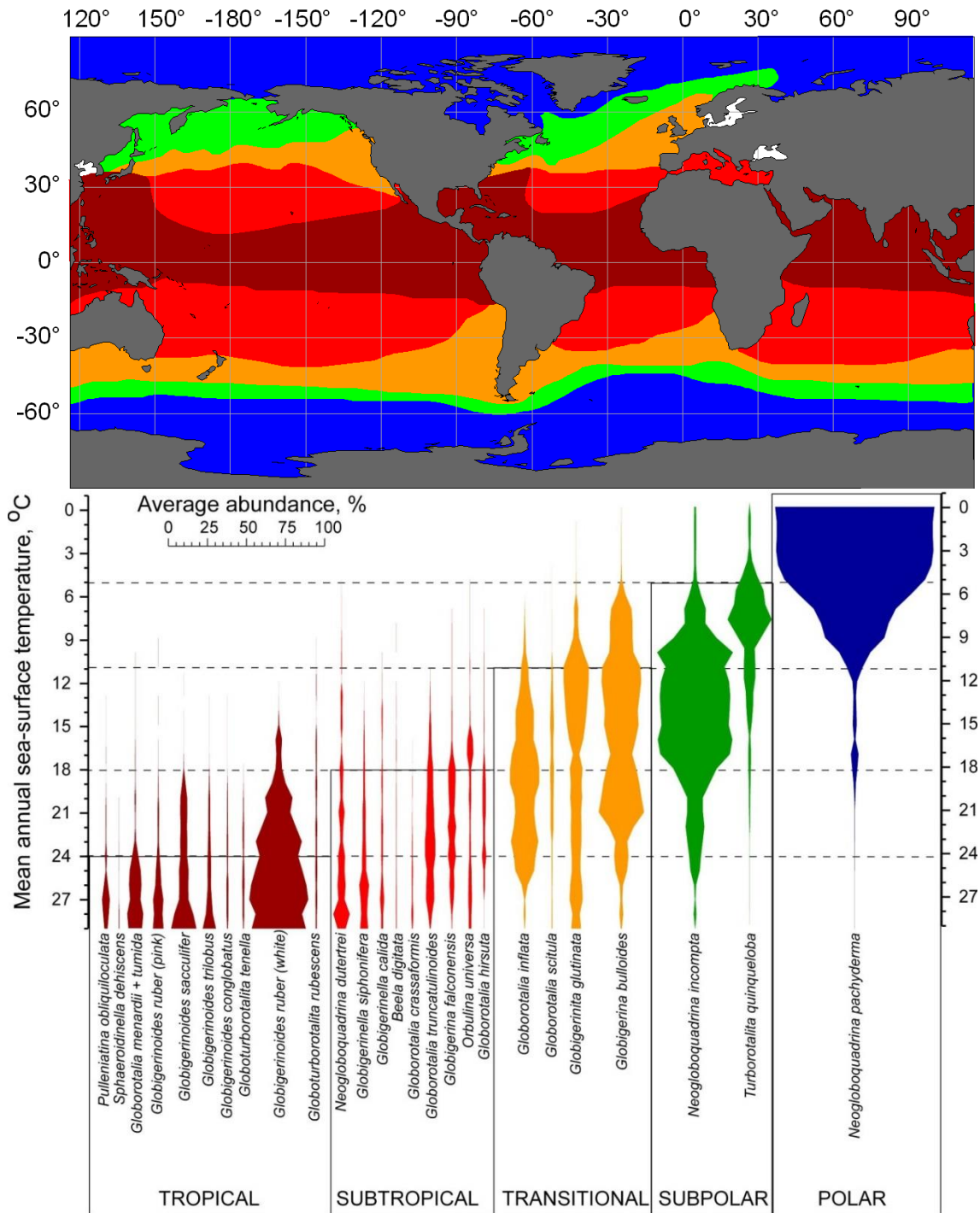
Figure 3.2: Planktonic foraminiferal provinces in the modern ocean, not including upwelling zones. The distribution of the provinces (Bé, 1977; Vincent and H., 1981) follows SST gradients, reflecting the strong relationship between SST and species abundance. The abundance plots are based on surface-sediment data from the Atlantic Ocean (Kučera et al., 2005a), averaged at one degree centigrade intervals. Dark red: Tropical; Red: Subtropical; Orange: Transitional; Green: Subpolar; Blue: Polar. Taken from Kučera (2007).

characteristic faunal assemblage and abundances. For example, *N. pachyderma* morphospecies is almost exclusively a (bi-)polar species especially in waters ≤9°C, although very minor occurrences can be found in waters with SST up to 24°C (Žarić *et al.*, 2005; Kučera, 2007). This is in comparison to the more restricted distribution of the tropical *G. ruber* pink, which has been observed in SSTs ranging between 16-29°C, but only in the Atlantic Ocean (Žarić *et al.*, 2005; Kučera, 2007). In addition, changes in species abundance, e.g. from tropical to subtropical species centred at 18-20°C, suggest overlapping assemblages form diverse ecotone communities at the transition of faunal provinces (Morey *et al.*, 2005), where they can be influenced by, and react to seasonal changes in hydrography, e.g. the Azores Front in the North Atlantic (Schiebel *et al.*, 2002a).

Global SST plays a crucial role in the latitudinal, abundance and diversity of planktonic foraminiferal in the world's oceans, but other ecological (e.g. productivity); hydrographic (e.g. currents, frontal systems, areas of upwelling) and geographic features can influence distribution both globally and regionally. In addition, biological requirements (presence/absence of symbionts; prey type, quality and abundance) and ecological preferences (depth; water column structure), as well as with the historical influence of restricting gene flow, e.g. the restriction of *G. ruber* pink to the Atlantic Ocean and Mediterranean Sea since MIS 5.5 (~120ka), all have an influence on the distribution, diversity and abundance of planktonic foraminifera (Thompson *et al.*, 1979; Arnold and Parker, 1999). These factors will be discussed in the following sections.

3.2.1   Abundance and diversity

Abundance, diversity and the distribution of planktonic foraminifera biomass is directly affected by SST, along with hydrological (depth, water column structure, salinity) and trophic conditions (chlorophyll-α concentration, nutrients, prey availability and quality) (Watkins *et al.*, 1996; Kučera, 2007; Schiebel and Hemleben, 2017). Foraminiferal biomass is dependent on the number and size of the individual species present and this can vary spatially, seasonally and even within the water column with high biomass in shallow waters to decreasing values in deeper waters. Average global standing stocks of planktonic foraminifera are low in comparison to other protozoans or zooplankton, but range from 10-100 ind./m^3 (Schiebel and Hemleben, 2017), which is in contrast to ~1.42 ind./10m^{-3} values reported in late spring plankton tows of the mainly oligotrophic

Mediterranean Sea (Mallo *et al.*, 2017).

Mean annual SST and mean annual temperature at depth (i.e. thermocline) are the main factors governing diversity, along with hydrodynamic and ecological effects of upwelling and stratification of the water column. In oligotrophic subtropical gyres of the middle latitudes, diversity peaks in areas with a deep permanent thermocline and SSTs of less than 27°C, where vertical niche partitioning allows for species to become ecological specialists (Rutherford *et al.*, 1999; Al-Sabouni *et al.*, 2007). For example, shallow species such as *G. ruber* and *T. sacculifer* inhabit the mixed layer, *N. dutertrei* and *G. menardii* are present in the upper thermocline, followed by the deeper species *G. scitula* in the mid-thermocline, with *G. truncatulinoides* and *G. hirsuta* occupying the deepest part of the thermocline (Rutherford *et al.*, 1999). This is in comparison to the cooler homogenous waters of high latitudes that have little or no thermocline, high productivity and a short productive season; or tropical waters (>27°C) that have a sharp shallow based thermocline that inhibit the development of extensive vertical niche separation of the faunal community. Diversity decreases in areas of upwelling due to the negative effects of high primary productivity, chlorophyll concentration and increased turbidity on symbiont-bearing species (Bé and Tolderlund, 1971; Ottens and Nederbragt, 1992; Al-Sabouni *et al.*, 2007; Schiebel and Hemleben, 2017).

3.2.2 Preservation

When utilising census counts of planktonic foraminiferal assemblages for palaeoenvironmental studies, preservation of fossil tests is an issue that must be addressed. Following early death or reproduction, empty tests of planktonic foraminifera descend towards the sea floor, either to be buried within the sediment or they can be dissolved within the water column. Biological decomposition can begin quite quickly within the upper 700m of the water column and is caused by bacterial decomposition of the remaining cytoplasm and increasing acidification within the test (Schiebel and Hemleben, 2005). This bacterial decomposition is greater in well-oxygenated waters, therefore chances of preservation is greater in anoxic environments (Schiebel and Hemleben, 2005).

Dissolution of calcite tests is governed by the degree of $CaCO_3$ saturation in the seawater. With increasing depth, especially below the photic zone, the partial pressure of CO_2 increases (with decreasing rates of photosynthesis and temperature, and increasing water pressure), leading to a lowering of pH from approximately 8.2 to 7

(Armstrong and Brasier, 2009). Although the effects of dissolution <3000m is noticeable, they are deemed to be minor (Berger *et al.*, 1982). The depth at which thermodynamic dissolution rates rapidly increase is called the lysocline (between 3-5km) and can be identified in fossil assemblages by the preservation of tests in sediment cores (Berger *et al.*, 1982; Kučera, 2007). The point where $CaCO_3$ in solution equals the supply of $CaCO_3$ is called the calcium carbonate compensation depth (CCD) and beyond this point, little calcite is preserved, e.g. <3% of the planktonic foraminifera assemblage is preserved at depths >4000m in the Arabian Sea (Conan *et al.*, 2002).

In comparison to most undersaturated deep open ocean settings, the Mediterranean Sea is strongly supersaturated in both calcite and aragonite throughout the water column (Schneider *et al.*, 2007). A number of reasons have been proposed for this, including the high salinity of Mediterranean waters, the inflow of highly alkaline waters from rivers and the Black Sea, and the proximal locations of areas of deep water formation, which enable the quick redistribution of this excess $CaCO_3$ down to deeper waters (Schneider *et al.*, 2007). Therefore, carbonate dissolution of foraminiferal tests is not a significant factor in the Mediterranean Sea. However, this supersaturation in $CaCO_3$ may lead to some diagenetic overgrowths of inorganic calcite crusts on the primary test calcite that was precipitated during the foraminifera's life cycle, which may affect the geochemical signature of the test wall (van Raden *et al.*, 2011).

3.3 Ecological Factors

On a more mesoscale, foraminifera abundance, flux and distribution are governed by species specific biological requirements and preferences, and regional hydrological or trophic factors, such as SST, food quality and availability, nutrient availability, depth preference and seasonality.

3.3.1 Sea surface temperature

Sea Surface Temperature (SST) is regarded as the most important influencing factor in the distribution, diversity and size of planktonic foraminifera. Morey *et al.* (2005) determined the relationship between mean annual SST and faunal distribution to be more significant than the 34 other environmental variables analysed. Accounting for 30.4% of the faunal variance, the close correlation of species with SST reflected the latitudinal variability among species. In addition, SST explains approximately 90% of the geographic variation in diversity of the Atlantic Ocean (Rutherford *et al.*, 1999).

Species	Bé and Tolderlund (1971)				Tolderlund and Bé (1971)*				Bé and Hutson (1977)*	Bijma et al. (1990)			Hilbrecht (1996)				Žarić et al. (2005)			
	Range (°C)		Optimum (°C)		Range (°C)		Optimum (°C)		Optimum (°C)	Range (°C)		Optimum (°C)	Range (°C)		Optimum** (°C)		Range (°C)		Optimum (°C)	
	Min	Max	Min	Max	Min	Max	Min	Max		Min	Max		Min	Max	Min	Max	Min	Max	Min	Max
G. rubescens†									23.00				12.85	28.90	27.15	27.25				
G. tenella†													2.85	28.90	24.60	28.70				
G. ruber white	14	30	21	29	13.30	29.50		>21.3	24.20	14	32	26.50	2.75	28.95	22.80	26.80	9.80	31.00	21.80	30.60
G. ruber pink								>24.4					2.40	28.70	26.85	27.90	16.40	29.60	22.60	29.50
T. sacculifer†	15	30	24	30	15.00	29.50		>22.1	25.20	14	32	26.50	1.85	28.95	27.15	27.65	9.70	31.00	23.10	29.70
C. nitida	20	30											20.40	28.90	22.15	26.35				
G. calida													5.95	28.90	20.50	27.10				
G. siphonifera†	12	30	19	28	10.50	29.50	17.40	25.30	23.50	11	30		9.30	28.95	18.90	28.30	11.90	31.00	20.10	30.70
B. digitata†													9.15	28.95	15.20	28.30				
O. universa†	10	30	17	23	10.50	29.50		>18.2	21.70	12	31	23.50	2.85	28.95	14.80	15.55				
G. truncat. (s & d)	4	27	17	22	10.50	28.10	15.40	22.00	20.30				2.85	28.95	12.85	22.65				
G. falconensis													3.80	28.80	16.45	23.00				
G. inflata	1	27	13	19	2.20	26.90	10.40	19.90	16.50				2.15	28.95	12.55	20.30				
G. scitula									22.70				4.45	28.90	12.85	20.05				
G. bulloides	0	27	3	19	2.10	23.30	9.00	11.00	13.40				0.35	28.95	6.45	12.05	1.90	31.00	1.40	29.80
T. humilis													12.85	28.30	12.85	19.95				
G. glutinata	3	30	24	27	2.50	29.50	10.60 / 18.50	13.40 / 22.00	22.20				1.85	28.95	6.90	27.15				
T. quinq.	1	21		<12	2.20	16.00	4.60	10.80	9.90				-0.35	28.90	4.45	8.50				
N. incompta	10	24	10	18	2.20	23.30	2.20	6.50	4.80				-0.35	28.75	9.00	17.95	-1.80	29.80	5.80	23.60
N. pachy.	7.20	9		<4									-0.35	28.95	-0.35	9.85	-1.18	23.70		<0.9/<6.8‡

*Table 3.3: SST ranges and optima (°C). Species are grouped by faunal provinces, as defined in Figure 3.2 (Kučera, 2007). * Studies where N. pachyderma and N. incompta not differentiated. † SPRUDTS group (missing H. pelagica) as defined by Rohling et al. (1993) as warm subtropical water indicator. ‡ Optimum SST based on 75% of population, as defined by Hilbrecht (1996) (Žarić et al., 2005). ** SST Optimum = >75%. G. truncat. = G. truncatulinoides; T. quinq. = T. quinqueloba; N. pachy = N. pachyderma; s = sinistral; d = dextral.*

Most morphospecies have broad thermal ranges, e.g. the "warm" spinose species *G. ruber* white inhabits waters with SSTs between 9.8 and 31°C, but most species have a preferred optimum abundance range defined by their highest relative abundances, which for *G. ruber* white is 21.8-30.6°C (Žarić *et al.*, 2005). These global thermal ranges were originally calculated from SSTs at sediment traps or plankton tow stations where species were recorded and are summarised in Table 3.3 (Bé and Tolderlund, 1971; Tolderlund and Bé, 1971; Bé and Hutson, 1977; Bijma *et al.*, 1990; Hilbrecht, 1996; Žarić *et al.*, 2005). Note, most thermal ranges are indicative of surface water temperature only and may not encompass the absolute water temperature that the species may live in, e.g. the preferred SST range of *N. incompta* or *N. pachyderma* is 5.8-23.6°C and <0.9°C respectively however, these deeper dwelling species live within the DCM which may be several degrees cooler, therefore their true thermal range could be several degrees lower (Fairbanks and Wiebe, 1980; Žarić *et al.*, 2005). Distribution of *N. pachyderma* and *G. ruber* pink are closely aligned to SST, with the lowest optimum SST (<0.9°C) and narrowest SST range (16-29°C) respectively (Žarić *et al.*, 2005). Once beyond their optimum tolerance temperature range, planktonic foraminifera display a gradual reduction in rates of growth and reproduction, as well as nutrient uptake (Arnold and Parker, 1999).

It has been demonstrated that there is a progressive increase in growth rate within well-defined optimal thermal ranges, where the maximal growth rate is near the upper end of each species specific thermal niche (Table 3.4) (Lombard *et al.*, 2009). Above or below these optimal growth limits, growth appears to stop.

Species	Optimal thermal range (°C)		Maximal growth limits (°C)	
	Min	Max	Min	Max
G. ruber white	11	32	20	29
T. sacculifer	11	32	20	29
G. siphonifera	11	32	20	29
O. universa	11	32	20	29
G. bulloides	7	28	9	25
N. incompta	4	23	6	20
N. pachyderma		<12		<5

Table 3.4: Optimal temperature ranges and maximal growth limits (Lombard et al., 2009).

In general, test size increases from the poles towards the equator, with the highest correlations occurring between test size, the mean annual temperatures at the surface and at 200m, and the degree of stratification of the water column (Schmidt *et al.*, 2004).

Ambient water temperature influences cell physiology, enzymatic activity and calcification of the test. Larger test sizes in tropical/subtropical warm waters occur through the potential combination of greater stratification, enhanced calcification of tests in carbonate supersaturated warmer waters and increased irradiance, which promote algal symbiotic activity and photosynthesis. This equatorward increase is not consistent however, as shell size minima were observed at 2°C and 17°C for most species, except for the more resilient *G. inflata* (Schmidt *et al.*, 2004). These temperatures coincide with polar and subtropical fronts, which have unfavourable environmental conditions for symbiont-bearing species (such as increased turbidity, homogenised water column, vertical displacement of individuals by currents among others), leading to low diversity and smaller test sizes in these regions (Schmidt *et al.*, 2004). This pattern is seen in upwelling regions too, as the number of larger spinose symbiont-bearing species decrease in the turbid waters, accompanied by the dominance of the smaller *G. bulloides* (Schmidt *et al.*, 2004).

3.3.2   Salinity

Salinity was considered a factor in planktonic foraminifera spatial distribution, as it may have osmotic effects on the foraminifera cell, as well as the effect of density and flotation (Bé and Hutson, 1977; Hemleben *et al.*, 1987). In modern oceans, foraminifera inhabit waters ranging from 32.7 – 37.3‰, with *N. pachyderma* inhabiting the most hyposaline waters (Hilbrecht, 1996). However, laboratory studies by Bijma *et al.* (1990) determined that most species have a wide but differing salinity tolerance, ranging from 22 to 49‰ and it was concluded that salinity did not limit the biogeographic variation of species.

3.3.3   Depth ranges

Early studies using stratified plankton tows or analysis of shell geochemistry noted that living planktonic foraminifera had variable depth habitats; they calcified their shells at different depths and in general, the abundance of species decreased from surface waters to the base of the mixed layer (~200m) (Emiliani, 1954; Fairbanks *et al.*, 1980; Fairbanks *et al.*, 1982). Unlike other motile phytoplankton and zooplankton, there is no evidence of diel vertical migration in planktonic foraminifera communities (Greco *et al.*, 2019; Meilland *et al.*, 2019). It has been suggested that the vertical distribution of specific species varied during their life cycle, indicating that they migrate in response to changing ecological requirements and potentially due to specific depth habitats during

ontogeny (Figure 3.3) (Fairbanks *et al.*, 1980; Hemleben *et al.*, 1989; Schiebel and Hemleben, 2005; Iwasaki *et al.*, 2017; Rebotim *et al.*, 2017; Kretschmer *et al.*, 2018; Greco *et al.*, 2019; Pracht *et al.*, 2019; Lessa *et al.*, 2020). However, vertical migration during ontogeny is difficult to observe or to model (Kretschmer *et al.*, 2018). In a recent study of planktonic foraminifera depth variation in stations spanning the subtropical South Atlantic, Lessa *et al.* (2020) determined that environmental parameters were the primary factor in the vertical variation of species, and there was little statistical evidence of reproductive or ontogenetic factors.
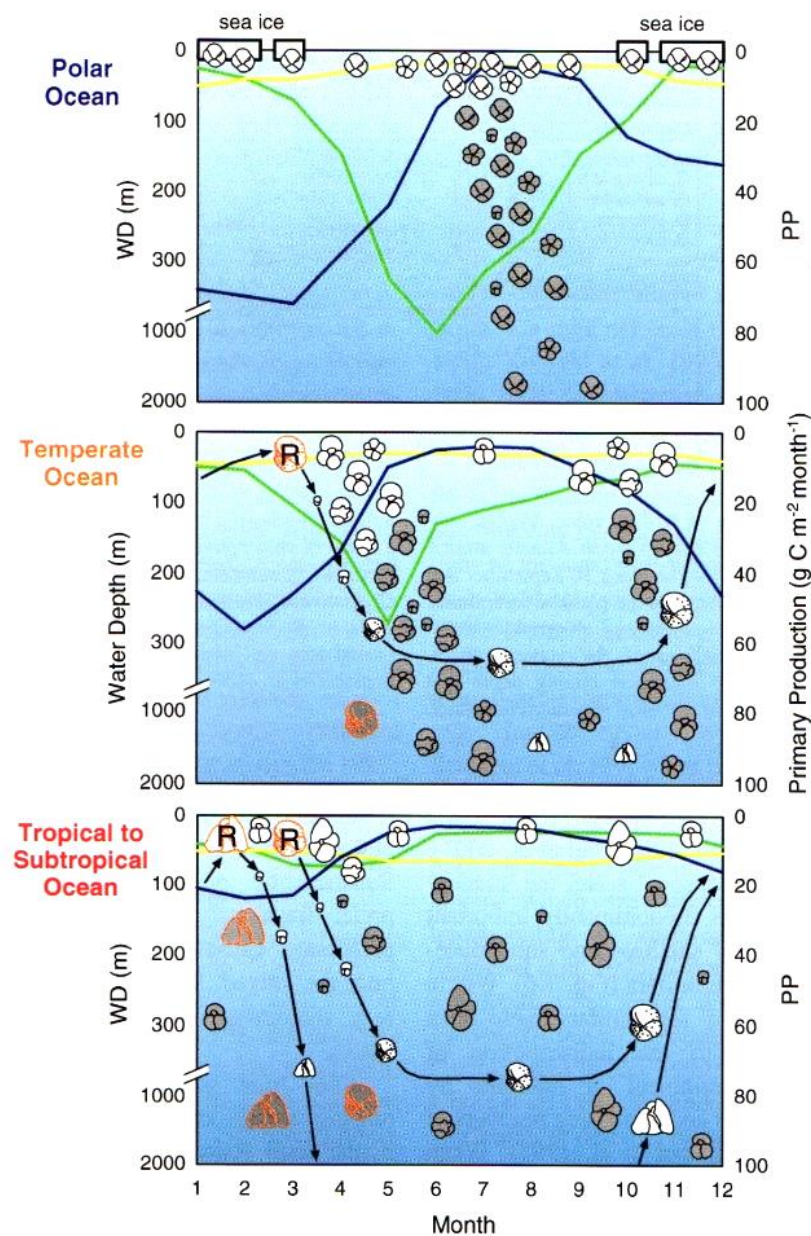
Figure 3.3: Seasonality of living depth (white tests) and sedimentation of empty tests (grey tests) of polar, temperate and tropical/subtropical species. Mixed layer water (blue line) and maximum photic depths (1% isolume; yellow line) are given on the left y-axis, and integrated primary production (PP, green line) is given on the right y-axis. The reproductive cycle of intermediate (e. g. G. hirsuta) and deep-dwelling planktic foraminiferal species (G. truncatulinoides) as they ascend to the photic zone before the spring bloom (black "R"), and empty tests settle to the seabed after reproduction (white "R"). Taken from Schiebel and Hemleben (2017).

Depth habitat (m)	Species	ALD (m)	Depth habitat	Yearly cycle	Monthly cycle
Surface (<100)	*G. ruber* pink	39.51	S		B-W
	G. tenella	52.16	v		M
	G. ruber white	57.84	V		B-W
	T. sacculifer	60.71	V	May-Jul	NM
Surface – subsurface (50-200)	*G. calida*	73.33	V	-	-
	G. glutinata	78.62	V	May-Jul	NM
	O. universa	79	S		M
	N. incompta	80.93	V	May-Jul	
	G. siphonifera	83.78	V		M
	G. falconensis	92.92	V	-	-
	G. truncatulinoides	96.36	V	May-Jul	NM
	G. bulloides	102.35	V		M
	G. inflata	104.35	V		M
	G. rubescens	107.41	V	-	-
	N. pachyderma	113.35	ND		M
Sub-surface (130–230)	*T. quinqueloba*	143.9	V		M
	G. scitula	224.28	V	May-Jul	M

Table 3.5: Average living depth (ALD) of modern planktonic foraminifera. Species with a yearly cycle: months with the deepest ALD. Monthly cycle: B-W = bi-weekly; M = monthly; NM = new moon. Algal symbionts: F = facultative algal symbionts; B = bacterial symbionts. ND = No data; S = Stable: V = Variable. Based on Rebotim et al. (2017) and Schiebel and Hemleben (2017).
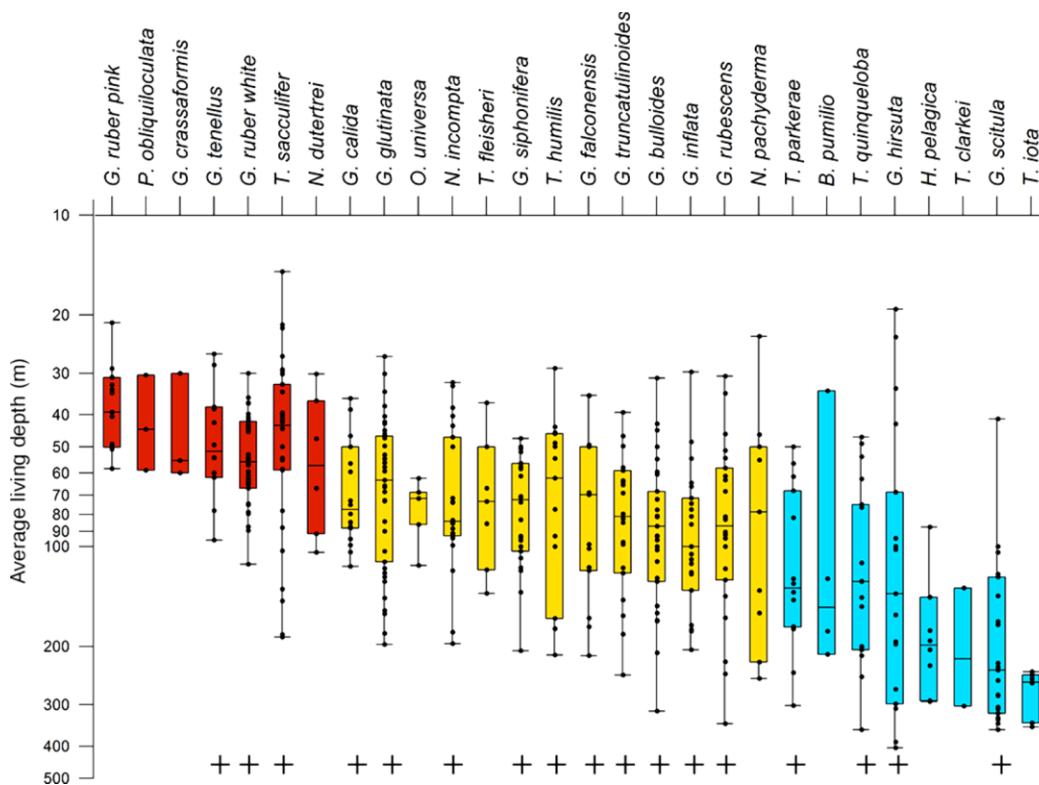
Figure 3.4: Average living depths (ALD) of the living planktonic foraminifera. The box and whiskers plots highlight the median and the upper-lower quartiles. Species are ordered according to their mean ALD. Colours are used to highlight species with similar depth preferences. Taken from Rebotim et al. (2017).

Depths habitats of foraminifera can be divided into three broad categories: a) surface

species that live within the photic zone (<100m) and have an average living depth of 40-60m; b) surface to subsurface species that range from 50-200m, and c) subsurface species that have an average living depth of >70m, but range from 130 to >230m (Figure 3.4; Table 3.5) (Rebotim *et al.*, 2017). The extent and patterns of any vertical migration is specific to each species. Species such as *G. ruber* pink and *O. universa* have relatively narrow living depth ranges, but have broad temperature ranges, which enables them to maintain a stable depth habitat regardless of changing thermal conditions (Field, 2004; Rebotim *et al.*, 2017). Others display variable vertical migration in response to changing ecological or hydrological conditions, such as light intensity (e.g. symbiont-bearing *T. sacculifer*); temperature (e.g. *G. calida* and *G. rubescens* deepen with increasing water temperatures) or food availability (e.g. *N. incompta*) (Field, 2004; Kuroyanagi and Kawahata, 2004; Rebotim *et al.*, 2017). Species also display seasonal ontogenetic patterns in depth habitat (as discussed in Section 3.1.3), such as annual (e.g. *G. truncatulinoides* deepest in summer months) or synodic lunar cycles (e.g. *G. ruber* or *G. glutinata*, which are deepest around the new moon), which are superimposed on their primary depth habitats (Figure 3.1; Figure 3.3) (Schiebel and Hemleben, 2005; Rebotim *et al.*, 2017). Hydrological changes in the water column, such as the location of the pycnocline, deepening of the mixed layer, stratification, development of a DCM, periods of upwelling or eddies can influence their depth habitat (Schiebel *et al.*, 2002a; Field, 2004; Kuroyanagi and Kawahata, 2004; Al-Sabouni *et al.*, 2007; Salmon *et al.*, 2015).

3.3.4 Seasonality

Interannual seasonal changes in SST, as well as water-column structure and influx of food sources and nutrients, can influence the temporal and spatial dynamics of a planktonic foraminiferal population. When tropical/subtropical spinose species, such as *G. ruber* white, *G. ruber* pink, *T. sacculifer*, *O. universa*, *G. siphonifera*, *G. rubescens* and *G. tenella* inhabit shallow waters within their optimum temperature range (>25°C), there is little annual flux in their abundances. In cooler waters however, seasonal peaks in abundance occur in warmer more stratified waters during the summer (e.g. *G. ruber* pink in July-September) or autumn (*G. ruber* white in September to October), indicating that temperature is the key factor governing their abundance rather than food, due to the presence of endosymbionts (Jonkers and Kučera, 2015; Salmon *et al.*, 2015; Schiebel and Hemleben, 2017). It is inferred that such species have preferred thermal niches, i.e. a preferred temperature range for the optimal balance between growth and respiration,

which correlate specific temperature ranges per species with increased reproductive success (Jonkers and Kučera, 2015).

Cooler/temperate (mostly) symbiont-barren or deeper dwelling species *G. bulloides*, *G. glutinata*, *T. quinqueloba*, *N. incompta*, *N. pachyderma*, *G. scitula* and *G. calida* display strong, consistent uni- or bimodal peaks during both the autumn/winter and the more significant spring bloom (especially in the mid latitudes), coinciding with cooler waters, periods of maximum chlorophyll-α, deepening of the mixed layer and redistribution of nutrients to the euphotic zone, leading to heightened primary productivity and increased seasonal planktonic foraminifera flux (Kuroyanagi and Kawahata, 2004; Jonkers and Kučera, 2015; Salmon *et al.*, 2015; Schiebel and Hemleben, 2017).

Finally, deep water species such as *G. inflata* and *G. truncatulinoides* have a single short peak during the winter/spring that is not linked to productivity, but may be linked to their long reproductive cycle and shallowing to warmer more dynamic surface waters to reproduce (Jonkers and Kučera, 2015). Of the deeper species, only *G. scitula* shows a seasonal pattern similar to that of cold-water and temperate species.

3.3.5   Food preferences

Availability and distribution of food directly influence the spatial and temporal distribution of planktonic foraminifera, as it affects their growth rates, longevity and timing and success of reproduction (Schiebel and Hemleben, 2017). Most planktonic foraminifera are omnivorous, though this differs significantly between spinose and non-spinose species, and within the groups themselves. Prey includes i) zooplankton: mainly copepods and ciliates, and include among others, tunicates, radiolarians and pteropods; ii) phytoplankton: mainly diatoms, but also include dinoflagellates, eukaryotic and thecate algae and iii) bacteria. Studies of contents of food vacuoles in the cytoplasm of spinose species demonstrate that they are preferentially carnivorous, though they do feed on phytoplankton.

The highest abundances of symbiont-bearing spinose species are generally found in oligotrophic waters in subtropical gyres, where food is not readily available, but the waters are clear, allowing maximum light penetration in the photic zone (Watkins *et al.*, 1996; Žarić *et al.*, 2005; Kučera, 2007). It was found that *G. ruber* was less dependent on zooplankton than other spinose species such as *T. sacculifer* and *G. siphonifera*, suggesting that it is more adapted and successful in low productivity regions, where it

can more efficiently utilise nutrition from primary producers (Anderson, 1983).

Non-spinose species are preferentially herbivorous (mainly diatoms), therefore inhabit more eutrophic waters with high phytoplankton productivity, such as upwelling areas or in waters that experience seasonal phytoplankton blooms (Hemleben *et al.*, 1989; Schiebel and Hemleben, 2005). Non-spinose species are not suited to capture large live prey, though zooplankton prey remains are found in their food vacuoles and it has been suggested that they can feed on particulate organic, i.e. matter inactive or dead animal prey, e.g. *G. truncatulinoides* utilise their rhizopodial net to entrain small pieces of animal protein (Anderson *et al.*, 1979). More recently, it was found that Gammaproteobacteria within particular organic matter formed a significant proportion of the diet of *N. incompta* type II from stratified waters along the Californian coast, with more limited feeding on phytoplankton (Bird *et al.*, 2018). It should be noted that the trophic requirements for most genotypes have not yet been resolved, therefore how it fully impacts their abundance and distribution remains an unknown (Bird *et al.*, 2018).

Food availability during ontogeny can affect both the size of the chambers (i.e. the greater the food availability, the larger the chamber size) and longevity of the foraminifera (i.e. if food is scarce, the foraminifera will delay gametogenesis until more favourable conditions return, thus they will live longer). Growth rates are different for carnivorous (higher) and herbivorous (lower) species, possibly indicating the response to the energetic content differences of their prey (Lombard *et al.*, 2009).

3.3.6 Nutrients

For most non-algal symbiont bearing species, nutrient availability plays a significant role in governing their distribution, abundance and test size (Schiebel and Hemleben, 2017). These species feed mainly on phytoplankton (e.g. diatoms or dinoflagellates). In turn, phytoplankton primary productivity is controlled by their own specific biological, physical and trophic demands, including availability of nutrients, including organic and inorganic carbon and nitrate (NO_3), as well as nitrogen dioxide (NO_2), phosphate (PO_4) and silicate (SiO_4) (Schiebel *et al.*, 2004). Morey *et al.* (2005) determined that a fertility or nutrient gradient was the 2nd most influential parameter for variability of tropical/subtropical fauna (7.9%). A canonical correspondence analysis (CCA) analysis of global sediment and water-column samples inferred an inverse relationship between SST and salinity to a nutrient and fertility gradient between fertile tropical/subtropical upwelling areas (e.g. *N. dutertrei*) and low fertility oligotrophic waters (e.g. *G. ruber*)

(Morey *et al.*, 2005).

Globally, primary productivity gradually increases with temperature from the subpolar to temperate zones, in comparison to highly variable fertility gradients in warmer subtropical and tropical zones (Schmidt *et al.*, 2004). However, upwelling zones display the greatest fertility gradient. When nutrient levels increase within the upper water column, this can lead to an increase in the productivity of primary producers and within a few days, trigger changes in the foraminiferal assemblage and flux rates at specific times of the year (Schiebel *et al.*, 1995). In temperate waters, there can be two seasons of enhanced primary productivity (spring and autumn blooms) caused by a combination of deep vertical mixing of the water column, which entrains nutrient-rich waters from below the pycnocline into the nutrient depleted euphotic zone, nutrient recycling and light intensity. This is also seen in low latitude stratified oligotrophic waters, where regional seasonal effects of monsoons or upwelling increase nutrient availability and increase primary productivity (Schiebel and Hemleben, 2005). In addition, more proximal areas with high terrestrial input from either delta or river plumes, or nearshore canyon heads also have high nutrient availability (Retailleau *et al.*, 2012).

Increased homogenisation of the water column and higher prey densities affect quality and penetration of light into the euphotic zone, which directly impacts on symbiont bearing species (Bijma *et al.*, 1992). In upwelling areas, symbiont-bearing species generally have smaller shell sizes, caused by the effects of under-saturation of O_2 in deeper waters and low light levels on symbionts that restrict host respiration and metabolism. This is in comparison to fertile waters in river plumes that are enriched in O_2 and are associated with larger test sizes (Bijma *et al.*, 1992).

In oligotrophic waters, such as the Mediterranean Sea, a well-developed DCM can occur when the pycnocline and nutricline lie within or close to the base of the euphotic zone. The maximum depth of the DCM is correlated to the position of the seasonal pycnocline and the depth of minimum light intensity needed for phytoplankton to grow (Fairbanks and Wiebe, 1980). With the development of a DCM and the entrainment of nutrients into waters with higher light intensities, phytoplankton biomass significantly increases (Fairbanks and Wiebe, 1980). Neogloboquadrina species such as *N. incompta* and *N. dutertrei* have been found to be closely associated with the high productivity of a DCM (Fairbanks *et al.*, 1982; Rohling and Gieskes, 1989; Field, 2004; Kuroyanagi and Kawahata, 2004).

The response of planktonic foraminifera to enhanced productivity has been noted in numerous studies of upwelling areas, temperate waters and following storm events (Schiebel *et al.*, 1995; Schiebel *et al.*, 2001; Schiebel *et al.*, 2004; Retailleau *et al.*, 2012). Schiebel *et al.* (2001) observed the effect of changes in nutrient availability and chlorophyll-α redistribution within the BIOTRANS research area, located in the eastern North Atlantic (20°W, 47°N). Late summer stratified waters with a well-defined DCM were dominated by *N. incompta*, and associated warm water species such as *G. ruber*, *O. universa*, *T. sacculifer* and *G. siphonifera*. Following the southerly tracking of a frontal zone and storm induced deep water-column mixing, there was increased chlorophyll-α redistribution and entrainment of nitrates from below the nutricline. The subsequent faunal assemblage was dominated mainly by *G. bulloides* and the deeper *T. quinqueloba*. This dominance of *G. bulloides* and *T. quinqueloba* was also observed during the autumn bloom in the Bay of Biscay and was associated to riverine nutrient input, increased turbidity and associated enhanced primary productivity (Retailleau *et al.*, 2012). In several studies, primary productivity pulses characterised by diatoms coincide with a strong swift response by *G. glutinata* (Schiebel and Hemleben, 2000; Schiebel *et al.*, 2001).

In addition to influencing the abundance and distribution of foraminiferal species, increased deep mixing of the water column, re-suspension of fine particulate organic matter and nutrients, and the associated increase in phytoplankton following intensive storm events has been associated with an increase growth rates of the planktonic assemblage (Schiebel *et al.*, 1995).

3.4 Distribution of planktonic foraminifera in the Mediterranean Sea

As planktonic foraminifera are the main proxy used to reconstruct Late Pleistocene SST and hydrological conditions in the Mediterranean Sea, it is important to review the modern distribution of planktonic foraminifera. What species currently inhabit the Mediterranean Sea? How do modern hydrological conditions impact on the structure of faunal communities, and is there any seasonality in their annual flux? Understanding how the living assemblage is adapted to modern conditions in the Mediterranean Sea will help to determine to what extent foraminifera were impacted by rapid palaeoenvironmental changes during the deglacial. How did they respond to variations in SSTs? Did their responses differ on a basin-wide scale? Can we decipher any other factors that influenced their distribution, such as changes in hydrological structure and

trophic conditions, particularly in the Gulf of Lion? In turn, can we identify the main mechanisms of deglaciation in the Mediterranean? A detailed understanding of the modern Mediterranean assemblage will help us address these questions.

The spatial distribution of modern planktonic foraminifera in the Mediterranean Sea has been investigated in a number of studies over the past 50 years. These studies include plankton tows taken along transects spanning the Mediterranean Sea, time-series sediment traps and core-top surface sediment samples. Plankton tows studies include Cifelli (1974), Pujol and Vergnaud Grazzini (1995) and Mallo *et al.* (2017) (Figure 3.5). The main benefits of plankton tows are that they provide a snapshot of the living assemblage and hydrological conditions at given depths, at specific times in the year, and have good spatial distribution across the Mediterranean Sea. However, this specificity of time and place is also a limiting factor, especially when applying their results to sediment cores. In addition, they are further constrained by the size fraction of the plankton nets used (e.g. 150 μm), which will not capture the full size range of smaller species, e.g. *T. quinqueloba*.

Sediment trap data are available for the Gulf of Lion (Rigual-Hernández *et al.*, 2012), Alboran Sea (Bárcena *et al.*, 2004; Hernández-Almeida *et al.*, 2011) and most recently, the Levantine Sea (Avnaim-Katav *et al.*, 2020). Generally, sediment trap studies span 1+ year(s). They are deployed at specific depths and sample the flux of all species (regardless of size) at regular timescales. Variations in the composition and flux of the full assemblage through the year(s) can provide evidence of seasonality in response to bloom events or short-term hydrological events, which is invaluable when deciphering the complex signals in sediment cores. Unfortunately, sediment trap studies that report planktonic foraminifera counts are poorly distributed across the Mediterranean Sea. In addition, results are specific to the sediment trap site location and may be significantly influenced by specific events that occurred during the study period, e.g. 1997–1998 El Niño-Southern Oscillation event recorded in the Alboran Sea (Bárcena *et al.*, 2004; Hernández-Almeida *et al.*, 2011).

Finally, the study by Thunell (1978) utilised core-top surface sediments to map the distribution of modern planktonic foraminifera across the Mediterranean. Surface sediments are collected from core-tops or box-cores and represent an averaging of species abundance and flux over years, decades to centuries, depending on sedimentation rates and taphonomic effects at the site (Morey *et al.*, 2005; Siccha and

Kucera, 2017). Although they lack the temporal constraints or hydrological data of plankton tows or sediment trap studies, their generalised abundance data is more comparable with sediment core data. In the Mediterranean, surface sediment sites are more abundant and have greater spatial distribution than either plankton tows or sediment trap sites (Thunell, 1978). Therefore, they provide a good overview of species distribution across the modern Mediterranean.

Cifelli (1974) published the first reported results of plankton tows from a summer cruise in 1969. This cruise track extended from the Ionian Sea in the eastern Mediterranean Sea to east of Madeira Island in the Atlantic Ocean (Figure 3.5). This study provided a snapshot of the late spring/early summer faunal assemblages. In the western basin, Cifelli (1974) determined that the assemblage was composed of an equal mix of cooler "northern" and subtropical species. "Northern" (i.e. "North Atlantic") species included *G. bulloides*, *N. incompta*, *T. quinqueloba* and *G. inflata*, whereas subtropical species comprised of *G. siphonifera*, *G. ruber*, *G. tenella*, *T. sacculifer*, *G. truncatulinoides* and *O. universa*. In contrast, "northern" species were replaced by greater numbers of subtropical fauna in the eastern basin, though there was a noticeable increase in cooler subpolar and transitional species in areas of intermediate water formation.

Thunell (1978) published the first study to map the spatial distribution and inferred faunal preferences of 16 key planktonic foraminiferal species within the Mediterranean Sea. The study utilised 66 core-top samples located throughout both the eastern and western basins, though with the exception of the Adriatic Sea or the seas north of Libya (Figure 3.5). As with Cifelli (1974), this study documented a noticeably cooler, grazing assemblage in the western basin, and a warmer predatory eastern assemblage. Many aspects of this study are now outdated, such as the lack of differentiation of certain morphospecies (*N. pachyderma* and *N. incompta*; *G. ruber* white and *G. ruber* pink, and *G. truncatulinoides* sinistral and dextral). In light of the identification of planktonic foraminifera genotypes, there is the added complexity that the distribution of certain genotypes display an apparent seasonal signal and/or niche competition in the Mediterranean, e.g. *G. ruber* subtypes IIa1 and IIa2 (Aurahs *et al.*, 2009). However, Thunell (1978) remains the only study that has mapped the spatial distribution of modern morphospecies across the Mediterranean Sea. This allows for a basic comparison with the spatial distribution of morphospecies during the Late Pleistocene. In addition, the core top dataset has formed the basis of the training dataset for Artificial Neural Networks for the Mediterranean Sea (Hayes *et al.*, 2005). This will be discussed

further detail in the Chapter 5.

A seminal work investigating the abundance and distribution of living planktonic foraminifera across a NW-SE transect of the Mediterranean was published by Pujol and Vergnaud Grazzini (1995). This study utilised a series of plankton tows deployed at 5 depth intervals within the top 350m at 14 stations in winter (Feb-Mar 1986), late summer (Sep-Oct 1986) and early spring (Apr 1990) in the Alboran Sea only (Figure 3.5). As with the previous studies, it was clear that the composition and diversity of species changed from the more productive west to oligotrophic east. However, these variations were also reported across the seasons and at different depths. The averaged flux of planktonic foraminifera (0-350m) in the Mediterranean Sea was lower in the summer than in the winter. Again, this varied across the basins and seasonally, e.g. in the Gulf of Lion, summer tows varied from <200 to 3700 ind./1000m^3 from summer to winter, whereas the opposite was observed in the south-eastern basin. The recent sediment trap study in the Levantine Sea contradicts this and will be discussed further below.
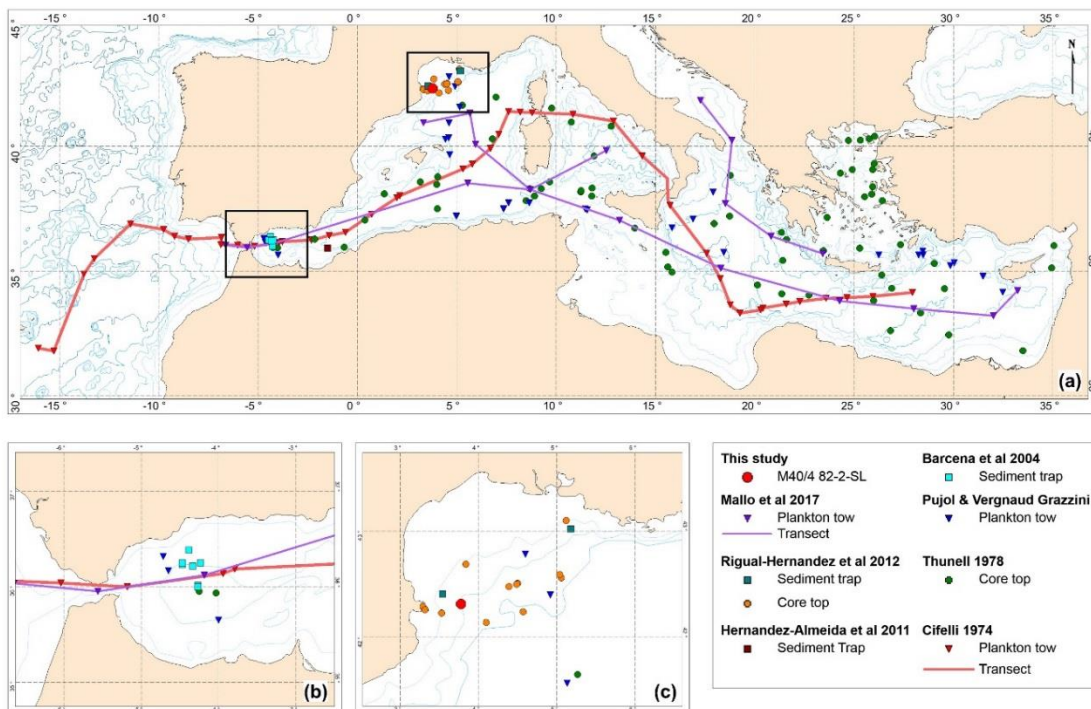
Figure 3.5: Distribution of plankton tow, core top and sediment trap site locations a) the Mediterranean Sea, b) Alboran Sea and c) Gulf of Lion, as published by Cifelli (1974); Thunell (1978); Pujol and Vergnaud Grazzini (1995); Bárcena et al. (2004); Hernández-Almeida et al. (2011); Rigual-Hernández et al. (2012); Mallo et al. (2017).

This study demonstrated that although the Mediterranean experiences extremes in SST and SSS, it is food availability and hydrological structure of the water column that are

the driving forces for the spatial and seasonal distribution of planktonic foraminifera. SSTs <13°C were only seen as a notable factor in the presence of *N. incompta* at all sampled depths in the Gulf of Lion. Increased productivity and abundance of grazing species were linked to periods of winter upwelling and deep-water formation (e.g. north-west Mediterranean, Alboran Sea, Cyprus) and fronts/eddies along current systems (e.g. the MAW along the north African coast to the east of the Strait of Gibraltar). The presence of a DCM was associated with a mixed assemblage of deeper grazers. In the northwest Mediterranean, the DCM was situated at ~75m during the summer, but shallowed to 40-50m during the winter, coinciding to the peak at that depth in *N. incompta*, along with *G. bulloides* and *G. inflata*. In the summer, the stratified oligotrophic waters were dominated by shallow dwelling, symbiont-bearing predator species (primarily *G. ruber* white, *G. ruber* pink and *T. sacculifer*) that thrive in the well-lit photic zone, with *G. truncatulinoides* at greater depths in the western basin.

The most recent basin-wide study was conducted by Mallo *et al.* (2017) in May 2013 using BONGO nets at 20 stations sampling the upper 200m of the water column (Figure 3.5). This research presented the absolute and relative abundance of planktonic foraminifera in relation to SST, SSS, productivity and water geochemistry. Absolute abundance of planktonic foraminifera was extremely low during summer months (an average of 1.42 ± 1.43 ind./$10m^3$), which is comparable to the summer abundances reported by Pujol and Vergnaud Grazzini (1995). In addition, Mallo *et al.* (2017) reported low diversity with only 12 morphospecies recorded. This was significantly lower than the diversity reported in Cifelli (1974), Thunell (1978) and Pujol and Vergnaud Grazzini (1995), who all reported between 18 and 20 morphospecies. Notable absences were *G. truncatulinoides*, the Neogloboquadrinids, *T. quinqueloba*, *G. glutinata* and many of the SPRUDTS groups. This low diversity may reflect the seasonality or life cycles of the species, or the size of specimens may have been too small to be captured in the nets (150µm).

In general, the early summer faunal distribution support older summer plankton tows (Cifelli, 1974; Pujol and Vergnaud Grazzini, 1995) and as well as data from sediment trap studies (discussed below) (Bárcena *et al.*, 2004; Hernández-Almeida *et al.*, 2011; Rigual-Hernández *et al.*, 2012; Avnaim-Katav *et al.*, 2020). *G. ruber* white was the most abundant species along with *O. universa*, particularly in the eastern basin. *G. inflata* and *G. bulloides* were the main species in the western basin, along with *T. sacculifer*. As would be expected, cooler SSTs and food availability were the governing

factors for eutrophic species. The distribution of *G. ruber* white and *G. ruber* pink coincided with the west to east temperature and salinity gradient and their ability to thrive in oligotrophic waters. Interestingly, the high percentage of *G. ruber* white in Tyrrhenian Sea was linked to greater food availability, inferring that once *G. ruber* is in suitably warm waters, food a key determinant for their distribution. Similarly, food and nutrient rich upwelling areas were factors for *T. sacculifer* and *O. universa*.

Within the mainly oligotrophic Mediterranean Sea, the cooler surface waters in the Gulf of Lion and the Alboran Sea basin are the most productive. These high productivity regions have been studied in detail using a comparison of sediment trap and surface sediments by Rigual-Hernández *et al.* (2012) in the Gulf of Lion, and Bárcena *et al.* (2004) and Hernández-Almeida *et al.* (2011) in the Alboran Sea.

Rigual-Hernández *et al.* (2012) analysed data from two sediment trap stations located either side of the gulf in the Gulf of Lion over a 12 year period (1993-2006) (Figure 3.5). Both stations displayed a unimodal pattern that accounted for approximately 80% of the total average annual flux. This peak occurred during the coldest part of the year (SSTs ranged 13 to 14.5˚C) and coincided with the highest annual chlorophyll-a concentrations and the late winter/early spring phytoplankton bloom (Rigual-Hernández *et al.*, 2012). This typical winter-spring assemblage was dominated by *G. bulloides*, along with *G. truncatulinoides*, *N. incompta* and *G. inflata*. During the spring-summer and early autumn when the waters were warmer and more stratified, there were minor peaks of *O. universa*, *G. siphonifera*, *T. sacculifer* and *G. ruber* white and *G. ruber* pink, accounting for just 4 to 6% of the relative abundance.

Comparisons were made with core top data located along a transect between the two stations (Figure 3.5). The same four eutrophic species dominated the core top assemblages. However, the relative abundances differed from within the highly productive Rhone Delta plume (dominated by *G. bulloides*), to the more distal less productive sites, where species diversity increased and higher relative abundances of *N. incompta* and *G. truncatulinoides*. These more distal results are similar to those reported by Pujol and Vergnaud Grazzini (1995) in their Gulf of Lion stations. Importantly, it was inferred by Rigual-Hernández *et al.* (2012) that given the unimodal planktonic foraminiferal signal recorded in both sediment traps, the fossil assemblage in the core tops in this region would reflect primarily the high productivity, cooler water winter-spring bloom assemblage.

Results from a series of sediment traps and surface sediments located along the productive margins of the Alboran Sea gyres were published by Bárcena *et al.* (2004) and Hernández-Almeida *et al.* (2011) (Figure 3.5Figure 3.5). The sampling period of the sediment traps incorporated the intense seasonal upwelling experienced in the Alboran Sea, but also coincided with the global 1997-1997 El Niño-Southern Oscillation (ENSO) event (Bárcena *et al.*, 2004; Hernández-Almeida *et al.*, 2011).

The Western Alboran Gyres (WAG) region was dominated by *G. bulloides*, with *G. inflata* and minor *G. ruber* white (>90% of the total population); whereas *T. quinqueloba* and *G. bulloides* dominated the Almeria-Oran Front (AOF) (~85% of the total population), along with *G. inflata* and *G. ruber* white (Bárcena *et al.*, 2004; Hernández-Almeida *et al.*, 2011). There was a unimodal peak during the winter-spring bloom, which was delayed due to the extended warming of the late summer/autumn SSTs of the ENSO event. When the gyres finally were re-established, *G. bulloides* dominated the assemblage, driven by the increase in upwelling/wind-driven productivity and food availability (Bárcena *et al.*, 2004). This was in contrast to the relative abundance from core top sediments, where *G. bulloides* accounted for <40% of the total population. *G. inflata* was present throughout the sampling period (<20%), but it had the highest annual relative abundance (43%) in surface sediments. The mean annual relative abundance of *G. ruber* white in surface sediments was low (<3.3%), but it formed a significant component of the assemblage during the autumn and unseasonably warm early winter. Interestingly, the spring plankton tow data reported by Pujol and Vergnaud Grazzini (1995) for this region has greater similarity to the core top data than the spring patterns recorded in sediment traps. This disconnect between the sediment trap data from 1997/1998 and surface samples illustrate the considerable influence of the ENSO event that winter, where the opportunistic *G. bulloides* flourished in comparison to *G. inflata* (Bárcena *et al.*, 2004).

The faunal assemblage and flux patterns recorded in the sediment trap deployed in the AOF region was markedly different to the WAG (Hernández-Almeida *et al.*, 2011). There were three substantial seasonal peaks during the summer, late autumn/winter and spring, coinciding with cold upwelling/productive periods. *T. quinqueloba* (~20%) and *G. bulloides* (~18%) were the dominant species during these productive periods. During the unseasonably warm late summer/early autumn period, stratification, low productivity and deepening of the thermocline lead to a peak of both *G. inflata* and *G. ruber*. These results are similar to the summer assemblage of Cifelli (1974) and core top

data from Thunell (1978).

The recent sediment trap study by Avnaim-Katav *et al.* (2020) in the ultra-oligotrophic Levantine Sea is the sole planktonic foraminifera sediment trap study in the eastern Mediterranean. During the sampling period in 2017/2018, oligotrophic conditions were observed throughout the year. Similar to Mallo *et al.* (2017), species diversity in this region was very low. 96% of species were comprised of symbiont bearing predatory species, primarily *G. ruber* white, with *G. rubescens*, *G. tenella*, *O. universa*, *G. ruber* pink, *G. calida*, and *G. siphonifera*. The average annual planktonic foraminifera flux was extremely low and displayed short-lived winter and late summer peaks. The main peak in February (dominated by *G. ruber* white, *G. rubescens* and *G. calida*, accounting for 46% of the annual flux) coincided with the lowest annual SST and minor increase in chlorophyll. This was followed by a minor late summer peak (*G. ruber* white, *G. ruber* pink and *O. universa*) when SSTs ≥28°C. The greater abundance during winter contrasts Pujol and Vergnaud Grazzini (1995). In general, this seasonal assemblage was similar to plankton tows and nearby core-top samples, with the exception of the marked decreased in *G. bulloides* and unexpectedly, *G. ruber* pink (Pujol and Vergnaud Grazzini, 1995; Mallo *et al.*, 2017; Siccha and Kucera, 2017). The decrease in *G. bulloides* was attributed to increasing SSTs and oligotrophy in the modern Levantine Sea, whereas the reasons for the decrease in *G. ruber* pink was less clear (Avnaim-Katav *et al.*, 2020).

Chapter 4.

4   Palaeoclimatic signals of the Late Pleistocene

The Quaternary Period spans the last 2.58 Ma and is subdivided into the Early (from 2.58 Ma), Middle (from 773 kyr BP) and Late Pleistocene stages (from 126 kyr BP), and the Holocene Epoch (from 11.7 kyr to the present) (Cohen *et al.*, 2013). It is characterised by a series of long-term glacial and interglacial periods, where the waxing and waning of vast ice sheets dominated much of the northern hemisphere continents, interspersed with shorter term stadial and interstadial periods. This predominantly cold period began as a gradual cooling in the Paleogene, with more pronounced cooling during the Miocene and Pliocene (Bell and Walker, 2005). These fluctuations in climate are evident globally in a wide range of proxies, such as deep-sea, ice and lake cores, coral reefs and pollen archives.

The focus of this chapter will be on the latter part of the Late Pleistocene, a period of significant short-term climate oscillations following the Last Glacial Maximum. This section will outline the proposed forcings and feedbacks of long-term climate change, as well as the drivers for millennial-scale variability observed in the Late Pleistocene, both globally and within the Mediterranean region. This will provide the context for understanding how and why these climate forcings are observed in the geological archives of the Mediterranean Sea.

4.1   Mechanisms of long-term climate change

Astronomical theories, known as Milankovitch cycles, have been identified and used to account for the periodicity and timing of long-term climate change. The main mechanisms illustrated in Figure 4.1, as summarised by Bell and Walker (2005) are: i) "Precession of the equinoxes" describes the direction of the tilt of the earth's axis, which can "wobble" over time, thus effecting the distribution of radiation received by the northern and southern hemispheres during the perihelion and aphelion. It has two interconnected periodicities, a major cycle of ~23 kyr and minor one of ~19 kyr; ii) "Obliquity of the ecliptic" is the degree of the tilt of the earth's axis, which has a cyclical range of 21.5° to 24.5° and a periodicity of ~41 kyr; iii) "Eccentricity of the orbit" is the change from an elliptical to a more circular orbit of the earth around the sun, which impacts the amount of radiation received during the summer and winter. The

shape of the orbit has a periodicity of 95 to 136 kyr (~100 kyr average), along with an additional longer-term and more significant 413 kyr cycle.
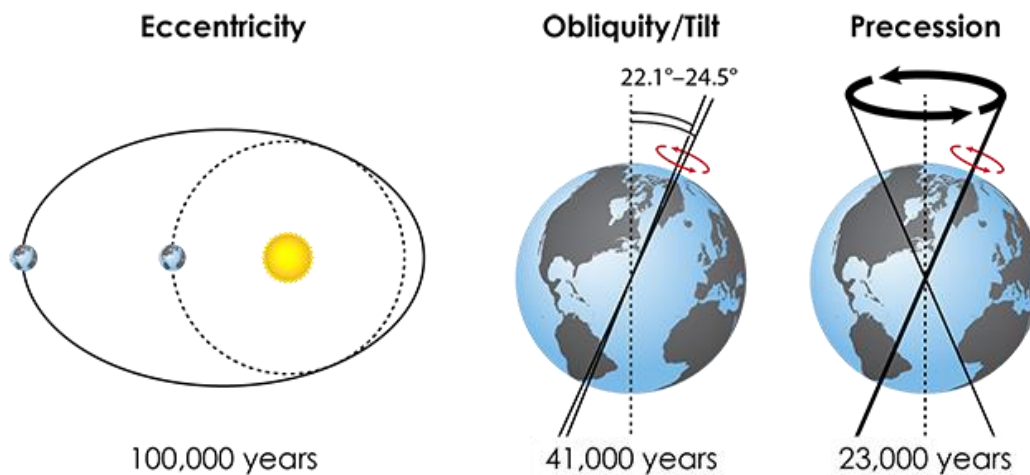
Figure 4.1: Illustration of the main mechanisms of Milankovitch cycles, i.e. eccentricity, obliquity, and precession. Taken from Astrophysics Team University of Lincoln (n.d.).

Precession and obliquity affect the latitudinal and seasonal distribution of solar insolation, whereas eccentricity alone impacts global and annual mean insolation (Berger, 1978; Berger and Loutre, 1991). In addition, eccentricity has a key role in modulating the seasonal and latitudinal effects of precession and obliquity, e.g. during periods of low eccentricity (more circular orbit), changes in seasonal insolation due to precession are weaker than periods of higher eccentricity (more elliptical) (Jansen *et al.*, 2007; McCarroll, 2015). The Milankovitch theory proposes that the growth and shrinkage of ice sheets is controlled by high northern latitude boreal insolation changes (Milankovitch, 1941; Milanković, 1998). During periods of summer insolation minima at 65°N, snow and ice persist throughout the year, enabling the growth of northern hemisphere ice sheets (Figure 1.2) (Berger and Loutre, 1991; Imbrie *et al.*, 1993; Jansen *et al.*, 2007; Vettoretti and Peltier, 2011; Yin and Berger, 2011; Past Interglacials Working Group of PAGES, 2016). In its most simplistic form, this enhanced build-up of snow then ice would trigger its own feedback mechanisms through increasing albedo; changes in atmospheric circulation, e.g. the southern displacement of the polar front jet stream and the paths of storm tracks across the North Atlantic; surface and deep water circulation changes, e.g. the strength and pathway of North Atlantic currents and deep water formation (DWF). These feedbacks would also impact on atmospheric composition of gasses and particulates, e.g. reduce CO_2, CH_4 and water vapour, and increase dust; all of which would finally impact on reducing precipitation rates, thus leading to the cessation of ice growth (Maslin, 2009). These shorter-term feedbacks will

be discussed in more detail in section 4.2 Short-term climate change.
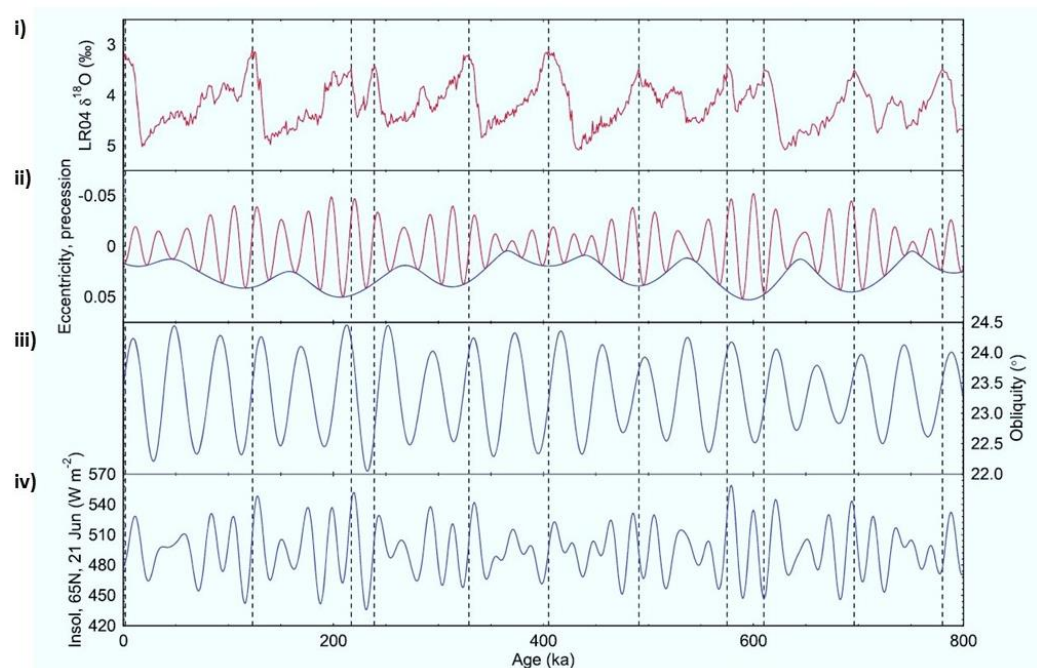
Figure 4.2: Interglacial Peaks (dashed line) correlated with: i) LR04 stack of marine benthic foraminifera $\delta^{18}O$ (Lisiecki and Raymo, 2005); insolation parameters ii) precession (red) with eccentricity (blue) (negative plotted high); iii) obliquity (in degrees); iv) calculated insolation at 65°N for the summer solstice. Taken from Past Interglacials Working Group of PAGES (2016).

Increasing summer insolation and insolation seasonality, which occurs when the precession minima (i.e. northern hemisphere summer occurs at perihelion) and maximum obliquity are in phase, were key triggers for the onset of the last deglaciation around 19-20 kyr, and peaked in the early Holocene (Clark *et al.*, 2009). This increase in northern hemisphere summer insolation led to enhanced summer ablation, rapid ice mass loss in many northern hemisphere ice sheets and mountain glaciers, and rising sea levels. In addition, insolation is a key forcing for variations in precipitation and northern high latitude temperatures, sea ice and vegetation during the deglacial period (Yin and Berger, 2011). Sea level rise and certain melt water pulse (MWP) events can be linked to the onset of rising summer insolation at ~19 kyr, when there was 5-10 m rise in sea-level (19 kyr MWP), and MWP-1B occurred during the insolation maxima of the early Holocene (~11.5-11 kyr) (Clark *et al.*, 2004; Stanford *et al.*, 2011b; Carlson and Clark, 2012; Abdul *et al.*, 2016). However, the relationship of these responses with insolation are not always linear. The observed lagged response of sea level to deglacial insolation changes were attributed to the more complex interactions between northern hemisphere ice volume and the strength of Asian Summer Monsoons with insolation (Grant *et al.*, 2014).

It is evident that astronomical theories account for the "rhythm" of glacial cycles (Hays

et al., 1976). However, there remains many unanswered questions, e.g. when minimum precession/obliquity maxima are in phase and insolation in Northern Hemisphere summer is heightened, it would be expected that this would correlate with or produce strong interglacials, but this is not always the case (Figure 4.2) (Yin and Berger, 2010; Paillard, 2015; Past Interglacials Working Group of PAGES, 2016). In addition, regional and seasonal responses to changing insolation need to be accounted for (Past Interglacials Working Group of PAGES, 2016). The initial cyclicity of ~41 kyr during the early- to mid-Pleistocene reflects a potential influence of the obliquity cycle; however by the late Pleistocene, the duration of glacial cycles slowed and lengthened, and were followed by shorter interglacials so that their periodicity became ~100 kyr, equating more to an influence of eccentricity (McCarroll, 2015; Paillard, 2015). Finally, astronomical forcing cannot account for this shift from 41 to 100 kyr periodicity, the intensification of glacial cycles in the last 800ka or the marked increase in cooling that began in the Late Miocene.
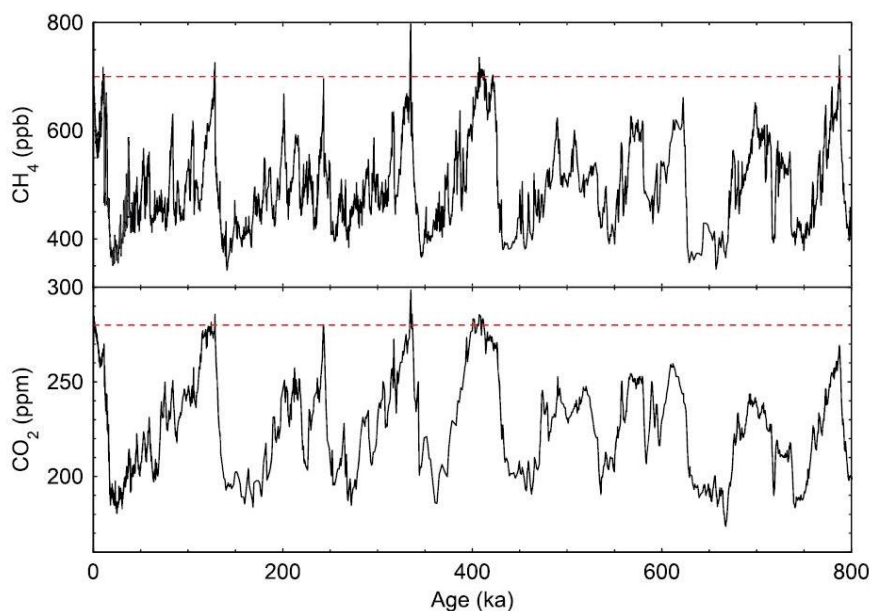
Figure 4.3: Atmospheric carbon dioxide (CO_2) and methane (CH_4) concentrations over last 800ka. Dashed red lines represent the considered typical preindustrial values. Taken from Past Interglacials Working Group of PAGES (2016).

Variations in other forcing factors, such as greenhouse gasses (i.e. carbon dioxide (CO_2), methane (CH_4) and nitrous oxide (N_2O)) (Figure 4.3) and albedo (from variations in the extent of ice sheets, sea level and vegetation, and dust/aerosols in the atmosphere) have been found to be of significant internal feedback mechanisms (PALAEOSENS Project Members, 2012; McCarroll, 2015). The effects of albedo have been modelled for the LGM and researchers have determined that ice sheets are responsible for ~50% of cooling during the LGM (Jansen *et al.*, 2007). Atmospheric

CO_2 levels during glacial periods were ~100ppm lower than interglacial periods (180 to 300 ppm); during the LGM, CO_2 levels were closely correlated with $\delta^{18}O$ records from Antarctic ice cores, thus were attributed as a driver for the other ~50% of cooling during the LGM (Jansen *et al.*, 2007; Paillard, 2015). There is a strong link between ice sheet growth rates and greenhouse gasses. The development of larger northern hemisphere ice sheets is associated with sequestering significant amounts of atmospheric CO_2 by the oceans and storing it at depth, through DWF, nutrient driven planktonic productivity and amount of ice sheet cover (McCarroll, 2015).

Throughout the Quaternary period, it is evident that external/internal forcings and feedback mechanisms do not operate in isolation. The Late Pleistocene cycles (i.e. ~100 kyr interglacial/glacial periods, followed by an abrupt termination) can be attributed to a combination of linear and non-linear responses to ice sheet growth; changing sea levels, oceanic circulation and atmospheric CO_2; effects of albedo, moisture availability and insolation from astronomical forcings.

4.2   Short-term climate change

Short-term climate oscillations can be defined as changes over millennial, centenary or decadal timescales. In general, the late glacial to the early Holocene period (~18 to 11.7 kyr BP) represents the gradual return to interglacial conditions. However, it is punctuated by short-term changes including Heinrich Stadial 1 (HS1), the Bølling-Allerød (BA) and Younger Dryas (YD), followed by the more stable warmer early Holocene, which also experience more discrete cold events at 11.2 kyr and 8.2 kyr (Figure 4.4). During this timeframe, the Northern Hemisphere was dominated by the release of ice sheet armadas into the North Atlantic; the retreat and wasting of the great Laurentide and Fennoscandian ice sheets and subsequent meltwater discharge; changes in sea surface circulation and DWF in the North Atlantic; rising sea levels and eustatic uplift.

4.2.1   Mechanisms for short-term climate change

4.2.1.1   North Atlantic Ocean Circulation

The Atlantic Ocean has many unique characteristics including DWF occurring at both poles; latitudinal exchange of surface, intermediate and deep waters; it has higher rates of evaporation, thus higher SSTs, salinity (1 to 2psu) and density than the Pacific Ocean (Craig *et al.*, 2017). The ocean is made up of three main water masses: i) the cold deep

nutrient-rich Antarctic Bottom Waters (AABW) that are formed around Antarctica, flow northward, and sink to the abyssal plain (>4000m) from where they travel through the tropics to the North Atlantic basin; ii) the dense warmer, nutrient poor and saline North Atlantic Deep Waters (NADW) that form east of Greenland and in the Labrador Sea, and flow southward between 1500 to 3500m deep; iii) the uppermost cool, nutrient rich and oxygen-poor Antarctic Intermediate Waters (AAIW) also formed near the Antarctic and flow northward above the NADW, as they are less dense (Figure 4.5).
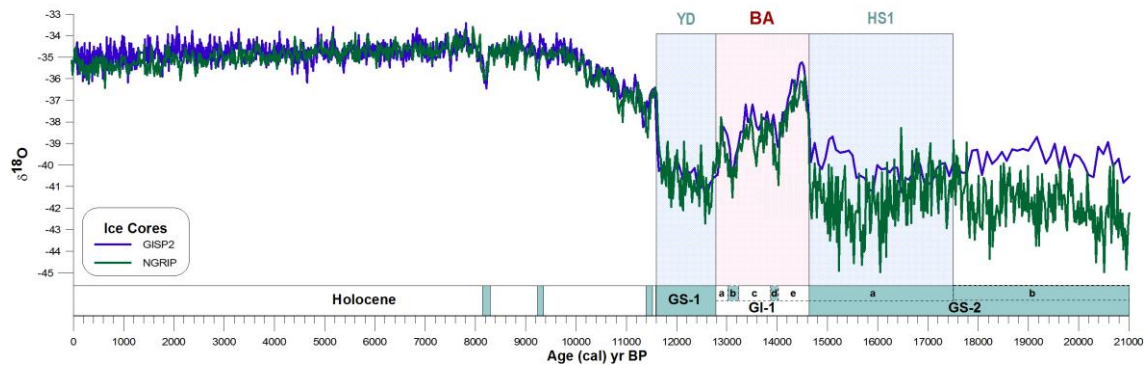
Figure 4.4: Late Pleistocene and Holocene ice core GISP2 and NGRIP Greenland δ18O profiles, displaying INTIMATE event stratigraphy (GS = Greenland stadial; GI = Greenland Interstadial) with the corresponding location of HS1, BA and YD (Grootes and Stuiver, 1999; Alley, 2004; NGRIP dating group, 2008; Rasmussen et al., 2014). Colder periods highlighted in blue.

Warm saline surface waters flow north from the tropics as the North Atlantic Current (NAC), driven mainly by wind, tides and eddies, and transports heat from the Southern Hemisphere and tropics towards the Nordic and Arctic Seas (Maslin, 2009). As the NAC flows north, it loses heat to the atmosphere through evaporation, enabling this cool dense water to sink at around 60°N to form NADW. In addition, the dense hypersaline (36.5 to 37.5 psu) Mediterranean Outflow Water (MOW) exits the Straits of Gibraltar and flows northward at depths between300 to 1400m to Arctic Sea, where the injection of dense salty waters aids the creation of NADW (van Dijk *et al.*, 2018). This process of mixing, cooling and DWF releases a significant amount of energy into the atmosphere, equivalent to an additional 25% to the insolation received within the North Atlantic region each year (Broecker and Denton, 1989). This thermohaline circulation pattern forms part of the Atlantic Meridional Overturning Circulation (AMOC), a conveyor system that enables heat exchange and carbon sequestering between the lower and higher latitudes in the North Atlantic. The strength and pathways of the AMOC system are driven by mechanisms such as surface heat exchange, evaporation, salinity, atmospheric winds, the extent of sea-ice and input of freshwater from melting ice (Figure 4.6) (Broecker *et al.*, 1985; Rahmstorf, 2006; Bakke *et al.*, 2009; Sherriff-

Tadano *et al.*, 2017; van Dijk *et al.*, 2018; Frajka-Williams *et al.*, 2019; Kostov *et al.*, 2019).
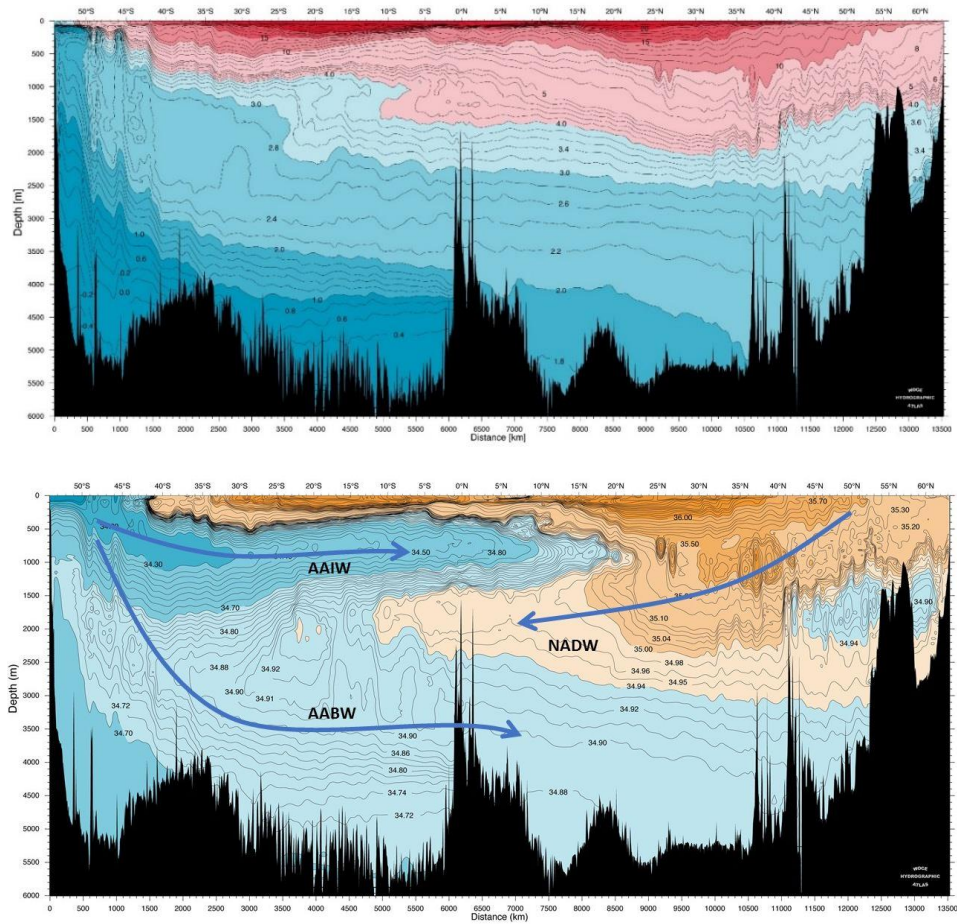
Figure 4.5: Longitudinal cross section through the North Atlantic, displaying the potential temperature variations (top panel) and salinities, with the main waters masses and direction of flow highlighted (bottom panel). From the "WOCE Atlantic Ocean Atlas" (Koltermann et al., 2011).
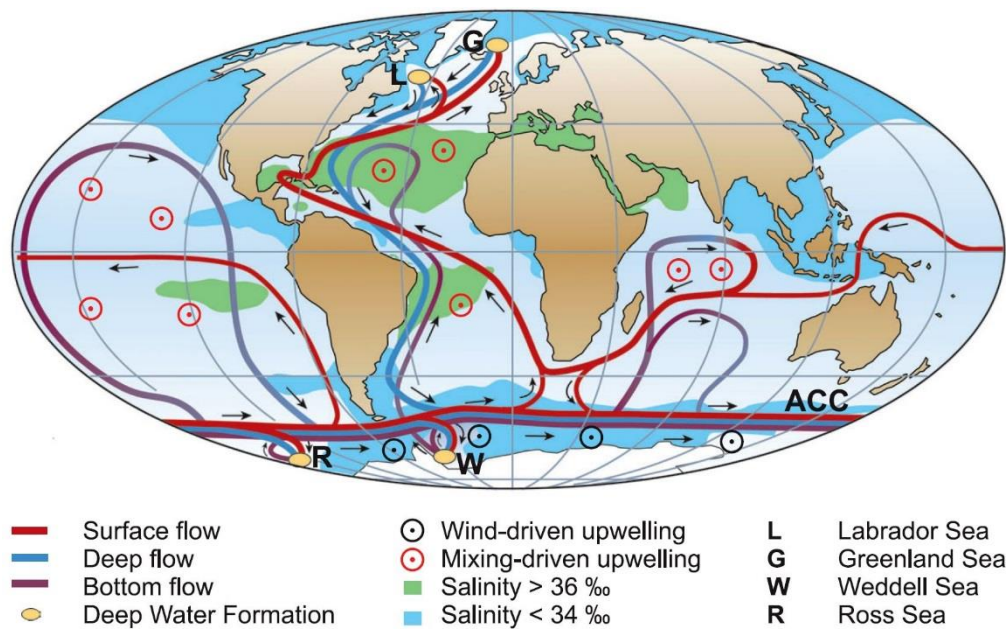
Figure 4.6: Schematic of global thermohaline circulation, indicating areas of deep water formation, upwelling and surface water salinities. Taken from Rahmstorf (2006).

Other fundamental components of North Atlantic circulation include the Polar and Azores Fronts. Oceanic fronts are usually classified as zones of convergence of different water masses, where the largest horizontal gradients of different water properties occur, e.g. temperature and salinity. The polar front forms the boundary where the NAC and Arctic waters meet and follows the Greenland and eastern Canadian continental margins close to the sea ice edge (Bashirova *et al.*, 2014). It acts as a physical barrier, constraining sea ice and iceberg drifting, and forms an ecological barrier for marine fauna. Further south, the warm Azores Currant is a branch of the Gulf Stream that flows eastward towards the Gulf of Cadiz, along the Azores Front (35 to 37°N), which demarks the northern limit of the 18°C water mass associated with the subtropical Eastern North Atlantic Central Water (Gould, 1985; Rogerson *et al.*, 2004; Martin-Garcia, 2019).

Changes in ocean circulation have several climate forcing and non-linear feedback mechanisms that impact short-term global climate patterns. In the North Atlantic, these include the significant transport of heat into the Arctic by the AMOC; regulation of carbon storage at depth; the location of the warm surface water currents which impact both the amount of sea-ice in the Arctic and the influence of albedo; the influence of the "bipolar seesaw" on cross-equatorial heat partitioning and the positioning of the inter-tropical convergence zone (ITCZ); and sea levels, where a weakened or shutdown of the AMOC has the potential to rapidly increase regional sea levels by ~1m, due to the barotropic pressure balance between surface currents and sea surface slopes (Rahmstorf, 2006). Southerly migrations of the polar front have been documented in the North Atlantic during the LGM and HEs, bringing cold waters as far south as 40°N, along the western European margin (McIntyre *et al.*, 1972; Ruddiman, 1977; CLIMAP Project Members, 1981; Bard *et al.*, 1987; Cortijo *et al.*, 2005; Eynaud *et al.*, 2009; Bashirova *et al.*, 2014).

It is therefore evident that variations in the strength of the AMOC or the location of NADW formation has impacts on the global amount of heat and CO_2 available in the oceans and the atmosphere. Numerous studies have determined that the AMOC plays a central role in short term climate change in the northern hemisphere, especially since the LGM through to the Holocene (Heinrich, 1988; Broecker and Denton, 1989; Bond *et al.*, 1992; Broecker, 1998; Alley, 2007). However, the exact mechanisms of AMOC induced climate are still being determined for key events over the past 20 kyr. For example, three simplified modes of AMOC have been proposed for during this period:

i) during interstadial periods, deep mixing and NADW formation occurs in Arctic Seas around Greenland and Labrador; ii) a reduction of the depth of mixing and the area of NADW formation is relocated further south to the Irminger Sea, south of Iceland during stadial periods; iii) significant weakening or the complete shutdown of the NADW can occur during HE (Rahmstorf, 2002, 2006; Alley, 2007). These proposed mode changes are linked to variations in the density of surface waters due to the influx of large volumes of freshwater causing latitudinal shifts or shutdowns of the AMOC. However, the situation is inherently more complex. Deglacial events show individual and unique characteristics and responses that complicate this simplified view. For example during HE1 (~19 to 15 kyr BP), the catastrophic release of iceberg armadas from disintegrating northern hemisphere ice shelves caused a freshening and increase in the buoyancy of North Atlantic waters, inhibiting/reducing NADW formation and weakening/offsetting the AMOC (Bond *et al.*, 1992; Rahmstorf, 2002; McManus *et al.*, 2004; Ivanovic *et al.*, 2018).

In more recent studies, variations in the AMOC and strength of NADW in the Nordic Sea were identified to have begun ~400 years prior to the termination of both GI-1 (BA) and GS-1 (YD) events, as defined in Greenland ice cores (Lane *et al.*, 2013; Barker *et al.*, 2015; Muschitiello *et al.*, 2019). During the latter stages of the of the BA, with increasing inflow of meltwaters, SSTs began to cool and there was an expansion of sea-ice and southern migration of the oceanic polar front (Muschitiello *et al.*, 2015; Muschitiello *et al.*, 2019). Similarly, the resumption of the NADW prior to the termination of the YD was correlated to a gradual increase in SST, decrease in meltwater production, sea-ice extent and iceberg discharge, along with the northward migration of the oceanic polar front (Muschitiello *et al.*, 2019). In addition, atmospheric circulation (i.e. wind strength and direction) is inherently linked to AMOC strength, enhanced NADW formation and ice sheet extent (Sherriff-Tadano *et al.*, 2017). During the early GS-1, the cooling of SSTs and the expansion of sea ice in Nordic Seas allowed large-scale anticyclonic atmospheric blocking systems to be established in north-eastern Atlantic and over the Fennoscandian ice sheet (Bakke *et al.*, 2009). This high-pressure system displaced the polar front jet to the south, allowing cold air and North Atlantic storm tracks towards north-western Europe (Bakke *et al.*, 2009; Lane *et al.*, 2013; Renssen *et al.*, 2015; Renssen *et al.*, 2018; Schenk *et al.*, 2018). It was proposed that this atmospheric blocking pattern impeded the northern heat transfer by the AMOC, further weakening NADW (Muschitiello *et al.*, 2019). The mid-YD strengthening of the

AMOC was accompanied by the asynchronous migration of the polar front jet stream northward over north-western Europe (Lane *et al.*, 2013).

4.2.1.2 *Atmospheric greenhouse gasses*

Variations in atmospheric greenhouse gasses such as carbon dioxide (CO_2), methane (CH_4) and nitrous oxide (N_2O) are not only important for influencing long-term climate signals, but changes in the sources and sinks of atmospheric gasses have a bearing on shorter term climate oscillations. As seen in Section 4.1, levels of CO_2 varied greatly between glacial/interglacial periods (from ~180 to 280 ppm) and it has been suggested that CO_2 increase is the primary mode for the onset of a deglacial period (Shakun and Carlson, 2010; Shakun *et al.*, 2012; Shao *et al.*, 2019). Indeed, changes in atmospheric CO_2 are required to account for the globalisation of climate signals and have been estimated to contribute between a third to two-thirds of global cooling events, along with orbital and insolation variations, and more regional influences of ice albedo and ice sheet extent (Shakun *et al.*, 2012). The main CO_2 reservoirs include: i) the atmosphere; ii) the terrestrial biosphere and biomass uptake; iii) the oceans. Within the oceans, variations in CO_2 occur through CO_2 exchange between the atmosphere and surface waters; CO_2 chemistry within surface waters, driven by deep sea ventilation; pH, salinity, temperature and productivity changes; absorption of carbon by marine biota and sequestering of dissolved inorganic carbon to the deep ocean (Broecker, 1981; Marcott *et al.*, 2014).

Antarctica ice cores are generally used to analyse trends in greenhouse gasses over the past 800 kyr, as they have less impurities than Greenland cores and provide a more reliable continuous record, though generally at a lower resolution and precision than Greenland ice cores (Jouzel, 2013; Marcott *et al.*, 2014). Data from the well-constrained West Antarctic Ice Sheet Divide ice core (WDC) have been used as a good analogue to data from Greenland and provide sub-centennial records of global CO_2 levels (Marcott *et al.*, 2014). Between the LGM and mid-Holocene, there was an increase in global CO_2 (~80ppm), with three proposed shorter-term modes in CO_2 variations: i) there was a gradual increase in CO_2 during HS1 and the YD (~10ppm/kry^{-1}); ii) three rapid increases in CO_2 occur within HS1 and at the start of both the BA and Holocene (10 to 15ppm in 100 to 200 years); iii) there are 1 to i kyr stable periods during the latter part of HS1, BA and early Holocene, where there were no significant changes in global CO_2 (Figure 4.7) (Shakun *et al.*, 2012; Marcott *et al.*, 2014). These modes of CO_2 variation

have been linked to changes to deep water ventilation and temperature variations recorded between the northern and southern hemispheres (Shakun *et al.*, 2012).
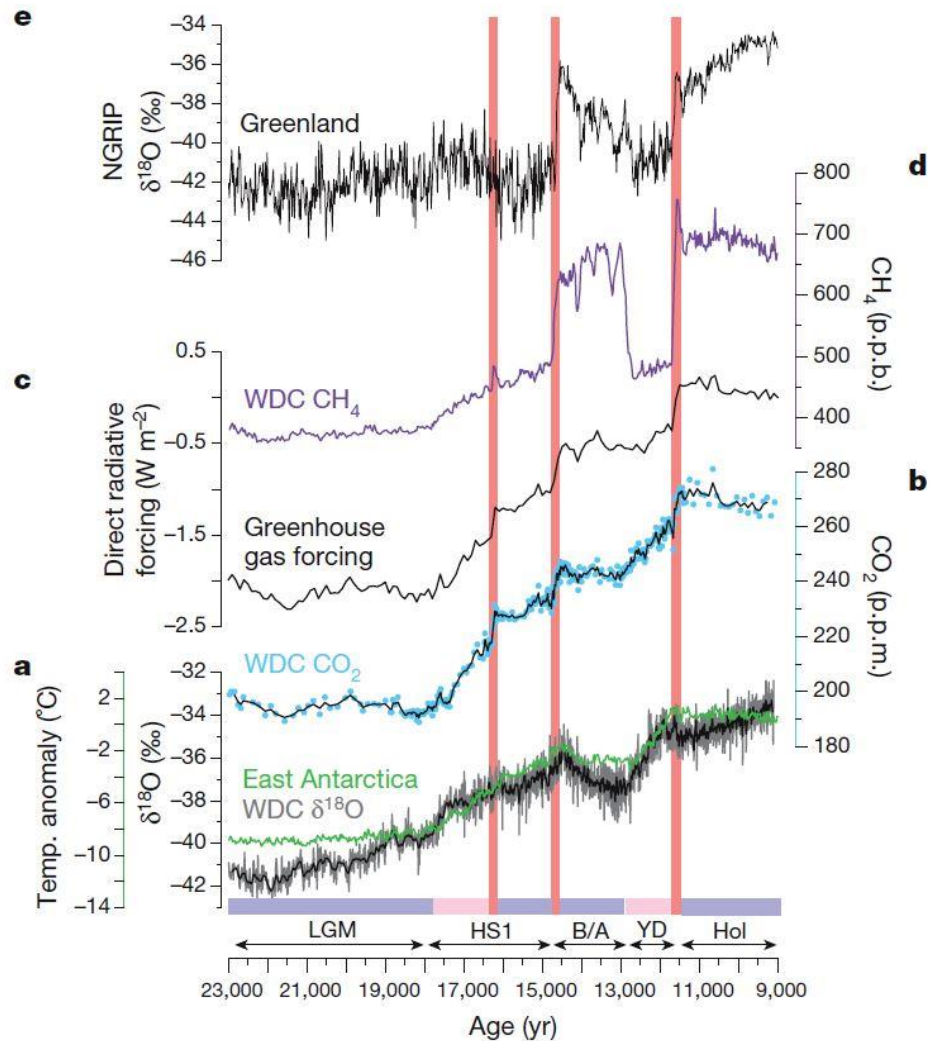
Figure 4.7: Greenhouse gasses and $\delta^{18}O$ values from Greenland and Antarctica. a) $\delta^{18}O$ from West Antarctic Ice Sheet Divide ice core (WDC) (grey/black) and water $\delta^{18}O$ temperature composite from East Antarctica (green). b) Atmospheric CO_2 concentrations. c) Direct radiative forcing of CO_2, CH_4 and N_2O. d) Atmospheric CH_4 concentrations. e) NGRIP $\delta^{18}O$. Coloured bands at bottom indicate times when CO_2 is stable (blue), slowly increasing (pink) or rapidly increasing (red). Taken from Marcott et al. (2014).

During the LGM, DWF in the North Atlantic is assumed to have shoaled and reduced, and Antarctic and northern Pacific waters become strongly stratified, allowing enhanced carbon sequestering in the deep oceans (Sigman *et al.*, 2007; Shao *et al.*, 2019). During the initial deglacial stages (HS1), the slow increase in CO_2 coincided with variations in the "bipolar seesaw", where a cooling of the North Atlantic and an injection of iceberg armadas into the North Atlantic triggered a reduction in the strength of the AMOC, inhibiting latitudinal transfer of heat between the hemispheres (Shakun *et al.*, 2012; Marcott *et al.*, 2014). This had the effect of warming the southern hemisphere, increasing Antarctic wind-driven overturning and buoyancy, allowing sequestered CO_2

to be released to the atmosphere, thus enhancing postglacial global warming (Sigman *et al.*, 2007; Shakun *et al.*, 2012; Marcott *et al.*, 2014). The associated jumps in CO_2 observed at the start of the BA and Holocene are correlated to the resumption of the AMOC, and changes to terrestrial carbon storage during these warm periods (Marcott *et al.*, 2014). The longer plateaux in CO_2 observed during the latter HS1, BA and early Holocene are associated with a strong AMOC, enhanced latitudinal heat exchange and cooling in the Antarctic, possibly causing a stratification and reduction of degassing of the Southern Oceans (Marcott *et al.*, 2014).

Analysis of Greenland $\delta^{13}C$ ice core records show that both N_2O and CH_4 levels peaked at the beginning of interglacial warming events (i.e. an increase of 50%), then slowly fell during the subsequent slow decline into the glacial period, as well as fluctuating within millennium timescales (Flückiger *et al.*, 2004; Alley, 2007; Wolff *et al.*, 2010). Both gasses have a wide range of sources, such as wetlands or peat for CH_4, and soil and productive regions in oceans for N_2O, thus how and the magnitude of their influence on short-term climate change is different (Flückiger *et al.*, 2004; Schilt *et al.*, 2013; McCarroll, 2015).

CH_4 is both responsive to changes in its source and only requires small quantities to be added to the atmosphere for it to act as a powerful climate forcer (Nisbet, 2002). The main pre-anthropogenic source of CH_4 were wetlands, particularly in tropical to boreal regions (Matthews, 2000; Flückiger *et al.*, 2004). CH_4 emissions are strongly impacted by the extent and productivity of these wetlands, with a positive correlation with increasing rates of precipitation and temperature (Matthews, 2000). Other factors that influence CH_4 variability include orbital variations, such as precession and degree of summer insolation; and input from methane hydrate sources, such as seasonal thawing of permafrost regions and organic rich deep sea sediments, following changes to sea level, SST or pressure in the waters above (Nisbet, 2002; Flückiger *et al.*, 2004; Huber *et al.*, 2006; Ruddiman, 2006). Within the past 65 kyr, variations in CH_4 concentrations are seen to be in close correlation with the temperature changes observed at the beginning of DO Events (DO 9 to 17), though with a 25 to 75 ± 25 year lag, as well as observed over millennial/sub-millennial timescales (Huber *et al.*, 2006). Records of CH_4 from the WDC during the Late Pleistocene show a gradual increase in CH_4 after the LGM up to the beginning of the BA, where there was a rapid increase until the YD, when it decreased, followed by a rapid increase again at the beginning of the Holocene (Figure 4.7) (Marcott *et al.*, 2014).

The dominant N_2O source during the Late Pleistocene was terrestrial soils mainly in the tropics and to a lesser extent in temperate regions (Flückiger *et al.*, 2004). Emissions of terrestrial N_2O were governed mainly by rates of precipitation and temperature. In the oceans, N_2O can be sourced from changes in the rates of denitrification in upwelling areas and nitrification of the open ocean influenced by periods of stratification (Flückiger *et al.*, 2004). Since the LGM, rates of N_2O were seen to decrease during HS1 and the YD, which has been attributed to a reduction in the AMOC; while levels began to rise several centuries prior to the beginning of the DO, due to an intensification of terrestrial emissions caused by higher rates of precipitation and temperature, and increased denitrification due to enhanced upwelling at the beginning of a DO event (Flückiger *et al.*, 2004; Schilt *et al.*, 2013).

4.2.1.3   *Solar output variations*

Several mechanisms for the variation in insolation and the quality of solar energy have been observed and attributed as drivers for short-term changes to global climate over decadal to centennial timescales, e.g. in modern times a 0.1% variation in insolation has been observed over a 11 year cycle (Jansen *et al.*, 2007). Mechanisms for insolation variations include sunspots (i.e. dark patches in the photosphere, leading to a decline in solar output) and solar flares (i.e. brief violent eruptions of solar energy). The 11 year periodicity in the number of sunspots and irradiance have been associated with, e.g. temperature records in north-west Europe; and variations in solar flares can cause changes in atmospheric circulation, precipitation, storminess and SSTs (Bell and Walker, 2005). Over longer timeframes, changes in solar output can be correlated with fluctuations of the ^{14}C and ^{10}Be isotopes in the atmosphere, which are modulated by ionised gasses ejected from the sun's surface (i.e. solar winds) (Stuiver and Braziunas, 1993; van Geel *et al.*, 2003). Solar periodicities of 88, ~200 and ~2500 years have been identified from a range of palaeo proxies, such as terrestrial, deep sea and ice cores and have been suggested as potential trigger mechanisms for the rapid climate events in the Late Pleistocene (Bond *et al.*, 2001; van Geel *et al.*, 2003; Mayewski *et al.*, 2004). During warm periods, atmospheric $\Delta^{14}C$ values decrease and increase during cold periods such as GS-1/"Younger Dryas", GI-1d "Older Dryas" or the 8.2ka event, and these variations have been associated (in part) to changes in solar activity (van Geel *et al.*, 2003; Mayewski *et al.*, 2004; Wiersma and Renssen, 2006).

The mechanisms that enable variations in ^{14}C include UV radiation and cosmic ray flux.

An increase (decrease) in UV radiation increases (decreases) the production of ozone in the stratosphere, thus warming (cooling) the stratosphere (Haigh, 1994). This has the effect of varying upper atmospheric winds, leading to latitudinal changes to the descending arm of Hadley Cells and location of mid-latitude storm tracks (Haigh, 1996; van Geel *et al.*, 2003). In addition, variations in cosmic ray flux influence cloud cover (i.e. aerosol formation and cloud nucleation are positively affected by ionisation by cosmic rays), which can increase albedo and impact rates of precipitation, which is thought to have occurred in the early Holocene cool period (van Geel *et al.*, 2003).

4.2.1.4 *Volcanism and volcanic aerosols*

Following the LGM, the retreat and wastage of the large Northern Hemisphere ice sheets resulted in significant isostatic rebound and crustal fracturing (Kutterolf *et al.*, 2013; Praetorius *et al.*, 2016). Rates of volcanic activity at ~12,000 yr BP in areas such as Iceland, were ~100 times that of the preceding glacial or subsequent Holocene period, with global rates estimated to be between two and six times above that of background levels during the last deglaciation (Maclennan *et al.*, 2002; Huybers and Langmuir, 2009; Brown *et al.*, 2014). This heightened period of volcanism led to an increase of volcanic ash, dust and gasses such as sulphur dioxide (SO_2) and hydrogen sulphide (H_2S) being ejected into the atmosphere (Maclennan *et al.*, 2002; Timmreck, 2012). In regions such as Iceland, eruptions primarily occurred beneath the ice, thus were much more explosive and allowed for greater distribution of the dark mafic ash across the Fennoscandian ice sheet, leading to an ash-induced decrease in albedo and enhanced melting (Muschitiello *et al.*, 2017).

In contrast, oxidisation of volcanic gasses SO_2 and H_2S in the stratosphere form sulphuric acid (H_2SO_4) and sulphuric aerosols, which increase both albedo and the diffusion of solar radiation in the troposphere, with a potential global cooling of 0.2 to 0.3°C in the years following an eruption (Bell and Walker, 2005; Timmreck, 2012). Halogen-rich volcanic eruptions in the Western Antarctic (~17.7 kyr BP) have been proposed as a mechanism that may have triggered the rapid deglacial in the southern hemisphere, as halogen aerosols ejected into the stratosphere can deplete ozone and increase UV radiation reaching the earth's surface (McConnell *et al.*, 2017).

Impacts of volcanism have also been noted on global oceanography, circulation and precipitation rates (Iles *et al.*, 2015). Following major periods of tropical volcanism, models suggest that the AMOC in the North Atlantic can intensify and delay continental

winter warming of the Northern Hemisphere ~10 years after the eruptions, as is suggested for the onset of the Little Ice Age in the late 13th century (Timmreck, 2012).

4.3 Mechanisms of Late Pleistocene short-term climate change

Generalised patterns of Late Pleistocene short-term climatic oscillations can be identified in ice cores, deep-sea sediment cores and in a range of terrestrial proxies across the northern hemisphere. This next section will introduce the main short-term events that occurred since the LGM in the North Atlantic region, discuss the main triggers and drivers of these events, and detail how these events impacted the Mediterranean region.

4.3.1 Heinrich Stadial 1

In North Atlantic marine sediments, Heinrich Events (HE) can be identified as short intense cold pulses, characterised by layers of ice-rafted debris (IRD) found in deep sea marine sediment cores (Heinrich, 1988; Bond *et al.*, 1992; Alley and MacAyeal, 1994; Alley and Clark, 1999). This IRD is comprised of a heterogeneous lithic sediment with grain sizes that range from fine silts and clay (<63 µm) up to occasional rock fragments (>3000 µm) (Heinrich, 1988; Andrews, 2000; Hodell *et al.*, 2017). This sediment was entrained by ice originating primarily from the North American Laurentide ice sheet, but also from the Greenland, Fennoscandian and British-Irish ice sheets. The sediments were redeposited as detrital carbonate rich sediments by melting sea ice and glacial meltwater in areas more proximal to the ice sheets, with more distal IRD layers deposited by floating icebergs (Heinrich, 1988; Bond *et al.*, 1992; Andrews, 2000; Hodell *et al.*, 2017). Seven HE (HE6 to HE1, although some researchers assign HE0 to the Younger Dryas) have been identified in the North Atlantic over the past 65 kyr (Andrews and Voelker, 2018).

Before proceeding however, the terminology surrounding this period requires clarification. For this study, the term Heinrich Event (HE) represent the climatic event that triggered the release of the iceberg armadas and the subsequent deposition of IRD in the North Atlantic, and HE can be variable in duration. The term Heinrich Stadial (HS) has been utilised to describe the longer chronostratigraphic interval that contains the actual Heinrich Event (or multiple Heinrich Events), as well as encompassing the associated cold period (which may be longer than the HE), decreased SST and glacial advances (Sanchez Goñi and Harrison, 2010; Hodell *et al.*, 2017). However, Andrews

and Voelker (2018) recently recommend that the use of the term "stadial" for this chronozone should be discontinued to prevent confusion with its usage for a period of glacial advance. They recommended replacing the use of HS with the Greenland stadial (GS) and Interstadial (GI) nomenclature, i.e. Heinrich Stadial 1 (HS1) would equate to GS-2.1a (Rasmussen *et al.*, 2014). However, in regions that are more distal from Greenland such as the Mediterranean Sea, one cannot assume synchronicity in the timing of these events over such distances. Therefore, in terms of this research HS1 is used to describe the period between the LGM and the onset of the BA, i.e. the "mystery interval" of Denton *et al.* (2006) (~17.5 to 14.7 kyr BP).

Following the LGM, with an increase in summer insolation and heightened SST, the northern hemisphere ice sheets began to recede (Figure 4.8) (Denton *et al.*, 2010). Melting of European ice sheets from the English channel into the north-eastern Atlantic began around 20 kyr, peaking between 18.3 to 7 kyr BP (Denton *et al.*, 2010; Hodell *et al.*, 2017; Ivanovic *et al.*, 2018). This influx of large volumes of freshwater and rising sea levels from accelerated melting of the Eurasian ice sheet is linked to the beginning of HS1, and potentially was a trigger for AMOC weakening and the HE (Hodell *et al.*, 2017).
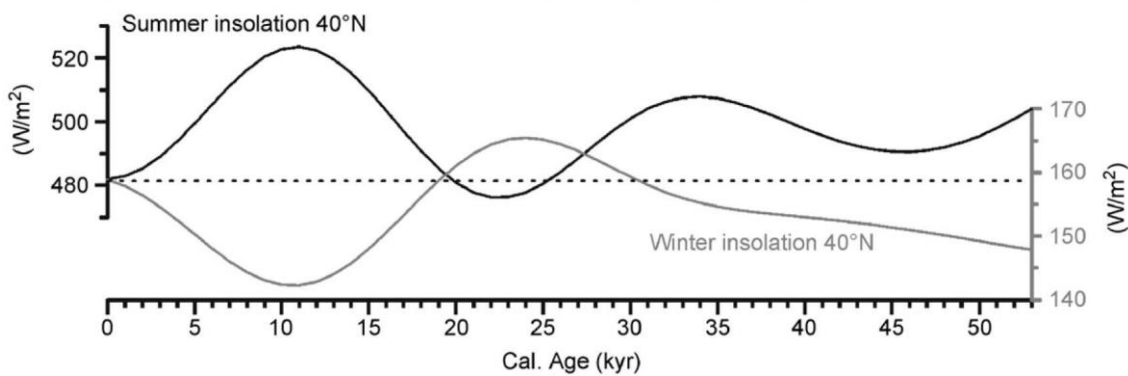
Figure 4.8: Summer and winter insolation curves at 40°N for the last 50 kyr. Taken from Frigola et al. (2008).

Evidence from global proxies for HS1 reflect the complexity of this period. Numerous studies in the northern hemisphere record cold conditions in the north-western Atlantic; a weakening/shutdown of NADW and AMOC; expansion of sea ice; enhanced seasonality (i.e. greater summer insolation with extremely cold winters (Figure 4.8)) and recession of global mountain glaciers from ~17.5 kyr BP; the ITCZ was displaced to the south; the Asian monsoon weakened, which is in contrast with an increase in both CO_2 and CH_4, and warmer conditions in Antarctic (Monnin *et al.*, 2001; McManus *et al.*, 2004; Denton *et al.*, 2006; Barker *et al.*, 2009; Denton *et al.*, 2010; Hodell *et al.*,

2017). In distal cores taken in the North Atlantic as far south as subtropical waters off the Iberian margin, two HE have been identified (HE1a: ~16.2 kyr BP and HE1b ~15.1 kyr BP) and are associated with the southern displacement of the oceanic polar front (as far south as ~40°N) leading to a pronounced cooling phase, and a decrease in both SST and salinity (Bard *et al.*, 2000; Eynaud *et al.*, 2009; Denton *et al.*, 2010; Martins *et al.*, 2015; Hodell *et al.*, 2017).

The exact mechanism(s) for triggering HE is still unclear. MacAyeal (1993) proposed the "binge-purge model" caused by the internal mechanical failure of the large Laurentide ice sheet. This theory suggests that geothermal and heat generated from friction at the base of the ice sheet thawed the basal sediments grounding the ice sheet, leading to the rapid surge towards the ice margins, releasing catastrophic floods of cold meltwater and huge armadas of icebergs into the North Atlantic. In contrast, Denton *et al.* (1999) believe global cooling a result of external climate forcing in the millennia prior to the HE resulted in increased precipitation, ice sheet growth and ablation of icebergs from expanding sea ice. Rodgers *et al.* (2003) proposed that SST warming in the tropics, as a result of increasing insolation or CO_2 greenhouse gasses prior to HE, allowed warm, moist air from the Pacific Ocean to be advected over continental North America, leading to enhanced summer melting of the Laurentide ice sheets (Lohmann, 2016; Zhang *et al.*, 2017; Oughton and Urrego, 2021). Other theories include: deglacial increases in sea levels that destabilised the margins of sea ice shelves triggering the HE; the "bipolar" seesaw, where changes in hemisphere heat transfer triggered increases in meltwater discharge, impacting on sea levels, AMOC strength and NADW formation; synchronicity of HE events with ^{14}C and [10]Be records infer that variations in solar output may influence the SST and salinity of Arctic waters, thus impacting on NADW formation; or ice-sheet collapse linked to basin-wide subsurface warming in the North Atlantic (~2°C) due to the slowdown of AMOC 1 to 2 kyr prior to the HE events (Alley and MacAyeal, 1994; Hemming, 2004; Maslin, 2009; Marcott *et al.*, 2011; Bassis *et al.*, 2017). Regardless of the internal or external triggering mechanism(s), the release of ice and cold meltwaters from the disintegrating ice shelves was equivalent to an increase of ~4 m/kyr global mean sea level rise, and caused a freshening and increase in the buoyancy of North Atlantic waters, inhibiting NADW formation and weakening or shutdown of the AMOC (McManus *et al.*, 2004; Ivanovic *et al.*, 2018).

4.3.2   Bølling-Allerød

Initially identified by Dansgaard *et al.* (1993), 25 Dansgaard-Oeschger (DO) events - including the Bølling-Allerød (BA) - have been identified from $\delta^{18}O$ records in the GRIP and GISP2 Greenland ice cores during the last interglacial (~120 kyr) (GI-25 to GI-1) (Dansgaard *et al.*, 1984; Oeschger *et al.*, 1984; Dansgaard *et al.*, 1985; Johnsen *et al.*, 1992; Dansgaard *et al.*, 1993; Grootes *et al.*, 1993; Maslin, 2009; Wolff *et al.*, 2010; McCarroll, 2015). DO events are defined as significant millennial-scale shifts from stadial to interstadial periods, with temperature changes in the order of 8 to 16°C that initiated very rapidly (within decadal timescales) and are followed by a more gradual return to stadial conditions (Bond *et al.*, 1999; Li and Born, 2019). Data from Greenland ice cores indicate that the estimated annual accumulation rates of snow doubled from 5.5cm/yr during the stadial to 10.1cm/yr during interstadial periods (e.g. GI-10 to GI-3), CH_4 and N_2O values increased, and sea salt and dust levels decreased (Monnin *et al.*, 2001; Andersen *et al.*, 2006; Li and Born, 2019). DO events have an average periodicity of ~1500 yr, though the duration and the magnitude of warming/cooling varies, e.g. GI-3 lasted only 300 years in contrast to GI-23 which lasted 2,500 years (Wolff *et al.*, 2010). Most have the characteristic asymmetrical sawtooth pattern of rapid warming followed by gradual cooling, with some DO events followed by a HE (Wolff *et al.*, 2010; Li and Born, 2019). Bond *et al.* (1993) suggested that certain DO events could be grouped together into cycles with increasingly cooler interstadials, followed by a terminal HE, e.g. GI-12 to GI-9 were followed by HE4, and GI-8 to GI-5 were followed by HE3. However, as this does not always occur, e.g. from 23 to 15 kyr BP, the sequence was GI-2, LGM, then HE1, this cannot be regarded as a general characteristic of DO events.

Evidence of DO events can be most clearly identified in Greenland ice cores, though deep sea sediment cores in the surrounding Arctic seas and the North Atlantic also display the DO signals (Broecker *et al.*, 1985; Bond *et al.*, 1993; Dansgaard *et al.*, 1993; Alley and Clark, 1999; Voelker, 2002; Alley, 2007). The mechanisms for triggering DO events and the subsequent return to stadial conditions has not yet been fully resolved due to the short duration of some DO events and the resolution of the proxy data (Lynch-Stieglitz, 2017). The dominant mechanism is believed to be linked to fresh meltwater input or salinity variations that increased deep water ventilation, strengthened the AMOC and meridional heat transport from the equator towards Arctic waters, thus warming the northern hemisphere (Broecker *et al.*, 1985; Lynch-Stieglitz, 2017; Li and

Born, 2019). The influx of meltwater is believed to have been triggered by an increased in summer 65°N insolation, sea levels and greenhouse gasses, which led to the BA warming (Maslin, 2009). However, more recent models propose a "spontaneous" or unforced oscillation of combined atmosphere-ice-ocean system, i.e. positive feedbacks from variations in atmospheric wind patterns, the location and strength of the Atlantic subpolar gyre, sea ice extent, ocean mixing and heat exchange in northern hemisphere seas (Li and Born, 2019). Other factors include the displacement of the ITCZ to the north, enhanced evaporation and precipitation in the northern hemisphere, strengthening Asian and African monsoons and increased CH_4 emissions from tropical wetlands (Wang *et al.*, 2001; Erhardt *et al.*, 2019).

The BA (~14.7 to 12.8 kyr BP) is the most recent DO event (DO-1) following HS1. It broadly equates to warmer GI-1 defined from Greenland ice cores, though the BA chronozone is not synonymous with GI-1 (Rasmussen *et al.*, 2014). In the northern hemisphere, the BA has the characteristic initial rapid DO warming, followed by a slow oscillating cooling towards the Younger Dryas. However, this warming was not a global event. In the southern hemisphere there was a return to stadial conditions, known as the Antarctic Cold Reversal (14.5 to 12.9 kyr) (Broecker *et al.*, 2010; Fiedel, 2011). The BA chronozone has been subdivided into the Bølling warm period, "Older Dryas" (OD) cold period (~14.4-14 kyr) and the Allerød warm period, which is briefly interrupted by the "Intra-Allerød Cold Period" (IACP) (Menviel *et al.*, 2011). However, the OD and IACP are terms not used by INTIMATE event ice core stratigraphy, as these short chronozones cannot be accurately correlated to specific cold events evident in Greenland cores (Rasmussen *et al.*, 2014; Head and Gibbard, 2015). Brief intra-interstadial cold periods are recorded during the gradual $\delta^{18}O$ decline during GI-1, and are subdivided as GI-1e to GI-1a (with a further subdivision of GI-1c: GI-1c3 to GI-1c1) (Figure 4.4) (Rasmussen *et al.*, 2014). These interruptions are said to represent amplified cooling from brief meltwater pulses from the Laurentide ice sheet (Menviel *et al.*, 2011; Deschamps *et al.*, 2012).

During the early BA, the southern limit of winter ice and position of the oceanic polar front receded to near Iceland, the Azores Front moved northwards to its modern position, and there was an estimated ~15°C atmospheric warming over Greenland during the initial Bølling warming (Bell and Walker, 2005; Liu *et al.*, 2009; Repschläger *et al.*, 2015; Cowling *et al.*, 2020). The rapid recovery of the AMOC after HS1 and increasing CO_2 are the proposed triggers for the BA event (Monnin *et al.*,

2001; Liu *et al.*, 2009; Menviel *et al.*, 2011). It is estimated that CO_2 increased by 20 to 35 ppmv in less than 200 years, and it was proposed that ~10°C of the BA warming was as a result of CO_2 induced warming (Liu *et al.*, 2009; Köhler *et al.*, 2011; Marcott *et al.*, 2014). Other greenhouse gasses also increased, with sources of enhanced CH_4 attributed to the tropics and boreal regions, with N_2O originating from more productive or expanded wetlands (Monnin *et al.*, 2001; Alley, 2007). From the initial peak in AMOC strength in the Bølling, the AMOC gradually slowed as it progressed through the Allerød period, interspersed with brief periods of enhanced ice sheet melting that further weakening the AMOC, e.g. the OD and IACP chronozones (Menviel *et al.*, 2011; Yasuhara *et al.*, 2019). A key feature of the early BA is a short but substantial meltwater pulse known as Meltwater Pulse 1A (MWP-1A), which had a significant impact on global sea levels, e.g. ~14 to 18m in the Pacific and ~20m in the North Atlantic (Fairbanks, 1989; Peltier and Fairbanks, 2006; Deschamps *et al.*, 2012). However, its chronology and role during the BA is debated (Stanford *et al.*, 2006; Stanford *et al.*, 2011a; Rigual-Hernández *et al.*, 2017). Earlier studies correlated the MWP-1A to the OD chronozone (Peltier and Fairbanks, 2006; Stanford *et al.*, 2006; Thornalley *et al.*, 2010; Menviel *et al.*, 2011). However, Stanford *et al.* (2011a) reanalysed multi-proxy global datasets and suggested MWP-1A was part of a multi-centennial to millennial event that began 14.6 kyr BP and peaked ~13.8 kyr BP. In the Pacific, Deschamps *et al.* (2012) dated MWP-1A in Tahitian coral reefs to 14.65 to 14.31 kyr, coinciding with the onset of the Bølling. In addition, the origin of these MWP-1A meltwaters is also under debate, with potential sources attributed to the Laurentide, Fennoscandian and/or Antarctic ice sheets (Peltier and Fairbanks, 2006; Deschamps *et al.*, 2012; Rigual-Hernández *et al.*, 2017; Yeung *et al.*, 2019). Another important feature of the BA was that the ITCZ was relocated to the north, which increased precipitation in the mid latitudes of the northern hemisphere (Menviel *et al.*, 2011). Snow accumulation rates increased from 6.2 cm/yr to 12.6cm/yr in Greenland between GS-2 and GI-1, which was greater than recorded for the preceding stadial/interstadial cycles (Andersen *et al.*, 2006; Menviel *et al.*, 2011).

4.3.3 Younger Dryas

The final Late Pleistocene cold period (GS-1) recorded in Greenland ice cores has been dated to 12.9 to 11.7 kyr b2k (Rasmussen *et al.*, 2014). The Younger Dryas (YD) chronozone has been widely documented in the North Atlantic and north-west Europe and broadly equates to GS-1, but it is not a synonym for this interstadial event (Bell and

Walker, 2005; Rasmussen *et al.*, 2014). The YD is so named due to the proliferation of the arctic flower *Dryas octopetala* that accompanied a return to tundra vegetation in north-west Europe and open steppe to the south (Carlson, 2013; McCarroll, 2015). The YD chronozone has also been called H0, due to its similarities to Heinrich Events (Andrews *et al.*, 1995). Paradoxically, the YD cold dry period occurred when the deglacial northern hemisphere was warming as it approached the summer insolation maxima (Figure 4.8) (Carlson, 2013). There was a rapid return to cooler waters in the North Atlantic, an expansion of sea-ice, re-location of the polar front south to the north-western Iberian Peninsula, a re-advance of alpine glaciers and air temperatures fell by ~8°C along coastal north-west Europe (Ruddiman and McIntyre, 1981; Bell and Walker, 2005; Ivy-Ochs *et al.*, 2007). Mean annual air temperatures recorded in Greenland ice cores cooled by ~16°C during GS-1, with seasonal variations of 4 to 6°C cooler during the summer and extremes of 26 to 28°C cooler during winter, temperatures comparable to HS1 cooling (Severinghaus *et al.*, 1998; Denton *et al.*, 2005; Liu *et al.*, 2012). Indeed, enhanced seasonality is a noted feature of the northern hemisphere during the YD (Denton *et al.*, 2005; Lie and Paasche, 2006). Precipitation values decreased by ~40%, with an associated increase in dust and winds (Alley, 2000). Atmospheric CO_2 rose from ~240ppm to ~260ppm and has been linked to the slowdown of the AMOC (Monnin *et al.*, 2001; Marcott *et al.*, 2014). CH_4 rates decoupled from CO_2 and began to decrease by 200ppb ~200 years before the start of the YD (Marcott *et al.*, 2014).

Global sea levels were ~60m below modern values, though rates of sea level rise fell from 20mm/yr^{-1} during the mid-Allerød, to just 7 to 4 mm/yr^{-1} during the YD, and has been attributed to the re-advance of the Fennoscandian ice sheet (Fairbanks, 1989; Bard *et al.*, 2010; Lambeck *et al.*, 2014; Abdul *et al.*, 2016). Sediment cores and speleothems from the tropics and China record the southern displacement of the ITCZ and weakening of the Indo-Asian monsoon (Chiang *et al.*, 2003; Carlson, 2010; Renssen *et al.*, 2018).

The global mean cooling was estimated to be ~0.6°C, approximately ~10% of the global cooling during the LGM (Rahmstorf, 2002; Shakun and Carlson, 2010). As seen during HS1 and BA, the temperature regimes varied between and within the hemispheres, with an average cooling of ~2°C in the mid latitudes and ~5°C cooling in the high latitudes of the northern hemisphere, in comparison to an average warming of 1 to 2°C below ~45°S (Shakun and Carlson, 2010). Both the magnitude of cooling in the northern

hemisphere and the global 0.6°C cooling suggest that an AMOC slowdown, which coincided with the termination of the Antarctic Cold Reversal, was the trigger for the YD event, rather than global atmospheric forcing (Shakun and Carlson, 2010). To allow for the extremes in summer/winter temperatures recorded in Greenland, sea ice filled the Norwegian Sea and extended as far south as ~40°N along the eastern seaboard of North America and ~50°N along the west coast of Europe (Broecker, 2006; Brauer *et al.*, 2008; Abdul *et al.*, 2016; Muschitiello *et al.*, 2019). Sea ice formed due to the fresh cold surface waters, inhibiting the release of oceanic heat and increased albedo (Brauer *et al.*, 2008; Broecker *et al.*, 2010; Abdul *et al.*, 2016; Rea *et al.*, 2020). In addition, patterns of northern hemisphere YD atmospheric circulation were strongly influenced by ice sheet topography (in particular the Laurentide ice sheet) and persistent atmospheric blocking over the north-eastern Atlantic and Fennoscandian ice sheet (Raible *et al.*, 2015; Schenk *et al.*, 2018). The polar front jet was displaced to the south, directing cold Westerly winds and storm tracks towards continental Europe in winter, increasing cyclogenesis and precipitation, in particular towards the eastern Mediterranean Sea (Rea *et al.*, 2020). These blocking regimes and the expanse of winter sea ice led to extreme cold, dry conditions during the winter. There is recent evidence from palaeobotanical studies that warm summer temperatures were experienced in both north and south-eastern Europe during the YD (Schenk *et al.*, 2018; Magyari *et al.*, 2019; Schenk *et al.*, 2020). While it is clear winter cooling was greater than summer (modelled July air temperature anomalies range from -1 in southern Europe to -4 towards the Scandinavia), these proposed warm YD summer conditions are debated (Renssen *et al.*, 2015; Renssen, 2020).

Terrestrial records in north-west Europe have recorded two distinct phases in the YD, an initial cold stable phase, followed by a more unstable phase with spring snow melts, the resumption of the AMOC and the gradual improvement of the climate towards the warmer Holocene (Lane *et al.*, 2013). The timing of these phases are not synchronous in terrestrial proxies across north-west Europe when plotted against the Icelandic Vedde Ash layer (a well-known stratigraphic marker ~12.1 kyr), and the regional representations of the YD phases have been linked to the position of the polar front jet stream (and cold Westerly winds), which gradually made a slow oscillating retreat north from ~12.3 kyr (Bakke *et al.*, 2009; Lane *et al.*, 2013; Muschitiello *et al.*, 2019; Cowling *et al.*, 2020).

Although the YD period is well documented and studied, the trigger for the slowdown

of the AMOC is still debated (Carlson, 2010). Several theories have been developed to account for this rapid return to glacial conditions in the high latitudes of the northern hemisphere, despite rising CO_2 and increasing summer insolation. The most prominent proposed mechanism was a catastrophic input of meltwater, IRD and detrital carbonate rich sediments originating from the proglacial Lake Agassiz, which were redirected from the Gulf of Mexico into the eastern North Atlantic via the St. Lawrence estuary (Broecker *et al.*, 1989; Broecker, 2006; Carlson, 2013; Pearce *et al.*, 2015). This input of cold fresh meltwater would have decreased surface water densities in the North Atlantic, slowing or even briefly shutting down the AMOC and impacting NADW formation (Broecker *et al.*, 1989; Alley and Clark, 1999; McManus *et al.*, 2004; Broecker, 2006; Carlson, 2013). However, there are still some significant unanswered questions relating to this catastrophic flooding hypothesis. For example, a gradual cooling trend is evident in some proxies at the start of the YD, which would be unlikely during a catastrophic flood event; also the location of an eastern meltwater channel from Lake Agassiz to the St. Lawrence River or an alternative northern route to the Arctic Sea has yet to be identified (Broecker *et al.*, 2010; Carlson, 2013).

Firestone *et al.* (2007) proposed an alternative catastrophic trigger, i.e. the Younger Dryas Boundary Impact Hypothesis. This theory suggests that an extra-terrestrial object hit or exploded just above the Laurentide ice sheet ~12.9 kyr, triggering the onset of YD cooling. This impact/airburst was said to have generated enough heat to destabilise the ice sheet, releasing meltwaters into the eastern North Atlantic and initiating continental-scale wildfires, Late Pleistocene megafauna extinctions and a decline of the North American Clovis culture. This hypothesis is still actively debated, with new supporting research, e.g. a recently discovered impact crater in north-western Greenland suggested as a potential impact site; while much of the original evidence, chronology and assertions have been re-evaluated and discounted, and cast doubt on the impact hypothesis as a trigger for the YD (Pinter *et al.*, 2011; Holliday *et al.*, 2014; van Hoesel *et al.*, 2014; Kjær *et al.*, 2018; Thackeray *et al.*, 2019).

More recently, there is evidence of enhanced meltwater released from the Fennoscandian ice sheet and Baltic Ice Lake in southern Sweden in the late Allerød chronozone (Björck, 2007; Muschitiello *et al.*, 2015; Muschitiello and Wohlfarth, 2015; Muschitiello *et al.*, 2016). This incursion of meltwater from the eastern North Atlantic may have led to the gradual changes observed for deep-water ventilation and NADW formation in the Nordic Sea ~400 years before the pCO^2 cooling signal was recorded in

Greenland (Muschitiello *et al.*, 2015; Muschitiello *et al.*, 2019). This slowdown potentially acted as a precursor to the later rapid YD climate change, i.e. sea ice distribution, increasing wind intensities and shifting of the jet stream south, which redirected wind and moisture from the Arctic (cooling them as they flowed over sea ice) into north-west Europe (Brauer *et al.*, 2008; Rach *et al.*, 2014; Muschitiello *et al.*, 2015; Abdul *et al.*, 2016; Muschitiello *et al.*, 2019).

4.4 Late Pleistocene short-term climate change in the Mediterranean Sea: signals and drivers

4.4.1 Heinrich Stadial 1 in the Mediterranean region

In modern oceans, *N. pachyderma* forms ~100% of the population in Arctic waters (Darling *et al.*, 2006; Kretschmer *et al.*, 2016). During HE1, the total abundance of planktonic foraminifera reduce significantly in the North Atlantic and the population was dominated almost exclusively by *N. pachyderma* (Heinrich, 1988; Hodell *et al.*, 2017). Therefore, heightened percentages of *N. pachyderma* have been used to track changes in the location in the polar front in the North Atlantic during the glacial/deglacial period (McIntyre *et al.*, 1972; Ruddiman *et al.*, 1977; Bard *et al.*, 1987; Bond *et al.*, 1992). During HS1, *N. pachyderma* recorded off the Iberian margin (ranging from >90% to the north and >10% in the Gulf of Cádiz) indicate the relatively stable southerly position of the polar front (~40°N) during this chronozone (Figure 4.9) (Cayre *et al.*, 1999; Eynaud *et al.*, 2009; Martins *et al.*, 2015). The presence of these cold waters and periodic IRD deposits during HS1 had significant impacts on both the hydrology and atmospheric circulation patterns of the western Mediterranean Sea.

Naughton *et al.* (2016) identified a complex 3-phase signal to HS1 along the western margin of the Iberian Peninsula, where SSTs, air temperatures and precipitation varied with changes in both the polar front jet stream and oceanic polar front. The initial phase is characterised by minimal IRD deposits (HE1a), a significant decrease in both SST and air temperatures (10 to 16°C and ~6°C respectively), an increase in Westerlies, precipitation and fluvial discharge, and *Pinus* and temperate forests in the Iberian Peninsula began to recede (Naughton *et al.*, 2009; Martins *et al.*, 2015; Naughton *et al.*, 2016). The suggested cause of this cold-wet phase was that the southern displacement of the North Atlantic subtropical gyre, and the polar jet stream was located as far south as the Gulf of Cádiz (Naughton *et al.*, 2009; Repschläger *et al.*, 2015; Naughton *et al.*,

2016). The middle phase had a slight warming of SST, though the waters were still cold enough for *N. pachyderma*, but there was little IRD deposited. The terrestrial environment became slightly warmer, with a slight increase in *Pinus* and became increasingly dry, with a change to semi-desert vegetation, especially in western Iberian and in the Pyrenees (Naughton *et al.*, 2016). This phase also displayed an intensification of the trade winds, all indicating that the polar jet stream was displaced further north (Naughton *et al.*, 2009; Naughton *et al.*, 2016). During the final phase, there was a moderate warming of surface waters (as attested by a decrease in *N. pachyderma* and an increase in *T. quinqueloba*) with deposition of IRD (HE1b) in the region (Naughton *et al.*, 2009; Naughton *et al.*, 2016). Air temperatures increased slightly, as indicated by

Figure 4.9: Interpolated position of the polar front (PF) and subarctic waters along the Iberian margin during the Last Glacial Maximum (LGM), Heinrich Event 1 (HE1), Younger Dryas (YD) and the 8.2 kyr cold event. (left) Relative abundance of N. pachyderma in the sediments (modern values in the area <5%). (right) δ18O signal of G. bulloides. Taken from Eynaud et al. (2009).

the increase in *Pinus*, and were accompanied by an increase in precipitation and Westerly winds (Naughton *et al.*, 2016). These patterns indicate that the polar jet stream had moved to a more southerly position again.

In general, terrestrial studies based pollen, lake and speleothem profiles, as well as cosmogenic exposure ages from glacial landforms, support this pattern of cooling, with periods of enhanced aridity in the western Mediterranean. The existing temperate forests declined to be replaced by semi-desert, open ground and coniferous steppe taxa (Combourieu Nebout *et al.*, 2002; Combourieu Nebout *et al.*, 2009; Fletcher *et al.*, 2010; Desprat *et al.*, 2013). Lakes from the Iberian Peninsula show a period (with either one or two pulses, depending on the resolution of the proxy) of reduced sedimentation and increased salinity, indicating reduced precipitation during the period (Moreno *et al.*, 2012). Speleothem records record a hiatus during HS1, when conditions were too cold and/or dry to allow speleothem deposition (Moreno *et al.*, 2010). The aridity experienced during HSs over the past 100 kyr was deemed a limiting factor in the growth of glaciers in the Mediterranean region (Allard *et al.*, 2021). However, glacial advances were recorded in the mountainous regions on the Iberian Peninsula, Pyrenees and southwestern Alps, pointing to the southerly position of the polar front jet, which funnelled North Atlantic storm tracks and increased precipitation over the north-western Mediterranean (Hughes and Woodward, 2017; Palacios *et al.*, 2017; Reixach *et al.*, 2021).

Marine sediment core records corroborate the evidence of a cold HS1 climate, with the southward displacement of both the polar front jet stream and ITCZ. In the western basin, foraminifera, alkenones, surface water $\delta^{18}O$, deep water $\delta^{13}C$ values, peaks in aeolian dust and terrestrial biomarkers indicate that surface water densities were high, SSTs were cold, westerlies were enhanced, strengthening cyclonic activity and promoting greater WMDW formation and upwelling in the Alboran Sea (Kallel *et al.*, 1997b; Rohling *et al.*, 1998; Cacho *et al.*, 1999; Cacho *et al.*, 2000; Sierro *et al.*, 2005; Frigola *et al.*, 2008; Rodrigo-Gámiz *et al.*, 2011; Martinez-Ruiz *et al.*, 2015; Bazzicalupo *et al.*, 2018). This pattern of enhanced DWF is antiphase to that of the North Atlantic, where NADW formation was supressed, and upwelling and productivity were reduced along the Iberian margin (Sierro *et al.*, 2005; Ausín *et al.*, 2020). SSTs during HS1 were colder than that of the LGM, with summer SST in the Gulf of Lion indicating that temperatures were 5°C cooler than present day (~22°C), with estimates of 4°C decreases in the Alboran Sea and up to 8°C in the Tyrrhenian Sea (Kallel *et al.*,

1997b; Rohling *et al.*, 1998; Cacho *et al.*, 1999; Cacho *et al.*, 2001).

However, this pattern of enhanced WMDW formation was not constant throughout the HS1 period. After the initial phase of enhanced DWF during the beginning of HS1, over a period of <1ka coinciding with HE1, cold meltwaters from the North Atlantic (which may have included icebergs) are believed to have entered the western Mediterranean (Cacho *et al.*, 1999; Sierro *et al.*, 2005; Bazzicalupo *et al.*, 2018). Associated peaks of *N. pachyderma*, variations in redox conditions, decrease in salinity and negative anomalies in $\delta^{18}O$ in planktonic and $\delta^{13}C$ in benthic foraminifera are evident throughout the western basin (Kallel *et al.*, 1997b; Rohling *et al.*, 1998; Cacho *et al.*, 1999; Kallel *et al.*, 2004; Sierro *et al.*, 2005; Cacho *et al.*, 2006; Melki, 2011; Rodrigo-Gámiz *et al.*, 2011; Martinez-Ruiz *et al.*, 2015). This influx of cold fresh meltwater maintained the cold SST, but would have decreased the salinity and density of surface waters, causing a collapse of WMDW formation during HE1, mirroring the NADW formation slowdown/cessation in the North Atlantic at this time (Sierro *et al.*, 2005; Martinez-Ruiz *et al.*, 2015). Benthic foraminifera assemblages, Ba/Al proxies and total organic carbon analysis of HE1 sediments were correlated to the deposition of an Organic Rich Layer (ORL), known as pre-ORL1 in the western Mediterranean (Cacho *et al.*, 2002; Rogerson *et al.*, 2008; Melki, 2011; Rodrigo-Gámiz *et al.*, 2011; Martinez-Ruiz *et al.*, 2015). This pre-ORL1 layer occurred as a result of reduction in the thermohaline circulation and ventilation of deep-water, with heightened marine productivity in surface waters (Rogerson *et al.*, 2008; Rodrigo-Gámiz *et al.*, 2011; Martinez-Ruiz *et al.*, 2015). Once the inflow of cold meltwaters subsided during the final phase of HS1, there was a return to deep convection of the western basin, as seen by the return of high $\delta^{18}O$ surface water and $\delta^{13}C$ deep water values (Sierro *et al.*, 2005; Melki, 2011).

$\delta^{18}O$ and $\delta^{13}C$ spikes (~16 kyr BP) in speleothems and decreasing lake levels both located in Israel, indicate the cold arid conditions were also experienced in the eastern Mediterranean Sea during HS1 (Bar-Matthews *et al.*, 1997; Bar-Matthews *et al.*, 1999; Bartov *et al.*, 2003). Sedimentological analysis of the Nile discharge demonstrated that the main Nile drainage network was cut-off from the White and Blue Nile headwaters (Lake Victoria and Lake Tana) due to reduced river levels, inferring a reduction in the African Monsoon at the time (Box *et al.*, 2011). In deep sea marine records in the Straits of Sicily, HS1 is marked by cool SST (ranging from winter temperatures of 8 to 10°C and summer 9 to 11°C), lower salinity waters and the presence of *N. pachyderma*, though at low abundances (1 to 3%) (Essallami *et al.*, 2007; Rouis-Zargouni *et al.*,

2010). In the Ionian and Aegean Seas, HS1 is identified from an enrichment in $\delta^{18}O$ and lower SST inferred from alkenone-based paleothermometry and planktonic foraminifera assemblages (Geraga *et al.*, 2008; Geraga *et al.*, 2010). In the Levantine Basin, SST decreased to reflect the cold period (~16°C), however, in contrast to the western and central basins, eastern waters were noticeably more saline, due a higher excess of evaporation over precipitation during this arid period (Essallami *et al.*, 2007).

In summary, the increased aridity and cooling experienced in the Mediterranean Region during HS1 was driven by the southern position of the polar front jet to a position along the Iberian margin (Eynaud *et al.*, 2009; Martins *et al.*, 2015; Naughton *et al.*, 2016; Reixach *et al.*, 2021). However, the north-west Mediterranean experienced periods of enhanced cyclogenesis as cold North Atlantic storms were funnelled through the neighbouring mountains (Reixach *et al.*, 2021). SSTs and the hydrology of the western basin were greatly influenced by these heightened winds, with periods of enhanced WMDW formation, upwelling and productivity (Rohling *et al.*, 1998; Cacho *et al.*, 1999). In the eastern basin, the presence of this cold polar air, as well as the reduction of the African Monsoon kept SSTs cool and the region dry (Bartov *et al.*, 2003);Box, 2011 #196}. In addition to atmospheric drivers, the periodic inflow of cold fresher waters from the North Atlantic associated with HEs, was another key driver for the low SST and reduced deep water ventilation in the western basin during HS1 (Sierro *et al.*, 2005; Rogerson *et al.*, 2008; Martinez-Ruiz *et al.*, 2015).

4.4.2   Bølling-Allerød in the Mediterranean region

The response of the Mediterranean region to the BA warm humid period is observed in both terrestrial and marine proxies. However, the signal is complex and is spatially variable across the region. Pollen records from western Mediterranean show an increase in temperate forest species, similar to the modern vegetation of the western Mediterranean. Many of these records indicate increasingly warm humid conditions during the Bølling period that peak towards the end of the Allerød (Combourieu Nebout *et al.*, 2002; Combourieu Nebout *et al.*, 2009; Dormoy *et al.*, 2009; Fletcher *et al.*, 2010; García-Alix *et al.*, 2014; Naughton *et al.*, 2016). However, this pattern contrasts the GI-1 signal in Greenland ice cores (i.e. initial peak followed by a slow oscillating decline towards the end of the chronozone) (Combourieu Nebout *et al.*, 2009; Fletcher *et al.*, 2010; Naughton *et al.*, 2016). Interestingly, an abrupt BA initiation similar to the GI-1 signal, is observed in speleothem records in southern France and eastern Alps, whereas

other caves in northern Iberian and Adriatic Peninsulas show the more gradual increase in temperature and humidity during the BA (Frisia *et al.*, 2005; Genty *et al.*, 2006; Moreno *et al.*, 2010; Belli *et al.*, 2013). It was inferred with the strengthening of the AMOC, the western Mediterranean experienced extended periods negative "North Atlantic Oscillation (NAO)-like" conditions, i.e. anomalously low pressure that allowed more winter storms and Westerly winds to be tracked into the basin during the Bølling warm period (Genty *et al.*, 2006; Moreno *et al.*, 2010; Rodrigo-Gámiz *et al.*, 2011; García-Alix *et al.*, 2014; Naughton *et al.*, 2016). The OD and IACP chronozone signals are evident in the pollen record, where multi-centennial scale forest declines occur along with a return of semi-desert, coniferous and open ground species (centred ~14 and ~13.3 kyr BP), indicating brief returns to drier and/or colder conditions (Combourieu Nebout *et al.*, 2009; Dormoy *et al.*, 2009; Fletcher *et al.*, 2010).

In the north and eastern Mediterranean, the signal is very similar. Temperate forests were prevalent, and lake levels show an increase in precipitation/temperature ratios indicating that both warm and wetter conditions were experienced in this region (Rossignol-Strick, 1995; Robinson *et al.*, 2006; Langgut *et al.*, 2011; Panagiotopoulos *et al.*, 2013; de Beaulieu *et al.*, 2017). This is in agreement with sedimentological analysis in both the Aegean and eastern Mediterranean basin, where there a decrease in aeolian dust, increased deposition of fine grained sediment from enhanced riverine input, and geochemical ratios all indicate a sharp increase in wet conditions, peaking between 13.8 and 13.7 kyr BP (Hamann *et al.*, 2008; Heymann *et al.*, 2013). The OD and IACP chronozones are recorded in the eastern basin, however the western Mediterranean signals have greater precipitation gradients, suggesting that these cold events were potentially stronger and drier in the eastern basin (Dormoy *et al.*, 2009). As in the western basin, speleothems in Israel indicated a gradual warming and increase in precipitation rates during the BA (Bar-Matthews *et al.*, 1997; Bar-Matthews *et al.*, 1999). In contrast, although temperate forests did increase in the central Mediterranean during this period, the assemblage was still dominated by semi-desert species, indicating that while temperatures did increase, the region remained relatively dry in comparison to both the western and eastern basins (Desprat *et al.*, 2013). This pattern of aridity is also evident in aeolian and terrigenous sediments from the southern Mediterranean and North Africa (Bout-Roumazeilles *et al.*, 2012).

Marine records along the Iberian margin indicate that the BA signal is closely linked to the retreating position of the polar front and the northward migration of subtropical

waters (Cacho *et al.*, 2001). Along west coast of the Iberian peninsula, deep sea sediment cores recorded patterns of high fluvial input, decreasing $\delta^{18}O$ values and polar/subpolar foraminifera species and greater influence of warmer waters from North Atlantic subtropical gyre (Rodrigues *et al.*, 2010; Repschläger *et al.*, 2015; Naughton *et al.*, 2016). SSTs in the early Bølling ranged from 15 to 17°C, though in sites that were under greater influence of cold freshwater terrestrial runoff decreased to ~11°C during the late Allerød (Rodrigues *et al.*, 2010).
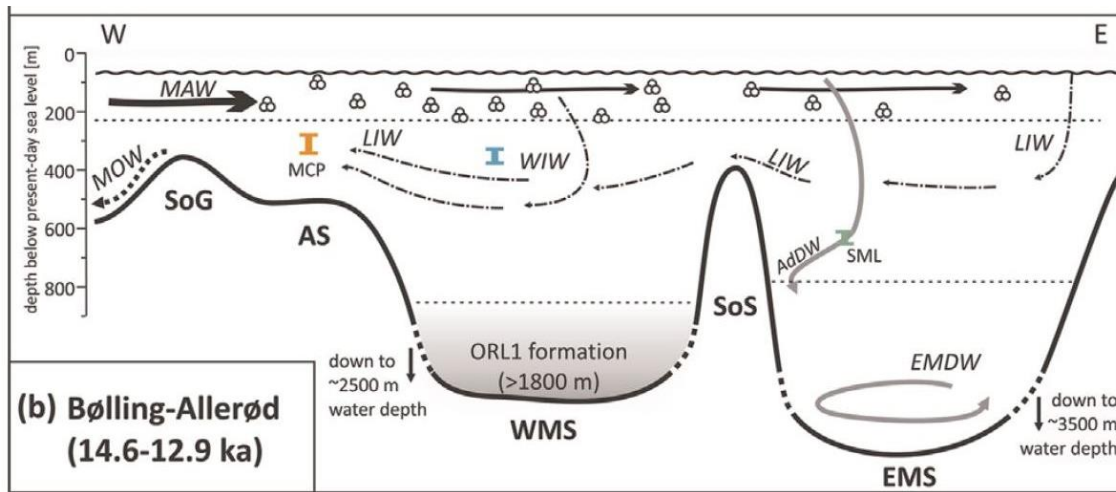
Figure 4.10: Schematic of west-east profile of the Mediterranean Sea during the BA (14.6-12.9 kyr). Black arrows: Surface water comprising MAW and freshwater discharge from onshore (i.e. melt water discharge, river discharge). Dashed-dotted black arrows: LIW and WIW. Grey arrows: EMDW. Dotted black arrows: MOW. Dashed black lines indicate roughly the water mass boundaries. SoG = Straits of Gibraltar; AS = Alboran Sea; Strait of Sicily = Strait of Sicily; WMS = Western Mediterranean Sea; EMS = Eastern Mediterranean Sea. Taken from Fink et al. (2015).

An important feature of the BA chronozone in the deep-sea basins of the western Mediterranean and the Alboran Sea is Organic Rich Layer 1 (ORL1), which was deposited between ~14.35 and 8.9 kyr BP (Cacho *et al.*, 2002; Rogerson *et al.*, 2008; Martinez-Ruiz *et al.*, 2015; Pérez-Asensio *et al.*, 2020). This ORL1 deposit is a dark organic-rich sediment with >0.8% total organic carbon (TOC) and is characterised by a "saddle" pattern to alkenone accumulation maxima, as defined by Rogerson *et al.* (2008) (Martrat *et al.*, 2014; Pérez-Asensio *et al.*, 2020). Although similar to sapropels from the eastern Mediterranean, sapropels such as Sapropel 1 (S1) have significantly more TOC (~2% carbon), they occur at different time intervals and durations (S1 began ~ 10kyr BP) and ORLs are not linked to precession maxima (Rogerson *et al.*, 2008; Pérez-Asensio *et al.*, 2020). During the BA various aluminium (Al) and uranium/thorium (U/Th) ratios indicate higher precipitation and fluvial input, enhanced surface water productivity, reduced aeolian sediment deposition, variations in bottom water oxygenation and a decrease in thermohaline circulation (Rogerson *et al.*, 2008; Melki, 2011; Rodrigo-Gámiz *et al.*, 2011; Martinez-Ruiz *et al.*, 2015). Sea levels were

estimated to have risen from -100 to -70m in the Mediterranean Sea at a rate of as 60 mm/yr during MWP-1A (Fink *et al.*, 2015; Zecchin *et al.*, 2015). The input of both alpine meltwater from Rhône and freshwater from monsoon flooding that was transported in from the eastern basin by the LIW, reduced surface water density, leading to a reduction in in Wester Mediterranean Deep Water (WMDW) formation and promoted Western Intermediate Water (WIW) formation in the Gulf of Lion (Figure 4.10) (Rogerson *et al.*, 2008; Fink *et al.*, 2015; Rohling *et al.*, 2015). All these factors were fundamental in developing and sustaining ORL1, which lasted until the Early Holocene.

As with the terrestrial signals, the response of marine proxies to the BA climate amelioration also display this complexity and variability across the Mediterranean Sea. In the Alboran Sea, the onset of the BA was rapid, with a stepwise increase in SST until the Allerød period (Cacho *et al.*, 2001). Some estimates of SST in the Alboran Sea range from ~13.5 to 14.5°C during the initial phase of the BA, increasing up to ~15.5°C around 14.5 kyr BP (Cacho *et al.*, 2001), while other estimates from Mg/Ca and $U^{K'}_{37}$ temperature profiles suggest a rapid increase to almost full interglacial SST (~18°C) were achieved (Rodrigo-Gámiz *et al.*, 2014a; Jiménez-Amat and Zahn, 2015). The lower SST estimates were said to reflect the influence of the intensification of seasonal deep mixing in the Alboran Sea during the initial phase of the BA leading to enhanced productivity, which began to wane during the Allerød (Cacho *et al.*, 2001). This seasonal upwelling and enhanced productivity of warm surface waters is reflected in the dominance of *G. bulloides*, *G. inflata*, *G. ruber* and SPRUDTS (Bazzicalupo *et al.*, 2018). The establishment of the ORL1 environment in the Alboran Sea had an impact on the planktonic foraminiferal assemblage. *G. inflata* is a deeper water eutrophic species that usually thrives along the gyre margins in the Alboran Sea (Bárcena *et al.*, 2004; Hernández-Almeida *et al.*, 2011). However, during the late BA period the percentage of *G. inflata* decreased as the shoaling of the pycnocline and a reduction in deep vertical mixing allowed nutrients into the photic zone forming a DCM, enabling *N. incompta* to flourish (Bazzicalupo *et al.*, 2018).

In the Gulf of Lion, the boundary between HS1 and the BA is highlighted by the rapid fall in *G. bulloides* and an initial peak, then slow decline of *G. ruber* and *O. universa*, suggesting a decrease in upwelling, with a rapid increase (by ~6°C) then fall in SST (Melki *et al.*, 2009). Benthic foraminifera indicate dysoxic deep water conditions (a possible ORL1 signal?) and $\delta^{18}O$ differences between benthic and planktonic species

indicate WMDW formation was supressed (Frigola *et al.*, 2008; Melki *et al.*, 2009; Melki *et al.*, 2010). This reduction in WMDW allowed the formation of WIW, stratification of the water column and the creation of a DCM (Rogerson *et al.*, 2008; Fink *et al.*, 2015). This pattern of changing water column structure and heightened eutrophication, with the initial dominance in *G. inflata*, followed by *N. incompta*, are similar to the observations in the Alboran Sea (Melki *et al.*, 2009). In other areas of the western basin, SST in the Balearic Sea and Tyrrhenian Sea were estimated at ~14°C and 14 to 17.5°C respectively and surface water salinity was reduced, in comparison to the HS1 (Kallel *et al.*, 1997b; Cacho *et al.*, 2001; Di Donato *et al.*, 2009; Dubois-Dauphin *et al.*, 2017). The foraminiferal assemblage in the Tyrrhenian Sea was dominated by *G. ruber* and *G. inflata* with a fall in *G. bulloides*, suggesting enhanced seasonality and productivity due to heightened precipitation and fluvial runoff (Kallel *et al.*, 1997b; Cacho *et al.*, 2001; Di Donato *et al.*, 2008; Di Donato *et al.*, 2009; Lirer *et al.*, 2013). It has been suggested that the clearer OD and IACP signals in the Tyrrhenian Sea, in comparison to analogous records in the Alboran Sea, was due to the greater influence of north-westerly winds in this region (Cacho *et al.*, 2001).

ORL1 deposits do not occur in the eastern Mediterranean. However, the eastern basin was under the influence of the African Humid Period (AHP) (14.8 to 5.5 kyr) (deMenocal *et al.*, 2000; Kontakiotis, 2016). During the AHP, increasing northern hemisphere summer insolation increased the intensity and northward expansion of precipitation from African monsoons (Figure 4.8) (deMenocal *et al.*, 2000; Shanahan *et al.*, 2015). This intensification in precipitation, riverine discharge (especially the Nile), along with the combination of rising sea levels, meltwater from the Alps and increased NASW inflow, led to summer stratification of the water column, more sluggish deep water ventilation and a decrease in eutrophic benthic foraminifera species in many areas of the eastern Mediterranean (Asioli *et al.*, 2001; Schmiedl *et al.*, 2010; Cornuault *et al.*, 2016; Dubois-Dauphin *et al.*, 2017; Cornuault *et al.*, 2018). As seen in many of the western basin cores, the HS1/BA transition is clearly identified in many cores by the characteristic appearance of *G. inflata*, *O. universa* and *G. ruber* (Geraga *et al.*, 2008; Rouis-Zargouni *et al.*, 2010). In the Sicilian Strait, SSTs were estimated at ~17°C, while both the Adriatic and Aegean Seas are characterised by an initial rapid increase in SST (~13 to 17°C spring/autumn range) and gradual cooling, with evidence of the cooler OD and IACP events (Asioli *et al.*, 2001; Rouis-Zargouni *et al.*, 2010; Sicre *et al.*, 2013; Kontakiotis, 2016). Both sub-basins indicate increasingly productive surface waters

with enhanced summer stratification and a strong DCM (Asioli *et al.*, 2001; Geraga *et al.*, 2008; Triantaphyllou *et al.*, 2009; Kontakiotis, 2016). However, further south and in the Ionian Sea, there are localised areas of winter upwelling and weakening of the DCM, which has been linked to sea level rise and strengthening winds (Asioli *et al.*, 2001; Geraga *et al.*, 2008; Kontakiotis, 2016). The Levantine basin recorded SST comparable to the Holocene during the BA (~21°C) and lower salinity surface waters (Essallami *et al.*, 2007; Castañeda *et al.*, 2010).

As discussed, the response of the Mediterranean to the BA warming is complex and asynchronous across the region, making deciphering and resolving the differences between these signals quite difficult. Rising sea levels, the retreat of the polar front to the north and inflow of warm subtropical waters impacted SSTs, productivity, density and WMDW formation, leading to the onset of the deposition of ORL-1 in the western Mediterranean Sea (Kallel *et al.*, 1997b; Cacho *et al.*, 2001; Rogerson *et al.*, 2008; Melki, 2011; Naughton *et al.*, 2016). The period was also humid, with seasonal variability in winds and storm tracks incoming from the North Atlantic, as well as the displacement to the north of the ITCZ allowing greater influence from the monsoons, and elevated fluvial and meltwater discharge into the Sea (deMenocal *et al.*, 2000; Genty *et al.*, 2006; Di Donato *et al.*, 2008; Fletcher *et al.*, 2010; Kontakiotis, 2016).

4.4.3 Younger Dryas in the Mediterranean region

In the Mediterranean Sea, the complex signal of the YD period is spatially varied and contrasting between marine and terrestrial proxies. Off the north-western Iberian Peninsula, SST during the YD fell by 2 to 4°C, but this decrease was not as extreme as in HS1 and no IRD sediments were recorded (Eynaud *et al.*, 2009; Naughton *et al.*, 2016). The oceanic polar front and polar front jet stream were not displaced as far south as during the HS1, and their positions oscillated throughout the YD as evidenced in the variability and intensity of both winter precipitation and Westerly winds along the north-south Iberian Peninsula, as well as within the Mediterranean region (Figure 4.9) (Eynaud *et al.*, 2009; Naughton *et al.*, 2016). These milder SSTs along the coast also reflect the greater influence and mixing by warmer subtropical waters from the south (Eynaud *et al.*, 2009).

In general, nannofossil productivity proxies off the south-western Iberian coast indicate a drop in SST of ~4°C, a stratified water column with low productivity and a deepening nutricline, which was linked to the weakened AMOC and southward displacement of

the Subpolar Front (Ausín *et al.*, 2020). However, when examined in detail, the two YD phases seen in many terrestrial records in north-west Europe were identified in this region: i) the colder "YDa" (dated 13.4 to 12.5 kyr) had weaker upwelling, a shallower nutricline and higher productivity, ii) followed by a warmer "YDb" period (12.5 to 11.4 kyr), which experienced more upwelling, had a deeper nutricline and less productivity than earlier in the YD (Ausín *et al.*, 2020). These two main phases were further subdivided into four subdivisions using both pollen and alkenone-based SST proxies from the south-western Iberian Peninsula (Naughton *et al.*, 2019). The onset of GS-1 "GS-1a" (12.89 to 12.72 kyr) was increasingly cold (SST ~9°C) and dry, peaking in "GS-1b" (SST ~8°C; 12.72 to 12.39 kyr). "GS-1c" (12.39 to 12.03 kyr) became progressively warmer (SST ~8.5 to ~10°C) and wetter. GS-1 termination "GS-1d" (12.03 to 11.77 kyr) was an unsettled phase with alternating rapid cool/wet and cold/dry phases (SSTs oscillating between ~9 to 16°C) (Naughton *et al.*, 2019).

Within the Mediterranean Region, these subdivisions can be recognised in both terrestrial and marine high-resolution records, especially the variations in the late and terminal YD. However, most researchers do not subdivide the early YD. Throughout the remainder of this section, the phases of YD variability will be referred to as YD-1 for the early YD and YD-2 for the later YD (further subdivided YD-2a and YD-2b). However, these subdivided chronozones make no reference to the chronology of these phases, as their occurrences vary spatially and temporally within the region, or they have not been dated in the literature.

Pollen records from the northern Iberian Peninsula characterise YD-1 as a cold and dry period, with the decrease in temperate Mediterranean forest species and increase in steppe and semi-desert species; followed by a gradual increase in *Pinus, Cedrus* and heath species indicating greater precipitation, heightened westerlies and terrestrial runoff during winter months in YD-2 (Combourieu Nebout *et al.*, 2009; Fletcher *et al.*, 2010; Naughton *et al.*, 2016). However, this two-phase signal is not evident in many sites to the south or east, away from the Atlantic margin or in more mountainous regions. These regions record persistent cold and drier conditions, though the occurrence of temperate species in these sites indicate the continued presence of winter precipitation and Westerly winds throughout the YD (Combourieu Nebout *et al.*, 2009; Dormoy *et al.*, 2009; Fletcher *et al.*, 2010; Moreno *et al.*, 2012; Naughton *et al.*, 2019).

This variability may be explained by a recent study that reconstructed atmospheric

circulation patterns during the YD. Rea *et al.* (2020) interpolated precipitation patterns over western Europe using palaeoglacier equilibrium line altitudes (i.e. the elevation where annual ablation equals accumulation) for the coldest period of the YD, which the authors attributed to the early YD (Figure 4.11). A high-pressure blocking system over the Fennoscandian ice sheet into central Europe, along with expanded sea-ice in the North Atlantic, pushed the polar front jet stream southwards towards north-western Mediterranean (Figure 4.11). The resultant precipitation reconstruction is similar to the modern Scandinavian (SCAND) circulation, where precipitation increases in spring and autumn in the north western Mediterranean, shifting to winter over the Iberian Peninsula and across the rest of the Mediterranean Sea (Rea *et al.*, 2020). Geochemical proxies from the Alboran and Balearic Seas indicate that fluvial input was high during YD-2 indicating a strong seasonal precipitation signal (Jimenez-Espejo *et al.*, 2007). Pollen records from other areas in the western Mediterranean, such as the Tyrrhenian Sea, again show this decline in temperate forests and establishment of semi-desert species (Rossignol-Strick, 1995).
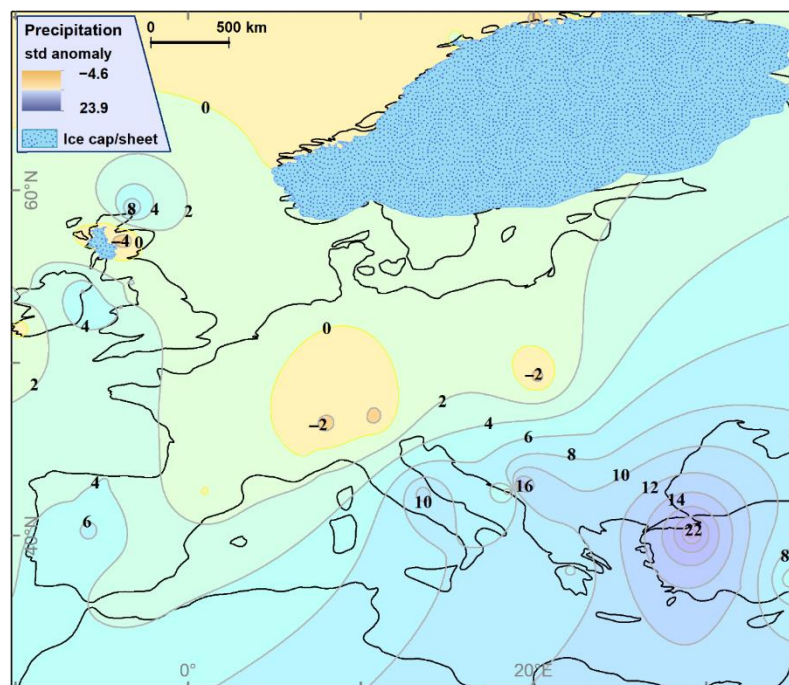
Figure 4.11: Interpolated precipitation anomalies in comparison to modern day in Europe during the YD. Taken from Rea et al. (2020).

There is little indication of YD glacial re-advance in the Iberian Peninsula, though rock glaciers (linked to cold dry periods) were present in Spain (Hughes and Woodward, 2017). The Egesen Stadial in the Alps equates to the YD chronozone, where there were the development and growth of small valley glaciers, and cirque advances, with the final phase of moraine development dated ~11.9kyr (Ivy-Ochs, 2015). There is evidence of a

YD glacial re-advance in the Maritime Alps, Greece and Morocco, indicating an excess in precipitation in the form of snow in these areas (Hughes *et al.*, 2006; Hughes and Woodward, 2017). Speleothem records in the north of Spain show an abrupt positive shift in $\delta^{13}C$ records, indicating intense cooling and enhanced aridity, comparable to glacial times (Moreno *et al.*, 2010). Air temperatures estimates from caves in northern and eastern Spain showed a decrease of ~7°C (winter) to ~4°C (summer) compared to the BA period (Baldini *et al.*, 2019). Precipitation rates were higher in summer than in winter months, which was attributed to reduced moisture uptake by winter Westerlies, due to increased sea ice in the North Atlantic (Baldini *et al.*, 2019). ORL-1 deposition continued through the YD in the deep basins of the Western Mediterranean. WMDW strength was still reduced, with WIW in the Gulf of Lion and Levantine Intermediate Water (LIW) dominant throughout the western basin (Figure 4.12) (Cacho *et al.*, 2002; Rogerson *et al.*, 2008; Martinez-Ruiz *et al.*, 2015; Dubois-Dauphin *et al.*, 2017; Pérez-Asensio *et al.*, 2020). In general, it was a eutrophic period with high productivity, heightened organic matter influx and sediment deposition from both aeolian dust (from north Africa) and rivers (Martinez-Ruiz *et al.*, 2015; Pérez-Asensio *et al.*, 2020).
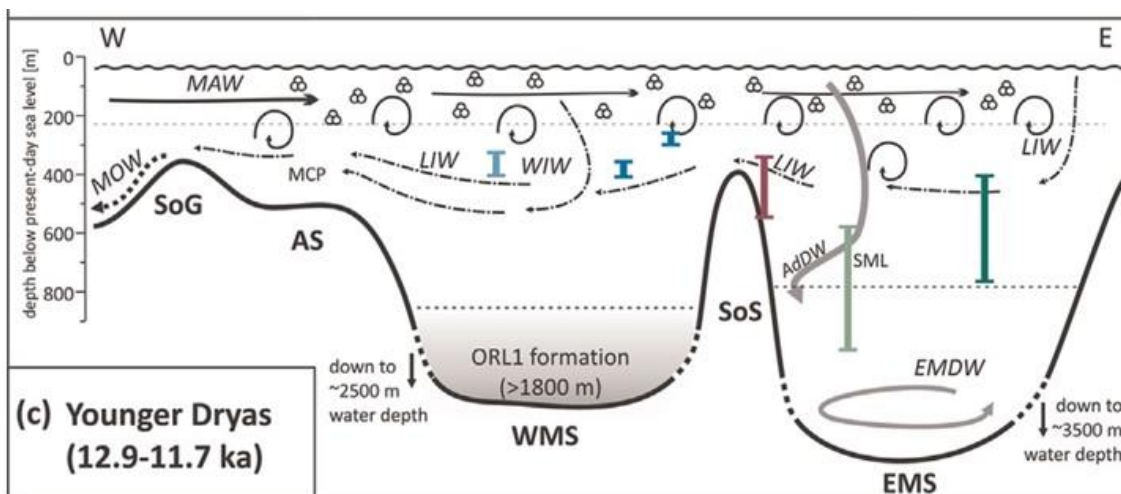
Figure 4.12: Schematic of west-east profile of the Mediterranean Sea during the Younger Dryas (12.9-11.7 kyr). Black arrows: Surface water comprising MAW and freshwater discharge from onshore (i.e. melt water discharge, river discharge). Dashed-dotted black arrows: LIW and WIW. Grey arrows: EMDW. Dotted black arrows: MOW. Dashed black lines indicate roughly the water mass boundaries. SoG = Straits of Gibraltar; AS = Alboran Sea; Strait of Sicily = Strait of Sicily; WMS = Western Mediterranean Sea; EMS = Eastern Mediterranean Sea. Taken from Fink et al. (2015).

Alkenone-based SSTs suggest the Alboran Sea cooled by ~4°C, with YD-1 cooling co-incident to the GS-1 atmospheric cooling and YD-2 SST increase ~600 years prior to the Holocene warming in Greenland ice cores (~12.25 kyr) (Cacho *et al.*, 2001; Cacho *et al.*, 2002; Rodrigo-Gámiz *et al.*, 2014a; Ausin *et al.*, 2015a; Jiménez-Amat and Zahn, 2015). Prior to the YD termination, a small drop in SST (~1°C) was recorded and

equates to the instability of the YD-2b period (Cacho *et al.*, 2001). These oscillations in SST in the Alboran sea were attributed to the shifting position of the polar front, which impacted on the strength and flow paths of incoming Westerly winds, NASW inflow, regional variations in fluvial input and upwelling intensities (Cacho *et al.*, 2001; Ausin *et al.*, 2015a; Pérez-Asensio *et al.*, 2020). Both productivity ratios (determined from Ba ratios) and nannofossils (especially coccolithophore species that thrive in turbid fresher surface waters and fresh-water diatoms) peaked in YD-1 in the Alboran Sea, along with the dominance of *N. incompta* throughout the YD (Bárcena *et al.*, 2001; Jimenez-Espejo *et al.*, 2007; Bazzicalupo *et al.*, 2018). The strong influence of LIW and WIW and weakened WMDW is evident by the decoupling of the epifaunal and deep infaunal benthic foraminifera δ^{13}C signal (Pérez-Asensio *et al.*, 2020).

In the Gulf of Lion, δ^{18}O SST estimates fell to ~9°C (summer) in YD-1, but had recovered to ~16°C by the end of YD-2 (Melki *et al.*, 2009; Dubois-Dauphin *et al.*, 2017). Surface water salinity was estimated to have decreased by ~2‰ from the BA to ~35 to 35.5‰ during this period. Planktonic foraminifera assemblages are dominated by *N. incompta*, *T. quinqueloba*, *G. glutinata* and *G. bulloides*, with rare *G. ruber*, with the highest accumulation rates in YD-1 (Melki *et al.*, 2009). Benthic accumulation rates were also very high (~4600 individuals/cm^2/kyr), with an increase in shallow infaunal opportunistic eutrophic species that responded to an influx of organic matter to the sea floor (Melki *et al.*, 2009). δ^{13}C values showed productivity was similar to that of today in the Gulf of Lion (Melki, 2011). This heightened primary productivity associated with this influx of organic matter and low δ^{13}C were attributed to enhanced winter vertical mixing – driven by the intensification of the Mistral winds, along with freshwater input from the River Rhône or possible deep-water cascade events (Figure 4.12) (Melki *et al.*, 2009; Melki, 2011).

Further south, SST estimates in the Balearic Sea were comparable to those in the Gulf of Lion and productivity was high, with continued fluvial input (Frigola *et al.*, 2008; Fink *et al.*, 2015; Dubois-Dauphin *et al.*, 2017). Neodymium isotopic composition (ϵNd) on foraminifera and cold water corals show a greater influence from an intermediate water mass (WIW or LIW) than WMDW during YD-1 though this decreased towards the YD-2 termination (Dubois-Dauphin *et al.*, 2017).

In the Tyrrhenian Sea, surface waters in YD-1 were cold (~10°C), highly productive, with a well-developed DCM, as reflected by a peak in dinocyst species and eutrophic

planktonic foraminiferal species *N. incompta*, *T. quinqueloba* and *G. glutinata* (Capotondi, 1995; Capotondi *et al.*, 1999; Rouis-Zargouni *et al.*, 2010; Morabito *et al.*, 2014). This was followed by a peak in *G. bulloides*, *G. inflata* and *G. ruber* indicating the increased mixing of surface waters during the warmer YD-2. The influence of the LIW was strong in the Tyrrhenian Sea during the YD and it was suggested that the cool dry conditions during the YD favoured enhanced net evaporation and LIW production the in eastern Mediterranean (Toucanne *et al.*, 2012).

Pollen data from marine and lacustrine cores from the Aegean and Ionian Seas and adjacent region, show a fall in forest species and dominance of semi-desert species, indicating dry conditions (estimates of annual precipitation <150mm in lowland regions, with a significant fall in winter precipitation) and air temperatures falling below freezing (Rossignol-Strick, 1995; Robinson *et al.*, 2006; Dormoy *et al.*, 2009; Panagiotopoulos *et al.*, 2013). In detail, Dormoy *et al.* (2009) identified the three phases of YD: YD-1 (dated 12.6 to 12.4 kyr) indicates air temperature ~5°C cooler; YD-2a (12.4 to 12.2 kyr) records an increase of 3–5°C; YD-2b (12.2 to 11.7 kyr) identified a return to colder conditions (~1°C cooler). Semi-desert pollen in a marine core taken off the south central Mediterranean document this dry arid period, though there is still a significant presence of deciduous forests (*Quercus*, *Cedrus* and *Pinus*) (Desprat *et al.*, 2013). Although cold, upland areas in north-western Tunisia and lowland areas in southern Italy were humid enough to act as refugia for temperate forest species during the YD (Desprat *et al.*, 2013; de Beaulieu *et al.*, 2017).

Speleothems in north-eastern Italy record high seasonality in YD-1 speleothem growth, but in contrast to the wetter summers seen in northern Spain, precipitation was greater during the autumn and long winters, which then became drier with less seasonality in YD-2 (Belli *et al.*, 2013; Baldini *et al.*, 2019). These patterns in seasonality and increasing aridity were linked to increasing Bora wind strength during the YD. Although there is an overestimation of precipitation anomalies in the Dinaric Alps and over Turkey, the reconstruction of Rea *et al.* (2020) supports these findings, and suggests that there was heightened winter cyclogenesis and precipitation in the eastern basin in YD-1, when the incoming cold polar front jet stream met the warm eastern Mediterranean Sea (Figure 4.11). In Soreq Cave in Israel, δ^{18}O values peak around the YD period (dated 13.2 to 11.4 kyr), with an associated increase in δ^{13}C, indicating cold dry conditions in the eastern Mediterranean region (Bar-Matthews *et al.*, 1997; Bar-Matthews *et al.*, 1999). Inflow from the Nile deceased during the YD due to the

southern offset of the ITCZ, weakened monsoons and a brief hiatus in the AHP (deMenocal *et al.*, 2000; Mojtahid *et al.*, 2015; Shanahan *et al.*, 2015). Analysis of sediments in south central Mediterranean indicate significant aeolian deposition from an arid Tunisia (Bout-Roumazeilles *et al.*, 2012; Desprat *et al.*, 2013). This aeolian sedimentation influence is also observed in other regions of the eastern Mediterranean, though the pattern varies (Hamann *et al.*, 2008). A gradual cooling occurred over ~2 kyr, with an initial reduction in Saharan dust that progressively increased during the YD, indicating that the North African region exerted more control over the SE Mediterranean during YD-2 (Castañeda *et al.*, 2010).

Around the Strait of Sicily and southern Adriatic Sea, MAT SST estimates range from ~9.5°C (Apr/May) to ~11°C (Oct/Nov) (Essallami *et al.*, 2007; Sicre *et al.*, 2013). The three YD phases were identified in the cool eutrophic waters of the northern Adriatic from planktonic foraminifera (Asioli *et al.*, 2001). The assemblage alternates from a stratified YD-1 dominated by *T. quinqueloba*; YD-2a represented by a peak of the upwelling species *G. bulloides*, and finally YD-2b, where a return of *T. quinqueloba* and minor peak of *G. inflata* indicate more seasonally stratified surface waters (Asioli *et al.*, 2001). The southern Adriatic is also dominated by eutrophic species, especially *N. incompta* in YD-1, which was replaced by warm oligotrophic species *G. ruber* in YD-2 (Geraga *et al.*, 2008). The YD-1 assemblage in the Aegean Sea is dominated by *N. incompta*, followed by the more gradual transition to *G. ruber*, *G. bulloides*, *G. glutinata* and *T. quinqueloba* in YD-2 (Geraga *et al.*, 2010). As in the southern Adriatic, this indicated eutrophic waters with a DCM in YD-1, becoming increasingly seasonal and warm in YD-2. It was inferred that DWF was limited in the eastern basin, with LIW dominating the ventilation of the surface waters driven by strong winter convection, and minor seasonal fluvial input in YD-1, though falling by YD-2 (Asioli *et al.*, 2001; Schmiedl *et al.*, 2010; Kontakiotis, 2016). The Levantine Basin was significantly warmer, with minimum SST MAT estimates ranging from ~16°C (Apr/May) to ~20°C (Oct/Nov), though the warming of SST following the YD was more gradual than elsewhere in the Mediterranean (Essallami *et al.*, 2007; Castañeda *et al.*, 2010). *G. ruber* and other warm water species decreased in YD-1 and there was an increase in the eutrophic species *N. incompta*, *G. truncatulinoides* and *G. inflata*; YD-2 was characterised by an increase in *G. bulloides* and *G. ruber* indicating warmer water with increased seasonal upwelling (Mojtahid *et al.*, 2015).

Although not as extreme as HS1, in general, the YD in the Mediterranean was cold and

dry. However, oscillations in the southerly position of the oceanic polar front, expansion of Arctic sea ice and changes in North Atlantic atmospheric circulation are all key drivers in the variability of the YD signal observed throughout the Mediterranean region (Eynaud *et al.*, 2009; Geraga *et al.*, 2010; Ausin *et al.*, 2015a; Jiménez-Amat and Zahn, 2015; Naughton *et al.*, 2016). During the early YD, air temperatures were cold, precipitation rates were spatially variable and the sea was cool and productive, with continued weakening of deep-water ventilation in the western basin (Cacho *et al.*, 2001; Melki *et al.*, 2009; Dubois-Dauphin *et al.*, 2017; Pérez-Asensio *et al.*, 2020). In the latter half of the YD, as the polar front began its retreat northward, SSTs began to increase and terrestrial proxies point to increased variability of precipitation and seasonality between the basins (Sbaffi *et al.*, 2004; Combourieu Nebout *et al.*, 2009; Belli *et al.*, 2013; Ausin *et al.*, 2015a).

In summary, late Pleistocene oscillations in northern hemisphere climate are clearly represented throughout the Mediterranean Sea, though they are spatially and chronologically complex. Although the global climate became significantly more stable in the Holocene period, several short-term deteriorations, such as the 11.4, 9.3 and 8.2 kyr events, are recorded in Greenland ice cores (Rasmussen *et al.*, 2014). These early Holocene events and their impact in the north-western Mediterranean Sea will be discussed in more detail in Chapter 7.

Chapter 5.

5 Materials and methods

This chapter will present the materials and methodology used for both micropalaeontological and chronological analysis of core M40/4 82-2SL, as well as the data requirements and chronological controls applied when collating the planktonic foraminifera census count data for the Late Pleistocene events within the Mediterranean Sea. The analytical, statistical and spatial interpolation methods used for both the Late Pleistocene databases and M40/4 82-2SL, including Artificial Neural Networks (ANN), palaeoenvironmental proxies and Principal Component Analysis (PCA), will be discussed in detail.

5.1 Late Pleistocene datasets

In order to conduct a basin wide reconstruction of the Mediterranean Sea during HS1, the BA and YD, a comprehensive and spatially widespread compilation of planktonic foraminifera count data had to be generated for each chronozone. Initially, the chronology of HS1, the BA and YD in the Mediterranean needed to be defined, to determine what sample intervals in each core dataset needed to be targeted. Once potential marine sediment cores were identified, a series of data requirements and quality control parameters need to be met prior to the inclusion of data into the compilation. These chronological and database requirements will be discussed in detail below.

5.1.1 Chronology of the Late Pleistocene chronozones in the Mediterranean Sea

The most recent INTIMATE Stratigraphy Research group chronostratigraphic framework for Late Pleistocene events, as recorded in the NGRIP and GISP2 Greenland ice cores, was published in 2014 (Rasmussen *et al.*, 2014). A series of significant events were evident in both ice cores, alternating between stadial (GS) and interstadials (GI) and sub-events (Table 5.1a). However, synchronicity of these events cannot be assumed to be correlated to regions beyond Greenland (Austin and Hibbert, 2012; Blaauw, 2012). There is no definitive consensus for the exact onset or end dates for Heinrich Stadial 1 (HS1), the Bølling-Allerød (BA) or the Younger Dryas (YD) within the Mediterranean Sea (Cacho *et al.*, 2002; Geraga *et al.*, 2005; Frigola *et al.*, 2008).

Therefore, to begin to define the chronology of the Late Pleistocene chronozones within the Mediterranean Sea, a literature review was conducted for research based on marine microfossils, corals and deep-sea sediment cores. Terrestrial records or proxies were not used, as the effects of climate change may not be diachronous or comparable between proxies (Blaauw, 2012; Lowe and Walker, 2014). Between 18 and 24 published articles were reviewed, with the average onset and end dates for each chronozone summarised in Table 5.1b.

In addition, as M40/4 82-2SL is such a high-resolution core, the chronology of the Late Pleistocene events is well constrained, though as the core only extends to ~15.5 cal kyr BP, the start date of HS1 was not recorded (discussed further in Section 5.2.2 below). Therefore, the interpolated date ranges of the YD, BA and end of HS1 from M40/4 82-2SL were used to supplement the dates obtained from the literature (see Table 5.1b). There is close correlation across all sources to the onset and end of most chronozones, with the main differences observed at the end of both the BA and HS1. However, as both these events were so clearly defined in M40/4 82-2SL, the date ranges for the YD (12800 to 11550 ± 50 cal yr BP), the BA (14700 to 12800 ± 50 cal yr BP), and HS1 end date (14700 ± 50 cal yr BP) chronozones were taken from M40/4 82-2SL. The start date of HS1 was obtained from the literature and is defined as 17100 ± 50 cal yr BP. A confidence interval of ± 50 years was added to all chronozones to allow for calibration or correlation errors arising from older datasets or lower resolution cores.

a) INTIMATE Event Stratigraphy		b) Mediterranean Stratigraphy		
Event Onset	Age with definition uncertainty (yr b2k)	Chronozone Start / End	Mean dates from published sources (cal yr BP)	M40/4 82-2SL (cal yr BP)
Holocene Start	11703 ± 4	YD End	11500 ± 600	11550
GS-1 Start	12896 ± 4	YD Start	12850 ± 850	12800
GI-1 Start	14692 ± 4	BA End	13075 ± 825	12800
		BA Start	14725 ± 1225	14700
GS-2.1a Start	17480 ± 200	HS1 End	14950 ± 950	14700
		HS1 Start	17100 ± 900	-

Table 5.1: Comparison of INTIMATE Event Stratigraphy (yr b2k) (Rasmussen et al., 2014), (a) the average chronozone start and end dates (cal yr BP), (b) obtained from published Mediterranean Sea marine datasets and the interpolated chronozone dates (cal yr BP) from M40/4 82-2SL. Note: the Bølling-Allerød chronozone is not a synonym for GI-1 or Younger Dryas chronozone for GS-1 (Rasmussen et al., 2014).

5.1.2 Data requirements

To source potential Mediterranean Sea datasets, a literature review was conducted to identify articles that used deep-sea marine sediment cores with counts of planktonic foraminifera. The online Open Access library Pangaea® (http://www.pangaea.de/) was utilised to search for published datasets, both for cores identified in the literature and other potential datasets. For datasets not available on Pangaea®, corresponding authors were contacted, requesting the original planktonic foraminifera counts and chronological control points. Furthermore, Dr Cloke-Hayes supplied several unpublished chronologically constrained datasets.

Potential datasets had to meet a defined set of criteria prior to compilation in the Late Pleistocene databases. As the ANN training dataset used by Hayes *et al.* (2005) incorporated the 150 µm fraction core top dataset of Thunell (1978), all planktonic foraminifera census counts had to belong to >150 µm fraction. Both total and percentage counts were acceptable, but the complete faunal assemblage had to be recorded. Due to the taxonomic criteria used by Thunell (1978), the following species were grouped together: i) *N. incompta* and 'P/D integrades' are 'P/D integrade + *N. incompta*', ii) *G. ruber* white and pink are *G. ruber* (total); iii) *G. siphonifera* and *G. calida* are 'siphon+calida'; iv) *G. truncatulinoides* sinistral and dextral are '*G. truncatulinoides* (total)' and v) *G. sacculifer* plexus remain undifferentiated. For some older datasets published on Pangaea®, the SPRUDTS group were not differentiated (see Appendix 3) (Jorissen *et al.*, 1993). However, if the SPRUDTS data formed only a minor component of the total percentage (<3% average within the entire chronozone), the SPRUDTS data was included and assigned to *G. sacculifer,* as this morphospecies was on average the most significant SPRUDTS species during the Late Pleistocene.

It should be noted that the datasets collated were from a diverse range of studies from the late 1970s through to 2017 and as such, this can introduce some discrepancies within the data (Table 5.2). Over these 40 years, taxonomic definitions for many morphospecies has changed, e.g. *N. pachyderma* sinistral and dextral are now reclassified as *N. pachyderma* and *N. incompta*; and there have been the substantial progress in identifying morphologically similar genotypes (Darling *et al.*, 2006; Darling and Wade, 2008; Aurahs *et al.*, 2009; Ujiié *et al.*, 2010; Aurahs *et al.*, 2011; Morard *et al.*, 2011; André *et al.*, 2013; André *et al.*, 2014; Schiebel and Hemleben, 2017). Therefore, there was little consistency with the naming convention or classification of

species. In some studies, *G. ruber* morphospecies was subdivided into *G. ruber* white, *G. ruber* pink and *G. elongatus*, in others it was just *G. ruber*. Therefore, some generalisations in morphospecies were made for the spatial distribution analysis (see 5.1.4 Spatial analysis). *G. ruber* plexus includes *G. ruber* white, *G. ruber* pink and *G. elongatus*; all Neogloboquadrina species merges *N. pachyderma* sinistral, *N. pachyderma* dextral and/or *N. incompta*; "P/D intergrades" and *N. dutertrei*; *G. truncatulinoides* includes both dextral and sinistral coiling varieties; and *G. sacculifer* contains both "with sac" and "without sac" variants.

In total, data from 67 cores was collated, with 60, 62 and 63 cores compiled in the YD, BA and HS1 databases respectively (Table 5.2, Figure 5.1).

Region	Core	Longitude (WGS84)	Latitude (WGS84)	Water depth (m)	Coring device	^{14}C AMS dates	Citation
Alboran Sea (n = 5)	CEUTA10PC08	-4.87	36.02	914	PC	Yes	Ausin *et al.* (2015a)
	KS 310	-1.57	35.55	1900	NS	Yes	Hayes *et al.* (1999)
	MD 95-2043	-2.62	36.14	1841	CC	Yes	Cacho *et al.* (1999); Cacho *et al.* (2001); Sbaffi *et al.* (2001); Pérez-Folgado *et al.* (2003)
	ODP 977	-1.96	36.03	1984	NS	Yes	Pérez-Folgado *et al.* (2003); Pérez-Folgado *et al.* (2004)
	SU81-07	-3.48	35.57	1375	PC	No	Kallel *et al.* (1997a)
Balearic Sea (n = 2)	MD99-2343	4.03	40.50	2391	PC	Yes	Sierro *et al.* (2005)
	ODP 975B	4.51	38.90	2400	APC & XCB	Yes	González-Donoso *et al.* (2000) Jimenez-Espejo *et al.* (2007)
Gulf of Lion (n = 3)	BC 15	5.93	41.95	2500	NS	Yes	Rohling *et al.* (1998); Hayes *et al.* (1999)
	M40/4 82-2SL	3.78	42.31	1079	PC	Yes	This thesis
	MD 99-2346	4.15	42.04	2100	NS	Yes	Melki *et al.* (2009)
Tyrrhenian Sea (n = 10)	AC 85-4	11.77	41.75	662	PC	Yes[†]	Capotondi *et al.* (1989)
	BS 78-12	9.82	42.67	626	PC	Yes	Jorissen *et al.* (1993); Hayes *et al.* (1999)
	BS 79-22	14.38	38.39	1449	GC	No	Sbaffi *et al.* (2001)
	BS 79-33	14.03	38.26	1282	GC	Yes	Cacho *et al.* (2001); Sbaffi *et al.* (2001)
	BS 79-37	13.42	38.30	1400	GC	Yes	Sbaffi *et al.* (2004)
	BS 79-38	13.58	38.41	1489	GC	No	Cacho *et al.* (2001); Sbaffi *et al.* (2001); Sbaffi *et al.* (2004)
	GNS 84-c106	14.71	40.48	292	NS	Yes	Di Donato *et al.* (2008)
	KET 80-03	13.35	40.55	1920	NS	Yes	Kallel *et al.* (1997b) Zachariasse *et al.* (1997); Paterne *et al.* (1999)
	KET 80-19	13.21	40.33	1920	PC	No	Kallel *et al.* (1997b); Kallel *et al.* (2004)
	LC 07	10.07	38.14	488	PC	No	Hayes *et al.* (1999); Dinarès-Turell *et al.* (2003); Incarbona *et al.* (2008)
Strait of Sicily (n = 5)	Chain61-19	13.10	35.78	1475	PC	No	Muerdter and Kennett (1983/84); Muerdter (1984)
	CS72-37	12.28	36.68	1304	PC	No	Kallel *et al.* (1997a)
	KET 80-39	11.41	36.32	290	NS	No	Hayes *et al.* (2005)
	MD 04-2797 CQ	11.67	36.95	771	CASQ	Yes	Rouis-Zargouni *et al.* (2010)
	TRI171-15	13.95	36.73	820	PC	No	Muerdter and Kennett (1983/84); Muerdter (1984)

Region	Core	Longitude (WGS84)	Latitude (WGS84)	Water depth (m)	Coring device	^{14}C AMS dates	Citation
Adriatic Sea (n = 8)	IN 68-3	18.75	40.70	868	PC	Yes	Jorissen *et al.* (1993)
	IN 68-5	18.53	41.23	1030	PC	Yes	Jorissen *et al.* (1993); Hayes *et al.* (1999)
	IN 68-7	18.23	41.93	1225	PC	Yes	Jorissen *et al.* (1993)
	IN 68-9	17.91	41.79	1234	PC	Yes	Jorissen *et al.* (1993); Rohling *et al.* (1997); Hayes *et al.* (1999)
	IN 68-21	14.78	42.88	252	PC	Yes	Jorissen *et al.* (1993)
	IN 68-28	16.92	41.98	396	PC	No	
	IN 68-29	17.13	42	797	PC	No	
	IN 68-38	17.57	41.12	716	PC	No	
Aegean Sea (n = 18)	AEG-3	24.85	40.13	685	BGC	Yes	Aksu *et al.* (1995b)
	AEG-4	25.93	37.40	404	BGC	No	
	AEG-5	26.16	37.33	430	BGC	Yes	
	AEG-19	24.83	39.27	380	BGC	Yes	
	AEG-20	24.97	38.43	630	BGC	Yes	
	AEG-22	26.75	35.75	820	BGC	Yes	
	C40	24.08	36.94	852.80	NS	Yes	Geraga *et al.* (2000)
	C69	24.21	36.55	632	NS	Yes	Geraga *et al.* (2005)
	LC 21	26.58	35.66	1522	PC	Yes	Hayes *et al.* (1999); Casford *et al.* (2002)
	MAR03-02	26.37	38.07	398	PC	No	İşler *et al.* (2016a); İşler *et al.* (2016b)
	MAR03-03	25.82	37.86	720	PC	No	
	MAR03-25	26.44	37.17	494	PC	Yes	
	MAR03-27	25.32	38.31	651	PC	Yes	
	MAR03-28	25.02	39.02	453	PC	Yes	
	MNB3	25.00	39.26	800	GC	No	Geraga *et al.* (2010)
	SK1	23.60	39	1041	PC	Yes	Zachariasse *et al.* (1997); Casford *et al.* (2007); Kontakiotis (2016)
	SL-11	25.80	39.10	258	GC	No	Casford *et al.* (2007)
	SL-21	25.42	39.02	317	GC	No	
Ionian Sea (n = 12)	75KS76	22.11	35.91	2890	PC	Yes	Znaidi-Rivault (1982)
	BC 02	21.42	35.29	3349	BC	No	Principato (2003); Principato *et al.* (2003)
	BC 06	21.12	34.88	2539	BC	No	

Region	Core	Longitude (WGS84)	Latitude (WGS84)	Water depth (m)	Coring device	^{14}C AMS dates	Citation
	BC 07	20.54	35.76	3022	BC	No	
	LynchII-3	16.70	35.03	2432	PC	No	Muerdter (1984)
	ODP 964A	17.75	36.27	3658	PC	Yes	Barry (2017)
	ODP 969A	24.88	33.84	2200.30	PC	Yes	Barry (2017)
	ODP 973A	18.01	35.01	3695	NS	Yes	Hessler *et al.* (2014)
	P4	18.93	36.23	3560	NS	No	Hayes *et al.* (1999)
	T87/2/20G	23.75	34.97	707	GC	Yes	Znaidi-Rivault (1982); Rohling *et al.* (1993);
	T87/2/27G	23.02	35.08	607	GC	Yes	Zachariasse *et al.* (1997); Hayes *et al.* (1999)
	Z1	19.87	39.25	1160	GC	Yes	Geraga *et al.* (2008)
Levantine Sea (n = 4)	LC-31	31.17	35	2298	PC	Yes	Casford *et al.* (2007)
	MD 84-641	33.63	33.03	1375	NS	Yes	Melki *et al.* (2010)
	TRI172-22	29.02	35.32	3150	PC	No	Thunell *et al.* (1977); Thunell and Williams (1983)
	75KS5	31.75	34.83	1560	PC	Yes	Znaidi-Rivault (1982)

Table 5.2: Details of cores collated for the Late Pleistocene chronozones, including their location, water depth, coring device, if they include valid ^{14}C AMS dates and citations. Coring Device: BC = Box core; CASQ = Calypso Square core; CC = Calypso Corer; GC = Gravity Core; BGC = Benthos Gravity Core; PC = Piston Core; APC & XCB = Triple APC & double XCB coring. †^{14}C AMS dates, but no sample depth reported.
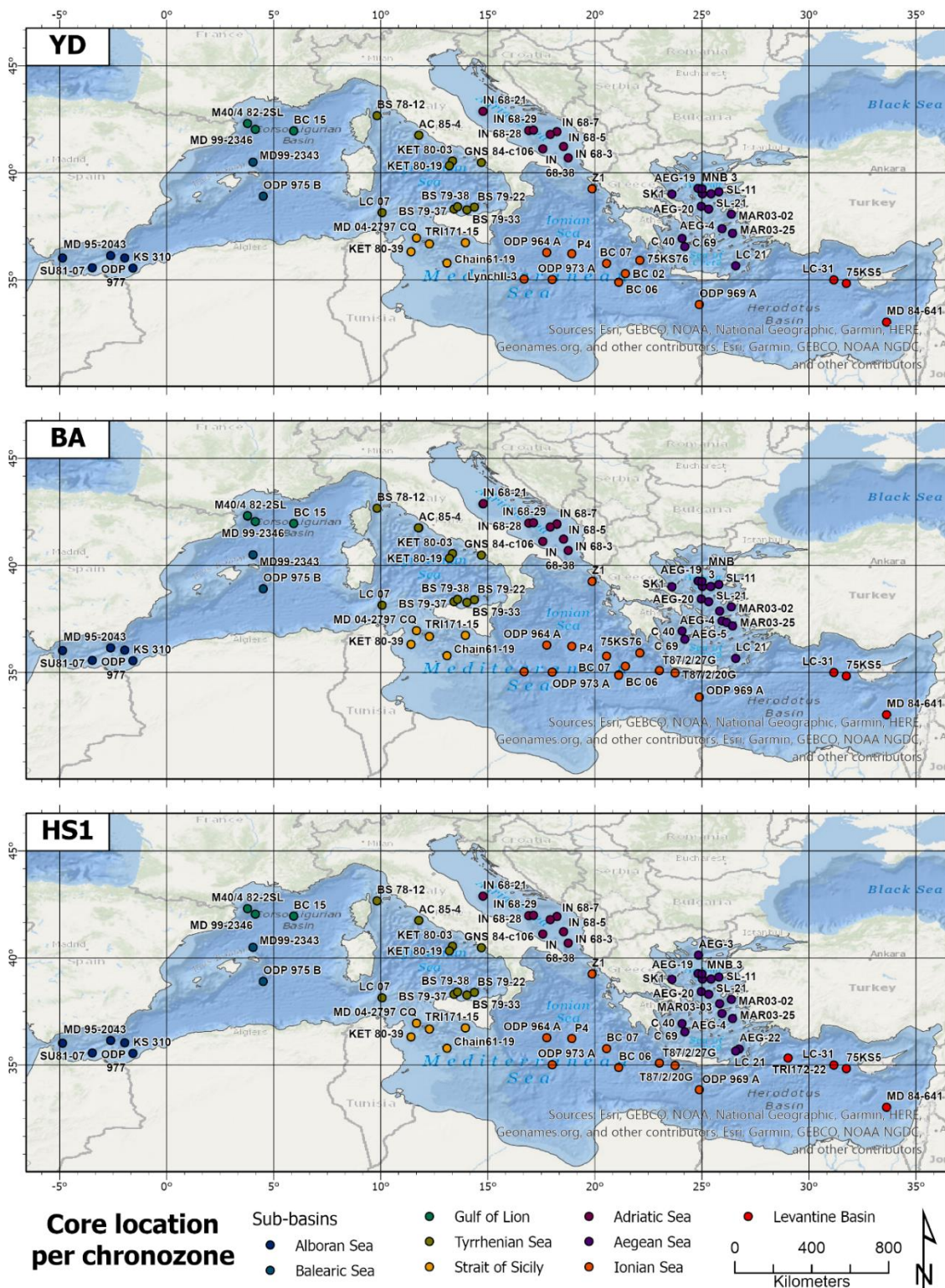
Figure 5.1: Distribution of cores used for Late Pleistocene datasets.

5.1.3 Chronological framework and data compilation

As the Late Pleistocene datasets ranged from a variety of authors over the past 30 years, the methods used to date and calibrate control points varied greatly. Some older studies used uncalibrated radiocarbon years (Jorissen *et al.*, 1993). In more recent studies, ^{14}C AMS dates were recalibrated using software such as Calib (Stuiver *et al.*, 2017) or

OxCal (Ramsey and Lee, 2013) and a ∆R value may/may not have been applied (Sbaffi *et al.*, 2004; Geraga *et al.*, 2010; Melki *et al.*, 2010; Rouis-Zargouni *et al.*, 2010). Therefore, direct comparison between the original datasets is not possible. To enable reliable and consistent comparison between these datasets, a set of criteria and metadata requirements, proposed by recent palaeoecological studies were adapted and applied to this database (Thomopoulos *et al.*, 2010; Giesecke *et al.*, 2014; Flantua *et al.*, 2016; Borreggine *et al.*, 2017). For each site the following information was recorded: site name; year of data preparation; control point type; depth of sample; non-^{14}C dates or control points ages; for ^{14}C samples, the original age model, calibration method and software used, the ^{14}C date (min, max, errors), reservoir correction, the published calibrated age (min, max, best age, errors); and any additional relevant comments from authors, such as presence of outliers, turbidites, hiatuses etc. In addition, the mean Mediterranean Sea ∆R value of 58 ± 15 ^{14}C years was applied to all recalibrated ^{14}C AMS dates (Reimer and McCormac, 2002; Faivre *et al.*, 2015). Once the data was compiled, all ^{14}C AMS dates with reported errors and the mean ∆R value were recalibrated using Calib v.7.0.2 and the Marine13 calibration curve (Reimer *et al.*, 2013; Stuiver *et al.*, 2017). The full list of control points is listed in Appendix 1.

5.1.3.1 *Age quality level*

It should be noted that the nature of chronological and age model generation and reporting over the past ~30 years has been inconsistent. In many instances the original ^{14}C dates, corrections or depth of samples used for dating were not published. Numerous studies with limited or no ^{14}C dates used a variety of different methods to provide a chronostratigraphic framework for their cores, such as independently dated event ages (e.g. the start and end dates for S1) that are biostratigraphically "tuned" to the results of the planktonic foraminifera abundance curves (Capotondi *et al.*, 1989; Aksu *et al.*, 1995a); biostratigraphic correlation to well-dated cores, such as MD 95-2043 in the Alboran Sea, originally published by Cacho *et al.* (1999) (Jorissen *et al.*, 1993; Sbaffi *et al.*, 2001); tuning against other proxies, e.g. *G. bulloides* δ^{18}O curves to the Greenland ice cores (Jimenez-Espejo *et al.*, 2007), as well as utilising dated tephra layers (Kallel *et al.*, 1997a). In most instances, the ages of these control points were reported without errors. Many of these methods can be quite subjective and potentially can add additional biases and errors to the data. Using control points in a core in the Mediterranean Sea that are tuned to Greenland ice cores or biostratigraphically to cores located in different Mediterranean sub-basins or hydrographic regimes are also

problematic, mainly as they assume synchronicity of events both globally and/or within the Mediterranean region (Blaauw, 2012).

To account for the variations in quality of geochronology of the data, for each chronozone an age quality (AQ) level was assigned based on methodology defined by Mix *et al.* (2001) and adapted by the MARGO working group for the LGM (Hayes *et al.*, 2005; Kučera *et al.*, 2005a) . However, the two radiometric dates that were required within the LGM chronozone was reduced to just one for the YD, BA and HS1 chronozones, as the extent of these intervals are more discrete than the LGM chronozone (19-23 cal kyr BP). For the Late Pleistocene chronozones, the AQ criteria applied were as follows:

- *Level 1:* Chronological control was based on at least one of the following: i) a radiometric date within the target interval, most commonly a reservoir-corrected ^{14}C year date adjusted to calendar years using CALIB v 7.0.4; ii) a U/Th date or dated tephra layer with reported uncertainties.

- *Level 2:* Characterised by at least one of the following: i) at least one the radiometric date occurring within ±3 kyr of the chronozones; ii) correlated with an adjacent Level 1 core, using bio- or δ^{18}O stratigraphic data. Biostratigraphy was based mainly on the abundant *G. inflata* and *N. incompta*, as both have distinct Late Pleistocene profiles in the Mediterranean (Ruddiman and McIntyre, 1981; Margreth *et al.*, 2011).

- *Level 3:* Chronological control was based on: i) at least one radiometric date (> 3 kyr) within the core dataset; ii) correlated with an adjacent Level 2 core, using bio- or δ^{18}O stratigraphic data; iii) a dated tephra layer without reported uncertainties.

- *Level 4:* Datasets with no radiometric dates but were chronologically constrained using: i) stratigraphic markers (e.g. Sapropel 1 start and end dates of ~6-9 kyr); ii) bio- or δ^{18}O stratigraphic correlation to a further removed Level 1 core.

The AQ level and number of samples per core are listed in Appendix 1 and displayed in Figure 5.2.
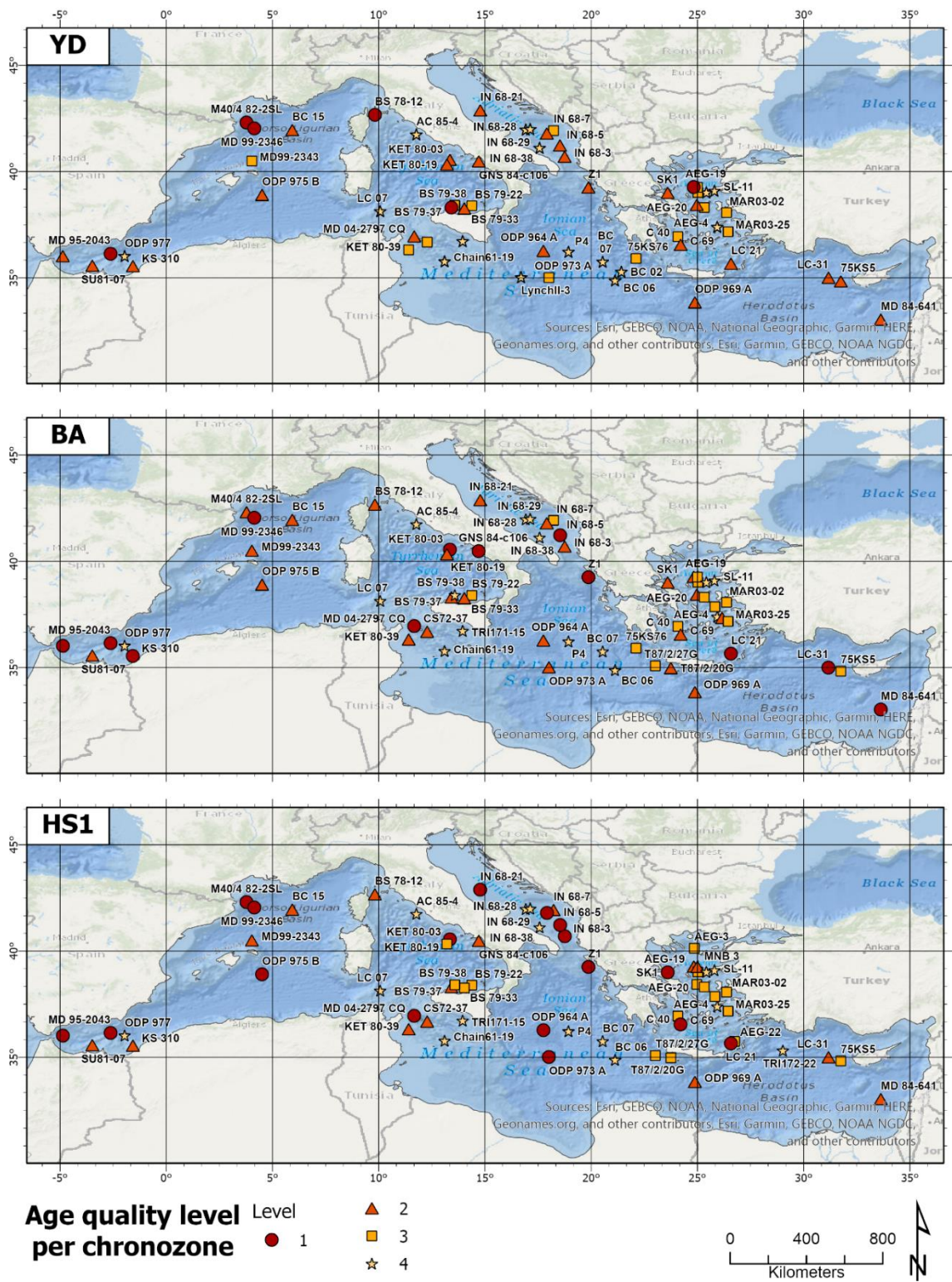
Figure 5.2: Age quality scores for cores collated for the Late Pleistocene datasets.

5.1.3.2 Age models

Revised age models were generated for all cores, where possible. For a limited number of cores, the investigators did not report sample depths or the original ^{14}C AMS dates with their errors, therefore the original age model was retained with a reduced AQ value (see Appendix 1 and Appendix 2). Most original chronologies were based on linear interpolation, which assumes that changes in sedimentation rates only occur only at the depth of the control points used. However, in recent years more rigorous age modelling software such Bacon, Bchron, Clam and OxCal have been developed, which provide more realistic accumulation curves (Telford *et al.*, 2004; Blaauw, 2010a, b). The non-Bayesian, 'classical' age depth modelling software Clam v.2.2 software (run in the program "R") was selected to generate the revised age models, as in many instances the number of control points per core was less than 4, therefore unsuitable for more sophisticated Bayesian age-modelling curves (Blaauw, 2010a, b). For those cores with four or more control points, a 'classical' smooth weighted spline interpolation (smooth: 0.3), reported with 95% confidence intervals was used, while those with less than four control points or those reported without analytical errors, a linear interpolation between neighbouring samples, with 95% confidence intervals were generated (Appendix 1) (Blaauw, 2010a, b).

The revision of age models allowed for direct comparison between datasets, especially for those cores with recalibrated ^{14}C AMS dates were problematic "tuned" control points were removed (Giesecke *et al.*, 2014; Flantua *et al.*, 2016; Alberico *et al.*, 2017). It should be noted that these revised age models are not designed to replace the original chronology, as the authors' original interpretation of the chronology will have been informed by their in-depth understanding of the local depositional environment (Flantua *et al.*, 2016).

5.1.4 Spatial analysis

For each chronozone, a number of variables were mapped within the Mediterranean Region. For each dataset, the mean abundance of the main morphospecies were classified and mapped. To allow direct comparison with the spatial distribution of modern species, the arbitrary percentage ranges utilised by Thunell (1978) were used for the majority of species. More concise ranges were used for low abundance taxa to allow for a more meaningful display of their more limited occurrences and this change of range is noted in the legend. The mean predicted annual, summer and winter SSTs,

and seasonal SST variability for each chronozone were also displayed spatially. The ranges used by Hayes *et al.* (2005) were utilised to classify these datasets. Finally, the mean eutrophication (E-Index) and stratification (S-Index) indices values were also mapped for each core. These palaeoenvironmental proxies are discussed in further detail below (see section 5.3.3 Palaeoenvironmental proxies). This data was presented as classified data points.

In addition, an interpolated surface was created for each variable and classified using the same ranges as the data points. Spatial interpolation is a common technique used to generate a continuous surface between disparate points within a region (Mallick *et al.*, 2014; Kusuma *et al.*, 2018). There are a number of methods available, such as Inverse Distance Weighted (IDW), natural/spatial neighbour, spline and kriging (Kusuma *et al.*, 2018). A number of interpolation methods, such as IDW and spatial neighbour, were tested then discounted due to the limitations caused by the uneven distribution of data points, the inability to either extend the interpolation beyond the extent of the data points, or constrain the interpolation with the Mediterranean coastline. Clearly the physical geography of the Mediterranean region has a direct bearing on the spatial distribution of species and other environmental parameters, i.e. data points from cores taken from different sub-basins (e.g. Tyrrhenian and Adriatic Seas), should not have direct influence on the interpolation on the other side of the Italian peninsula. Therefore, a minimum curvature, regularized spline interpolation was used (i.e. the "Spline with barriers" tool in Esri ArcPro v.2.5.2) (Briggs, 1974; Zoraster, 2003). This method creates a surface that passes through the data points, but can extend beyond the limit of the data points to create a smooth surface (Figure 5.3). In addition, it had the added benefit to allowing the interpolation to extend to, and be constrained by, the coastline. A similar analysis method was used by Thomopoulos *et al.* (2010) to display the spatial distribution of specific taxa and SST variability every 1 kyr over the past 18 kyr in the Mediterranean Sea.
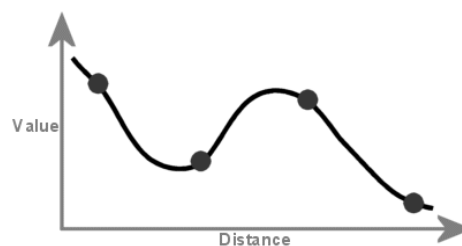
Figure 5.3: Spline interpolation. The surface bends through the data points, which allows the surface to exceed the range of the dataset (GIS Resources, 2020).

There are a number of caveats with these interpolations to be aware of. It is clear from Figure 5.1 that the spatial distribution of cores collated for the three chronozones is not homogeneous across the Mediterranean Sea. The eastern basin is better represented in the dataset with 47 cores, in comparison to 20 cores in the western Mediterranean. In addition, there are a number of areas, such as along the North African coast (in particularly off the north/north-east of Tunisia and Libya coast) where no cores exist, or they did not meet the data requirements for this study. The results of the interpolation in these regions should be viewed with caution. In areas that have few or no data points, the spline interpolation can overshoot the extent of neighbouring data points and introduce artefacts in the interpolation, which can suggest enhanced or reduced values. Finally, the AQ scores of the core datasets for each chronozone should be kept in mind, as minor anomalies in the interpolation may be due to a lower quality core of the dataset and should be treated with caution. For all maps, AQ is represented by variations in symbol size and is noted in the legends. The basemap is the Esri World Ocean Base (Esri, 2014).

5.2   M40/4 82-2SL

M40/4 82-2SL was a known high resolution core from the Gulf of Lion, as sections from it that spanned the mid to late Holocene, were utilised as part of a study on the application of *G. truncatulinoides* sinistral and dextral as biostratigraphic markers in the western Mediterranean Sea (Broggy, 2011). Palaeoenvironmental analysis of the mid to late Holocene identified three phases of climate variability, as well as a series of cool periods that could be linked with North Atlantic cooling events (Broggy, 2011). However, the older sections of this core were unprocessed and unanalysed. Therefore, the potential of this core to answer the research question of how the Gulf of Lion was impacted by deglacial extreme events was clear.

The 532 cm deep-sea sediment gravity core M40/4 82-2SL (42.31˚N, 3.78˚E, water depth 1079m) was taken during the RV Meteor cruise (M40/4) to the Mediterranean Sea in Jan-Feb 1998 (Figure 5.4). The core was located in the Gulf of Lion, and was part of a E-W transect of gravity cores intended to aid reconstruction of sapropels in the eastern basin and Mediterranean Sea palaeoenvironments from the Last Glacial Maximum (LGM) to the present (Emeis *et al.*, 1999; Hieke *et al.*, 1999). The lithology was predominantly an olive grey homogenous nannofossil/foraminiferal ooze, with minor bioturbation observed between 70-80 cm, periodic silt lamination from 470-360 cm and

no signs of turbidites (Figure 5.5) (Hieke *et al.*, 1999).
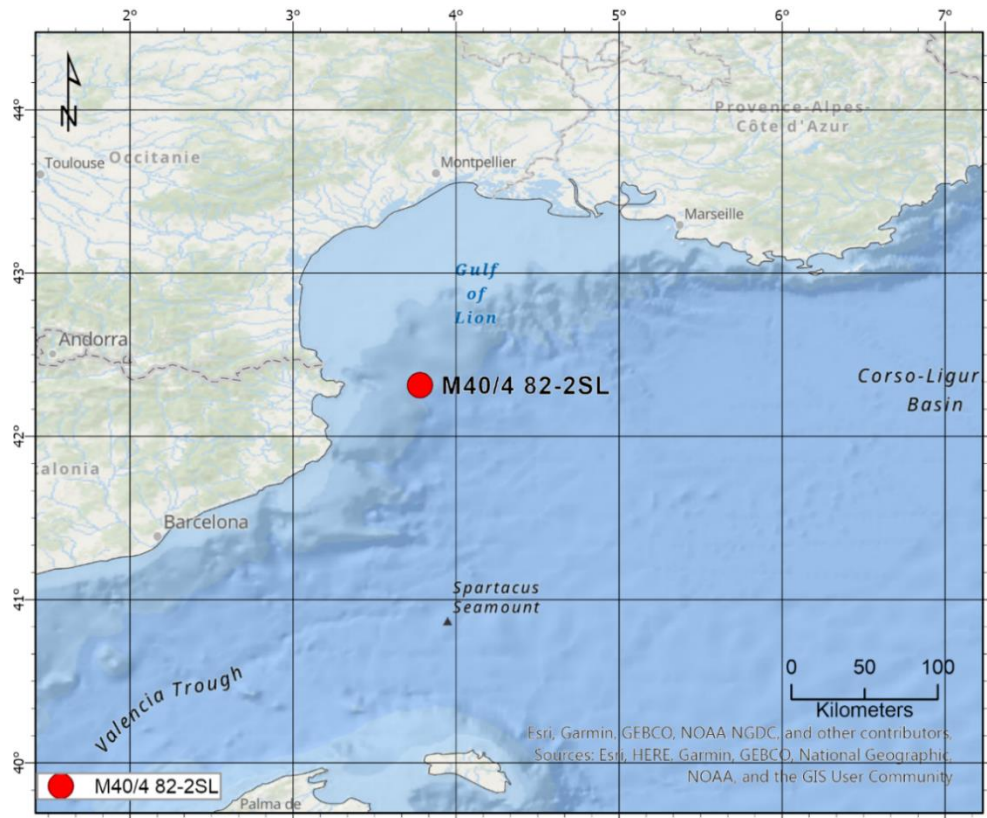
Figure 5.4: Location of M40/4 82-2SL in the Gulf of Lion, taken during the RV Meteor cruise (M40/4) to the NW Mediterranean Sea in Jan-Feb 1998.

5.2.1   Laboratory procedures

Onboard, the gravity core was cut into 1 m sections (1 [oldest] to 6 [youngest]) and subsequently a U channel sub-sample was taken by Dr. Cloke-Hayes in Tubingen, Germany (Figure 5.5). The U channel was sliced into 1 cm samples and processed using the standard micropaleontological preparation techniques (e.g. de Vernal *et al.* (2010)). All samples were placed into clean labelled weighed petri dishes and oven-dried at <40°C for 24 hours. A low oven temperature is important to prevent cracking of the foraminifera tests, as well as stopping clay sediments becoming baked and difficult to disaggregate (Thomas and Murney, 1985). Once dried, each sample was weighed to obtain a total dry weight. Samples were soaked in deionised water to disaggregate the sediment, before being wet sieved through a 63 µm mesh sieve. Deionised water is used to ensure that samples are not contaminated by carbonates and other minerals, which may impact their use for geochemical analysis. The >63 µm residue was placed in a weighed petri dish, oven-dried at <40°C for 24 hours, before being weighed to obtain the >63µm dry weight. Finally, each sample was dry sieved through a 150 µm mesh sieve and stored in glass bottles as separate size fractions (<150 µm and >150 µm).
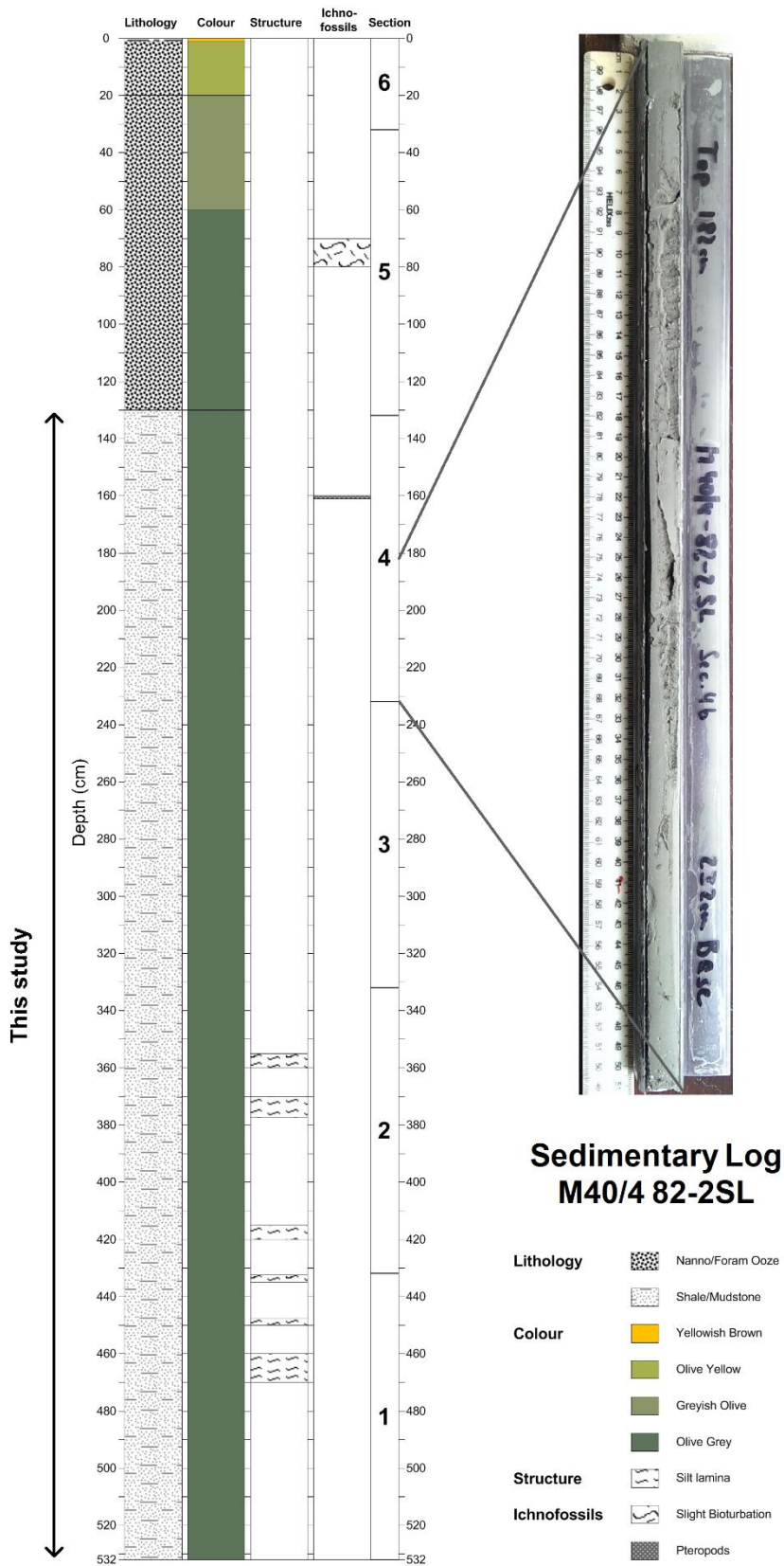
Figure 5.5: Sedimentary log of M40/4 82-2SL, including a photograph of U channel Section 4b (182 to 232 cm). Log redrawn from Hieke et al. (1999).

There is much debate regarding the recommended sieve size fraction used for palaeoenvironmental research (Peeters *et al.*, 1999; Al-Sabouni *et al.*, 2007; Kučera, 2007; Di Donato *et al.*, 2011; Di Donato *et al.*, 2015). Many researchers now use 63, 90, 106 or 125 µm size fractions to ensure capture of smaller cooler-water species (such as *T. quinqueloba*) and achieve maximum diversity (Buccheri *et al.*, 2002; Lirer *et al.*, 2013; Morabito *et al.*, 2014; Kuhlmann *et al.*, 2015; Capotondi *et al.*, 2016); though this smaller fraction also includes difficult to identify juvenile forms.

For many of the large-scale global palaeoclimatic studies which use transfer functions, such as Imbrie and Kipp (1971); CLIMAP Project Members (1976); Ortiz and Mix (1997), it was necessary to establish default procedures and 150 µm was adopted as the standard sieve-size for planktonic foraminifera. Furthermore, the calibration dataset for the ANN analysis was based on MARGO protocols, which used datasets of >150 µm counts (see section: 5.3.1 Sea surface temperature reconstruction) (Hayes *et al.*, 2005; Kučera *et al.*, 2005a; Kučera *et al.*, 2005b). Therefore, the >150 µm size fraction was employed in this study. This allows for direct comparison of results to key studies from the Mediterranean, such as modern planktonic foraminifera distribution (Thunell, 1978; Pujol and Vergnaud Grazzini, 1995; Rigual-Hernández *et al.*, 2012) and palaeoenvironmental studies (Rohling *et al.*, 1998; Cacho *et al.*, 1999; Geraga *et al.*, 2000; Pérez-Folgado *et al.*, 2003; Melki, 2011; İşler *et al.*, 2016a), all of which used the >150 µm size fraction.

For this study, sections 1 to 4 (132 to 519 cm) of M40/4 82-2SL were used; sections 5 to 6 (0 to 131 cm) were analysed as part of research undertaken by Broggy (2011). A total of 200 >150 µm samples were picked for the full planktonic assemblage and counted. The sample interval was every 2 cm, except for specific sections that were targeted as ^{14}C AMS control points. Here, if necessary, samples every 1 cm were picked and counted to achieve the minimum sample weight needed to be dated – see Chronological framework section. A minimum of N>300 specimens were picked to achieve a statistically representative population, calculated to be an estimated <8% deviation from the total population, or within a 95% confidence interval (Phleger, 1960; Peeters *et al.*, 1999; Al-Sabouni *et al.*, 2007). If necessary, the sample was split with a micro-splitter to obtain a representative aliquot of at least N>300 specimens, to achieve a quantitative census count. All planktonic foraminiferal data is presented as a percentage of total population.

Morphospecies taxonomy was based on Hemleben *et al.* (1989) and verified with Schiebel and Hemleben (2017). Specific morphotypes such as *G. ruber* white, *G. ruber* pink, *G. siphonifera*, *G. calida*, *G. truncatulinoides* dextral and *G. truncatulinoides* sinistral were counted separately. However, Thunell (1978) grouped these morphospecies together and this data was used for the ANN calibration dataset (Hayes *et al.*, 2005). Therefore, for the ANN analysis only, these morphospecies counts were grouped together to form *G. ruber* (total), *G. siphonifera* + *G. calida*, and *G. truncatulinoides* (total). In addition, although counted separately, *G. siphonifera*, *H. pelagica*, *G. rubescens*, *O. universa*, *B. digitata*, *G. tenella* and *G. sacculifer* have been grouped together to form the SPRUDTS group for display purposes and as an indicator of warm subtropical water (see Appendix 3) (Rohling *et al.*, 1993).

5.2.2 Chronological framework

The chronology of M40/4 82-2SL was established using nine accelerator mass spectroscopy (AMS) radiocarbon control points, including five ^{14}C AMS dates from 0-131 cm by Broggy (2011) and four ^{14}C AMS dates obtained during the present study from 132-519 cm (Table 5.3). A minimum weight of >10mg per sample was needed for each ^{14}C AMS control point. Therefore, due to the small size of the U channel samples, the ^{14}C AMS control points ranged from 1 cm to 3 cm in width in order to achieve the minimum weight required and were composed of a mixed planktonic foraminiferal assemblage.

Lab. ID	Depth (cm)	Radiocarbon age (yr BP)	Calibrated age range (2δ) Lower | Upper		Calendar age* (cal yr BP)	Sed. Rate (cm/kyr)	Source
231534[†]	0 - 3	820 ± 40	269	524	404	15.21	1
231535[†]	24 - 25	3980 ± 40	3694	4140	3923	15.38	1
231536[†]	36 - 39	4620 ± 40	4534	4976	4776	16.05	1
231537[†]	42 - 45	4770 ± 40	4809	5234	4979	16.85	1
231538[†]	68 - 69	5980 ± 40	6190	6528	6352	18.6	1
458586[†]	180 - 182	7820 ± 30	8061	8380	8241	50.55	2
UBA - 33948[‡]	352 - 354	10459 ± 44	11226	11860	11526	53.24	2
UBA - 33949[‡]	422 - 424	11347 ± 53	12614	12962	12775	55.51	2
UBA - 33950[‡]	502 - 504	13098 ± 56	14546	15315	15013	36.31	2

*Table 5.3: Results of ^{14}C radiocarbon dates on a mixed planktonic foraminifera assemblage for M40/4 82-2SL. *Calendar age is the Median Probability. Laboratory: [†]Beta Analytic Ltd, London BioScience Innovation Centre; [‡]14CHRONO Centre, Queen's University Belfast; Source: (1) Broggy (2011) and (2) this study.*
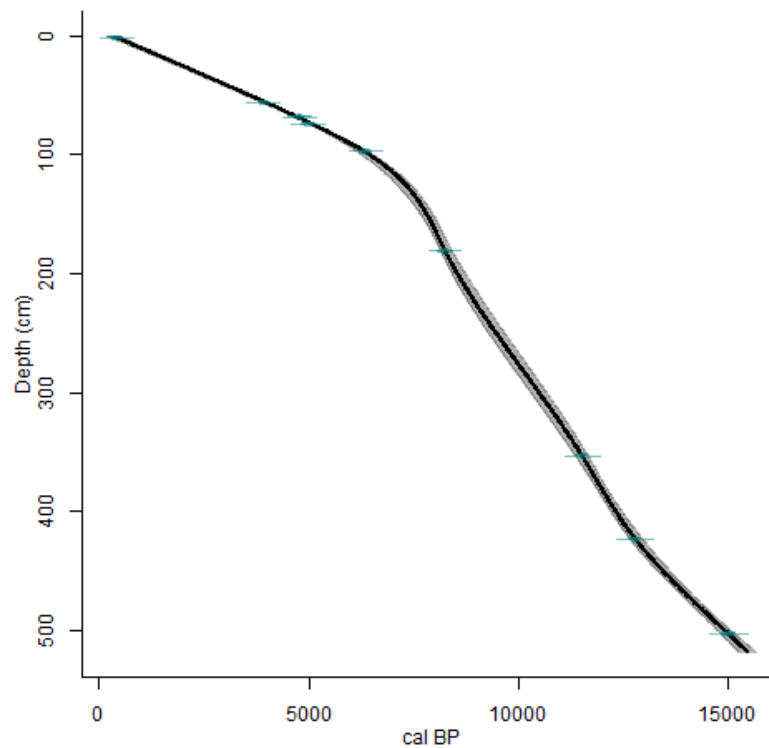
Figure 5.6: Age-depth model created using Clam v.2.2 (Blaauw, 2010a, b). This is a non-Bayesian, 'classical' smooth weighted spline interpolation (smooth: 0.3; number of iterations: 10,000; goodness-of-fit: 6.24), with reported 95% confidence intervals. Calibrated age distributions are in blue; the confidence ranges are in transparent grey and the weighted average 'best fit' line of the age-depth model derived ages is in black.

Calendar ages (reported as cal yr BP) for all ^{14}C AMS dates were calibrated using Calib v.7.0.2, applying the Marine13 calibration curve (surface water marine reservoir age (R(t)) = 405 ± 22 ^{14}C yrs) (Reimer *et al.*, 2013; Stuiver *et al.*, 2017). The average R(t) of the Mediterranean Sea was estimated to be 400 ± 16yrs BP (Siani *et al.*, 2000; Reimer and McCormac, 2002; Faivre *et al.*, 2015). In addition, the local reservoir correction (ΔR) (i.e. the regional offset from the global R(t)) across the Mediterranean Sea was deemed to be statistically homogeneous, with an average of 58 ± 15 ^{14}C yrs when calibrated with the 1998 marine calibration dataset (Reimer and McCormac, 2002; Faivre *et al.*, 2015). Using the Marine Reservoir Correction Database (http://calib.org/marine/, accessed 31/03/18), the ΔR of 19 samples located within the western Mediterranean (original data from Siani *et al.* (2000); Reimer and McCormac (2002)) was calculated to be 46 ± 68 ^{14}C yrs (compared to the 2004 marine calibration dataset), and this ΔR was applied to the Calib ^{14}C AMS date calibration. It should be noted, the ΔR from the LGM to the Holocene is not constant, especially during HS1 and the BA, when the R(t) has been estimated to have increased up to ~400 yrs (Siani *et al.*, 2001). As the ΔR has not yet been fully constrained for these periods, the ΔR value of 46 ± 68 ^{14}C yrs has been applied to all ^{14}C AMS dates for M40/4 82-2SL (Casford *et al.*, 2007; Fletcher *et al.*, 2010).

The age model was generated in Clam v.2.2 software (run in the program "R") (Blaauw, 2010a, b; R Core Team, 2017). It is based on a non-Bayesian, 'classical' smooth weighted spline interpolation (smooth: 0.3) and reported with the 95% confidence intervals (Blaauw, 2010a, b) (Figure 5.6). Sedimentation rates (cm/kyr) were calculated as an average of the interpolated sedimentation rates between ^{14}C AMS control points.

5.3   Methods

5.3.1   Sea surface temperature reconstruction

To enable past sea surface temperature (SST) reconstructions for global palaeoclimate studies, e.g. the 'Climate: long range investigation, mapping and prediction' (CLIMAP) Project (CLIMAP Project Members, 1976, 1981), transfer functions such as the Imbrie-Kipp Transfer Function were first developed to quantify the relationship of fossil planktonic foraminifera assemblages with past SST (Imbrie and Kipp, 1971). Additional methods have been developed over the last 50 years, including the Modern Analog Technique (MAT), MAT with Similarity Index (SIMMAX), Revised Analog Method (RAM) and Artificial Neural Networks (ANN) (Hutson, 1980; Prell, 1985; Pflaumann *et al.*, 1996; Kallel *et al.*, 1997a; Malmgren and Nordlund, 1997; Waelbroeck *et al.*, 1998; Malmgren *et al.*, 2001; Kučera and Darling, 2002; Hayes *et al.*, 2005; Kučera *et al.*, 2005b).

Neural networks were first developed in the 1940s and they aimed to mimic the basic functionality of the biological neuron (Wasserman, 1989; Malmgren and Nordlund, 1997). In essence, Artificial Neural Networks (ANN) are a self-learning computer system that can establish the complex relationship between a set of input variables to determine an output vector (Wasserman, 1989; Malmgren and Nordlund, 1997). To do this, the backpropagation neural network uses a system of input vectors (e.g. assemblage data) that are attached to a series of layers of interconnected neurons, which have a weighted connection to each neuron of the subsequent layer. The output layer contains the parameters of the network that give the lowest prediction error for the target vector; in this case, annual, summer (July to September) and winter (January to March) SST estimates (Hayes *et al.*, 2005; Kučera *et al.*, 2005a). In comparison to other methods such as MAT, ANN is not as depend on the size of the calibration dataset and permits extrapolation outside the range of parameter values in the calibration data set (Malmgren and Nordlund, 1997; Kučera *et al.*, 2005a). However, the main disadvantage

of ANN is that it is more difficult to determine the contribution of different variables on the resulting predictions.

As part of the 'Multiproxy approach for the reconstruction of the glacial ocean surface' (MARGO) project, Hayes *et al.* (2005) used ANNs to reconstruct LGM SST. To train the ANN, a calibration dataset was created to learn the relationships between recent planktonic foraminifera assemblages from core-tops and modern SST (Hayes *et al.*, 2005; Kučera *et al.*, 2005a; Kučera *et al.*, 2005b). This dataset comprises of 23 planktonic foraminifera species from 274 samples taken from recent core-top samples from the Mediterranean Sea (analogous of an interglacial/interstadial assemblage) and the North Atlantic (representing a glacial/stadial assemblage). To assess the accuracy of the calibration dataset results against recently recorded SST, Hayes *et al.* (2005) compared the ANN results against the annual SST from the World Ocean Atlas v.2 "NODC_WOA98" dataset (10m depth) (WOA, 1998; Kučera *et al.*, 2005a). The root mean square error of prediction (RMSEP) was calculated as the square root of the sum of the squared differences between the observed and predicted values of each sample in a test subset, divided by the number of samples in this subset (Hayes *et al.*, 2005; Kučera *et al.*, 2005b). This comparison established that ANN can successfully estimate SST, with average error rates ranging from 0.5°C in winter months, to 1.1°C during the summer (Hayes *et al.*, 2005). The more successful winter SST prediction was attributed to the reduced variability of species (e.g. dominance of *N. pachyderma*) in colder waters of the calibration dataset (Hayes *et al.*, 2005; Kučera *et al.*, 2005b). In contrast, the higher prediction error rates for summer ANN predictions were attributed to a combination of the potential effects of "lumping" of the greater number of morphospecies in warmer waters, taxonomic inconsistences between the different sources of calibration datasets and insufficient core-top data in the calibration dataset for specific areas (Hayes *et al.*, 2005; Kučera *et al.*, 2005b). More recently, the effects of taxonomic inconsistences between researchers on transfer functions was tested using ANN (Al-Sabouni *et al.*, 2018). It was found that although there was significant taxonomic variation between researchers (~77%), the deviation of the resulting ANN SST predictions was less than the prediction error (<1°C) (Al-Sabouni *et al.*, 2018).

It should be noted that relying solely on transfer functions that use species abundance and distribution to reconstruct specific SSTs can be problematic (Hessler *et al.*, 2014; Jonkers and Kučera, 2019). As generating or collating other independent proxies was outside the scope of these research project, predicted SSTs are discussed in relation to

the ecological preferences and biogeographical patterns of the morphospecies to infer the general palaeoecological conditions that prevailed during these chronozones.

For this study, ANN analysis was completed using the NeuroGenetic Optimizer (NGO) (v2.6) program. The NGO software first randomly split the data (x 10 times) into a larger training set (80%) and a smaller test subset (20%), then ran the analysis for each partition. The best network from each of the 10 partitions for the separate annual, summer and winter analysis were retained and the average SST predictions (+1SD) were calculated for each.

5.3.2 Spectral analysis

Spectral analysis is used in palaeoenvironmental analysis to help decipher and understand the physical processes which generate the variability recorded in a time series. Periodicities in SSTs variation was determined using a bias-corrected REDFIT power spectrum analysis in the statistical software PAST v4.02, which was specifically designed for unevenly spaced time series data (Hammer *et al.*, 2001; Schulz and Mudelsee, 2002). REDFIT attempts to fit the spectrum to a red-noise model and uses a first-order autoregressive process (AR(1)) to explain this red noise signature, in order to estimate the confidence levels at which periodicity can be considered significant (above the 90% confidence interval).

5.3.3 Palaeoenvironmental proxies

In the absence of independent variables (e.g. [13]C), using the interpretation of the ecological variability of the morphospecies has been used as a proxy for palaeoenvironmental parameters (Sbaffi *et al.*, 2004; Kontakiotis, 2016). A range of established palaeoenvironmental proxies were utilised to determine what factors may have influenced the distribution of planktonic foraminifera, such as food availability, food type, sea surface productivity and the hydrology in the Mediterranean Sea during the Late Pleistocene and Early Holocene. Hydrological conditions were determined using eutrophication (E-Index), deep-mixing (DM-index) and different stratification (S-Index) indices. While it is acknowledged that they are not as robust as independent quantitative methods, but as indicators of environmental conditions, they provide an insight for the interpretation of the ANN and PCA analysis.

The E-Index is calculated from a comparison of eutrophic and oligotrophic species

using the formula: e / (e + o) * 100, where *e* represents the sum of eutrophic species (*N. incompta* dextral and sinistral, *G. bulloides*, *T. quinqueloba*, *G. inflata*), and *o* signifies oligotrophic species (*G. ruber* white and pink, *G. rubescens*, *G. sacculifer*, *O. universa*, *G. siphonifera*) (Kontakiotis, 2016). As the opportunistic species *G. bulloides* thrives in episodes of heightened productivity and food availability driven by upwelling and deep mixing, the total percentage abundance of *G. bulloides* has commonly been used as a proxy for upwelling (U-Index) (Thiede, 1975). However, as Gulf of Lion is an area of deep water formation rather than true upwelling, it has been termed a "deep-mixing" index (DM-Index) for M40/4 82-2SL. The ratio between *G. bulloides*/*G. ruber* has been used as a proxy for summer water stratification when dominated by *G. ruber* (S-Index) (Sbaffi *et al.*, 2004; Kontakiotis, 2016). This method has been used to determine the stratification across the Mediterranean Sea during HS1, BA and YD chronozones. However, as *G. ruber* is absent for extensive periods in the Late Pleistocene in the Gulf of Lion, it was determined that that the *G. bulloides*/*G. ruber* ratio would not be suitable to determine stratification variability in M40/4 82-2SL. *G. inflata* is one of the main eutrophic species present throughout much of the timeframe of this study (except HS1). Its presence in the Western Mediterranean is closely linked to the annual winter-spring bloom in seasonally stratified stable waters (Giraudeau, 1993; Bárcena *et al.*, 2004; Lončarić *et al.*, 2007; Hernández-Almeida *et al.*, 2011). Therefore, for M40/4 82-2SL the percentage abundance of *G. inflata* was used as a seasonal (winter) stratification indicator.

5.3.4 Principal component analysis

Principal Component Analysis (PCA) is an ordination statistical method used to reduce the dimensionality of multivariate data to determine the variables or principal components (PC) that govern variance of that dataset (Dale and Dale, 2002; McKillup and Dyar, 2010; Jolliffe and Cadima, 2016). The method assumes that data such as planktonic foraminifera abundance can provide an insight to the ecological factors that determine the distribution of that population in nature (Dale and Dale, 2002). PCA identifies closely correlated variables and creates a series of new components (listed in decreasing order of importance) that illustrate the differences within the sample points (McKillup and Dyar, 2010). A standardised PCA was completed on the planktonic foraminifera abundance data from M40/4 82-2SL sections 1 to 4, using PAST v.4.0 (variance-covariance matrix, bootstrap no: 1000) (Hammer *et al.*, 2001). The data comprised of all species that were >3% abundance/sample, with low abundance warm

water species *G. siphonifera*, *G. rubescens*, *O. universa*, *B. digitata*, *G. tenella* and *G. sacculifer* combined and incorporated into the dataset as the SPRUDTS group.

PCA is a robust method in reducing the complexity of multivariable data, identifying correlations between the variables (morphospecies in this instance) and quantifying their contribution to the PC. However, care must be taken with datasets that contain zero values, as this may overestimate redundancy (i.e. correlation) of variables (McKillup and Dyar, 2010). Although not ideal, for this analysis zero values were replaced with their column average (default mean value imputation setting in PAST v.4.0.) (Hammer *et al.*, 2001). With complex species abundance datasets, the main limitation of this method is deciphering the palaeoenvironmental and/or ecological variables represented by the PCs. The interpretation of these PCs is only as good as the in-depth understanding of the original data.

Chapter 6.

6 Late Pleistocene sea surface temperatures and planktonic foraminifera distribution in the Mediterranean Sea

Late Pleistocene climate signals are clearly recorded in both terrestrial and marine proxies in and around the Mediterranean Sea (Kallel *et al.*, 1997b; Bar-Matthews *et al.*, 1999; Cacho *et al.*, 2001; Cacho *et al.*, 2002; Casford *et al.*, 2002; Combourieu Nebout *et al.*, 2002; Sbaffi *et al.*, 2004; Hayes *et al.*, 2005; Moreno *et al.*, 2005; Fletcher and Sánchez Goñi, 2008; Castañeda *et al.*, 2010; Baldini *et al.*, 2015; Bazzicalupo *et al.*, 2018). However, the records are highly complex, with many contradictions and significant spatial and chronological variability across the Sea. This makes it difficult to decipher the magnitude and drivers of climate and oceanographic changes during these chronozones in the Mediterranean Sea.

LGM	Annual (°C)	Summer (°C)	Winter (°C)	Seasonality (°C)
Mediterranean Sea	14.24	17.11	12.08	5.03
Western Basin	11.80	13.98	10.29	3.69
Eastern Basin	17.10	20.80	14.19	6.61
Variability between basins	5.31	6.82	3.90	

Table 6.1: Mean predicted SSTs, using ANN and seasonality (°C) (calculated from mean summer less winter SSTs) during the LGM across the Mediterranean Sea, and separately for the western and eastern basins (Hayes et al., 2005). Variability between basins was the difference between the western and eastern mean SST.

This information is available for the LGM, where predicted mean annual SSTs were 14.24°C (Table 6.1; Figure 6.1) (Hayes *et al.*, 2005). However, this level of detail is missing for the deglacial in the Mediterranean Sea. Proxy data from individual cores provide localised SST estimates and palaeoenvironmental interpretations for their sites (Kallel *et al.*, 1997b; Rohling *et al.*, 1998; Cacho *et al.*, 1999; Cacho *et al.*, 2000; Asioli *et al.*, 2001; Sbaffi *et al.*, 2004; Essallami *et al.*, 2007; Melki *et al.*, 2009; Castañeda *et al.*, 2010; Kontakiotis, 2016; Bazzicalupo *et al.*, 2018; Cornuault *et al.*, 2018). However, there is no basin-wide consensus for annual or seasonal variations in SSTs, or a comprehensive visualisation of the variability of SSTs during the HS1, BA and YD chronozones.
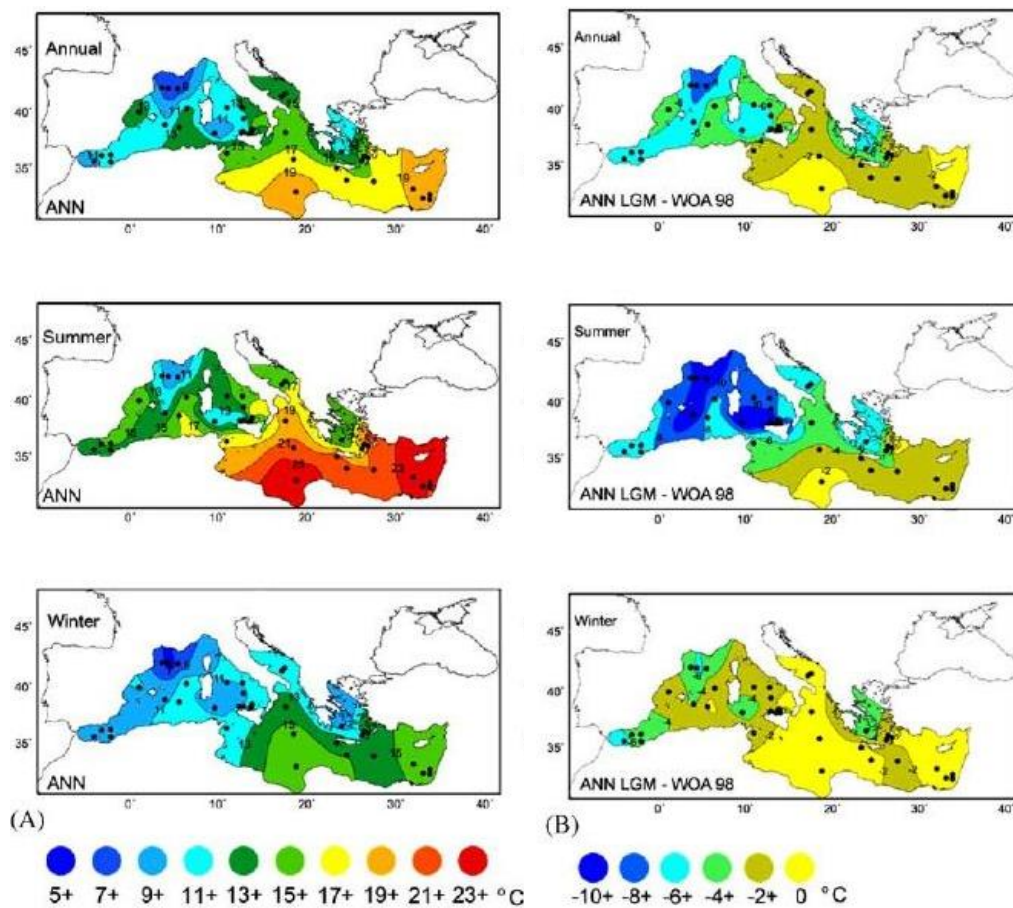
Figure 6.1: (a) Predicted annual, summer and winter SST and (b) SST anomalies during the LGM in the Mediterranean Sea, based on ANN. Taken from Hayes et al. (2005).

The only comparative study of SST reconstruction of the deglacial period was conducted by Thomopoulos *et al.* (2010). The deglacial period was divided into 12 time slices (each spanning 1 kyr), and the distribution of published SST estimates (based on $\delta^{18}O$ values) and four key planktonic foraminifera morphospecies (*G. ruber*, *G. bulloides*, *G. inflata* and *N. pachyderma*) were interpolated for the Mediterranean Sea. While this paper illustrates changing patterns over these 1 kyr time slices, there is some generalisation or dilution of the results for specific chronozones that spanned these 1 kyr time slices. For example, as the BA is only represented by the 13 kyr time slice, the rapid increase in temperatures during the early Bølling is not represented in this dataset, therefore the reported BA $\delta^{18}O$ values are cooler than expected.

Having reliable and rigorous SST predictions for these extreme events is an invaluable resource for marine researchers working in the Mediterranean region. It provides researchers with independent SST predictions to compare their research with, and palaeoenvironmental interpretations for these extreme events placing their work in context to the wider Mediterranean region. In addition, it is a valuable resource for

122

climate scientists, to test the main mechanisms of deglacial climate change and determine to what extent they impacted this transitional zone.

Fossil assemblages are not only useful in predicting past SSTs, they are ideal proxies for reconstructing sea surface palaeoenvironmental conditions and factors that controlled them. As outlined in Chapter 3, the distribution and abundance of planktonic foraminifera are governed by a range of parameters, mainly SST, as well as hydrographic factors, such as depth preferences, water column structure and salinity; and trophic conditions, such as chlorophyll-α concentration, nutrients, prey availability and quality (Watkins *et al.*, 1996; Kučera, 2007; Schiebel and Hemleben, 2017). The distribution and abundance of extant planktonic foraminifera across the Mediterranean Sea have been investigated using core-top sediments, sediment traps and plankton tow profiles (Cifelli, 1974; Thunell, 1978; Pujol and Vergnaud Grazzini, 1995; Bárcena *et al.*, 2004; Hernández-Almeida *et al.*, 2011; Rigual-Hernández *et al.*, 2012; Mallo *et al.*, 2017; Avnaim-Katav *et al.*, 2020). In the Mediterranean, seasonal food availability and hydrological structure of the water column, rather than SST, were determined to be the main controls for the modern distribution and flux of planktonic foraminifera (Pujol and Vergnaud Grazzini, 1995; Bárcena *et al.*, 2004; Hernández-Almeida *et al.*, 2011; Rigual-Hernández *et al.*, 2012). The mapped modern distribution of 16 key morphospecies by Thunell (1978) is a useful comparison to test differences during the deglacial (Figure 6.2). The only comparison are the interpolated distributions of the 4 morphospecies that were mapped during the deglacial by Thomopoulos *et al.* (2010).

However, it should be kept in mind that populations in sediments are a decadal or centennial average of the annual flux at the site, e.g. strong winter-spring bloom in the western basin or a bimodal winter and smaller summer bloom in the far eastern basin (Bárcena *et al.*, 2004; Hernández-Almeida *et al.*, 2011; Rigual-Hernández *et al.*, 2012; Avnaim-Katav *et al.*, 2020). In addition, depending on the species, peaks in flux can occur earlier/later in warmer/cooler periods or in different hydrological conditions, which may impact of the palaeoenvironmental interpretation of fossil communities (Jonkers and Kučera, 2015).
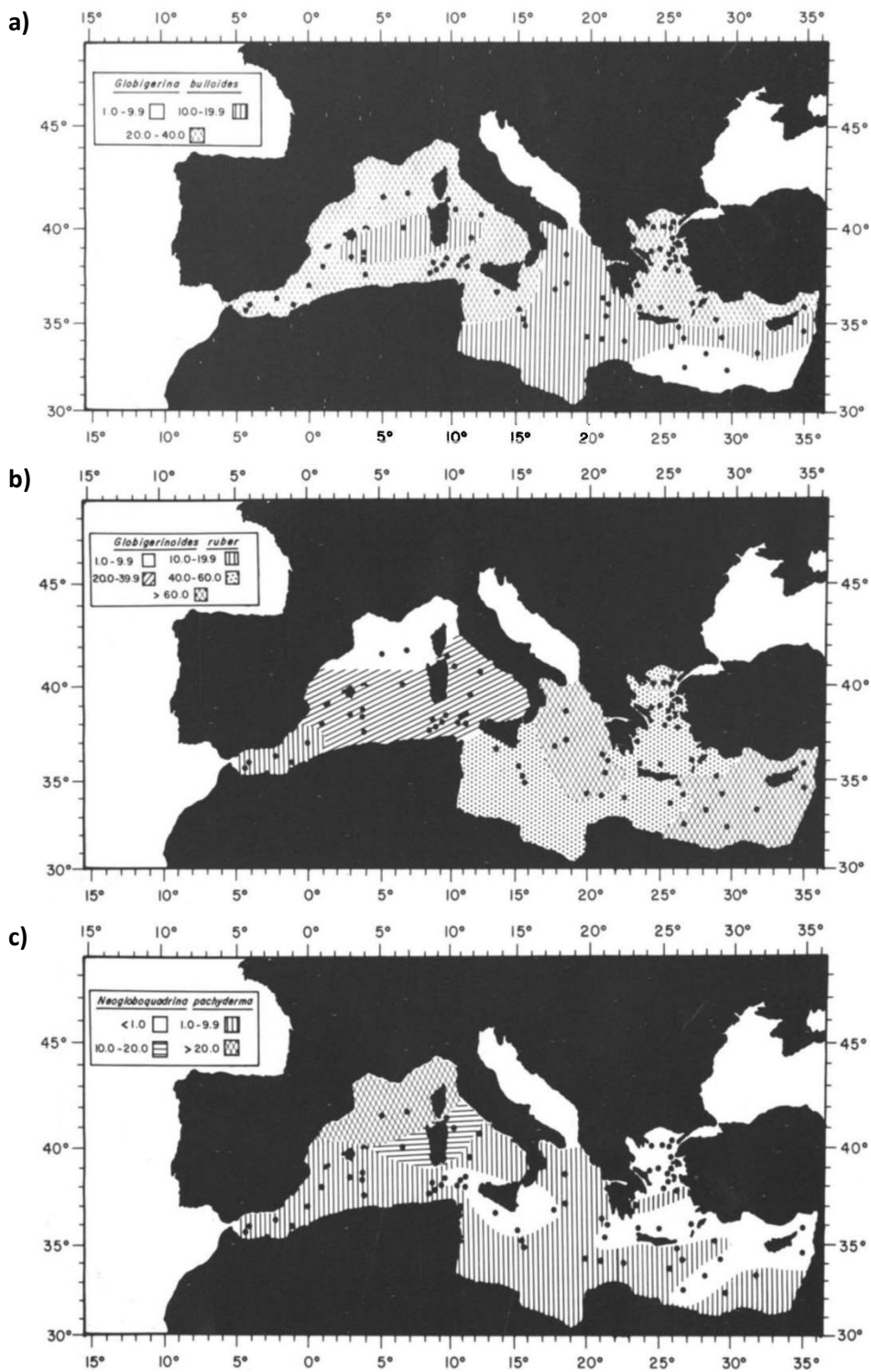
Figure 6.2: Distribution of a) G. bulloides, b) G. ruber and c) N. pachyderma (sinistral and dextral), 3 of the 16 morphospecies mapped from modern surface sediments in the Mediterranean Sea (Thunell, 1978).

124

To enhance our understanding of this time period and assess the impact on the hydrological systems in the Mediterranean Sea, this chapter addresses the following two fundamental research questions:

1. To what extent did sea surface temperatures (SSTs) change during these periods of rapid climate change during the deglaciation across the Mediterranean Sea? The reconstruction of SSTs will allow an examination of the magnitude of these events, drawing on SST comparisons from the Last Glacial Maximum and the modern day. In addition, SST reconstructions will also provide a spatial context addressing questions such as, how did SSTs differ on a basin wide scale? Was the western basin always colder than the eastern basin? How did conditions in the Adriatic and Aegean Seas vary in relation to the wider eastern basin during these chronozones? It is anticipated that the answers to these questions will provide an insight into the potential drivers of SST variability in the Mediterranean Sea during the period of deglaciation.

2. To what extent did planktonic foraminifera respond to climatic variability during the deglacial? What governed their response? Was it the variations in SSTs? Or was their distribution and abundance impacted by other hydrological parameters?

To answer these two research questions, the results of planktonic foraminifera count data collated from 67 cores spanning the Mediterranean Sea, for the HS1, BA and YD chronozones are presented. Annual, summer and winter SSTs were reconstructed using ANN, utilising the methods outlined in Hayes *et al.* (2005). Interpretation of the reconstructed SSTs and distribution of planktonic foraminifera during the HS1, BA and YD will be discussed in relation to the potential mechanisms of climate change experienced in the region during the deglacial period.

6.1 Results

6.1.1 Planktonic foraminifera distribution

The nine most abundant morphospecies/genera were mapped to illustrate their abundances and distribution across the Mediterranean during periods of extreme climate change following the LGM (Table 6.2). In addition, maps of lower abundance SPRUDTS group morphospecies that are mentioned in the text, are provided in

Appendix 2.

Species	HS1	BA	YD
Neogloboquadrina (total)	37.80	33.58	31.46
G. bulloides	20.50	20.14	18.52
G. ruber **plexus**	10.73	16.90	17.00
G. glutinata	9.74	8.53	11.87
T. quinqueloba	11.91	6.27	7.80
G. scitula	6.31	3.02	1.52
G. inflata	1.74	7.69	6.89
SPRUDTS	0.80	1.47	1.56
G. sacculifer[†]	0.52	0.27	0.59
G. siphonifera[†]	0.14	0.42	0.29
O. universa[†]	0.11	0.86	0.52
G. truncatulinoides **(total)**	0.28	1.03	1.02

Table 6.2: Mean abundance (%) of the main planktonic foraminifera during HS1, BA and YD. Neogloboquadrina (total) includes N. pachyderma sinistral, N. pachyderma dextral and/or N. incompta; "P/D intergrades" and N. dutertrei; G. ruber plexus includes G. ruber white, G. ruber pink and G. elongatus; G. truncatulinoides (total) contains both dextral and sinistral species; †Maps of the distribution of these low abundance SPRUDTS species are in Appendix 2.

6.1.1.1 *Neogloboquadrina species*
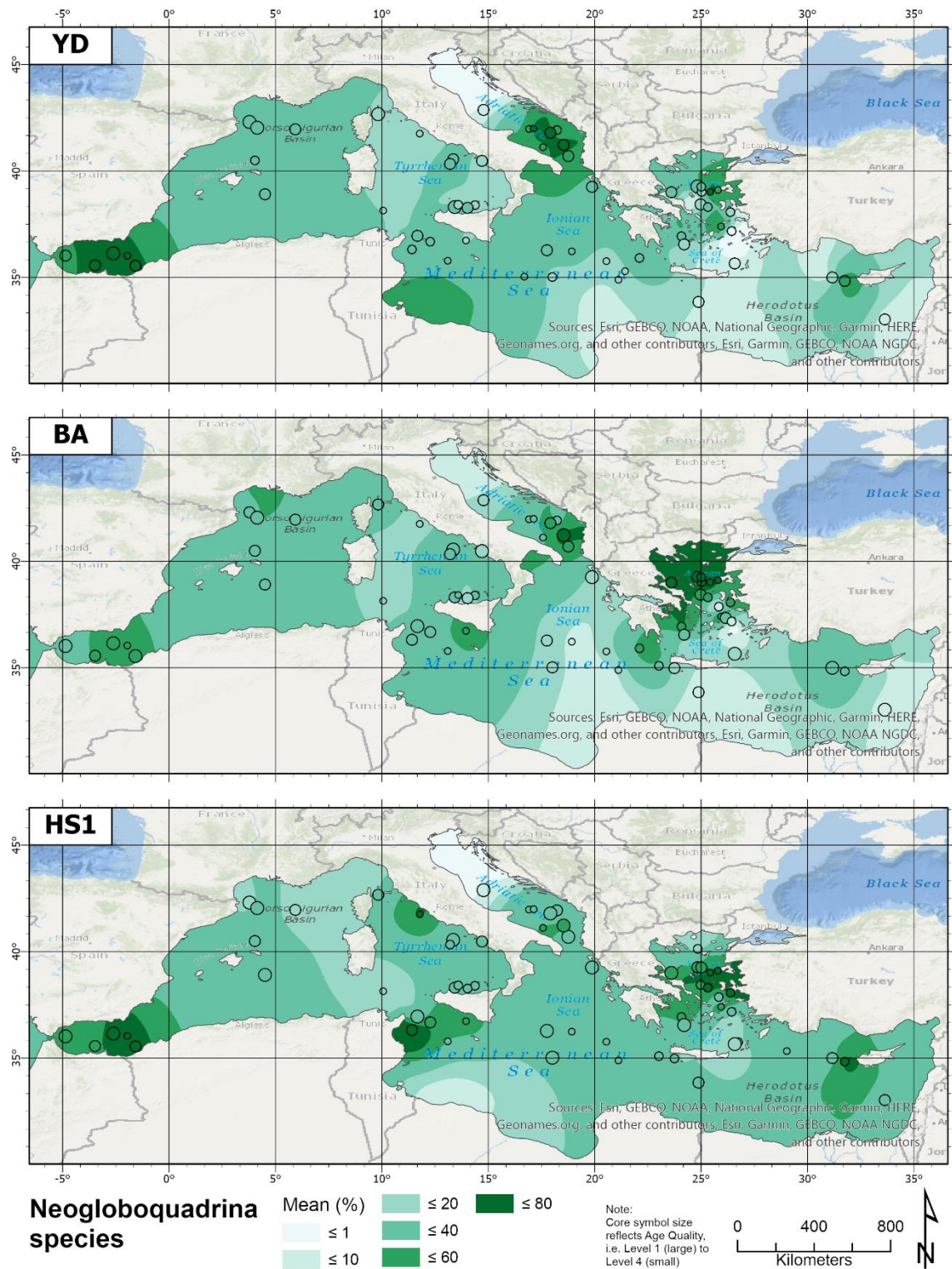
Figure 6.3: Spatial distribution of Neogloboquadrina species (%) during HS1, BA and YD. Neogloboquadrina species includes N. pachyderma sinistral, N. pachyderma dextral and/or N. incompta; "P/D intergrades" and N. dutertrei.

As outlined in Chapter 5, due to inconsistencies in taxonomy and generalisation of morphospecies classification, it was necessary to combine any or all occurrences of *N. pachyderma* sinistral, *N. pachyderma* dextral and/or *N. incompta*, "P/D intergrades" and *N. dutertrei* to a singular Neogloboquadrina species. This allows us to see the generalised patterns of this genus, but unfortunately it does not allow us to see more discrete variations in, for example, the extent of the incursion of cold water *N. pachyderma* into the Mediterranean with IRD events during HS1 (Cacho *et al.*, 1999; Cacho *et al.*, 2001; Cacho *et al.*, 2002; Pérez-Folgado *et al.*, 2003; Sierro *et al.*, 2005; Frigola *et al.*, 2008).

This cooler water eutrophic genus is generally indicative of enhanced food and the presence of a DCM and was the most prolific group in the Mediterranean through all chronozones (Table 6.2; Figure 6.3) (Rohling and Gieskes, 1989; Rohling *et al.*, 1993; Schiebel and Hemleben, 2017). During HS1, they accounted for 37.8% of the population. As would be expected, there is a peak of >50% in the Alboran Sea, which decreased through the central and north-western basin, increasing again in the Tyrrhenian Sea and Strait of Sicily. Their distribution in the eastern basin, especially the Ionian Sea was consistently >20%, peaking in DWF areas of the Aegean and the Levantine Sea. The northern Adriatic had the lowest abundances during this period.

The distribution of Neogloboquadrina species in the BA chronozone remained extensive (33.58%), though more diminished in the eastern basin. The western basin had a more evenly distributed population (≤40%), though with a heightened population in the eastern Alboran Sea (≤ 60%) decreasing to ≤10% in the Tyrrhenian Sea. The major difference to HS1 is evident in the eastern basin, where their distribution dropped to <20% along the Mediterranean Ridge, Ionian and eastern Levantine Seas. However, the Aegean Sea and southern Adriatic reached values >60%.

Mean abundance of Neogloboquadrina species reduced slightly during the YD (31.46%), again with a more substantial decrease in the eastern basin (Table 6.2; Figure 6.3). The western basin formed a similar pattern to the BA, though the peak in the Alboran Sea was more intensive (≤80%), decreasing to ≤20% through much of the Tyrrhenian Sea. From the Strait of Sicily into the Ionian Sea, the population increased to ≤40%, then steadily decreased towards the Levantine Sea. The southern Adriatic, eastern Aegean and northern Aegean Seas had discrete elevated peaks (>40%).

6.1.1.2 G. bulloides
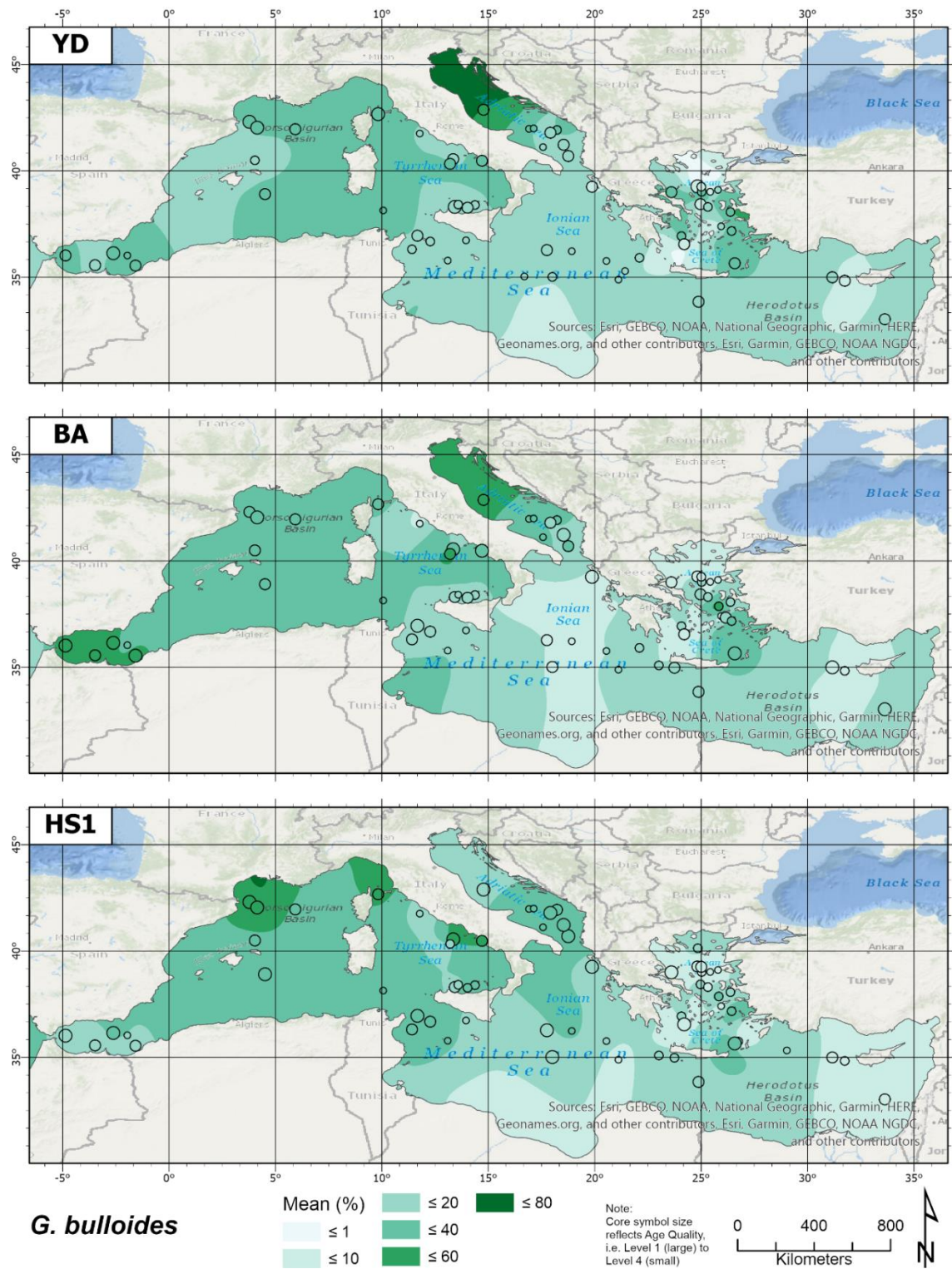
Figure 6.4: Spatial distribution of G. bulloides (%) during HS1, BA and YD.

In HS1, *G. bulloides* were widely distributed throughout both basins, with a mean of 20.5% (Table 6.2; Figure 6.4). *G. bulloides* is a cooler water, opportunistic eutrophic species, with a close association to high primary production and periods of upwelling (Sautter and Thunell, 1991; Conan and Brummer, 2000; Schiebel *et al.*, 2001; Schiebel and Hemleben, 2017). It was more prevalent in the western basin, ranging from ≤20% in the Alboran Sea, increasing northwards towards the Gulf of Lion and northern Tyrrhenian Sea. There is a clear demarcation at the Strait of Sicily, where their abundance decreases to between <10 to ≤40% in the eastern basin. The highest abundances occur in DWF areas of the Adriatic and southern Aegean Sea extending southwards into the Ionian and Levantine Seas.

During the warmer BA chronozone, the mean abundance of *G. bulloides* was similar to HS1 (20.14%), but their distribution pattern was quite different. The Alboran Sea had an elevated population (≤60%). The mean abundance in the western basin is ≤40%, decreasing to the east towards the Strait of Sicily. The distribution of *G. bulloides* in the eastern basin is more variable, with abundance in the Ionian and Levantine Seas decreasing to ≤10 to ≤20%. Again, the DWF areas of the eastern basin show greater abundance (≤40%), though their distribution was more tightly constrained, and they did not extend southward as seen in HS1.

G. bulloides decreased in overall abundance during the YD to 18.52% (Table 6.2) and its distribution in both western and eastern basins was more disparate (Figure 6.4). Relative abundance in the western basin ranged from ≤11 to ≤40%, which is much lower compared to both the BA and HS1. The southern Tyrrhenian Sea and Strait of Sicily recorded populations of ≤20%. In comparison, their distribution in the eastern basin was more uniform, decreasing to ≤10% in parts of the Levantine and Aegean Seas. *G. bulloides* reached its highest abundance (≤60%) during the BA in the Adriatic and in the DWF area of the Aegean Sea.

6.1.1.3 *G. ruber plexus*
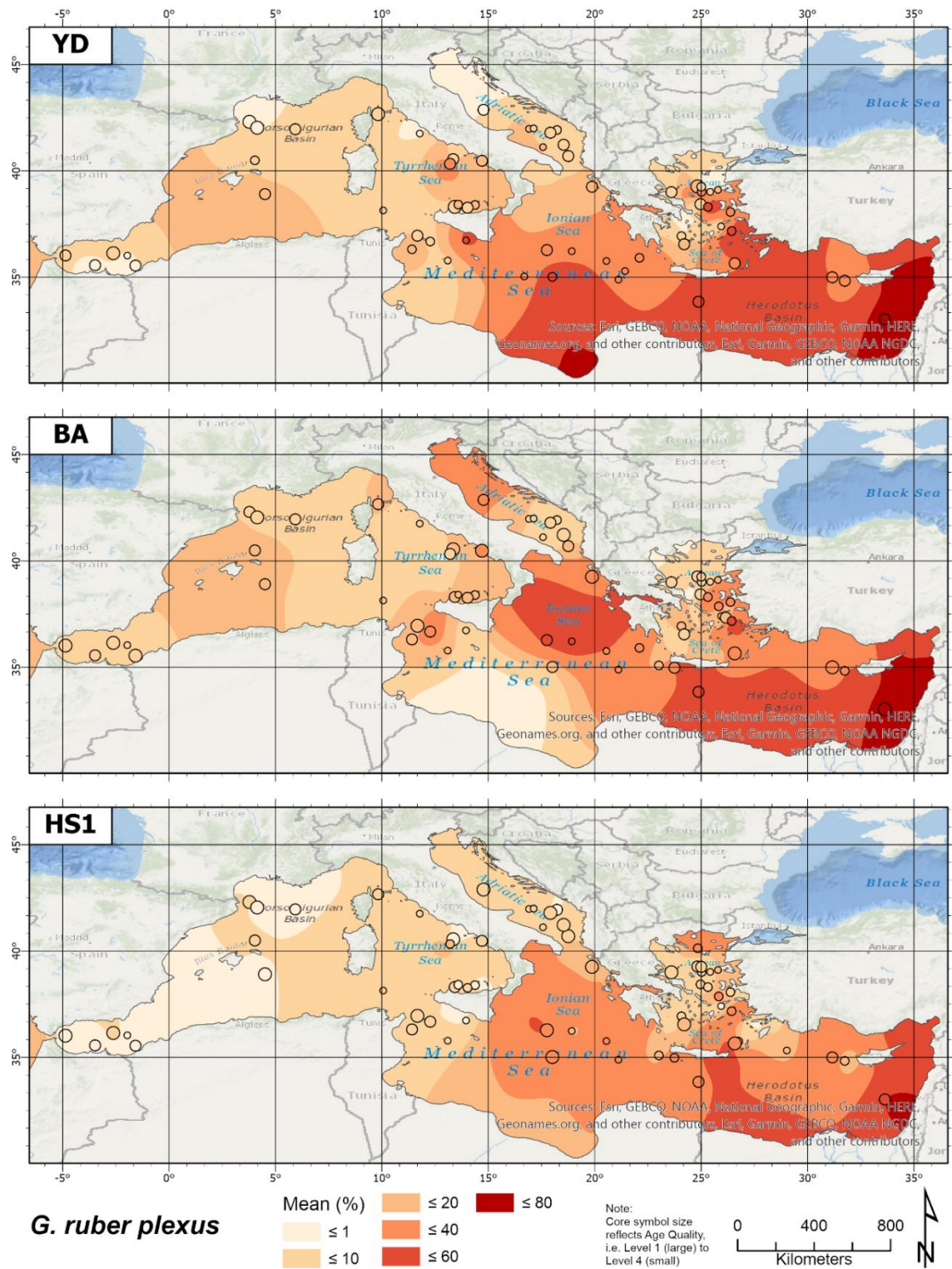
Figure 6.5: Spatial distribution of G. ruber plexus (%) during HS1, BA and YD. G. ruber plexus includes G. ruber white, G. ruber pink and G. elongatus.

As mentioned in Chapter 5, all variants of *G. ruber* have been amalgamated into a *G. ruber* plexus grouping. *G. ruber* is an important group in the Mediterranean. Although mainly indicative of warmer summer waters and oligotrophic conditions, its range can extend into more eutrophic mixed shallow waters (Anderson, 1983; Seears *et al.*, 2012; Schiebel and Hemleben, 2017). In addition, there are variations in the ecological preferences between the genotypes in this group (Numberger *et al.*, 2009). *G. ruber* is generally abundant in all chronozones (Table 6.2; Figure 6.5). In HS1, it formed 10.73% of the population, however, there was a clear east/west divide in their distribution. *G. ruber* species only reached ≤5% across the western basin into the Strait of Sicily. However, the pattern was very different in the eastern basin, where abundances in the central Ionian and Levantine Sea ranged from >20 to ≤60%. The population was more limited in areas of DWF in the northern Levantine, Adriatic and Aegean Seas.

In the BA chronozone, there was an expansion of *G. ruber* into the western basin and a significant increase in abundance in the eastern basin. It formed 16.9% of the overall Mediterranean planktonic foraminifera population, but there were very different distribution patterns in the two basins. The western basin varied from ≤10% in the Alboran Sea to ≤20% in the Balearic and Tyrrhenian Seas, and into the Strait of Sicily. The population remained low in the Gulf of Lion and in the central western Mediterranean. The eastern basin saw a significant increase in *G. ruber* species in the Ionian and south-eastern Levantine Seas (≤40% to ≤80%). The population of *G. ruber* remained lower in the northern Levantine, Adriatic and Aegean Seas, but even in these areas, their abundance increased to between ~5 to ≤40%. Note, the low abundance in the southern Ionian Sea is an artefact caused by the lack of data points in this area influencing the spline interpolation process and should be treated with caution.

The YD population of *G. ruber* plexus remained high, forming ~17% of the population across the Mediterranean Sea. The distribution of *G. ruber* in the western basin was similar to the BA. However, they were virtually absent from the southern Alboran Sea and the Gulf of Lion. The central Tyrrhenian Sea saw a minor increase in abundance. East of the Strait of Sicily, the population remained high, though with more moderate values in areas of DWF. There is a distinct north/north-westerly decrease in abundance of *G. ruber* species from the Levantine Sea towards the northern regions of the Aegean and Adriatic Seas.

6.1.1.4   G. glutinata
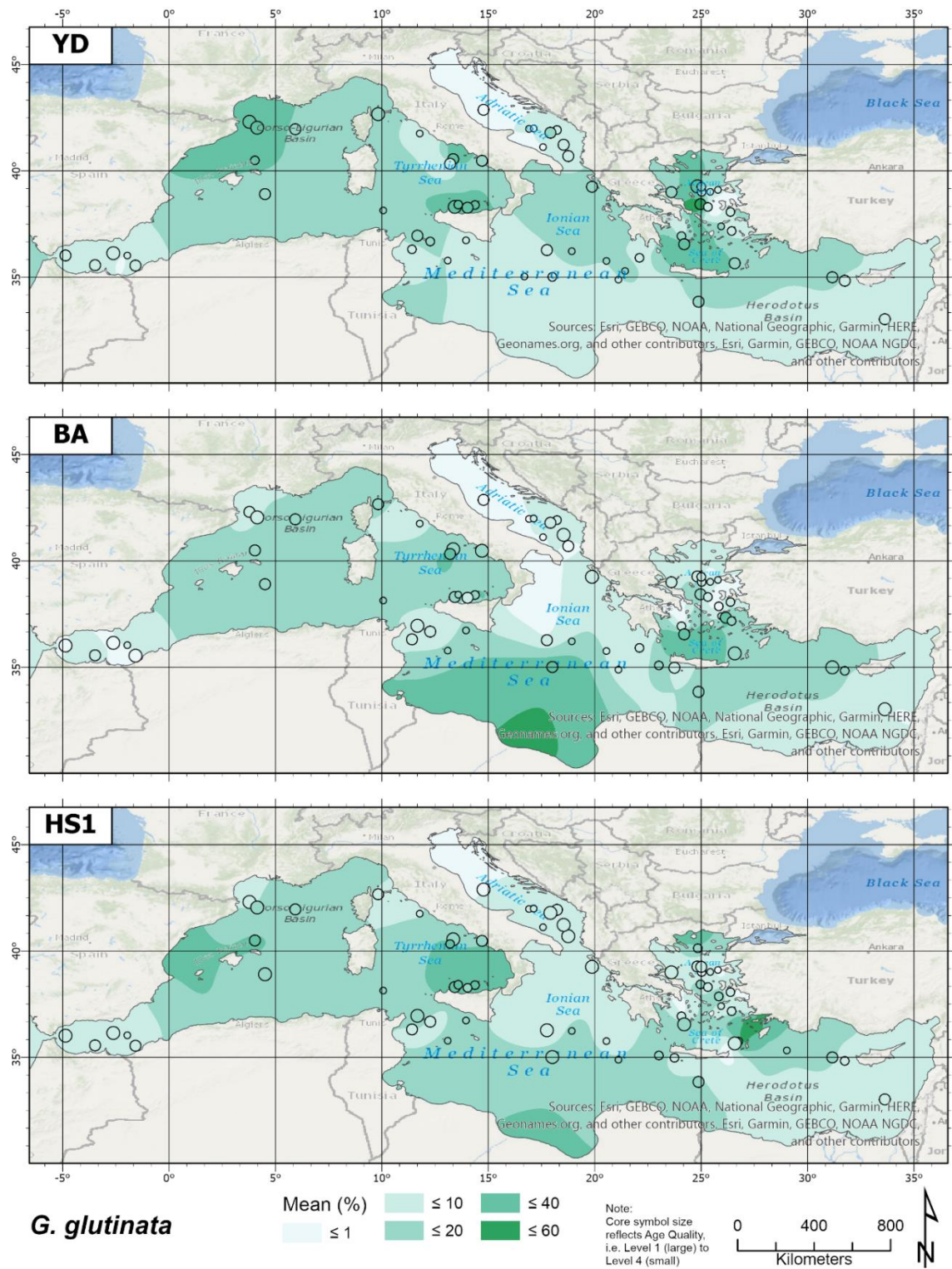
Figure 6.6: Spatial distribution of G. glutinata (%) during HS1, BA and YD.

The ubiquitous *G. glutinata* was evenly distributed through all the chronozones in the Late Pleistocene (Table 6.2; Figure 6.6). This shallower eutrophic species is indicative of fresh food (diatoms) and has wide tolerances to SST variation (Bé and Tolderlund, 1971; Thunell and Reynolds, 1984; Hemleben *et al.*, 1989; Rebotim *et al.*, 2017). During HS1, it reached 9.74% of the population, though it was more prevalent in the western basin. It ranged from ≤10% to ≤20% through the majority of the western basin, peaking in the southern Tyrrhenian Sea (≤40%). A similar population extended into the southern Ionian Sea, penetrating as far as Crete (≤20%), then fell to ≤10% over the remainder of the eastern basin, except for a minor peak in the DWF area in the southern Aegean.

Overall, the *G. glutinata* population decreased to 8.53% during the BA. However, their distribution and abundance were broadly similar to HS1 in the western basin, though not as prevalent in the Alboran and southern Tyrrhenian Sea. The lower abundance (≤10%) of *G. glutinata* at the Strait of Sicily had expanded, though the population just east of this region and along the Mediterranean ridge remained ≤20%. *G. glutinata* also flourished in the waters north of Crete (>20%), expanding into the Aegean and western Levantine Sea. Only the north western Adriatic and north-western Ionian Sea contained trace amounts of the species.

G. glutinata increased in abundance during the YD (11.87%), particularly in the north western Mediterranean around the Gulf of Lion and northern Balearics, with more discrete elevations in parts of the Tyrrhenian Sea (≤40%). The remainder of the western basin had a population of ≥20%, except for the Alboran Sea and parts of the northern and central Tyrrhenian Sea. East of the Strait of Sicily, the population fell to ≤10% for the majority of the southern eastern basin into the eastern Levantine Sea. *G. glutinata* was abundant in the Aegean (peaking ~50%) and northern Ionian and Levantine Seas (ranging from 10 to ~30%) but was absent through most of the northern and western Adriatic Sea.

6.1.1.5   T. quinqueloba
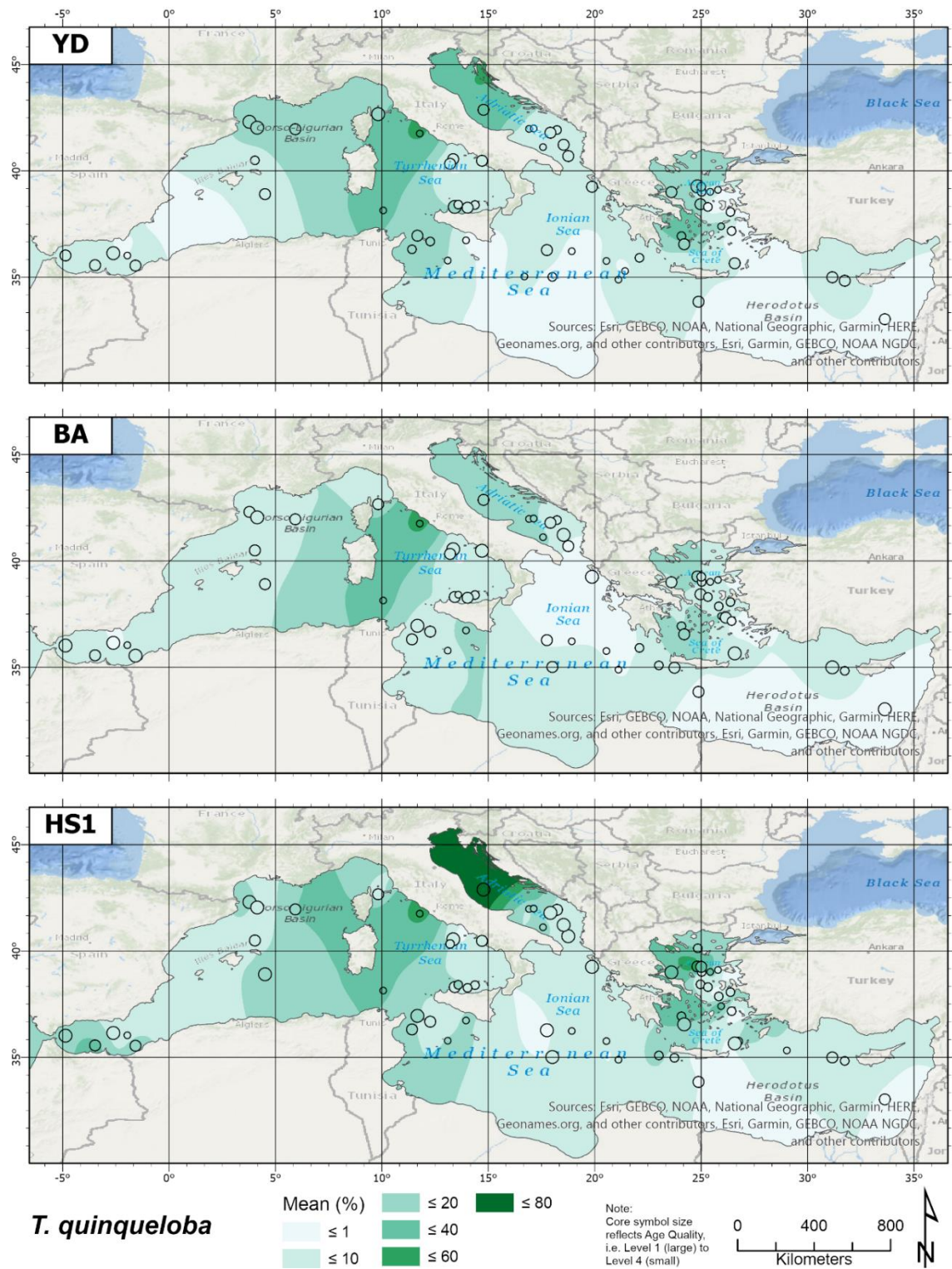
Figure 6.7: Spatial distribution of T. quinqueloba (%) during HS1, BA and YD.

T. quinqueloba is a small, cool water, opportunistic eutrophic species that inhabits deeply mixed water columns and areas of high productivity (Sautter and Thunell, 1991; Conan and Brummer, 2000; Schiebel *et al.*, 2001; Schiebel and Hemleben, 2017). During the HS1 chronozone, *T. quinqueloba* formed 11.91% of the population throughout the Mediterranean Sea (Table 6.2; Figure 6.7). However, this signal is influenced by a core in the northern Adriatic, which had a significant peak (~78%) of *T. quinqueloba*. In the western Mediterranean, *T. quinqueloba* is an important species, ranging from ≤10% in the Balearic Sea, increasing towards the east, where they peak in the eastern Tyrrhenian Sea. The Alboran Sea, Gulf of Lion and parts of the Strait of Sicily have moderate populations (~10 to 20%). In the eastern basin, the population ranged from trace amounts to ≤5%, except for the sizable peak in the northern Adriatic and in parts of the Aegean Sea.

The population significantly decreases during the BA (6.27%) (Table 6.2; Figure 6.7). The population in the western half of the western Mediterranean was ≤10%, though once again increasing towards the central Tyrrhenian Sea. The south-eastern Tyrrhenian and Strait of Sicily also decreased to ≤10%. In the Ionian and southern Levantine Sea, the extent of *T. quinqueloba* contracted, with more areas recording only trace amounts. However, its abundance shows an increase in some western areas of both the Adriatic and Aegean Seas (≤20%).

The YD saw a small increase in *T. quinqueloba* (7.8%). Their distribution was primarily confined to the northern regions of both basins (ranging from >10 to ~40%), i.e. the Gulf of Lion, Tyrrhenian Sea, northern Adriatic and Aegean Seas, though they extended into the southern Tyrrhenian Sea and Strait of Sicily. *T. quinqueloba* was absent or ≤10% through the remaining south-western half of the western basin and the Ionian and Levantine Seas.

6.1.1.6 G. inflata
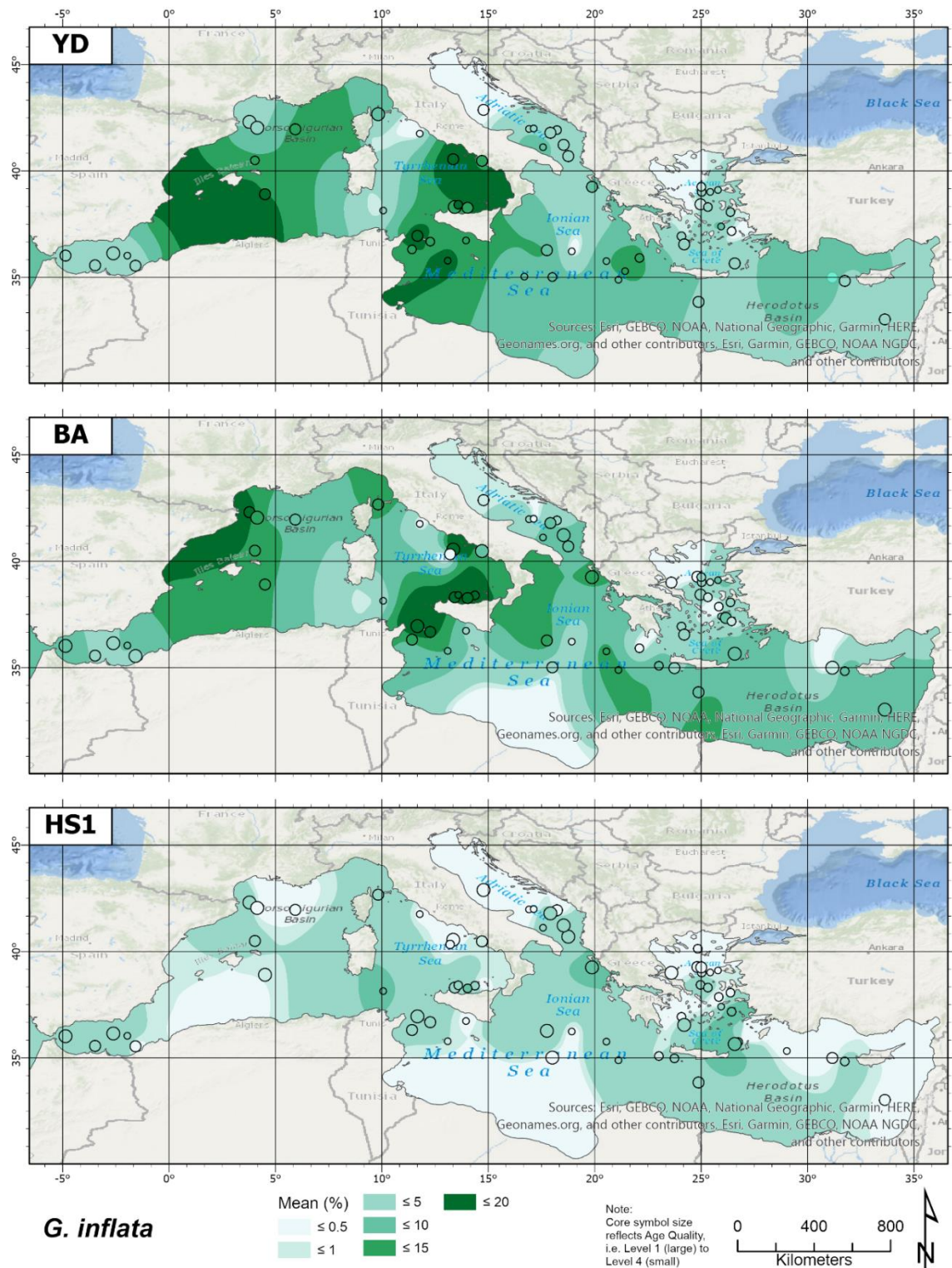
*Figure 6.8: Spatial distribution of G. inflata (%) during HS1, BA and YD. **Note** the reduction in classification intervals for this group.*

G. inflata is a key deep dwelling meso- to eutrophic species of the modern western Mediterranean, indicative of uniform temperatures in deep, stable mixed layers (Cifelli, 1974; Thunell, 1978; Pujol and Vergnaud Grazzini, 1995; Mallo *et al.*, 2017). However, its abundance from the Late Pleistocene was generally low and variable between the chronozones (Table 6.2; Figure 6.8). A notable feature of the HS1 assemblage is the very low abundance or absence of *G. inflata* and this pattern is reflected in these results, where it formed only 1.74% of the population. This low abundance was consistent throughout both basins and it reached only between 2 and 4% in the Alboran Sea and central regions of both basins.

The population increased during the BA chronozone (7.69%), especially in the Balearic to Gulf of Lion region (≤20%) and southern Tyrrhenian Sea and Strait of Sicily (≤40%). The distribution of *G. inflata* remained low throughout the majority of the eastern basin (<10%), except for small pockets in the Ionian Sea.

Although the mean population throughout the Mediterranean remained low during the YD (6.89%), its population was consistently elevated in the central western basin, eastern Tyrrhenian Sea and into the Strait of Sicily (≤20%). However, the population of *G. inflata* was reduced in the Alboran Sea, Gulf of Lion and in the waters around Sardinia and Corsica (≤10%). The population in the eastern basin was more limited (ranging from <1 to ≤5%) with only a small area in the central Ionian Sea that reached ≤10%.

6.1.1.7 G. scitula
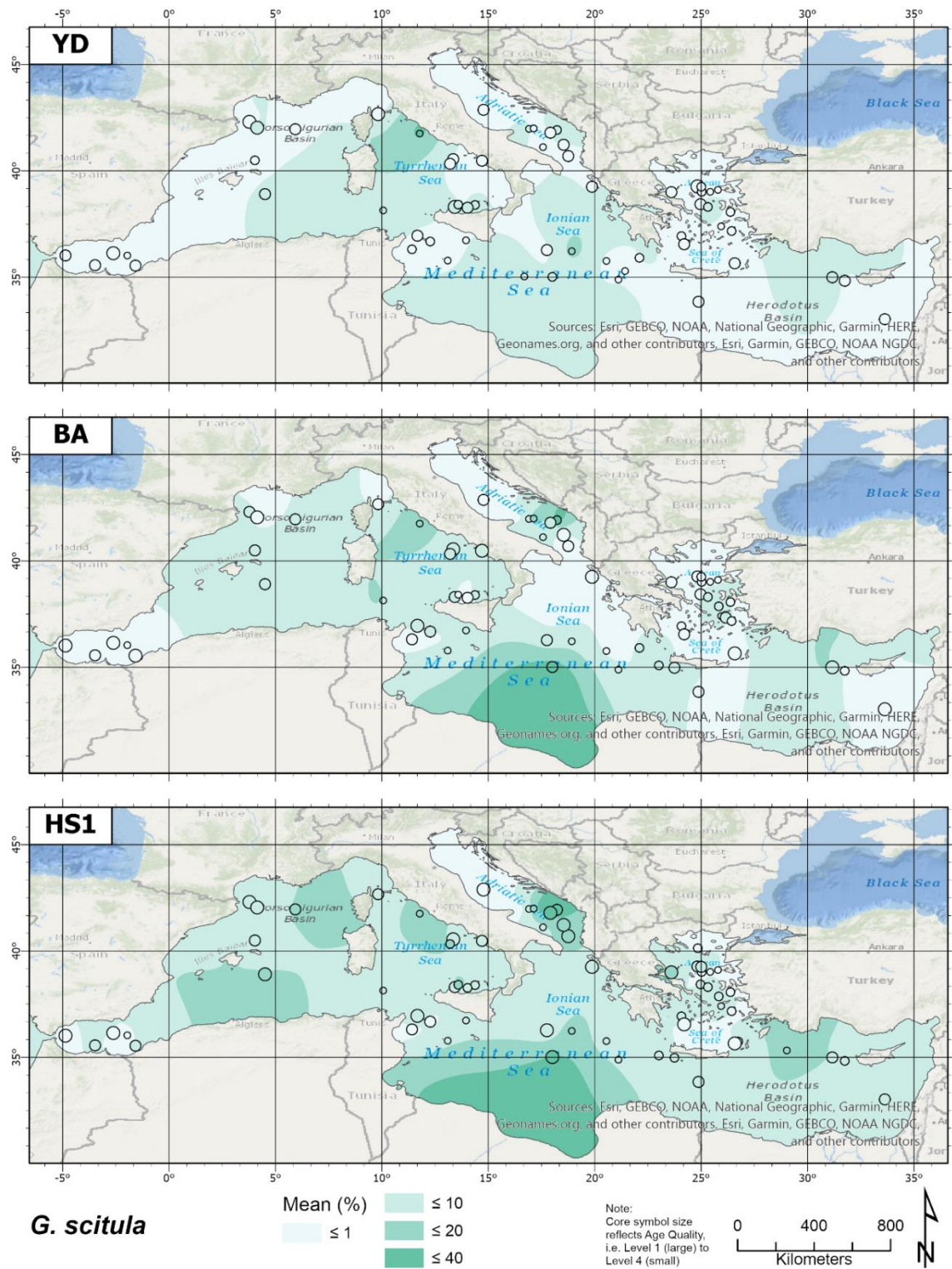
Figure 6.9: Spatial distribution of G. scitula (%) during HS1, BA and YD.

The cool, deep dwelling eutrophic *G. scitula* is a rare species in modern Mediterranean waters, as well as through most of the Late Pleistocene (Thunell, 1978; Pujol and Vergnaud Grazzini, 1995; Itou *et al.*, 2001; Chapman, 2010; Schiebel and Hemleben, 2017). However, it was more abundant during HS1 (6.31%) (Table 6.2; Figure 6.9). During this cold period, *G. scitula* inhabited the western basin (≤10%), with small areas in the central basin and eastern Tyrrhenian Sea, where it reached ≤20%. Lowest abundances were in the southern Alboran Sea (≤1%). The population of *G. scitula* in the eastern basin was more varied. The majority of the basin had abundances that ranged from ≤5 to ≤20%. However, the distribution patterns in the Aegean and Adriatic were more variable. Areas where *G. scitula* occurred in trace amounts in the north western Adriatic, and eastern and southern Aegean, were adjacent to more discrete areas where it reached ≤40%.

During the BA, both the abundance and distribution of *G. scitula* decreased (3.02%). In the western basin, *G. scitula* was absent from the Alboran Sea, though it slowly increased towards the Tyrrhenian Sea (≤10%). In the eastern basin, *G. scitula* was absent in much of the Ionian, southern Levantine, Adriatic and Aegean Seas. When it occurred (the Mediterranean ridge, northern Levantine Sea and south-east Adriatic), it varied from ≤5% to ≤40%.

The population further decreased during the YD (1.52%) and was absent from much of the western half of the western basin, again increasing eastward towards the northern Tyrrhenian Sea (≤10 to ≤20%). Similarly, it was absent from much of the eastern basin, occurring mainly along the Mediterranean ridge, northern Levantine and small areas of the central Adriatic and Aegean Seas (≤10%).

6.1.1.8   SPRUDTS
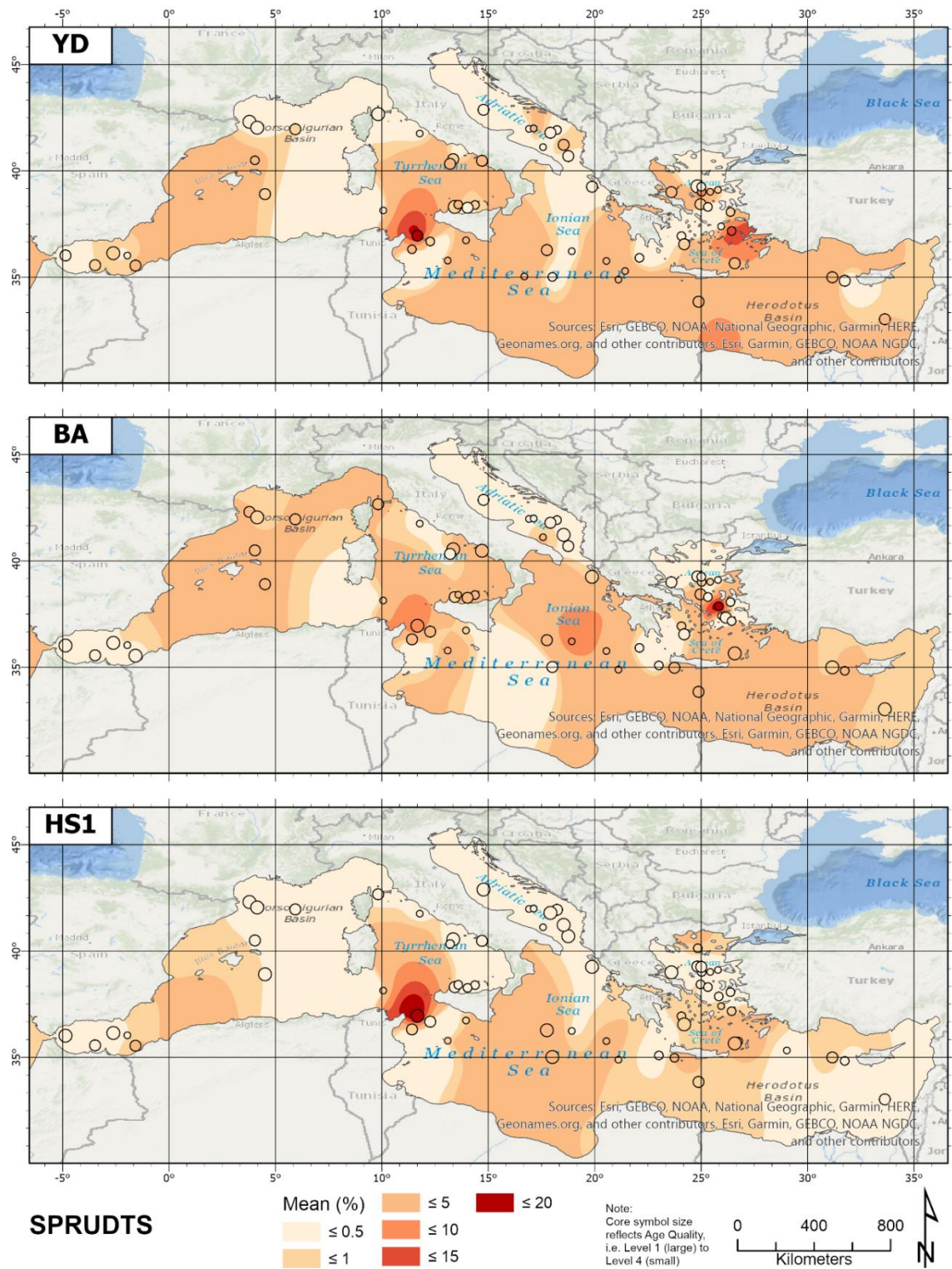
*Figure 6.10: Spatial distribution of SPRUDTS species (%) during HS1, BA and YD. **Note** the reduction in classification intervals for this group.*

Figure 6.10 displays the distribution of the collective SPRUDTS group. SPRUDTS represent warm water, though there are differences in their individual ecological requirements. Although they form only a small component of the total population (Table 6.2), they are regionally important. Of the SPRUDTS species reported, maps of species that reached >3% (i.e. *O. universa*; *G. siphonifera* and *G. sacculifer*) are provided in Appendix 2. These species will be discussed, when relevant.

As would be expected, the SPRUDTS population in the Mediterranean is low during HS1 (~0.8%). They are virtually absent in the western basin, except for a noticeable peak in the Strait of Sicily, representing an isolated peak in *G. sacculifer* at this location (≤20%) (Appendix 2). In the eastern basin, the SPRUDTS population is low, though there are minor (≤5%) occurrences of *G. siphonifera* and *G. sacculifer* in the western Ionian Sea and in areas of DWF in the southern Aegean.

SPRUDTS increased to 1.47% during the BA. Although still in low abundance (<5%), their distribution had expanded. In the western basin, the population is comprised mainly of *O. universa*, with limited *G. siphonifera* and *G. sacculifer* (Appendix 2). SPRUDTS species are absent or at trace amounts in the Alboran Sea and parts of the Tyrrhenian Sea. Once again, there is a peak of *G. sacculifer* (≤10%) in the Strait of Sicily, with minor occurrences of *O. universa*. In the eastern basin, the SPRUDTS species expanded their range and became more abundant, though they did not extend to the far eastern edge of the Levantine Sea, where *G. ruber* plexus had peaked. Both *O. universa* and *G. siphonifera* became more widespread, both peaking in the central Ionian Sea (≤10%). The Adriatic and Aegean only contained trace amounts of the SPRUDTS group during the BA.

There was a marked contraction in the range of SPRUDTS in both basins during the YD, though regionally their numbers increased, thus their overall abundance increased to 1.56%. The eastern Alboran Sea and northwards through the Balearics had trace amounts of the more common SPRUDTS species (≤5%), in addition to minor *G. tenella* and *G. rubescens*. A minor elevation in *O. universa* in the Tyrrhenian Sea and a peak (≤20%) of *G. sacculifer* in the Strait of Sicily heighten the SPRUDTS signal in this region. The distribution of SPRUDTS in the eastern basin became more variable in the YD, with more elevated occurrences of *O. universa* and *G. siphonifera* in the southern Ionian and Levantine Seas and in areas of DWF in the Aegean (Appendix 2).

6.1.1.9   *G. truncatulinoides (total)*
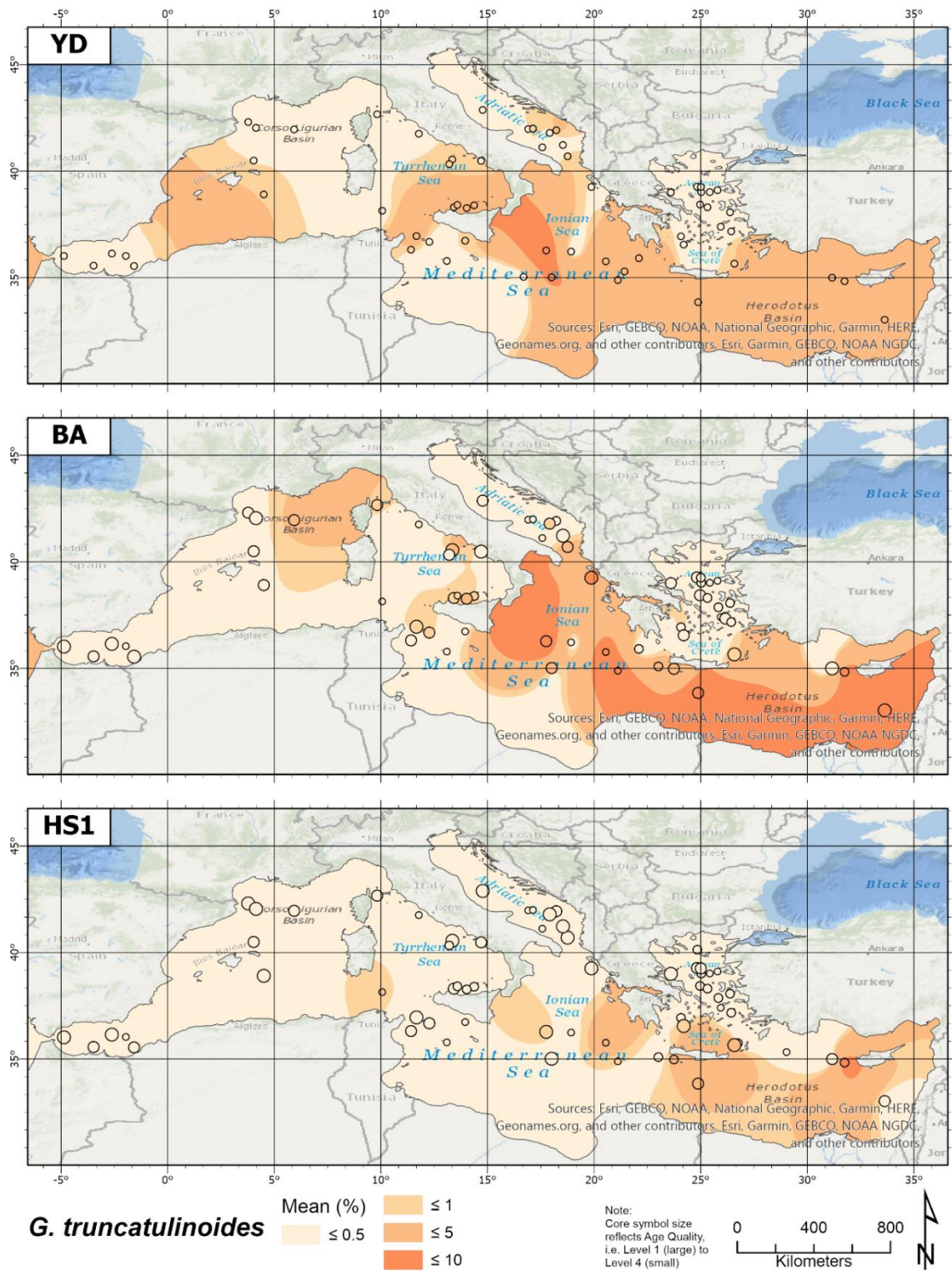
Figure 6.11: Spatial distribution of G. truncatulinoides (total) (%) during HS1, BA and YD. G. truncatulinoides (total) includes both sinistral and dextral variants. **Note** *the reduction in classification intervals for this group.*

Due to constraints with the original datasets, *G. truncatulinoides* (total) includes both dextral and sinistral coiling varieties. In general, it occurs in low abundances, but was regionally significant, particularly in the eastern basin (Table 6.2; Figure 6.11). During the HS1 chronozone, it is virtually absent (0.28%), especially in the western basin, and was identified in the central Ionian and Levantine Seas, reaching a maximum of between ≤1 and ≤5%.

However, during the BA (1.03%), there is a notable increase in abundance and expansion in their distribution in the central eastern basin, reaching ≤10% in the Levantine and central Ionian Seas. In addition, there is a minor increase in the northern margin of the western basin (≤1%).

There was a similar abundance of *G. truncatulinoides* during the YD (1.02%) and was more widely distributed in the western basin, primarily in the southern Tyrrhenian Sea into the Strait of Sicily, though in low abundances (≤1 to ≤5%). The heightened interpolated values in the southern Balearic Sea is most certainly an artefact of spline interpolation in this area. In the eastern basin, *G. truncatulinoides* is present throughout the Levantine and Ionian Seas (<5%), peaking around the Mediterranean Ridge (~6.5%).

6.1.2   Palaeoenvironmental proxies

To aid interpretation of the faunal results, the eutrophication (E-Index) and stratification (S-Index) palaeoenvironmental proxies were utilised Chapter 5. The mean values of both proxies for each chronozone are listed in Table 6.3.

Chronozone	E-index	S-Index
YD	77.91	40.76
BA	78.27	44.03
HS1	85.66	32.53

Table 6.3: Mean Eutrophication Index (E-Index; higher values are more eutrophic, lower are more oligotrophic) and Stratification Index (S-Index: G. bulloides/G. ruber; lower values represent weaker stratification, higher values represent stronger stratification) during HS1, BA and YD.

6.1.2.1 Eutrophication Index (E-Index)
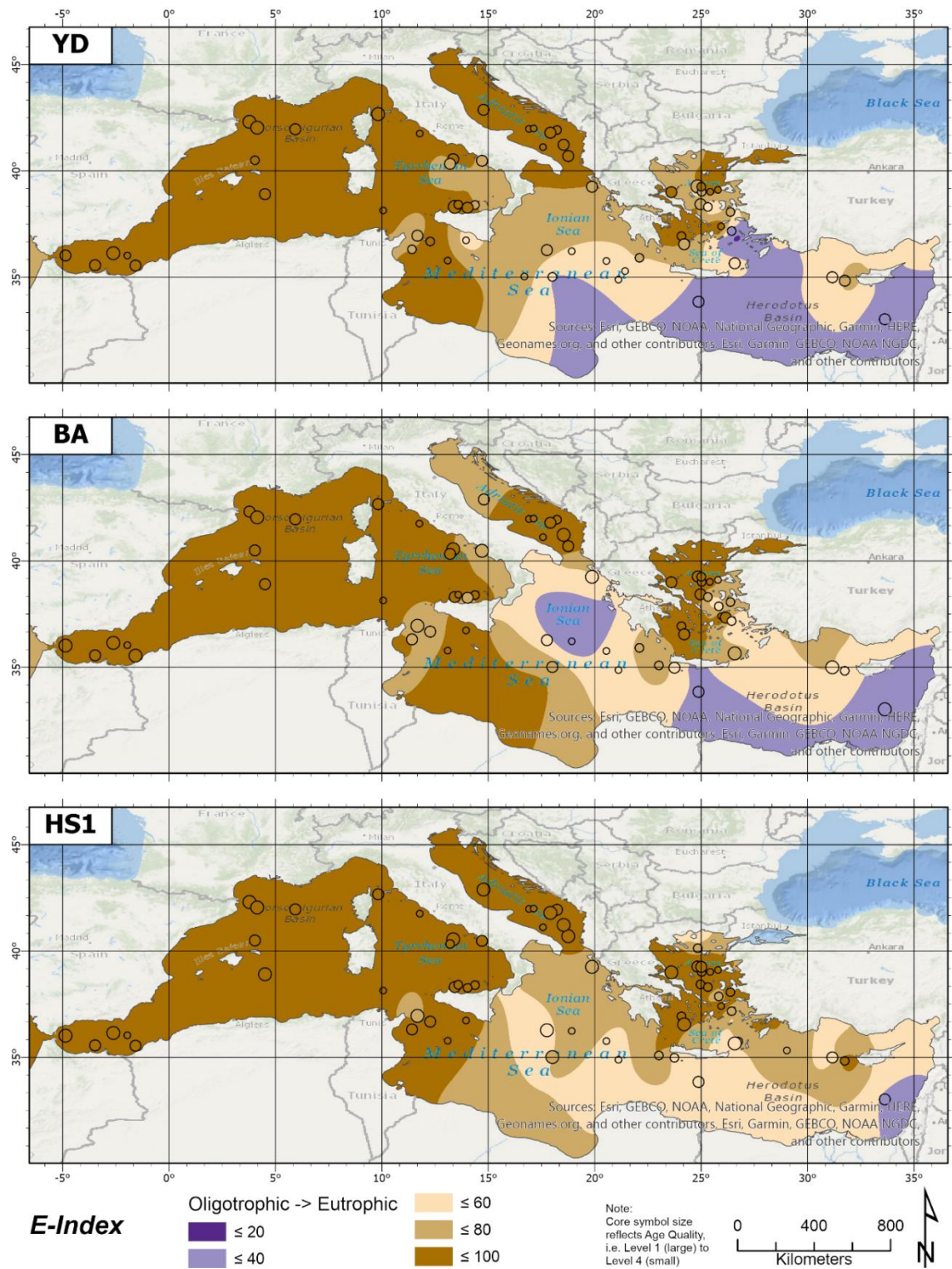
Figure 6.12: Eutrophication Index (E-Index) during HS1, BA and YD.

As discussed in Chapter 5, the E-Index quantifies the variations of eutrophic and oligotrophic species (Kontakiotis, 2016). It is clear from Table 6.3 and Figure 6.12 that eutrophication is quite high through all chronozones in the Late Pleistocene. This is especially true for the western basin, with was dominated by eutrophic species throughout the majority of the basin. The pattern in the eastern basin is more variable through these chronozones.

The HS1 chronozone in the western basin was overwhelmingly eutrophic, with only a minor decrease in the E-Index at the Strait of Sicily. In the eastern basin, both northern sub-basins had a high E-Index. However, oligotrophic conditions strengthened towards the south and east, predominantly in the Ionian Sea, along the Mediterranean Ridge and into the Levantine Sea, where they peaked along the eastern margin.

The E-Index during the BA in the western basin was similar to HS1, except that there was a slight decrease in eutrophic conditions in the eastern Tyrrhenian Sea and an expansion of the lower E-Index region at the Strait of Sicily. In the eastern basin, there was greater variability in the signal. Oligotrophic conditions became firmly established in the central Ionian Sea and along the southern margin of the Levantine Sea. The Aegean Sea retained its high E-Index score, whereas the northern regions in the Adriatic had decreased slightly.

The E-Index in the western basin during the YD had greater similarity to the BA than the cold HS1 chronozone, though the less eutrophic area in the Tyrrhenian Sea had expanded since the BA. In addition, oligotrophic conditions had expanded from the southern Ionian to the Levantine Sea. The entire Adriatic Sea once again had a high E-Index, whereas the signal was much more variable in the Aegean Sea and northern Levantine Sea.

6.1.2.2 Stratification Index (S-Index)
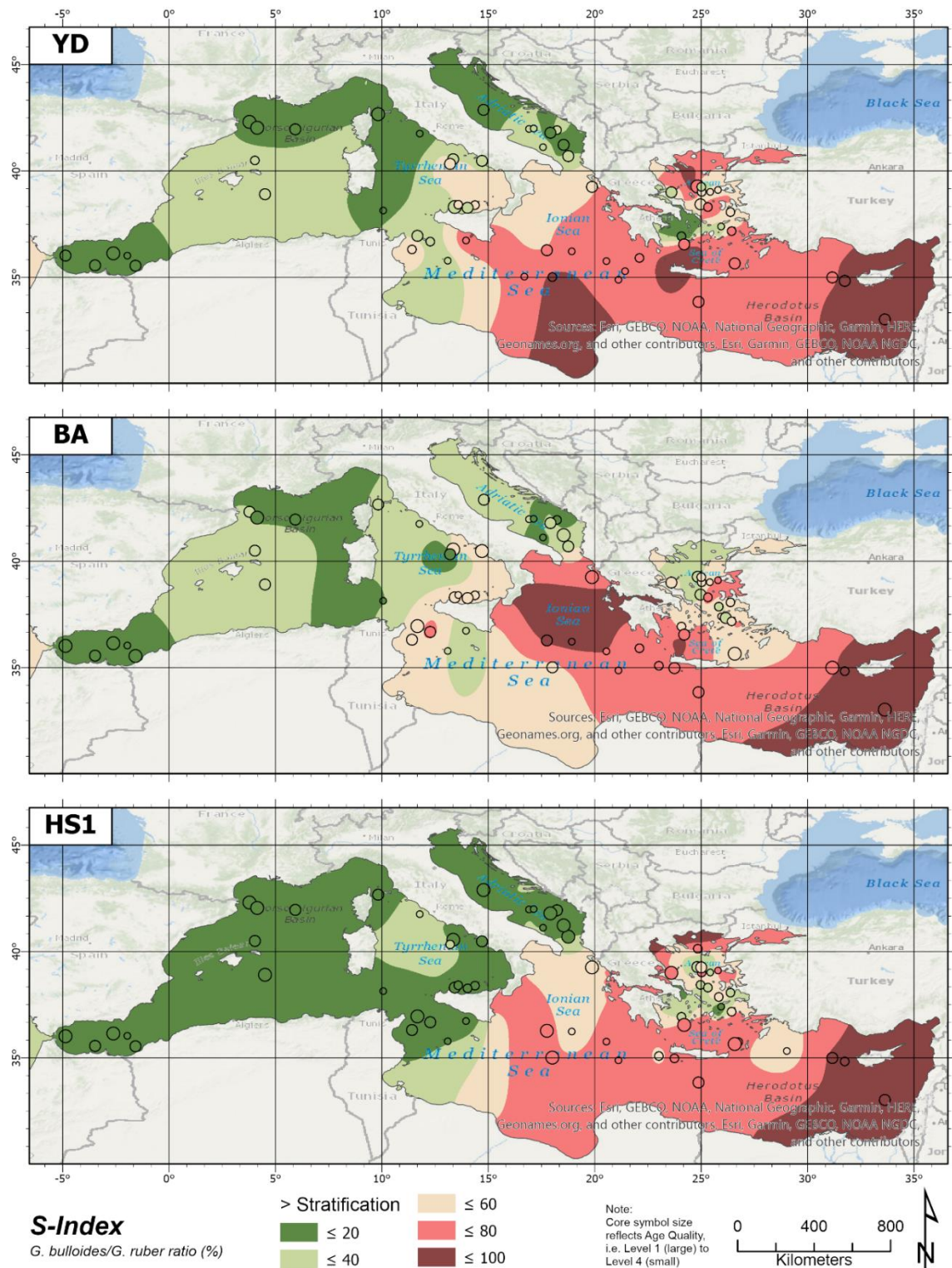
Figure 6.13: Stratification Index (S-Index) during HS1, BA and YD. S-Index is based on a ratio between G. bulloides/G. ruber, which is used as a proxy for summer stratification (Sbaffi et al., 2004).

The ratio of *G. bulloides*/*G. ruber* has been utilised as a summer stratification proxy for the three chronozones of the Late Pleistocene and the mean values have been summarised in Table 6.3. The spatial distribution of the S-Index during these periods, illustrate a clear east/west divide in stratification, especially during HS1 (Figure 6.13). During this cool period, the western basin had little or no seasonal stratification, except for the central Tyrrhenian Sea. The Strait of Sicily acted as a barrier and east of the straits, there was a rapid and easterly increase in stratification. There was little or no seasonal stratification in the Adriatic, whereas it was variable in the Aegean Sea. Weakened stratification was observed in the Ionian Sea and in the area of DWF in the northern Levantine Sea.

During the BA, weak seasonal stratification was established in the central western basin and Tyrrhenian Sea. The Strait of Sicily no longer acted as a barrier to stratification and moderate levels are evident in the eastern Tyrrhenian Sea and south into the Strait of Sicily. East of the Strait of Sicily and south of the Mediterranean Ridge, stratification remained moderate to low. Further north, strong levels of stratification extended from the Ionian Sea towards the Levantine Sea. The stratification signal in the Adriatic and Aegean Seas became more variable, with weak to moderate stratification occurring in different regions of the sub-basins.

Weak summer stratification in the western basin became more widespread during the YD, except for the Alboran Sea, northern regions and south into the western Tyrrhenian Sea. However, summer stratification in the eastern Tyrrhenian Sea remained moderately high, though it had decreased in intensity around the Strait of Sicily, in comparison to the BA. The strength of stratification in the eastern basin was more variable, strengthening south of the Mediterranean Ridge and into the eastern Levantine basin. The Adriatic had little or no seasonal stratification, whereas stratification had increased throughout the Aegean Sea, but remained low in the southern Aegean, west of the Cyclades Islands.

6.1.3 Sea surface temperatures

Artificial Neural Networks (ANN) were utilised to predict the variations in SST across the Mediterranean Sea during the Late Pleistocene chronozones. The mean annual, summer and winter SSTs (°C) for the Mediterranean Sea and separately for the west and east basin, along with the variability and seasonality of SSTs are given in Table 6.4 and displayed in Figure 6.14 to Figure 6.18. To aid interpretation of the extent of SST variability during the Late Pleistocene in comparison to modern conditions (Figure 2.5), SST anomalies were mapped for each chronozone (Figure 6.15). The anomalies for each chronozone were calculated as the difference between the annual SST for each core (predicted using ANN) and the interpolated World Ocean Atlas (2018) annual SST value (depth 10m) at each core site (Table 6.4) (Locarnini, 2018).

	Chrono-zone	Annual (°C)	Annual anomaly (°C)	Summer (°C)	Winter (°C)	Season-ality (°C)
Mediterranean Sea	YD	14.19	-4.48	17.38	11.49	5.89
	BA	15.03	-3.63	18.26	12.32	5.95
	HS1	13.57	-5.09	16.16	11.46	4.71
Western Basin	YD	12.37	-5.83	15.07	10.23	4.84
	BA	13.70	-4.50	16.69	11.30	5.39
	HS1	11.01	-7.19	13.06	9.65	3.41
Eastern Basin	YD	15.11	-3.81	18.53	12.12	6.42
	BA	15.66	-3.22	19.01	12.80	6.21
	HS1	14.76	-4.11	17.60	12.29	5.31
SST variability between basins	YD	2.74	2.02	3.46	1.89	
	BA	1.95	1.28	2.32	1.50	
	HS1	3.75	3.08	4.54	2.64	

Table 6.4: Mean annual, summer and winter SST for the Mediterranean Sea and both western and eastern basins, as predicted using ANNs during HS1, BA and YD. Annual SST anomaly is the annual SST - World Ocean Atlas (2018) annual SST (depth 10m) (Locarnini, 2018). SST seasonality is mean summer - winter SSTs. Variability between the basins is the different between the mean SSTs in the western and eastern basin.

6.1.3.1 Annual SSTs
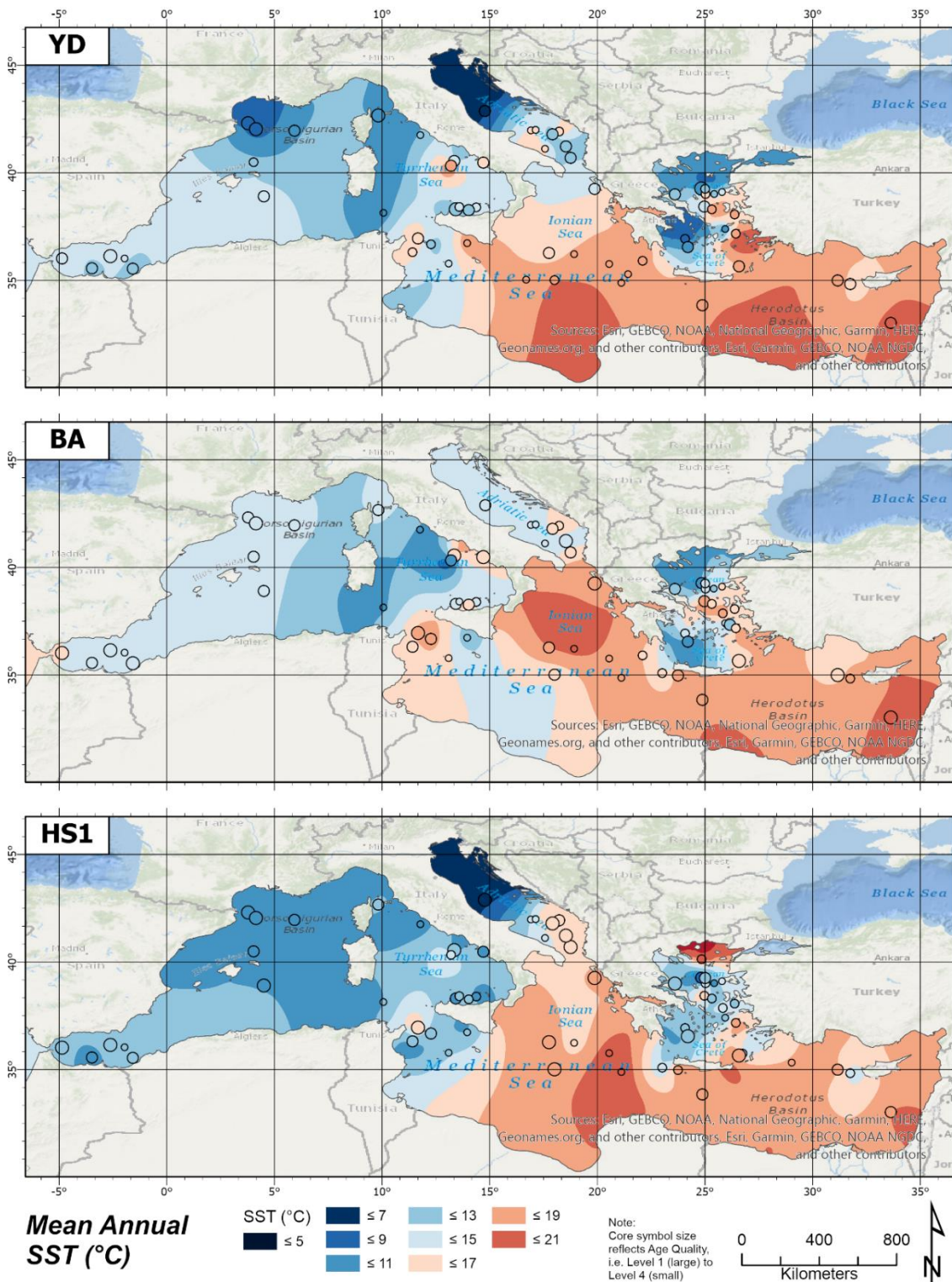
Figure 6.14: Mean Annual SSTs (°C) predicted using ANN during HS1, BA and YD.

Annual SSTs during HS1 were as low as 13.57°C. There is a clear SST increase from west to east, recording a variation of 14.12°C between the lowest and highest temperatures (Table 6.4). In the western basin, the north-south increase in SSTs was low, ranging from ≤11°C in the Gulf of Lion to ≤13°C in the Alboran Sea (Figure 6.14). The warmest annual SSTs were recorded in the central Tyrrhenian Sea (≤15°C) and south in the Strait of Sicily (≤17°C). In the eastern basin, annual SSTs in the southern Ionian and Levantine Sea reached values ≤21°C. The Adriatic was cold, with SSTs ranging from ≤7°C in the far north to ≤17°C further south. The central Aegean Sea ranged from ≤9°C to ≤15°C. Note, a solitary low age quality (AQ) data point in the northern margins of the Aegean Sea predicted SSTs ≤21°C, and this should be treated with caution.

Predicted annual SSTs in the BA increased to ~15°C, though the range in SST values decreased to 10.47°C. The signal became more complex in the western basin; instead of the modern north-west/south-east SST gradient, SSTs were warmer in the western half of the basin and cooler towards the eastern half. SSTs peaked (≤17°C) in the most westerly Alboran Sea, then decreased to ≤15°C as far as the Gulf of Lion. In contrast, SSTs in the central Tyrrhenian Sea and south within the North African current fell to ≤9°C. These annual SSTs are cooler than those predicted during HS1 in this region. SSTs along the coast of central Italy reached ≤17°C and the Strait of Sicily was warm (≤19°C), though a low AQ core south of Sicily predicted SST ≤13°C. Throughout the Ionian Sea and into the southern Levantine Sea, predicted SSTs ranged from ≤19 to ≤21°C. The Adriatic remained cool (≤15 to ≤17°C), though in contrast to HS1, these cool waters did not extend outside of the basin to influence the northern Ionian Sea. SSTs in the central Aegean were elevated (≤19°C) but were flanked to the north and south by colder waters (<11°C).

Annual SSTs again decreased during the YD (14.19°C), though the pattern in the western basin was different to that experienced during HS1, and the seasonal range was not as extreme (12.73°C). The Gulf of Lion was significantly colder than the rest of the western basin, decreasing to ≤9°C. There was a gradual increase in SSTs towards the Alboran Sea (≤13 to ≤15°C). As seen during the BA, cold waters (≤11°C) extended from the north-western Tyrrhenian Sea, south towards the Tunisian coast. However, SSTs reached ≤17°C further east in the central Tyrrhenian Sea and Strait of Sicily. Eastern basin annual SSTs gradually increase from north to south, ranging from ≤7°C in the Adriatic and Aegean Seas, to ≤21°C in the southern Ionian and Levantine Seas.

It is clear from (Table 6.4) that SSTs during all three chronozones were cooler than modern SSTs. HS1 reveals the greatest mean cooling (-7.19°C), followed by the YD (-4.48°C) and the BA (-3.63°C) (Table 6.4), though the spatial distribution of these SST anomalies varied across each chronozone (Figure 6.15). The cooling observed in the eastern basin was more stable across the three chronozones, varying only 0.89°C between the chronozones. This is in comparison to the western basin, where cooling during HS1 (-7.19°C) was much more extensive than experienced during both the BA (-4.50°C) and YD (-5.83°C) (Table 6.4).

In detail, the extreme cooling during HS1 is especially evident across the majority of the western basin, as well as the northern Adriatic Sea and SW Aegean Sea, whereas the cooling was more moderate in the southern Adriatic, Ionian and Levantine Seas.

During the BA, the greatest SST anomalies were located primarily in the Tyrrhenian Sea, east of the Straits of Sicily and in the Aegean Sea (-4 to -6°C). However, there was only a 1.28°C difference between the two basins (Table 6.4), with SST anomalies in northern regions comparable to the cooling seen in the central eastern basin (-3.22°C).

With the return of enhanced cooling during the YD, SST anomalies are focused in the northern sub-basins (both the Gulf of Lion and Adriatic experienced their deepest cooling events during the YD, i.e. -7.58 and -4.86°C respectively), as well as the central Tyrrhenian Sea (Table 6.4; Figure 6.15). However, in comparison to HS1, SST anomalies were 2 to 3°C less in the Alboran Sea and Strait of Sicily, and SSTs throughout much of the southern eastern basin are only ≤2°C cooler than experienced in modern times.
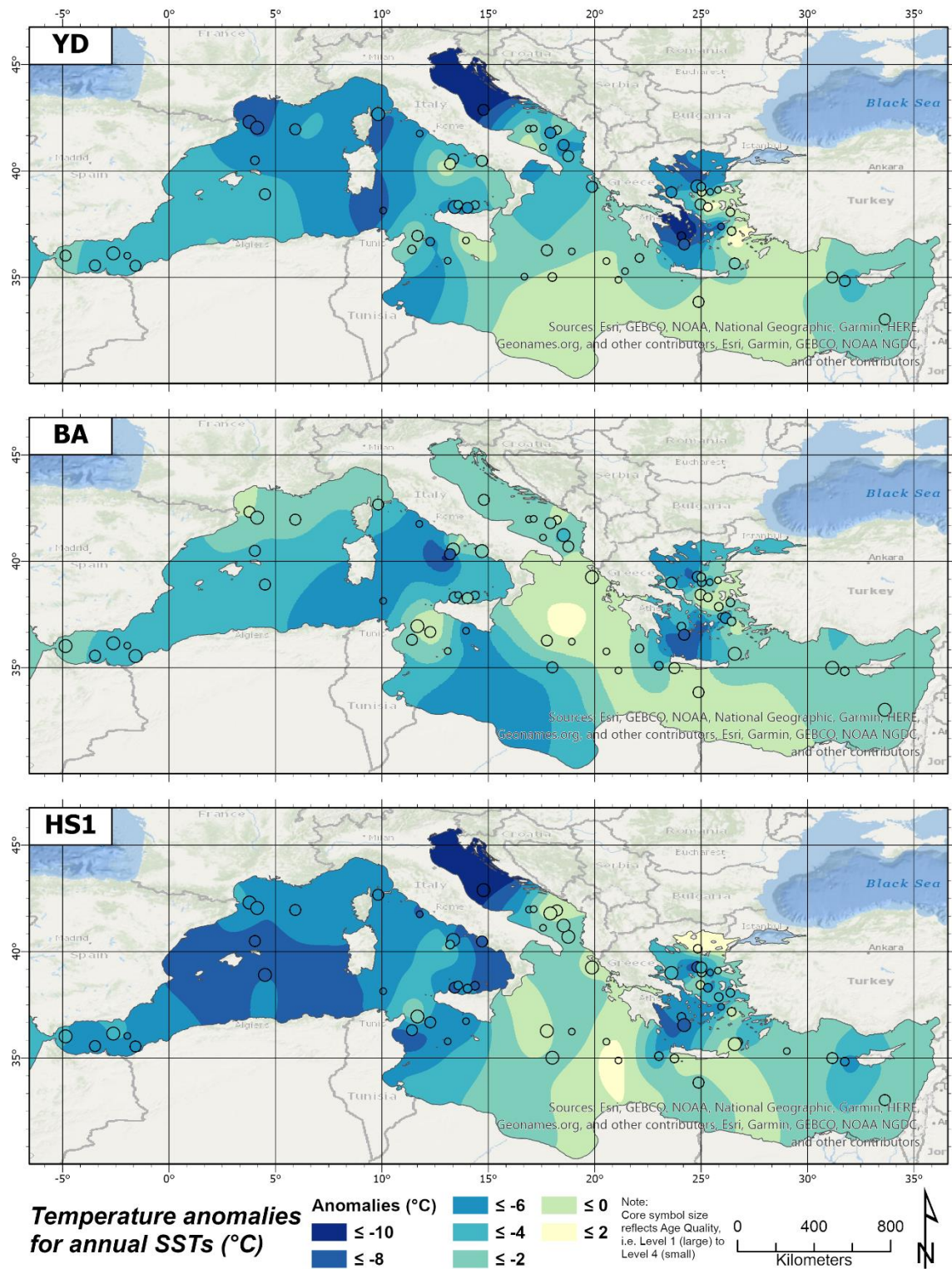
Figure 6.15: Annual SST anomalies (°C) during HS1, BA and YD. The SST anomalies for each core was calculated as the annual SST (predicted using ANN) - World Ocean Atlas (2018) annual SST (depth 10m) (Locarnini, 2018).

6.1.3.2 Summer SSTs
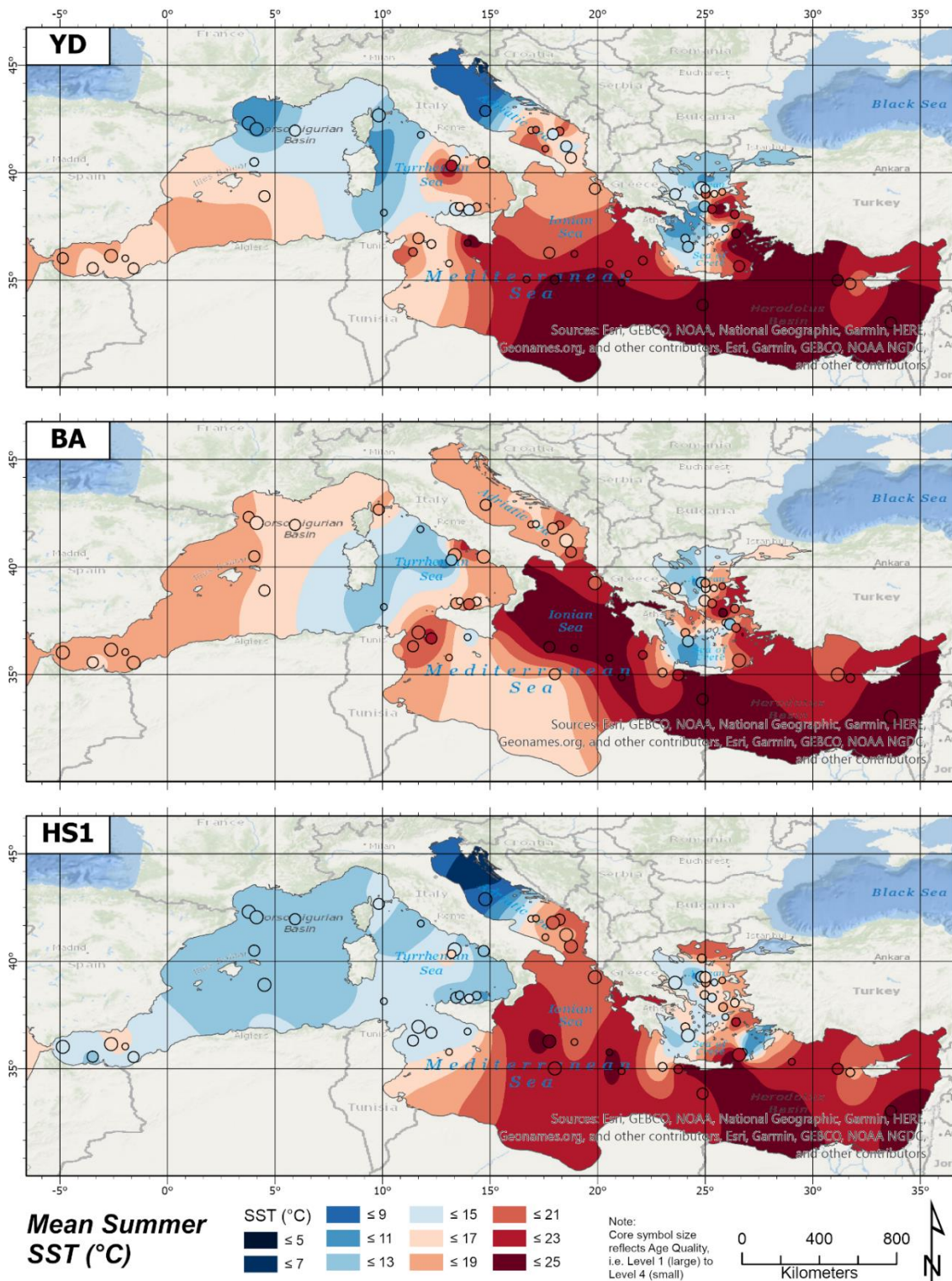
Figure 6.16: Mean Summer SSTs (°C) predicted using ANN during HS1, BA and YD.

During HS1, the average summer SST across the Mediterranean Sea was 16.16°C (Table 6.4; Figure 6.16). However, there is a clear disconnect between the western basin (≤11°C, with minor areas that reached ≤17°C) and southern parts of the eastern basin (≤17 to ≤25°C), with the sharp division in SSTs positioned to the east of the Strait of Sicily. Summer SSTs were highly variable in the Adriatic and Aegean Seas (ranging from ≤9 to ≤21°C), with cooler waters extending south into the Ionian and northern Levantine Sea.

The pattern in mean summer SST was significantly different during the BA (18.26°C). As observed for the mean annual SSTs, the Alboran Sea to Gulf of Lion was significantly warmer (≤19°C) then the waters around Sardinia (≤13°C), though SSTs warmed again along the eastern margin of the Tyrrhenian Sea and into the Strait of Sicily. The central eastern basin was very warm (≤19 to 25°C), cooler in the Adriatic (≤19°C), and much colder (≤15°C) in the northern and southern sections of the Aegean Sea.

On average, predicted summer SSTs were warmer in the YD than HS1 (17.38°C). There was also a discernible north/south variability in SST, with the Gulf of Lion, northern Tyrrhenian, northern Adriatic and Aegean Seas all displaying decreased SSTs (≤9 to ≤15°C). Southern regions were noticeably warmer, reaching ≤19°C in the Alboran and southern Balearic Seas, and ≤25°C in southern waters of the eastern basin.

6.1.3.3 Winter SSTs

Mean winter SSTs fell to 11.46°C in HS1, with the majority of the western basin ≤11°C, the lowest SSTs in the north-western Mediterranean (Figure 6.17). SSTs in the eastern basin ranged from ≤5 to ≤17°C, warming towards the south. Areas of DWF are evident by their lower SSTs in the southern Aegean and northern Levantine Sea.

Again, moderately warmer winter SSTs (12.33°C) were evident along the western half of the western basin. In comparison, waters east of Sardinia and Corsica and within the Tyrrhenian Sea fell to ≤11°C. The central and southern eastern basin had SSTs that only reached ≤17°C. The Adriatic and Aegean also remained cold during the BA winter seasons.

Mean winter SSTs during the YD (11.49°C) were similar to HS1, there is a definite north-west/south-east variability across the Mediterranean Sea. SSTs in the Gulf of Lion

and northern Adriatic and regions in the Aegean fell to ≤7 to ≤9°C (≤11°C in the Alboran Sea), whereas SSTs in the southern eastern basin ranged between ≤15 to ≤17°C.
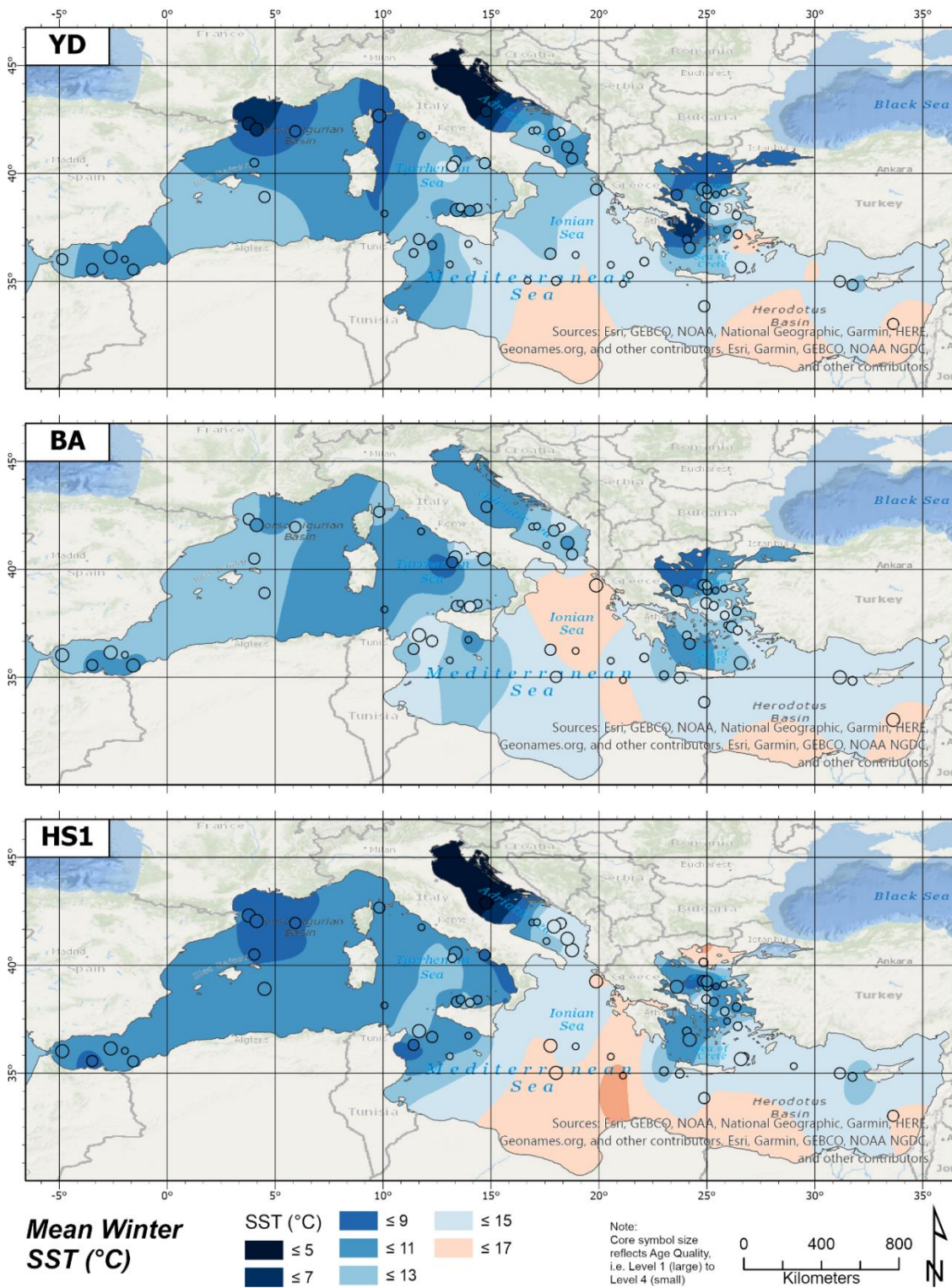
Figure 6.17: Mean Winter SSTs (°C) predicted using ANN during HS1, BA and YD.

6.1.3.4 Seasonality
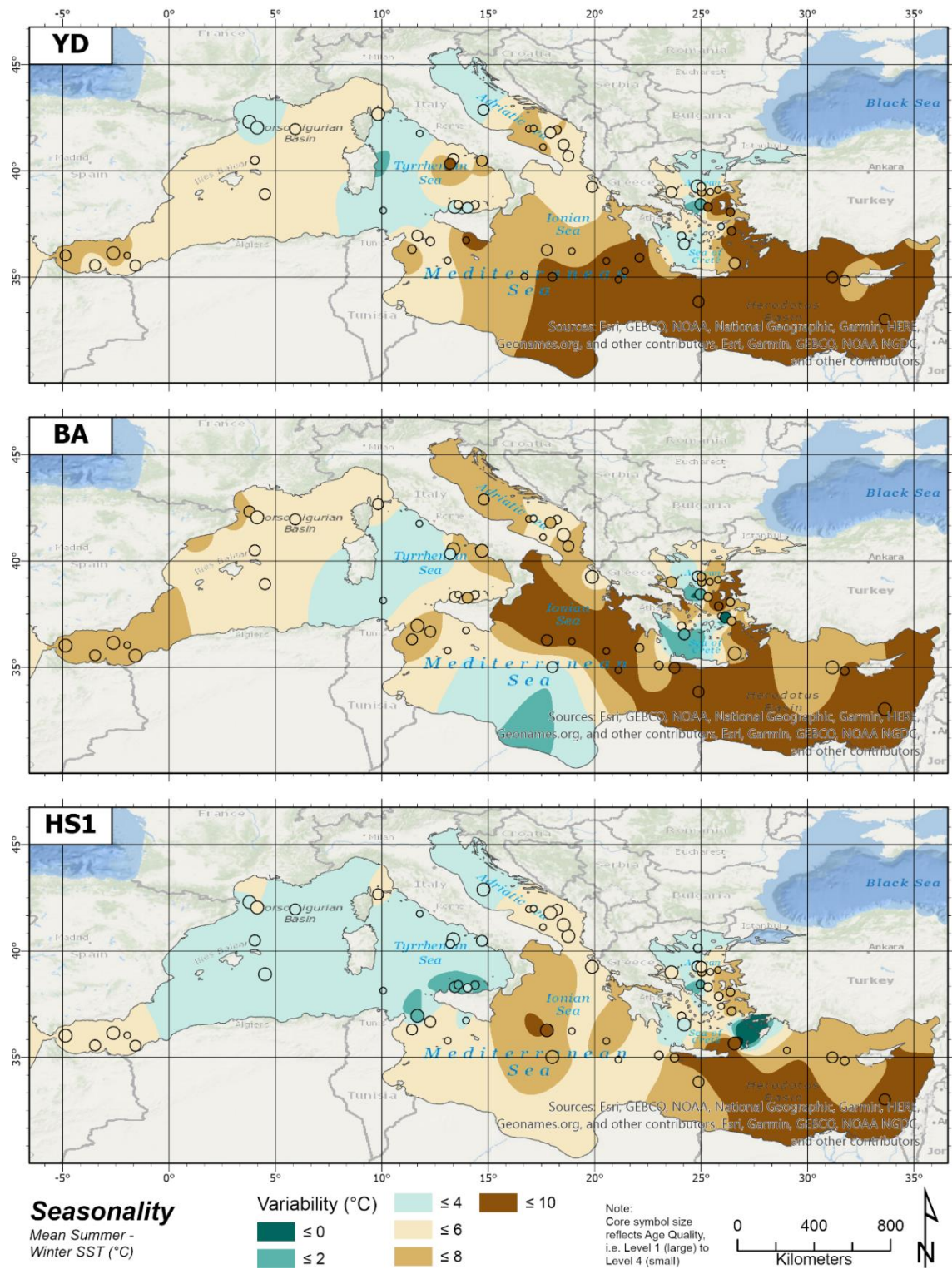
Figure 6.18: Seasonal variation (°C) during HS1, BA and YD. Seasonality variability = Mean summer SST – mean winter SST.

Patterns in seasonality were calculated as the difference between the predicted mean summer SST and mean winter SST (Table 6.4; Figure 6.18). The variation between summer and winter SSTs during HS1 was on average 4.71°C, primarily in the eastern basin (5.31°C). However, in contrast, seasonality was low in areas of the Adriatic and Aegean Seas. The mean variability in the western basin was 3.41°C, with some regional variation, e.g. in the Alboran (≤6°C) and southern Tyrrhenian (≤2°C) Seas.

Seasonal SST variations increased during the BA (5.95°C) and occurred extensively across both basins. Mean SSTs in the western basin were 5.39°C, with extensive areas in the central and eastern basin varied by ≤10°C (mean SSTs in the eastern basin were 6.21°C). Only the Tyrrhenian Sea, sections of the Aegean Sea and southern Mediterranean Ridge area showed more moderate SST variability (≤4°C).

Seasonality remained high during the YD (5.89°C) across the Mediterranean. This is especially true along the Mediterranean Ridge into the Levantine Sea, where seasonal SST varied ≤8 to 10°C (mean seasonal variation in the eastern basin was 6.42°C). Seasonal SST variation in the western basin was on average 4.84°C. However, there is a noticeable decrease in many northerly regions, i.e. the Gulf of Lion and northern Adriatic, and in the western Tyrrhenian Sea and DWF areas of the Aegean Sea.

6.2   Discussion

6.2.1   Heinrich Stadial 1

The decrease in SSTs during HS1 (~17.1 to 14.7 kyr BP) is substantial, especially in the western basin and the northern Adriatic Sea, which experienced a mean ~7°C cooling in comparison to the modern day (Table 6.4; Figure 6.19). SSTs were markedly different between the two basins, particularly during summer months (3.75°C), with a clear transition in the waters to the south of Sicily (~15°E), as well as in the central Adriatic Sea (~42°N) (Table 6.4, Figure 6.14; Figure 6.15). Mean annual SSTs for the chronozone are broadly comparable to those reported for the Gulf of Lion (Melki *et al.*, 2009), Balearic Sea (Dubois-Dauphin *et al.*, 2017), Alboran Sea (Cacho *et al.*, 1999; Cacho *et al.*, 2001; Martrat *et al.*, 2014; Bazzicalupo *et al.*, 2018), Tyrrhenian Sea (Sbaffi *et al.*, 2004; Di Donato *et al.*, 2008) and the southern Aegean Sea (Geraga *et al.*, 2005). It should be noted that as SSTs are reconstructed using a variety of methods, direct comparison between different transfer functions and proxies can be problematic. For example, Modern Analogue Technique (MAT) transfer functions predicts SSTs

during April–May (Kallel *et al.*, 1997b), whereas C_{37} alkenone production in *E. huxleyi* is seasonally variable, peaking in the spring and autumn in the modern western Mediterranean and Adriatic Sea (Essallami *et al.*, 2007; Sicre *et al.*, 2013; Rodrigo-Gámiz *et al.*, 2014a). Additionally, it was found that alkenone SSTs estimates during cold periods such as HS1 and the YD in the southern Adriatic were higher than those predicted using MAT, as it is believed that alkenone production was delayed until the short warmer summer season when surface waters were stratified, therefore there was little reflection of the cold deeper waters below (Sicre *et al.*, 2013). Therefore, these differences in SST estimates may reflect the variable impact of seasonality and/or palaeoecology of the foraminiferal assemblage in comparison with alkenone producers (Jiménez-Amat and Zahn, 2015). There are some more substantial variations between the ANN predictions and some reported SST values, e.g. MAT April-May estimates of ~9°C in the Tyrrhenian Sea is much cooler than the ~11 to ~13°C predicted annual SSTs using ANN (in this study) (Kallel *et al.*, 1997b). Also, predicted annual SSTs for the southern Adriatic Sea (≤17°C) are not as cool as the MAT estimates (~12°C) reported by Siani *et al.* (2001) and are closer to the winter predictions.

Figure 6.19: Scatter plot of the annual SST anomalies (°C) for HS1 cores against Latitude (°N). The SST anomalies for each core was calculated as the annual SST for HS1 (predicted using ANN) - World Ocean Atlas (2018) annual SST (depth 10m) (Locarnini, 2018).

When comparing against the LGM, mean annual SSTs for the Mediterranean Sea were lower (13.57°C) than during those predicted for the LGM (14.24°C) (Figure 6.1; Table

6.1) (Hayes *et al.*, 2005). Indeed, there was less variability in SSTs across the western basin in comparison to the LGM (Figure 6.1), though a similar extensive cold signal was noted during previous glacial stages in the western basin (Hayes *et al.*, 1999). Seasonality was low in the western basin; this enhanced cooling was maintained during both the summer and winter seasons (Table 6.4; Figure 6.18). The similarity of estimated SSTs off the Iberian coast (10 to 16°C) to those predicted for the Alboran Sea (~11.6°C) show the connectivity of the two regions during this period (Naughton *et al.*, 2009; Martins *et al.*, 2015; Naughton *et al.*, 2016). These low SSTs, as well as the lack of seasonality both support evidence of the relatively stable southerly position of the polar front (~40°N) along the western Iberian margin during HS1, which had a direct impact on cooling the western basin (Figure 4.9) (Eynaud *et al.*, 2009; Martins *et al.*, 2015). The polar front was located further north during the LGM, which would account for the more moderate SSTs in the western basin at that time (Figure 4.9; Figure 6.1).

The greater abundance and distribution pattern of Neogloboquadrina species in the western basin (Figure 6.3) illustrate the periodic inflow of cold North Atlantic Surface Waters (NASW) during Heinrich Events (HE) into the western basin (Rohling *et al.*, 1998; Cacho *et al.*, 1999; Cacho *et al.*, 2000; Sierro *et al.*, 2005). Peaks of *N. pachyderma* (>10%) reported in the Gulf of Cádiz, Alboran Sea and up into the Gulf of Lion were associated with these cold fresher NASW (Rohling *et al.*, 1998; Cacho *et al.*, 1999; Cayre *et al.*, 1999; Eynaud *et al.*, 2009; Melki *et al.*, 2009; Bassetti *et al.*, 2010; Martins *et al.*, 2015). Although this data compilation cannot differentiate between *N. pachyderma* and *N. incompta* (especially from older datasets), it can be safely assumed that the elevated rates in Neogloboquadrina species centred in the Alboran Sea would include these signature peaks of *N. pachyderma*. The patterns of both the low winter SSTs and Neogloboquadrina distribution in the western basin suggests that these cold NASW cooled the MAW, which spread through the western basin and flowed through the Straits of Sicily (Figure 6.3; Figure 6.17).

In addition, the cold winter SSTs in the Gulf of Lion point to the southern expansion of the polar jet stream, which allowed cold dry polar air to be funnelled deep into the north-west basin, enhancing periods of increased cyclogenesis (Naughton *et al.*, 2009; Naughton *et al.*, 2016). These cold winds would have contributed to the seasonal cooling of surface waters and increasing densities that would have led to periods of enhanced Western Mediterranean Deep Water (WMDW) formation (Rohling *et al.*, 1998). However, this signal of enhanced deep mixing masks the more subtle suggestion

of periods of reduced deep water ventilation that were associated with the deposition of Pre-ORL1 in the western basin (Sierro *et al.*, 2005; Rogerson *et al.*, 2008; Melki, 2011).

The Straits of Sicily is an area of transition between the colder west and more moderate eastern basin. Cores in the region report spring SSTs ranging from 8 to ~16°C from the early to late HS1, similar to the ~6°C seasonal variation in the region (Rouis-Zargouni *et al.*, 2010). The response of the eastern basin was much more measured, with cold winter SSTs and warm moderately to highly stratified summer waters in the Ionian and Levantine Seas that are comparable to both the modern day SSTs and the LGM (Figure 6.1; Figure 6.19) (Hayes *et al.*, 2005). In the south east, predicted SSTs are similar to the ~4.5°C cooling from geochemically reconstructed SSTs adjacent to the Nile River delta (Castañeda *et al.*, 2010). Therefore, it can be concluded that the influence of the oceanic polar front and incoming polar air did not extend as far as this region. This decreasing influence has been observed in cores in the Strait of Sicily and southern Aegean (Geraga *et al.*, 2005). The Aegean Sea has the greatest range in SST anomalies, ranging from the mildest SSTs to ~9°C cooler in comparison to modern SSTs (Figure 6.15; Figure 6.19). However, the solitary high SST datapoint in the northern Aegean is a poorly constrained, low AQ core, therefore should be treated with caution. Outflow of cold Adriatic and Aegean waters are clearly evident extending south into the main basin. These cold winter SSTs in the northern Adriatic, southern Aegean Sea, as well as cooler waters in the northern Levantine Sea equate to areas of deep or intermediate water formation (Figure 6.15). This suggests that the Bora and Etesian winds were consistently strong during HS1, as a consequence of increased cyclogenesis in the Gulf of Genoa (that trigger low pressure in the Adriatic, heightening the Bora winds), or strong Siberian ridge systems were present in winter in central Europe (Grisogono and BeluŠIĆ, 2009). These cold winds were actively cooling surface waters in the northern margins of the eastern basin, triggering intermediate and deep ventilation in the eastern basin (Figure 6.17). As with the western basin, annual SSTs in the eastern basin were cooler (~2.3°C) than predicted for LGM (Table 6.1; Table 6.4). However, the LGM reconstructions unfortunately did not include data points from the northern Adriatic, which consistently experienced the coldest SSTs during all chronozones, so the LGM prediction may be underestimated (Hayes *et al.*, 2005).

Along the northern margin, summer SSTs remained cool indicating the probable seasonal influx of cold meltwaters from the mountain glaciers that fringed the northern Mediterranean Sea. This is especially evident in the northern Adriatic, where the

significant peak in *T. quinqueloba* along with heightened levels of *G. bulloides* suggest these opportunistic species responded to the heightened productivity triggered by the discharge of cold Alpine waters from the River Po (Jorissen *et al.*, 1993). Indeed, it has been suggested that due to lower sea levels, these northern Adriatic cores would have been located closer to the mouth of the River Po at this time (Jorissen *et al.*, 1993; Zecchin *et al.*, 2015).

With lower sea levels during the LGM, the Strait of Sicily acted as a physical barrier to the exchange of water masses between the two basins (Cornuault *et al.*, 2018). Global sea levels were estimated to be -90m rsl at this time (Jouet *et al.*, 2006; Stanford *et al.*, 2011a). Although still low, the increase in sea level would have allowed the re-establishment of hydrological exchange between the two basins. As mentioned above, the west-east SST divide between the basins was less defined in the winter, as cold waters extended through the Strait of Sicily into the eastern basin. $\delta^{13}C$ values and neodymium (Nd) isotopic composition illustrate this increased influence of MAW in the eastern Mediterranean (Cornuault *et al.*, 2018). In addition, the outflow of the slightly warmer, saline LIW can be traced by the more moderate SSTs ($\leq 13°C$) that extend up into the central Tyrrhenian Sea, as well as the presence of deeper species such as *T. quinqueloba* and minor frequencies of *G. inflata* and *G. scitula*.

The HS1 planktonic foraminifera community was dominated by cooler water, eutrophic assemblages (Neogloboquadrina species, *G. bulloides*, *T. quinqueloba*, *G. glutinata* and *G. scitula*) with *G. ruber* as the only significant warm water representative. This is quite different to the modern assemblage, which is composed of *G. ruber* white, *G. ruber* pink, *G. elongatus* and *O. universa*, primarily in the eastern basin and decreasing towards the south-western basin; whereas *G. bulloides*, *N. incompta*, *G. inflata* and *G. truncatulinoides* sinistral dominate the western basin, peaking mainly during the winter-spring bloom (Thunell, 1978; Pujol and Vergnaud Grazzini, 1995; Bárcena *et al.*, 2004; Hernández-Almeida *et al.*, 2011; Rigual-Hernández *et al.*, 2012; Mallo *et al.*, 2017; Avnaim-Katav *et al.*, 2020). Also, in the modern Mediterranean Sea, *T. quinqueloba* are only regionally significant in certain cooler water regions, and *G. glutinata* and *G. scitula* are rare (<5% of any assemblage) (Thunell, 1978; Pujol and Vergnaud Grazzini, 1995).

In general, as HS1 conditions were cold and dry, precipitation and fluvial input were reduced in the region (Bar-Matthews *et al.*, 1997; Bar-Matthews *et al.*, 1999; Bartov *et*

al., 2003; Moreno *et al.*, 2010; Box *et al.*, 2011). However, the southerly position of the Atlantic jet stream, strengthened katabatic winter winds and increased cyclogenesis were key to increasing deep mixing and productivity in the Gulf of Lion (WMDW), Adriatic and Aegean Seas (EMDW), and within the Rhodes Gyre (LIW) (Figure 6.12). This higher productivity allowed the opportunistic *G. bulloides* and *T. quinqueloba*, as well as Neogloboquadrina species and more modest amounts of *G. glutinata* to flourish. As mentioned above, deep convection was not constant during HS1. This strong eutrophication signal across the western basin agrees with other proxies that suggest the surface water productivity remained high, even when accompanied with decreased deep convection, and led to the deposition of the pre-ORL1 layer during HS1 (Cacho *et al.*, 2002; Rogerson *et al.*, 2008; Melki, 2011; Rodrigo-Gámiz *et al.*, 2011; Martinez-Ruiz *et al.*, 2015).

The warmer water assemblage is comprised of *G. ruber* plexus, with just minor SPRUDTS. *G. ruber* plexus is the is one of the dominant groups in the warm, stratified oligotrophic waters of the modern Mediterranean, especially in the eastern basin (Cifelli, 1974; Thunell, 1978; Pujol and Vergnaud Grazzini, 1995; Mallo *et al.*, 2017; Avnaim-Katav *et al.*, 2020). However, it only forms ~11% of the population during HS1. *G. ruber* plexus inhabited the south and east of the Ionian and Levantine Seas, in a similar distribution pattern for the equivalent period as mapped by Thomopoulos *et al.* (2010). Modern studies have identified specific genotypes within *G. ruber* plexus, and to a more limited degree *G. siphonifera*, that are able to flourish in more productive late spring to early autumn waters than other predatory species (Numberger *et al.*, 2009; Mallo *et al.*, 2017). In the modern Levantine Sea, *G. ruber* peaks in the winter during short periods with the coolest SSTs (~18°C) and maximum in chlorophyll concentrations, followed by minor peaks of *O. universa* and *G. ruber* pink in the warm (~25°C) ultraoligotrophic summer waters (Pujol and Vergnaud Grazzini, 1995; Avnaim-Katav *et al.*, 2020). However, winter SSTs in the central and eastern basin were much cooler than the preferred thermal range (21.8 to 30.6°C) of *G. ruber* white (Bijma *et al.*, 1990; Žarić *et al.*, 2005). Therefore, it can be suggested that the *G. ruber* plexus population peaked later in the season coinciding with warmer waters. In the modern western basin, *G. ruber* white is generally a minor element of the population, peaking in the summer/early autumn stratified waters in the Gulf of Lion, though it can form a minor part of the spring assemblage in the Alboran Sea (Bárcena *et al.*, 2004; Hernández-Almeida *et al.*, 2011; Rigual-Hernández *et al.*, 2012). Similarly, *G. ruber*

plexus is only a minor component of the HS1 assemblage and was found mainly in the Tyrrhenian Sea, suggesting that SSTs were too cold for it during most of the chronozone.

Despite the inflow of cold NASWs during HEs, predicted summer SSTs were not as cold in the Alboran Sea in comparison to the northern regions of the Mediterranean (Figure 6.16). Both these slightly warmer summer SSTs and presence of minor *G. ruber* in the northern Alboran Sea suggest that there may have been limited inflow of subtropical NASW through the Strait of Gibraltar, possibly nearing the final stages of HS1 (Bazzicalupo *et al.*, 2018; Ausín *et al.*, 2019). These periodic warmer waters would have extended along the North African coast as the Modified Atlantic Water (MAW), then split to enter the southern Tyrrhenian Sea and eastwards through the Strait of Sicily. In the Strait of Sicily, there was a notable peak of *G. sacculifer*, which is a common member of the modern assemblage in this region (Pujol and Vergnaud Grazzini, 1995). Although summer SSTs ($\leq 15°C$) were on the lower end of their optimum temperature preference, as a euryhaline species it would have tolerated the lower salinities of the MAW, potentially at the expense of other oligotrophic mixed layer species such as *G. ruber* white (Pujol and Vergnaud Grazzini, 1995; Schiebel and Hemleben, 2017). Further east however, *G. sacculifer* was replaced by the prevalence of *G. ruber* plexus.

Although they occur in lower abundances, the distribution of the deeper *G. scitula* and *G. truncatulinoides* is interesting, as both are more prevalent in the eastern basin during HS1. *G. scitula* is predominantly described as a cooler water species and rare in modern Mediterranean (Pujol and Vergnaud Grazzini, 1995; Itou *et al.*, 2001; Chapman, 2010; Schiebel and Hemleben, 2017). However, during HS1 it is more commonly found in association with warmer *G. ruber* and SPRUDTS species. In addition, in modern waters *G. truncatulinoides* sinistral is a key species in the western basin and largely absent from the eastern basin (Thunell, 1978; Pujol and Vergnaud Grazzini, 1995). It can be inferred that these species were able to inhabit the deeper cooler productive waters of the eastern basin during periods of seasonal stratification.

G. inflata is regarded as a transitional species and is very rare/absent during cold periods such as the HS1 and its appearance usually marks the transition to the BA (Bé and Tolderlund, 1971; Thunell and Williams, 1983; Muerdter and Kennett, 1983/84; Jorissen *et al.*, 1993Rohling, 1998 #641). In the western Mediterranean, it is a

ubiquitous late autumn to spring deep-dwelling species, with a diverse range of habitats. In the modern Gulf of Lion, *G. inflata* formed ≤10% of the winter/spring bloom assemblage, peaking in March when cool surface waters are deeply mixed (Thunell, 1978; Pujol and Vergnaud Grazzini, 1995; Rigual-Hernández *et al.*, 2012). In contrast, it is a dominant species in the modern Alboran Sea, peaking in the late autumn/winter (November to January) and minor fluxes in the early summer (May to August), and was associated with stable, mesotrophic to oligotrophic waters, with deep thermoclines (Pujol and Vergnaud Grazzini, 1995; Bárcena *et al.*, 2004; Hernández-Almeida *et al.*, 2011). Further east, *G. inflata* is found in north African coastal waters along the path of the MAW, into the south-eastern Tyrrhenian Sea and through the Strait of Sicily, as well in the western flow of the LIW (Thunell, 1978; Pujol and Vergnaud Grazzini, 1995). As expected, the distribution of *G. inflata* is low (<2%) during HS1. Therefore, its virtual absence from the western basin suggests that conditions were potentially too cold for this species, or during periods of increased water column instability and heightened productivity, it was out competed by the opportunistic *G. bulloides* and *T. quinqueloba* (Bárcena *et al.*, 2004).

Interpolating the mean E- and S-Indices values for each chronozone is a novel way of using foraminifera proxy data as palaeoenvironmental indicators. These indices have been applied to downcore analysis, particularly in the eastern basin, but have not applied to a dataset such as this, or interpolated to map their distribution over a wide geographic area (Sbaffi *et al.*, 2004; Kontakiotis, 2016; Giamali *et al.*, 2020). As expected, the dominance of Neogloboquadrina species, *G. bulloides* and *T. quinqueloba* in the western basin, as well as both Adriatic and Aegean Seas produced a strong E-Index (Figure 6.12). This is also supported by the very low S-Index, suggesting that these cool waters were deeply mixed (Figure 6.13). It can be assumed that the peak flux of fauna occurred during the winter/spring bloom period similar to modern oceans, though with winter SSTs so cold, the timing of these bloom periods may have been later in the season (Bárcena *et al.*, 2004; Hernández-Almeida *et al.*, 2011; Rigual-Hernández *et al.*, 2012; Jonkers and Kučera, 2015).

While there are many similarities between the indices, i.e. eutrophication and seasonal stratification are indelibly linked, there are differences in their distribution that allow a deeper understanding of the potential changes to the water column during the deglacial. SSTs in parts of the Ionian and Levantine seas are comparable to today and waters are moderate to highly stratified (Figure 6.15; Figure 6.19). However, the E-Index is also

elevated across the southern basin, clearly illustrating these waters experienced periods of heightened seasonal productivity, which are very different to the modern stratified ultraoligotrophic waters (Avnaim-Katav *et al.*, 2020). Only coastal waters off Lebanon and Israel experienced any significant oligotrophic conditions. Seasonality across the Mediterranean decreased from the LGM (Table 6.1; Table 6.4) and is evident primarily in the Levant region, where SSTs varied by ~10°C and seasonal stratification of the water column is apparent (Figure 6.13; Figure 6.18). This suggests that the impact of diverging summer and winter insolation curves was not yet a significant factor in the Mediterranean Sea during this chronozone (Figure 4.8).

6.2.2 Bølling/Allerød

With the increase in atmospheric temperatures and the strengthening of the AMOC in the North Atlantic during the BA (14.7 to 12.8 kyr BP), mean annual SSTs across the Mediterranean Sea improved (~15°C). However, they were only ~1.5°C warmer than those predicted for HS1 and 3.63°C lower in comparison to modern SSTs (Table 6.4). The distribution of SSTs across the sea was quite different to the west-east divide during HS1, or the north-west to south-east warming of the modern sea (Figure 2.5). Variability between the basins was <2°C (Table 6.4) and the Gulf of Lion and Adriatic Sea experienced a similar degree of cooling as the Ionian and Levantine Seas (-4 to -5°C). In contrast, the Aegean and Tyrrhenian Seas experienced the greatest variability and coolest annual SSTs during the BA, with anomalies reaching -9.5°C compared to the modern sea (Figure 6.20). Again, when compared with previous studies, these predicted SSTs are comparable to the generalised SST estimates, e.g. in the Alboran Sea (Cacho *et al.*, 1999; Cacho *et al.*, 2001; Martrat *et al.*, 2014; Rodrigo-Gámiz *et al.*, 2014a; Bazzicalupo *et al.*, 2018), the Gulf of Lion (Melki *et al.*, 2009), Balearic Sea (Dubois-Dauphin *et al.*, 2017); Tyrrhenian Sea (Sbaffi *et al.*, 2004; Di Donato *et al.*, 2008), the southern Aegean Sea (Geraga *et al.*, 2005) and Levantine Sea (Castañeda *et al.*, 2010). However, SSTs estimated using alkenones for the Straits of Sicily and the Southern Adriatic were ~3°C cooler and were more similar to ANN winter or April-May MAT estimates (Essallami *et al.*, 2007; Sicre *et al.*, 2013).
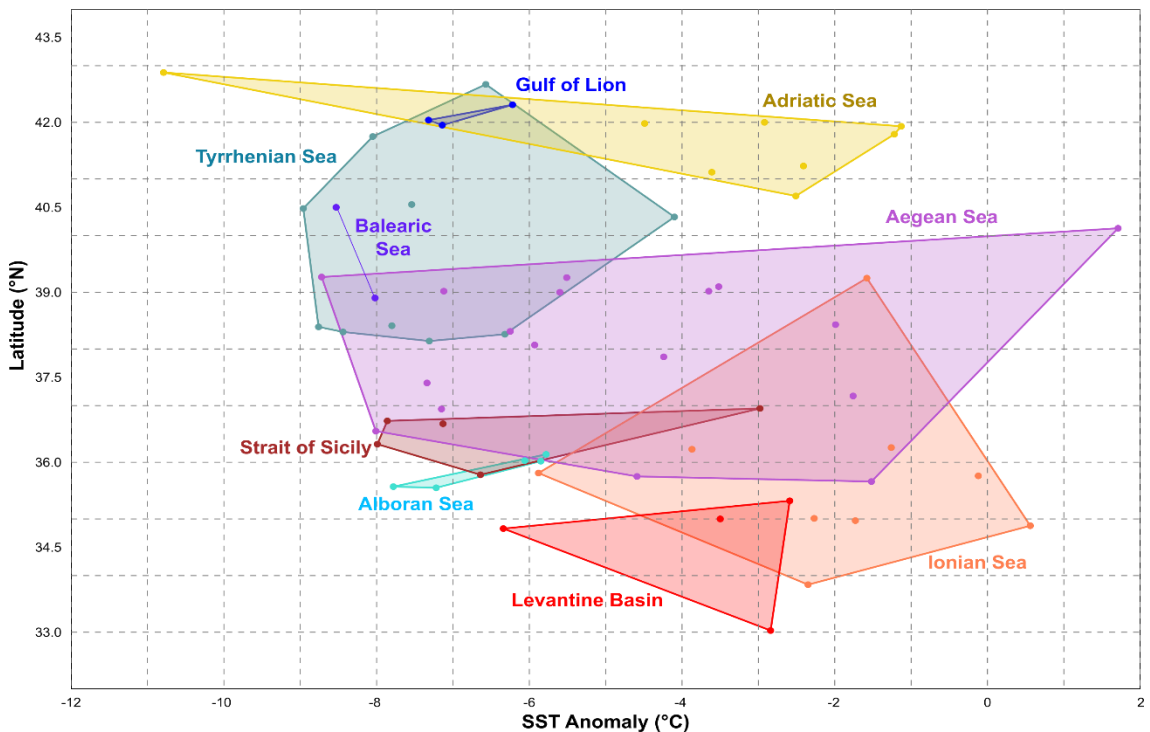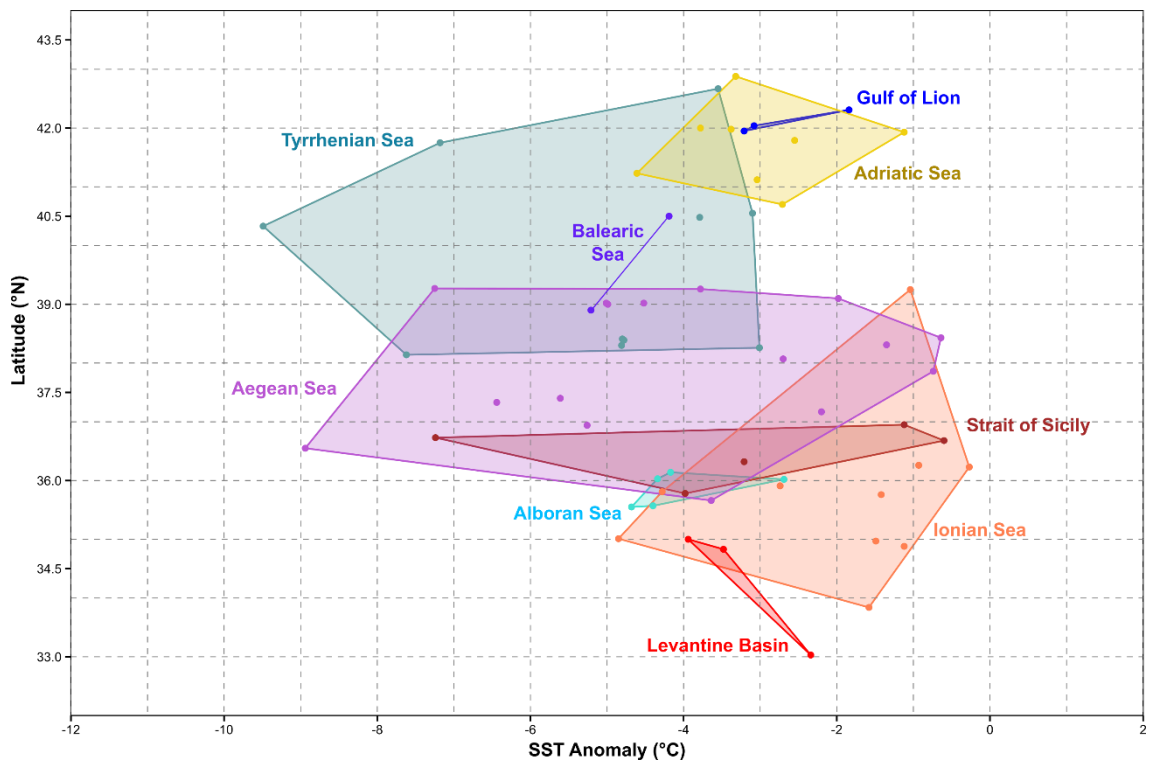
Figure 6.20: Scatter plot of the annual SST anomalies (°C) for BA cores against Latitude (°N). The SST anomalies for each core was calculated as the annual SST for BA (predicted using ANN) - World Ocean Atlas (2018) annual SST (depth 10m) (Locarnini, 2018).

As discussed in Chapter 4, temperatures recorded in Greenland ice cores during GI-1 (Figure 4.4) exhibit the classic DO sawtooth pattern (Li and Born, 2019). However, the response and timing of SST change to the BA warming varied across the Mediterranean (Cacho *et al.*, 2001; Rodrigo-Gámiz *et al.*, 2014a; Jiménez-Amat and Zahn, 2015). Given the generalised nature of these SST predictions, both warm and the brief cold climate oscillations within the BA may/may not be represented, or overrepresented. This may be a factor for the variability observed for areas such as the Aegean Sea, where some cores have a low number of samples per chronozone Appendix 1b) (Aksu *et al.*, 1995b; İşler *et al.*, 2016a; İşler *et al.*, 2016b).

With the strengthening of the AMOC and the northern retreat of the polar front during the BA, the western basin was under greater influence of incoming warmer waters from the North Atlantic subtropical gyre (Schwab *et al.*, 2012; Jiménez-Amat and Zahn, 2015; Repschläger *et al.*, 2015). This is especially evident in the summer SST predictions in the western basin, where warm water extends from the Alboran Sea to the Gulf of Lion (Figure 6.16). The cool winter SSTs predicted in the Southern Alboran Sea may reflect the periodic inflow of cooler fresher waters during the short GI-1b or GI-1d or the resumption of deep mixing associated with the gyres (Cacho *et al.*, 2001). The more moderate winter SSTs in the north-west basin and southern Adriatic Sea suggest

milder winters with less influence from cold seasonal winds from the North Atlantic (Dubois-Dauphin *et al.*, 2017). The reduced winds would have consequences for DWF in these regions, reducing deep ventilation of the western basin, which contributed to the deposition of ORL1 during the BA (Cacho *et al.*, 2002; Rogerson *et al.*, 2008; Martinez-Ruiz *et al.*, 2015; Pérez-Asensio *et al.*, 2020).

Predicted SSTs in the western Tyrrhenian Sea are much reduced in comparison to the rest of the western basin, presumably due to the increased abundance of *T. quinqueloba* in two low AQ cores. Although rare in the modern Mediterranean, this species is relatively common in the cool, eutrophic well mixed water of the Alboran Sea, as well as Ligurian Sea and south of Sardinia (Cifelli, 1974; Thunell, 1978). During the BA, *T. quinqueloba* flourished in coastal locations along the Italian coast, suggesting that it was under the influence of enhanced fluvial/meltwater discharge and increased precipitation (Kallel *et al.*, 1997b; Cacho *et al.*, 2001; Di Donato *et al.*, 2008; Di Donato *et al.*, 2009; Lirer *et al.*, 2013). In addition, it has been noted that the Older Dryas and Inter-Allerød Cold Period were clearly documented in both terrestrial and marine proxies in the region (Cacho *et al.*, 2001; Combourieu Nebout *et al.*, 2009; Dormoy *et al.*, 2009; Fletcher *et al.*, 2010). This suggests the reorganisation of atmospheric circulation during these short cold periods allowed cold Westerly winds from the North Atlantic to be funnelled into the region, cooling SSTs (Cacho *et al.*, 2001). Therefore, these cooler SSTs may be a closer approximate of the periodic cold events, rather than reflective of the mean values experienced during the full chronozone.

One of the main influences during the summer in the BA, in particular the eastern basin, was the initiation of the African Humid Period (AHP) (deMenocal *et al.*, 2000; Kontakiotis, 2016). The AHP was driven by a combination of rising summer insolation, the northern position of the ITCZ, which allowed the African Monsoons to penetrate further north into the Mediterranean, and increased riverine input (Asioli *et al.*, 2001; Schmiedl *et al.*, 2010; Cornuault *et al.*, 2016; Dubois-Dauphin *et al.*, 2017; Cornuault *et al.*, 2018). In addition, rising sea levels and increased meltwater input (e.g. MWP-1A or seasonal meltwater fed from alpine regions) would have contributed to a decrease in surface water density and deep ventilation, and enhanced stratification (Rogerson *et al.*, 2008; Fink *et al.*, 2015; Rohling *et al.*, 2015). In the eastern basin, both the S-Index and E-Index reflect this strengthened stratification and expanded oligotrophic signal. SSTs in the eastern basin also show increasing seasonality (Figure 6.18), as a result of the increasing disconnect between the summer and winter insolation values (Figure 4.8).

There was a change in the distribution and greater diversity of the planktonic foraminiferal assemblage from HS1 to the BA. Once again, there was a dominance in the high productivity Neogloboquadrina species and *G. bulloides*, with lower percentages of *G. glutinata*. Both *T. quinqueloba* and *G. scitula* decreased in abundance, and *G. inflata* made an appearance. *G. ruber* plexus increased, accompanied by low, but regionally abundant SPRUDTS. Although the composition of the dominant fauna was similar to the col HS1 chronozone, there is a definite expansion of the habitats of warmer species into the western basin and Adriatic and Aegean seas, as well as a reorganisation of the eutrophic species.

Neogloboquadrina species and *G. bulloides* form more than 50% of the population. In modern waters, e.g. the Gulf of Lion, both species are abundant in sediment traps during periods of peak annual chlorophyll-*α* and phytoplankton blooms (Rigual-Hernández *et al.*, 2012). In general, *G. bulloides* is widespread, mainly in the western basin, but also in low abundances in the eastern basin (Figure 6.2) (Thunell, 1978; Pujol and Vergnaud Grazzini, 1995; Mallo *et al.*, 2017). In the Gulf of Lion, *G. bulloides* was the most abundant species in the deeply mixed waters from February to April, demonstrating clear opportunistic behaviours in response to the outflow of nutrient rich waters in the Rhône delta plum (Rigual-Hernández *et al.*, 2012). In the Alboran Sea, it was associated with *T. quinqueloba*, peaking during seasonal upwelling events (Bárcena *et al.*, 2004; Hernández-Almeida *et al.*, 2011). In sediment traps and plankton tows in the Ionian and Levantine seas, very low numbers of *G. bulloides* were observed in winter waters, where eddies were able to sustain phytoplankton blooms (Mallo *et al.*, 2017; Avnaim-Katav *et al.*, 2020). *N. incompta* is largely restricted to the cooler waters of the north-western basin, though it does occur in lower abundances elsewhere across the sea, whereas *N. pachyderma* is forms <1% of the modern Mediterranean assemblage (Figure 6.2) (Thunell, 1978; Pujol and Vergnaud Grazzini, 1995). In the Gulf of Lion, *N. incompta* was positively correlated to deeply mixed bloom periods, peaking in March, but it was also more abundant in more distal core top traps and plankton tow stations, where primary productivity was less intense (Pujol and Vergnaud Grazzini, 1995; Rigual-Hernández *et al.*, 2012). *N. incompta* was present at all depths in the Gulf of Lion plankton tows, but peaked ~50m, coinciding with maximum chlorophyll concentrations (Pujol and Vergnaud Grazzini, 1995). However, given the association of *N. incompta* with cooler waters of the north west and also with mesopelagic depths along the North African coastline, Pujol and Vergnaud Grazzini (1995) suggest that

SSTs may also be a limiting factor in their abundance.

Therefore, while both *G. bulloides* and *N. incompta* are eutrophic species, their response to trophic events, hydrological structure and SSTs are subtly different. In modern waters, *G. bulloides* is opportunistic, resilient over longer bloom periods and can take advantage of heightened productivity over a wide range of habitats. In contrast, *N. incompta* is much more reliant on cooler, productive waters, with more discrete flux peaks and can be associated with pycnocline depth and chlorophyll concentrations (Fairbanks and Wiebe, 1980; Rohling and Gieskes, 1989; Pujol and Vergnaud Grazzini, 1995; Kuroyanagi and Kawahata, 2004; Rohling *et al.*, 2004).

During the BA, the distribution of *G. bulloides* and Neogloboquadrina species was broadly similar to their modern distribution, though with some variations (Thunell, 1978; Pujol and Vergnaud Grazzini, 1995). *G. bulloides* is elevated in both the Alboran Sea and northern Adriatic, along with more modest occurrences of *G. ruber* plexus, *G. inflata* (in the Alboran Sea) and *T. quinqueloba* (in the Adriatic). These species are important components of the modern annual Alboran Sea assemblage, though there are no modern analogues for the winter assemblage in the northern Adriatic Sea (Cifelli, 1974; Thunell, 1978; Pujol and Vergnaud Grazzini, 1995; Mallo *et al.*, 2017). Therefore, in the Alboran Sea during the BA, there was a return to more modern conditions, indicative of high winter productivity triggered by upwelling, along with seasonally stratified, more oligotrophic conditions during warmer summer/autumn months (Cacho *et al.*, 2001; Bárcena *et al.*, 2004; Hernández-Almeida *et al.*, 2011).

The distribution of *G. bulloides* and Neogloboquadrina species the rest of the western basin, into the eastern basin, clearly show heightened productivity during the cooler winter/spring season. The strong eutrophic signal in the western basin is in agreement with the heightened productivity associated with enhanced precipitation and freshwater inflow during the BA, which led to a shoaling of the LIW, switch to WIW formation in the Gulf of Lion and initiated the deposition of ORL1(Cacho *et al.*, 2002; Rogerson *et al.*, 2008; Martinez-Ruiz *et al.*, 2015; Pérez-Asensio *et al.*, 2020). Seasonal monsoonal inflow would have added nutrient rich waters that supported the eutrophic community in the eastern basin (Castañeda *et al.*, 2010). With rising sea levels, the inflow of cooler, nutrient rich, euryhaline waters allowed Neogloboquadrina species to flourish, when the northern Aegean reconnected with the Black Sea (Vidal *et al.*, 2010). In the northern Adriatic Sea, the peak of *G. bulloides* and *T. quinqueloba* is a clear fluvial/meltwater

signal from the River Po (Jorissen *et al.*, 1993).

As mentioned above (section 6.2.1), *G. inflata* was largely absent in HS1, but formed a minor but locally significant member of the BA winter/spring assemblage (<8%). Its presence, in association with *G. ruber* plexus, suggest that the Gulf of Lion and Balearic Sea experienced more stable periods (i.e. reduced deep mixing associated with weakened WMDW formation), where the thermocline was deeper and meso- to eutrophic conditions prevailed (Bárcena *et al.*, 2001; Hernández-Almeida *et al.*, 2011). This is reflected in the seasonal stratification signal in these areas. *G. inflata* avoided the cooler waters of the western Tyrrhenian Sea (≤11°C), though its distribution in the south-eastern Tyrrhenian Sea and Strait of Sicily is similar to modern observations, where it is linked to the flow of the MAW and LIW (Thunell, 1978; Pujol and Vergnaud Grazzini, 1995). Milder winter SSTs and monsoon driven productivity allowed for it to form part of the eastern Mediterranean assemblage.

G. truncatulinoides (total) is a minor component of the BA assemblage, yet its distribution is interesting. In the modern sea, the deep dwelling *G. truncatulinoides* sinistral is primarily a western basin species, where it flourishes in winter and is correlated to deeply mixed productive waters (Thunell, 1978; Pujol and Vergnaud Grazzini, 1995). Therefore, its occurrence in the Ligurian Sea (≤5%) during the BA is similar to that of modern times. However, *G. truncatulinoides* (total) was widespread in the Ionian and Levantine Seas (≤10%), correlating with more stratified waters. This would suggest that this population was mainly *G. truncatulinoides* dextral, which are more abundant when the thermocline is shallow (Lohmann and Schweitzer, 1990; Darling and Wade, 2008; Ujiié *et al.*, 2010; Billups *et al.*, 2016). Unfortunately, we cannot be certain, as most datasets do not differentiate the coiling direction of the *G. truncatulinoides* morphospecies.

The warmer water assemblage was primarily dominated by *G. ruber* plexus, with low to moderate frequencies of the SPRUDTS group. These groups illustrate the expansion of warm SSTs and influence of the AHP, which allowed for seasonal stratification and oligotrophic conditions in the eastern basin (Cornuault *et al.*, 2016; Cornuault *et al.*, 2018). In modern waters, *G. ruber* plexus is widespread, particularly in the east and southern western basin (Cifelli, 1974; Thunell, 1978; Pujol and Vergnaud Grazzini, 1995; Mallo *et al.*, 2017). Sediment trap and plankton tow studies in the Levantine Sea and across the eastern basin demonstrate that the ubiquitous *G. ruber* white had a

bimodal peak, peaking in the winter (February) with *G. rubescens* and *G. calida*, followed by a smaller peak in summer (August/September), accompanied by *G. ruber* pink and *O. universa* (Cifelli, 1974; Pujol and Vergnaud Grazzini, 1995; Mallo *et al.*, 2017; Avnaim-Katav *et al.*, 2020). Different *G. ruber* genotypes have been seen to thrive in productive waters, e.g. *G. elongatus* inhabits higher productivity shallow waters (Numberger *et al.*, 2009). In comparison to HS1, alkenone production is estimated to have returned to the April-May period (Sicre *et al.*, 2013). As winter SSTs were still relatively cool in the eastern basin (≤17°C) and moderately productive, it can be assumed that *G. ruber* plexus may have peaked later in the late spring/early summer. In the western basin, these morphospecies are also evident in the Balearic, Alboran and eastern Tyrrhenian Seas, areas where they are common in the modern summer assemblage (Cifelli, 1974; Thunell, 1978; Pujol and Vergnaud Grazzini, 1995; Mallo *et al.*, 2017). With weakened surface water densities and deep-water ventilation in the western basin, seasonal stratification could become established, allowing them to expand their ranges. Once again, *G. sacculifer* occurred in in the Strait of Sicily to northern Tyrrhenian Sea, correlating to seasonal stratification in these waters.

6.2.3 Younger Dryas

The return to cold dry conditions during the YD chronozone (~12.8 to 11.55 kyr BP) in the northern hemisphere saw a decrease in sea and air temperatures in the North Atlantic, an expansion of sea ice and alpine glaciers, a reduction in precipitation and the southerly displacement of both the PF and ITCZ (Ruddiman and McIntyre, 1981; Bell and Walker, 2005; Ivy-Ochs *et al.*, 2007).

In the Mediterranean Sea, mean annual SSTs decreased to ~14.2°C. While not as low as those experienced during HS1, they were comparable to the predicted annual SSTs experienced during the LGM (Table 6.1; Table 6.4) (Hayes *et al.*, 2005). When examined in detail, winter SSTs were as cool as those experienced in HS1, but warmer during the summer. This strong seasonality signal could be expected, with the approach of the maximum differentiation between summer and winter insolation (Figure 4.8; Table 6.4; Figure 6.18) (Carlson, 2013). Indeed, these warm summer SSTs in the eastern basin support the warm summer temperatures suggested by terrestrial proxies in parts of northern and south central Europe (Schenk *et al.*, 2018; Magyari *et al.*, 2019; Schenk *et al.*, 2020).

When compared with previous studies in areas such as the Alboran Sea, southern Tyrrhenian Sea, the Straits of Sicily and central Adriatic Sea, mean annual SST predictions are not as cool as previously reported (Kallel *et al.*, 1997b; Cacho *et al.*, 1999; Cacho *et al.*, 2001; Essallami *et al.*, 2007; Rouis-Zargouni *et al.*, 2010; Sicre *et al.*, 2013). For example, from YD-1 to YD-2, alkenones SST estimates ranged from ~12 to ~15°C in the Alboran Sea and 11 to 16/18°C in the southern Tyrrhenian Sea (Cacho *et al.*, 2001). This is in comparison to the mean annual value of ≤15°C predicted for both areas in this study (Figure 6.14). As discussed in Chapter 4, YD-1 was primarily cold and dry and was followed by warmer, more humid conditions in YD-2 (Cacho *et al.*, 1999; Cacho *et al.*, 2001; Sbaffi *et al.*, 2004; Jimenez-Espejo *et al.*, 2007; Naughton *et al.*, 2016; Bazzicalupo *et al.*, 2018; Naughton *et al.*, 2019; Ausín *et al.*, 2020). Although the variability of the YD is not as extreme as experienced during the BA chronozone, there will be a similar generalisation of the complex YD signal in many areas of the Mediterranean Sea. However, the published ranges in SSTs from YD-1 to YD-2 are similar to the predicted summer/winter predictions in this study (Figure 6.18), therefore it is possible that seasonality signal in these regions may be an artefact of the SST variability experienced during the chronozone, rather than a true seasonality signal. In more northerly and easterly regions, there is greater agreement with the ANN SST predictions, e.g. Balearic Sea (Dubois-Dauphin *et al.*, 2017), Gulf of Lion (Melki *et al.*, 2009), northern Tyrrhenian Sea (Di Donato *et al.*, 2008) and the Levantine Sea (Essallami *et al.*, 2007; Castañeda *et al.*, 2010).

As discussed above (section 6.2.1), there was a clear differentiation between the cold western basin / warmer eastern basin during HS1, denoting the cooling influence of relatively stable southerly position of the polar front on the western basin. In contrast, the dominant cold SST anomalies (≤ -6°C) during the YD were primarily along northern margins and central Tyrrhenian Sea (Figure 6.21). There was a generalised north-south increase in annual SSTs, i.e. ~9°C in northern waters, increasing to ~15 and 21°C along the southern western and eastern basins respectively (Figure 6.14). In the western basin, these cold anomalies are more discrete than during HS1 and are closer to the anomaly patterns reconstructed for the LGM, whereas SSTs in the southern Adriatic and the Aegean Sea were colder than both HS1 and the LGM (Figure 6.1; Figure 6.15) (Hayes *et al.*, 1999; Hayes *et al.*, 2005). This strong cooling in northern waters suggests that heightened winds were the primary driver of this cooling. Cold westerly winds were funnelled deep into the north-western Mediterranean region, as a result of expanded sea

ice and reorganisation of atmospheric circulation patterns in the North Atlantic, which displaced the polar front jet stream to the south (Repschläger *et al.*, 2015; Naughton *et al.*, 2016; Rea *et al.*, 2020).
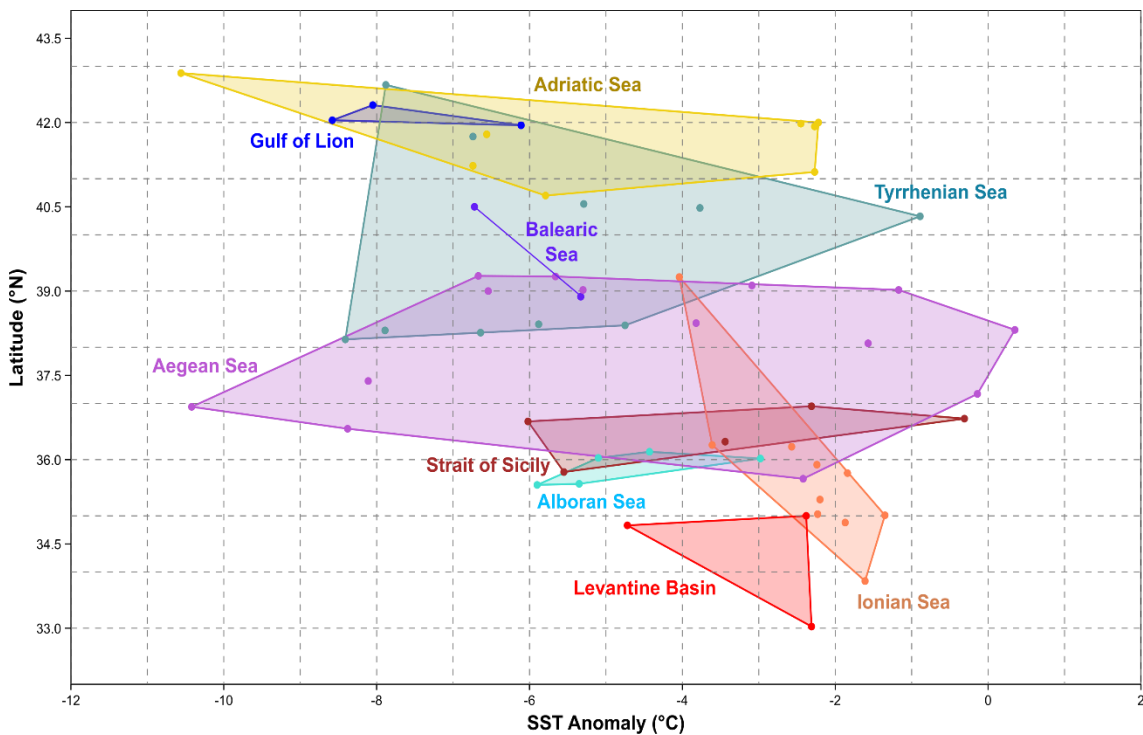
Figure 6.21: Scatter plot of the annual SST anomalies (°C) for YD cores against Latitude (°N). The SST anomalies for each core was calculated as the annual SST for YD (predicted using ANN) - World Ocean Atlas (2018) annual SST (depth 10m) (Locarnini, 2018).

Further south, annual SSTs in the Alboran and Balearic seas were warmer than experienced during the LGM and HS1 periods (Figure 6.21), and comparable to SSTs estimated off the south-western coast of Portugal at this time (Hayes *et al.*, 2005; Ausín *et al.*, 2020). The oceanic polar front was not positioned as far south as during HS1, though subarctic waters extended to ~40°N along the Iberian Margin, redirecting the Azores Front further south towards the Gulf of Cadiz (Eynaud *et al.*, 2009; Schwab *et al.*, 2012; Martins *et al.*, 2015; Ausín *et al.*, 2020). Predicted winter SSTs suggest subarctic waters did penetrate the Alboran Sea (during YD-1?) (Figure 6.17), with the periodic inflow of warmer subtropical waters (possibly in YD-2?) is certainly evident in warmer summer SSTs predictions (17 to 19°C), which spread from the Alboran Sea into the southern Balearic Sea (Figure 6.16). In the eastern basin, mean annual SSTs were 15.11°C, again moderately warmer that the HS1, though ~2°C cooler than the LGM (Table 6.1; Table 6.4) (Hayes *et al.*, 2005). This cooler signal comes from the cold waters in the Adriatic and Aegean Seas that expanded southwards into the main eastern basin. Only the southern half of the basin and eastern Levantine Sea saw annual SSTs

reach ≤19°C.

The planktonic foraminiferal assemblage reflects these cool, though seasonally variable SSTs. Neogloboquadrina species, *G. bulloides* and *G. glutinata*, with *T. quinqueloba* and *G. inflata* flourished, as the cooler water eutrophic assemblage, while *G. ruber* and minor SPRUDTS expanded their ranges in seasonally warmer and stratified waters.

The widespread distribution of eutrophic species in the western basin, in particular Neogloboquadrina species and more moderate *G. bulloides* in the Alboran Sea, suggest heightened productivity, deep mixing and the presence of a seasonal DCM (Bárcena *et al.*, 2001; Cacho *et al.*, 2001; Ausin *et al.*, 2015a; Bazzicalupo *et al.*, 2018; Pérez-Asensio *et al.*, 2020). However, *G. bulloides* and *T. quinqueloba* were less widespread in the Balearic Sea when compared to the previous periods, implying that deep mixing was more variable or weaker during this period. Shallower waters remained productive with an abundance of *G. glutinata* and Neogloboquadrina species. This combination of productive surface waters with more moderate deep mixing and shallowed pycnocline would be expected, as the deposition of ORL1 continued through this period (Jimenez-Espejo *et al.*, 2007; Rogerson *et al.*, 2008; Dubois-Dauphin *et al.*, 2017; Pérez-Asensio *et al.*, 2020). The distribution of *G. truncatulinoides* became a little more widespread during the YD, though at very low abundances. In the western basin, its distribution moved further south away from the colder northern waters into the Balearic Sea and the Strait of Sicily into the southern Tyrrhenian Sea. In addition, the decrease in Neogloboquadrina species and increase of *G. inflata*, *T. quinqueloba* and minor *G. scitula* in the eastern Tyrrhenian Sea and Strait of Sicily indicate that more mesotrophic to eutrophic deep mixed layer conditions prevailed in the winter. The presence of these deeper species may support the heightened influence of shallower LIW in the Tyrrhenian Sea during the YD (Thomopoulos *et al.*, 2010; Toucanne *et al.*, 2012).

The cooler water assemblage in the eastern basin was concentrated mainly in the cold eutrophic waters of the Adriatic and Aegean Seas, in particular in areas of deep and intermediate water formation. The range of these eutrophic species expanded south, within the outflow of cooler waters from both sub-basins. Neogloboquadrina species dominated, along with *G. bulloides*, *G. glutinata* and *T. quinqueloba*. The increase in precipitation, seasonal meltwater / riverine influence can be traced by the cold summer SSTs and elevated *G. bulloides* and *T. quinqueloba* in the northern basins (Jorissen *et al.*, 1993; Asioli *et al.*, 2001; Rea *et al.*, 2020). Similarly, heightened *T. quinqueloba*

and other eutrophic species in the northern Aegean point to the inflow of euryhaline, organic rich waters from the continued connection with the Black Sea (Vidal *et al.*, 2010). These fresher dense waters in the sub-basins were further cooled by cold westerly winds penetrating the north-western region, along with cold air descending the surrounding upland regions. For the remainder of the southern eastern basin, Neogloboquadrina species, *G. bulloides*, *G. inflata* and *G. glutinata* were present, though decreasing progressively towards the warmer waters in the south east. As the AHP weakened briefly during the YD, this more moderate, seasonal surface water productivity signal is more likely linked to the increase in precipitation predicted for the eastern basin, rather than inflow from the River Nile (deMenocal *et al.*, 2000; Mojtahid *et al.*, 2015; Shanahan *et al.*, 2015; Rea *et al.*, 2020).

The habitats of warmer species further expanded and were widespread in the southern eastern basin, though they were more restricted in the western basin compared to the BA. *G. ruber* plexus reached its highest abundances during the YD (17%), though the SPRUDTS group remained ≤5%. It has been suggested that alkenone production in the central Mediterranean Sea once again shifted to the short summer season (Sicre *et al.*, 2013). Given there was high seasonality during the YD period especially across the Levantine and Ionian Seas (summer SSTs >21°C; winter SSTs ≤17°C), a similar delay in the bloom of e.g. *G. ruber* white can be assumed, therefore this assemblage most likely reflects the late spring/summer period, when these warmer waters were seasonally stratified (Figure 6.13; Figure 6.16; Figure 6.18). Similar to the BA, the low abundance of *G. truncatulinoides* was widespread throughout the eastern basin, correlating with these more oligotrophic, stratified waters, again suggesting the population was primarily the dextral variant. As would be expected, *G. ruber* plexus and SPRUDTS were poorly represented in the Adriatic and Aegean Seas and the Gulf of Lion due to the low summer SSTs. Their distribution in the Ionian Sea and Mediterranean Ridge was influenced by these cooler waters exiting the northern sub-basins, as well as incoming from the west through the Strait of Sicily (though, once again, *G. sacculifer* peaked again at the Strait of Sicily). It should be noted that the YD distribution of *G. ruber* in Thomopoulos *et al.* (2010) was much more limited in the northern Levantine Sea in comparison to Figure 6.5, which may indicate the over estimation of *G. ruber* in this area in the interpolation. Similar to the BA, the similar distribution of *G. ruber* plexus and SPRUDTs species to *G. inflata* in the Balearic Sea, again suggests seasonal late summer/autumn stratification, with periods of deep, stable mesotrophic mixed layer in

the early winter period (Bárcena *et al.*, 2001; Hernández-Almeida *et al.*, 2011).

When the SPRUDTS assemblage is examined in detail, it is primarily composed of *G. siphonifera* and *O. universa*. Both are cosmopolitan, deeper dwelling species, which have specific genotypes in the modern Mediterranean that can inhabit higher productivity areas and mesotrophic DCMs (de Vargas *et al.*, 1999; de Vargas *et al.*, 2002; Darling and Wade, 2008; Mallo *et al.*, 2017; Schiebel and Hemleben, 2017). Therefore, the combination of these species along with *G. ruber* plexus suggest that these warmer surface waters across the Mediterranean may have been periodically or moderately productive during the YD (Pujol and Vergnaud Grazzini, 1995; Numberger *et al.*, 2009; Rigual-Hernández *et al.*, 2012).

6.3   Conclusion

This study affords us a unique opportunity to reconstruct the SST and palaeoenvironmental conditions across the Mediterranean Sea during HS1, BA and YD. Mapping the spatial distribution of the main morphospecies, SSTs and palaeoenvironmental proxies is a novel way of visualising and interpolating how complex signals from regionally disparate studies changed through each chronozone. This new dataset is an excellent resource that can help identify the primary drivers of these deglacial events within the Mediterranean region, as well as how they relate to global changes occurring at the time.

It is clear that the Mediterranean Sea experienced significant cooling during the deglacial. Compared to the modern day, mean annual SSTs were significantly cooler during HS1 (~5°C) and YD (~4.5°C). Indeed, both HS1 and YD were cooler than the LGM. Cooling in the BA were not as extreme, but SSTs were still ~3.6°C cooler than modern conditions. The spatial variability across and within each basin indicate the strong connection with changes in the North Atlantic oceanic circulation. The stable southerly position of the polar front along the Iberian Peninsula margin during HS1 allowed polar waters to enter the Mediterranean Sea, significantly cooling the western basin, though it had less impact on the eastern basin. During the YD, the polar front was not located as far south, and its position was less stable. Therefore, the influence of incoming subarctic waters can be been traced in the cold winter SSTs in the south-west basin, whereas warmer waters from the Northern Atlantic subtropical gyre are evident from the warmer summer SSTs.

Cold air temperatures, the expansion of sea ice and the subsequent reorganisation of atmospheric circulation patterns over the North Atlantic during HS1 and YD offset the polar front jet stream towards the Mediterranean region. This led to reorganisation of precipitation patterns; significant wind-driven surface water cooling and deep mixing in the north-western basin, Adriatic and Aegean Seas, particularly during the YD. In contrast, the increase in air temperatures and the greater influence of the ITCZ on precipitation and riverine discharge (e.g. the AHP) are evident during the BA. In addition, the northerly retreat of the oceanic polar front and inflow of warm waters from North Atlantic subtropical gyre can be seen in the milder winter and warm summer SSTs in both basins, particularly the eastern basin. The increasing seasonality experienced in eastern basin during the BA and YD suggest the stronger influence of the continual divergence of the summer and winter insolation values. However, regional controls such as periodic meltwater events and changes to fluvial discharge are also very important along the north-west basin and Adriatic Sea. Rising sea levels and the reconnection with the Black Sea can be traced in the cooler SSTs and increased productivity in the Aegean Sea during the BA, continuing into the YD.

Mapping morphospecies distribution and palaeoenvironmental proxies allow us to gain a unique insight to how planktonic foraminifera responded to deglacial climate change across the Mediterranean Sea, as well as aid us to reconstruct the palaeohydrological conditions during these events. It is clear that SSTs are an important factor in governing planktonic foraminifera distribution and abundance. The cooler waters of the western basin, along with Adriatic and Aegean Seas are dominated by cooler water species throughout the deglacial, whereas the habitat of *G. ruber* plexus only expanded once summer SSTs begin to increase from the BA.

However, as Pujol and Vergnaud Grazzini (1995) suggested for the modern assemblage, the response and adaptation of morphospecies to the unique hydrological structure and food availability during each chronozone, are key to explain the complexities of their distribution. The cooler western basin was dominated by Neogloboquadrina species and *G. bulloides*, indicating that it remained strongly eutrophic throughout the deglacial. However, the peak of *G. bulloides* in the Alboran Sea during the BA is associated with the resumption of more modern winter upwelling conditions due to the inflow of warmer subtropical waters, whereas they flourished in the Gulf of Lion during HS1 during periods of wind driven deep winter mixing and WMDW formation. The inflow of polar waters during HS1 can be traced by the pattern of Neogloboquadrina species

(*N. pachyderma*?) as they expanded out from the Alboran Sea into the western basin. From the BA onwards, the stable population of Neogloboquadrina species in Gulf of Lion and Balearic Sea can be correlated with a shallowing of the pycnocline and the productive surface waters associated with the deposition of ORL1. However, the more modest association of *G. inflata* and *G. ruber* in the Balearic Sea suggest that this region also experienced periods where summer surface waters were stratified, followed by a cooler late autumn-early winter deep, but stable, mesotrophic mixed layer.

In contrast, the assemblage of the eastern basin in the early deglacial was much more diverse than modern waters and experienced greater seasonal extremes in SSTs. There was a greater percentage of eutrophic species, though surface waters became increasingly oligotrophic during the short warm summers of the BA and YD, as *G. ruber* plexus and other warmer spinose species were able to expand their habitats. The assemblage was very different to modern waters, e.g. seasonal stratification in the central eastern basin was correlated with a small population of *G. truncatulinoides* species (dextral variant?). In the modern Mediterranean, the population of *G. truncatulinoides* is mainly the sinistral variant and most commonly found in the north-west basin. The cool waters of the Adriatic and Aegean were more similar to the western basin throughout the deglacial, with a strong eutrophic signal in areas of deep and intermediate water formation. Also *T. quinqueloba*, *G. bulloides* and Neogloboquadrina species were indicators of enhanced outflow of the River Po and the reconnection with the Black Sea.

Therefore, while SSTs are a strong governing factor on the distribution of planktonic foraminifera during the deglacial, hydrological structure and productivity also key limiting factors during HS1, the BA and YD.

Chapter 7.

7 Late Pleistocene to early Holocene palaeoenvironmental variability in the Gulf of Lion

7.1 Introduction

The Mediterranean Region has been termed a climate change hotspot and is at significant risk of increasing sea surface temperatures (SSTs) from anthropogenic global warming (Giorgi, 2006; Lionello *et al.*, 2012b). Mean air temperatures across the Mediterranean Basin are 1.4°C warmer since the late 19th century, especially during summer months, and SSTs are increasing 0.35°C per decade (Shaltout and Omstedt, 2014; Cramer *et al.*, 2018). The western Mediterranean Sea is particularly sensitive to climate change, with SSTs increasing ~2°C/100 yr in the past century (Lionello *et al.*, 2012b; Sicre *et al.*, 2016). As atmospheric CO_2 and SSTs increase, the modern north-western basin is becoming increasingly stratified and less productive, which is already impacting both the planktonic foraminifera assemblage (e.g. decrease in *G. bulloides*) and the $\delta^{13}C$ signature of their tests (Pallacks *et al.*, 2021a; Pallacks *et al.*, 2021b).

The Gulf of Lion is unique to the western Mediterranean basin, as it is an area of deep-water formation (DWF) and surface waters are both cool and highly productive. The World Ocean Atlas (WOA, 2018) estimates mean annual SSTs of 16.83°C in the modern Gulf of Lion, which are noticeably cooler than those experienced throughout the rest of the Mediterranean Sea (Table 7.1) (Locarnini, 2018). As discussed in Chapter 2, one of main controlling factors for modern SSTs in the Gulf of Lion are the cold dry winter katabatic Mistral and Tramontane winds that cool surface waters and trigger the formation of the Western Mediterranean Deep Water (WMDW) (Medoc, 1970; Petrenko, 2003). Given its location at the transitional zone between the mid-latitudes and the tropics, winter precipitation, direction of storm tracks and SST in the northern/north-western Mediterranean are impacted by northern hemisphere mid-latitude teleconnection patterns (Trigo *et al.*, 2006; Ulbrich *et al.*, 2012). The southerly position of polar front jet steer North Atlantic winter depression systems and storm tracks towards the north-western Mediterranean, increasing cyclogenesis and precipitation in the region (Trigo *et al.*, 2006; Baldi *et al.*, 2008). Annual variability and interconnectivity in modes of atmospheric circulation in the North Atlantic, such as the

East Atlantic pattern (EA) and North Atlantic Oscillation (NAO) have significant bearing on SSTs and rates of winter precipitation; i.e. variations in the modes can impact the strength of local winds, and the intensity and frequency of cyclogenesis (Hurrell, 1995; Josey *et al.*, 2011; Rodrigo, 2021).

a) Modern SSTs

Region	Annual (°C)	Summer (°C)	Winter (°C)	Seasonality (°C)
Mediterranean Sea	19.41	24.35	15.19	9.15
Western Basin	18.28	23.33	14.08	9.25
Eastern Basin	20.07	24.94	15.847	9.09
Gulf of Lion	16.83	21.33	13.08	8.25

b) LGM SSTs

Region	Annual (°C)	Summer (°C)	Winter (°C)	Seasonality (°C)
Gulf of Lion	8.11	7.13	10.23	-3.10

Table 7.1: a) Modern mean annual and seasonal SST from the World Ocean Atlas (2018) (Locarnini, 2018). WOA (2018) values were located within 200km of the Gulf of Lion coast and are derived from the statistical mean annual and seasonal temperature (1955 to 2017) in 1° latitude/longitude grids. b) Mean predicted SSTs, using ANN and seasonality (°C) (calculated from mean summer less winter SSTs) during the LGM in the Gulf of Lion (Hayes et al., 2005).

The Gulf of Lion is a crescent shaped stable continental margin, located at the mouth of the River Rhône and is ~60km wide in the central part of the continental shelf (Figure 7.1). Sediments deposited on the inner shelf during the Late Pleistocene and Holocene have been extensively utilised to measure post-glacial sea level rise, meltwater pulse events and the retreat of the River Rhône and deltaic system (Berné *et al.*, 2004; Berné *et al.*, 2007; Sierro *et al.*, 2009). The catchment of the Rhône includes the Alps, Massif Central and Jura mountain ranges (Révillon *et al.*, 2011). The river contributes ~90% of the freshwater and sediment budget to the Gulf of Lion, which has been consistent over the past 16 kyr (Palanques *et al.*, 2006; Révillon *et al.*, 2011). Sediments from the Rhône are deposited onto the north-eastern part of the inner shelf, where the anti-clockwise direction of the Northern Current redistributes these sediments causing them to thicken towards the west-south-west (Berné *et al.*, 2004; Berné *et al.*, 2007). Other smaller rivers and streams that discharge into the Gulf of Lion only contribute ~10% to the overall sediment budget (Berné *et al.*, 2007). The highest outflow occurs during the spring and autumn periods (Palanques *et al.*, 2006). Due to the combination of strong winter winds, intense deep mixing, DWF and seasonal peak discharge from the River Rhône, the Gulf of Lion is classed as one of the most productive regions in the Mediterranean Sea, with chlorophyll-*a* pigment ranging between 1 and 2 mg/m^3/yr

(Estrada, 1985; Cartes *et al.*, 2004; Rigual-Hernández *et al.*, 2010; Lazzari *et al.*, 2012; Rigual-Hernández *et al.*, 2012; Rigual-Hernandez *et al.*, 2013; Mazzocchi *et al.*, 2014).
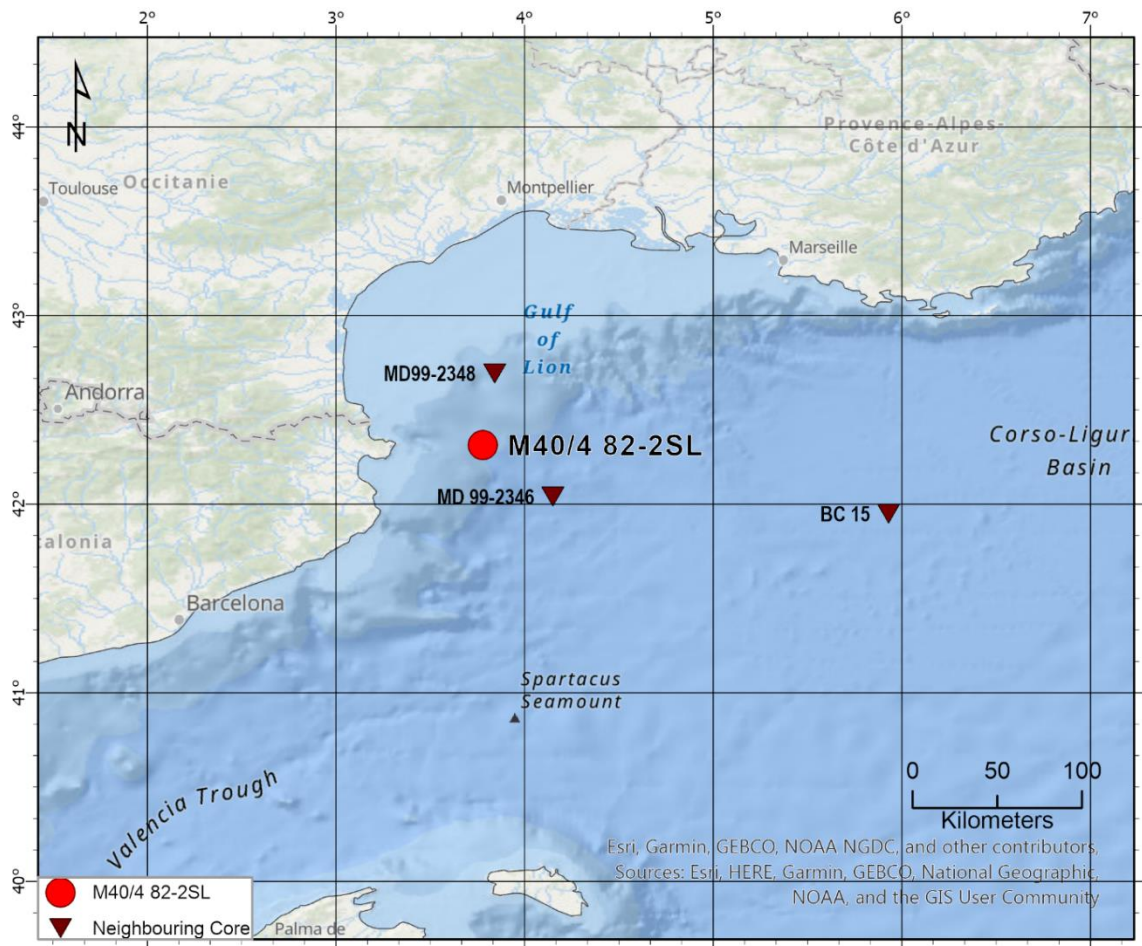
Figure 7.1: Map of the north-western Mediterranean and Gulf of Lion, illustrating the location of M40/4 82-2SL and neighbouring cores BC15, MD99-2346 and MD99-2348 (Rohling et al., 1998; Melki et al., 2009; Bassetti et al., 2010).

The modern planktonic foraminiferal assemblage in the Gulf of Lion was studied in detail by Rigual-Hernández *et al.* (2012). This study comprised of two sediment trap stations sampled over a 12 year period (1993-2006) and core top samples taken along a transect between both stations (Figure 3.5). Both stations recorded unimodal seasonal patterns of planktonic foraminifera influx during the coldest part of the year (average seasonal SST 13.2 to 14.5°C), which coincided with the highest annual chlorophyll-a concentrations and the late winter/early spring phytoplankton bloom (Rigual-Hernández *et al.*, 2012). During these high productivity periods, the winter-spring bloom accounted for approximately 80% of the total average annual flux of planktonic foraminifera. This typical winter-spring assemblage was dominated by just four species, *G. bulloides*, *G. truncatulinoides*, *N. incompta* and *G. inflata*. In addition, there were minor peaks (between 4.4 and 6.4%) of spinose species (*O. universa*, *G. siphonifera*, *G. sacculifer*

and *G. ruber*) recorded during the spring-summer and early autumn, when the waters in the Gulf were warmer and more stratified. A comparison of faunal results between sediment traps and core tops located nearby confirmed that the core top assemblage were analogous to the living assemblage above, though dominated by species from the strong winter-spring bloom (Rigual-Hernández *et al.*, 2012). This suggests core M40/4 82-2SL will provide an accurate reflection of the planktonic foraminifera species that inhabited the surrounding surface waters. However, it should be kept in mind that the assemblage may overrepresent species associated with peak production, rather than be a true reflection of the "annual" flux in species. The assemblage will clearly reflect the dominant SSTs, palaeoecological and trophic conditions during the sample timeframe, thus the assemblage will be discussed in relation to these potential factors.

	Chronozone	Event	From	To	Duration
Holocene	Early NG		8236	7433	803
	GL	8.2 kyr	8308	8265	43
		9.3 kyr	9282	9243	39
		11.4 kyr	11437		
			11535	8236	3299
Late Pleistoce	YD		12842	11535	1307
	BA	OD	13998	13883	115
			14656	12842	1814
	Late HS1		15481	14656	825

Table 7.2: Chronology of the Late Pleistocene chronozones, early Holocene stages and cold events (as defined from Greenland ice cores) observed in M40/4 82-2SL (Rasmussen et al., 2014; Walker et al., 2019a). Heinrich Stadial 1 (HS1); Bølling-Allerød (BA); Older Dryas (OD); Younger Dryas (YD); Greenlandian (GL); Northgrippian (NG).

As outlined in Chapter 5, M40/4 82-2SL was extracted from a terrace (1079 m water depth) situated on the southern side of the Gulf of Lion (Figure 7.1). Results from the mid to late Holocene (sections 5 and 6) are available in Broggy (2011) and will not be discussed as part of this thesis. The chronology of M40/4 82-2SL (sections 1 to 4) ranged between 15.48 to 7.4 kyr cal BP and the high resolution of the core allows clear identification of the main Late Pleistocene climatic events, including late Heinrich Stadial 1 (HS1), the Bølling-Allerød (BA) and the Younger Dryas (YD) (Table 7.2). It is possible to identify more discrete cold events, such as the Older Dryas (OD), the Intra-Allerød Cold Period (IACP) and the 11.4, 9.3 and 8.2 kyr Holocene cold events (Table 7.2). However, with the inherent errors associated with ^{14}C AMS dates (Table 5.3) as well as potential bias of using the weighted average 'best fit' line of the age model (Figure 5.6), correlating with these centennial scale events should be undertaken with caution. The early-mid Holocene was subdivided using the recently defined

Greenlandian (GL) (11.7 to 8.236 kyr b2k) and Northgrippian (NG) (8.236 kyr b2k) stages (Walker *et al.*, 2018; Walker *et al.*, 2019a; Walker *et al.*, 2019b).

Existing research based in the Gulf of Lion that utilise planktonic foraminiferal assemblages as a proxy to assess Late Pleistocene palaeoenvironmental change is limited, in comparison to other sites in the western Mediterranean, such as the Alboran Sea and Tyrrhenian Sea. The only studies that span the same timeframe and provide a comparison are MD99-2346 and the low resolution core BC15 (Figure 7.1) (Rohling *et al.*, 1998; Melki *et al.*, 2009). Other research in the Gulf of Lion focus on different faunal proxies, sedimentological analysis or do not cover the period in question here (Beaudouin *et al.*, 2004; Berné *et al.*, 2004; Bassetti *et al.*, 2006; Jouet *et al.*, 2006; Berné *et al.*, 2007; Sierro *et al.*, 2009; Bassetti *et al.*, 2010; Lombo Tombo *et al.*, 2015; Bassetti *et al.*, 2016).

Given the sensitivity of the modern western basin to anthropogenic climate change, this chapter aims to answer the research question: how did the north-western Mediterranean Sea respond to rapid climate change during the deglacial? In detail, i) were these events recorded in the planktonic foraminifera archive from a high resolution sediment core in the Gulf of Lion? ii) How did SSTs vary during these periods? iii) What were the impacts of these events, if any, on the structure of the planktonic foraminifera assemblage? iv) Is it possible to reconstruct the palaeoenvironmental and palaeoecological changes in surface waters during the deglacial? v) What were the suggested mechanisms that governed these changes in the Gulf of Lion?

Therefore, M40/4 82-2SL provides a very welcome, high-resolution record of planktonic foraminifera for this key location, spanning the late Heinrich Stadial 1 to the late Holocene. It provides an ideal archive that can be used to address these research questions. Results and analysis of the detailed faunal assemblage, reconstructed SSTs, palaeoenvironmental proxies and statistical analysis will be discussed in relation to the potential climate mechanisms that impacted the Gulf of Lion during the deglacial to early Holocene period.

7.2 Results

7.2.1 Sedimentation rates

Sedimentation rates were not constant during the Late Pleistocene to early Holocene (Figure 7.2). Mean sedimentation rates during HS1 were 32.7 cm/kyr (Table 7.3).

They only marginally increased during the BA (36.6 cm/kyr), though sedimentation rates had begun to increase during the mid to late Allerød period (from 13.5 kyr). Rates rapidly increased during the YD (54.88 cm/kyr), reaching a peak of ~60 cm/kyr between 12 and 11.7 kyr, then falling again towards the early Holocene (Figure 7.2). There was a gradual weakening during the GL period (53.54 cm/kyr). Sedimentation rates during the mid-GL period were relatively stable for an extended period, but from ~9.5 kyr, rates began to slowly increase, then more rapidly after 9 kyr. The mean sedimentation rate for the NG was 63.87 cm/kyr, but it is composed of a peak around 8.1 kyr (~74 cm/kyr), which then fell rapidly to 45 cm/kyr at 7.4 kyr.

Chronozone	Mean Sedimentation Rate (cm/kyr)
NG	63.87
GL	53.54
YD	54.88
BA	36.60
Late HS1	32.70

Table 7.3: Mean sedimentation rate for main chronozones in M40/4 82-2SL. Heinrich Stadial 1 (HS1); Bølling-Allerød (BA); Younger Dryas (YD); Greenlandian (GL); Northgrippian (NG).

7.2.2 Distribution of planktonic foraminifera

In total, 21 planktonic foraminifera morphospecies were identified in core M40/4 82-2SL and are listed in Table 3.1. Of these, 15 species have a minimum of 3% abundance per sample and the results are displayed in Figure 7.3. Neogloboquadrina species were picked and counted by coiling direction. As there were <3% left coiling specimens in all samples, they have been referred to as *N. incompta* sinistral, not *N. pachyderma*, and included with *N. incompta* as per Darling *et al.* (2006). For the purposes of this chapter, the combination of *N. incompta* and *N. incompta* sinistral will be referred to as *N. incompta*. The *G. ruber* plexus includes the genotypes *G. ruber* pink and *G. ruber* white Type Ia, IIa (which has been reclassified by Aurahs *et al.* (2011) as *G. elongatus*) and IIb (Table 3.1) (Darling and Wade, 2008; Aurahs *et al.*, 2009; Aurahs *et al.*, 2011; André *et al.*, 2014). For this study, the *G. ruber* plexus specimens were subdivided and
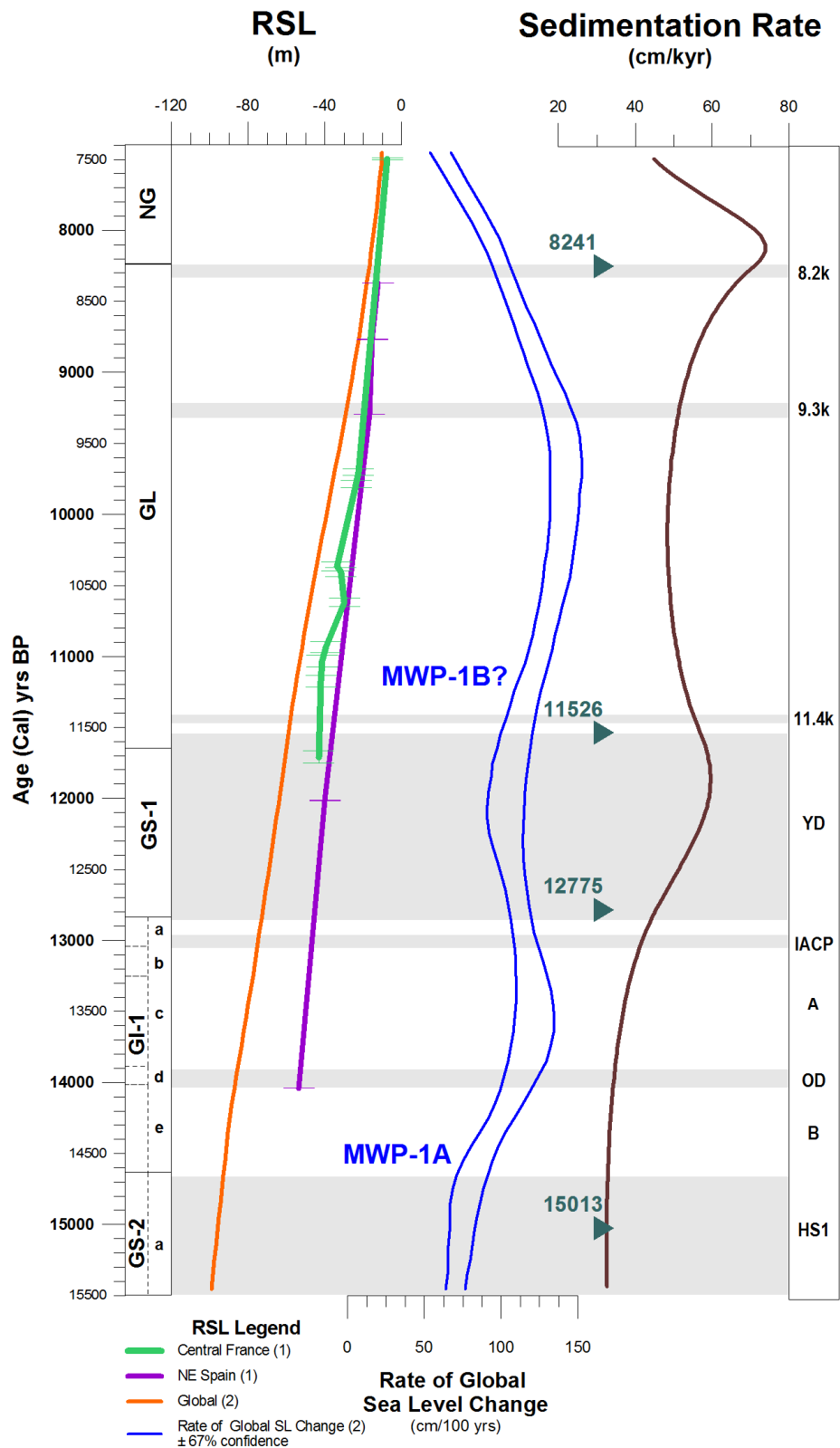
Figure 7.2: Late Pleistocene to early Holocene global and Gulf of Lion sea levels and global rates of sea level change, with sedimentation rates for M40/4 82-2SL sections 1 to 4. Green triangles are ^{14}C AMS control points. Data for sea level: (1) Vacchi et al. (2016) and (2) Stanford et al. (2011a). Location of MWP-1A and approximate location of MWP-1B (Stanford et al., 2011a; Abdul et al., 2016; Tian et al., 2020). INTIMATE event stratigraphy (Alley, 2004; NGRIP dating group, 2008; Rasmussen et al., 2014). Colder periods highlighted in grey. Heinrich Stadial 1 (HS1); Bølling (B); Older Dryas (OD); Allerød (A); Inter-Allerød Cold Period (IACP); Younger Dryas (YD); Greenlandian (GL); Northgrippian (NG).

counted as *G. ruber* white and *G. ruber* pink. Therefore, *G. ruber* white counts include genotypes *G. elongatus*, Ia and IIb. The SPRUDTS group (excluding *H. pelagica* which was not present in this assemblage) has collectively been plotted, along with separate plots of those members of the group that have values >3% (i.e. *G. siphonifera*, *G. rubescens*, *O. universa* and *B. digitata*) (Figure 7.3).

Species	Late HS1	BA	YD	GL	Early NG
G. ruber white	1	8.4	0.6	10.3	6
G. ruber pink	0	0.02	0	1.3	0.6
SPRUDTS	0.02	1.3	0.04	4.5	4.3
G. truncatulinoides d	0	0.3	0.01	0.2	0
G. truncatulinoides s	0	0.1	0	1.04	0
G. bulloides	52.8	26.4	20.2	23.5	22.3
G. glutinata	8.1	3.3	26	12.5	2.2
G. inflata	2.2	19.4	3.8	17.1	14.4
N. incompta	18	32.8	32.8	17.3	46.2
T. quinqueloba	12.5	6.5	16	9.5	3.4
G. scitula	5.1	1.3	0.5	2.4	0.03

Table 7.4: Mean planktonic foraminifera abundances (%) in M40/4 82-2SL sections 1 to 4 during the Late Pleistocene chronozones and early Holocene stages. Heinrich Stadial 1 (HS1); Bølling-Allerød (BA); Younger Dryas (YD); Greenlandian (GL); Northgrippian (NG).

	G. ruber w	G. ruber p	SPRUDTS	G. truncat. s	G. truncat. d	G. inflata	G. bulloides	G. glutinata	N. incompta	T. quinq.	G. scitula
G. ruber w	1										
G. ruber p	0.48	1									
SPRUDTS	0.47	**0.76**	1								
G. truncat. s	0.25	-0.12	-0.05	1							
G. truncat. d	0.33	-0.12	-0.09	0.10	1						
G. inflata	**0.67**	0.19	0.32	0.43	0.32	1					
G. bulloides	-0.22	-0.30	-0.33	0.06	-0.03	-0.23	1				
G. glutinata	-0.27	-0.24	-0.38	0.26	-0.05	-0.26	-0.21	1			
N. incompta	-0.41	-0.04	0.01	**-0.60**	-0.22	-0.42	-0.31	-0.37	1		
T. quinq.	-0.37	-0.22	-0.38	0.01	-0.07	-0.45	0.14	**0.50**	-0.29	1	
G. scitula	0.17	-0.15	-0.12	0.43	0.12	0.24	0.39	0.10	**-0.63**	0.05	1

Table 7.5: Pearson's r correlation matrix for all species >3% abundance, with combined SPRUDTS group (G. siphonifera, G. rubescens, O. universa and B. digitata). Values ≤-0.5 and ≥0.5 are highlighted. G. truncat. = G. truncatulinoides; T. quinq. = T. quinqueloba; w = white; p = pink; s = sinistral; d = dextral.

In general, the faunal assemblage of M40/4 82-2SL is dominated by eutrophic grazers,

mainly *G. bulloides*, *N. incompta G. glutinata*, *G. inflata* and *T. quinqueloba* (Table 7.4) *G. ruber* white is the main spinose predatory species, with only minor limited occurrences of SPRUDTS species. A Pearson's *r* correlation shows a high positive correlation between *G. ruber* pink and the SPRUDTS group (0.76), moderate correlations between *G. ruber* white and *G. inflata* (0.67), and *G. glutinata* and *T. quinqueloba* (0.50) (Table 7.5). In addition, *N. incompta* is negatively correlated with both *G. scitula* and *G. truncatulinoides* sinistral (-0.63 and -0.60 respectively).

The correlation between *G. ruber* pink and the SPRUDTS group would be expected, as they are all key warm oligotrophic species (Schiebel and Hemleben, 2017). *G. inflata* is often indicative of eutrophic deep mixed layers. However, the correlation between *G. ruber* white and *G. inflata* is suggestive of the seasonal correction between the species in the modern Alboran Sea (Bárcena *et al.*, 2004). This occurs when *G. ruber* white flourishes in stratified oligotrophic summer waters, followed by *G. inflata* in the cooler deeply mixed mesotrophic winter/spring waters (Giraudeau, 1993; Bárcena *et al.*, 2001; Lončarić *et al.*, 2007). The correlation between *G. glutinata* and *T. quinqueloba* is logical, as both have a preference for eutrophic waters and diatoms as a food source (Hemleben *et al.*, 1989; Schiebel *et al.*, 2001). The negative correlation between *N. incompta* and both *G. scitula* and *G. truncatulinoides* sinistral is interesting. These species spend some or all of their life-cycle feeding in the deep chlorophyll maximum (DCM), but generally *G. scitula* and *G. truncatulinoides* sinistral are deeper dwelling species that display vertical niche partitioning in warm oligotrophic waters, whereas *N. incompta* is a shallow dwelling grazer, more indicative of cooler eutrophic waters (Rutherford *et al.*, 1999; Schiebel and Hemleben, 2017).

Approximately 90% of the late HS1 assemblage is composed of just four species *G. bulloides*, *N. incompta*, *T. quinqueloba* and *G. glutinata* (Figure 7.3; Table 7.4). *G. bulloides* is the dominant species representing ~50% of the faunal assemblage. This species peaked at ~15 kyr then slowly decreased towards the end of HS1. A small decrease is noted between 15.25 and 15.05 kyr, which is negatively correlated with a minor peak in *G. glutinata*, then *N. incompta*. *T. quinqueloba*, comprising ~15% of the faunal assemblage, records a degree of variability but becomes more stable towards the end of HS1.
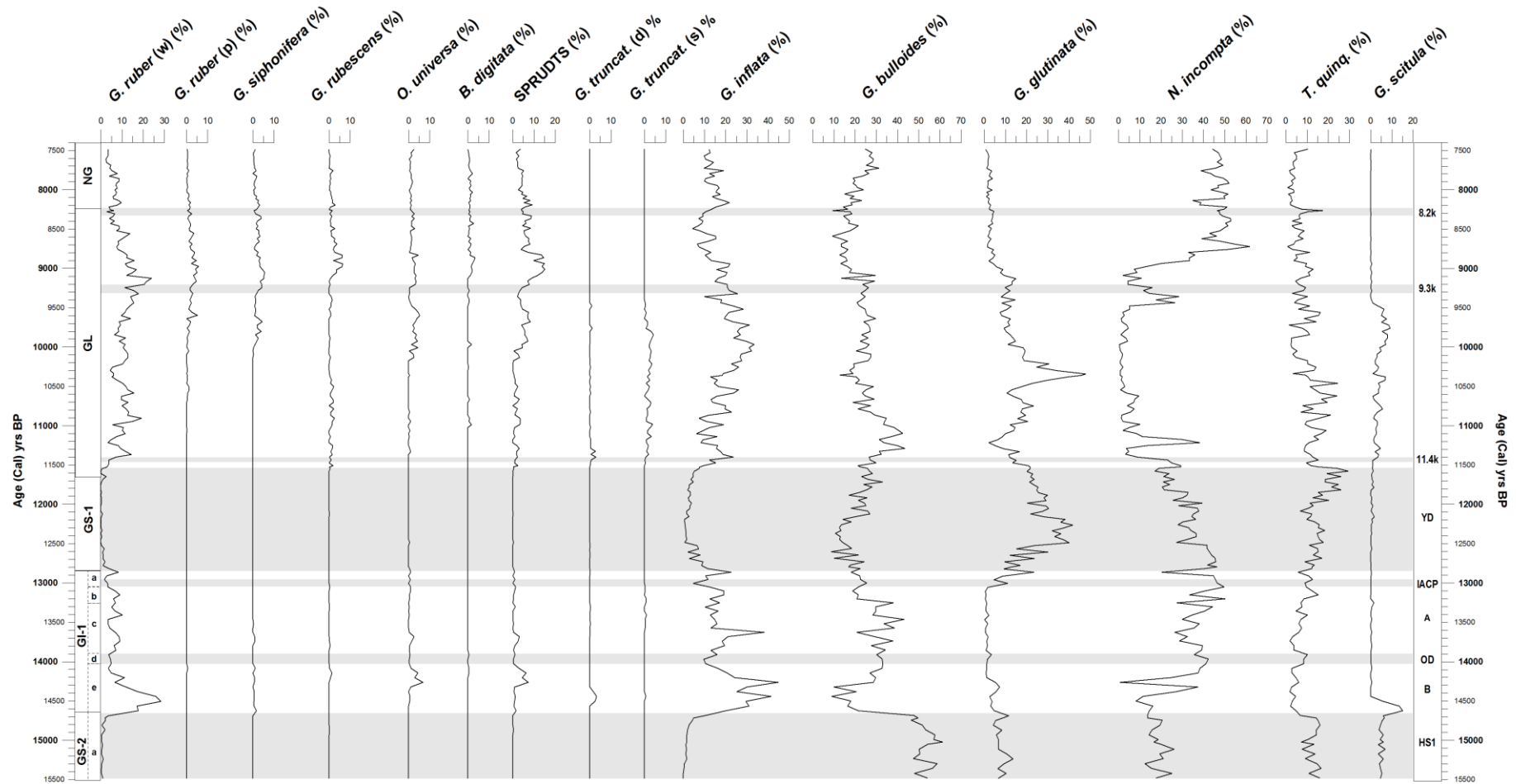
Figure 7.3: Faunal assemblage of M40/4 82-2SL sections 1 to 4 (7.5r to 15.5 kyr (cal) BP). SPRUDTS group = G. *s*iphonifera, H. *p*elagica (not present), G. *r*ubescens, O. *u*niversa, B. *d*igitata, G. *t*enella and G. *s*acculifer (Rohling et al., 1993); N. incompta = N. incompta + N. incompta sinistral; d = dextral; s = sinistral. INTIMATE event stratigraphy (Alley, 2004; NGRIP dating group, 2008; Rasmussen et al., 2014). Colder periods highlighted in grey. Heinrich Stadial 1 (HS1); Bølling (B); Older Dryas (OD); Allerød (A); Inter-Allerød Cold Period (IACP); Younger Dryas (YD); Greenlandian (GL); Northgrippian (NG).

190

The BA assemblage is certainly more diverse and variable in abundance than the late HS1. The transition to the BA occurs over ~60 years and is clearly illustrated by an abrupt turnover of most eutrophic species, especially *G. bulloides* and *T. quinqueloba*. They are replaced by *G. inflata* and *G. scitula*, along with warm oligotrophic species *G. ruber* white and minor SPRUDTS (Figure 7.3; Table 7.4). The early Bølling sees the highest abundance of both *G. ruber* white (~28%) and *G. scitula* (15.2%) over the entirety of the record, as well as significant peaks in *G. inflata*. However, the peak in *G. scitula* is brief and the species disappears ~14.3 kyr, followed by a decrease in *G. ruber* white then *G. inflata* by. These declines coincide with a rapid increase in *N. incompta* and *G. bulloides*, along with minor peaks in the SPRUDTS group (mainly *O. universa* with minor *G. siphonifera* and *G. rubescens*).

The faunal signal is subtle for the period coinciding with GI-1d, which has been attributed to the OD chronozone in this study. There is very little variation in most species, though *G. inflata* reaches its lowest abundance in the early Bølling and there are minor peaks in both *N. incompta* and *T. quinqueloba*.

The Allerød chronozone is dominated by *N. incompta* (~33%) and *G. bulloides* (~30%) with a relatively low variable population of *G. ruber* white (~7.5%), *G. inflata* (~22%) and *T. quinqueloba* (<4%). There are only trace amounts of SPRUDTS, *G. truncatulinoides* sinistral and dextral, *G. glutinata* and *G. scitula*. Around 13.6 kyr, there is a brief sharp peak in *G. inflata* (~38%) and associated dip in *G. bulloides* (~21%). The later Allerød chronozone is marked by a drop in *G. bulloides* (falling from 38 to 18%), while both *N. incompta* and *T. quinqueloba* began a slow variable increase in population (reaching maximum values of ~49 and ~15% respectively). Around 13 kyr (the IACP event?), there is a brief turnover of species, with a dip in *G. ruber* white and *G. inflata* and minor peaks in *G. bulloides* and *G. glutinata*. The Allerød/YD transition period sees a brief final peak in *G. ruber* (~8%), *G. inflata (22.5%)* and *G. glutinata* (23.4%), and short-term decline in *N. incompta* and *T. quinqueloba*.

The YD begins at ~12.8 kyr and again we see a reorganisation of the faunal community. 95% of the total population is composed of *N. incompta*, *G. glutinata*, *G. bulloides*, *T. quinqueloba* and limited *G. inflata* (Figure 7.3; Table 7.4). During the early YD, the population of *G. ruber* white significantly declined (~1.5%), *G. inflata* quickly dropped from its peak at the BA/YD transition (to lows of ~2%) and there is a variable decline in *G. bulloides* (ranging from 24 to 8%). The signal from *G. glutinata* and *T. quinqueloba*

is also highly variable, though gradually increasing and again, *N. incompta* remains stable (~43%). From ~12.5 to ~12.2 kyr, *G. glutinata* dominates the assemblage (~37%), along with *N. incompta* (~32%) and *T. quinqueloba* (~15%), while *G. bulloides* (13.6%) and *G. inflata* (~1%) reach their minimum abundances of the Late Pleistocene and early Holocene. The second half of the YD records a variable recovery of *G. bulloides* (~25%), with an increase in *T. quinqueloba* (an average of ~18%, but peaking at ~30%, its highest percentage in the core) and decreases in both *N. incompta* (~28%) and *G. glutinata* (~25%).

The assemblage of the Greenlandian (GL) stage has greater diversity and is highly variable in comparison to the YD. The main species are *G. bulloides*, *G. inflata*, *N. incompta*, *G. glutinata*, *G. ruber* white, *T. quinqueloba* and minor occurrences of the SPRUDTS group, *G. scitula* and *G. truncatulinoides* sinistral (Figure 7.3; Table 7.4). The transition from the late YD to the GL is gradual for most species, though is evident by the rapid fall in *T. quinqueloba* (falling from the 30% peak in the late YD to lows of <10%). This transition is quickly followed by the 11.4 kyr cold event, which seems to have little influence on species distribution, aside for a very minor increase in *T. quinqueloba* (15%). Following the 11.4 kyr event however, there is a significant drop, then a short strong peak in *N. incompta* (ranging from lows of ~3.5% to a peak of ~38% between 11.4 to 11.2 kyr).

The faunal pattern of the early GL chronozone is highly variable, with many species experiencing cyclical peaks and troughs, especially *G. inflata*, *T. quinqueloba*, *G. scitula* and *G. truncatulinoides* sinistral. Around 10.3 kyr there was a significant peak of *G. glutinata* (48%), which coincided with a minor increase in *G. scitula* (~7%) and a decrease in *G. ruber* white, *G. inflata*, *G. bulloides* and *T. quinqueloba*.

Most notably for the entire core, between 10.6 and 9.5 kyr, the population of the usually prolific *N. incompta* was decimated (<2%). This near total disappearance of *N. incompta* coincided with an elevation in several deeper dwelling species, i.e. *G. inflata* (~15%), *T. quinqueloba* (~13%), *G. scitula* (~3%) and very minor *G. truncatulinoides* sinistral (~1.5%) and *G. rubescens* (<1%). Warm species were present throughout, though variable in abundance (*G. ruber* white was ~10% and SPRUDTS <1.5%). There are many instances where an initial peak in *G. ruber* white was subsequently replaced by a minor peak in the SPRUDTS group. During this mid GL period, *G. bulloides*, *G. inflata* and *T. quinqueloba* were relatively stable (~23%, ~24% and 10% respectively),

while *G. glutinata* rapidly fell, then tapered out by ~9 kyr. Around 9.5 kyr, *N. incompta* made a sudden reappearance (~24%), while *G. scitula* and *G. truncatulinoides* sinistral disappeared.

The 9.3 kyr cold event does not have a significant impact in this core, though there is a coincident increase in *T. quinqueloba* (~9%) and a decrease in *N. incompta* (~14%) and warm species. Again, after this GL cold event, there is a decrease in *N. incompta* (<6%) and re-establishment of warm species (*G. ruber* white reached an average of ~18%). From 9.0 to 8.7 kyr, *N. incompta* peaks to its highest abundance (60.5%) and remains dominant until the end of the GL (~50%).

In Greenland ice cores, the transition from the GL to the NG stage occurs at the 8.2 kyr cold event. The assemblage of the early NG period (8.2 to 7.5 kyr) is less diverse than during the GL and is dominated by *N. incompta* (~46%). In addition, *G. bulloides* (~22%), *G. inflata* (~14.5%) and *G. ruber* white (~6%) occur, with minor SPRUDTS (4.3%) (Figure 7.3; Table 7.4). As with the 11.4 and 9.3 kyr events, the 8.2 kyr event is marked by a very brief sharp peak in *T. quinqueloba* (reaching ~17%) and a brief dip in warm species. *N. incompta* dips again after the cold event (~37%) but recovers its dominance quickly. Of the warm species, both *G. ruber* white and the SPRUDTS group decreased in abundance in comparison to the GL.

7.2.3 Principal Component Analysis

A standardised Principal Component Analysis (PCA) was completed for M40/4 82-2SL sections 1 to 4 to assist determining the main factors governing the distribution of species within this location in the Gulf of Lion. A summary of eigenvalues and variance for each principal component (PC) are listed in Table 7.6. The three main factors (PC1 to PC3) account for 92.52% of the total variance of the population. The rankings and loadings for the main planktonic foraminifera for PC1 to PC3 are displayed in Table 7.7.

PC1 accounts for 51% of the total variance, with very strong negative loadings for *N. incompta* (Table 7.7). *G. glutinata*, *G. inflata* and *G. bulloides* have more modest positive loadings. As these species are all eutrophic grazers, food is obviously an important factor. For *N. incompta*, the food availability, quality and type are the principal factors governing its abundance (Rohling and Gieskes, 1989; Schiebel *et al.*, 2001). *N. incompta* prefers cooler, productive waters above the pycnocline

PC	Eigenvalue	% Variance	Cumulative % of Total Variance
1	356.08	51.03	51.03
2	153.41	21.99	73.02
3	136.75	19.60	92.62
4	23.05	3.30	95.92
5	15.78	2.26	98.18
6	7.41	1.06	99.24
7	4.09	0.59	99.83
8	0.56	0.08	99.91
9	0.46	0.07	99.97
10	0.17	0.02	99.99
11	0.01	0.00	100.00

Table 7.6: PCA factors and their percentages of the total variability for core M40/4 82-2SL sections 1 to 4.

Species	PC1 (51.03%)	Species	PC2 (21.99%)	Species	PC3 (19.60%)
N. incompta	-0.92	*G. inflata*	-0.54	*G. glutinata*	-0.34
SPRUDTS	-0.01	*G. ruber* w	-0.30	*G. inflata*	-0.32
G. ruber p	0.00	SPRUDTS	-0.14	*G. ruber* w	-0.18
G. truncat. d	0.01	*G. ruber* p	-0.03	SPRUDTS	-0.09
G. truncat. s	0.03	*G. scitula*	-0.02	*G. ruber* p	-0.03
G. scitula	0.09	*G. bulloides*	-0.02	*G. truncat.* s	-0.01
T. quinq	0.09	*G. truncat.* d	-0.01	*G. truncat.* d	0.00
G. ruber w	0.11	*G. truncat.* s	-0.01	*N. incompta*	0.01
G. bulloides	0.18	*N. incompta*	0.07	*G. scitula*	0.05
G. inflata	0.19	*T. quinq.*	0.31	*T. quinq.*	0.07
G. glutinata	0.24	*G. glutinata*	0.71	*G. bulloides*	0.86

Table 7.7: Planktonic foraminifera rankings and factor loadings for PC1, PC2 and PC3 for M40/4 82-2SL sections 1 to 4. G. truncat. = G. truncatulinoides; T. quinq. = T. quinqueloba; w = white; p = pink; s = sinistral; d = dextral.

and is strongly associated with chlorophyll concentrations, but is also frequently found along the margins of subtropical upwelling regions or frontal zones, or within the DCM of stratified waters (Rohling and Gieskes, 1989; Schiebel *et al.*, 2001; Kuroyanagi and Kawahata, 2004). In highly productive regions, it is outcompeted by the opportunistic *G. bulloides* and *T. quinqueloba* (Schiebel *et al.*, 2002b). As discussed in section 3.4, in the modern Gulf of Lion, *N. incompta* flourished during the spring bloom, peaking at depths associated with shallow chlorophyll concentrations, when surface waters were deeply mixed and phytoplankton and nutrients from the Rhône Delta Plume are at their maximum (Pujol and Vergnaud Grazzini, 1995; Rigual-Hernández *et al.*, 2012). It is also more common in more distal sites where primary productivity was less intense and *G. bulloides* had decreased in abundance (Rigual-Hernández *et al.*, 2012). The positive loadings for other eutrophic species reflect different trophic requirements, their

preference for deeper mixed surface waters or periods of deep mixing (Schiebel *et al.*, 2001; Schiebel *et al.*, 2002b). Therefore, the close association of PC1 with *N. incompta* suggest that food availability and the depth of this food (linked to chlorophyll concentrations and pycnocline depth) are the primary factors for PC1.
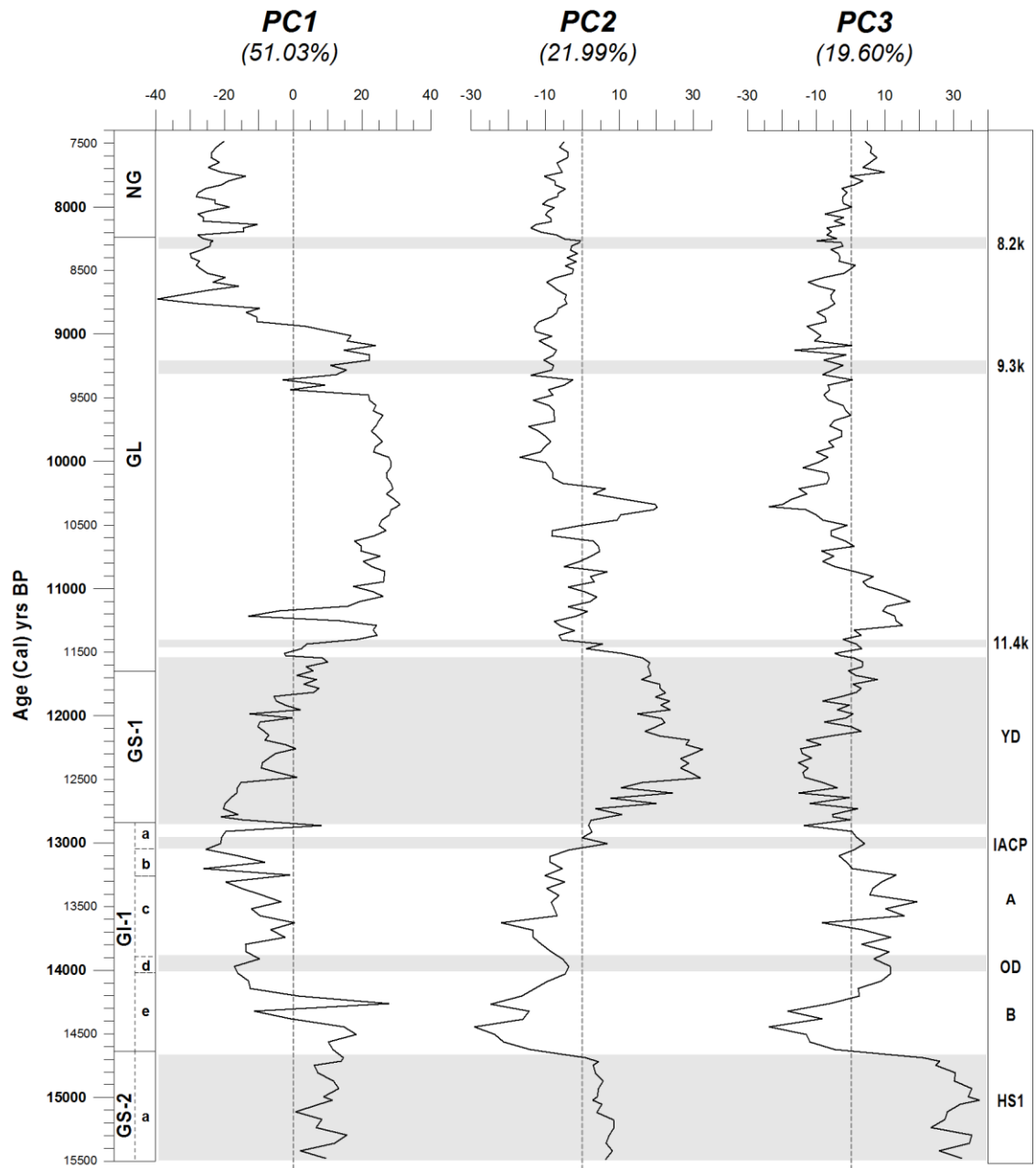
Figure 7.4: PC1, PC2 and PC3 results for M40/4 82-2SL sections 1 to 4. INTIMATE event stratigraphy (Alley, 2004; NGRIP dating group, 2008; Rasmussen et al., 2014). Colder periods highlighted in grey. Heinrich Stadial 1 (HS1); Bølling (B); Older Dryas (OD); Allerød (A); Inter-Allerød Cold Period (IACP); Younger Dryas (YD); Greenlandian (GL); Northgrippian (NG).

PC2 (~22% total variance) is strongly linked to the positive loading of the eutrophic species *G. glutinata* and *T. quinqueloba*, with more moderate negative loadings from *G. inflata*, also a deeper dwelling eutrophic species and the warm water oligotrophic species *G. ruber* white and minor SPRUDTS (Table 7.7). This PC result is a more

complex signal to decipher than PC1. The main species *G. glutinata*, *T. quinqueloba* and *G. inflata* all have surface to subsurface depth preferences (Table 3.5) and a cool deep mixed eutrophic water column (Pujol and Vergnaud Grazzini, 1995; Schiebel and Hemleben, 2005; Rebotim *et al.*, 2017). Therefore, it is difficult to separate out the key drivers for this component. However, the inclusion of *G. ruber* and minor SPRUDTS that are indicative of warm stratified summer waters, along with *G. inflata* may suggest periods of temperature driven enhanced seasonal stratification combined with mesotrophic winter productivity versus a well-mixed deep-water productivity signal.

Finally, PC3 (19.6% total variance) is dominated by a strong positive loading of *G. bulloides*, and moderate negative loadings from *G. glutinata*, *G. inflata* and minor *G. ruber* white (Table 7.7). As *G. bulloides* is an opportunistic species strongly linked to deep mixing, it could be suggested that deep mixing was the governing factor for PC3. However, *G. glutinata* and *G. inflata* are both deep mixed layer species and flourish when productive waters have been firmly established. Therefore, their association with *G. ruber* white (warm stratified summer waters) suggest that PC3 is indicative of strength and stability of the seasonal deep mixing and mixing of the water column. The downcore results for PC1, PC2 and PC3 are illustrated in Figure 7.4.

Figure 7.5 plots the scores for PC1 and PC2 with the loadings for each species, grouped by chronozone. There is clear a correlation during the YD and early NG with specific components represented by PC1 and PC2. The YD is characterised by periods where potentially the chlorophyll maximum shallowed, as a result of weakened seasonal stratification, correlating with *G. glutinata* and *N. incompta*. The early NG has a discrete signal, with abundant food availability that was accessible to *N. incompta*, and moderate seasonal stratification (*G. inflata* and *G. ruber* white and SPRUDTS). In contrast, the BA signal is more varied. Seasonal stratification is the dominant signal through the majority of the chronozone, with high variability in food accessibility for *N. incompta* in comparison to *G. inflata*. Finally, the GL signal is the most variable, with two distinct periods. The absence of *N. incompta* in the early GL, suggests that available food was too deep to be accessed by *N. incompta*, followed by the later GL period when *N. incompta* dominated, as trophic conditions became more favourable for them and is closely correlated to the early NG signal. The majority of the GL results show heightened stratification, with more discrete periods where stratification weakened, illustrating the greater influence of *G. glutinata* and *T. quinqueloba* in the mid GL. In contrast to the rest of the later chronozones, the late HS1 is less influenced by either

PC1 or PC2, with little correlation to seasonal stratification or the depth of available food. As we have seen in Figure 7.4, the late HS1 period is almost exclusively closely correlated to the positive deep mixing signal in PC3 (*T. quinqueloba* and *G. bulloides*).
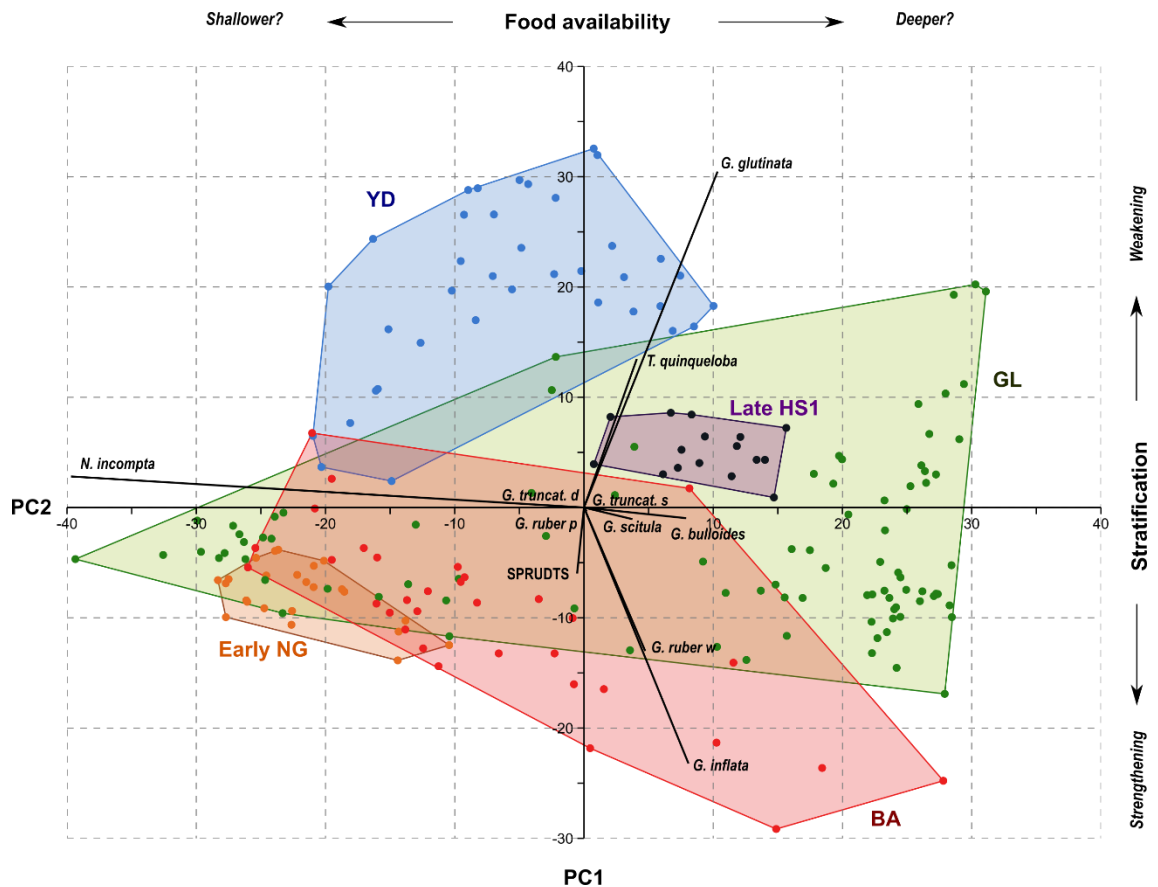
Figure 7.5: Scatter plot of PC1 and PC2 scores for M40/4 82-2SL sections 1 to 4, grouped by the main chronozones. The 'Biplot' lines illustrate the PC1 and PC2 loadings for the main planktonic foraminifera species. The colour of the samples points and the convex hulls are defined by chronozone grouping: Late Heinrich Stadial 1 (HS1) = purple; Bølling-Allerød (BA) = red; Younger Dryas (YD) = blue; Greenlandian (GL) = green and early Northgrippian (NG) = orange. G. truncat. = G. truncatulinoides; w = white; p = pink; s = sinistral; d = dextral.

7.2.4 Sea Surface Temperatures

The predicted mean annual, summer and winter SST (±1 SD) for the main late Pleistocene and early-mid Holocene chronozones are listed in Table 7.8 and the results downcore are displayed in Figure 7.6. During the late HS1, mean annual SSTs remained stable and very low (10.18°C ± 0.97°C), with only 3.83°C difference between summer and winter SSTs. In comparison to Greenland $\delta^{18}O$ ice core records, NGRIP displays more variation in air temperature, though a similar minor increase in SST at ~15.1 kyr is also evident in the GISP2 data, though more muted.
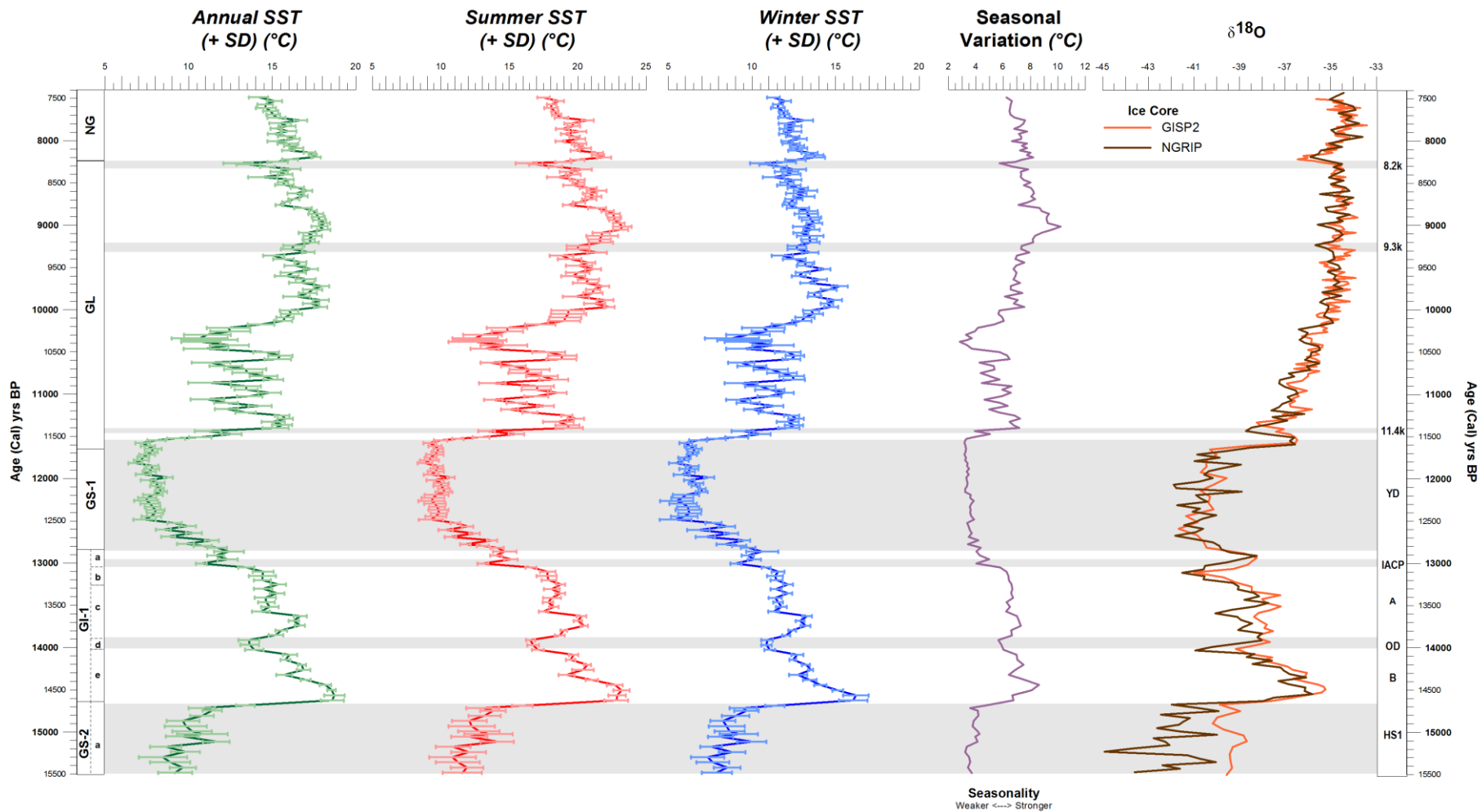
Figure 7.6: Annual, summer and winter SST (°C) for M40/4 82-2SL sections 1 to 4, as predicted by ANN. Seasonal variation is the mean summer less winter SST (°C). As a comparison, the δ¹⁸O profiles GISP2 and NGRIP Greenland ice cores are displayed. INTIMATE event stratigraphy (Alley, 2004; NGRIP dating group, 2008; Rasmussen et al., 2014). Colder periods highlighted in grey. Heinrich Stadial 1 (HS1); Bølling (B); Older Dryas (OD); Allerød (A); Inter-Allerød Cold Period (IACP); Younger Dryas (YD); Greenlandian (GL); Northgrippian (NG).

Chrono-zone	Annual		Summer		Winter		Season-ality (°C)
	SST (±1 SD) (°C)	Range (°C)	SST (±1 SD) (°C)	Range (°C)	SST (±1 SD) (°C)	Range (°C)	
Early NG	15.76 ±0.45	3.45	19.58 ±0.42	4.42	12.40 ±0.43	2.47	7.18
GL	15.06 ±0.67	8.88	18.65 ±0.83	12.04	12.12 ±0.65	7.38	6.53
YD	8.30 ±0.47	4.87	10.27 ±0.55	5.28	6.78 ±0.50	4.36	3.49
BA	15.19 ±0.48	7.96	18.64 ±0.47	10.12	12.20 ±0.37	7.17	6.44
Late HS1	10.18 ±0.97	4.94	12.58 ±1.33	5.10	8.75 ±0.85	4.02	3.83

Table 7.8: Mean annual, summer and winter SST (+1 SD) as predicted using ANN for the main chronozones in M40/4 82-2SL sections 1 to 4, in the Late Pleistocene and Early-Mid Holocene. Annual, summer and winter SST ranges are calculated as the maximum less minimum SST for each period. Seasonal variation is the mean summer less winter SST. Heinrich Stadial 1 (HS1); Bølling-Allerød (BA); Younger Dryas (YD); Greenlandian (GL); Northgrippian (NG).

The HS1/BA transition is rapid, with an increase of ~5.2°C annual SST in ~60 years (Figure 7.6). The mean annual SST during the initial Bølling period was 18.5°C (up to 14.4 kyr), which was the highest SST recorded in the Late Pleistocene and early Holocene in this core. SST decreased towards the OD by 3.3°C, then recovered in the early Allerød (~16°C). Around 13.6 kyr, there is a sharp decrease in SST followed by a relatively stable period with a mean SST of ~14.6°C. SST briefly drops (~10.8°C) around 13 kyr (the IACP?), with a minimal recovery before the start of the YD. The BA is also characterised by an increased seasonality, with the range of SST between the summer and winter ranging from 7.5°C in the early Bølling to 4.4°C in the late Allerød. The BA SST profile broadly follows that of the Greenland ice cores, though the signal of the OD cold event appears to occur slightly later, though this may be within the margin of error of the chronology. In addition, the cooling during the mid to late Allerød that is observed in the Greenland cores is not observed in this Gulf of Lion core.

Mean SSTs during the YD fall to a low of 8.3°C, almost 2°C cooler than the late HS1 and a drop of ~6.9°C from the mean BA SST (Figure 7.6). The early YD is a period of extreme SST variability until ~12.5 kyr, coinciding with a generalised cooling in the NGRIP record. SSTs stabilise during the mid YD and remain cold until the end of the YD. Summer SSTs fall to 10.3°C. As with the late HS1, the mean seasonal variation decreases to just 3.5°C.

SST predictions for the early GL period show a period of extreme variability until 10.3 kyr. On average, SSTs are ~13°C, but range from 9.25°C to 15.8°C (Figure 7.6). After 10.3 kyr, SSTs steadily increase to ~16.2°C, before decreasing slightly to 15.8°C in the

early NG stage. There is some coincidence between falling SST around the 11.4, 9.3 and more substantially, the 8.2 kyr cold events. However, the low SSTs around the 8.2 kyr event (~13.75°C) seemingly precedes that cold event, once again suggesting a discrepancy due to inherent errors of the core chronology for correlating to centennial scale events. As during the BA warm period, once again summer-winter seasonality increases from a variation of 6.5°C in the GL to 7.2°C during the early NG.

7.3 Discussion

7.3.1 Late Heinrich Stadial 1 (~15.5 to 14.7 kyr BP)

In the absence of independent palaeo-productivity proxies from this core and relatively limited palaeo-discharge estimates for the River Rhône (Kettner and Syvitski, 2009), changes to sedimentation rates are discussed in relation to the interaction of sea level change in the Gulf of Lion with rates of deposition from the River Rhône. During the LGM, sediments on the inner continental shelf in the Gulf of Lion were largely exposed and actively eroded due to an estimated lowered relative sea-level (rsl) of 110-115m (to a max of 140m rsl) between 20 to 15 kyr (Figure 7.2) (Bassetti *et al.*, 2006; Jouet *et al.*, 2006). This would be comparable to the global sea level estimates of -90m rsl at this time (Jouet *et al.*, 2006; Stanford *et al.*, 2011a). Initial post LGM sedimentation rates on the northern inner shelf were very high (2.5 m/kyr) as the pro-delta seaward limit of the Rhône Deltaic System was ~40km from the modern coast and river mouths were closer to the shelf edge, allowing terrigenous sediments to be deposited further out beyond the shelf edge (Sierro *et al.*, 2009). However, a transgressive sequence began in earnest ~18 kyr ago and the sea level had risen to between 98-105m rsl, though this slowed down between 17 and 15.9 kyr (Jouet *et al.*, 2006). The lower mean sedimentation rates (32.7 cm/kyr) recorded in M40/4 82-2SL reflect this slow-down in sea level rise, drier terrestrial conditions and evidentially little variation in discharge from the Rhône (Table 7.3; Figure 7.2) (Combourieu Nebout *et al.*, 2002; Sierro *et al.*, 2005; Combourieu Nebout *et al.*, 2009; Fletcher *et al.*, 2010; Moreno *et al.*, 2010; Moreno *et al.*, 2012).

7.3.1.1 *Sea Surface Temperatures*

The predicted mean annual SST (~10.2°C) during the late HS1 was ~6.65°C lower than modern SSTs (Table 7.9; Figure 7.6), which are equivalent to SST estimates during the same period in neighbouring core MD99-2346 (Melki *et al.*, 2009). SSTs were ~2°C warmer than those experienced during the LGM (~8.2°C) (Table 7.1) (Hayes *et al.*,

2005). In comparison to the rest of the western Mediterranean, SSTs in the late HS1 in the Gulf of Lion were cooler than previously proposed for the entire HS1 (Kallel *et al.*, 1997b; Cacho *et al.*, 1999; Cacho *et al.*, 2001). The low seasonality in SSTs (~3.8°) indicate that waters remained cool throughout the year, with summer SSTs ~8.75°C cooler than modern SSTs (Table 7.8; Table 7.9). Orbitally driven summer and winter insolation differences at 40°N were still at a minimum (Frigola *et al.*, 2008). Therefore, these persistently cool SSTs in the Gulf of Lion reflect the southerly position of the ocean polar front and polar front jet stream during HS1, which enabled cold winds to penetrate into the north-western Mediterranean (Rohling *et al.*, 1998; Eynaud *et al.*, 2009; Martinez-Ruiz *et al.*, 2015; Naughton *et al.*, 2016).

Chronozone	Annual Anomaly (°C)	Summer Anomaly (°C)	Winter Anomaly (°C)
Early NG	-1.07	-1.75	-0.68
GL	-1.77	-2.68	-0.96
YD	-8.53	-11.06	-6.30
BA	-1.64	-2.69	-0.88
Late HS1	-6.65	-8.75	-4.33

Table 7.9: Mean annual, summer and winter SST anomalies for the main chronozones in the Late Pleistocene and Early-Mid Holocene. Anomaly values were calculated by subtracting modern World Ocean Atlas (2018) values (Table 7.1) from the mean ANN annual, summer and winter SST reconstructions for each chronozone. Heinrich Stadial 1 (HS1); Bølling-Allerød (BA); Younger Dryas (YD); Greenlandian (GL); Northgrippian (NG).

To the south, MD99-2343 in the Balearic Sea showed an increase in the $\delta^{18}O$ of both benthic and planktonic foraminifera as would be expected with the lower observed SSTs and decreased freshwater input during this dry period (Sierro *et al.*, 2005). However, between 16.2 and 15.7 kyr there was a notable decrease in $\delta^{18}O$, attributed to an influx of North Atlantic Surface Waters (NASW), associated with incoming ice rafted debris (IRD) and meltwater pulses (Sierro *et al.*, 2005; Frigola *et al.*, 2008). Inflow of low $\delta^{18}O$ water from meltwaters from Eurasian ice sheets and the Alps was discounted, as Rhône discharge at this time did not record lower $\delta^{18}O$ values (Sierro *et al.*, 2005). This incoming fresher NASW would have had a lower salinity and density, thus minimising mixing with the MAW, allowing greater penetration into the western basin. Indeed, these lower salinities are evident from benthic foraminiferal communities in the Gulf of Lion at this time (Melki *et al.*, 2009; Melki, 2011).

7.3.1.2 *Planktonic foraminiferal assemblage*

The defining faunal characteristic of the late HS1 was the dominance of *G. bulloides* (52.8%), accompanied only by other cool water eutrophic species. There was an

absence of both *G. inflata* and all warm oligotrophic species. This low diversity during late HS1 is also seen in neighbouring core MD99-2346 (Melki *et al.*, 2009). To aid interpretation of the planktonic foraminifera assemblage in M40/4 82-2SL, a range of palaeoenvironmental proxies were utilised, including the eutrophication (E-Index) and stratification (S-Index) (Figure 7.7) (Sbaffi *et al.*, 2004; Kontakiotis, 2016). As would be expected, the E-Index is very strong and seasonal stratification was not a feature during HS1.

As the Gulf of Lion is a site of deep surface water mixing and WMDW formation, the percentage of *G. bulloides* has been used as a "Deep mixing" index (DM-Index), rather than the traditional "Upwelling" Index (U-Index) (see Section 5.3.3) (Hemleben *et al.*, 1989; Kontakiotis, 2016). During HS1, the DM-Index is at its strongest throughout the whole core (Figure 7.7). As an opportunistic species, *G. bulloides* is known to invade a region once the phyto and zooplankton bloom has begun and food availability is high (mainly algae, but it can feed on any particulate organic matter) (Pujol and Vergnaud Grazzini, 1995; Schiebel and Hemleben, 2005, 2017). High frequencies of *G. bulloides* reflect abundant food availability, rather than on temperature or depth preferences (Schiebel and Hemleben, 2017). As mentioned above, sedimentation rates were relatively low, therefore this productivity signal was not as a result of increased discharge nutrient rich waters from the Rhône. The dominance of *G. bulloides* and inferred deep-mixing signal along with the cold SSTs strongly suggest that enhanced westerlies, wind-driven cooling and cyclogenesis were the main drivers of conditions in the Gulf of Lion at this time.

The remaining assemblage is composed of cool water eutrophic grazers *N. incompta*, *T. quinqueloba* and minor *G. glutinata* (Table 7.4). As would be expected, *T. quinqueloba* would form part of this assemblage, as it is commonly found in close association with *G. bulloides* in strongly eutrophic, deeply mixed waters (Sautter and Thunell, 1991; Conan and Brummer, 2000; Schiebel *et al.*, 2001; Schiebel and Hemleben, 2017). Also, *T. quinqueloba* occurs alongside minor peaks in *G. glutinata*, which have a similar preference for diatoms, and are negatively correlated to peaks of *N. incompta* (Figure 7.3). Clearly *N. incompta* was able to survive in this late HS1 environment, but it did not flourish (~18%).

The negative correlation between the two species suggests that the more opportunistic *T. quinqueloba* was more adapted to periods of higher productivity than *N. incompta*

(Schiebel *et al.*, 2001; Schiebel and Hemleben, 2017). The *G. bulloides* population
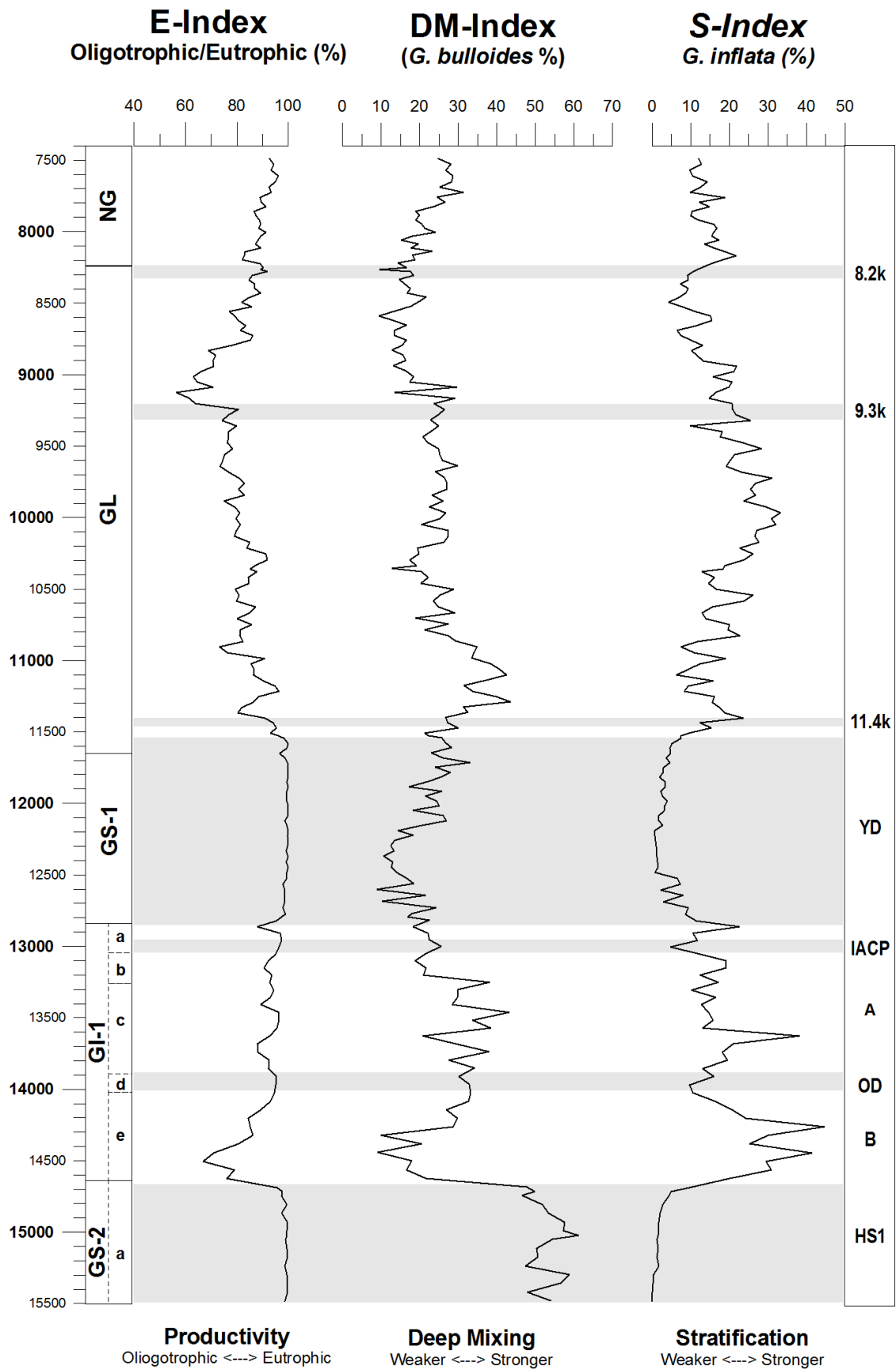
Figure 7.7: Palaeoenvironmental indices for M40/4 82-2SL sections 1 to 4. INTIMATE event stratigraphy (Alley, 2004; NGRIP dating group, 2008; Rasmussen et al., 2014). Colder periods highlighted in grey. Heinrich Stadial 1

began to wane in the final ~300 years prior to the HS1/BA transition, whereas the *T. quinqueloba* population remained stable at around 15%. This suggests the strong Westerly winds began to weaken as the polar jet stream began to retreat northward, or an increasing riverine signal, correlated to increasing precipitation on the Iberian Peninsula (Naughton *et al.*, 2016).

As left coiling Neogloboquadrina species form less than 1.5% of the population during the late HS1 in M40/4 82-2SL, they are counted as *N. incompta* sinistral and not *N. pachyderma* (Darling *et al.*, 2006). However, *N. pachyderma* were found in other sites in the western basin indicating an influx of cold meltwaters into the western Mediterranean at this time (Cacho *et al.*, 1999; Cacho *et al.*, 2001; Cacho *et al.*, 2002; Combourieu Nebout *et al.*, 2002; Pérez-Folgado *et al.*, 2003; Sierro *et al.*, 2005; Frigola *et al.*, 2008). *N. pachyderma* (~5 to 10%) were recorded during mid HS1 in neighbouring cores, MD99-2346, MD99-2348 and BC15 (Rohling *et al.*, 1998; Melki *et al.*, 2009; Bassetti *et al.*, 2010). However, as M40/4 82-2SL only extends into the later part of HS1, unfortunately it was not long enough to record any earlier influx of *N. pachyderma* relating to the inflow of cold NASW in the early to mid HS1.

7.3.1.3 *Palaeoenvironmental Reconstruction*

It is evident that deep mixing and ventilation were significant features of the late HS1 in the Gulf of Lion. In modern subtropical zones, upwelling systems and areas of DWF are highly seasonal and are characterised by cooler water winter/spring eutrophic species, such as *G. bulloides*, *G. glutinata*, *T. quinqueloba*, *N. dutertrei* and *N. incompta* (Thiede, 1975; Conan and Brummer, 2000; Field, 2004; Fraile *et al.*, 2009; Retailleau *et al.*, 2012; Darling *et al.*, 2017). Following an upwelling/deep mixing event, entrained nutrients in the photic zone are depleted and the summer assemblage is dominated by warm water predators such as *G. ruber* and the SPRUDTS group (Conan and Brummer, 2000; Darling *et al.*, 2017). However, there is no definitive "upwelling" faunal assemblage, as there can be significant regional variations (Darling *et al.*, 2017). This is true when comparing modern assemblages in upwelling and or DWF regions in the western Mediterranean, such the Gulf of Lion in comparison with, and even between the gyres of the Alboran Sea (Bárcena *et al.*, 2004; Hernández-Almeida *et al.*, 2011; Rigual-Hernández *et al.*, 2012).

The signal of the late HS1 period in the Gulf of Lion clearly shows cold annual SSTs, intense deep surface water mixing and heightened nutrification of surface to sub-surface waters due to enhanced Westerly winds over the western Mediterranean. This is in direct opposition to the reduced deep water ventilation experienced in the North Atlantic (Sierro *et al.*, 2005; Frigola *et al.*, 2008). During HS1, the WMDW formation intensified due to strengthened Westerly winds, except for a brief weakening coinciding with the influx of cold fresh NASW pulses from HE1 and subsequent deposition of the pre-ORL in the western basin (Sierro *et al.*, 2005; Frigola *et al.*, 2008; Rogerson *et al.*, 2008; Rodrigo-Gámiz *et al.*, 2011; Martinez-Ruiz *et al.*, 2015). However, this brief mid HS1 weakening of deep ventilation is not evident in M40/4 82-2SL, therefore it can be assumed that WMDW formation had resumed by the start of the M40/4 82-2SL record.

7.3.2   Bølling-Allerød (14.7 to 12.8 kyr BP)

During the BA chronozone, both pollen and speleothem proxies from the western Mediterranean region record an increase in the rates of precipitation (Combourieu Nebout *et al.*, 2002; Combourieu Nebout *et al.*, 2009; Dormoy *et al.*, 2009; Fletcher *et al.*, 2010; Moreno *et al.*, 2010; Belli *et al.*, 2013; Naughton *et al.*, 2016). Global sea levels during the BA chronozone rapidly increased from approximately -100 to -60m rsl (Jouet *et al.*, 2006; Lombo Tombo *et al.*, 2015). This rapid rise is attributed to MWP-1A (between ~14.6 and 14.3 kyr BP) and increasing sea levels in the Mediterranean Sea by ~30m (Figure 7.2) (Deschamps *et al.*, 2012; Fink *et al.*, 2015; Zecchin *et al.*, 2015). Modelling of the River Rhône determined that discharge since the LGM was relatively stable, though meltwater discharge and sediment flux were negatively impacted by Alpine glacial growth and positively by glacial ablation (Kettner and Syvitski, 2009). It is also proposed that there was a sustained period of Alpine meltwater release through the River Rhône (~15 to 13 kyr), which impacted WMDW formation strength and contributed to the initiation of the Organic Rich Layer 1 (ORL1) deposition in the western basin (Rohling *et al.*, 2015). These meltwaters would have inundated the shelf in the Gulf of Lion, causing the coast to retreat landward and increase sedimentation rates (from 14.8 kyr), initiating the deposition of the Rhône pro-delta (particularly between 14.5 and 7 kyr) (Berné *et al.*, 2004; Berné *et al.*, 2007; Sierro *et al.*, 2009; Rigual-Hernández *et al.*, 2017). Although sedimentation rates in M40/4 82-2SL slowly increased during the BA, they were not as high as expected (Table 7.3; Figure 7.2). While sea levels were increasing on the Gulf of Lion continental shelf, the site of M40/4 82-2SL may have been further away from the active sediment lobe of the Rhône pro-

delta.

7.3.2.1 Sea Surface Temperatures

The distinctive asymmetrical sawtooth GI-1 temperature signal in the Greenland $\delta^{18}O$ isotope records is mirrored in the M40/4 82-2SL SST predictions for the BA chronozone (Figure 7.8) (Wolff *et al.*, 2010; Li and Born, 2019). In general, mean annual SST for the entire BA chronozone (15.19°C) are ~1.64°C cooler than modern SSTs (Table 7.1; Table 7.8; Table 7.9). Seasonal variation increased during the BA (~6.4°C), though they were not as high as modern values (Table 7.8). Winter SST predictions in M40/4 82-2SL are comparable to both the estimated winter SST for the BA chronozone in MD99-2346 and are just ~1°C cooler than modern winter SSTs (Melki *et al.*, 2009). However, summer SSTs are ~2.7°C cooler than modern summer SST values (Table 7.9). This is reflected in the broadly typical modern winter-spring assemblage during the BA, yet a more limited warmer water assemblage. Winter SSTs in the Gulf of Lion were significantly cooler than sites in the rest of the western Mediterranean, e.g. ~16°C for the Tyrrhenian Sea (Kallel *et al.*, 1997b; Cacho *et al.*, 1999; Cacho *et al.*, 2001).
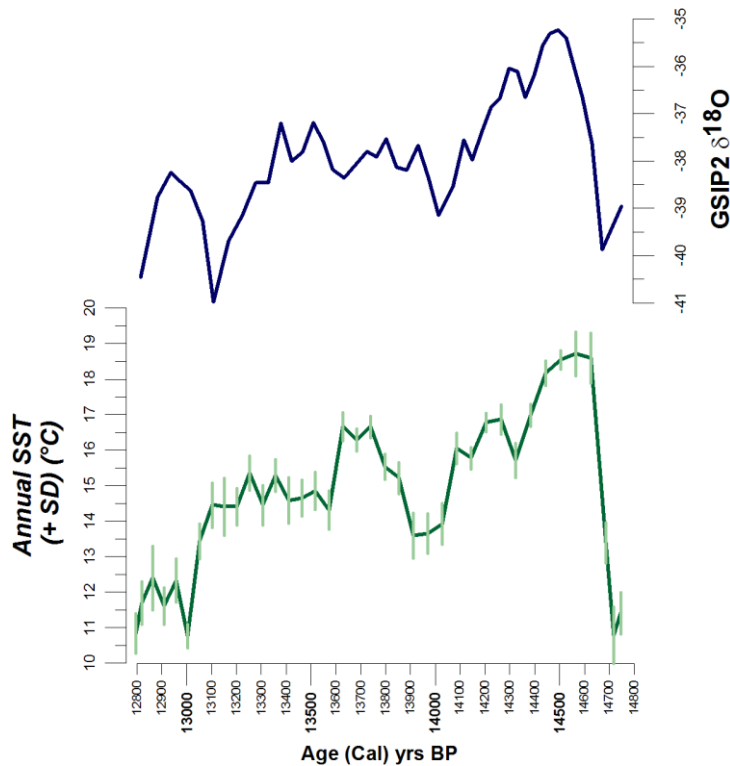
Figure 7.8: Mean annual SSTs (°C) for M40/4 82-2SL and $\delta^{18}O$ profile from the GISP2 Greenland ice core for the Bølling-Allerød chronozone (Grootes et al., 1993).

The strong similarity between $\delta^{18}O$ isotope signals from Greenland ice cores and M40/4

82-2SL is also seen in MD99-2346, as well as in $\delta^{18}O$ values from speleothems in Chauvet Cave in southern France and Grotta Savi in the south-eastern Alps (Frisia *et al.*, 2005; Genty *et al.*, 2006). This suggests a strong teleconnection between the North Atlantic and the north-west Mediterranean basin (Figure 7.8). SSTs in the modern Gulf of Lion are particularly sensitive to post-Industrial CO_2 warming (Pallacks *et al.*, 2021b). Therefore, it suggests that atmospheric warming from rapidly increasing CO_2 during the early Bølling is recorded in these north-western Mediterranean archives.

This early warming during the Bølling is in contrast with the stepwise increase in SSTs in the Alboran and southern Tyrrhenian, which peak during the Allerød (Cacho *et al.*, 2001). With the resumption of the AMOC and rising sea levels, the western basin was under greater influence of incoming warmer waters from the North Atlantic subtropical gyre (Schwab *et al.*, 2012; Jiménez-Amat and Zahn, 2015; Repschläger *et al.*, 2015). Changes in atmospheric pressure regime in the North Atlantic, similar to the modern negative NAO mode, steered weakened Westerlies and greater rates of precipitation into the south-western Mediterranean region, leading to enhanced vertical mixing in the Alboran Sea gyres and cooling of incoming subtropical waters (Moreno *et al.*, 2010 ; Rodrigo-Gámiz *et al.*, 2011; García-Alix *et al.*, 2014; Naughton *et al.*, 2016). However, the warm early Bølling signal in the north-west suggests that a high-pressure blocking system over western Europe may have deflected these weaker Westerly winds further south over the southern Iberian Peninsula, rather than over north-west basin.

The cooling signal in M40/4 82-2SL from ~14.3 kyr is coincident with the timing of MWP-1A in the Mediterranean Sea (Zecchin *et al.*, 2015). MWP-1A waters identified in the Arctic are known to be cold and were linked to an expansion of seasonal sea-ice cover (Rigual-Hernández *et al.*, 2017). However, SSTs in the Alboran Sea were not significantly impacted by the event (Rodrigues *et al.*, 2010). This suggests that MWP-1A would have had little effect on SSTs in the Gulf of Lion. However, the suggested enhanced outflow of Alpine meltwaters into the Gulf of Lion around this time would certainly have much greater impact on cooling surface waters in the Gulf of Lion (Rohling *et al.*, 2015). The rapid fall in SST at 13.6 kyr is coincident with a brief cooling in the Greenland δ18O isotope record (during GI-1c). Across the Mediterranean, it appears as a cold dry period in terrestrial proxies and marks the onset of mid-Allerød cooling in the neighbouring MD99-2346 as well as other cores across the Mediterranean (Cacho *et al.*, 2001; Dormoy *et al.*, 2009; Melki *et al.*, 2009).

7.3.2.2 *Planktonic foraminiferal assemblage*

With the rapid increase in SSTs, diversity increased, suggesting a restructuring of the hydrological system and seasonal structure of the water column (Table 7.4; Figure 7.3). All palaeoenvironmental indices suggest strong, seasonally stratified and oligotrophic conditions were established in the early Bølling until ~14.3 kyr (Figure 7.7). However, from ~14.3, the increase in Alpine meltwaters suggested by cooler SSTs is supported by the re-establishment of winter/spring eutrophic conditions and the moderate and somewhat variable deep mixing signal for the remainder of the BA.

Inflow of warmer subtropical waters from the North Atlantic subtropical gyre into the western basin, along with the increased SSTs in the Gulf of Lion allowed a warm assemblage to become established. The abundance of *G. ruber* white during the early Bølling mimics the Greenland $\delta^{18}O$ isotope records and similar patterns, though at more modest rates, are recorded in BC15 and MD99-2346 (Rohling *et al.*, 1998; Melki *et al.*, 2009). In the recent Mallo *et al.* (2017) study on the modern Mediterranean summer assemblage, *G. ruber* white (plus *G. elongatus*) was the dominant summer species. Its presence was determined mainly by heightened SSTs, then by enhanced primary productivity. It was also noted that in oligotrophic waters, low food availability inhibited their presence (Mallo *et al.*, 2017). The SPRUDTS group form a small, but significant component of the early BA assemblage, reaching a brief peak (~7%) in the mid Bølling following the decrease in *G. ruber* white. This peak is comprised primarily of *O. universa*, a deeper species that also is positively associated with more productive warm stratified waters, also evident in similarly aged minor peaks in the neighbouring cores (Rohling *et al.*, 1998; Melki *et al.*, 2009).

In tandem with the warmer water assemblage, *G. inflata* formed the primary winter-spring bloom species, indicating seasonally moderately productive waters and a deepening of the pycnocline. *G. inflata* was almost absent from the Mediterranean Sea during the LGM to the HS1 period, when winter SSTs decreased below their optimum preference (Table 7.8). Its reappearance at the beginning of the BA is a biomarker for the HS1/BA transition, and is clearly evident in M40/4 82-2SL, as well as in neighbouring cores BC15 and MD99-2346 (Bé and Tolderlund, 1971; Muerdter and Kennett, 1983/84; Rohling *et al.*, 1998; Melki *et al.*, 2009; Bazzicalupo *et al.*, 2018). As mentioned in section 7.2.2, *G. ruber* white and *G. inflata* are positively correlated in the Pearson's r correlation matrix (Table 7.5). This correlation occurs when *G. ruber* white

inhabits the summer oligotrophic stratified waters and *G. inflata* the cooler deepened mixed layer during mesotrophic winter/spring periods (Giraudeau, 1993; Bárcena *et al.*, 2001; Bárcena *et al.*, 2004; Lončarić *et al.*, 2007).

A brief peak in *G. scitula* coincides with the elevated *G. ruber* white and *G. inflata* in the early Bølling. This brief peak is unusual during this early warm phase, especially as it was virtually absent for the remainder of the BA chronozone. Traditionally, *G. scitula* is classified as a polar / subpolar species (Bé, 1977). However, more recently it is found to be a more cosmopolitan opportunistic species, typical of intensely mixed eutrophic temperate waters, especially during the spring bloom (Itou *et al.*, 2001; Chapman, 2010; Schiebel and Hemleben, 2017). This peak is evident in BC15, but not in MD99-2346 (Rohling *et al.*, 1998; Melki *et al.*, 2009). *G. scitula* is rare (<1%) in the modern Mediterranean, occurring only in the Aegean Sea and the north-western Mediterranean (Thunell, 1978; Pujol and Vergnaud Grazzini, 1995). It is one of the deepest dwelling species in this assemblage with an ALD of ~224m (Table 3.5) (Rebotim *et al.*, 2017). When found in combination with warmer shallow-dwelling predatory species such as *G. ruber* white or *O. universa*, it is indicative of stratification and vertical niche partitioning (Rutherford *et al.*, 1999; Schiebel *et al.*, 2002b; Schiebel and Hemleben, 2005).

As SSTs begin to cool from ~14.2 kyr, productivity increased and the pycnocline shallowed, allowing *N. incompta* to dominate the assemblage, which was also recorded in both MD99-2346 and BC15 (Rohling *et al.*, 1998; Melki *et al.*, 2009). The more modest and variable abundances of *G. bulloides* and *T. quinqueloba* support periods of weaker wind intensity during the BA, though the peak in *T. quinqueloba* during the OD chronozone suggests an increase in winds during this brief cold snap (Figure 7.3; Table 7.4).

7.3.2.3   *Palaeoenvironmental Reconstruction*

It is clear that the BA chronozone was a warm period, but the palaeoenvironment conditions fluctuated substantially over the ~1.8 kyr, influencing both the fauna and the ecological factors that governed their abundance (Figure 7.3; Figure 7.5). Reorganisation of North Atlantic atmospheric circulation patterns and a decrease in wind intensity over the Gulf of Lion allowed the atmospheric warming to rapidly increase SSTs by ~8°C during the initial ~200 years of the early Bølling (Figure 7.6). This warming was accompanied by a swift turnover of the fauna to a more diverse

warm water assemblage, and deeper dwelling eutrophic species. The strongly negative PC2 and the positive S-Index indicate that surface waters had a distinct annual variation, with warm oligotrophic waters during summer/autumn months, with a deep eutrophic mixed layer during the winter/spring. In addition, rising sea levels from the HS1/BA transition in the Alboran Sea allowed greater inflow of NASW into the western basin, freshening the MAW and leading to a deepening of the pycnocline (Bárcena *et al.*, 2004; Bazzicalupo *et al.*, 2018). This deepening of the pycnocline meant that cool stable eutrophic winter waters (~15°C) could support the reappearance of deeper dwelling *G. inflata* and *G. scitula* in the Gulf of Lion.

As discussed in section 4.4.2, the BA chronozone coincided with the onset of ORL1 deposition in the western basin between 14.5 and 9 kyr BP (Cacho *et al.*, 2002; Rogerson *et al.*, 2008; Martinez-Ruiz *et al.*, 2015; Bazzicalupo *et al.*, 2018; Pérez-Asensio *et al.*, 2020). The deposition of ORL1 is associated with an influx of freshwaters, such as an increase in meltwater discharge from the River Rhône, combined with a decrease in winter westerlies (Rohling *et al.*, 2015). All these factors would have enhanced surface water productivity in the Gulf of Lion, but reduced surface water density and deep mixing, leading to a reduction in WMDW and promoted Western Intermediate Water (WIW) formation and deposition of ORL1 (Frigola *et al.*, 2008; Rogerson *et al.*, 2008; Melki, 2011; Fink *et al.*, 2015; Rohling *et al.*, 2015). As with planktonic species, there was a turnover in benthic foraminifera species following the HS1/BA transition, and the community was composed primarily of deep and intermediate taxa, indicative of enhanced laterally advected, low-quality organic carbon to the sea floor (Melki *et al.*, 2009).

The timing of the beginning of the deposition of ORL1 (14.35 kyr BP) coincided with a series of faunal changes in M40/4 82-2SL. *G. scitula* had already disappeared and *G. ruber* white was declining, to be replaced by the opportunistic, deeper dwelling *O. universa*. There was a recovery of eutrophic species, first *G. bulloides*, then *N. incompta*. *G. inflata* was still present, but it was soon replaced by *N. incompta* indicative of the shallowing of the pycnocline (negative PC1), which was also seen in the Alboran at this time (Bazzicalupo *et al.*, 2018). All patterns suggest this was a period with enhanced seasonality (PC2), where the warm summer waters were still stratified and the shallowing pycnocline (negative PC1) from 14.15 kyr, which became a fixture for the remainder of the BA chronozone (Figure 7.4; Figure 7.5).

The OD chronozone in M40/4 82-2SL is identifiable by the drop in mean annual SST (~13.6°C) for <150 years around 13.9 kyr and correlates well to the GI-1d cold event. The planktonic foraminiferal community was less responsive to this cooling event and is only evident from a decrease in *G. inflata* and moderate peak in *T. quinqueloba*. Summer SSTs decreased more substantially than winter, thus seasonality (PC2) weakened during this brief cooling. This would suggest that changes in the North Atlantic atmospheric circulation redirected colder winter Westerlies back into the north-west Mediterranean Sea. While the OD faunal signal is subtle, this strengthening of winds is supported by the brief peak in *T. quinqueloba*.

The rapid fall in SST at 13.6 kyr is accompanied by a sharp peak in *G. inflata* and decrease in *G. bulloides*, *O. universa* and *N. incompta*. This initial cooling event is unusual in that most cool water eutrophic species fall in abundance, while *G. inflata* has a strong positive response. It can be assumed that although temperatures were cool and productive (stable E-Index), the pycnocline deepened and the water column became more stable, allowing *G. inflata* to flourish. One possible cause is a freshening of surface waters coinciding with the peak in MWP-1A in the Gulf of Lion, as this event occurs shortly after the suggested global peak in MWP-1A (~13.8 kyr) (Stanford *et al.*, 2011a).

Waters in the mid to late Allerød became more unsettled, with elevated *G. bulloides*, then moderate increases in *T. quinqueloba* (positive PC3). This is in contrast to MD99-2346, where *G. bulloides* fell and *N. incompta* and *G. glutinata* were the dominant species (Melki *et al.*, 2009). As sea levels continued to rise, this suggests variability in rates of Alpine meltwater or changing position of the Rhône Delta plume towards the site of M40/4 82-2SL.

The end of the Allerød is marked by another brief fall in mean annual SST (at 10.76°C) that could be attributed to the IACP chronozone, though it does lag the GI-1b cold event recorded in Greenland ice cores. This may be a function of age model and/or chronology errors discussed above, or that the Mediterranean was slower to respond to this cooling event. As with the OD, the faunal signal is subtle, with a small peak in *G. glutinata* and *G. bulloides* and a dip in both *G. inflata* and *G. ruber* white. Again, this cold snap was potentially caused by a brief increase in Westerly winds. The recovery following this brief cold snap was terminated by the transition to the YD.

7.3.3   Younger Dryas (12.8 to 11.55 kyr BP)

Rates of global sea level rise decelerated during the YD from 20 mm/yr^{-1}to 4 mm/yr^{-1} (Bard *et al.*, 2010; Abdul *et al.*, 2016). This stillstand in sea level rise in the Gulf of Lion enabled sedimentation rates to significantly rise and initiate the deposition of the Early Rhône Deltaic Complex (Berné *et al.*, 2007). This is evident in M40/4 82-2SL, where sedimentation rates reached ~55 cm/kyr (Table 7.3; Figure 7.2). In general in the Mediterranean region, the YD period was cold and dry, though there were seasonal increases in winter precipitation and Westerly winds by the latter half of the chronozone (Combourieu Nebout *et al.*, 2009; Fletcher *et al.*, 2010; Naughton *et al.*, 2016).

7.3.3.1   *Sea Surface Temperatures*

The predicted mean annual SST were ~8.5°C cooler than modern annual SSTs in the Gulf of Lion (Table 7.8; Table 7.9). In addition, annual SSTs were approximately ~2°C cooler than in the late HS1 and comparable to those experienced during the LGM in the Gulf of Lion (Table 7.1) (Hayes *et al.*, 2005). Similar to HS1, seasonality was low (<4°C) and SSTs remained cool throughout the year. This signal does not reflect the warm summers suggested by terrestrial proxies elsewhere in northern and south-eastern Europe (Schenk *et al.*, 2018; Magyari *et al.*, 2019; Schenk *et al.*, 2020). SSTs in M40/4 82-2SL are significantly cooler than elsewhere in the western basin (Kallel *et al.*, 1997b; Paterne *et al.*, 1999; Cacho *et al.*, 2001; Cacho *et al.*, 2002; Beaudouin *et al.*, 2004; Di Donato *et al.*, 2008; Rogerson *et al.*, 2008; Martrat *et al.*, 2014; Rodrigo-Gámiz *et al.*, 2014a; Ausin *et al.*, 2015a). As discussed in section 4.4.3, the location of the oceanic polar front was variable and did not reach as far south, in comparison to HS1, though subarctic waters were mapped as far south as ~40°N (Eynaud *et al.*, 2009). Changes in atmospheric circulation patterns steered cold Westerly winds and winter storm tracks towards continental Europe, increasing cyclogenesis and precipitation, especially in the eastern Mediterranean Sea (Naughton *et al.*, 2016; Rea *et al.*, 2020). With the reorganisations of atmospheric and oceanic systems, there was considerable variability in the response of different regions in the western basin to the YD cooling.

Both marine and terrestrial proxies identify three subdivisions to the YD signals in the Mediterranean Region. in the M40/4 82-2SL record, two main phases are evident, though they display different characteristics compared to elsewhere in the western Mediterranean Sea. YD-1 (12.8 to 12.5 kyr) is distinct phase, with highly variable SSTs (ranging from 11.7 to 8.5°C). This slow oscillating cooling contrasts the abrupt onset of the YD cooling recorded in the nearby speleothem records southern France but is

comparable to summer SST estimates in the nearby MD99-2346 (Genty *et al.*, 2006; Melki *et al.*, 2009).

Mean annual SSTs remained relatively stable for the remainder of the YD-2 (mean ~7.7°C). However, variations in winter SSTs in particular, suggest that YD-2 can be further subdivided into YD-2a (12.5 to 12.2 kyr) where there was a decrease in winter SSTs, and YD-2b (12.2 to 11.5 kyr BP), which displayed a minor increase in winter SSTs (~1.5°C). Interestingly, there was a brief decrease in $\delta^{18}O$ in the speleothem record from Chauvet Cave in the south of France ~12.15 kyr, just prior to YD-2b, though the cause of this brief warming was unclear (Genty *et al.*, 2006). The stability of cold SSTs in YD-2a and YD-2b in M40/4 82-2SL contrast the SST increase estimated in MD99-2346 and elsewhere in the western basin(Melki *et al.*, 2009). Many of these SST estimates (based on alkenones) indicate a recovery ~700 years prior to the YD termination (Cacho *et al.*, 2001; Sbaffi *et al.*, 2001; Essallami *et al.*, 2007). However, it has been suggested that this SST increase may reflect a change to the timing of alkenone production (i.e. from spring/autumn to warmer summer months) rather than represent a true recovery in SST (Essallami *et al.*, 2007; Sicre *et al.*, 2013; Rodrigo-Gámiz *et al.*, 2014a). The YD signal in the Gulf of Lion also contrasts the Greenland $\delta^{18}O$ isotope records (Figure 7.6). For example, the results from M40/4 82-2SL does not record this mid YD climatic amelioration following the resumption of the AMOC (Lane *et al.*, 2013). Therefore, it can be assumed that the site of M40/4 82-2SL was influenced by more regional controls during the YD.

7.3.3.2 *Planktonic foraminiferal assemblage*

These three distinct YD subdivisions are even clearer in the faunal assemblage, and PC2 and PC3 analysis (Figure 7.3; Figure 7.4). In general, the YD faunal record is marked by the disappearance of *G. ruber* white, SPRUDTS and the slow decline in *G. inflata* by the mid YD (Table 7.4; Figure 7.3). The assemblage is dominated by eutrophic species *N. incompta*, *G. glutinata*, *G. bulloides* and *T. quinqueloba*. This explains the strong stable E-Index scores throughout the chronozone, confirming the continued presence of highly eutrophic waters (Figure 7.7). Interestingly, the DM-Index is weaker than expected, declining during YD-1 towards a stable period in YD-2a and is followed by a variable, but gradual strengthening of the deep mixing signal in YD-2b. *G. bulloides* was present in these eutrophic waters, but it did not dominate the assemblage as it did during HS1, suggesting that wind strength was much less (especially in YD-2b). The S-

Index signal was also weak throughout the YD, especially in YD-2a and YD-2b.

Of these species not already discussed in detail above, *G. glutinata* occupied a dominant role during YD-2a (~36%), then slowly decreased again in YD-2b. Comparable signals in *G. glutinata* were recorded in BC15 and MD99-2346 during the YD, as well as in other regions such as the Tyrrhenian and Aegean Seas (Rohling *et al.*, 1998; Carboni *et al.*, 2005; Melki *et al.*, 2009; Geraga *et al.*, 2010). In the modern Mediterranean Sea, *G. glutinata* is regarded as a cosmopolitan species and is present in low abundances (<5%) in surface sediments in most areas of the western and eastern basins (Cifelli, 1974; Thunell, 1978; Rigual-Hernández *et al.*, 2012). It has been recorded in low abundances in surface waters during the late summer, but it is more prolific in deeper waters during the winter/spring bloom periods, when fresh food (diatoms) are available (Pujol and Vergnaud Grazzini, 1995; Hilbrecht, 1996). In the Gulf of Lion, *G. glutinata* is present in the modern assemblage, but in very low abundances (<2%) (Thunell, 1978; Pujol and Vergnaud Grazzini, 1995; Rigual-Hernández *et al.*, 2012).

7.3.3.3 *Palaeoenvironmental Reconstruction*

Surface waters were extremely cold and strongly eutrophic during the YD in the Gulf of Lion. PC1 in YD-1 suggest that the a relatively stable shallow pycnocline, which allowed *N. incompta* to dominate. Seasonal stratification (PC2) decreased in YD-1 and remained low through the remainder of the chronozone (Figure 7.5). This YD-1 assemblage is similar to other regions of the western basin, which record cold SST, heightened productivity and development of a DCM (Bárcena *et al.*, 2001; Cacho *et al.*, 2001; Cacho *et al.*, 2002; Jimenez-Espejo *et al.*, 2007; Melki *et al.*, 2009; Rodrigo-Gámiz *et al.*, 2014a; Ausin *et al.*, 2015a; Jiménez-Amat and Zahn, 2015; Bazzicalupo *et al.*, 2018).

PC3 factor loadings are governed by the negative correlation between *G. bulloides* and *G. glutinata* (Table 7.7). As discussed in section 3.3.6, both species are known to thrive on the margins of productive zones, though they have different feeding strategies (Bé and Hutson, 1977; Bijma *et al.*, 1992). *G. bulloides* is first to respond to deep mixing and redistribution of nutrients and chlorophyll, but once the mixed layer deepens and there is a phytoplankton bloom, the less opportunistic *G. glutinata* becomes established (Hilbrecht, 1996; Schiebel *et al.*, 2001; Schiebel *et al.*, 2004). The cyclicity in *G. bulloides* and *G. glutinata* suggests that there was a variability in food availability and quality, as well as the depth of vertical mixing, potentially caused by variable wind

strengths. Stable isotope analysis of tree-ring cellulose located in the southern foothills of the French Alps record an intensification of winter cyclones and precipitation, along with decreasing temperatures during YD-1 (Pauly *et al.*, 2018). Similar to M40/4 82-2SL, this region was located along the more southerly, oscillating position of the polar front during the YD. Therefore, it was determined that Mediterranean cyclogenesis increased in intensity, as more frequent cold mid-latitude seasonal low pressure systems penetrated the north-western Mediterranean Sea, as well as increasing incursion of intense precipitation events and extreme cold sweeping in from the North Atlantic (Pauly *et al.*, 2018). This signal of increasing winds and precipitation concur with the cool, mixed eutrophic waters in the Gulf of Lion during YD-1.

The increase of *G. glutinata*, with smaller amounts of *T. quinqueloba* in YD-2a indicate the development of a deep highly eutrophic mixed layer and a proliferation of fresh diatom prey. This heightened productivity is supported by benthic communities in MD99-2346, where the community changed to shallow infaunal species that specialised in the influx of fresh organic matter (Melki *et al.*, 2009). This elevated peak in *G. glutinata* was coincident with a *G. bulloides* minima, suggesting there was little wind-driven deep mixing at this time (Figure 7.3). There was little seasonal stratification, implied by the strong positive PC2 loadings (the strongest recorded in M40/4 82-2SL) (Figure 7.4; Figure 7.5). MD99-2346 showed a decrease in salinity values at this time, attributed to inflow of cold fresher NASW into the western Mediterranean (Cacho *et al.*, 2001; Melki *et al.*, 2009). This freshening and cooling of surface waters indicate a sustained period of deep mixing of the surface water, breakdown of the thermocline and an increase in the depth of the pycnocline (PC1). With the onset of global climatic amelioration during YD-2a, SSTs had begun to recover elsewhere in the western Mediterranean and there is evidence of heightened wind, deep mixing, precipitation and productivity at this time (Genty *et al.*, 2006; Combourieu Nebout *et al.*, 2009; Melki *et al.*, 2009; Fletcher *et al.*, 2010; Naughton *et al.*, 2016; Dubois-Dauphin *et al.*, 2017). However, as mentioned above M40/4 82-2SL did not record an early recovery in SST and wind strength was at a minimum. Therefore, it is proposed that surface waters remained cold and very productive throughout the year due to the increase in precipitation, inflow of NASW and increase discharge from the River Rhône.

Both *G. bulloides* and *T. quinqueloba* slowly replace *G. glutinata* in YD-2b (Figure 7.3). The faunal changeover occurs as winter SSTs warm slightly and pollen records in the northern Iberian Peninsula report a strengthened seasonal precipitation (Genty *et al.*,

2006; Combourieu Nebout *et al.*, 2009; Fletcher *et al.*, 2010; Naughton *et al.*, 2016). A coincident peak in sedimentation rates (Figure 7.2) and *T. quinqueloba* (the highest in the record) strongly suggest that this slight warming and increase in precipitation led to an increase in discharge from the Rhône, allowing the opportunistic *G. bulloides* and *T. quinqueloba* to thrive in the deep mixed layer. In addition, this increase in *T. quinqueloba* also correlates to coincident peaks observed in cores along the north-western margin of the Iberian Peninsula, which may also indicate the continued injection of cooler NASW deep into the western Mediterranean (Naughton *et al.*, 2016).

7.3.4 Early Holocene (11.55 to 7.5 kyr BP)

Although different stages, the palaeoenvironmental variations between the GL and NG stages were less extreme than those experienced between the Late Pleistocene chronozones, thus will be discussed together in the following section.

The early Holocene in northern mid latitudes is defined by a global warming of ~0.6°C between 11.5 and 9.5 kyr, followed by a stable warm period until ~5 kyr (Holocene Thermal Maximum) (Marcott *et al.*, 2013). This warming is interspersed with cold events triggered by variations in solar insolation, greenhouse gasses, solar activity minima and increasing volcanic aerosols (Mayewski *et al.*, 2004; Wanner *et al.*, 2015). For example, freshwater discharge events and sea-ice expansion led to a periodic decrease in the AMOC and has been attributed to the 8.2 kyr cold event (where air temperature in Greenland cooled by ~5°C), as well as smaller events such as the 11.4, 10.3 and 9.3 kyr events (Bond *et al.*, 1997; Wiersma and Renssen, 2006; Fleitmann *et al.*, 2008; Born and Levermann, 2010; Walker *et al.*, 2019a). The early Holocene amelioration in the western Mediterranean region is evident as warmer humid periods interspersed with cold arid events in both terrestrial and marine studies (Cacho *et al.*, 2001; Casford *et al.*, 2001; Frigola *et al.*, 2007; Dormoy *et al.*, 2009; Bout-Roumazeilles *et al.*, 2012; Ausin *et al.*, 2015b; Jalali *et al.*, 2016; Zielhofer *et al.*, 2017; Bazzicalupo *et al.*, 2018; Baldini *et al.*, 2019).

Rates of sea level change began to rapidly increase in the early Holocene, with global sea levels rising by ~50m by the early NG (Figure 7.2) (Stanford *et al.*, 2011a). Gulf of Lion sea levels rose from -43m at the base of the GL to approximately -30m at 10.6 kyr, then to -7.4 m by 7.5 kyr (Bassetti *et al.*, 2016; Vacchi *et al.*, 2016). Deposition of the Early Rhône Deltaic Complex continued for another ~1 kyr into the GL stage despite the increase in sea level rise, as the influx of meltwaters and sediment (from MWP-1B?)

was in phase with the rate of sea-level rise (Berné *et al.*, 2007). MWP-1B is a debated deglacial meltwater event that followed the YD cold period. Barbados corals record a total sea level rise of ~14m and date the MWP-1B event to between 11.45 and 11.1 kyr (Abdul *et al.*, 2016). However, many global sea level records do not register this meltwater pulse (Stanford *et al.*, 2011a; Lambeck *et al.*, 2014). It is believed that with summer insolation reaching its zenith during the early Holocene, MWP-1B was triggered by glacio-eustatic sea-level rise following the YD period (Stanford *et al.*, 2011a; Zecchin *et al.*, 2015; Abdul *et al.*, 2016; Tian *et al.*, 2020).

In the Gulf of Lion, the source of incoming sediments is attributed to meltwaters from Alpine glaciers and increased precipitation (Berné *et al.*, 2007). Models have suggested that there was a sustained release of cool Alpine fresh meltwaters between 11.5 and 9.5 kyr, which inhibited WMDW development and enabled the continued deposition of ORL-1 until ~9 kyr (Cacho *et al.*, 2002; Rogerson *et al.*, 2008; Ausin *et al.*, 2015b; Rohling *et al.*, 2015). Faunal and geochemical proxies from the Alboran Sea also suggest enhanced humidity and riverine input at this time (Martinez-Ruiz *et al.*, 2015; Bazzicalupo *et al.*, 2018). Speleothems from the northern Iberian Peninsula record wetter summers and drier winters (between 11 to 10.8 kyr), then becoming more arid in the summer and wetter in the winter by 8.9 kyr (Baldini *et al.*, 2019).

In M40/4 82-2SL, mean sediment rates for the GL and early NG stages were similar to those of the YD (Table 7.3). However, Figure 7.2 illustrates the variability of the sedimentation rates during these stages. The early-mid GL saw a slowing in sedimentation rates, correlating to a shallow marine transgressive sequence in the Gulf of Lion. This was followed by the period of maximum flooding of the continental shelf (between 8.5 and 7.5 kyr), which is seen as a rapid increase in sedimentation rates in M40/4 82-2SL (Bassetti *et al.*, 2016; Fanget *et al.*, 2016). As air temperatures and humidity increased during from ~10 kyr, vegetation cover increased, stabilising both the rates of terrestrial erosion and sediment load of the River Rhône (Kettner and Syvitski, 2009; Bassetti *et al.*, 2016). In the Gulf of Lion, sediment deposition slowed during the early NG, as it coincided with the peak of the transgressive sequence and subsequent sediment starvation (Fanget *et al.*, 2016). This can been seen in the sharp fall in sedimentation rates at ~8 kyr in M40/4 82-2SL (Figure 7.2). As rates of sea level rise and river discharge began to decline, followed by the slow decline in SST (from ~8.8 kyr in M40/4 82-2SL, see Figure 7.2; Figure 7.6), there was an increase in the density of surface waters, summer stratification and reestablishment of winter deep-water

ventilation from ~9 kyr (Rogerson *et al.*, 2008; Kettner and Syvitski, 2009; Ausin *et al.*, 2015a; Bassetti *et al.*, 2016).

7.3.4.1   Sea Surface Temperatures

The predicted annual SST in M40/4 82-2SL during the Early Holocene increased to 15.2°C. However, this value is cooler than expected, i.e. SSTs were ~1.8°C cooler than modern SSTs (Table 7.9), as it is strongly influenced by the strong cyclical pattern between 11.5 and 10 kyr, where SSTs ranged from ~10.6 to 15.8°C. This early GL signal differs from many SST estimates in the Gulf of Lion and the western Mediterranean. Most record a relatively steady rise in SST following the YD termination (with a small dip correlated to the 11.4 kyr event) and stabilising ~11 kyr (e.g. spring SST were ~16°C in MD99-2346) (Kallel *et al.*, 1997b; Cacho *et al.*, 2001; Sbaffi *et al.*, 2004; Frigola *et al.*, 2007; Jimenez-Espejo *et al.*, 2007; Rogerson *et al.*, 2008; Melki *et al.*, 2009; Bazzicalupo *et al.*, 2018; Català *et al.*, 2019). Only a limited number of cores in the Alboran Sea display slower rates of SST increase, with similar patterns of SST variability and seasonality during the early Holocene (Pérez-Folgado *et al.*, 2003; Rodrigo-Gámiz *et al.*, 2014a; Ausin *et al.*, 2015b).

There was a significant reduction in seasonality during the cold periods of these cycles, as summer SSTs experienced greater degree of cooling compared to winter SSTs (Figure 7.6). Around this period, seasonal precipitation patterns changed wetter summers/drier winters, with a strong influence of precipitation systems originating from the North Atlantic (Jalali *et al.*, 2017; Baldini *et al.*, 2019). Records from benthic foraminifera record a decrease in surface water salinity in the Gulf of Lion, which support salinity modelling that suggests that the decrease in WMDW formation during this period was triggered by sustained periods (~2kyr) of Alpine meltwater outflow from the River Rhône (Melki *et al.*, 2009; Rohling *et al.*, 2015; Jalali *et al.*, 2017). As this period coincides with peak summer / minimum winter insolation values, melting of Alpine glaciers would have been greater summer months, leading to an influx of colder meltwaters waters and enhanced summer cooling in the Gulf of Lion. Therefore, the combination of meltwater pulses and enhanced precipitation increased the seasonal outflow of the Rhône, creating this cyclical signal, with cooler summer SSTs.

To clarify if this early GL signal was truly cyclical, a spectral analysis was completed and three cycles of 385, 140 and 81 years were identified (>90% confidence level) (Figure 7.9). It is possible that some of these cycles may be linked to changes in solar

activity, e.g. the 81 year cycle may equate to the Gleissberg–Yoshimura cycle (50-100 years) (Soon *et al.*, 2014). Variations in solar cycles are thought to impact modern atmospheric circulation and pressure gradients in the North Atlantic, which in turn would influence cyclogenesis and precipitation rates in the north-west Mediterranean region (Matthes *et al.*, 2021). During the Holocene, short-term solar variability superimposed on longer-term insolation changes are believed to be a primary driving force of Holocene rapid climate change events (Mayewski *et al.*, 2004). Across the Mediterranean Region, a number of marine and terrestrial studies have identified potential solar cycles in both foraminifera and geochemical proxies during the Holocene (Heymann *et al.*, 2013; Rodrigo-Gámiz *et al.*, 2014b; Le Houedec *et al.*, 2020). For example, early Holocene centennial-scale solar minima were correlated with cold periods in the North Atlantic, which led to winter rain minima in lake sediments in the Middle Atlas Mountains to the south, and an increased precipitation further north towards the north-west Mediterranean (Zielhofer *et al.*, 2019).
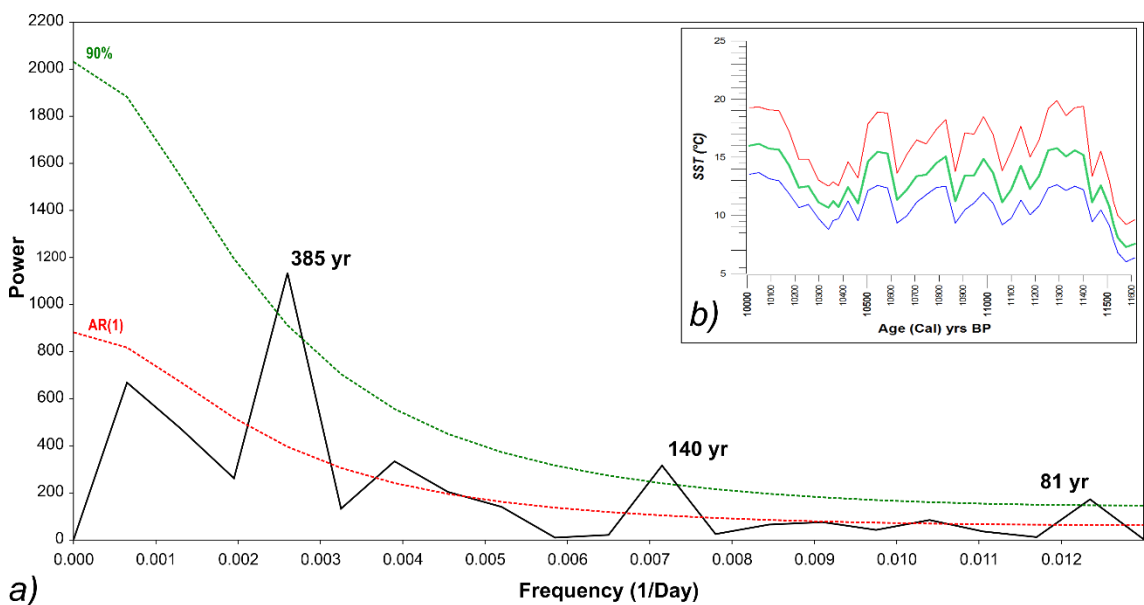
Figure 7.9: a) Bias-corrected spectral analysis (REDFIT) in the Early Holocene (11.6 to 10 kyr). The dashed green line indicates the 90% confidence level. The dotted red line indicates the theoretical first-order autoregressive (AR1) process that explains the "red-noise" signature (Schulz and Mudelsee, 2002). b) Mean annual (green), winter (blue) and summer (red) SSTs for the same period.

The 11.4 kyr cold period only registers as a minor dip in SST, followed by a significant recovery in SST (Figure 7.6). However, the most sustained cold period at the time centres around 10.3 kyr, when annual SSTs fell to <11°C (Figure 7.6). Although not classified as a major cold snap globally, it has been recorded as a cold, dry period in the Greenland $\delta^{18}O$ isotope records, as an IRD event in the North Atlantic (i.e. North Atlantic Cold Event 7) and also in other proxies across global sites (dates ranging from

10.5 to 10 kyr) (Bond *et al.*, 1997; Mayewski *et al.*, 2004; Wang *et al.*, 2013; Zielhofer *et al.*, 2017). This period marks the final minor mountain glacier re-advance in the Alps (~10.5 kyr), and inhibition of WMDW correlated to the onset of monsoonal flooding associated with Sapropel 1 deposition in the eastern basin (Ivy-Ochs, 2015; Rohling *et al.*, 2015).

During the mid to late GL, SSTs increased, then stabilised between 10 and 8 kyr (mean annual SST ~16.6°C) (Figure 7.6). Seasonal variation was significant, reflecting the difference in summer and winter insolation at this time (Figure 7.6; Table 7.8). Decreases in SSTs can be seen around 9.3 and the 8.2 kyr, though the minor SST decrease ~9.3 kyr is within the variability seen at the time and may not be a true signal of the North Atlantic cold event. The expression of 8.2 kyr cold event is more substantial, with a decrease of ~3°C in SST and reduced seasonality, again reflecting greater degree of cooling of summer SSTs. Following the cold 8.2 kyr event, there was a swift recovery in SST. Predicted annual SSTs for the early NG stage were 15.76°C, only ~1.1°C cooler than modern SSTs (Table 7.8, Table 7.9). However, this was the beginning of a sequence of slow SST decline towards 7.5 kyr (Figure 7.6). Although many western Mediterranean marine proxy studies record this cooling from ~8 to 7 kyr (Cacho *et al.*, 2001; Jalali *et al.*, 2016; Jalali *et al.*, 2017), a similar cooling trend (towards ~4.2 kyr) was observed some studies in the Alboran sea (Marchal *et al.*, 2002; Ausin *et al.*, 2015b; Català *et al.*, 2019). This cooling was attributed a decrease in the inflow of warmer subtropical waters, as the North Atlantic subtropical gyre moved northward towards higher latitudes in the Mid Holocene and a strengthening of Westerly winters into the region (Català *et al.*, 2019).

7.3.4.2 *Planktonic foraminiferal assemblage and palaeoenvironmental reconstruction*

The transition from the YD to early GL was not immediate for most species. It was not until after the 11.4 kyr cold event that we see a decrease in shallow eutrophic species and an increase in warm oligotrophic species and deep grazers. Although annual SSTs were still ~1.75°C cooler than modern SSTs, they were warm enough for allow for this more diverse assemblage (Table 7.8; Table 7.9). The establishment of this more modern seasonal assemblage reflect significant changes to the hydrological structure that were occurring in the Gulf of Lion.

The early GL was characterised by a variable, cyclical abundance in *G. inflata* and *G.*

ruber white and minor *G. truncatulinoides* sinistral, suggesting periods with warm, seasonally stratified summer/autumn waters, followed by a cooler deep mixed layer during mesotrophic winter/spring periods (more moderate E-Index and peaks in PC2 and PC3, as well as the S-Index). In addition, *G. ruber* white was accompanied by *G. rubescens*, the first of the SPRUDTS species to inhabit the early GL period (Figure 7.3). *G. rubescens* is a rare, small species, inhabiting surface to sub-surface temperate to tropical oligotrophic waters (Table 3.5) (Bé, 1977; Bé and Hutson, 1977; Hilbrecht, 1996; Conan and Brummer, 2000; Schiebel and Hemleben, 2017).

Although *T. quinqueloba* had decreased in abundance since the YD, it displays an inverse pattern of peaks to *G. inflata*/*G. ruber* white. At the same time, *G. bulloides* had increased in abundance. The combination of these opportunistic species, along with eutrophic benthic foraminifera species that flourish with pulsed flux of organic matter, both agrees with the suggestion of increased discharge of nutrient rich fresh waters from the Rhône at this time (Melki *et al.*, 2009). Also, the peaks in PC3 and the DM-Index in the early GL (up to ~10.9 kyr) suggest there may be an increase in winter wind strength at this time, which was also seen in elemental ratio proxies in the Alboran Sea (Martinez-Ruiz *et al.*, 2015). At the same time, sea levels were rapidly increasing (MWP-1B?), surface water salinity and density were decreasing and the pycnocline was deepening (Berné *et al.*, 2007; Melki *et al.*, 2009; Rohling *et al.*, 2015; Jalali *et al.*, 2017). This is reflected by the generally lower percentages of *N. incompta* (and PC1). These cyclical faunal patterns match those of the predicted SSTs (Figure 7.6). Therefore, as global temperatures began to recover in the early GL period (up to ~10.3 kyr), the Gulf of Lion also experienced an increase in SSTs, with seasonally stratified/deeply mixed eutrophic waters and strengthening of winter winds. However, periodic pulses of enhanced riverine discharge and meltwater pulses cooled summer surface waters, and injected nutrient rich waters, which supported an opportunistic eutrophic assemblage.

In comparison to the Late Pleistocene chronozones, the diversity of the GL eutrophic assemblage increased, with varying amounts of *G. bulloides*, *G. inflata*, *N. incompta*, *G. glutinata*, *T. quinqueloba*, *G. scitula* and both *G. truncatulinoides* dextral and sinistral (Figure 7.3; Table 7.4). However, one of the most striking faunal signals in the entire core was the rapid and sustained collapse of *N. incompta* (<5%) between 10.6 and 9.5 kyr. This reduction is seen elsewhere in the Gulf of Lion and the western Mediterranean, though not as pronounced or for as long (Pérez-Folgado *et al.*, 2003;

Sprovieri *et al.*, 2003; Sbaffi *et al.*, 2004; Di Donato *et al.*, 2009; Melki *et al.*, 2009; Morabito *et al.*, 2014). This period was coincident with the increase in shallower *G. glutinata* and deep grazers *G. truncatulinoides* sinistral, *G. inflata*, *T. quinqueloba* and *G. scitula*. It also coincided with the cessation of MWP-1B, but the region was still experiencing the continuing effects of the rapid rates of sea level increase (Figure 7.2) (Stanford *et al.*, 2011a). Clearly, waters remained productive and food was available, but the structure of the winter water column no longer favoured *N. incompta* (strongly positive PC1). Instead deep grazers accounted for ~40% of the eutrophic assemblage, as the winter/spring bloom period experienced deep vertical mixing and the nutricline and pycnocline deepened in response to the freshened surface waters.

In addition to the collapse of *N. incompta*, there was a substantial peak in *G. glutinata* (>45%) and reduction of both *G. ruber* white and the SPRUDTS group correlating to the 10.3 kyr cold event (Figure 7.3; Figure 7.6). *G. bulloides*, *T. quinqueloba* and *G. inflata* all decreased at this time. Therefore, this cold period was not accompanied by heightened winds or deep mixing. *G. truncatulinoides* sinistral and *G. scitula* were still present, though in low abundances. There was no evidence of this peak in *G. glutinata* in MD99-2346, where abundances steadily decreased towards the end of the GL stage (Melki *et al.*, 2009). However, elevated rates or minor peaks of *G. glutinata* can been seen in cores from western, central and the eastern Mediterranean in the early Holocene (Sbaffi *et al.*, 2001; Sprovieri *et al.*, 2003; Favaretto *et al.*, 2008; Geraga *et al.*, 2010; Morabito *et al.*, 2014). This sustained peak in the shallower dwelling *G. glutinata*, positive PC2, along with minor abundances in deeper dwelling species in M40/4 82-2SL suggest a deep thermocline and that winter deep mixing was firmly established, allowing *G. glutinata* to dominate the cold shallow productive waters at the expense of opportunistic *G. bulloides* and *T. quinqueloba*, with *G. truncatulinoides* and *G. scitula* seasonally inhabiting deeper waters.

There is a similar turnover of warmer oligotrophic species, indicating a change to the structure of warmer summer/autumn waters, Following the decline of *G. rubescens* and a brief fall in *G. ruber* white during the 10.3 kyr cold event, *O. universa* reappeared in the mid GL, followed by *G. siphonifera* (~10 kyr) (Figure 7.3). Both are deeper dwelling species, governed by warmer SST and more mixed, productive waters (de Vargas *et al.*, 2002; Darling and Wade, 2008; Rigual-Hernández *et al.*, 2012; Rebotim *et al.*, 2017; Schiebel and Hemleben, 2017). In addition, the *G. ruber* plexus in the modern Mediterranean includes the high productivity *G. elongatus* (Types IIa1 and

IIa2) (Darling and Wade, 2008; Aurahs *et al.*, 2009; Aurahs *et al.*, 2011; André *et al.*, 2014). Therefore, the similar occurrences of both *O. universa* and *G. siphonifera*, along with *G. ruber* white morphospecies in the mid GL indicate that late spring to early autumn waters were more productive, where *G. ruber* white inhabited shallower waters (~60m) and *G. siphonifera* and *O. universa* in deeper waters (~80m). At the same time, seasonal stratification and SST seasonality were both increasing, which is evident from the negative PC2 and elevated *G. inflata*. Interestingly, the E-Index is decreasing at this point (Figure 7.7). However, this index utilises the traditional interpretation of these spinose species to indicate warm oligotrophic water. It does not consider the full range of their ecological tolerances; therefore, it may lose some of the nuance that the presence of these species may imply, especially in productive areas such as the Gulf of Lion.

The initial peak during the recovery of *N. incompta* (~9.5 kyr) correlated to the disappearance of both *G. truncatulinoides* sinistral and *G. scitula*, which was also recorded in the Tyrrhenian Sea (Di Donato *et al.*, 2009). It can be assumed that deep mixing of the water column weakened and there was a reestablishment of a shallower pycnocline (PC1). This initial peak was brief and following the 9.3 kyr cold event, *N. incompta* briefly declined again, to the advantage of *T. quinqueloba*, *G. inflata* and *G. glutinata*, again pointing to deep winter mixing and deepening of the pycnocline. From ~9 kyr *N. incompta* made its final recovery and dominated the remainder of the late GL assemblage (PC1), while the populations of both *G. bulloides* and *G. inflata* declined and *G. glutinata* was reduced to a more modern Mediterranean Sea abundance (<5%) (Figure 7.3) (Thunell, 1978). This recovery of *N. incompta* occurred close to the termination of deposition of ORL1 ~9 kyr in the western basin when WMDW formation resumed, sea level rise slowed, sedimentation rates peaked in the Gulf of Lion, SSTs began to cool and precipitation decreased (Jalut *et al.*, 1997; Jalut *et al.*, 2000; Rogerson *et al.*, 2008; Bassetti *et al.*, 2016). In general, productivity in the western basin decreased from this period, but it is clear that the Gulf of Lion remained productive for the remainder of this mid-Holocene period (Fink *et al.*, 2013; Fink *et al.*, 2015).

In the warm water assemblage, there was a peak in *G. ruber* white (>20%) following the 9.3 kyr event, then it slowly declined along with decreasing SSTs towards the GL termination at 8.2 kyr. At the same time, SPRUDTS species formed 6.25% of the assemblage. *O. universa* and *G. siphonifera* were still present along with *B. digitata*, another more productive warm water species (Figure 7.3) (Schiebel and Hemleben,

2017). The tropical, oligotrophic *G. ruber* pink increased slightly, and for the remainder of the late GL stage, there were modest rates of this genotype when summer SST were consistently >19°C (Figure 7.3). Therefore, this more complex summer assemblage in the late GL suggests that while there were periods of higher productivity in the early and/or late summer/early autumn, there were seasonally stronger oligotrophic conditions during the height of the summer (E-Index) (Figure 7.7).

The 8.2 kyr cold event, which marks the transition from GL to NG has little impact on the assemblage, except for a peak in *T. quinqueloba* and decrease in SPRUDTS species. The early NG marks the establishment of the more modern Gulf of Lion assemblage, dominated by *N. incompta*, *G. bulloides*, *G. inflata*, which formed >80% of the NG assemblage (Table 7.4) (Broggy, 2011). *G. ruber* pink almost disappeared, while *G. ruber* white and SPRUDTS species account for 6% and 4.3% of the population, respectively. Similarly, the benthic assemblage became more representative of modern conditions (Melki *et al.*, 2009). This suggests a more modern hydrographic structure was established during the NG stage, i.e. a seasonally well-developed DCM (PC1) and oligotrophic conditions in the summer to late summer months (PC2), with decreasing periods of heightened productivity in surface/subsurface waters in the early summer and early autumn broadly. Winter conditions were comparable, with high productivity, wind-driven winter deep mixing events (PC3) associated with WMDW formation.

7.4   Conclusion

Core M40/4 82-2SL has provided a high-resolution and sub-centennial record of the Gulf of Lion between 15.48 to 7.4 kyr. The climate and hydrographical changes experienced during each chronozone are clearly identifiable, and the detailed nature of the record illustrates the complexity of these extreme periods. Indeed, this marine core has recorded climate trends and patterns for certain periods that are usually only evident in terrestrial proxies (e.g. Chauvet speleothem in southern France). In-depth analysis of this planktonic foraminifera data, has made it possible to resolve some of the complex regional and global mechanisms and interactions that governed the deglacial Gulf of Lion region (see Table 7.10 below).

Clearly, the Gulf of Lion is an inherently complex region. During the Late Pleistocene into early Holocene, the region was under the influence of localised discharge from the River Rhône, Alpine meltwater pulses, localised winds and winter cyclogenesis. There is also evidence of strong teleconnections with North Atlantic oceanic and atmospheric

circulation patterns and low pressure systems, which impacted surface temperatures and salinity, and further intensified wind strength, precipitation and winter cyclogenesis. For example, the late HS1 and YD in the Gulf of Lion were both extremely cold periods, much colder than elsewhere in the western Mediterranean basin, and temperatures during the YD comparable with the LGM. The southerly position of polar front was a controlling factor for both periods, where cold pulses of polar and subpolar NASWs cooled SSTs, and winds were strengthened, especially during the late HS1. However, the variability of the position of the oceanic polar front during the YD meant that the region was under greater influence of storm and precipitation events incoming from the North Atlantic or locally occurring cyclogenesis.

The early Bølling SST signal bears striking resemblance to $\delta^{18}O$ signal of Greenland ice cores, reflecting the strong teleconnection with North Atlantic, where the rise in CO_2 and air temperatures in early Bølling equated to the sharp increase in SSTs in the Gulf of Lion. It also points to the resumption of North Atlantic deep water circulation and the inflow of warmer waters from the North Atlantic Subtropical Gyre. However, during the later Bølling to Allerød period, there is increasing evidence of freshwater and Alpine and MWP-1A meltwaters that cooled and freshened surface waters. Periodic increases in river discharge and meltwater pulses were also key drivers for the early Holocene, where SSTs display a strong cyclicity, which were cooler than expected when compared to other areas in the western basin. This evidence strongly supports the existence of meltwater pulses in the early Holocene that were needed for continued deposition of ORL1. As these meltwater pulses diminished, SSTs began to recover by the mid GL. However, the late GL saw an earlier cooling trend in comparison to other areas in the Mediterranean (from ~9 kyr) as WMDW formation resumed and this cooling continued until the early NG. In addition, rapid cooling events such as the OD, 10.3 and 8.2 kyr are also evident in the record, linked to brief increase in cold winds and freshwater events in the region.

Interpretation of the planktonic foraminifera assemblage has allowed for detailed reconstruction of the palaeoecology and hydrology during these events. It is clear that the fauna responded to the changes in SSTs. For example, in response to the warmer SSTs and increase in seasonality during the early Bølling, the assemblage rapidly reorganised to become seasonally variable, with a peak in *G. ruber* white during warmer more oligotrophic summer/autumn season, and deeper dwelling *G. inflata* and *G. scitula* peaking during the more eutrophic, deeply mixed winter/spring surface waters.

However, although SSTs broadly governed the assemblage, they do not explain the more detailed variability within the record. The assemblage is strongly eutrophic through the majority of the chronozones, which is similar to modern conditions. However, the structure of the assemblage signpost variabilities in trophic and hydrological conditions during these events. For example, it is interesting to compare the cooler water eutrophic assemblages of the late HS1 and the YD. Both have cool waters and low seasonality, however the variations in the associated assemblages clearly indicate differences in surface water conditions. The dominance of *G. bulloides*, along with *T. quinqueloba* and *N. incompta* imply strong wind-driven deep mixing during HS1, whereas distinctions in the abundances in *N. incompta*, *G. glutinata*, *G. bulloides* and *T. quinqueloba* enable the subdivision of the YD, mapping changes in the depth of the pycnocline in response to weaken wind strength, inflow of cold NASWs, and the increasing precipitation influence during the late YD. This is also evident in the early Holocene, as the cyclicity in SSTs is clearly as a response to the variability of *G. inflata* and *G. ruber* white alternating with *T. quinqueloba* and *G. bulloides*. The disappearance of *N. incompta* is one of the most striking faunal responses during the early to mid Holocene. Although surface waters were strongly eutrophic, the pycnocline deepened due to rapidly increasing sea levels and freshwater discharge, allowing deeper dwelling eutrophic species to flourish.

Chronozone		Planktonic Foraminifera Assemblage		Mean SSTs (Seasonality) (°C)	Palaeoenvironmental interpretation		Mechanisms
		Warmer	Cooler		Summer/Autumn	Winter/Spring	
Early NG		*G. ruber* white SPRUDTS	*N. incompta* *G. bulloides* *G. inflata*	15.76 (7.18)	Warm, with continued cooling trend; Strong seasonality; Stratified and oligotrophic in high summer months; Higher productivity in early/late summer	Eutrophic; Deep mixing; Increased productivity; Establishment of modern fauna	Cold winter winds and cyclogenesis
GL	Late GL	*G. ruber* white SPRUDTS	*G. bulloides* *N. incompta* *G. inflata* *G. glutinata* *T. quinqueloba*	15.06 (6.53)	Warm, but beginning to cool; Stratified and oligotrophic in high summer months; Higher productivity in early/late summer	Shallow pycnocline; Eutrophic, Seasonal deep mixing; Increased productivity	Resumption of WMDW formation; Cold winter winds and cyclogenesis
	Early-Mid GL				Warm; Stratified and oligotrophic in high summer months; Higher productivity in early/late summer	Deep thermocline and pycnocline; Deep mixing; Increased productivity	Rapid sea level rise; discharge from River Rhône
					Warming, interspersed with periodic cooling		Increase in precipitation; periodic meltwater pulses and discharge from River Rhône
					Increased seasonality; Stratified and oligotrophic; Periods increased summer cooling	Deep thermocline and pycnocline; Deep mixing; Increased productivity	
YD	YD-2b	*N. incompta* *G. glutinata* *G. bulloides* *T. quinqueloba*		8.30 (3.49)	Cold, though winter SSTs not as low; Productive; Deeping of mixed layer		Increase in seasonal precipitation, inflow of cold NASW and river discharge; Variable winds
	YD-2a				Cold; Weak winds; Increase in shallow water productivity; Deepening of mixed layer		Weaker winds; Inflow of cold NASW
	YD-1				Gradual cooling;		Variable position of oceanic

Chronozone		Planktonic Foraminifera Assemblage		Mean SSTs (Seasonality) (°C)	Palaeoenvironmental interpretation		Mechanisms
		Warmer	Cooler		Summer/Autumn	Winter/Spring	
					Low seasonality; Productive		Polar Front, periodic inflow of cold NASW; Variable winds
BA	Allerød	*G. ruber* white	*G. bulloides* *N. incompta* *G. inflata*	15.19 (6.44)	Warm with stepwise cooling; Stratified	Productive; Increasing deep mixing	Increase in sea level, Alpine meltwaters and River Rhône discharge
	OD				Cooler; Stratified	Cool and unstable waters	Strong winds incoming from the North Atlantic
	Mid-Late Bølling				Still warm, but cooling; Stratified and oligotrophic in high summer months; higher productivity in early/late summer	Cooler eutrophic waters; Shallowing of pycnocline	Inflow of warm NASW; Increased in Alpine meltwaters and MWP-1A, discharge from River Rhône
	Early Bølling				Rapid warming; Warm stratified, oligotrophic waters; Increased seasonality	Stable eutrophic waters; Deep pycnocline; No deep mixing	Weak winds; Inflow of warm NASW; Atmospheric warming due to rapid increase in CO_2
Late HS1		*G. bulloides* *N. incompta* *T. quinqueloba* *G. glutinata* *G. scitula*		10.18 (3.83)	Highly productive; Low SST and seasonality; Intense deep surface water mixing and WMDW formation		Inflow of cold NASW due to southerly position of ocean polar front; Strong North Atlantic winds

Table 7.10: Dominant planktonic foraminifera species, palaeoenvironmental interpretation and proposed mechanisms of climate change during the main Late Pleistocene chronozones and early Holocene stages in the Gulf of Lion. Heinrich Stadial 1 (HS1); Bølling-Allerød (BA); Younger Dryas (YD); Greenlandian (GL); Northgrippian (NG). SPRUDTS group = G. siphonifera, G. rubescens, O. universa and B. digitata.

Chapter 8.

8 Conclusion

Following the Last Glacial Maximum (LGM), the deglacial was a period of extreme climatic and environmental change in the northern hemisphere. Evidence of these changes have been recorded in the North Atlantic marine sediments, Greenland ice cores and terrestrial proxies across the northern hemisphere. They have also been observed in studies across the Mediterranean Sea. However, given the transitional nature of the Mediterranean region, these signals are spatially disparate and inherently complex. Sea surface temperatures (SSTs) for the LGM in the Mediterranean Sea were reconstructed using the Artificial Neural Networks (ANN) transfer function, but there were no equivalent regional SST reconstructions for the deglacial Heinrich Stadial 1 (HS1), the Bølling/Allerød (BA) and Younger Dryas (YD) chronozones.

Therefore, the first of the aims for this study was to reconstruct the basin-wide palaeoecology and palaeoclimate of the Mediterranean Sea during HS1, the BA and YD. In order to achieve this, a comprehensive database of planktonic foraminifera counts was compiled from 67 cores that were widely distributed across the Mediterranean Sea. A number of research questions were addressed using this dataset. How did the Mediterranean Sea respond to rapid change during HS1, the BA and YD and to what extent did these changes impact the hydrology and distribution of planktonic foraminifera. Annual, summer and winter SSTs were reconstructed using ANN, and the distribution of these SSTs and key planktonic foraminifera morphospecies were mapped and analysed for each chronozone. Eutrophic and stratification indices, calculated from the planktonic foraminifera assemblage were also mapped, which is a novel application of these palaeoenvironmental indices.

The impact of these three extreme periods is certainly evident across the Mediterranean Sea. Mean annual SSTs for the HS1 were 13.57°C, 15.03°C during the BA and 14.16°C in the YD. Both the HS1 and YD were cooler than the LGM. Although warmer, the BA was still ~3.5°C cooler than modern conditions. However, all chronozones display unique distribution patterns of SST, faunal and hydrological variability. The western basin, along with the Adriatic and Aegean Seas were generally cooler, especially during HS1 and the YD and had strongly eutrophic assemblages. SSTs in the southern eastern basin was less impacted by the deglacial cold periods. The basin was certainly more

eutrophic and less stratified in comparison to modern-day ultra-oligotrophic conditions, though as surface waters warmed during the BA and YD, they became increasingly oligotrophic. This enabled the warm water spinose assemblage to diversify and expand their ranges into the western basin.

The impact of a number of drivers can be identified for these events. The strong year-round cooling of the western basin during HS1 reflects the stable southerly position of the oceanic polar front. This enabled cold North Atlantic Surface Waters (NASW) to penetrate the western basin, which is reflected by the distribution of Neogloboquadrina species that extended from the Strait of Gibraltar into the western basin. During the BA and YD, changing pressure systems over the Fennoscandian ice sheet and associated variability in North Atlantic atmospheric circulation would have impacted wind strength and precipitation rates in the Mediterranean region. These variations can be seen in the cooler SSTs in the western basin and along northern margins, as well as changes to the productivity and deep mixing of surface waters. At the same time, the northward migration of the Intertropical Convergence Zone and increasing summer insolation led to warmer SSTs and enhanced seasonality in the eastern Mediterranean. Increases in freshwater discharge, meltwater events and rising sea levels in the Gulf of Lion, Adriatic and Aegean Seas were also identified by cooler SSTs and the increase in *G. bulloides*, *T. quinqueloba* and Neogloboquadrina species.

These SST and palaeoenvironmental reconstructions present a broad, basin-wide summary of conditions during the HS1, BA and YD that was previously unavailable for the Mediterranean Sea. Although signals for each chronozone are generalised, they provide evidence of the main factors that governed each extreme period. They also clearly display the spatial variability of these signals across the Mediterranean Sea. Finally, they demonstrate the sensitivity of the Mediterranean Sea to rapid climate change.

The second aim of this thesis was to test how the north-west Mediterranean Sea responded to extreme changes during the deglacial period. In the modern-day, this region is under the influence of North Atlantic depressions and winter cyclogenesis, and surface water productivity is strongly correlated with seasonal discharge of nutrient rich waters from the River Rhône. Therefore, the associated high sedimentation rates and sensitivity of the region to climate change makes it an ideal location to examine the impact of extreme events. However, micropalaeontological studies based in this region

are somewhat limited.

M40/4 82-2SL was a known high resolution sediment core collected from the Gulf of Lion and was selected to address the objective of reconstructing the north-western Mediterranean Sea during the deglacial period. The sections of M40/4 82-2SL utilised for this study spanned the late HS1 to the mid Holocene (~15.5 to 7.4 kyr). SSTs were predicted using ANN, and a combination of the faunal abundance, multivariate statistics (PCA) and palaeoenvironmental proxies were utilised to reconstruct the palaeoenvironment. As the core was located within the Rhône Delta Plume, sedimentation rates throughout this period were generally high, thus the foraminiferal record proved to be an excellent archive of the global and regional factors that influenced the Gulf of Lion.

The BA, YD and early to mid Holocene variability and complexity are distinctly recorded, though only the end stage of HS1 was captured in the core. There is close correlation of annual SSTs with Greenland $\delta^{18}O$ ice core records, especially during the BA. Cooling during the late HS1 and especially during the YD was more extreme than the LGM. SSTs during the BA were almost comparable to modern SSTs in the Gulf of Lion. However, the SST record was highly variable in the early Holocene due to periods of enhanced Rhône discharge and periodic meltwater events, which provides strong support for an Alpine meltwater contribution to the continued ORL1 deposition during the early Holocene.

The assemblage throughout was strongly eutrophic. *N. incompta*, *G. bulloides*, *G. inflata* and *T. quinqueloba* were the dominant species, with only more limited periodic peaks of *G. ruber* white in the warmer BA and Holocene. In detail, variations in the planktonic foraminifera community structure allowed for a detailed reconstruction of the changes to the productivity and hydrological structure of surfaces waters. For example, the dominance of *G. bulloides* in the late HS1 points to extreme wind-driven deep mixing. This contrasts the rapid reorganisation and diversification of the assemblage in the early Bølling as atmospheric temperatures rose. As SSTs rapidly increased, there was a change to a more seasonal assemblage, with warm stratified oligotrophic summer waters, followed by cooler mesotrophic winter-spring surface waters with a stable deep mixed layer. The inflow of nutrient-rich fresher waters during the early Holocene led to a deepening of the pycnocline. This triggered a ~1000-year period where *N. incompta* was near absent and was replaced by a diverse deeper-

dwelling eutrophic assemblage.

M40/4 82-2SL undoubtedly demonstrates the effects of variable discharge from the River Rhône, meltwater pulses and rising sea levels during the transition from the Late Pleistocene to early Holocene. It also records the impact of North Atlantic atmospheric circulation, precipitation and wind strength on SSTs, trophic conditions and the hydrological structure of the Gulf of Lion. In turn, the resulting conditions shaped the diversity and abundance of the planktonic foraminifera assemblage. Given the detail of the M40/4 82-2SL record, it is a welcome addition to the limited collection of palaeoenvironmental reconstructions for the north-west Mediterranean Sea.

8.1 Limitations and future work

The use of published datasets for wide ranging palaeoenvironmental studies comes with a number of considerations that have to be acknowledged and addressed when possible. These issues include variations in identification, classification and generalisation of morphospecies between researchers. This is becoming increasingly pertinent, in light of the emerging complexity of genotypes that may have different ecological niches. Invariably, this means that much of the nuance of the ecological and hydrological factors that govern the distribution of these species may be lost. However, the addition of greater numbers of core data points help identify and minimise any errant signals in the datasets. Also, the distribution of morphospecies were not regarded in isolation, they were analysed in relation to other species, palaeoenvironmental proxies and SSTs. In addition, issues around core chronology, poor reporting of control points and variable age model quality can decrease the confidence of observed results. In this study, this issue was addressed by the recalibration of all ^{14}C AMS radiocarbon ages, generating new age models where possible, and assigning an age quality level to all datasets. For future publications, I plan to recalibrate all ^{14}C radiocarbon dates, in light of the newly published Marine20 marine radiocarbon age calibration curve and updated ΔR values (Reimer and McCormac, 2002; Heaton *et al.*, 2020; Reimer *et al.*, 2020) and regenerate the age model for any cores that have four or more age control points, using the more rigorous BACON Bayesian age-depth model approach (Blaauw and Christen, 2011).

As SSTs and productivity in the Gulf of Lion were so strongly influenced by meltwater events and enhanced outflow from the River Rhône, it is my intention to obtain stable isotope measurements (i.e. δ^{18}O and δ^{13}C) for specific sections of M40/4 82-2SL (e.g.

the early Holocene). This analysis will provide independent proxies for the SST reconstructions and productivity signals indicated by the planktonic foraminifera assemblage in M40/4 82-2SL. This will support further investigation of these freshwater discharge signals, which is of interest to researchers in the western Mediterranean Sea, especially in relation to the deposition of ORL1 and associated changes in the deep ventilation in the Gulf of Lion.

The final extreme event of the deglacial in the Mediterranean Sea is related to the deposition of Sapropel 1 (S1) (~6-10 kyr BP) in the eastern basin. S1 is correlated with anoxic conditions that are associated with the monsoon maximum and sea level rise (Rossignol-Strick, 1985; Rohling *et al.*, 2015; Grant *et al.*, 2016). This event has been extensively researched across the eastern basin and in the limited footprint in the Tyrrhenian Sea (Rohling *et al.*, 2015). However, this event has never been investigated on a basin-wide scale, therefore there is limited information regarding its effects on SSTs, intermediate and deep water ventilation in the western basin and planktonic foraminifera communities across both basins. Also, how did S1 compare to periods of ORL1 deposition in the western basin during the BA and YD datasets (Rogerson *et al.*, 2008; Rohling *et al.*, 2015; Pérez-Asensio *et al.*, 2020)? Therefore, it is proposed that a similar basin-wide planktonic foraminifera dataset for S1 be compiled, in order to reconstruct the impact of S1 on SSTs and planktonic foraminifera across the Mediterranean Sea.

References

Abdul, N.A., Mortlock, R.A., Wright, J.D. and Fairbanks, R.G. (2016) 'Younger Dryas sea level and meltwater pulse 1B recorded in Barbados reef crest coral *Acropora palmata*', *Paleoceanography*, 31(2), 330-344, available: http://dx.doi.org/10.1002/2015pa002847.

Aksu, A.E., Yaşar, D. and Mudie, P.J. (1995a) 'Paleoclimatic and paleoceanographic conditions leading to development of sapropel layer S1 in the Aegean Sea', *Palaeogeography, Palaeoclimatology, Palaeoecology*, 116(1), 71-101, available: http://dx.doi.org/10.1016/0031-0182(94)00092-M.

Aksu, A.E., Yaşar, D., Mudie, P.J. and Gillespie, H. (1995b) 'Late glacial-Holocene paleoclimatic and paleoceanographic evolution of the Aegean Sea: micropaleontological and stable isotopic evidence', *Marine Micropaleontology*, 25(1), 1-28, available: http://dx.doi.org/10.1016/0377-8398(94)00026-J.

Al-Sabouni, N., Fenton, I.S., Telford, R.J. and Kučera, M. (2018) 'Reproducibility of species recognition in modern planktonic foraminifera and its implications for analyses of community structure', *Journal of Micropalaeontology*, 37(2), 519-534, available: http://dx.doi.org/10.5194/jm-37-519-2018.

Al-Sabouni, N., Kucera, M. and Schmidt, D.N. (2007) 'Vertical niche separation control of diversity and size disparity in planktonic foraminifera', *Marine Micropaleontology*, 63(1-2), 75-90, available: http://dx.doi.org/10.1016/j.marmicro.2006.11.002.

Alberico, I., Giliberti, I., Insinga, D.D., Petrosino, P., Vallefuoco, M., Lirer, F., . . . Ferraro, L. (2017) 'Marine sediment cores database for the Mediterranean Basin: a tool for past climatic and environmental studies', *Open Geosciences*, 9(1), available: http://dx.doi.org/10.1515/geo-2017-0019.

Allard, J.L., Hughes, P.D. and Woodward, J.C. (2021) 'Heinrich Stadial aridity forced Mediterranean-wide glacier retreat in the last cold stage', *Nature Geoscience*, 14(4), 197-205, available: http://dx.doi.org/10.1038/s41561-021-00703-6.

Alley, R.B. (2000) 'The Younger Dryas cold interval as viewed from central Greenland', *Quaternary Science Reviews*, 19(1–5), 213-226, available: http://dx.doi.org/10.1016/S0277-3791(99)00062-1.

Alley, R.B. (2004) 'GISP2 Ice Core Temperature and Accumulation Data [dataset]' in IGBP PAGES/World Data Center for Paleoclimatology, ed., *Data Contribution Series #2004-013*, Boulder CO, USA: NOAA/NGDC Paleoclimatology Program.

Alley, R.B. (2007) 'Wally Was Right: Predictive Ability of the North Atlantic "Conveyor Belt" Hypothesis for Abrupt Climate Change', *Annual Review of Earth and Planetary Sciences*, 35(1), 241-272, available: http://dx.doi.org/10.1146/annurev.earth.35.081006.131524.

Alley, R.B. and Clark, P.U. (1999) 'The Deglaciation of the Northern Hemisphere: A Global Perspective', *Annual Review of Earth and Planetary Sciences*, 27(1), 149-182, available: http://dx.doi.org/10.1146/annurev.earth.27.1.149.

Alley, R.B. and MacAyeal, D. (1994) 'Ice-rafted debris associated with binge/purge oscillations of the Laurentide Ice Sheet', *Paleoceanography*, 9(4), 503-511.

Almazroui, M., Awad, A.M. and Nazrul Islam, M. (2017) 'Characteristics of the internal and external sources of the Mediterranean synoptic cyclones for the period 1956–2013',

Theoretical and Applied Climatology, 133(3-4), 811-827, available: http://dx.doi.org/10.1007/s00704-017-2218-2.

Alpert, P., Baldi, M., Ilani, R., Krichak, S., Price, C., Rodó, X., . . . Xoplaki, E. (2006) 'Relations between climate variability in the Mediterranean region and the tropics: ENSO, South Asian and African monsoons, hurricanes and Saharan dust' in Lionello, P., Malanotte-Rizzoli, P. and Boscolo, R., eds., *Mediterranean Climate Variability*, Amsterdam: Elsevier, 149-177.

Amitai, Y., Ashkenazy, Y. and Gildor, H. (2018) 'The effect of wind-stress over the Eastern Mediterranean on deep-water formation in the Adriatic Sea', *Deep Sea Research Part II: Topical Studies in Oceanography*, available: http://dx.doi.org/10.1016/j.dsr2.2018.11.015.

Andersen, K.K., Svensson, A., Johnsen, S.J., Rasmussen, S.O., Bigler, M., Röthlisberger, R., . . . Dahl-Jensen, D. (2006) 'The Greenland Ice Core Chronology 2005, 15–42ka. Part 1: constructing the time scale', *Quaternary Science Reviews*, 25(23-24), 3246-3257, available: http://dx.doi.org/10.1016/j.quascirev.2006.08.002.

Anderson, O., Spindler, M., Bé, A. and Hemleben, C. (1979) 'Trophic activity of planktonic foraminifera', *Journal of the Marine Biological Association of the United Kingdom*, 59(3), 791-799.

Anderson, O.R. (1983) *Radiolaria*, New York: Springer-Verlag.

André, A., Quillévére, F., Morard, R., Ujiié, Y., Escarguel, G., de Vargas, C., . . . Douady, C.J. (2014) 'SSU rDNA divergence in planktonic foraminifera: molecular taxonomy and biogeographic implications', *PloS one*, 9(8), e104641, available: http://dx.doi.org/10.1371/journal.pone.0104641.

André, A., Weiner, A., Quillévéré, F., Aurahs, R., Morard, R., Douady, C.J., . . . Kucera, M. (2013) 'The cryptic and the apparent reversed: lack of genetic differentiation within the morphologically diverse plexus of the planktonic foraminifer Globigerinoides sacculifer', *Paleobiology*, 39(01), 21-39, available: http://dx.doi.org/10.1666/0094-8373-39.1.21.

Andrews, J. (2000) 'Icebergs and Iceberg Rafted Detritus (IRD) in the North Atlantic: Facts and Assumptions', *Oceanography*, 13(3), 100-108, available: http://dx.doi.org/10.5670/oceanog.2000.19.

Andrews, J.T., Jennings, A.E., Kerwin, M., Kirby, M., Manley, W., Miller, G.H., . . . MacLean, B. (1995) 'A Heinrich-like event, H-0 (DC-0): Source(s) for detrital carbonate in the North Atlantic during the Younger Dryas Chronozone', *Paleoceanography*, 10(5), 943-952, available: http://dx.doi.org/10.1029/95pa01426.

Andrews, J.T. and Voelker, A.H.L. (2018) '"Heinrich events" (& sediments): A history of terminology and recommendations for future usage', *Quaternary Science Reviews*, 187, 31-40, available: http://dx.doi.org/10.1016/j.quascirev.2018.03.017.

Appeltans, W., Ahyong, S.T., Anderson, G., Angel, M.V., Artois, T., Bailly, N., . . . Blazewicz-Paszkowycz, M., et al. (2012) 'The magnitude of global marine species diversity', *Curr Biol*, 22(23), 2189-202, available: http://dx.doi.org/10.1016/j.cub.2012.09.036.

Armstrong, H. and Brasier, M. (2009) *Microfossils*, Oxford, UK: Wiley.

Arnau, P., Liquete, C. and Canals, M. (2004) 'River Mouth Plume Events and Their Dispersal in the Northwestern Mediterranean Sea', *Oceanography*, 17(3), 22-31.

Arnold, A.J. and Parker, W.C. (1999) 'Biogeography of planktonic foraminifera' in Gupta, B. K. S., ed., *Modern foraminifera*, 103-122.

Arnone, R.A., Wiesenburg, D.A. and Saunders, K.D. (1990) 'The origin and characteristics of the Algerian Current', *Journal of Geophysical Research: Oceans*, 95(C2), 1587-1598.

Asioli, A., Trincardi, F., Lowe, J.J., Ariztegui, D., Langone, L. and Oldfield, F. (2001) 'Sub-millennial scale climatic oscillations in the central Adriatic during the Lateglacial: palaeoceanographic implications', *Quaternary Science Reviews*, 20(11), 1201-1221, available: http://dx.doi.org/10.1016/S0277-3791(00)00147-5.

Astrophysics Team University of Lincoln (n.d.) *Enhanced Milankovitch Cycles*, available: https://astrophysics-lincoln.org/projects/ [accessed 24/04/2021].

Aurahs, R., Grimm, G.W., Hemleben, V., Hemleben, C. and Kucera, M. (2009) 'Geographical distribution of cryptic genetic types in the planktonic foraminifer Globigerinoides ruber', *Molecular Ecology*, 18(8), 1692-1706.

Aurahs, R., Treis, Y., Darling, K. and Kučera, M. (2011) 'A revised taxonomic and phylogenetic concept for the planktonic foraminifer species Globigerinoides ruber based on molecular and morphometric evidence', *Marine Micropaleontology*, 79(1-2), 1-14, available: http://dx.doi.org/10.1016/j.marmicro.2010.12.001.

Ausin, B., Flores, J.A., Sierro, F.J., Bárcena, M.A., Hernández-Almeida, I., Francés, G., . . . Cacho, I. (2015a) 'Coccolithophore productivity and surface water dynamics in the Alboran Sea during the last 25 kyr', *Palaeogeography, Palaeoclimatology, Palaeoecology*, 418, 126-140, available: http://dx.doi.org/10.1016/j.palaeo.2014.11.011.

Ausin, B., Flores, J.A., Sierro, F.J., Cacho, I., Hernandez-Almeida, I., Martrat, B. and Grimalt, J.O. (2015b) 'Atmospheric patterns driving Holocene productivity in the Alboran Sea (Western Mediterranean): A multiproxy approach', *The Holocene*, 25(4), 583-595, available: http://dx.doi.org/10.1177/0959683614565952.

Ausín, B., Haghipour, N., Wacker, L., Voelker, A.H.L., Hodell, D., Magill, C., . . . Eglinton, T.I. (2019) 'Radiocarbon Age Offsets Between Two Surface Dwelling Planktonic Foraminifera Species During Abrupt Climate Events in the SW Iberian Margin', *Paleoceanography and Paleoclimatology*, 34, available: http://dx.doi.org/doi:10.1029/2018PA003490.

Ausín, B., Hodell, D.A., Cutmore, A. and Eglinton, T.I. (2020) 'The impact of abrupt deglacial climate variability on productivity and upwelling on the southwestern Iberian margin', *Quaternary Science Reviews*, 230, available: http://dx.doi.org/10.1016/j.quascirev.2019.106139.

Austin, W.E.N. and Hibbert, F.D. (2012) 'Tracing time in the ocean: a brief review of chronological constraints (60–8 kyr) on North Atlantic marine event-based stratigraphies', *Quaternary Science Reviews*, 36, 28-37, available: http://dx.doi.org/10.1016/j.quascirev.2012.01.015.

Avnaim-Katav, S., Herut, B., Rahav, E., Katz, T., Weinstein, Y., Alkalay, R., . . . Almogi-Labin, A. (2020) 'Sediment trap and deep sea coretop sediments as tracers of recent changes in planktonic foraminifera assemblages in the southeastern ultra-oligotrophic Levantine Basin', *Deep Sea Research Part II: Topical Studies in Oceanography*, 171, available: http://dx.doi.org/10.1016/j.dsr2.2019.104669.

Bakke, J., Lie, Ø., Heegaard, E., Dokken, T., Haug, G.H., Birks, H.H., . . . Nilsen, T. (2009) 'Rapid oceanic and atmospheric changes during the Younger Dryas cold period', *Nature Geoscience*, 2(3), 202-205, available: http://dx.doi.org/10.1038/ngeo439.

Baldi, M., Gaetani, M., Dalu, G. and Maracchi, G. (2008) 'Jetstream and seasonal anomalies in the Mediterranean', *Bollettino Geofisico*, 31, 51-69.

Baldini, L.M., Baldini, J.U.L., McDermott, F., Arias, P., Cueto, M., Fairchild, I.J., . . . Richards, D.A. (2019) 'North Iberian temperature and rainfall seasonality over the Younger Dryas and Holocene', *Quaternary Science Reviews*, 226, available: http://dx.doi.org/10.1016/j.quascirev.2019.105998.

Baldini, L.M., McDermott, F., Baldini, J.U.L., Arias, P., Cueto, M., Fairchild, I.J., . . . Richards, D.A. (2015) 'Regional temperature, atmospheric circulation, and sea-ice variability within the Younger Dryas Event constrained using a speleothem from northern Iberia', *Earth and Planetary Science Letters*, 419, 101-110, available: http://dx.doi.org/10.1016/j.epsl.2015.03.015.

Bar-Matthews, M., Ayalon, A. and Kaufman, A. (1997) 'Late Quaternary Paleoclimate in the Eastern Mediterranean Region from Stable Isotope Analysis of Speleothems at Soreq Cave, Israel', *Quaternary Research*, 47(2), 155-168, available: http://dx.doi.org/10.1006/qres.1997.1883.

Bar-Matthews, M., Ayalon, A., Kaufman, A. and Wasserburg, G.J. (1999) 'The Eastern Mediterranean paleoclimate as a reflection of regional events: Soreq cave, Israel', *Earth and Planetary Science Letters*, 166(1–2), 85-95, available: http://dx.doi.org/10.1016/S0012-821X(98)00275-1.

Barale, V., Jaquet, J.-M. and Ndiaye, M. (2008) 'Algal blooming patterns and anomalies in the Mediterranean Sea as derived from the SeaWiFS data set (1998–2003)', *Remote Sensing of Environment*, 112(8), 3300-3313.

Bárcena, M., Cacho, I., Abrantes, F., Sierro, F., Grimalt, J. and Flores, J. (2001) 'Paleoproductivity variations related to climatic conditions in the Alboran Sea (western Mediterranean) during the last glacial–interglacial transition: the diatom record', *Palaeogeography, Palaeoclimatology, Palaeoecology*, 167(3), 337-357.

Bárcena, M.A., Flores, J.A., Sierro, F.J., Pérez-Folgado, M., Fabres, J., Calafat, A. and Canals, M. (2004) 'Planktonic response to main oceanographic changes in the Alboran Sea (Western Mediterranean) as documented in sediment traps and surface sediments', *Marine Micropaleontology*, 53(3-4), 423-445, available: http://dx.doi.org/10.1016/j.marmicro.2004.09.009.

Bard, E., Arnold, M., Maurice, P., Duprat, J., Moyes, J. and Duplessy, J.-C. (1987) 'Retreat velocity of the North Atlantic polar front during the last deglaciation determined by 14C accelerator mass spectrometry', *Nature*, 328, 791, available: http://dx.doi.org/10.1038/328791a0.

Bard, E., Hamelin, B. and Delanghe, D. (2010) 'Deglacial Meltwater Pulse 1B and Younger Dryas Sea Levels Revisited with Boreholes at Tahiti', *Science (New York, N.Y.)*, 327, 1235-7, available: http://dx.doi.org/10.1126/science.1180557.

Bard, E., Rostek, F., Turon, J.-L. and Gendreau, S. (2000) 'Hydrological impact of Heinrich events in the subtropical northeast Atlantic', *Science*, 289(5483), 1321-1324.

Barker, S., Chen, J., Gong, X., Jonkers, L., Knorr, G. and Thornalley, D. (2015) 'Icebergs not the trigger for North Atlantic cold events', *Nature*, 520, 333, available: http://dx.doi.org/10.1038/nature14330.

Barker, S., Diz, P., Vautravers, M.J., Pike, J., Knorr, G., Hall, I.R. and Broecker, W.S. (2009) 'Interhemispheric Atlantic seesaw response during the last deglaciation', *Nature*, 457(7233), 1097-102, available: http://dx.doi.org/10.1038/nature07770.

Barry, D. (2017) *A palaeoecological analysis of Late Quaternary sapropels from the Mediterranean ridge*, unpublished thesis (PhD), Mary Immaculate College.

Bartov, Y., Goldstein, S.L., Stein, M. and Enzel, Y. (2003) 'Catastrophic arid episodes in the Eastern Mediterranean linked with the North Atlantic Heinrich events', *Geology*, 31(5), 439-442, available: http://dx.doi.org/10.1130/0091-7613(2003)031<0439:Caeite>2.0.Co;2.

Bashirova, L.D., Kandiano, E.S., Sivkov, V.V. and Bauch, H.A. (2014) 'Migrations of the North Atlantic Polar front during the last 300 ka: Evidence from planktic foraminiferal data', *Oceanology*, 54(6), 798-807, available: http://dx.doi.org/10.1134/s0001437014060010.

Bassetti, M.-A., Berné, S., Sicre, M.-A., Dennielou, B., Alonso, Y., Buscail, R., . . . Menniti, C. (2016) 'Holocene hydrological changes in the Rhône River (NW Mediterranean) as recorded in the marine mud belt', *Climate of the Past*, 12(7), 1539-1553, available: http://dx.doi.org/10.5194/cp-12-1539-2016.

Bassetti, M.A., Carbonel, P., Sierro, F.J., Perez-Folgado, M., Jouët, G. and Berné, S. (2010) 'Response of ostracods to abrupt climate changes in the Western Mediterranean (Gulf of Lions) during the last 30 kyr', *Marine Micropaleontology*, 77(1-2), 1-14, available: http://dx.doi.org/10.1016/j.marmicro.2010.06.004.

Bassetti, M.A., Jouet, G., Dufois, F., Berné, S., Rabineau, M. and Taviani, M. (2006) 'Sand bodies at the shelf edge in the Gulf of Lions (Western Mediterranean): Deglacial history and modern processes', *Marine Geology*, 234(1-4), 93-109, available: http://dx.doi.org/10.1016/j.margeo.2006.09.010.

Bassis, J.N., Petersen, S.V. and Mac Cathles, L. (2017) 'Heinrich events triggered by ocean forcing and modulated by isostatic adjustment', *Nature*, 542(7641), 332-334, available: http://dx.doi.org/10.1038/nature21069.

Bazzicalupo, P., Maiorano, P., Girone, A., Marino, M., Combourieu-Nebout, N. and Incarbona, A. (2018) 'High-frequency climate fluctuations over the last deglaciation in the Alboran Sea, Western Mediterranean: Evidence from calcareous plankton assemblages', *Palaeogeography, Palaeoclimatology, Palaeoecology*, 506, 226-241, available: http://dx.doi.org/10.1016/j.palaeo.2018.06.042.

Bé, A.W.H. (1977) 'An ecological, zoogeographic and taxonomic review of recent planktonic foraminifera' in Ramsey, A. T. S., ed., *Oceanic micropaleontology*, London: Academic Press., 1-100.

Bé, A.W.H. and Hutson, W.H. (1977) 'Ecology of Planktonic Foraminifera and Biogeographic Patterns of Life and Fossil Assemblages in the Indian Ocean', *Micropaleontology*, 23(4), 369-414, available: http://dx.doi.org/10.2307/1485406.

Bé, A.W.H. and Tolderlund, D. (1971) 'Distribution and ecology of living planktonic foraminifera in surface waters of the Atlantic and Indian Oceans' in Funnel, B. M. and Riedel, W. R., eds., *Micropaleontology of Oceans*, New York: Cambridge University Press,, 105-149.

Beaudouin, C., Dennielou, B., Melki, T., Guichard, F., Kallel, N., Berné, S. and Huchon, A. (2004) 'The Late-Quaternary climatic signal recorded in a deep-sea turbiditic levee (Rhône Neofan, Gulf of Lions, NW Mediterranean): palynological constraints', *Sedimentary Geology*, 172(1), 85-97.

Bell, M. and Walker, M.J.C. (2005) *Late Quaternary environmental change: physical and human perspectives*, 2nd ed. ed., Harlow: Pearson/Prentice Hall.

Belli, R., Frisia, S., Borsato, A., Drysdale, R., Hellstrom, J., Zhao, J.x. and Spötl, C. (2013) 'Regional climate variability and ecosystem responses to the last deglaciation in the northern hemisphere from stable isotope data and calcite fabrics in two northern Adriatic stalagmites', *Quaternary Science Reviews*, 72, 146-158, available: http://dx.doi.org/10.1016/j.quascirev.2013.04.014.

Bergamasco, A. and Malanotte-Rizzoli, P. (2010) 'The circulation of the Mediterranean Sea: a historical review of experimental investigations', *Advances in Oceanography and Limnology*, 1(1), 11-28, available: http://dx.doi.org/10.1080/19475721.2010.491656.

Berger, A. (1978) 'Long-Term Variations of Daily Insolation and Quaternary Climatic Changes', *Journal of the Atmospheric Sciences*, 35(12), 2362-2367, available: http://dx.doi.org/10.1175/1520-0469(1978)035<2362:Ltvodi>2.0.Co;2.

Berger, A. and Loutre, M.-F. (1991) 'Insolation values for the climate of the last 10 million years', *Quaternary Science Reviews*, 10, 297-317, available: http://dx.doi.org/10.1016/0277-3791(91)90033-Q.

Berger, W.H., Bonneau, M.C. and Parker, F.L. (1982) 'Foraminifera on the deep-sea floor-lysocline and dissolution rate', *Oceanologica Acta*, 5(2), 249-258.

Berné, S., Jouet, G., Bassetti, M.A., Dennielou, B. and Taviani, M. (2007) 'Late Glacial to Preboreal sea-level rise recorded by the Rhône deltaic system (NW Mediterranean)', *Marine Geology*, 245(1-4), 65-88, available: http://dx.doi.org/10.1016/j.margeo.2007.07.006.

Berné, S., Rabineau, M., Flores, J.A. and Sierro, F.J. (2004) 'The impact of Quaternary global changes on strata formation', *Oceanography*, 17(4), 92-103.

Bijma, J., Faber, W.W. and Hemleben, C. (1990) 'Temperature and salinity limits for growth and survival of some planktonic foraminifers in laboratory cultures', *Journal of foraminiferal research*, 20(2), 95-116.

Bijma, J., Hemleben, C., OBERHÄNsLI, H. and Spindler, M. (1992) 'The effects of increased water fertility on tropical spinose planktonic foraminifers in laboratory cultures', *Journal of foraminiferal research*, 22(3), 242-256.

Billups, K., Hudson, C., Kunz, H. and Rew, I. (2016) 'Exploring Globorotalia truncatulinoides coiling ratios as a proxy for subtropical gyre dynamics in the northwestern Atlantic Ocean during late Pleistocene Ice Ages', *Paleoceanography*, 31(5), 553-563, available: http://dx.doi.org/10.1002/2016pa002927.

Bird, C., Darling, K.F., Russell, A.D., Fehrenbacher, J.S., Davis, C.V., Free, A. and Ngwenya, B.T. (2018) '16S rRNA gene metabarcoding and TEM reveals different ecological strategies within the genus Neogloboquadrina (planktonic foraminifer)', *PloS one*, 13(1), e0191653, available: http://dx.doi.org/10.1371/journal.pone.0191653.

Björck, S. (2007) 'PALEOCLIMATE RECONSTRUCTION | Younger Dryas Oscillation, Global Evidence' in Elias, S. A., ed., *Encyclopedia of Quaternary Science*, 2nd ed., Oxford: Elsevier, 1985-1993.

Blaauw, M. (2010a) 'Clam, R code for classical (non-Bayesian) age-depth modelling', v. 2.2.

Blaauw, M. (2010b) 'Methods and code for 'classical' age-modelling of radiocarbon sequences', *Quaternary Geochronology*, 5(5), 512-518, available: http://dx.doi.org/10.1016/j.quageo.2010.01.002.

Blaauw, M. (2012) 'Out of tune: the dangers of aligning proxy archives', *Quaternary Science Reviews*, 36, 38-49, available: http://dx.doi.org/10.1016/j.quascirev.2010.11.012.

Blaauw, M. and Christen, J.A. (2011) 'Flexible paleoclimate age-depth models using an autoregressive gamma process', *Bayesian Analysis*, 6(3), 457-474.

Boltovskoy, D. and Correa, N. (2014) 'Foraminifers (Planktonic)' in Harff, J., Meschede, M., Petersen, S. and Thiede, J., eds., *Encyclopedia of Marine Geosciences*, Dordrecht: Springer Netherlands, 1-9.

Bond, G., Broecker, W., Johnsen, S., McManus, J., Labeyrie, L., Jouzel, J. and Bonani, G. (1993) 'Correlations between climate records from North Atlantic sediments and Greenland ice', *Nature*, 365(6442), 143-147.

Bond, G., Heinrich, H., Broecker, W., Labeyrie, L., McManus, J., Andrews, J., . . . Ivy-Ochs, S. (1992) 'Evidence for massive discharges of icebergs into the North Atlantic ocean during the last glacial period', *Nature*, 360, 245-249.

Bond, G., Kromer, B., Beer, J., Muscheler, R., Evans, M.N., Showers, W., . . . Bonani, G. (2001) 'Persistent solar influence on North Atlantic climate during the Holocene', *Science*, 294(5549), 2130-2136.

Bond, G., Showers, W., Cheseby, M., Lotti, R., Almasi, P., Priore, P., . . . Bonani, G. (1997) 'A pervasive millennial-scale cycle in North Atlantic Holocene and glacial climates', *Science*, 278(5341), 1257-1266.

Bond, G.C., Showers, W., Elliot, M., Evans, M., Lotti, R., Hajdas, I., . . . Johnson, S. (1999) 'The North Atlantic's 1-2 kyr climate rhythm: Relation to Heinrich Events, Dansgaard/Oeschger cycles and the little ice age', *Geophysical Monograph-American Geophysical Union*, 112, 35-58.

Born, A. and Levermann, A. (2010) 'The 8.2 ka event: Abrupt transition of the subpolar gyre toward a modern North Atlantic circulation', *Geochemistry, Geophysics, Geosystems*, 11(6), n/a-n/a, available: http://dx.doi.org/10.1029/2009gc003024.

Borreggine, M., Myhre, S.E., Mislan, K.A.S., Deutsch, C. and Davis, C.V. (2017) 'A database of paleoceanographic sediment cores from the North Pacific, 1951-2016', *Earth System Science Data*, 9(2), 739-749, available: http://dx.doi.org/10.5194/essd-9-739-2017.

BouDagher-Fadel, M.K. (2015) *Biostratigraphic and geological significance of planktonic foraminifera*, Updated 2nd ed., UCL Press, available: http://www.ucl.ac.uk/ucl-press/browse-books/biostratigraphic-and-geological-significance-of-planktonic-foraminifera [accessed 03/11/15].

Bout-Roumazeilles, V., Combourieu-Nebout, N., Desprat, S., Siani, G. and Turon, J.L. (2012) 'Tracking atmospheric and riverine terrigenous supplies variability during the last

glacial and the Holocene in central Mediterranean', *Climate of the Past Discussions*, 8(4), 2921-2968, available: http://dx.doi.org/10.5194/cpd-8-2921-2012.

Box, M.R., Krom, M.D., Cliff, R.A., Bar-Matthews, M., Almogi-Labin, A., Ayalon, A. and Paterne, M. (2011) 'Response of the Nile and its catchment to millennial-scale climatic change since the LGM from Sr isotopes and major elements of East Mediterranean sediments', *Quaternary Science Reviews*, 30(3-4), 431-442, available: http://dx.doi.org/10.1016/j.quascirev.2010.12.005.

Brauer, A., Haug, G.H., Dulski, P., Sigman, D.M. and Negendank, J.F.W. (2008) 'An abrupt wind shift in western Europe at the onset of the Younger Dryas cold period', *Nature Geoscience*, 1(8), 520-523, available: http://dx.doi.org/10.1038/ngeo263.

Briggs, I.C. (1974) 'Machine contouring using minimum curvature', *Geophysics*, 39(1), 39-48.

Broecker, W.S. (1981) 'Glacial to Interglacial Changes in Ocean and Atmosphere Chemistry' in Berger, A., ed., *Climatic Variations and Variability: Facts and Theories: NATO Advanced Study Institute First Course of the International School of Climatology, Ettore Majorana Center for Scientific Culture, Erice, Italy, March 9–21, 1980*, Dordrecht: Springer Netherlands, 111-121.

Broecker, W.S. (1998) 'Paleocean circulation during the last deglaciation: a bipolar seesaw?', *Paleoceanography*, 13(2), 119-121.

Broecker, W.S. (2006) 'Abrupt climate change revisited', *Global and Planetary Change*, 54(3-4), 211-215, available: http://dx.doi.org/10.1016/j.gloplacha.2006.06.019.

Broecker, W.S., Andree, M., Wolfli, W., Oeschger, H., Bonani, G., Kennett, J. and Peteet, D. (1988) 'The chronology of the last Deglaciation: Implications to the cause of the Younger Dryas Event', *Paleoceanography*, 3(1), 1-19, available: http://dx.doi.org/10.1029/PA003i001p00001.

Broecker, W.S. and Denton, G.H. (1989) 'The role of ocean-atmosphere reorganizations in glacial cycles', *Geochimica et Cosmochimica Acta*, 53(10), 2465-2501, available: http://dx.doi.org/10.1016/0016-7037(89)90123-3.

Broecker, W.S., Denton, G.H., Edwards, R.L., Cheng, H., Alley, R.B. and Putnam, A.E. (2010) 'Putting the Younger Dryas cold event into context', *Quaternary Science Reviews*, 29(9-10), 1078-1081, available: http://dx.doi.org/10.1016/j.quascirev.2010.02.019.

Broecker, W.S., Kennett, J.P., Flower, B.P., Teller, J.T., Trumbore, S., Bonani, G. and Wolfli, W. (1989) 'Routing of meltwater from the Laurentide Ice Sheet during the Younger Dryas cold episode', *Nature*, 341(6240), 318.

Broecker, W.S., Peteet, D.M. and Rind, D. (1985) 'Does the ocean-atmosphere system have more than one stable mode of operation?', *Nature*, 315(6014), 21-26, available: http://dx.doi.org/10.1038/315021a0.

Broggy, T.C. (2011) *Planktonic foraminiferal response to the Last Glacial Termination and their application to Holocene biostratigraphy in the western Mediterranean Sea*, unpublished thesis, University of Limerick, available: https://dspace.mic.ul.ie/handle/10395/1027.

Brown, S.K., Crosweller, H.S., Sparks, R.S.J., Cottrell, E., Deligne, N.I., Guerrero, N.O., . . . Takarada, S. (2014) 'Characterisation of the Quaternary eruption record: analysis of the Large Magnitude Explosive Volcanic Eruptions (LaMEVE) database', *Journal of Applied Volcanology*, 3(1), available: http://dx.doi.org/10.1186/2191-5040-3-5.

Buccheri, G., Capretto, G., Di Donato, V., Esposito, P., Ferruzza, G., Pescatore, T., . . . Madonia, G. (2002) 'A high resolution record of the last deglaciation in the southern Tyrrhenian Sea: environmental and climatic evolution', *Marine Geology*, 186(3–4), 447-470, available: http://dx.doi.org/10.1016/S0025-3227(02)00270-0.

Cacho, I., Grimalt, J.O. and Canals, M. (2002) 'Response of the Western Mediterranean Sea to rapid climatic variability during the last 50,000 years: a molecular biomarker approach', *Journal of Marine Systems*, 33-34, 253-272.

Cacho, I., Grimalt, J.O., Canals, M., Sbaffi, L., Shackleton, N.J., Schönfeld, J. and Zahn, R. (2001) 'Variability of the western Mediterranean Sea surface temperature during the last 25,000 years and its connection with the Northern Hemisphere climatic changes', *Paleoceanography*, 16(1), 40-52.

Cacho, I., Grimalt, J.O., Pelejero, C., Canals, M., Sierro, F.J., Flores, J.A. and Shackleton, N. (1999) 'Dansgaard-Oeschger and Heinrich event imprints in Alboran Sea paleotemperatures', *Paleoceanography*, 14(6), 698-705.

Cacho, I., Grimalt, J.O., Sierro, F.J., Shackleton, N. and Canals, M. (2000) 'Evidence for enhanced Mediterranean thermohaline circulation during rapid climatic coolings', *Earth and Planetary Science Letters*, 183, 417-429.

Cacho, I., Shackleton, N., Elderfield, H., Sierro, F.J. and Grimalt, J.O. (2006) 'Glacial rapid variability in deep-water temperature and $\delta18O$ from the Western Mediterranean Sea', *Quaternary Science Reviews*, 25(23-24), 3294-3311, available: http://dx.doi.org/10.1016/j.quascirev.2006.10.004.

Camberlin, P. and Philippon, N. (2002) 'The East African March–May Rainy Season: Associated Atmospheric Dynamics and Predictability over the 1968–97 Period', *Journal of Climate*, 15(9), 1002-1019, available: http://dx.doi.org/10.1175/1520-0442(2002)015<1002:teammr>2.0.co;2.

Capotondi, L. (1995) 'Biostratigraphic changes and paleoceanographic record in Corsica Basin (Tyrrhenian Sea) during the last 18000 years', *Palaeopelagos*, 5, 215-226.

Capotondi, L., Borsetti, A., Vergnaud-Grazzini, C. and D'Onofrio, S. (1989) 'Biostratigrafia e stratigrafia isotopica della carota AC85-4: considerazioni sulla paleoceanografia tardo-quaternaria del Mar Tirreno orientale', *Giornale di Geologia, Serie 3a*, 51(1), 201-212.

Capotondi, L., Girone, A., Lirer, F., Bergami, C., Verducci, M., Vallefuoco, M., . . . De Lange, G.J. (2016) 'Central Mediterranean Mid-Pleistocene paleoclimatic variability and its association with global climate', *Palaeogeography, Palaeoclimatology, Palaeoecology*, 442, 72-83.

Capotondi, L., Maria Borsetti, A. and Morigi, C. (1999) 'Foraminiferal ecozones, a high resolution proxy for the late Quaternary biochronology in the central Mediterranean Sea', *Marine Geology*, 153(1–4), 253-274, available: http://dx.doi.org/10.1016/S0025-3227(98)00079-6.

Carboni, M.G., Bergamin, L., Di Bella, L., Landini, B., Manfra, L. and Vesica, P. (2005) 'Late Quaternary paleoclimatic and paleoenviromental changes in the Tyrrhenian Sea', *Quaternary Science Reviews*, 24(18-19), 2069-2082, available: http://dx.doi.org/10.1016/j.quascirev.2004.09.009.

Carlson, A.E. (2010) 'What Caused the Younger Dryas Cold Event?', *Geology*, 38, 383-384, available: http://dx.doi.org/doi:10.1130/focus042010.1.

Carlson, A.E. (2013) *The Younger Dryas Climate Event*, Amsterdam: Elsevier.

Carlson, A.E. and Clark, P.U. (2012) 'Ice sheet sources of sea level rise and freshwater discharge during the last deglaciation', *Reviews of Geophysics*, 50(4).

Cartes, J., Maynou, F., Sardà, F., Lloris, D., Tudela, S., Simard, F., . . . Guglielmi, P. (2004) 'Part I: The Mediterranean deep-sea ecosystems: an overview of their diversity, structure, functioning and anthropogenic impacts, with a proposal for their conservation' in WWF/IUCN, ed., *The Mediterranean deep-sea ecosystems : an overview of their diversity, structure, functioning and anthropogenic impacts, with a proposal for their conservation*, Málag, Rome: IUCN, WWF, 9-38.

Casford, J.S.L., Abu-Zied, R., Rohling, E.J., Cooke, S., Boessenkool, K.P., Brinkhuis, H., . . . Papatheodorou, G. (2001) 'Mediterranean climate variability during the Holocene', *Mediterranean marine science*, 2(1), 45-56.

Casford, J.S.L., Abu-Zied, R., Rohling, E.J., Cooke, S., Fontanier, C., Leng, M., . . . Thomson, J. (2007) 'A stratigraphically controlled multiproxy chronostratigraphy for the eastern Mediterranean', *Paleoceanography*, 22(4), PA4215, available: http://dx.doi.org/10.1029/2007pa001422.

Casford, J.S.L., Rohling, E.J., Abu-Zied, R., Cooke, S., Fontanier, C., Leng, M. and Lykousis, V. (2002) 'Circulation changes and nutrient concentrations in the late Quaternary Aegean Sea: A nonsteady state concept for sapropel formation', *Paleoceanography*, 17(2), 14-1-14-11.

Castañeda, I.S., Schefuß, E., Pätzold, J., Sinninghe Damsté, J.S., Weldeab, S. and Schouten, S. (2010) 'Millennial-scale sea surface temperature changes in the eastern Mediterranean (Nile River Delta region) over the last 27,000 years', *Paleoceanography*, 25(1), PA1208, available: http://dx.doi.org/10.1029/2009PA001740.

Català, A., Cacho, I., Frigola, J., Pena, L.D. and Lirer, F. (2019) 'Holocene hydrography evolution in the Alboran Sea: a multi-record and multi-proxy comparison', *Climate of the Past*, 15(3), 927-942, available: http://dx.doi.org/10.5194/cp-15-927-2019.

Cayre, O., Lancelot, Y., Vincent, E. and Hall, M.A. (1999) 'Paleoceanographic reconstructions from planktonic foraminifera off the Iberian Margin: Temperature, salinity, and Heinrich events', *Paleoceanography*, 14(3), 384-396, available: http://dx.doi.org/10.1029/1998pa900027.

Chaisson, W. and Pearson, P. (1997) 'Planktonic foraminifer biostratigraphy at Site 925: Middle Miocene-Pleistocene' in Shackleton, N. J., Curry, W. B., Richter, C. and Bralower, T. J., eds., *Proceedings of the Ocean Drilling Program, Scientific Results: College Station, TX (Ocean Drilling Program)*, 3-31.

Chapman, M.R. (2010) 'Seasonal production patterns of planktonic foraminifera in the NE Atlantic Ocean: Implications for paleotemperature and hydrographic reconstructions', *Paleoceanography*, 25(1), available: http://dx.doi.org/10.1029/2008pa001708.

Chiang, J.C.H., Biasutti, M. and Battisti, D.S. (2003) 'Sensitivity of the Atlantic Intertropical Convergence Zone to Last Glacial Maximum boundary conditions', *Paleoceanography*, 18(4), 1094, available: http://dx.doi.org/10.1029/2003pa000916.

Chiggiato, J., Schroeder, K. and Trincardi, F. (2016) 'Cascading dense shelf-water during the extremely cold winter of 2012 in the Adriatic, Mediterranean Sea: Formation, flow, and

seafloor impact', *Marine Geology*, 375, 1-4, available:
http://dx.doi.org/10.1016/j.margeo.2016.03.002.

Cifelli, R. (1974) 'Planktonic foraminifera from the Mediterranean and adjacent Atlantic waters (Cruise 49 of the Atlantis II, 1969)', *The Journal of Foraminiferal Research*, 4(4), 171-183.

Clark, P.U., Dyke, A.S., Shakun, J.D., Carlson, A.E., Clark, J., Wohlfarth, B., . . . McCabe, A.M. (2009) 'The Last Glacial Maximum', *Science*, 325(5941), 710-714, available: http://dx.doi.org/10.1126/science.1172873.

Clark, P.U., McCabe, A.M., Mix, A.C. and Weaver, A.J. (2004) 'Rapid Rise of Sea Level 19,000 Years Ago and Its Global Implications', *Science*, 304(5674), 1141-1144, available: http://dx.doi.org/10.1126/science.1094449.

CLIMAP Project Members (1976) 'The Surface of the Ice-Age Earth', *Science*, 191(4232), 1131-1137, available: http://dx.doi.org/10.1126/science.191.4232.1131.

CLIMAP Project Members (1981) 'Seasonal reconstructions of the Earth's surface at the last glacial maximum', *Geological Society of America, Map and Chart Series*, MC-36, 1-18.

Cohen, K., Finney, S., Gibbard, P. and Fan, J. (2013) 'The ICS International Chronostratigraphic Chart.', *Episodes*, 36, 199-204, available: http://dx.doi.org/10.18814/epiiugs/2013/v36i3/002.

Colella, S., Falcini, F., Rinaldi, E., Sammartino, M. and Santoleri, R. (2016) 'Mediterranean Ocean Colour Chlorophyll Trends', *PloS one*, 11(6), e0155756, available: http://dx.doi.org/10.1371/journal.pone.0155756.

Combourieu Nebout, N., Peyron, O., Dormoy, I., Desprat, S., Beaudouin, C., Kotthoff, U. and Marret, F. (2009) 'Rapid climatic variability in the west Mediterranean during the last 25000 years from high resolution pollen data', *Climate of the Past*, 5(3), 503-521.

Combourieu Nebout, N., Turon, J.L., Zahn, R., Capotondi, L., Londeix, L. and Pahnke, K. (2002) 'Enhanced aridity and atmospheric high-pressure stability over the western Mediterranean during the North Atlantic cold events of the past 50 k.y.', *Geology*, 30(10), available: http://dx.doi.org/10.1130/0091-7613(2002)030<0863:Eaaahp>2.0.Co;2.

Conan, S.M.H. and Brummer, G.J.A. (2000) 'Fluxes of planktic foraminifera in response to monsoonal upwelling on the Somalia Basin margin', *Deep Sea Research Part II: Topical Studies in Oceanography*, 47(9), 2207-2227, available: http://dx.doi.org/10.1016/S0967-0645(00)00022-9.

Conan, S.M.H., Ivanova, E.M. and Brummer, G.J.A. (2002) 'Quantifying carbonate dissolution and calibration of foraminiferal dissolution indices in the Somali Basin', *Marine Geology*, 182(3–4), 325-349, available: http://dx.doi.org/10.1016/S0025-3227(01)00238-9.

Cornuault, M., Tachikawa, K., Vidal, L., Guihou, A., Siani, G., Deschamps, P., . . . Revel, M. (2018) 'Circulation changes in the Eastern Mediterranean Sea over the past 23,000 years inferred from authigenic Nd isotopic ratios', *Paleoceanography and Paleoclimatology*, available: http://dx.doi.org/10.1002/2017pa003227.

Cornuault, M., Vidal, L., Tachikawa, K., Licari, L., Rouaud, G., Sonzogni, C. and Revel, M. (2016) 'Deep water circulation within the eastern Mediterranean Sea over the last 95kyr: New insights from stable isotopes and benthic foraminiferal assemblages',

Palaeogeography, Palaeoclimatology, Palaeoecology, 459, 1-14, available: http://dx.doi.org/10.1016/j.palaeo.2016.06.038.

Cortijo, E., Duplessy, J.-C., Labeyrie, L., Duprat, J. and Paillard, D. (2005) 'Heinrich events: hydrological impact', *Comptes Rendus Geoscience*, 337(10-11), 897-907, available: http://dx.doi.org/10.1016/j.crte.2005.04.011.

Cowling, O.C., Thomas, E.K., Svendsen, J.I., Mangerud, J., Vasskog, K. and Haflidason, H. (2020) 'Northward Shifts in the Polar Front Preceded Bølling and Holocene Warming in Southwestern Scandinavia', *Geophysical Research Letters*, 47(14), available: http://dx.doi.org/10.1029/2020gl088153.

Craig, P.M., Ferreira, D. and Methven, J. (2017) 'The contrast between Atlantic and Pacific surface water fluxes', *Tellus A: Dynamic Meteorology and Oceanography*, 69(1), available: http://dx.doi.org/10.1080/16000870.2017.1330454.

Cramer, W., Guiot, J., Fader, M., Garrabou, J., Gattuso, J.-P., Iglesias, A., . . . Xoplaki, E. (2018) 'Climate change and interconnected risks to sustainable development in the Mediterranean', *Nature Climate Change*, 8(11), 972-980, available: http://dx.doi.org/10.1038/s41558-018-0299-2.

Culver, S.J. (1991) 'Early cambrian foraminifera from west Africa', *Science*, 254(5032), 689-91, available: http://dx.doi.org/10.1126/science.254.5032.689.

Dale, A.L. and Dale, B. (2002) 'Application of ecologically based statistical treatments to micropalaeontology' in Haslett, S. K., ed., *Quaternary environmental micropalaeontology*, London: Arnold, 340.

Dansgaard, W., Clausen, H.B., Gundestrup, N., Johnsen, S.J. and Rygner, C. (1985) 'Dating and Climatic Interpretation of Two Deep Greenland Ice Cores' in *Greenland Ice Core: Geophysics, Geochemistry, and the Environment* American Geophysical Union, 71-76.

Dansgaard, W., Johnsen, S.J., Clausen, H.B., Dahl-Jensen, D., Gundestrup, N., Hammer, C.U. and Oeschger, H. (1984) 'North Atlantic Climatic Oscillations Revealed by Deep Greenland Ice Cores' in Hansen, J. E. and Takahashi, T., eds., *Climate Processes and Climate Sensitivity, 29*, 288-298.

Dansgaard, W., Johnsen, S.J., Clausen, H.B., Dahl-Jensen, D., Gundestrup, N.S., Hammer, C.U., . . . Bond, G. (1993) 'Evidence for general instability of past climate from a 250-kyr ice-core record', *Nature*, 364(6434), 218-220, available: http://dx.doi.org/10.1038/364218a0.

Darling, K.F., Kroon, D., Wade, C.M. and Leigh Brown, A.J. (1996) 'Molecular phylogeny of the planktic foraminifera', *The Journal of Foraminiferal Research*, 26(4), 324-330, available: http://dx.doi.org/10.2113/gsjfr.26.4.324.

Darling, K.F., Kučera, M., Kroon, D. and Wade, C.M. (2006) 'A resolution for the coiling direction paradox in Neogloboquadrina pachyderma', *Paleoceanography*, 21(2), PA2011, available: http://dx.doi.org/10.1029/2005PA001189.

Darling, K.F., Thomas, E., Kasemann, S.A., Seears, H.A., Smart, C.W. and Wade, C.M. (2009) 'Surviving mass extinction by bridging the benthic/planktic divide', *Proceedings of the National Academy of Sciences*, 106(31), 12629-12633, available: http://dx.doi.org/10.1073/pnas.0902827106.

Darling, K.F. and Wade, C.M. (2008) 'The genetic diversity of planktic foraminifera and the global distribution of ribosomal RNA genotypes', *Marine Micropaleontology*, 67(3–4), 216-238, available: http://dx.doi.org/10.1016/j.marmicro.2008.01.009.

Darling, K.F., Wade, C.M., Kroon, D., Brown, A.J.L. and Bijma, J. (1999) 'The diversity and distribution of modern planktic foraminiferal small subunit ribosomal RNA genotypes and their potential as tracers of present and past ocean circulations', *Paleoceanography*, 14(1), 3-12.

Darling, K.F., Wade, C.M., Siccha, M., Trommer, G., Schulz, H., Abdolalipour, S. and Kurasawa, A. (2017) 'Genetic diversity and ecology of the planktonic foraminifers Globigerina bulloides , Turborotalita quinqueloba and Neogloboquadrina pachyderma off the Oman margin during the late SW Monsoon', *Marine Micropaleontology*, 137, 64-77, available: http://dx.doi.org/10.1016/j.marmicro.2017.10.006.

Davis, C.V., Livsey, C.M., Palmer, H.M., Hull, P.M., Thomas, E., Hill, T.M. and Benitez-Nelson, C.R. (2020) 'Extensive morphological variability in asexually produced planktic foraminifera', *Science Advances*, 6(28), eabb8930.

de Beaulieu, J.-L., Brugiapaglia, E., Joannin, S., Guiter, F., Zanchetta, G., Wulf, S., . . . Magny, M. (2017) 'Lateglacial-Holocene abrupt vegetation changes at Lago Trifoglietti in Calabria, Southern Italy: The setting of ecosystems in a refugial zone', *Quaternary Science Reviews*, 158, 44-57, available: http://dx.doi.org/10.1016/j.quascirev.2016.12.013.

de Vargas, C., Audic, S., Henry, N., Decelle, J., Mahé, F., Logares, R., . . . Carmichael, M., et al. (2015) 'Eukaryotic plankton diversity in the sunlit ocean', *Science*, 348(6237), available: http://dx.doi.org/10.1126/science.1261605.

de Vargas, C., Bonzon, M., Rees, N.W., Pawlowski, J. and Zaninetti, L. (2002) 'A molecular approach to biodiversity and biogeography in the planktonic foraminifer Globigerinella siphonifera (d'Orbigny)', *Marine Micropaleontology*, 45(2), 101-116, available: http://dx.doi.org/10.1016/S0377-8398(02)00037-3.

de Vargas, C., Norris, R., Zaninetti, L., Gibb, S.W. and Pawlowski, J. (1999) 'Molecular Evidence of Cryptic Speciation in Planktonic Foraminifers and Their Relation to Oceanic Provinces', *Proceedings of the National Academy of Sciences of the United States of America*, 96(6), 2864-2868.

de Vargas, C., Renaud, S., Hilbrecht, H. and Pawlowski, J. (2001) 'Pleistocene adaptive radiation in Globorotalia truncatulinoides: genetic, morphologic, and environmental evidence', *Paleobiology*, 27(1), 104-125, available: http://dx.doi.org/10.1666/0094-8373(2001)027<0104:PARIGT>2.0.CO;2.

de Vargas, C., Zaninetti, L., Hilbrecht, H. and Pawlowski, J. (1997) 'Phylogeny and Rates of Molecular Evolution of Planktonic Foraminifera: SSU rDNA Sequences Compared to the Fossil Record', *Journal of Molecular Evolution*, 45(3), 285-294, available: http://dx.doi.org/10.1007/pl00006232.

de Vernal, A., Henry, M. and Bilodeau, G. (2010) 'Micropaleontological preparation techniques and analyses, 3rd Ed.', *Les Cahiers du Geotop*, 3, 32.

deMenocal, P., Ortiz, J., Guilderson, T. and Sarnthein, M. (2000) 'Coherent High- and Low-Latitude Climate Variability During the Holocene Warm Period', *Science*, 288(5474), 2198-2202, available: http://dx.doi.org/10.1126/science.288.5474.2198.

Denton, G., Alley, R., Comer, G. and Broecker, W. (2005) 'The role of seasonality in abrupt climate change', *Quaternary Science Reviews*, 24(10-11), 1159-1182, available: http://dx.doi.org/10.1016/j.quascirev.2004.12.002.

Denton, G.H., Anderson, R.F., Toggweiler, J.R., Edwards, R.L., Schaefer, J.M. and Putnam, A.E. (2010) 'The last glacial termination', *Science*, 328(5986), 1652-6, available: http://dx.doi.org/10.1126/science.1184119.

Denton, G.H., Broecker, W.S. and Alley, R.B. (2006) 'The mystery interval 17.5 to 14.5 kyrs ago', *PAGES news*, 14(20), 14-16.

Denton, G.H., Heusser, C.J., Lowel, T.V., Moreno, P.I., Andersen, B.G., Heusser, L.E., . . . Marchant, D.R. (1999) 'Interhemispheric Linkage of Paleoclimate During the Last Glaciation', *Geografiska Annaler: Series A, Physical Geography*, 81(2), 107-153, available: http://dx.doi.org/10.1111/1468-0459.00055.

Deschamps, P., Durand, N., Bard, E., Hamelin, B., Camoin, G., Thomas, A.L., . . . Yokoyama, Y. (2012) 'Ice-sheet collapse and sea-level rise at the Bølling warming 14,600 years ago', *Nature*, 483(7391), 559-564.

Desprat, S., Combourieu-Nebout, N., Essallami, L., Sicre, M.-A., Dormoy, I., Peyron, O., . . . Turon, J. (2013) 'Deglacial and Holocene vegetation and climatic changes in the southern Central Mediterranean from a direct land-sea correlation', *Climate of the Past*, 9(2), 767-787.

Di Donato, V., Daunis-i-Estadella, J., Martín-Fernández, J.A. and Esposito, P. (2015) 'Size Fraction Effects on Planktonic Foraminifera Assemblages: A Compositional Contribution to the Golden Sieve Rush', *Mathematical Geosciences*, 47(4), 455-470, available: http://dx.doi.org/10.1007/s11004-014-9529-y.

Di Donato, V., Esposito, P., Garilli, V., Naimo, D., Buccheri, G., Caffau, M., . . . Stanzione, D. (2009) 'Surface–bottom relationships in the Gulf of Salerno (Tyrrhenian Sea) over the last 34 kyr: Compositional data analysis of palaeontological proxies and geochemical evidence', *Geobios*, 42(5), 561-579, available: http://dx.doi.org/10.1016/j.geobios.2009.02.005.

Di Donato, V., Esposito, P., Russo-Ermolli, E., Scarano, A. and Cheddadi, R. (2008) 'Coupled atmospheric and marine palaeoclimatic reconstruction for the last 35 ka in the Sele Plain–Gulf of Salerno area (southern Italy)', *Quaternary International*, 190(1), 146-157, available: http://dx.doi.org/10.1016/j.quaint.2008.05.006.

Di Donato, V., Martín-Fernández, J., Daunis-i-Estadella, J. and Esposito, P. (2011) 'Analysis of fossil planktonic foraminifera: the sieve mesh effect', in *Proceedings of the 4th International Workshop on Compositional Data Analysis*, Sant Feliu de Guíxols, Spain, CoDaWork 2011.

Dinarès-Turell, J., Hoogakker, B.a.a., Roberts, A.P., Rohling, E.J. and Sagnotti, L. (2003) 'Quaternary climatic control of biogenic magnetite production and eolian dust input in cores from the Mediterranean Sea', *Palaeogeography, Palaeoclimatology, Palaeoecology*, 190, 195-209, available: http://dx.doi.org/10.1016/S0031-0182(02)00605-3.

Dormoy, I., Peyron, O., Combourieu Nebout, N., Goring, S., Kotthoff, U., Magny, M. and Pross, J. (2009) 'Terrestrial climate variability and seasonality changes in the Mediterranean region between 15 000 and 4000 years BP deduced from marine pollen records', *Climate of the Past*, 5(4), 615-632.

Dubois-Dauphin, Q., Montagna, P., Siani, G., Douville, E., Wienberg, C., Hebbeln, D., . . . Colin, C. (2017) 'Hydrological variations of the intermediate water masses of the western Mediterranean Sea during the past 20 ka inferred from neodymium isotopic composition in foraminifera and cold-water corals', *Climate of the Past*, 13(1), 17-37, available: http://dx.doi.org/10.5194/cp-13-17-2017.

El-Geziry, T.M. and Bryden, I.G. (2014) 'The circulation pattern in the Mediterranean Sea: issues for modeller consideration', *Journal of Operational Oceanography*, 3(2), 39-46, available: http://dx.doi.org/10.1080/1755876x.2010.11020116.

Emeis, K.-C., Berger, L., Endler, R., Leipe, T., Struck, U. and Wien, K. (1999) 'Sapropels, Alkenones and Stable Isotopes' in Hieke, W., Hemleben, C., Linke, M., Türkay, M. and Weikert, H., eds., *Mittelmeer 1997/98: Cruise No. 40, 28 October 1997-10 February 1998*, Institut für Meereskunde der Universität Hamburg: Leitstelle Meteor, 157-159.

Emeis, K.-C., Struck, U., Schulz, H.-M., Rosenberg, R., Bernasconi, S., Erlenkeuser, H., . . . Martinez-Ruiz, F. (2000) 'Temperature and salinity variations of Mediterranean Sea surface waters over the last 16,000 years from records of planktonic stable oxygen isotopes and alkenone unsaturation ratios', *Palaeogeography, Palaeoclimatology, Palaeoecology*, 158(3), 259-280.

Emiliani, C. (1954) 'Depth habitats of some species of pelagic foraminifera as indicated by oxygen isotope ratios', *American Journal of Science*, 252(3), 149-158.

Erhardt, T., Capron, E., Rasmussen, S.O., Schüpbach, S., Bigler, M., Adolphi, F. and Fischer, H. (2019) 'Decadal-scale progression of the onset of Dansgaard–Oeschger warming events', *Climate of the Past*, 15(2), 811-825, available: http://dx.doi.org/10.5194/cp-15-811-2019.

Esri (2014) *"World Ocean Base" [basemap]*, available: https://services.arcgisonline.com/ArcGIS/rest/services/Ocean/World_Ocean_Base/Map Server [accessed 25/07/20].

Essallami, L., Sicre, M.A., Kallel, N., Labeyrie, L. and Siani, G. (2007) 'Hydrological changes in the Mediterranean Sea over the last 30,000 years', *Geochemistry, Geophysics, Geosystems*, 8(7), Q07002, available: http://dx.doi.org/10.1029/2007gc001587.

Estrada, M. (1985) 'Deep Phytoplankton and Chlorophyll Maxima in the Western Mediterranean' in Moraitou-Apostolopoulou, M. and Kiortsis, V., eds., *Mediterranean Marine Ecosystems*, Boston, MA: Springer US, 247-277.

Estrada, M. (1996) 'Primary production in the northwestern Mediterranean', *SCIENTIA MARINA*, 60, 55-64.

Estrada, M., Marrasé, C., Latasa, M., Berdalet, E., Delgado, M. and Riera, T. (1993) 'Variability of deep chlorophyll maximum characteristics in the Northwestern Mediterranean', *MARINE ECOLOGY PROGRESS SERIES*, 289-300.

Estrada, M., Vives, F. and Alcaraz, M. (1985) 'Life and the productivity of the open sea' in Margalef, R., ed., *Western Mediterranean*, Oxford: Pergamon Press.

Eynaud, F., de Abreu, L., Voelker, A., Schönfeld, J., Salgueiro, E., Turon, J.-L., . . . Cacho, I. (2009) 'Position of the Polar Front along the western Iberian margin during key cold episodes of the last 45 ka', *Geochemistry, Geophysics, Geosystems*, 10(7), Q07U05, available: http://dx.doi.org/10.1029/2009gc002398.

Fairbanks, R.G. (1989) 'A 17, 000-year glacio-eustatic sea level record: influence of glacial melting rates on the Younger Dryas event and deep-ocean circulation', *Nature*, 342(6250), 637-642.

Fairbanks, R.G., Sverdlove, M., Free, R., Wiebe, P.H. and Be, A.W.H. (1982) 'Vertical distribution and isotopic fractionation of living planktonic foraminifera from the Panama Basin', *Nature*, 298(5877), 841-844.

Fairbanks, R.G. and Wiebe, P.H. (1980) 'Foraminifera and Chlorophyll Maximum: Vertical Distribution, Seasonal Succession, and Paleoceanographic Significance', *Science*, 209(4464), 1524-1526.

Fairbanks, R.G., Wiere, P.H., Allan, W.H.B. and xe (1980) 'Vertical Distribution and Isotopic Composition of Living Planktonic Foraminifera in the Western North Atlantic', *Science*, 207(4426), 61-63.

Faivre, S., Bakran-Petricioli, T., Barešić, J. and Horvatinčić, N. (2015) 'New Data on Marine Radiocarbon Reservoir Effect in the Eastern Adriatic Based on Pre-Bomb Marine Organisms from the Intertidal Zone and Shallow Sea', *Radiocarbon*, 57(04), 527-538, available: http://dx.doi.org/10.2458/azu_rc.57.18452.

Fanget, A.-S., Bassetti, M.-A., Fontanier, C., Tudryn, A. and Berné, S. (2016) 'Sedimentary archives of climate and sea-level changes during the Holocene in the Rhône prodelta (NW Mediterranean Sea)', *Climate of the Past*, 12(12), 2161-2179, available: http://dx.doi.org/10.5194/cp-12-2161-2016.

Favaretto, S., Asioli, A., Miola, A. and Piva, A. (2008) 'Preboreal climatic oscillations recorded by pollen and foraminifera in the southern Adriatic Sea', *Quaternary International*, 190(1), 89-102, available: http://dx.doi.org/10.1016/j.quaint.2008.04.005.

Fiedel, S.J. (2011) 'The mysterious onset of the Younger Dryas', *Quaternary International*, 242(2), 262-266, available: http://dx.doi.org/10.1016/j.quaint.2011.02.044.

Field, D.B. (2004) 'Variability in vertical distributions of planktonic foraminifera in the California Current: Relationships to vertical ocean structure', *Paleoceanography*, 19(2), n/a-n/a, available: http://dx.doi.org/10.1029/2003pa000970.

Fink, H.G., Wienberg, C., De Pol-Holz, R. and Hebbeln, D. (2015) 'Spatio-temporal distribution patterns of Mediterranean cold-water corals (Lophelia pertusa and Madrepora oculata) during the past 14,000 years', *Deep Sea Research Part I: Oceanographic Research Papers*, 103, 37-48, available: http://dx.doi.org/10.1016/j.dsr.2015.05.006.

Fink, H.G., Wienberg, C., De Pol-Holz, R., Wintersteller, P. and Hebbeln, D. (2013) 'Cold-water coral growth in the Alboran Sea related to high productivity during the Late Pleistocene and Holocene', *Marine Geology*, 339, 71-82, available: http://dx.doi.org/10.1016/j.margeo.2013.04.009.

Firestone, R.B., West, A., Kennett, J.P., Becker, L., Bunch, T.E., Revay, Z.S., . . . Wolbach, W.S. (2007) 'Evidence for an extraterrestrial impact 12,900 years ago that contributed to the megafaunal extinctions and the Younger Dryas cooling', *Proceedings of the National Academy of Sciences*, 104(41), 16016-16021, available: http://dx.doi.org/10.1073/pnas.0706977104.

Flantua, S.G.A., Blaauw, M. and Hooghiemstra, H. (2016) 'Geochronological database and classification system for age uncertainties in Neotropical pollen records', *Climate of the Past*, 12(2), 387-414, available: http://dx.doi.org/10.5194/cp-12-387-2016.

Fleitmann, D., Mudelsee, M., Burns, S.J., Bradley, R.S., Kramers, J. and Matter, A. (2008) 'Evidence for a widespread climatic anomaly at around 9.2 ka before present', *Paleoceanography*, 23(1), n/a-n/a, available: http://dx.doi.org/10.1029/2007PA001519.

Fletcher, W.J. and Sánchez Goñi, M.F. (2008) 'Orbital- and sub-orbital-scale climate impacts on vegetation of the western Mediterranean basin over the last 48,000 yr', *Quaternary Research*, 70(3), 451-464, available: http://dx.doi.org/10.1016/j.yqres.2008.07.002.

Fletcher, W.J., Sanchez Goñi, M.F., Peyron, O. and Dormoy, I. (2010) 'Abrupt climate changes of the last deglaciation detected in a Western Mediterranean forest record', *Climate of the Past*, 6(2), 245-264.

Flückiger, J., Blunier, T., Stauffer, B., Chappellaz, J., Spahni, R., Kawamura, K., . . . Dahl-Jensen, D. (2004) 'N2O and CH4 variations during the last glacial epoch: Insight into global processes', *Global Biogeochemical Cycles*, 18(1), GB1020, available: http://dx.doi.org/10.1029/2003gb002122.

Fraile, I., Mulitza, S. and Schulz, M. (2009) 'Modeling planktonic foraminiferal seasonality: Implications for sea-surface temperature reconstructions', *Marine Micropaleontology*, 72(1-2), 1-9, available: http://dx.doi.org/10.1016/j.marmicro.2009.01.003.

Frajka-Williams, E., Ansorge, I.J., Baehr, J., Bryden, H.L., Chidichimo, M.P., Cunningham, S.A., . . . Wilson, C. (2019) 'Atlantic Meridional Overturning Circulation: Observed Transport and Variability', *Frontiers in Marine Science*, 6(260), available: http://dx.doi.org/10.3389/fmars.2019.00260.

Frigola, J., Moreno, A., Cacho, I., Canals, M., Sierro, F.J., Flores, J.A. and Grimalt, J.O. (2008) 'Evidence of abrupt changes in Western Mediterranean Deep Water circulation during the last 50 kyr: A high-resolution marine record from the Balearic Sea', *Quaternary International*, 181(1), 88-104, available: http://dx.doi.org/10.1016/j.quaint.2007.06.016.

Frigola, J., Moreno, A., Cacho, I., Canals, M., Sierro, F.J., Flores, J.A., . . . Curtis, J.H. (2007) 'Holocene climate variability in the western Mediterranean region from a deepwater sediment record', *Paleoceanography*, 22(2), n/a-n/a, available: http://dx.doi.org/10.1029/2006PA001307.

Frisia, S., Borsato, A., SpÖTl, C., Villa, I.M. and Cucchi, F. (2005) 'Climate variability in the SE Alps of Italy over the past 17 000 years reconstructed from a stalagmite record', *Boreas*, 34(4), 445-455, available: http://dx.doi.org/10.1080/03009480500231336.

Funk, C., Hoell, A., Shukla, S., Husak, G. and Michaelsen, J. (2016) 'The East African Monsoon System: Seasonal Climatologies and Recent Variations' in de Carvalho, L. M. V. and Jones, C., eds., *The Monsoons and Climate Change: Observations and Modeling*, Cham: Springer International Publishing, 163-185.

Gačić, M., Lascaratos, A., Manca, B.B. and Mantziafou, A. (2001) 'Adriatic Deep Water and Interaction with the Eastern Mediterranean Sea' in Cushman-Roisin, B., Gacic, M., Poulain, P.-M., Artegiani, A., ed., *Physical Oceanography of the Adriatic Sea: Past, Present and Future*, Netherlands: Springer 111-142.

García-Alix, A., Jiménez-Moreno, G., Jiménez-Espejo, F.J., García-García, F. and Delgado Huertas, A. (2014) 'An environmental snapshot of the Bølling interstadial in Southern Iberia', *Quaternary Research*, 81(2), 284-294, available: http://dx.doi.org/10.1016/j.yqres.2014.01.009.

Garzoli, S. and Maillard, C. (1979) 'Winter circulation in the Sicily and Sardinia straits region', *Deep Sea Research Part A. Oceanographic Research Papers*, 26(8), 933-954, available: http://dx.doi.org/10.1016/0198-0149(79)90106-7.

Genty, D., Blamart, D., Ghaleb, B., Plagnes, V., Causse, C., Bakalowicz, M., . . . Wainer, K. (2006) 'Timing and dynamics of the last deglaciation from European and North African δ13C stalagmite profiles—comparison with Chinese and South Hemisphere stalagmites', *Quaternary Science Reviews*, 25(17-18), 2118-2142, available: http://dx.doi.org/10.1016/j.quascirev.2006.01.030.

Geraga, M., Ioakim, C., Lykousis, V., Tsaila-Monopolis, S. and Mylona, G. (2010) 'The high-resolution palaeoclimatic and palaeoceanographic history of the last 24,000 years in the central Aegean Sea, Greece', *Palaeogeography, Palaeoclimatology, Palaeoecology*, 287(1–4), 101-115, available: http://dx.doi.org/10.1016/j.palaeo.2010.01.023.

Geraga, M., Mylona, G., Tsaila-Monopoli, S., Papatheodorou, G. and Ferentinos, G. (2008) 'Northeastern Ionian Sea: Palaeoceanographic variability over the last 22 ka', *Journal of Marine Systems*, 74(1–2), 623-638, available: http://dx.doi.org/10.1016/j.jmarsys.2008.05.019.

Geraga, M., Tsaila-Monopolis, S., Ioakim, C., Papatheodorou, G. and Ferentinos, G. (2000) 'Evaluation of palaeoenvironmental changes during the last 18,000 years in the Myrtoon basin, SW Aegean Sea', *Palaeogeography, Palaeoclimatology, Palaeoecology*, 156(1–2), 1-17, available: http://dx.doi.org/10.1016/S0031-0182(99)00123-6.

Geraga, M., Tsaila-Monopolis, S., Ioakim, C., Papatheodorou, G. and Ferentinos, G. (2005) 'Short-term climate changes in the southern Aegean Sea over the last 48,000 years', *Palaeogeography, Palaeoclimatology, Palaeoecology*, 220(3–4), 311-332, available: http://dx.doi.org/10.1016/j.palaeo.2005.01.010.

Gertman, I., Ovchinnikov, I.M. and Popov, Y.I. (1990) 'Deep water formation in the Aegean Sea', *Journal of Physical Oceanography*, 32.

Giamali, C., Kontakiotis, G., Koskeridou, E., Ioakim, C. and Antonarakou, A. (2020) 'Key Environmental Factors Controlling Planktonic Foraminiferal and Pteropod Community's Response to Late Quaternary Hydroclimate Changes in the South Aegean Sea (Eastern Mediterranean)', *Journal of Marine Science and Engineering*, 8(9), available: http://dx.doi.org/10.3390/jmse8090709.

Giesecke, T., Davis, B., Brewer, S., Finsinger, W., Wolters, S., Blaauw, M., . . . Bradshaw, R.H.W. (2014) 'Towards mapping the late Quaternary vegetation change of Europe', *Vegetation History and Archaeobotany*, 23(1), 75-86, available: http://dx.doi.org/10.1007/s00334-012-0390-y.

Giorgi, F. (2006) 'Climate change hot-spots', *Geophysical Research Letters*, 33(8), available: http://dx.doi.org/10.1029/2006gl025734.

Giraudeau, J. (1993) 'Planktonic foraminiferal assemblages in surface sediments from the southwest African continental margin', *Marine Geology*, 110(1), 47-62, available: http://dx.doi.org/10.1016/0025-3227(93)90104-4.

GIS Resources (2020) *Types of interpolation methods*, available: http://www.gisresources.com/types-interpolation-methods_3/ [accessed 28/07/20].

Giunta, S., Negri, A., Morigi, C., Capotondi, L., Combourieu-Nebout, N., Emeis, K.C., . . . Vigliotti, L. (2003) 'Coccolithophorid ecostratigraphy and multi-proxy paleoceanographic reconstruction in the Southern Adriatic Sea during the last deglacial

time (Core AD91-17)', *Palaeogeography, Palaeoclimatology, Palaeoecology*, 190, 39-59, available: http://dx.doi.org/10.1016/S0031-0182(02)00598-9.

Givon, Y., Keller Jr, D., Pennel, R., Drobinski, P. and Raveh-Rubin, S. (2021) 'Synoptic-scale drivers of the Mistral wind: link to Rossby wave life cycles and seasonal variability', *Weather and Climate Dynamics Discussions*, 1-37, available: http://dx.doi.org/10.5194/wcd-2021-7.

González-Donoso, J.M., Serrano, F. and Linares, D. (2000) 'Sea surface temperature during the Quaternary at ODP Sites 976 and 975 (western Mediterranean)', *Palaeogeography, Palaeoclimatology, Palaeoecology*, 162(1–2), 17-44, available: http://dx.doi.org/10.1016/S0031-0182(00)00103-6.

Goswami, B.N. (2012) 'South Asian monsoon' in W. K. M. Lau and Waliser, D. E., eds., *Intraseasonal Variability in the Atmosphere–Ocean Climate System*, Second ed., Berlin Heidelberg: Springer-Verlag, 21-72.

Gould, W.J. (1985) 'Physical oceanography of the Azores front', *Progress in Oceanography*, 14, 167-190, available: http://dx.doi.org/10.1016/0079-6611(85)90010-2.

Grant, K.M., Grimm, R., Mikolajewicz, U., Marino, G., Ziegler, M. and Rohling, E.J. (2016) 'The timing of Mediterranean sapropel deposition relative to insolation, sea-level and African monsoon changes', *Quaternary Science Reviews*, 140, 125-141, available: http://dx.doi.org/10.1016/j.quascirev.2016.03.026.

Grant, K.M., Rohling, E.J., Ramsey, C.B., Cheng, H., Edwards, R.L., Florindo, F., . . . Williams, F. (2014) 'Sea-level variability over five glacial cycles', *Nat Commun*, 5, 5076, available: http://dx.doi.org/10.1038/ncomms6076.

Greco, M., Jonkers, L., Kretschmer, K., Bijma, J. and Kucera, M. (2019) 'Depth habitat of the planktonic foraminifera *Neogloboquadrina pachyderma* in the northern high latitudes explained by sea-ice and chlorophyll concentrations', *Biogeosciences*, 16(17), 3425-3437, available: http://dx.doi.org/10.5194/bg-16-3425-2019.

GRID-Arendal (2013a) *Chlorophyll-a concentration,* available: http://www.grida.no/resources/5912

GRID-Arendal (2013b) *River discharge of freshwater into the Mediterranean,* available: http://www.grida.no/resources/5897

Grisogono, B. and BeluŠIĆ, D. (2009) 'A review of recent advances in understanding the meso- and microscale properties of the severe Bora wind', *Tellus A*, 61(1), 1-16, available: http://dx.doi.org/10.1111/j.1600-0870.2008.00369.x.

Grootes, P.M. and Stuiver, M. (1999) *GISP2 Oxygen Isotope Data* [dataset], available: 10.1594/PANGAEA.56094.

Grootes, P.M., Stuiver, M., White, J.W.C., Johnsen, S. and Jouzel, J. (1993) 'Comparison of oxygen isotope records from the GISP2 and GRIP Greenland ice cores', *Nature*, 366(6455), 552-554, available: http://dx.doi.org/10.1038/366552a0.

Gupta, B.K.S. ed. (1999) *Modern foraminifera*, Dordrecht: Kluwer Academic Publishers.

Haigh, J.D. (1994) 'The role of stratospheric ozone in modulating the solar radiative forcing of climate', *Nature*, 370(6490), 544-546, available: http://dx.doi.org/10.1038/370544a0.

Haigh, J.D. (1996) 'The Impact of Solar Variability on Climate', *Science*, 272(5264), 981-984, available: http://dx.doi.org/10.1126/science.272.5264.981.

Hamann, Y., Ehrmann, W., Schmiedl, G., Krüger, S., Stuut, J.B. and Kuhnt, T. (2008) 'Sedimentation processes in the Eastern Mediterranean Sea during the Late Glacial and Holocene revealed by end-member modelling of the terrigenous fraction in marine sediments', *Marine Geology*, 248(1-2), 97-114, available: http://dx.doi.org/10.1016/j.margeo.2007.10.009.

Hammer, Ø., Harper, D.A.T. and Ryan, P.D. (2001) 'PAST: Paleontological Statistics Software Package for Education and Data Analysis', *Palaeontologia Electronica*, 4(1), 9.

Harding, A., Palutikof, J. and Holt, T. (2009) 'The climate system' in Woodward, J., ed., *The Physical Geography of the Mediterranean* Oxford University Press Oxford, 69-88.

Hayes, A., Kučera, M., Kallel, N., Sbaffi, L. and Rohling, E.J. (2005) 'Glacial Mediterranean sea surface temperatures based on planktonic foraminiferal assemblages', *Quaternary Science Reviews*, 24(7–9), 999-1016, available: http://dx.doi.org/10.1016/j.quascirev.2004.02.018.

Hayes, A., Rohling, E.J., De Rijk, S., Kroon, D. and Zachariasse, W.J. (1999) 'Mediterranean planktonic foraminiferal faunas during the last glacial cycle', *Marine Geology*, 153(1–4), 239-252, available: http://dx.doi.org/10.1016/S0025-3227(98)00019-X.

Hays, J.D., Imbrie, J. and Shackleton, N.J. (1976) 'Variations in the Earth's orbit: pacemaker of the ice ages', *Science*, 194(4270), 1121-1132.

Head, M.J. and Gibbard, P.L. (2015) 'Formal subdivision of the Quaternary System/Period: Past, present, and future', *Quaternary International*, 383, 4-35.

Heaton, T.J., Köhler, P., Butzin, M., Bard, E., Reimer, R.W., Austin, W.E.N., . . . Skinner, L.C. (2020) 'Marine20—The Marine Radiocarbon Age Calibration Curve (0–55,000 cal BP)', *Radiocarbon*, 62(4), 779-820, available: http://dx.doi.org/10.1017/rdc.2020.68.

Heinrich, H. (1988) 'Origin and consequences of cyclic ice rafting in the Northeast Atlantic Ocean during the past 130,000 years', *Quaternary Research*, 29, 142-152, available: http://dx.doi.org/10.1016/0033-5894(88)90057-9.

Hemleben, C., Spindler, M. and Anderson, O.R. (1989) 'Modern planktonic foraminifera' in, Berlin: Springer-Verlag, 363.

Hemleben, C., Spindler, M., Breitinger, I. and Ott, R. (1987) 'Morphological and physiological responses of Globigerinoides sacculifer (Brady) under varying laboratory conditions', *Marine Micropaleontology*, 12(0), 305-324, available: http://dx.doi.org/10.1016/0377-8398(87)90025-9.

Hemming, S.R. (2004) 'Heinrich events: Massive late Pleistocene detritus layers of the North Atlantic and their global climate imprint', *Reviews of Geophysics*, 42(1), available: http://dx.doi.org/10.1029/2003rg000128.

Hernández-Almeida, I., Bárcena, M.A., Flores, J.A., Sierro, F.J., Sanchez-Vidal, A. and Calafat, A. (2011) 'Microplankton response to environmental conditions in the Alboran Sea (Western Mediterranean): One year sediment trap record', *Marine Micropaleontology*, 78(1-2), 14-24, available: http://dx.doi.org/10.1016/j.marmicro.2010.09.005.

Herrle, J.O., Bollmann, J., Gebuhr, C., Schulz, H., Sheward, R.M. and Giesenberg, A. (2018) 'Black Sea outflow response to Holocene meltwater events', *Sci Rep*, 8(1), 4081, available: http://dx.doi.org/10.1038/s41598-018-22453-z.

Hess, D. and Tasa, D. (2010) *McKnight's Physical Geography: A Landscape Appreciation*, 10 ed., Boston: Prentice Hall.

Hessler, I., Harrison, S.P., Kučera, M., Waelbroeck, C., Chen, M.T., Anderson, C., . . . Londeix, L. (2014) 'Implication of methodological uncertainties for mid-Holocene sea surface temperature reconstructions', *Climate of the Past*, 10(6), 2237-2252, available: http://dx.doi.org/10.5194/cp-10-2237-2014.

Heymann, C., Nelle, O., Dörfler, W., Zagana, H., Nowaczyk, N., Xue, J. and Unkel, I. (2013) 'Late Glacial to mid-Holocene palaeoclimate development of Southern Greece inferred from the sediment sequence of Lake Stymphalia (NE-Peloponnese)', *Quaternary International*, 302, 42-60, available: http://dx.doi.org/10.1016/j.quaint.2013.02.014.

Hieke, W., Hemleben, C., Linke, M., Türkay, M. and Weikert, H. (1999) *Mittelmeer 1997/98: Cruise No. 40, 28 October 1997-10 February 1998*, Institut für Meereskunde der Universität Hamburg: Leitstelle Meteor.

Hilbrecht, H. (1996) *Extant planktic foraminifera and the physical environment in the Atlantic and Indian Oceans: an atlas based on Climap and Levitus (1982) data*, Mitteilungen aus dem Geologischen Institut der Eidgen. Technischen Hochschule und der Universität Zürich, Neue Folge, No. 300, pp 93, available: https://www.ngdc.noaa.gov/mgg/geology/hh1996/ [accessed 16 Feb 2017].

HMSO (1962) *Weather in the Mediterranean I: General Meteorology*, 2nd ed., London: Her Majesty's Stationery Office.

Hodell, D.A., Nicholl, J.A., Bontognali, T.R.R., Danino, S., Dorador, J., Dowdeswell, J.A., . . . Röhl, U. (2017) 'Anatomy of Heinrich Layer 1 and its Role in the Last Deglaciation', *Paleoceanography*, 32(3), available: http://dx.doi.org/10.1002/2016pa003028.

Holliday, V.T., Surovell, T., Meltzer, D.J., Grayson, D.K. and Boslough, M. (2014) 'The Younger Dryas impact hypothesis: a cosmic catastrophe', *Journal of Quaternary Science*, 29(6), 515-530, available: http://dx.doi.org/10.1002/jqs.2724.

Huber, C., Leuenberger, M., Spahni, R., Flückiger, J., Schwander, J., Stocker, T.F., . . . Jouzel, J. (2006) 'Isotope calibrated Greenland temperature record over Marine Isotope Stage 3 and its relation to CH4', *Earth and Planetary Science Letters*, 243(3), 504-519, available: http://dx.doi.org/10.1016/j.epsl.2006.01.002.

Hughes, P., Woodward, J. and Gibbard, P. (2006) 'Quaternary glacial history of the Mediterranean mountains', *Progress in physical geography*, 30(3), 334-364, available: http://dx.doi.org/10.1191/0309133306pp481ra.

Hughes, P.D. and Woodward, J.C. (2017) 'Quaternary glaciation in the Mediterranean mountains: a new synthesis', *Geological Society, London, Special Publications*, 433(1), 1-23, available: http://dx.doi.org/10.1144/sp433.14.

Hurrell, J.W. (1995) 'Decadal trends in the North Atlantic Oscillation, regional temperatures and precipitation', *Science*, 269, 676-679.

Hutson, W.H. (1980) 'The agulhas current during the late pleistocene: analysis of modern faunal analogs', *Science*, 207(4426), 64-6, available: http://dx.doi.org/10.1126/science.207.4426.64.

Huybers, P. and Langmuir, C. (2009) 'Feedback between deglaciation, volcanism, and atmospheric CO2', *Earth and Planetary Science Letters*, 286(3-4), 479-491, available: http://dx.doi.org/10.1016/j.epsl.2009.07.014.

Iles, C.E., Hegerl, G.C. and Schurer, A.P. (2015) 'Volcanic eruptions and the global hydrological cycle', *Past Global Changes Magazine*, 23(2), 56-57.

Imbrie, J., Berger, A., Boyle, E.A., Clemens, S.C., Duffy, A., Howard, W.R., . . . Toggweiler, J.R. (1993) 'On the structure and origin of major glaciation cycles 2. The 100,000-year cycle', *Paleoceanography*, 8(6), 699-735, available: http://dx.doi.org/10.1029/93PA02751.

Imbrie, J. and Kipp, N.G. (1971) 'A new micropaleontological method for quantitative paleoclimatology: application to a late Pleistocene Caribbean core', *The late Cenozoic glacial ages*, 3, 71-181.

Incarbona, A., Di Stefano, E., Sprovieri, R., Bonomo, S., Censi, P., Dinarès-Turell, J. and Spoto, S. (2008) 'Variability in the vertical structure of the water column and paleoproductivity reconstruction in the central-western Mediterranean during the Late Pleistocene', *Marine Micropaleontology*, 69(1), 26-41, available: http://dx.doi.org/10.1016/j.marmicro.2007.11.007.

İşler, E.B., Aksu, A.E. and Hiscott, R.N. (2016a) 'Late Quaternary paleoceanographic evolution of the Aegean Sea: planktonic foraminifera and stable isotopes', *Turkish Journal of Earth Sciences*, 25, 19-45, available: http://dx.doi.org/10.3906/yer-1501-36.

İşler, E.B., Hiscott, R.N. and Aksu, A.E. (2016b) 'Late Quaternary chronostratigraphy of the Aegean Sea sediments: special reference to the ages of sapropels S1–S5', *Turkish Journal of Earth Sciences*, 25, 1-18, available: http://dx.doi.org/10.3906/yer-1501-37.

Itou, M., Ono, T., Oba, T. and Noriki, S. (2001) 'Isotopic composition and morphology of living Globorotalia scitula: a new proxy of sub-intermediate ocean carbonate chemistry?', *Marine Micropaleontology*, 42(3–4), 189-210, available: http://dx.doi.org/10.1016/S0377-8398(01)00015-9.

Ivanovic, R.F., Gregoire, L.J., Burke, A., Wickert, A.D., Valdes, P.J., Ng, H.C., . . . Dentith, J.E. (2018) 'Acceleration of Northern Ice Sheet Melt Induces AMOC Slowdown and Northern Cooling in Simulations of the Early Last Deglaciation', *Paleoceanography and Paleoclimatology*, available: http://dx.doi.org/10.1029/2017pa003308.

Ivy-Ochs, S. (2015) 'Glacier variations in the European Alps at the end of the last glaciation', *Cuadernos de Investigación Geográfica*, 41(2), available: http://dx.doi.org/10.18172/cig.2750.

Ivy-Ochs, S., Kerschner, H. and Schlüchter, C. (2007) 'Cosmogenic nuclides and the dating of Lateglacial and Early Holocene glacier variations: The Alpine perspective', *Quaternary International*, 164-165, 53-63, available: http://dx.doi.org/10.1016/j.quaint.2006.12.008.

Iwasaki, S., Kimoto, K., Kuroyanagi, A. and Kawahata, H. (2017) 'Horizontal and vertical distributions of planktic foraminifera in the subarctic Pacific', *Marine Micropaleontology*, 130, 1-14, available: http://dx.doi.org/10.1016/j.marmicro.2016.12.001.

Jalali, B., Sicre, M.-A., Kallel, N., Azuara, J., Combourieu-Nebout, N., Bassetti, M.-A. and Klein, V. (2017) 'High-resolution Holocene climate and hydrological variability from

two major Mediterranean deltas (Nile and Rhone)', *The Holocene*, 095968361668325, available: http://dx.doi.org/10.1177/0959683616683258.

Jalali, B., Sicre, M.-A., Klein, V., Schmidt, S., Maselli, V., Lirer, F., . . . Châles, F. (2018) 'Deltaic and Coastal Sediments as Recorders of Mediterranean Regional Climate and Human Impact Over the Past Three Millennia', *Paleoceanography and Paleoclimatology*, 33(6), 579-593, available: http://dx.doi.org/10.1029/2017pa003298.

Jalali, B., Sicre, M.A., Bassetti, M.A. and Kallel, N. (2016) 'Holocene climate variability in the North-Western Mediterranean Sea (Gulf of Lions)', *Climate of the Past*, 12(1), 91-101, available: http://dx.doi.org/10.5194/cp-12-91-2016.

Jallet, L. and Giresse, P. (2005) 'Construction of the Pyreneo-Languedocian Sedimentary Ridge and associated sediment waves in the deep western Gulf of Lions (Western Mediterranean)', *Marine and Petroleum Geology*, 22(6–7), 865-888, available: http://dx.doi.org/10.1016/j.marpetgeo.2005.03.008.

Jalut, G., Amat, A.E., Bonnet, L., Gauquelin, T. and Fontugne, M. (2000) 'Holocene climatic changes in the Western Mediterranean, from south-east France to south-east Spain', *Palaeogeography, Palaeoclimatology, Palaeoecology*, 160(3), 255-290.

Jalut, G., Amat, A.E., i Mora, S.R., Fontugne, M., Mook, R., Bonnet, L. and Gauquelin, T. (1997) 'Holocene climatic changes in the western Mediterranean: installation of the Mediterranean climate', *Comptes Rendus de l'Académie des Sciences-Series IIA-Earth and Planetary Science*, 325(5), 327-334.

Jansa, A., Alpert, P., Arbogast, P., Buzzi, A., Ivancan-Picek, B., Kotroni, V., . . . Speranza, A. (2014) 'MEDEX: a general overview', *Natural Hazards and Earth System Sciences*, 14(8), 1965-1984, available: http://dx.doi.org/10.5194/nhess-14-1965-2014.

Jansa, A., Genoves, A., Picornell, M.A., Campins, J., Riosalido, R. and Carretero, O. (2001) 'Western Mediterranean cyclones and heavy rain. Part 2: Statistical approach', *Meteorological Applications*, 8(1), 43-56, available: http://dx.doi.org/10.1017/S1350482701001049.

Jansen, E., Overpeck, J., Briffa, K.R., Duplessy, J.-C., Joos, F., Masson-Delmotte, V., . . . Zhang, D. (2007) 'Palaeoclimate' in Solomon, S., Qin, D., Manning, M., Chen, Z., Marquis, M., Averyt, K. B., Tignor, M. and Miller, H. L., eds., *Climate Change 2007: The Physical Science Basis. Contribution of Working Group I to the Fourth Assessment Report of the Intergovernmental Panel on Climate Change*, Cambridge: Cambridge University Press, 434-497.

Jiménez-Amat, P. and Zahn, R. (2015) 'Offset timing of climate oscillations during the last two glacial-interglacial transitions connected with large-scale freshwater perturbation', *Paleoceanography*, 30(6), 768-788, available: http://dx.doi.org/10.1002/2014PA002710.

Jimenez-Espejo, F.J., Martinez-Ruiz, F., Sakamoto, T., Iijima, K., Gallego-Torres, D. and Harada, N. (2007) 'Paleoenvironmental changes in the western Mediterranean since the last glacial maximum: High resolution multiproxy record from the Algero–Balearic basin', *Palaeogeography, Palaeoclimatology, Palaeoecology*, 246(2–4), 292-306, available: http://dx.doi.org/10.1016/j.palaeo.2006.10.005.

Johnsen, S.J., Clausen, H.B., Dansgaard, W., Fuhrer, K., Gundestrup, N., Hammer, C.U., . . . Steffensen, J.P. (1992) 'Irregular glacial interstadials recorded in a new Greenland ice core', *Nature*, 359(6393), 311-313, available: http://dx.doi.org/10.1038/359311a0.

Jolliffe, I.T. and Cadima, J. (2016) 'Principal component analysis: a review and recent developments', *Philos Trans A Math Phys Eng Sci*, 374(2065), 20150202, available: http://dx.doi.org/10.1098/rsta.2015.0202.

Jonkers, L. and Kučera, M. (2015) 'Global analysis of seasonality in the shell flux of extant planktonic Foraminifera', *Biogeosciences*, 12(7), 2207-2226, available: http://dx.doi.org/10.5194/bg-12-2207-2015.

Jonkers, L. and Kučera, M. (2019) 'Sensitivity to species selection indicates the effect of nuisance variables on marine microfossil transfer functions', *Climate of the Past*, 15(3), 881-891, available: http://dx.doi.org/10.5194/cp-15-881-2019.

Jonkers, L., Reynolds, C.E., Richey, J. and Hall, I.R. (2015) 'Lunar periodicity in the shell flux of planktonic foraminifera in the Gulf of Mexico', *Biogeosciences*, 12(10), 3061-3070, available: http://dx.doi.org/10.5194/bg-12-3061-2015.

Jorissen, F.J., Asioli, A., Borsetti, A.M., Capotondi, L., de Visser, J.P., Hilgen, F.J., . . . Zachariasse, W.J. (1993) 'Late Quaternary central Mediterranean biochronology', *Marine Micropaleontology*, 21(1–3), 169-189, available: http://dx.doi.org/10.1016/0377-8398(93)90014-O.

Josey, S.A., Somot, S. and Tsimplis, M. (2011) 'Impacts of atmospheric modes of variability on Mediterranean Sea surface heat exchange', *Journal of Geophysical Research*, 116(C2), available: http://dx.doi.org/10.1029/2010jc006685.

Jouet, G., Berné, S., Rabineau, M., Bassetti, M.A., Bernier, P., Dennielou, B., . . . Taviani, M. (2006) 'Shoreface migrations at the shelf edge and sea-level changes around the Last Glacial Maximum (Gulf of Lions, NW Mediterranean)', *Marine Geology*, 234(1-4), 21-42, available: http://dx.doi.org/10.1016/j.margeo.2006.09.012.

Jouzel, J. (2013) 'A brief history of ice core science over the last 50 yr', *Climate of the Past*, 9(6), 2525-2547, available: http://dx.doi.org/10.5194/cp-9-2525-2013.

Kallel, N., Duplessy, J.-C., Labeyrie, L., Fontugne, M. and Paterne, M. (2004) 'Mediterranean Sea palaeohydrology and pluvial periods during the Late Quaternary' in Battarbee, R. W., Gasse, F. and Stickley, C. E., eds., *Past Climate Variability through Europe and Africa* Springer, 307-324.

Kallel, N., Paterne, M., Duplessy, J., Vergnaudgrazzini, C., Pujol, C., Labeyrie, L., . . . Pierre, C. (1997a) 'Enhanced rainfall in the Mediterranean region during the last sapropel event', *Oceanolica Acta*, 20(5), 697-712.

Kallel, N., Paterne, M., Labeyrie, L., Duplessy, J.-C. and Arnold, M. (1997b) 'Temperature and salinity records of the Tyrrhenian Sea during the last 18,000 years', *Palaeogeography, Palaeoclimatology, Palaeoecology*, 135(1–4), 97-108, available: http://dx.doi.org/10.1016/S0031-0182(97)00021-7.

Kennett, J.P. and Srinivasan, M. (1983) *Neogene planktonic foraminifera: a phylogenetic atlas*, Stroudsburg: Hutchinson Ross.

Kettner, A.J. and Syvitski, J.P.M. (2009) 'Fluvial responses to environmental perturbations in the Northern Mediterranean since the Last Glacial Maximum', *Quaternary Science Reviews*, 28(23-24), 2386-2397, available: http://dx.doi.org/10.1016/j.quascirev.2009.05.003.

Kjær, K.H., Larsen, N.K., Binder, T., Bjørk, A.A., Eisen, O., Fahnestock, M.A., . . . MacGregor, J.A. (2018) 'A large impact crater beneath Hiawatha Glacier in northwest Greenland', *Science Advances*, 4(11), eaar8173, available: http://dx.doi.org/10.1126/sciadv.aar8173.

Klein, B., Roether, W., Manca, B.B., Bregant, D., Beitzel, V., Kovacevic, V. and Luchetta, A. (1999) 'The large deep water transient in the Eastern Mediterranean', *Deep Sea Research Part I: Oceanographic Research Papers*, 46(3), 371-414, available: http://dx.doi.org/10.1016/S0967-0637(98)00075-2.

Köhler, P., Knorr, G., Buiron, D., Lourantou, A. and Chappellaz, J. (2011) 'Abrupt rise in atmospheric CO_2 at the onset of the Bølling/Allerød: in-situ ice core data versus true atmospheric signals', *Climate of the Past*, 7(2), 473-486, available: http://dx.doi.org/10.5194/cp-7-473-2011.

Koltermann, K.P., Gouretski, V. and Jancke, K. (2011) *Hydrographic Atlas of the World Ocean Circulation Experiment (WOCE): Volume 3: Atlantic Ocean*, Southampton, UK: International WOCE Project Office.

Kontakiotis, G. (2016) 'Late Quaternary paleoenvironmental reconstruction and paleoclimatic implications of the Aegean Sea (eastern Mediterranean) based on paleoceanographic indexes and stable isotopes', *Quaternary International*, 401, 28-42, available: http://dx.doi.org/10.1016/j.quaint.2015.07.039.

Kostov, Y., Johnson, H.L. and Marshall, D.P. (2019) 'AMOC sensitivity to surface buoyancy fluxes: the role of air-sea feedback mechanisms', *Climate Dynamics*, available: http://dx.doi.org/10.1007/s00382-019-04802-4.

Kothe, S., Lüthi, D. and Ahrens, B. (2014) 'Analysis of the West African Monsoon system in the regional climate model COSMO-CLM', *International Journal of Climatology*, 34(2), 481-493, available: http://dx.doi.org/10.1002/joc.3702.

Kretschmer, K., Jonkers, L., Kucera, M. and Schulz, M. (2018) 'Modeling seasonal and vertical habitats of planktonic foraminifera on a global scale', *Biogeosciences*, 15(14), 4405-4429, available: http://dx.doi.org/10.5194/bg-15-4405-2018.

Kretschmer, K., Kučera, M. and Schulz, M. (2016) 'Modeling the distribution and seasonality of Neogloboquadrina pachyderma in the North Atlantic Ocean during Heinrich Stadial 1', *Paleoceanography*, 31, 986–1010, available: http://dx.doi.org/10.1002/2015pa002819.

Kučera, M. (2007) 'Planktonic Foraminifera as Tracers of Past Oceanic Environments' in Hillaire–Marcel, C. and De Vernal, A., eds., *Developments in Marine Geology* Elsevier, 213-262.

Kučera, M. and Darling, K.F. (2002) 'Cryptic species of planktonic foraminifera: their effect on palaeoceanographic reconstructions', *Philosophical Transactions of the Royal Society of London. Series A: Mathematical, Physical and Engineering Sciences*, 360(1793), 695-718.

Kučera, M., Rosell-Melé, A., Schneider, R., Waelbroeck, C. and Weinelt, M. (2005a) 'Multiproxy approach for the reconstruction of the glacial ocean surface (MARGO)', *Quaternary Science Reviews*, 24(7–9), 813-819, available: http://dx.doi.org/10.1016/j.quascirev.2004.07.017.

Kučera, M., Weinelt, M., Kiefer, T., Pflaumann, U., Hayes, A., Weinelt, M., . . . Cortijo, E. (2005b) 'Reconstruction of sea-surface temperatures from assemblages of planktonic foraminifera: multi-technique approach based on geographically constrained calibration data sets and its application to glacial Atlantic and Pacific Oceans', *Quaternary Science*

Reviews, 24(7-9), 951-998, available: http://dx.doi.org/10.1016/j.quascirev.2004.07.014.

Kuhlmann, J., Asioli, A., Trincardi, F., Klügel, A. and Huhn, K. (2015) 'Sedimentary response to Milankovitch-type climatic oscillations and formation of sediment undulations: evidence from a shallow-shelf setting at Gela Basin on the Sicilian continental margin', *Quaternary Science Reviews*, 108(0), 76-94, available: http://dx.doi.org/10.1016/j.quascirev.2014.10.030.

Kuroyanagi, A. and Kawahata, H. (2004) 'Vertical distribution of living planktonic foraminifera in the seas around Japan', *Marine Micropaleontology*, 53(1), 173-196, available: http://dx.doi.org/10.1016/j.marmicro.2004.06.001.

Kusuma, D., Murdimanto, A., Sukresno, B. and Jatisworo, D. (2018) 'Comparison of interpolation methods for sea surface temperature data D', *JFMR-Journal of Fisheries and Marine Research*, 2(2), 103-115, available: http://dx.doi.org/10.21776/ub.jfmr.2018.002.02.7.

Kutterolf, S., Jegen, M., Mitrovica, J.X., Kwasnitschka, T., Freundt, A. and Huybers, P.J. (2013) 'A detection of Milankovitch frequencies in global volcanic activity', *Geology*, 41(2), 227-230, available: http://dx.doi.org/10.1130/g33419.1.

Lambeck, K., Rouby, H., Purcell, A., Sun, Y. and Sambridge, M. (2014) 'Sea level and global ice volumes from the Last Glacial Maximum to the Holocene', *Proc Natl Acad Sci U S A*, 111(43), 15296-303, available: http://dx.doi.org/10.1073/pnas.1411762111.

Lane, C.S., Brauer, A., Blockley, S.P.E. and Dulski, P. (2013) 'Volcanic ash reveals time-transgressive abrupt climate change during the Younger Dryas', *Geology*, 41(12), 1251-1254, available: http://dx.doi.org/10.1130/g34867.1.

Langgut, D., Almogi-Labin, A., Bar-Matthews, M. and Weinstein-Evron, M. (2011) 'Vegetation and climate changes in the South Eastern Mediterranean during the Last Glacial-Interglacial cycle (86 ka): new marine pollen record', *Quaternary Science Reviews*, 30(27), 3960-3972.

Latasa, M., Cabello, A.M., Morán, X.A.G., Massana, R. and Scharek, R. (2017) 'Distribution of phytoplankton groups within the deep chlorophyll maximum', *Limnology and Oceanography*, 62(2), 665-685, available: http://dx.doi.org/10.1002/lno.10452.

Lazzari, P., Solidoro, C., Ibello, V., Salon, S., Teruzzi, A., Béranger, K., . . . Crise, A. (2012) 'Seasonal and inter-annual variability of plankton chlorophyll and primary production in the Mediterranean Sea: a modelling approach', *Biogeosciences*, 9(1), 217-233, available: http://dx.doi.org/10.5194/bg-9-217-2012.

Le Houedec, S., Mojtahid, M., Bicchi, E., Lange, G.J. and Hennekam, R. (2020) 'Suborbital Hydrological Variability Inferred From Coupled Benthic and Planktic Foraminiferal-Based Proxies in the Southeastern Mediterranean During the Last 19 ka', *Paleoceanography and Paleoclimatology*, 35(2), available: http://dx.doi.org/10.1029/2019pa003827.

Lessa, D., Morard, R., Jonkers, L., Venancio, I.M., Reuter, R., Baumeister, A., . . . Kucera, M. (2020) 'Distribution of planktonic foraminifera in the subtropical South Atlantic: depth hierarchy of controlling factors', *Biogeosciences*, 17(16), 4313-4342, available: http://dx.doi.org/10.5194/bg-17-4313-2020.

Li, C. and Born, A. (2019) 'Coupled atmosphere-ice-ocean dynamics in Dansgaard-Oeschger events', *Quaternary Science Reviews*, 203, 1-20, available: http://dx.doi.org/10.1016/j.quascirev.2018.10.031.

Lie, O. and Paasche, O. (2006) 'How extreme was northern hemisphere seasonality during the Younger Dryas?', *Quaternary Science Reviews*, 25(5-6), 404-407, available: http://dx.doi.org/10.1016/j.quascirev.2005.11.003.

Lionello, P., Abrantes, F., Congedi, L., Dulac, F., Gacic, M., Gomis, D., . . . Xoplaki, E. (2012a) 'Introduction: Mediterranean Climate—Background Information' in Lionello, P., ed., *The Climate of the Mediterranean Region*, Oxford: Elsevier, xxxv-xc.

Lionello, P., Bhend, J., Buzzi, A., Della-Marta, P.M., Krichak, S.O., Jansà, A., . . . Trigo, R. (2006a) 'Cyclones in the Mediterranean region: Climatology and effects on the environment' in Lionello, P., Malanotte-Rizzoli, P. and Boscolo, R., eds., *Mediterranean Climate Variability* Elsevier, 325-372.

Lionello, P., Gacic, M., Gomis, D., Garcia-Herrera, R., Giorgi, F., Planton, S., . . . Xoplaki, E. (2012b) 'Program focuses on climate of the Mediterranean region', *Eos, Transactions American Geophysical Union*, 93(10), 105-106, available: http://dx.doi.org/10.1029/2012EO100001.

Lionello, P., Malanotte-Rizzoli, P., Boscolo, R., Alpert, P., Artale, V., Li, L., . . . Xoplaki, E. (2006b) 'The Mediterranean climate: An overview of the main characteristics and issues' in Lionello, P., Malanotte-Rizzoli, P. and Boscolo, R., eds., *Mediterranean Climate Variability*, Amsterdam: Elsevier, 1-26.

Lirer, F., Sprovieri, M., Ferraro, L., Vallefuoco, M., Capotondi, L., Cascella, A., . . . Lubritto, C. (2013) 'Integrated stratigraphy for the Late Quaternary in the eastern Tyrrhenian Sea', *Quaternary International*, 292(0), 71-85, available: http://dx.doi.org/10.1016/j.quaint.2012.08.2055.

Lisiecki, L.E. and Raymo, M.E. (2005) 'A Pliocene-Pleistocene stack of 57 globally distributed benthic δ18O records', *Paleoceanography*, 20, PA1003, available: http://dx.doi.org/10.1029/2004pa001071.

Liu, Z., Carlson, A.E., He, F., Brady, E.C., Otto-Bliesner, B.L., Briegleb, B.P., . . . Zhu, J. (2012) 'Younger Dryas cooling and the Greenland climate response to CO2', *Proc Natl Acad Sci U S A*, 109(28), 11101-4, available: http://dx.doi.org/10.1073/pnas.1202183109.

Liu, Z., Otto-Bliesner, B.L., He, F., Brady, E.C., Tomas, R., Clark, P.U., . . . Cheng, J. (2009) 'Transient simulation of last deglaciation with a new mechanism for Bølling-Allerød warming', *Science*, 325(5938), 310-4, available: http://dx.doi.org/10.1126/science.1171041.

Locarnini, R.A., A. V. Mishonov, O. K. Baranova, T. P. Boyer, M. M. Zweng, H. E. Garcia, J. R. Reagan, D. Seidov, K. Weathers, C. R. Paver, and I. Smolyar (2018) 'World Ocean Atlas 2018, Volume 1: Temperature.' in Mishonov, A., ed., *NOAA Atlas NESDIS 81*, 52.

Lockwood, J.G. (1985) *World climatic systems*, London: Edward Arnold.

Loeblich, A.R.J. and Tappan, H. (1987) *Foraminiferal genera and their classification*, New York: Van Nostrand Reinhold.

Lohmann, G. (2016) 'Atmospheric bridge on orbital time scales', *Theoretical and Applied Climatology*, 128(3-4), 709-718, available: http://dx.doi.org/10.1007/s00704-015-1725-2.

Lohmann, G.P. and Schweitzer, P.N. (1990) 'Globorotalia truncatulinoides' Growth and chemistry as probes of the past thermocline: 1. Shell size', *Paleoceanography*, 5(1), 55-75, available: http://dx.doi.org/10.1029/PA005i001p00055.

Lombard, F., Labeyrie, L., Michel, E., Spero, H.J. and Lea, D.W. (2009) 'Modelling the temperature dependent growth rates of planktic foraminifera', *Marine Micropaleontology*, 70(1-2), 1-7, available: http://dx.doi.org/10.1016/j.marmicro.2008.09.004.

Lombo Tombo, S., Dennielou, B., Berné, S., Bassetti, M.A., Toucanne, S., Jorry, S.J., . . . Fontanier, C. (2015) 'Sea-level control on turbidite activity in the Rhone canyon and the upper fan during the Last Glacial Maximum and Early deglacial', *Sedimentary Geology*, 323, 148-166, available: http://dx.doi.org/10.1016/j.sedgeo.2015.04.009.

Lončarić, N., van Iperen, J., Kroon, D. and Brummer, G.-J.A. (2007) 'Seasonal export and sediment preservation of diatomaceous, foraminiferal and organic matter mass fluxes in a trophic gradient across the SE Atlantic', *Progress in Oceanography*, 73(1), 27-59, available: http://dx.doi.org/10.1016/j.pocean.2006.10.008.

Lowe, J.J. and Walker, M.J. (2014) *Reconstructing quaternary environments*, 3rd ed., Routledge.

Ludwig, W., Dumont, E., Meybeck, M. and Heussner, S. (2009) 'River discharges of water and nutrients to the Mediterranean and Black Sea: Major drivers for ecosystem changes during past and future decades?', *Progress in Oceanography*, 80(3-4), 199-217, available: http://dx.doi.org/10.1016/j.pocean.2009.02.001.

Lynch-Stieglitz, J. (2017) 'The Atlantic Meridional Overturning Circulation and Abrupt Climate Change', *Ann Rev Mar Sci*, 9, 83-104, available: http://dx.doi.org/10.1146/annurev-marine-010816-060415.

MacAyeal, D.R. (1993) 'Binge/purge oscillations of the Laurentide Ice Sheet as a cause of the North Atlantic's Heinrich events', *Paleoceanography*, 8(6), 775-784, available: http://dx.doi.org/10.1029/93pa02200.

Maclennan, J., Jull, M., McKenzie, D., Slater, L. and Grönvold, K. (2002) 'The link between volcanism and deglaciation in Iceland', *Geochemistry, Geophysics, Geosystems*, 3(11), 1-25, available: http://dx.doi.org/10.1029/2001gc000282.

Magyari, E.K., Pál, I., Vincze, I., Veres, D., Jakab, G., Braun, M., . . . Korponai, J. (2019) 'Warm Younger Dryas summers and early late glacial spread of temperate deciduous trees in the Pannonian Basin during the last glacial termination (20-9 kyr cal BP)', *Quaternary Science Reviews*, 225, available: http://dx.doi.org/10.1016/j.quascirev.2019.105980.

Malanotte-Rizzoli, P., Manca, B.B., D'Alcalà, M.R., Theocharis, A., Bergamasco, A., Bregant, D., . . . Souvermezoglou, E. (1997) 'A synthesis of the Ionian Sea hydrography, circulation and water mass pathways during POEM-Phase I', *Progress in Oceanography*, 39(3), 153-204, available: http://dx.doi.org/10.1016/S0079-6611(97)00013-X.

Mallick, J., Hasan, M.A., Alashker, Y. and Ahmed, M. (2014) 'Bathymetric and Geochemical Analysis of Lake Al-Saad, Abha, Kingdom of Saudi Arabia Using Geoinformatics

Technology', *Journal of Geographic Information System*, 06(05), 440-452, available: http://dx.doi.org/10.4236/jgis.2014.65038.

Mallo, M., Ziveri, P., Mortyn, P.G., Schiebel, R. and Grelaud, M. (2017) 'Low planktic foraminiferal diversity and abundance observed in a spring 2013 west–east Mediterranean Sea plankton tow transect', *Biogeosciences*, 14(9), 2245-2266, available: http://dx.doi.org/10.5194/bg-14-2245-2017.

Malmgren, B.A., Kučera, M., Nyberg, J. and Waelbroeck, C. (2001) 'Comparison of statistical and artificial neural network techniques for estimating past sea surface temperatures from planktonic foraminifer census data', *Paleoceanography*, 16(5), 520-530.

Malmgren, B.A. and Nordlund, U. (1997) 'Application of artificial neural networks to paleoceanographic data', *Palaeogeography, Palaeoclimatology, Palaeoecology*, 136(1), 359-373.

Manca, B.B., Kovaĉević, V., Gaĉić, M. and Viezzoli, D. (2002) 'Dense water formation in the Southern Adriatic Sea and spreading into the Ionian Sea in the period 1997–1999', *Journal of Marine Systems*, 33-34, 133-154, available: http://dx.doi.org/10.1016/S0924-7963(02)00056-8.

Mantziafou, A. and Lascaratos, A. (2004) 'An eddy resolving numerical study of the general circulation and deep-water formation in the Adriatic Sea', *Deep Sea Research Part I: Oceanographic Research Papers*, 51(7), 921-952, available: http://dx.doi.org/10.1016/j.dsr.2004.03.006.

Marchal, O., Cacho, I., Stocker, T., Grimalt, J., Calvo, E., Martrat, B., . . . van Kreveld, S. (2002) 'Apparent long-term cooling of the sea surface in the northeast Atlantic and Mediterranean during the Holocene', *Quaternary Science Reviews*, 21, 455.

Marcott, S.A., Bauska, T.K., Buizert, C., Steig, E.J., Rosen, J.L., Cuffey, K.M., . . . Brook, E.J. (2014) 'Centennial-scale changes in the global carbon cycle during the last deglaciation', *Nature*, 514(7524), 616-9, available: http://dx.doi.org/10.1038/nature13799.

Marcott, S.A., Clark, P.U., Padman, L., Klinkhammer, G.P., Springer, S.R., Liu, Z., . . . Schmittner, A. (2011) 'Ice-shelf collapse from subsurface warming as a trigger for Heinrich events', *Proc Natl Acad Sci U S A*, 108(33), 13415-9, available: http://dx.doi.org/10.1073/pnas.1104772108.

Marcott, S.A., Shakun, J.D., Clark, P.U. and Mix, A.C. (2013) 'A reconstruction of regional and global temperature for the past 11,300 years', *Science*, 339(6124), 1198-201, available: http://dx.doi.org/10.1126/science.1228026.

Margreth, S., Gennari, G., Rüggeberg, A., Comas, M.C., Pinheiro, L.M. and Spezzaferri, S. (2011) 'Growth and demise of cold-water coral ecosystems on mud volcanoes in the West Alboran Sea: The messages from the planktonic and benthic foraminifera', *Marine Geology*, 282(1–2), 26-39, available: http://dx.doi.org/10.1016/j.margeo.2011.02.006.

Marshall, J., Donohoe, A., Ferreira, D. and McGee, D. (2013) 'The ocean's role in setting the mean position of the Inter-Tropical Convergence Zone', *Climate Dynamics*, 42(7-8), 1967-1979, available: http://dx.doi.org/10.1007/s00382-013-1767-z.

Martin-Garcia, G. (2019) 'Oceanic Impact on European Climate Changes during the Quaternary', *Geosciences*, 9(3), available: http://dx.doi.org/10.3390/geosciences9030119.

Martinez-Ruiz, F., Kastner, M., Gallego-Torres, D., Rodrigo-Gámiz, M., Nieto-Moreno, V. and Ortega-Huertas, M. (2015) 'Paleoclimate and paleoceanography over the past 20,000 yr in the Mediterranean Sea Basins as indicated by sediment elemental proxies', *Quaternary Science Reviews*, 107(0), 25-46, available: http://dx.doi.org/10.1016/j.quascirev.2014.09.018.

Martins, M.V.A., Perretti, A.R., Salgueiro, E., Frontalini, F., Moreno, J., Soares, A.M., . . . Dias, J.A. (2015) 'Atlantic sea surface temperatures estimated from planktonic foraminifera off the Iberian Margin over the last 40 Ka BP', *Marine Geology*, 367, 191-201, available: http://dx.doi.org/10.1016/j.margeo.2015.06.001.

Martrat, B., Jimenez-Amat, P., Zahn, R. and Grimalt, J.O. (2014) 'Similarities and dissimilarities between the last two deglaciations and interglaciations in the North Atlantic region', *Quaternary Science Reviews*, 99(0), 122-134, available: http://dx.doi.org/10.1016/j.quascirev.2014.06.016.

Maslin, M. (2009) 'Quaternary Climate Transitions and Cycles' in Gornitz, V., ed., *Encyclopedia of Paleoclimatology and Ancient Environments*, Dordrecht: Springer Netherlands, 841-855.

Matthes, K., Haigh, J. and Hanslmeier, A. (2021) '1.2 The impact of solar variability on climate' in Matthes, K., Wit, T. D. d., Lilensten, J. and Collectif, eds., *Earth's climate response to a changing Sun*, Les Ulis: EDP Sciences, 13-18.

Matthews, E. (2000) 'Wetlands' in Khalil, M. A. K., ed., *Atmospheric Methane: Its Role in the Global Environment*, Berlin, Heidelberg: Springer Berlin Heidelberg, 202-233.

Mayewski, P.A., Rohling, E.E., Curt Stager, J., Karlén, W., Maasch, K.A., David Meeker, L., . . . Steig, E.J. (2004) 'Holocene climate variability', *Quaternary Research*, 62(3), 243-255, available: http://dx.doi.org/10.1016/j.yqres.2004.07.001.

Mazzocchi, M.G., Siokou, I., Tirelli, V., Bandelj, V., Fernandez de Puelles, M.L., Ak Örek, Y., . . . Terbiyik Kurt, T. (2014) 'Regional and seasonal characteristics of epipelagic mesozooplankton in the Mediterranean Sea based on an artificial neural network analysis', *Journal of Marine Systems*, 135(0), 64-80, available: http://dx.doi.org/10.1016/j.jmarsys.2013.04.009.

McCarroll, D. (2015) '"Study the past, if you would divine the future": a retrospective on measuring and understanding Quaternary climate change', *Journal of Quaternary Science*, 30(2), 154-187, available: http://dx.doi.org/10.1002/jqs.2775.

McConnell, J.R., Burke, A., Dunbar, N.W., Kohler, P., Thomas, J.L., Arienzo, M.M., . . . Winckler, G. (2017) 'Synchronous volcanic eruptions and abrupt climate change approximately 17.7 ka plausibly linked by stratospheric ozone depletion', *Proc Natl Acad Sci U S A*, 114(38), 10035-10040, available: http://dx.doi.org/10.1073/pnas.1705595114.

McIntyre, A., Ruddiman, W.F. and Jantzen, R. (1972) 'Southward penetrations of the North Atlantic polar front: faunal and floral evidence of large-scale surface water mass movements over the last 225,000 years', *Deep Sea Research and Oceanographic Abstracts*, 19(1), 61-77, available: http://dx.doi.org/10.1016/0011-7471(72)90073-3.

McKillup, S. and Dyar, M.D. (2010) *Geostatistics explained: an introductory guide for earth scientists*, Cambridge University Press.

McManus, J.F., Francois, R., Gherardi, J.M., Keigwin, L.D. and Brown-Leger, S. (2004) 'Collapse and rapid resumption of Atlantic meridional circulation linked to deglacial

climate changes', *Nature*, 428(6985), 834-837, available: http://dx.doi.org/10.1038/nature02494.

MEDEX (1996) *The MEDEX Project: An expert system for forecasting gale-force winds in the Mediterranean region*, available: http://www.nrlmry.navy.mil/medex [accessed 07 Dec 2012].

Medoc, G. (1970) 'Observation of Formation of Deep Water in the Mediterranean Sea, 1969', *Nature*, 227(5262), 1037-1040, available: http://dx.doi.org/10.1038/2271037a0.

Meilland, J., Siccha, M., Weinkauf, M.F.G., Jonkers, L., Morard, R., Baranowski, U., . . . Kucera, M. (2019) 'Highly replicated sampling reveals no diurnal vertical migration but stable species-specific vertical habitats in planktonic foraminifera', *Journal of plankton research*, 41(2), 127-141, available: http://dx.doi.org/10.1093/plankt/fbz002.

Melki, T. (2011) 'Variation of deepwater convection in the western Mediterranean Sea (Gulf of Lion) during the last 28 ka', *Quaternary International*, 241(1-2), 160-168, available: http://dx.doi.org/10.1016/j.quaint.2011.04.001.

Melki, T., Kallel, N. and Fontugne, M. (2010) 'The nature of transitions from dry to wet condition during sapropel events in the Eastern Mediterranean Sea', *Palaeogeography, Palaeoclimatology, Palaeoecology*, 291(3–4), 267-285, available: http://dx.doi.org/10.1016/j.palaeo.2010.02.039.

Melki, T., Kallel, N., Jorissen, F.J., Guichard, F., Dennielou, B., Berné, S., . . . Fontugne, M. (2009) 'Abrupt climate change, sea surface salinity and paleoproductivity in the western Mediterranean Sea (Gulf of Lion) during the last 28 kyr', *Palaeogeography, Palaeoclimatology, Palaeoecology*, 279(1–2), 96-113, available: http://dx.doi.org/10.1016/j.palaeo.2009.05.005.

Menviel, L., Timmermann, A., Timm, O.E. and Mouchet, A. (2011) 'Deconstructing the Last Glacial termination: the role of millennial and orbital-scale forcings', *Quaternary Science Reviews*, 30(9-10), 1155-1172, available: http://dx.doi.org/10.1016/j.quascirev.2011.02.005.

Milanković, M. (1998) 'Canon of Insolation and the Ice-age Problem (Translated From German Edition of 1941), 619 pp', *Agency for Textbooks, Belgrade*.

Milankovitch, M. (1941) 'Kanon der Erdbestrahlung und seine Anwendung auf das Eiszeitenproblem', *Royal Serbian Academy Special Publication*, 133, 1-633.

Millot, C. (1979) 'Wind induced upwellings in the Gulf of Lions', *Oceanologica Acta*, 2(3), 261-274.

Millot, C. (1999) 'Circulation in the Western Mediterranean Sea', *Journal of Marine Systems*, 20, 423-442.

Millot, C. and Taupier-Letage, I. (2005) 'Circulation in the Mediterranean Sea' in Saliot, A., ed., *The Mediterranean Sea. Handbook of Environmental Chemistry*, Berlin, Heidelberg: Springer, 29-66.

Mix, A.C., Bard, E. and Schneider, R. (2001) 'Environmental processes of the ice age: land, oceans, glaciers (EPILOG)', *Quaternary Science Reviews*, 20(4), 627-657.

Mojtahid, M., Manceau, R., Schiebel, R., Hennekam, R. and Lange, G.J. (2015) 'Thirteen thousand years of southeastern Mediterranean climate variability inferred from an integrative planktic foraminiferal-based approach', *Paleoceanography*, 30(4), 402-422.

Monnin, E., Indermuhle, A., Dallenbach, A., Fluckiger, J., Stauffer, B., Stocker, T.F., . . . Barnola, J.M. (2001) 'Atmospheric CO2 concentrations over the last glacial termination', *Science*, 291(5501), 112-4, available: http://dx.doi.org/10.1126/science.291.5501.112.

Morabito, S., Petrosino, P., Milia, A., Sprovieri, M. and Tamburrino, S. (2014) 'A multidisciplinary approach for reconstructing the stratigraphic framework of the last 40 ka in a bathyal area of the eastern Tyrrhenian Sea', *Global and Planetary Change*, 123, Part A(0), 121-138, available: http://dx.doi.org/10.1016/j.gloplacha.2014.10.005.

Morales-Molino, C. and García-Antón, M. (2014) 'Vegetation and fire history since the last glacial maximum in an inland area of the western Mediterranean Basin (Northern Iberian Plateau, NW Spain)', *Quaternary Research*, 81(1), 63-77, available: http://dx.doi.org/10.1016/j.yqres.2013.10.010.

Morard, R., Garet-Delmas, M.J., Mahe, F., Romac, S., Poulain, J., Kucera, M. and de Vargas, C. (2018) 'Surface ocean metabarcoding confirms limited diversity in planktonic foraminifera but reveals unknown hyper-abundant lineages', *Sci Rep*, 8(1), 2539, available: http://dx.doi.org/10.1038/s41598-018-20833-z.

Morard, R., Quillevere, F., Douady, C.J., de Vargas, C., de Garidel-Thoron, T. and Escarguel, G. (2011) 'Worldwide genotyping in the planktonic foraminifer Globoconella inflata: implications for life history and paleoceanography', *PloS one*, 6(10), e26665, available: http://dx.doi.org/10.1371/journal.pone.0026665.

Moreno, A., Cacho, I., Canals, M., Grimalt, J.O., Sánchez-Goñi, M.F., Shackleton, N. and Sierro, F.J. (2005) 'Links between marine and atmospheric processes oscillating on a millennial time-scale. A multi-proxy study of the last 50,000 yr from the Alboran Sea (Western Mediterranean Sea)', *Quaternary Science Reviews*, 24(14), 1623-1636.

Moreno, A., González-Sampériz, P., Morellón, M., Valero-Garcés, B.L. and Fletcher, W.J. (2012) 'Northern Iberian abrupt climate change dynamics during the last glacial cycle: A view from lacustrine sediments', *Quaternary Science Reviews*, 36, 139-153, available: http://dx.doi.org/10.1016/j.quascirev.2010.06.031.

Moreno, A., Stoll, H., Jiménez-Sánchez, M., Cacho, I., Valero-Garcés, B., Ito, E. and Edwards, R.L. (2010) 'A speleothem record of glacial (25–11.6kyr BP) rapid climatic changes from northern Iberian Peninsula', *Global and Planetary Change*, 71(3-4), 218-231, available: http://dx.doi.org/10.1016/j.gloplacha.2009.10.002.

Morey, A.E., Mix, A.C. and Pisias, N.G. (2005) 'Planktonic foraminiferal assemblages preserved in surface sediments correspond to multiple environment variables', *Quaternary Science Reviews*, 24(7-9), 925-950, available: http://dx.doi.org/10.1016/j.quascirev.2003.09.011.

Muerdter, D.R. (1984) 'Low-salinity surface water incursions across the Strait of Sicily during late Quaternary sapropel intervals', *Marine Geology*, 58(3), 401-414, available: http://dx.doi.org/10.1016/0025-3227(84)90210-X.

Muerdter, D.R. and Kennett, J.P. (1983/84) 'Late Quaternary planktonic foraminiferal biostratrigraphy, Strait of Sicily, Mediterranean Sea', *Marine Micropaleontology*, 8(5), 339-359, available: http://dx.doi.org/10.1016/0377-8398(84)90001-X.

Muschitiello, F., D'Andrea, W.J., Schmittner, A., Heaton, T.J., Balascio, N.L., deRoberts, N., . . . Dokken, T.M. (2019) 'Deep-water circulation changes lead North Atlantic climate

during deglaciation', *Nat Commun*, 10(1), 1272, available: http://dx.doi.org/10.1038/s41467-019-09237-3.

Muschitiello, F., Lea, J.M., Greenwood, S.L., Nick, F.M., Brunnberg, L., MacLeod, A. and Wohlfarth, B. (2016) 'Timing of the first drainage of the Baltic Ice Lake synchronous with the onset of Greenland Stadial 1', *Boreas*, 45(2), 322-334, available: http://dx.doi.org/10.1111/bor.12155.

Muschitiello, F., Pausata, F.S.R., Lea, J.M., Mair, D.W.F. and Wohlfarth, B. (2017) 'Enhanced ice sheet melting driven by volcanic eruptions during the last deglaciation', *Nat Commun*, 8(1), 1020, available: http://dx.doi.org/10.1038/s41467-017-01273-1.

Muschitiello, F., Pausata, F.S.R., Watson, J.E., Smittenberg, R.H., Salih, A.A.M., Brooks, S.J., . . . Wohlfarth, B. (2015) 'Fennoscandian freshwater control on Greenland hydroclimate shifts at the onset of the Younger Dryas', *Nat Commun*, 6, 8939, available: http://dx.doi.org/10.1038/ncomms9939.

Muschitiello, F. and Wohlfarth, B. (2015) 'Time-transgressive environmental shifts across Northern Europe at the onset of the Younger Dryas', *Quaternary Science Reviews*, 109(0), 49-56, available: http://dx.doi.org/10.1016/j.quascirev.2014.11.015.

Naughton, F., Costas, S., Gomes, S.D., Desprat, S., Rodrigues, T., Sanchez Goñi, M.F., . . . Abrantes, F. (2019) 'Coupled ocean and atmospheric changes during Greenland stadial 1 in southwestern Europe', *Quaternary Science Reviews*, 212, 108-120, available: http://dx.doi.org/10.1016/j.quascirev.2019.03.033.

Naughton, F., Sánchez Goñi, M.F., Kageyama, M., Bard, E., Duprat, J., Cortijo, E., . . . Turon, J.L. (2009) 'Wet to dry climatic trend in north-western Iberia within Heinrich events', *Earth and Planetary Science Letters*, 284(3-4), 329-342, available: http://dx.doi.org/10.1016/j.epsl.2009.05.001.

Naughton, F., Sanchez Goñi, M.F., Rodrigues, T., Salgueiro, E., Costas, S., Desprat, S., . . . Abrantes, F. (2016) 'Climate variability across the last deglaciation in NW Iberia and its margin', *Quaternary International*, 414, 9-22, available: http://dx.doi.org/10.1016/j.quaint.2015.08.073.

NGRIP dating group (2008) 'Greenland Ice Core Chronology 2005 (GICC05) 60,000 Year, 20 Year Resolution [dataset]' in IGBP PAGES / World Data Center for Paleoclimatology, ed., *Data Contribution Series # 2008-034*, Boulder CO, USA: NOAA/NCDC Paleoclimatology Program.

Nisbet, E. (2002) 'Have sudden large releases of methane from geological reservoirs occurred since the Last Glacial Maximum, and could such releases occur again?', *Philosophical transactions. Series A, Mathematical, physical, and engineering sciences*, 360, 581-607, available: http://dx.doi.org/10.1098/rsta.2001.0958.

Norris, R.D. (1996) 'Symbiosis as an Evolutionary Innovation in the Radiation of Paleocene Planktic Foraminifera', *Paleobiology*, 22(4), 461-480.

Numberger, L., Hemleben, C., Hoffmann, R., Mackensen, A., Schulz, H., Wunderlich, J.-M. and Kučera, M. (2009) 'Habitats, abundance patterns and isotopic signals of morphotypes of the planktonic foraminifer Globigerinoides ruber (d'Orbigny) in the eastern Mediterranean Sea since the Marine Isotopic Stage 12', *Marine Micropaleontology*, 73(1–2), 90-104, available: http://dx.doi.org/10.1016/j.marmicro.2009.07.004.

O'Hare, G., Sweeney, J. and Wilby, R. (2013) *Weather, climate and climate change : human perspectives*, New York: Routledge.

Oeschger, H., Beer, J., Siegenthaler, U., Stauffer, B., Dansgaard, W. and Langway, C. (1984) 'Late Glacial Climate History from Ice Cores' in Hansen, J. E. and Takahashi, T., eds., *Climate Processes and Climate Sensitivity, 29*, 299-306.

Ortiz, J.D. and Mix, A.C. (1997) 'Comparison of Imbrie-Kipp Transfer Function and modern analog temperature estimates using sediment trap and core top foraminiferal faunas', *Paleoceanography*, 12(2), 175-190.

Ortiz, J.D., Mix, A.C. and Collier, R.W. (1995) 'Environmental control of living symbiotic and asymbiotic foraminifera of the California Current', *Paleoceanography*, 10(6), 987-1009.

Ottens, J.J. and Nederbragt, A.J. (1992) 'Planktic foraminiferal diversity as indicator of ocean environments', *Marine Micropaleontology*, 19(1), 13-28, available: http://dx.doi.org/10.1016/0377-8398(92)90019-G.

Oughton, J.W. and Urrego, D.H. (2021) 'Testing the Tropical Trigger Hypothesis of Abrupt Climate Variability', *Frontiers in Earth Science*, 9, available: http://dx.doi.org/10.3389/feart.2021.669885.

Paillard, D. (2015) 'Quaternary glaciations: from observations to theories', *Quaternary Science Reviews*, 107(0), 11-24, available: http://dx.doi.org/10.1016/j.quascirev.2014.10.002.

Palacios, D., de Andrés, N., Gómez-Ortiz, A. and García-Ruiz, J.M. (2017) 'Evidence of glacial activity during the Oldest Dryas in the mountains of Spain', *Geological Society, London, Special Publications*, 433(1), 87-110, available: http://dx.doi.org/10.1144/sp433.10.

PALAEOSENS Project Members (2012) 'Making sense of palaeoclimate sensitivity', *Nature*, 491(7426), 683-91, available: http://dx.doi.org/10.1038/nature11574.

Palanques, A., Durrieu de Madron, X., Puig, P., Fabres, J., Guillén, J., Calafat, A., . . . Bonnin, J. (2006) 'Suspended sediment fluxes and transport processes in the Gulf of Lions submarine canyons. The role of storms and dense water cascading', *Marine Geology*, 234(1-4), 43-61, available: http://dx.doi.org/10.1016/j.margeo.2006.09.002.

Pallacks, S., Schiebel, R., Vonhof, H., Galbraith, E. and Ziveri, P. (2021a) 'Western Mediterranean marine cores show an imprint of anthropogenically enhanced CO2 emissions in planktic Foraminifera', in *Goldschmidt 2021 [Virtual]*, July 2021.

Pallacks, S., Ziveri, P., Martrat, B., Mortyn, P.G., Grelaud, M., Schiebel, R., . . . Anglada-Ortiz, G. (2021b) 'Planktic foraminiferal changes in the western Mediterranean Anthropocene', *Global and Planetary Change*, 204, available: http://dx.doi.org/10.1016/j.gloplacha.2021.103549.

Panagiotopoulos, K., Aufgebauer, A., Schäbitz, F. and Wagner, B. (2013) 'Vegetation and climate history of the Lake Prespa region since the Lateglacial', *Quaternary International*, 293, 157-169, available: http://dx.doi.org/10.1016/j.quaint.2012.05.048.

Papadopoulos, V.P., Josey, S.A., Bartzokas, A., Somot, S., Ruiz, S. and Drakopoulou, P. (2012) 'Large-Scale Atmospheric Circulation Favoring Deep- and Intermediate-Water Formation in the Mediterranean Sea', *Journal of Climate*, 25(18), 6079-6091, available: http://dx.doi.org/10.1175/jcli-d-11-00657.1.

Past Interglacials Working Group of PAGES (2016) 'Interglacials of the last 800,000 years', *Reviews of Geophysics*, 54(1), 162-219, available: http://dx.doi.org/10.1002/2015rg000482.

Paterne, M., Kallel, N., Labeyrie, L., Vautravers, M., Duplessy, J.-C., Rossignol-Strick, M., . . . Fontugne, M. (1999) 'Hydrological relationship between the North Atlantic Ocean and the Mediterranean Sea during the past 15-75 kyr', *Paleoceanography*, 14(5), 626-638, available: http://dx.doi.org/10.1029/1998pa900022.

Pauly, M., Helle, G., Miramont, C., Buntgen, U., Treydte, K., Reinig, F., . . . Brauer, A. (2018) 'Subfossil trees suggest enhanced Mediterranean hydroclimate variability at the onset of the Younger Dryas', *Sci Rep*, 8(1), 13980, available: http://dx.doi.org/10.1038/s41598-018-32251-2.

Pawlowski, J., Holzmann, M., Berney, C., Fahrni, J., Gooday, A.J., Cedhagen, T., . . . Bowser, S.S. (2003) 'The evolution of early Foraminifera', *Proc Natl Acad Sci U S A*, 100(20), 11494-8, available: http://dx.doi.org/10.1073/pnas.2035132100.

Pearce, C., Andrews, J., Bouloubassi, I., Hillaire-Marcel, C., Jennings, A., Olsen, J., . . . Seidenkrantz, M.S. (2015) 'Heinrich 0 on the east Canadian margin: Source, distribution and timing', *Paleoceanography*, 30, 1613–162 4.

Peeters, F., Ivanova, E., Conan, S., Brummer, G.-J., Ganssen, G., Troelstra, S. and van Hinte, J. (1999) 'A size analysis of planktic foraminifera from the Arabian Sea', *Marine Micropaleontology*, 36(1), 31-63.

Peltier, W.R. and Fairbanks, R.G. (2006) 'Global glacial ice volume and Last Glacial Maximum duration from an extended Barbados sea level record', *Quaternary Science Reviews*, 25(23-24), 3322-3337, available: http://dx.doi.org/10.1016/j.quascirev.2006.04.010.

Pérez-Asensio, J.N., Frigola, J., Pena, L.D., Sierro, F.J., Reguera, M.I., Rodríguez-Tovar, F.J., . . . Cacho, I. (2020) 'Changes in western Mediterranean thermohaline circulation in association with a deglacial Organic Rich Layer formation in the Alboran Sea', *Quaternary Science Reviews*, 228, available: http://dx.doi.org/10.1016/j.quascirev.2019.106075.

Pérez-Folgado, M., Sierro, F.J., Flores, J.A., Cacho, I., Grimalt, J.O., Zahn, R. and Shackleton, N. (2003) 'Western Mediterranean planktonic foraminifera events and millennial climatic variability during the last 70 kyr', *Marine Micropaleontology*, 48, 49-70.

Pérez-Folgado, M., Sierro, F.J., Flores, J.A., Grimalt, J.O. and Zahn, R. (2004) 'Paleoclimatic variations in foraminifer assemblages from the Alboran Sea (Western Mediterranean) during the last 150 ka in ODP Site 977', *Marine Geology*, 212(1–4), 113-131, available: http://dx.doi.org/10.1016/j.margeo.2004.08.002.

Petrenko, A.A. (2003) 'Variability of circulation features in the Gulf of Lion NW Mediterranean Sea. Importance of inertial currents', *Oceanologica Acta*, 26(4), 323-338, available: http://dx.doi.org/10.1016/s0399-1784(03)00038-0.

Pettersen, S. (1956) 'Weather Analysis and Forecasting' in *Motion and Motion Systems*, New York: McGraw-Hill, 428.

Pflaumann, U., Duprat, J., Pujol, C. and Labeyrie, L.D. (1996) 'SIMMAX: A modern analog technique to deduce Atlantic sea surface temperatures from planktonic foraminifera in deep-sea sediments', *Paleoceanography*, 11(1), 15-35, available: http://dx.doi.org/10.1029/95PA01743.

Phleger, F.B. (1960) *Ecology and Distribution of Recent Foraminifera.*, Baltimore,: John Hopkins Press.

Pinter, N., Scott, A.C., Daulton, T.L., Podoll, A., Koeberl, C., Anderson, R.S. and Ishman, S.E. (2011) 'The Younger Dryas impact hypothesis: A requiem', *Earth-Science Reviews*, 106(3-4), 247-264, available: http://dx.doi.org/10.1016/j.earscirev.2011.02.005.

Poulos, S.E., Drakopoulos, P.G. and Collins, M.B. (1997) 'Seasonal variability in sea surface oceanographic conditions in the Aegean Sea (Eastern Mediterranean): an overview', *Journal of Marine Systems*, 13(1), 225-244, available: http://dx.doi.org/10.1016/S0924-7963(96)00113-3.

Pracht, H., Metcalfe, B. and Peeters, F.J.C. (2019) 'Oxygen isotope composition of the final chamber of planktic foraminifera provides evidence of vertical migration and depth-integrated growth', *Biogeosciences*, 16(2), 643-661, available: http://dx.doi.org/10.5194/bg-16-643-2019.

Praetorius, S., Mix, A., Jensen, B., Froese, D., Milne, G., Wolhowe, M., . . . Prahl, F. (2016) 'Interaction between climate, volcanism, and isostatic rebound in Southeast Alaska during the last deglaciation', *Earth and Planetary Science Letters*, 452, 79-89, available: http://dx.doi.org/10.1016/j.epsl.2016.07.033.

Prell, W.L. (1985) *Stability of low-latitude sea-surface temperatures: an evaluation of the CLIMAP reconstruction with emphasis on the positive SST anomalies. Final report*: Brown Univ., Providence, RI (USA). Dept. of Geological Sciences, available: https://babel.hathitrust.org/cgi/pt?id=uc1.31822023311996;view=1up;seq=11 [accessed 07/04/2018].

Principato, M.S. (2003) 'Late Pleistocene-Holocene Planktonic Foraminifera from the Eastern Mediterranean Sea: towards a high-resolution planktonic foraminiferal assemblage zonation for the Late Quaternary of the Mediterranean', *Rivista Italiana di Paleontologia e Stratigrafia (Research In Paleontology and Stratigraphy)*, 109(1), 111-124, available: http://dx.doi.org/10.13130/2039-4942/5497.

Principato, M.S., Giunta, S., Corselli, C. and Negri, A. (2003) 'Late Pleistocene–Holocene planktonic assemblages in three box-cores from the Mediterranean Ridge area (west–southwest of Crete): palaeoecological and palaeoceanographic reconstruction of sapropel S1 interval', *Palaeogeography, Palaeoclimatology, Palaeoecology*, 190(0), 61-77, available: http://dx.doi.org/10.1016/S0031-0182(02)00599-0.

Pujol, C. and Vergnaud Grazzini, C. (1989) 'Palaeoceanography of the last deglaciation in the Alboran Sea (Western Mediterranean). Stable isotopes and planktonic foraminiferal records', *Marine Micropaleontology*, 15(1), 153-179.

Pujol, C. and Vergnaud Grazzini, C. (1995) 'Distribution patterns of live planktic foraminifers as related to regional hydrography and productive systems of the Mediterranean Sea', *Marine Micropaleontology*, 25(2–3), 187-217, available: http://dx.doi.org/10.1016/0377-8398(95)00002-I.

Quantic, R. (2008) *Climatology for airline pilots*, Oxford, UK: Blackwell Science Ltd.

R Core Team (2017) 'R: A Language and Environment for Statistical Computing', v3.3.3.

Rach, O., Brauer, A., Wilkes, H. and Sachse, D. (2014) 'Delayed hydrological response to Greenland cooling at the onset of the Younger Dryas in western Europe', *Nature Geoscience*, 7(2), 109-112, available: http://dx.doi.org/10.1038/ngeo2053.

Rahmstorf, S. (2002) 'Ocean circulation and climate during the past 120,000 years', *Nature*, 419(6903), 207-214.

Rahmstorf, S. (2006) 'Thermohaline ocean circulation', *Encyclopedia of quaternary sciences*, 5.

Raible, C.C., Merz, N. and Woollings, T. (2015) 'North Atlantic Eddy-Driven Jet in Interglacial and Glacial Winter Climates', *Journal of Climate*, 28(10), 3977-3997, available: http://dx.doi.org/10.1175/jcli-d-14-00525.1.

Ramsey, C.B. and Lee, S. (2013) 'Recent and planned developments of the program OxCal', *Radiocarbon*, 55(2), 720-730.

Rasmussen, S.O., Bigler, M., Blockley, S.P., Blunier, T., Buchardt, S.L., Clausen, H.B., . . . Winstrup, M. (2014) 'A stratigraphic framework for abrupt climatic changes during the Last Glacial period based on three synchronized Greenland ice-core records: refining and extending the INTIMATE event stratigraphy', *Quaternary Science Reviews*, 106, 14-28, available: http://dx.doi.org/10.1016/j.quascirev.2014.09.007.

Rea, B.R., Pellitero, R., Spagnolo, M., Hughes, P., Ivy-Ochs, S., Renssen, H., . . . Braithwaite, R.J. (2020) 'Atmospheric circulation over Europe during the Younger Dryas', *Science Advances*, 6(50), eaba4844, available: http://dx.doi.org/10.1126/sciadv.aba4844.

Rebotim, A., Voelker, A.H.L., Jonkers, L., Waniek, J.J., Meggers, H., Schiebel, R., . . . Kučera, M. (2017) 'Factors controlling the depth habitat of planktonic foraminifera in the subtropical eastern North Atlantic', *Biogeosciences Discussions*, 1-48, available: http://dx.doi.org/10.5194/bg-2016-348.

Reddaway, J.M. and Bigg, G. (1996) *Climatic change over the Mediterranean and links to the general atmospheric circulation*.

Reimer, P. and McCormac, F. (2002) 'Marine radiocarbon reservoir corrections for the Mediterranean and Aegean Seas', *Radiocarbon*, 44(1), 159-166.

Reimer, P.J., Austin, W.E.N., Bard, E., Bayliss, A., Blackwell, P.G., Bronk Ramsey, C., . . . Talamo, S. (2020) 'The IntCal20 Northern Hemisphere Radiocarbon Age Calibration Curve (0–55 cal kBP)', *Radiocarbon*, 62(4), 725-757, available: http://dx.doi.org/10.1017/rdc.2020.41.

Reimer, P.J., Bard, E., Bayliss, A., Beck, J.W., Blackwell, P.G., Ramsey, C.B., . . . van der Plicht, J. (2013) 'IntCal13 and Marine13 Radiocarbon Age Calibration Curves 0–50,000 Years cal BP', *Radiocarbon*, 55(04), 1869-1887, available: http://dx.doi.org/10.2458/azu_js_rc.55.16947.

Reixach, T., Delmas, M., Braucher, R., Gunnell, Y., Mahé, C. and Calvet, M. (2021) 'Climatic conditions between 19 and 12 ka in the eastern Pyrenees, and wider implications for atmospheric circulation patterns in Europe', *Quaternary Science Reviews*, 260, 106923, available: http://dx.doi.org/10.1016/j.quascirev.2021.106923.

Renssen, H. (2020) 'Comparison of Climate Model Simulations of the Younger Dryas Cold Event', *Quaternary*, 3(4), available: http://dx.doi.org/10.3390/quat3040029.

Renssen, H., Goosse, H., Roche, D.M. and Seppä, H. (2018) 'The global hydroclimate response during the Younger Dryas event', *Quaternary Science Reviews*, 193, 84-97, available: http://dx.doi.org/10.1016/j.quascirev.2018.05.033.

Renssen, H., Mairesse, A., Goosse, H., Mathiot, P., Heiri, O., Roche, D.M., . . . Valdes, P.J. (2015) 'Multiple causes of the Younger Dryas cold period', *Nature Geoscience*, 8(12), 946-949, available: http://dx.doi.org/10.1038/ngeo2557.

Repschläger, J., Weinelt, M., Kinkel, H., Andersen, N., Garbe-Schönberg, D. and Schwab, C. (2015) 'Response of the subtropical North Atlantic surface hydrography on deglacial and Holocene AMOC changes', *Paleoceanography*, 30(5), 456-476, available: http://dx.doi.org/10.1002/2014pa002637.

Retailleau, S., Eynaud, F., Mary, Y., Abdallah, V., Schiebel, R. and Howa, H. (2012) 'Canyon heads and river plumes: How might they influence neritic planktonic Foraminifera communities in the SE Bay of Biscay?', *Journal of foraminiferal research*, 42(3), 257-269.

Retailleau, S., Howa, H. and Schiebel, R. (2010) 'Impact of storms on planktic foraminiferal fauna in the south-eastern Bay of Biscay', in *Isobay12*, Brest, France.

Retailleau, S., Schiebel, R. and Howa, H. (2011) 'Population dynamics of living planktic foraminifers in the hemipelagic southeastern Bay of Biscay', *Marine Micropaleontology*, 80(3-4), 89-100, available: http://dx.doi.org/10.1016/j.marmicro.2011.06.003.

Révillon, S., Jouet, G., Bayon, G., Rabineau, M., Dennielou, B., Hémond, C. and Berné, S. (2011) 'The provenance of sediments in the Gulf of Lions, western Mediterranean Sea', *Geochemistry, Geophysics, Geosystems*, 12(8), n/a-n/a, available: http://dx.doi.org/10.1029/2011gc003523.

Rigual-Hernandez, A.S., Barcena, M.A., Jordan, R.W., Sierro, F.J., Flores, J.A., Meier, K.J.S., . . . Heussner, S. (2013) 'Diatom fluxes in the NW Mediterranean: evidence from a 12-year sediment trap record and surficial sediments', *Journal of plankton research*, 35(5), 1109-1125, available: http://dx.doi.org/10.1093/plankt/fbt055.

Rigual-Hernández, A.S., Bárcena, M.A., Sierro, F.J., Flores, J.A., Hernández-Almeida, I., Sanchez-Vidal, A., . . . Heussner, S. (2010) 'Seasonal to interannual variability and geographic distribution of the silicoflagellate fluxes in the Western Mediterranean', *Marine Micropaleontology*, 77(1-2), 46-57, available: http://dx.doi.org/10.1016/j.marmicro.2010.07.003.

Rigual-Hernández, A.S., Colmenero-Hidalgo, E., Martrat, B., Bárcena, M.A., de Vernal, A., Sierro, F.J., . . . Lucchi, R.G. (2017) 'Svalbard ice-sheet decay after the Last Glacial Maximum: New insights from micropalaeontological and organic biomarker paleoceanographical reconstructions', *Palaeogeography, Palaeoclimatology, Palaeoecology*, 465, 225-236, available: http://dx.doi.org/10.1016/j.palaeo.2016.10.034.

Rigual-Hernández, A.S., Sierro, F.J., Bárcena, M.A., Flores, J.A. and Heussner, S. (2012) 'Seasonal and interannual changes of planktic foraminiferal fluxes in the Gulf of Lions (NW Mediterranean) and their implications for paleoceanographic studies: Two 12-year sediment trap records', *Deep Sea Research Part I: Oceanographic Research Papers*, 66, 26-40, available: http://dx.doi.org/10.1016/j.dsr.2012.03.011.

Robinson, A.R., Leslie, W.G., Theocharis, A. and Lascaratos, A. (2001) 'Mediterranean Sea circulation' in *Encyclopedia of Ocean Sciences* Academic Press, 1689-1705.

Robinson, A.R., Malanotte-Rizzoli, P., Hecht, A., Michelato, A., Roether, W., Theocharis, A., . . . Osman, M. (1992) 'General circulation of the Eastern Mediterranean', *Earth-Science Reviews*, 32(4), 285-309, available: http://dx.doi.org/10.1016/0012-8252(92)90002-B.

Robinson, S.A., Black, S., Sellwood, B.W. and Valdes, P.J. (2006) 'A review of palaeoclimates and palaeoenvironments in the Levant and Eastern Mediterranean from 25,000 to 5000 years BP: setting the environmental background for the evolution of human civilisation', *Quaternary Science Reviews*, 25(13–14), 1517-1541, available: http://dx.doi.org/10.1016/j.quascirev.2006.02.006.

Rodgers, K.B., Lohmann, G., Lorenz, S., Schneider, R. and Henderson, G.M. (2003) 'A tropical mechanism for Northern Hemisphere deglaciation', *Geochemistry, Geophysics, Geosystems*, 4(5), n/a-n/a, available: http://dx.doi.org/10.1029/2003gc000508.

Rodrigo-Gámiz, M., Martínez-Ruiz, F., Jiménez-Espejo, F.J., Gallego-Torres, D., Nieto-Moreno, V., Romero, O. and Ariztegui, D. (2011) 'Impact of climate variability in the western Mediterranean during the last 20,000 years: oceanic and atmospheric responses', *Quaternary Science Reviews*, 30(15–16), 2018-2034, available: http://dx.doi.org/10.1016/j.quascirev.2011.05.011.

Rodrigo-Gámiz, M., Martínez-Ruiz, F., Rampen, S.W., Schouten, S. and Sinninghe Damsté, J.S. (2014a) 'Sea surface temperature variations in the western Mediterranean Sea over the last 20 kyr: A dual-organic proxy (UK′37 and LDI) approach', *Paleoceanography*, 29(2), 87-98, available: http://dx.doi.org/10.1002/2013PA002466.

Rodrigo-Gámiz, M., Martínez-Ruiz, F., Rodríguez-Tovar, F.J., Jiménez-Espejo, F.J. and Pardo-Igúzquiza, E. (2014b) 'Millennial- to centennial-scale climate periodicities and forcing mechanisms in the westernmost Mediterranean for the past 20,000 yr', *Quaternary Research*, 81(1), 78-93, available: http://dx.doi.org/10.1016/j.yqres.2013.10.009.

Rodrigo, F.S. (2021) 'Exploring Combined Influences of Seasonal East Atlantic (EA) and North Atlantic Oscillation (NAO) on the Temperature-Precipitation Relationship in the Iberian Peninsula', *Geosciences*, 11(5), available: http://dx.doi.org/10.3390/geosciences11050211.

Rodrigues, T., Grimalt, J.O., Abrantes, F., Naughton, F. and Flores, J.-A. (2010) 'The last glacial–interglacial transition (LGIT) in the western mid-latitudes of the North Atlantic: Abrupt sea surface temperature change and sea level implications', *Quaternary Science Reviews*, 29(15-16), 1853-1862, available: http://dx.doi.org/10.1016/j.quascirev.2010.04.004.

Rodwell, M.J. and Hoskins, B.J. (1996) 'Monsoons and the dynamics of deserts', *Quarterly Journal of the Royal Meteorological Society*, 122(534), 1385-1404.

Rodwell, M.J. and Hoskins, B.J. (2001) 'Subtropical Anticyclones and Summer Monsoons', *Journal of Climate*, 14(15), 3192-3211, available: http://dx.doi.org/10.1175/1520-0442(2001)014<3192:saasm>2.0.co;2.

Roether, W., Klein, B., Manca, B.B., Theocharis, A. and Kioroglou, S. (2007) 'Transient Eastern Mediterranean deep waters in response to the massive dense-water output of the Aegean Sea in the 1990s', *Progress in Oceanography*, 74(4), 540-571, available: http://dx.doi.org/10.1016/j.pocean.2007.03.001.

Roether, W., Manca, B.B., Klein, B., Bregant, D., Georgopoulos, D., Beitzel, V., . . . Luchetta, A. (1996) 'Recent changes in eastern Mediterranean deep waters', *Science*, 271(5247), 333-335.

Rogerson, M., Cacho, I., Jimenez-Espejo, F., Reguera, M.I., Sierro, F.J., Martinez-Ruiz, F., . . . Canals, M. (2008) 'A dynamic explanation for the origin of the western Mediterranean organic-rich layers', *Geochemistry, Geophysics, Geosystems*, 9(7), Q07U01, available: http://dx.doi.org/10.1029/2007gc001936.

Rogerson, M., Rohling, E.J., Weaver, P.P.E. and Murray, J.W. (2004) 'The Azores Front since the Last Glacial Maximum', *Earth and Planetary Science Letters*, 222(3-4), 779-789, available: http://dx.doi.org/10.1016/j.epsl.2004.03.039.

Rohling, E.J., Abu-Zied, R., Casford, J., Hayes, A. and Hoogakker, B. (2009) 'The marine environment: present and past' in Woodward, J. C., ed., *The Physical Geography of the Mediterranean*, New York: Oxford Regional Environments.

Rohling, E.J. and Gieskes, W.W.C. (1989) 'Late Quaternary changes in Mediterranean intermediate water density and formation rate', *Paleoceanography*, 4(5), 531-545, available: http://dx.doi.org/10.1029/PA004i005p00531.

Rohling, E.J., Hayes, A., De Rijk, S., Kroon, D., Zachariasse, W.J. and Eisma, D. (1998) 'Abrupt cold spells in the northwest Mediterranean', *Paleoceanography*, 13(4), 316-322, available: http://dx.doi.org/10.1029/98PA00671.

Rohling, E.J., Jorissen, F.J. and De Stigter, H.C. (1997) '200 year interruption of Holocene sapropel formation in the Adriatic Sea', *Journal of Micropalaeontology*, 16(2), 97-108.

Rohling, E.J., Jorissen, F.J., Grazzini, C.V. and Zachariasse, W.J. (1993) 'Northern Levantine and Adriatic Quaternary planktic foraminifera; Reconstruction of paleoenvironmental gradients', *Marine Micropaleontology*, 21(1–3), 191-218, available: http://dx.doi.org/10.1016/0377-8398(93)90015-P.

Rohling, E.J., Marino, G. and Grant, K.M. (2015) 'Mediterranean climate and oceanography, and the periodic development of anoxic events (sapropels)', *Earth-Science Reviews*, 143(0), 62-97, available: http://dx.doi.org/10.1016/j.earscirev.2015.01.008.

Rohling, E.J., Sprovieri, M., Cane, T., Casford, J.S.L., Cooke, S., Bouloubassi, I., . . . Hayes, A. (2004) 'Reconstructing past planktic foraminiferal habitats using stable isotope data: a case history for Mediterranean sapropel S5', *Marine Micropaleontology*, 50(1), 89-123.

Rossignol-Strick, M. (1985) 'Mediterranean Quaternary sapropels, an immediate response of the African monsoon to variation of insolation', *Palaeogeography, Palaeoclimatology, Palaeoecology*, 49(3), 237-263.

Rossignol-Strick, M. (1995) 'Sea-land correlation of pollen records in the Eastern Mediterranean for the glacial-interglacial transition: Biostratigraphy versus radiometric time-scale', *Quaternary Science Reviews*, 14(9), 893-915, available: http://dx.doi.org/10.1016/0277-3791(95)00070-4.

Rouis-Zargouni, I., Turon, J.-L., Londeix, L., Essallami, L., Kallel, N. and Sicre, M.-A. (2010) 'Environmental and climatic changes in the central Mediterranean Sea (Siculo–Tunisian Strait) during the last 30 ka based on dinoflagellate cyst and planktonic foraminifera assemblages', *Palaeogeography, Palaeoclimatology, Palaeoecology*, 285(1–2), 17-29, available: http://dx.doi.org/10.1016/j.palaeo.2009.10.015.

Roussiez, V., Aloisi, J.-C., Monaco, A. and Ludwig, W. (2005) 'Early muddy deposits along the Gulf of Lions shoreline: A key for a better understanding of land-to-sea transfer of sediments and associated pollutant fluxes', *Marine Geology*, 222, 345-358, available: http://dx.doi.org/10.1016/j.margeo.2005.06.023.

Ruddiman, W.F. (1977) 'Late Quaternary deposition of ice-rafted sand in the subpolar North Atlantic (lat 40 to 65 N)', *Geological Society of America Bulletin*, 88(12), 1813-1827.

Ruddiman, W.F. (2006) 'Orbital changes and climate', *Quaternary Science Reviews*, 25(23-24), 3092-3112, available: http://dx.doi.org/10.1016/j.quascirev.2006.09.001.

Ruddiman, W.F. and McIntyre, A. (1981) 'The North Atlantic Ocean during the last deglaciation', *Palaeogeography, Palaeoclimatology, Palaeoecology*, 35, 145-214.

Ruddiman, W.F., Sancetta, C.D., McIntryre, A., Manley, G., Dreimanis, A., Lamb, H.H., . . . West, R.G. (1977) 'Glacial/Interglacial response rate of subpolar North Atlantic waters to climatic change: the record in oceanic sediments', *Philosophical Transactions of the Royal Society of London. B, Biological Sciences*, 280(972), 119-142, available: http://dx.doi.org/doi:10.1098/rstb.1977.0102.

Rutherford, S., D'Hondt, S. and Prell, W. (1999) 'Environmental controls on the geographic distribution of zooplankton diversity', *Nature*, 400(6746), 749-753.

Ruti, P.M., Somot, S., Giorgi, F., Dubois, C., Flaounas, E., Obermann, A., . . . Vervatis, V. (2016) 'Med-CORDEX Initiative for Mediterranean Climate Studies', *Bulletin of the American Meteorological Society*, 97(7), 1187-1208, available: http://dx.doi.org/10.1175/bams-d-14-00176.1.

Sadekov, A.Y., Eggins, S.M. and De Deckker, P. (2005) 'Characterization of Mg/Ca distributions in planktonic foraminifera species by electron microprobe mapping', *Geochemistry, Geophysics, Geosystems*, 6(12), n/a-n/a, available: http://dx.doi.org/10.1029/2005gc000973.

Salmon, K.H., Anand, P., Sexton, P.F. and Conte, M. (2015) 'Upper ocean mixing controls the seasonality of planktonic foraminifer fluxes and associated strength of the carbonate pump in the oligotrophic North Atlantic', *Biogeosciences*, 12(1), 223-235, available: http://dx.doi.org/10.5194/bg-12-223-2015.

Sanchez Goñi, M.F. and Harrison, S.P. (2010) 'Millennial-scale climate variability and vegetation changes during the Last Glacial: Concepts and terminology', *Quaternary Science Reviews*, 29(21-22), 2823-2827, available: http://dx.doi.org/10.1016/j.quascirev.2009.11.014.

Sautter, L.R. and Thunell, R.C. (1991) 'Planktonic foraminiferal response to upwelling and seasonal hydrographic conditions; sediment trap results from San Pedro Basin, Southern California Bight', *The Journal of Foraminiferal Research*, 21(4), 347-363.

Sbaffi, L., Wezel, F.C., Curzi, G. and Zoppi, U. (2004) 'Millennial- to centennial-scale palaeoclimatic variations during Termination I and the Holocene in the central Mediterranean Sea', *Global and Planetary Change*, 40(1–2), 201-217, available: http://dx.doi.org/10.1016/S0921-8181(03)00111-5.

Sbaffi, L., Wezel, F.C., Kallel, N., Paterne, M., Cacho, I., Ziveri, P. and Shackleton, N. (2001) 'Response of the pelagic environment to palaeoclimatic changes in the central Mediterranean Sea during the Late Quaternary', *Marine Geology*, 178(1–4), 39-62, available: http://dx.doi.org/10.1016/S0025-3227(01)00185-2.

Schenk, F., Bennike, O., Väliranta, M., Avery, R., Björck, S. and Wohlfarth, B. (2020) 'Floral evidence for high summer temperatures in southern Scandinavia during 15–11 cal ka BP', *Quaternary Science Reviews*, 233, available: http://dx.doi.org/10.1016/j.quascirev.2020.106243.

Schenk, F., Valiranta, M., Muschitiello, F., Tarasov, L., Heikkila, M., Bjorck, S., . . . Wohlfarth, B. (2018) 'Warm summers during the Younger Dryas cold reversal', *Nat Commun*, 9(1), 1634, available: http://dx.doi.org/10.1038/s41467-018-04071-5.

Schiebel, R. (2002) 'Planktic foraminiferal sedimentation and the marine calcite budget', *Global Biogeochemical Cycles*, 16(4), 3-1-3-21, available: http://dx.doi.org/10.1029/2001gb001459.

Schiebel, R., Bijma, J. and Hemleben, C. (1997) 'Population dynamics of the planktic foraminifer Globigerina bulloides from the eastern North Atlantic', *Deep Sea Research Part I: Oceanographic Research Papers*, 44(9-10), 1701-1713.

Schiebel, R. and Hemleben, C. (2000) 'Interannual variability of planktic foraminiferal populations and test flux in the eastern North Atlantic Ocean (JGOFS)', *Deep Sea Research Part II: Topical Studies in Oceanography*, 47(9), 1809-1852.

Schiebel, R. and Hemleben, C. (2005) 'Modern planktic foraminifera', *Paläontologische Zeitschrift*, 79, 135-148, available: http://dx.doi.org/10.1007/BF03021758.

Schiebel, R. and Hemleben, C. (2017) *Planktic Foraminifers in the Modern Ocean: Ecology, Biogeochemistry, and Application*, Berlin: Springer.

Schiebel, R., Hiller, B. and Hemleben, C. (1995) 'Impacts of storms on Recent planktic foraminiferal test production and CaCO3 flux in the North Atlantic at 47 °N, 20 °W (JGOFS)', *Marine Micropaleontology*, 26(1), 115-129, available: http://dx.doi.org/10.1016/0377-8398(95)00035-6.

Schiebel, R., Schmuker, B., Alves, M. and Hemleben, C. (2002a) 'Tracking the Recent and late Pleistocene Azores front by the distribution of planktic foraminifers', *Journal of Marine Systems*, 37(1), 213-227.

Schiebel, R., Waniek, J., Bork, M. and Hemleben, C. (2001) 'Planktic foraminiferal production stimulated by chlorophyll redistribution and entrainment of nutrients', *Deep Sea Research Part I: Oceanographic Research Papers*, 48(3), 721-740.

Schiebel, R., Waniek, J., Zeltner, A. and Alves, M. (2002b) 'Impact of the Azores Front on the distribution of planktic foraminifers, shelled gastropods, and coccolithophorids', *Deep Sea Research Part II: Topical Studies in Oceanography*, 49(19), 4035-4050, available: http://dx.doi.org/10.1016/S0967-0645(02)00141-8.

Schiebel, R., Zeltner, A., Treppke, U.F., Waniek, J.J., Bollmann, J., Rixen, T. and Hemleben, C. (2004) 'Distribution of diatoms, coccolithophores and planktic foraminifers along a trophic gradient during SW monsoon in the Arabian Sea', *Marine Micropaleontology*, 51(3-4), 345-371, available: http://dx.doi.org/10.1016/j.marmicro.2004.02.001.

Schilt, A., Baumgartner, M., Eicher, O., Chappellaz, J., Schwander, J., Fischer, H. and Stocker, T.F. (2013) 'The response of atmospheric nitrous oxide to climate variations during the last glacial period', *Geophysical Research Letters*, 40(9), 1888-1893, available: http://dx.doi.org/10.1002/grl.50380.

Schmidt, D.N., Renaud, S., Bollmann, J., Schiebel, R. and Thierstein, H.R. (2004) 'Size distribution of Holocene planktic foraminifer assemblages: biogeography, ecology and adaptation', *Marine Micropaleontology*, 50(3-4), 319-338, available: http://dx.doi.org/10.1016/s0377-8398(03)00098-7.

Schmiedl, G., Kuhnt, T., Ehrmann, W., Emeis, K.-C., Hamann, Y., Kotthoff, U., . . . Pross, J. (2010) 'Climatic forcing of eastern Mediterranean deep-water formation and benthic ecosystems during the past 22 000 years', *Quaternary Science Reviews*, 29(23–24), 3006-3020, available: http://dx.doi.org/10.1016/j.quascirev.2010.07.002.

Schneider, A., Wallace, D.W. and Körtzinger, A. (2007) 'Alkalinity of the Mediterranean sea', *Geophysical Research Letters*, 34(15).

Schneider, T., Bischoff, T. and Haug, G.H. (2014) 'Migrations and dynamics of the intertropical convergence zone', *Nature*, 513(7516), 45-53, available: http://dx.doi.org/10.1038/nature13636.

Schulz, M. and Mudelsee, M. (2002) 'REDFIT: estimating red-noise spectra directly from unevenly spaced paleoclimatic time series', *Computers & Geosciences*, 28(3), 421-426, available: http://dx.doi.org/10.1016/s0098-3004(01)00044-9.

Schwab, C., Kinkel, H., Weinelt, M. and Repschläger, J. (2012) 'Coccolithophore paleoproductivity and ecology response to deglacial and Holocene changes in the Azores Current System', *Paleoceanography*, 27(3), n/a-n/a, available: http://dx.doi.org/10.1029/2012pa002281.

Seager, R., Osborn, T.J., Kushnir, Y., Simpson, I.R., Nakamura, J. and Liu, H. (2019) 'Climate Variability and Change of Mediterranean-Type Climates', *Journal of Climate*, 32(10), 2887-2915, available: http://dx.doi.org/10.1175/jcli-d-18-0472.1.

Seears, H.A., Darling, K.F. and Wade, C.M. (2012) 'Ecological partitioning and diversity in tropical planktonic foraminifera', *BMC Evolutionary Biology*, 12(1), 54, available: http://dx.doi.org/10.1186/1471-2148-12-54.

Severinghaus, J., Sowers, T., Brook, E., Alley, R. and Bender, M. (1998) 'Timing of abrupt climate change at the end of the Younger Dryas interval from thermally fractionated gases in polar ice', *Nature*, 391, 141-146, available: http://dx.doi.org/10.1038/34346.

Shakun, J.D. and Carlson, A.E. (2010) 'A global perspective on Last Glacial Maximum to Holocene climate change', *Quaternary Science Reviews*, 29(15-16), 1801-1816, available: http://dx.doi.org/10.1016/j.quascirev.2010.03.016.

Shakun, J.D., Clark, P.U., He, F., Marcott, S.A., Mix, A.C., Liu, Z., . . . Bard, E. (2012) 'Global warming preceded by increasing carbon dioxide concentrations during the last deglaciation', *Nature*, 484(7392), 49-54, available: http://dx.doi.org/10.1038/nature10915.

Shaltout, M. and Omstedt, A. (2014) 'Recent sea surface temperature trends and future scenarios for the Mediterranean Sea', *Oceanologia*, 56(3), 411-443, available: http://dx.doi.org/10.5697/oc.56-3.411.

Shanahan, T.M., McKay, N.P., Hughen, K.A., Overpeck, J.T., Otto-Bliesner, B., Heil, C.W., . . . Peck, J. (2015) 'The time-transgressive termination of the African Humid Period', *Nature Geoscience*, 8(2), 140-144, available: http://dx.doi.org/10.1038/ngeo2329.

Shao, J., Stott, L.D., Gray, W.R., Greenop, R., Pecher, I., Neil, H.L., . . . Rae, J.W.B. (2019) 'Atmosphere-Ocean CO2 Exchange Across the Last Deglaciation from the Boron Isotope Proxy', *Paleoceanography and Paleoclimatology*, available: http://dx.doi.org/10.1029/2018pa003498.

Sherriff-Tadano, S., Abe-Ouchi, A., Yoshimori, M., Oka, A. and Chan, W.-L. (2017) 'Influence of glacial ice sheets on the Atlantic meridional overturning circulation through surface wind change', *Climate Dynamics*, 50(7-8), 2881-2903, available: http://dx.doi.org/10.1007/s00382-017-3780-0.

Siani, G., Paterne, M., Arnold, M., Bard, E., Métivier, B., Tisnerat, N. and Bassinot, F. (2000) 'Radiocarbon reservoir ages in the Mediterranean Sea and Black Sea', *Radiocarbon*, 42(2), 271-280.

Siani, G., Paterne, M., Michel, E., Sulpizio, R., Sbrana, A., Arnold, M. and Haddad, G. (2001) 'Mediterranean sea surface radiocarbon reservoir age changes since the Last Glacial Maximum', *Science*, 294(5548), 1917-1920.

Siccha, M. and Kucera, M. (2017) 'ForCenS, a curated database of planktonic foraminifera census counts in marine surface sediment samples', *Sci Data*, 4, 170109, available: http://dx.doi.org/10.1038/sdata.2017.109.

Sicre, M.-A., Jalali, B., Martrat, B., Schmidt, S., Bassetti, M.-A. and Kallel, N. (2016) 'Sea surface temperature variability in the North Western Mediterranean Sea (Gulf of Lion) during the Common Era', *Earth and Planetary Science Letters*, 456, 124-133, available: http://dx.doi.org/10.1016/j.epsl.2016.09.032.

Sicre, M.A., Siani, G., Genty, D., Kallel, N. and Essallami, L. (2013) 'Seemingly divergent sea surface temperature proxy records in the central Mediterranean during the last deglaciation', *Climate of the Past*, 9(3), 1375-1383, available: http://dx.doi.org/10.5194/cp-9-1375-2013.

Sierro, F.J., Andersen, N., Bassetti, M.A., Berné, S., Canals, M., Curtis, J.H., . . . Schneider, R. (2009) 'Phase relationship between sea level and abrupt climate change', *Quaternary Science Reviews*, 28(25-26), 2867-2881, available: http://dx.doi.org/10.1016/j.quascirev.2009.07.019.

Sierro, F.J., Hodell, D.A., Curtis, J.H., Flores, J.A., Reguera, I., Colmenero-Hidalgo, E., . . . Canals, M. (2005) 'Impact of iceberg melting on Mediterranean thermohaline circulation during Heinrich events', *Paleoceanography*, 20(2), PA2019, available: http://dx.doi.org/10.1029/2004PA001051.

Sigman, D.M., de Boer, A.M. and Haug, G.H. (2007) 'Antarctic stratification, atmospheric water vapor, and Heinrich Events: A hypothesis for Late Pleistocene deglaciations' in *Ocean Circulation: Mechanisms and Impacts—Past and Future Changes of Meridional Overturning*, 335-349.

Soon, W., Velasco Herrera, V.M., Selvaraj, K., Traversi, R., Usoskin, I., Chen, C.-T.A., . . . Becagli, S. (2014) 'A review of Holocene solar-linked climatic variation on centennial to millennial timescales: Physical processes, interpretative frameworks and a new multiple cross-wavelet transform algorithm', *Earth-Science Reviews*, 134, 1-15, available: http://dx.doi.org/10.1016/j.earscirev.2014.03.003.

Spezzaferri, S., Kučera, M., Pearson, P.N., Wade, B.S., Rappo, S., Poole, C.R., . . . Stalder, C. (2015) 'Fossil and genetic evidence for the polyphyletic nature of the planktonic foraminifera "globigerinoides", and description of the new genus trilobatus', *PloS one*, 10(5), e0128108, available: [accessed 2015].

Spezzaferri, S., Olsson, R.K. and Hemleben, C. (2017) 'Taxonomy, biostratigraphy, and phylogeny of Oligocene to Lower Miocene Globigerinoides and Trilobatus', *Cushman Foundation Special Publication*, (46), 269-306.

Sprovieri, R., Di Stefano, E., Incarbona, A. and Gargano, M.E. (2003) 'A high-resolution record of the last deglaciation in the Sicily Channel based on foraminifera and calcareous nannofossil quantitative distribution', *Palaeogeography, Palaeoclimatology, Palaeoecology*, 202(1–2), 119-142, available: http://dx.doi.org/10.1016/S0031-0182(03)00632-1.

Stanford, J.D., Hemingway, R., Rohling, E.J., Challenor, P.G., Medina-Elizalde, M. and Lester, A.J. (2011a) 'Sea-level probability for the last deglaciation: A statistical analysis of far-field records', *Global and Planetary Change*, 79(3-4), 193-203, available: http://dx.doi.org/10.1016/j.gloplacha.2010.11.002.

Stanford, J.D., Rohling, E.J., Bacon, S., Roberts, A.P., Grousset, F.E. and Bolshaw, M. (2011b) 'A new concept for the paleoceanographic evolution of Heinrich event 1 in the North Atlantic', *Quaternary Science Reviews*, 30(9-10), 1047-1066, available: http://dx.doi.org/10.1016/j.quascirev.2011.02.003.

Stanford, J.D., Rohling, E.J., Hunter, S.E., Roberts, A.P., Rasmussen, S.O., Bard, E., . . . Fairbanks, R.G. (2006) 'Timing of meltwater pulse 1a and climate responses to meltwater injections', *Paleoceanography*, 21(4), available: http://dx.doi.org/10.1029/2006pa001340.

Struglia, M.V., Mariotti, A. and Filograsso, A. (2004) 'River discharge into the Mediterranean Sea: Climatology and spects of the Observed Variability', *Journal of Climate*, 17(24), 4740-4751, available: http://dx.doi.org/10.1175/jcli-3225.1.

Stuiver, M. and Braziunas, T.F. (1993) 'Modeling Atmospheric 14C Influences and 14C Ages of Marine Samples to 10,000 BC', *Radiocarbon*, 35(1), 137-189, available: http://dx.doi.org/10.1017/S0033822200013874.

Stuiver, M., Reimer, P.J. and Reimer, R.W. (2017) 'CALIB 7.1'.

Takagi, H., Kimoto, K., Fujiki, T., Saito, H., Schmidt, C., Kucera, M. and Moriya, K. (2019) 'Characterizing photosymbiosis in modern planktonic foraminifera', *Biogeosciences*, 16(17), 3377-3396, available: http://dx.doi.org/10.5194/bg-16-3377-2019.

Takagi, H., Kurasawa, A. and Kimoto, K. (2020) 'Observation of asexual reproduction with symbiont transmission in planktonic foraminifera', *Journal of plankton research*, 42(4), 403-410, available: http://dx.doi.org/10.1093/plankt/fbaa033.

Tanhua, T., Hainbucher, D., Schroeder, K., Cardin, V., Álvarez, M. and Civitarese, G. (2013) 'The Mediterranean Sea system: a review and an introduction to the special issue', *Ocean Science*, 9(5), 789-803, available: http://dx.doi.org/10.5194/os-9-789-2013.

Telford, R., Heegaard, E. and Birks, H. (2004) 'All age–depth models are wrong: but how badly?', *Quaternary Science Reviews*, 23(1-2), 1-5, available: http://dx.doi.org/10.1016/j.quascirev.2003.11.003.

Thackeray, J.F., Scott, L. and Pieterse, P. (2019) 'The Younger Dryas interval at Wonderkrater (South Africa) in the context of a platinum anomaly', *Palaeontologia Africana*, 54, 30–35.

Thiede, J. (1975) 'Distribution of foraminifera in surface waters of a coastal upwelling area', *Nature*, 253(5494), 712-714.

Thomas, F.C. and Murney, M.G. (1985) *Techniques for extraction of foraminifers and ostracodes from sediment samples*, Dartmouth, Nova Scotia: Canadian Technical Report of Hydrography and Ocean Sciences, 54.

Thomopoulos, K., Geraga, M., Fakiris, E., Papatheodorou, G. and Ferentinos, G. (2010) 'Palaeoclimatic and Palaeoceanographic Evolution of the Mediterranean Sea over the Last 18ka', *Bulletin of the Geological Society of Greece*, 43(2), 1064, available: http://dx.doi.org/10.12681/bgsg.11271.

Thompson, P.R., Be, A.W.H., Duplessy, J.-C. and Shackleton, N.J. (1979) 'Disappearance of pink-pigmented Globigerinoides ruber at 120,000 yr BP in the Indian and Pacific Oceans', *Nature*, 280(5723), 554-558, available: http://dx.doi.org/10.1038/280554a0.

Thornalley, D.J.R., McCave, I.N. and Elderfield, H. (2010) 'Freshwater input and abrupt deglacial climate change in the North Atlantic', *Paleoceanography*, 25(1), available: http://dx.doi.org/10.1029/2009pa001772.

Thunell, R.C. (1978) 'Distribution of recent planktonic foraminifera in surface sediments of the Mediterranean Sea', *Marine Micropaleontology*, 3(2), 147-173, available: http://dx.doi.org/10.1016/0377-8398(78)90003-8.

Thunell, R.C. and Reynolds, L.A. (1984) 'Sedimentation of Planktonic Foraminifera: Seasonal Changes in Species Flux in the Panama Basin', *Micropaleontology*, 30(3), 243-262, available: http://dx.doi.org/10.2307/1485688.

Thunell, R.C. and Williams, D.F. (1983) 'Paleotemperature and paleosalinity history of the eastern Mediterranean during the Late Quaternary', *Palaeogeography, Palaeoclimatology, Palaeoecology*, 44(1-2), 23-39.

Thunell, R.C., Williams, D.F. and Kennett, J.P. (1977) 'Late Quaternary paleoclimatology, stratigraphy and sapropel history in eastern Mediterranean deep-sea sediments', *Marine Micropaleontology*, 2, 371-388.

Tian, S.Y., Yasuhara, M., Hong, Y., Huang, H.-H.M., Iwatani, H., Chiu, W.-T.R., . . . Rasmussen, T.L. (2020) 'Deglacial–Holocene Svalbard paleoceanography and evidence of meltwater pulse 1B', *Quaternary Science Reviews*, 233, available: http://dx.doi.org/10.1016/j.quascirev.2020.106237.

Timmreck, C. (2012) 'Modeling the climatic effects of large explosive volcanic eruptions', *Wiley Interdisciplinary Reviews: Climate Change*, 3(6), 545-564, available: http://dx.doi.org/10.1002/wcc.192.

Tintore, J., La Violette, P., Blade, I. and Cruzado, A. (1988) 'A study of an intense density front in the eastern Alboran Sea: the Almeria–Oran front', *Journal of Physical Oceanography*, 18(10), 1384-1397.

Tolderlund, D.S. and Bé, A.W.H. (1971) 'Seasonal Distribution of Planktonic Foraminifera in the Western North Atlantic', *Micropaleontology*, 17(3), 297-329, available: http://dx.doi.org/10.2307/1485143.

Toucanne, S., Jouet, G., Ducassou, E., Bassetti, M.-A., Dennielou, B., Angue Minto'o, C.M., . . . Mulder, T. (2012) 'A 130,000-year record of Levantine Intermediate Water flow variability in the Corsica Trough, western Mediterranean Sea', *Quaternary Science Reviews*, 33, 55-73, available: http://dx.doi.org/10.1016/j.quascirev.2011.11.020.

Triantaphyllou, M.V., Antonarakou, A., Kouli, K., Dimiza, M., Kontakiotis, G., Papanikolaou, M.D., . . . Dermitzakis, M.D. (2009) 'Late Glacial–Holocene ecostratigraphy of the south-eastern Aegean Sea, based on plankton and pollen assemblages', *Geo-Marine Letters*, 29(4), 249-267, available: http://dx.doi.org/10.1007/s00367-009-0139-5.

Trigo, I.F., Bigg, G.R. and Davies, T.D. (2002) 'Climatology of Cyclogenesis Mechanisms in the Mediterranean', *Monthly Weather Review*, 130(3), 549-569, available: http://dx.doi.org/10.1175/1520-0493(2002)130<0549:cocmit>2.0.co;2.

Trigo, R., Xoplaki, E., Zorita, E., Luterbacher, J., Krichak, S.O., Alpert, P., . . . Mariotti, A. (2006) 'Relations between variability in the Mediterranean region and mid-latitude variability' in Lionello, P., Malanotte-Rizzoli, P. and Boscolo, R., eds., *Mediterranean Climate Variability*, Amsterdam: Elsevier, 179-226.

Tsimplis, M.N., Zervakis, V., Josey, S.A., Peneva, E.L., Struglia, M.V., Stanev, E.V., . . . Oguz, T. (2006) 'Changes in the oceanography of the Mediterranean Sea and their link to climate variability' in P. Lionello, Malanotte-Rizzoli, P. and Boscolo, R., eds., *Mediterranean Climate Variability*, Amsterdam: Elsevier, 227-283.

Tyrlis, E., Lelieveld, J. and Steil, B. (2012) 'The summer circulation over the eastern Mediterranean and the Middle East: influence of the South Asian monsoon', *Climate Dynamics*, 40(5-6), 1103-1123, available: http://dx.doi.org/10.1007/s00382-012-1528-4.

Uhle, M.E., Macko, S.A., Spero, H.J., Engel, M.H. and Lea, D.W. (1997) 'Sources of carbon and nitrogen in modern planktonic foraminifera: the role of algal symbionts as determined by bulk and compound specific stable isotopic analyses', *Organic Geochemistry*, 27(3), 103-113, available: http://dx.doi.org/10.1016/S0146-6380(97)00075-2.

Ujiié, Y., de Garidel-Thoron, T., Watanabe, S., Wiebe, P. and de Vargas, C. (2010) 'Coiling dimorphism within a genetic type of the planktonic foraminifer Globorotalia truncatulinoides', *Marine Micropaleontology*, 77(3-4), 145-153, available: http://dx.doi.org/10.1016/j.marmicro.2010.09.001.

Ujiie, Y. and Lipps, J.H. (2009) 'Cryptic Diversity in Planktic Foraminifera in the Northwest Pacific Ocean', *The Journal of Foraminiferal Research*, 39(3), 145-154, available: http://dx.doi.org/10.2113/gsjfr.39.3.145.

Ulbrich, U., Lionello, P., Belusic, D., Jacobeit, J., Knippertz, P., Kuglitsch, F.G., . . . Ziv, B. (2012) 'Climate of the Mediterranean: Synoptic Patterns, Temperature, Precipitation, Winds, and Their Extremes' in *The Climate of the Mediterranean Region*, Oxford: Elsevier, 301-346.

Vacchi, M., Marriner, N., Morhange, C., Spada, G., Fontana, A. and Rovere, A. (2016) 'Multiproxy assessment of Holocene relative sea-level changes in the western Mediterranean: Sea-level variability and improvements in the definition of the isostatic signal', *Earth-Science Reviews*, 155, 172-197, available: http://dx.doi.org/10.1016/j.earscirev.2016.02.002.

van Dijk, J., Ziegler, M., de Nooijer, L.J., Reichart, G.J., Xuan, C., Ducassou, E., . . . Lourens, L.J. (2018) 'A saltier Glacial Mediterranean Outflow', *Paleoceanography and Paleoclimatology*, 179–197, available: http://dx.doi.org/10.1002/2017PA003228.

van Geel, B., van der Plicht, J. and Renssen, H. (2003) 'Major Δ14C excursions during the late glacial and early Holocene: changes in ocean ventilation or solar forcing of climate change?', *Quaternary International*, 105(1), 71-76, available: http://dx.doi.org/10.1016/s1040-6182(02)00152-0.

van Hoesel, A., Hoek, W.Z., Pennock, G.M. and Drury, M.R. (2014) 'The Younger Dryas impact hypothesis: a critical review', *Quaternary Science Reviews*, 83(0), 95-114, available: http://dx.doi.org/10.1016/j.quascirev.2013.10.033.

Van Leeuwen, R.J.W. (1989) *Sea-floor distribution and Late Quaternary faunal patterns of planktonic and benthic foraminifers in the Angola Basin*, unpublished thesis, Utrecht University.

van Raden, U.J., Groeneveld, J., Raitzsch, M. and Kucera, M. (2011) 'Mg/Ca in the planktonic foraminifera Globorotalia inflata and Globigerinoides bulloides from Western Mediterranean plankton tow and core top samples', *Marine Micropaleontology*, 78(3-4), 101-112, available: http://dx.doi.org/10.1016/j.marmicro.2010.11.002.

Velaoras, D., Krokos, G., Nittis, K. and Theocharis, A. (2014) 'Dense intermediate water outflow from the Cretan Sea: A salinity-driven, recurrent phenomenon, connected to thermohaline circulation changes', *Journal of Geophysical Research: Oceans*, 119(8), 4797-4820, available: http://dx.doi.org/10.1002/2014JC009937.

Vettoretti, G. and Peltier, W.R. (2011) 'The impact of insolation, greenhouse gas forcing and ocean circulation changes on glacial inception', *The Holocene*, 21(5), 803-817, available: http://dx.doi.org/10.1177/0959683610394885.

Vidal, L., Ménot, G., Joly, C., Bruneton, H., Rostek, F., Çağatay, M.N., . . . Bard, E. (2010) 'Hydrology in the Sea of Marmara during the last 23 ka: Implications for timing of Black Sea connections and sapropel deposition', *Paleoceanography*, 25(1), available: http://dx.doi.org/10.1029/2009pa001735.

Vincent, E. and H., B.W. (1981) 'Planktonic foraminifera and their use in Paleoceanography' in Emiliani, C., ed., *The Oceanic Lithosphere: The Sea*, Hoboken, N. J.: Wiley-Interscience, 1025–1119.

Voelker, A.H.L. (2002) 'Global distribution of centennial-scale records for Marine Isotope Stage (MIS) 3: a database', *Quaternary Science Reviews*, 21(10), 1185-1212, available: http://dx.doi.org/10.1016/S0277-3791(01)00139-1.

Wade, C.M., Darling, K.F., Kroon, D. and Leigh Brown, A.J. (1996) 'Early evolutionary origin of the planktic foraminifera inferred from small subunit rDNA sequence comparisons', *Journal of Molecular Evolution*, 43(6), 672-677, available: http://dx.doi.org/10.1007/BF02202115.

Waelbroeck, C., Labeyrie, L., Duplessy, J.C., Guiot, J., Labracherie, M., Leclaire, H. and Duprat, J. (1998) 'Improving past sea surface temperature estimates based on planktonic fossil faunas', *Paleoceanography*, 13(3), 272-283.

Walker, M., Gibbard, P., Head, M.J., Berkelhammer, M., Björck, S., Cheng, H., . . . Weiss, H. (2019a) 'Formal Subdivision of the Holocene Series/Epoch: A Summary', *Journal of the Geological Society of India*, 93(2), 135-141, available: http://dx.doi.org/10.1007/s12594-019-1141-9.

Walker, M., Head, M.J., Berkelhammer, M., Björck, S., Cheng, H., Cwynar, L., . . . Weiss, H. (2018) 'Formal ratification of the subdivision of the Holocene Series/Epoch (Quaternary System/Period): two new Global Boundary Stratotype Sections and Points (GSSPs) and three new stages/subseries', *Episodes*, 41(4), 213-223, available: http://dx.doi.org/10.18814/epiiugs/2018/018016.

Walker, M., Head, M.J., Lowe, J., Berkelhammer, M., BjÖrck, S., Cheng, H., . . . Weiss, H. (2019b) 'Subdividing the Holocene Series/Epoch: formalization of stages/ages and subseries/subepochs, and designation of GSSPs and auxiliary stratotypes', *Journal of Quaternary Science*, 34(3), 173-186, available: http://dx.doi.org/10.1002/jqs.3097.

Wang, S., Ge, Q., Wang, F., Wen, X. and Huang, J. (2013) 'Abrupt climate changes of Holocene', *Chinese Geographical Science*, 23(1), 1-12, available: http://dx.doi.org/10.1007/s11769-013-0591-z.

Wang, Y.J., Cheng, H., Edwards, R.L., An, Z.S., Wu, J.Y., Shen, C.C. and Dorale, J.A. (2001) 'A high-resolution absolute-dated late Pleistocene Monsoon record from Hulu Cave, China', *Science*, 294(5550), 2345-8, available: http://dx.doi.org/10.1126/science.1064618.

Wanner, H., Mercolli, L., Grosjean, M. and Ritz, S.P. (2015) 'Holocene climate variability and change; a data-based review', *Journal of the Geological Society*, 172(2), 254-263, available: http://dx.doi.org/10.1144/jgs2013-101.

Wasserman, P.D. (1989) *Neural computing: theory and practice*, New York: Van Nostrand Reinhold.

Waterson, A.M., Edgar, K.M., Schmidt, D.N. and Valdes, P.J. (2017) 'Quantifying the stability of planktic foraminiferal physical niches between the Holocene and Last Glacial Maximum', *Paleoceanography*, 32(1), 74-89, available: http://dx.doi.org/10.1002/2016pa002964.

Watkins, J.M., Mix, A.C. and Wilson, J. (1996) 'Living planktic foraminifera: tracers of circulation and productivity regimes in the central equatorial Pacific', *Deep Sea Research Part II: Topical Studies in Oceanography*, 43(4-6), 1257-1282, available: http://dx.doi.org/10.1016/0967-0645(96)00008-2.

Weiner, A.K. (2014) *Genetic diversity, biogeography and the morpho-genetic relationship in extant planktonic forminifera*, unpublished thesis, Universität Bremen.

Weinkauf, M.F.G., Siccha, M. and Weiner, A.K.M. (2020) 'Reproduction of a marine planktonic protist: Individual success versus population survival', *bioRxiv*, available: http://dx.doi.org/10.1101/2020.11.04.368100.

Weldeab, S., Menke, V. and Schmiedl, G. (2014) 'The pace of East African monsoon evolution during the Holocene', *Geophysical Research Letters*, 41(5), 1724-1732, available: http://dx.doi.org/10.1002/2014gl059361.

Wiersma, A.P. and Renssen, H. (2006) 'Model–data comparison for the 8.2kaBP event: confirmation of a forcing mechanism by catastrophic drainage of Laurentide Lakes', *Quaternary Science Reviews*, 25(1-2), 63-88, available: http://dx.doi.org/10.1016/j.quascirev.2005.07.009.

WOA (1998) *NODC_WOA98 data provided by the NOAA/OAR/ESRL PSD, Boulder, Colorado, USA, from their Web site at https://www.esrl.noaa.gov/psd/* [dataset].

Wolff, E.W., Chappellaz, J., Blunier, T., Rasmussen, S.O. and Svensson, A. (2010) 'Millennial-scale variability during the last glacial: The ice core record', *Quaternary Science Reviews*, 29(21-22), 2828-2838, available: http://dx.doi.org/10.1016/j.quascirev.2009.10.013.

Wüst, G. (1961) 'On the vertical circulation of the Mediterranean Sea', *Journal of Geophysical Research (1896-1977)*, 66(10), 3261-3271, available: http://dx.doi.org/10.1029/JZ066i010p03261.

Xoplaki, E. (2002) *Climate variability over the Mediterranean*, unpublished thesis, University of Bern, Switzerland, available: http://sinus.unibe.ch/klimet/docs/phd_xoplaki.pdf.

Xoplaki, E., González-Rouco, J., Luterbacher, J. and Wanner, H. (2003) 'Mediterranean summer air temperature variability and its connection to the large-scale atmospheric circulation and SSTs', *Climate Dynamics*, 20(7-8), 723-739.

Yasuhara, M., deMenocal, P.B., Dwyer, G.S., Cronin, T.M., Okahashi, H. and May Huang, H.-H. (2019) 'North Atlantic intermediate water variability over the past 20,000 years', *Geology*, 47(7), 659-663, available: http://dx.doi.org/10.1130/g46161.1.

Yeung, N.K.H., Menviel, L., Meissner, K.J. and Sikes, E. (2019) 'Assessing the Spatial Origin of Meltwater Pulse 1A Using Oxygen-Isotope Fingerprinting', *Paleoceanography and Paleoclimatology*, 34(12), 2031-2046, available: http://dx.doi.org/10.1029/2019pa003599.

Yin, Q.Z. and Berger, A. (2010) 'Insolation and CO2 contribution to the interglacial climate before and after the Mid-Brunhes Event', *Nature Geoscience*, 3(4), 243-246, available: http://dx.doi.org/10.1038/ngeo771.

Yin, Q.Z. and Berger, A. (2011) 'Individual contribution of insolation and CO2 to the interglacial climates of the past 800,000 years', *Climate Dynamics*, 38(3-4), 709-724, available: http://dx.doi.org/10.1007/s00382-011-1013-5.

Zachariasse, W., Jorissen, F., Perissoratis, C., Rohling, E. and Tsapralis, V. (1997) 'Late Quaternary foraminiferal changes and the nature of sapropel S1 in Skopelos Basin', in *Proceedings of the 5th Hellenic symposium on Oceanography and Fisheries, Kavalla, Greece*, 15-18.

Žarić, S., Donner, B., Fischer, G., Mulitza, S. and Wefer, G. (2005) 'Sensitivity of planktic foraminifera to sea surface temperature and export production as derived from sediment trap data', *Marine Micropaleontology*, 55(1-2), 75-105, available: http://dx.doi.org/10.1016/j.marmicro.2005.01.002.

Zecchin, M., Ceramicola, S., Lodolo, E., Casalbore, D. and Chiocci, F.L. (2015) 'Episodic, rapid sea-level rises on the central Mediterranean shelves after the Last Glacial Maximum: A review', *Marine Geology*, 369, 212-223.

Zhang, X., Knorr, G., Lohmann, G. and Barker, S. (2017) 'Abrupt North Atlantic circulation changes in response to gradual CO2 forcing in a glacial climate state', *Nature Geoscience*, 10(7), 518-523, available: http://dx.doi.org/10.1038/ngeo2974.

Zielhofer, C., Fletcher, W.J., Mischke, S., De Batist, M., Campbell, J.F.E., Joannin, S., . . . Mikdad, A. (2017) 'Atlantic forcing of Western Mediterranean winter rain minima during the last 12,000 years', *Quaternary Science Reviews*, 157, 29-51, available: http://dx.doi.org/10.1016/j.quascirev.2016.11.037.

Zielhofer, C., Köhler, A., Mischke, S., Benkaddour, A., Mikdad, A. and Fletcher, W. (2019) 'Western Mediterranean hydro-climatic consequences of Holocene iceberg advances (Bond events)', *Climate of the Past Discussions*, 15, 463–475, available: http://dx.doi.org/10.5194/cp-15-463-2019.

Ziv, B., Saaroni, H. and Alpert, P. (2004) 'The factors governing the summer regime of the eastern Mediterranean', *International Journal of Climatology*, 24(14), 1859-1871, available: http://dx.doi.org/10.1002/joc.1113.

Znaidi-Rivault, J. (1982) *Les grands evenements climatiques du Quaternaire recent en Mediterranee Orientale: La reponse sedimentaire, microfaunique et isotopique*, unpublished thesis, PhD Thesis, University of Paris.

Zoraster, S. (2003) 'A surface modeling algorithm designed for speed and ease of use with all petroleum industry data', *Computers & Geosciences*, 29, 1175-1182.

Appendix 1

a) List of control points used for revised chronology and age models

Core	Material Dated	Depth (cm)	Non-¹⁴C AMS Control Point (yr BP)	¹⁴C AMS dates Radiocarbon Age ± error (yr BP)	Calendar age ± error (cal yr BP)	Revised Age Model
AC 85-4	PF	31.00	8000			L
(1)		65.00	10000			
		125.00	12000			
		181.00	14000			
		235.00	16000			
		301.00	18000			
		351.00	20000			
		391.00	22000			
AEG-19	S1 End	52.00	6400			L
	S1 Start	72.00	9600			
	F & PT	100.00		10860 ± 80	12276 ± 81	
AEG-20	S1 End	79.00	6400			L
	S1 Start	113.00	9600			
	F & PT	120.00		9830 ± 70	10685 ± 72	
AEG-22	S1 End	30.00	6400			L
	S1 Start	48.00	9600			
	F & PT	50.00		9670 ± 70	10489 ± 72	
AEG-3	S1 End	47.00	6400			L
	S1 Start	78.00	9600			
	F & PT	80.00		9820 ± 70	10673 ± 72	
AEG-4	S1 End	45.00	6400			L
	S1 Start	60.00	9600			
AEG-5	S1 End	51.00	6400			L

Core	Material Dated	Depth (cm)	Non-^{14}C AMS Control Point (yr BP)	^{14}C AMS dates Radiocarbon Age ± error (yr BP)	Calendar age ± error (cal yr BP)	Revised Age Model
	S1 Start	82.00	9600			
	F & PT	90.00		10190 ± 70	11131 ± 72	
BC02	PF3/PF4 boundary	33.00	9000			L
(2)	PF4/PF5 boundary	37.00	10875			
BC06	PF3/PF4 boundary	25.00	9000			L
(2)	PF4/PF5 boundary	29.00	10875			
BC07	PF3/PF4 boundary	25.50	9000			L
(2)	PF4/PF5 boundary	28.00	10875			
BC15	PF	4.25		10150 ± 800	11176 ± 800	SS
	PF	64.75		14670 ± 900	17109 ± 900	
	PF	175.25		27380 ± 240	31008 ± 240	
	PF	256.25		31600 ± 400	35059 ± 400	
BS 78-12	0 cm (I)	0.00	5400			L
	BF	147.00		10600 ± 200	11780 ± 201	
	BA/HS1 boundary (I)	243.00	14600			
	BF	283.00		13820 ± 190	16062 ± 191	
	BF	551.00		21100 ± 400	24840 ± 400	
BS79-22	BS: BS79-33	5.00	1261			L
(3)	BS: BS79-33	20.00	3626			
	BS: BS79-33	32.00	4993			
	BS: BS79-33	63.00	6808			
	BS: BS79-33	72.00	8058			
	BS: BS79-33	81.00	8450			
	BS: BS79-33	120.00	10881			
	BS: BS79-33	147.00	11753			
	BS: BS79-33	156.00	12674			
	BS: BS79-33	198.00	14013			
	BS: BS79-33	219.00	16443			
	BS: BS79-33	267.00	18110			

Core	Material Dated	Depth (cm)	Non-^{14}C AMS Control Point (yr BP)	^{14}C AMS dates Radiocarbon Age ± error (yr BP)	Calendar age ± error (cal yr BP)	Revised Age Model
	BS: BS79-33	288.00	19269			
	BS: BS79-33	324.00	20959			
	BS: BS79-33	366.00	24534			
	BS: BS79-33	425.00	26473			
	BS: BS79-33	449.00	28843			
	BS: BS79-33	461.00	29514			
	BS: BS79-33	508.00	33405			
BS79-33	EZ	57.00	2530			L
(4)	EZ	98.00	3985			
	PF	115.00		6310 ± 70	6704 ± 72	
	EZ	120.00	7656			
	PF	136.00		8160 ± 90	8581 ± 91	
	EZ	150.00	9615			
	EZ	175.00	10995			
	PF	185.00		10830 ± 110	12221 ± 111	
	EZ	204.00	12945			
	PF	225.00		12910 ± 110	14593 ± 111	
	EZ	249.00	15343			
	PF	295.00		15480 ± 130	18249 ± 131	
	PF	340.00		16990 ± 140	19934 ± 141	
	EZ	360.00	21968			
	PF	450.00		24120 ± 220	27772 ± 221	
BS79-37	PF	4.00		900 ± 35	474 ± 38	SS
	PF	36.00		2270 ± 30	1813 ± 34	
	PF	80.00		3960 ± 40	3879 ± 43	
	PF	128.00		6870 ± 40	7338 ± 43	
	PF	196.00		10950 ± 70	12414 ± 72	
BS79-38	BS: MD95-2043	5.00	950			L
(3)	BS: MD95-2043	10.00	1107			

Core	Material Dated	Depth (cm)	Non-14C AMS Control Point (yr BP)	Radiocarbon Age ± error (yr BP)	Calendar age ± error (cal yr BP)	Revised Age Model
	BS: MD95-2043	35.00	1877			
	BS: MD95-2043	55.00	3626			
	BS: MD95-2043	95.00	4777			
	BS: MD95-2043	125.00	6071			
	BS: MD95-2043	145.00	7020			
	BS: MD95-2043	205.00	10249			
	BS: MD95-2043	230.00	11303			
	BS: MD95-2043	265.00	12352			
	BS: BS79-33	320.00	14606			
	BS: MD95-2043	395.00	19014			
C40 (5)	PF	73.00		6830		No
	PF	82.50		7830		
	PF	131.00		12350		
C69 (5, 6)	Z2 Tephra	15.00				No
	PF	28.00		5810 ± 40	6178 ± 43	
	PF	40.00		8750 ± 70	9357 ± 72	
	PF	60.00		14470 ± 70	17013 ± 72	
	BZ6/7 boundary	64.00				
	BZ7/8a boundary	84.00				
	BZ8/9 boundary	111.00				
	PF	152.00		36070 ± 300	40216 ± 300	
	PF	189.00		44300 ± 2000	47065 ± 2000	
CEUTA10 PC08	PF	22.00		5870 ± 40	6234 ± 43	SS
	PF	46.00		7940 ± 40	8348 ± 43	
	PF	82.00		9190 ± 50	9893 ± 52	
	PF	122.00		9900 ± 30	10771 ± 34	
	PF	156.00		11410 ± 30	12807 ± 34	
	PF	174.00		12240 ± 70	13633 ± 72	

Core	Material Dated	Depth (cm)	Non-¹⁴C AMS Control Point	¹⁴C AMS dates		Revised Age Model
				Radiocarbon Age ± error	Calendar age ± error	
			(yr BP)	(yr BP)	(cal yr BP)	
	PF	281.50		14270 ± 40	16704 ± 43	
	PF	323.50		14920 ± 40	17620 ± 43	
	PF	406.00		16910 ± 40	19846 ± 43	
	PF	452.00		18110 ± 50	21346 ± 52	
	PF	474.00		18360 ± 50	21695 ± 52	
	PF	541.50		20170 ± 50	23738 ± 52	
	PF	579.50		20480 ± 60	24079 ± 62	
	PF	603.50		21100 ± 60	24860 ± 62	
	PF	615.50		21540 ± 60	25429 ± 62	
Chain61-19 (7)	T-IB	240.00	10000			L
	T-IA	490.00	13000			
	BS: Stage 1/2 boundary (G. inflata)	700.00	15000			
CS72-37	BS	69.00	3076			L
	BS	107.00	8264			
	BS	187.00	15889			
GNS 84-c106	PF	140.00		3470 ± 40	3281 ± 43	SS
	PF	200.00		5660 ± 40	5993 ± 43	
	PF	250.00		8160 ± 70	8571 ± 72	
	PF	276.00		9314 ± 41	10086 ± 44	
	PF	310.00		9870 ± 100	10748 ± 101	
	PF	370.00		12870 ± 100	14518 ± 101	
	PF	470.00		17110 ± 60	20085 ± 62	
	PF	583.00		26030 ± 150	29697 ± 151	
IN 68-9	BF	7.50		3160 ± 120	2901 ± 121	SS
	PF	38.50		6390 ± 60	6797 ± 62	
	BF	81.25		9280 ± 180	9985 ± 181	
	PF	157.50		13100 ± 200	14912 ± 201	
	PF	201.50		14200 ± 300	16615 ± 300	

Core	Material Dated	Depth (cm)	Non-^{14}C AMS Control Point (yr BP)	^{14}C AMS dates Radiocarbon Age ± error (yr BP)	Calendar age ± error (cal yr BP)	Revised Age Model
	PF/PT	247.50		17200 ± 300	20195 ± 300	
IN68-21	BF	1.00		830 ± 100	399 ± 101	SS
	MOL/BF	164.50		7160 ± 140	7586 ± 141	
	MOL	245.50		9510 ± 130	10314 ± 131	
	BF	441.00		13300 ± 400	15231 ± 400	
	BF	712.50		15800 ± 500	18581 ± 500	
IN68-28 (8)	Tephra	0.00	2800			L
	Tephra	12.50	4900			
	BZ: Zone I/II boundary	27.50	9600			
	BZ: Zone II/III boundary	82.50	12700			
	Tephra	175.00	17900			
IN68-29	0 cm (I)	0.00	2000			L
	Tephra	25.00	2800			
	Tephra	50.00	4900			
	Tephra	130.00	9600			
	Tephra	200.00	12700			
	300 cm (I)	300.00	16000			
IN68-3	0 cm (I)	0.00	8750			L
	MOL	224.00		13060 ± 190	14841 ± 191	
	MOL	340.50		13400 ± 200	15465 ± 201	
	BF	527.00		16300 ± 200	19129 ± 201	
IN68-38	0 cm (I)	0.00	2000			L
	Tephra	100.00	4900			
	Tephra	290.00	9600			
	Tephra	375.00	12700			
	Tephra	475.00	17900			
IN68-5	BF	0.15		5800 ± 100	6145 ± 101	SS
	PF	1.95		9870 ± 170	10749 ± 171	
	BF	3.35		11900 ± 300	13312 ± 300	

Core	Material Dated	Depth (cm)	Non-^{14}C AMS Control Point (yr BP)	^{14}C AMS dates Radiocarbon Age ± error (yr BP)	Calendar age ± error (cal yr BP)	Revised Age Model
	BF	4.65		13700 ± 300	15880 ± 300	
	BF	6.22		14700 ± 300	17290 ± 300	
IN68-7	PF	2.50		1290 ± 120	788 ± 121	L
	PF	182.50		15400 ± 200	18166 ± 201	
	PT	250.50		23200 ± 600	26944 ± 600	
KET80-03	PF	100.00		10270 ± 161	11256 ± 161	SS
	PF	130.00		12140 ± 181	13551 ± 181	
	PF	150.00		13100 ± 201	14912 ± 201	
	PF	190.00		15590 ± 191	18369 ± 191	
KET80-19	Tephra	45.00	3900±100			L
	Tephra	80.00	7000			
	Tephra	140.00	9800±300			
	Tephra	180.00	12300±300			
	Tephra	220.00	14400			
KET80-39 (9)	BS: MD 04-2797 CQ	1.25	7426			L
	BS: MD 04-2797 CQ	81.25	9992			
	BS: MD 04-2797 CQ	121.25	11270			
	BS: MD 04-2797 CQ	141.25	12782			
	BS: MD 04-2797 CQ	161.25	14083			
	BS: MD 04-2797 CQ	181.25	15070			
	BS: MD 04-2797 CQ	211.25	16970			
	BS: MD 04-2797 CQ	221.25	17886			
KS310	PF	12.00		2175 ± 37	1700 ± 40	SS
	PF	79.00		9247 ± 54	9991 ± 56	
	PF	140.00		12280 ± 60	13677 ± 62	
	PF	179.00		15290 ± 90	18039 ± 91	
	PF	251.00		18299 ± 91	21610 ± 92	
LC 21	PF	50.00		3370 ± 60	3154 ± 62	SS
	PF	95.50		4290 ± 60	4329 ± 62	

Core	Material Dated	Depth (cm)	Non-14C AMS Control Point	14C AMS dates		Revised Age Model
				Radiocarbon Age ± error	Calendar age ± error	
			(yr BP)	(yr BP)	(cal yr BP)	
	PF	137.50		5590 ± 60	5919 ± 62	
	PF	161.50		7480 ± 60	7882 ± 62	
	PF	174.25		8120 ± 60	8518 ± 62	
	PF	179.50		9085 ± 65	9716 ± 67	
	PF	209.00		11765 ± 80	13192 ± 81	
	PF	242.50		14450 ± 60	16983 ± 62	
LC07	δ18O	70.00	20000			L
	δ18O	100.00	28000			
LC31	PF	28.50		3450 ± 50	3259 ± 52	SS
	PF	60.50		6120 ± 50	6484 ± 52	
	PF	82.50		8740 ± 50	9355 ± 52	
	PF	91.50		8500 ± 50	9055 ± 52	
	PF	126.50		12040 ± 50	13424 ± 52	
LynchII-3	S1 End	2.00	7000			L
	S1 Start	6.00	9000			
	TI	16.00	11000			
MAR03-02	Z2 Tephra	80.00	3613			L
	S1 End	125.00	6600			
	S1 Start	181.00	9900			
	MIS 1/2 boundary	220.00	14000			
	MIS 2 max	259.00	18000			
	Y2 Tephra	286.00	21554			
MAR03-03	Z2 Tephra	33.00	3613			L
	S1 End	51.00	6600			
	S1 Start	66.00	9900			
	MIS 1/2 boundary	80.00	14000			
	MIS 2 max	100.00	18000			
	Y2 Tephra	113.00	21554			
MAR03-25	Z2 Tephra	20.00	3613			L

Core	Material Dated	Depth (cm)	Non-^{14}C AMS Control Point	^{14}C AMS dates		Revised Age Model
				Radiocarbon Age ± error	Calendar age ± error	
			(yr BP)	(yr BP)	(cal yr BP)	
	S1 End	50.00	6600			
	S1 Start	81.00	9900			
	MIS 1/2 boundary	110.50	14000			
	MIS 2 max	138.00	18000			
	Y2 Tephra	190.00	21554			
	F	320.00		32960 ± 280	36420 ± 280	
MAR03-27	Z2 Tephra	40.00	3613			L
	S1 End	104.00	6600			
	S1 Start	113.00	9900			
	MIS 1/2 boundary	142.00	14000			
	MIS 2 max	180.00	18000			
	Y2 Tephra	245.00	21554			
	F	245.00		35910 ± 370	40035 ± 370	
MAR03-28	Z2 Tephra	40.00	3613			L
	S1 End	65.00	6600			
	S1 Start	102.00	9900			
	MIS 1/2 boundary	120.00	14000			
	MIS 2 max	141.00	18000			
	Y2 Tephra	161.00	21554			
	Y5 Tephra	310.00	39280			
	F	410.00		39470 ± 1050	42961 ± 1050	
MD 84-641	PF	13.00		4390 ± 120	4470 ± 121	SS
	PF	22.00		6710 ± 100	7172 ± 101	
	PF	24.00		7070 ± 100	7505 ± 101	
	PF	28.00		7490 ± 100	7889 ± 101	
	PF	32.00		8200 ± 130	8653 ± 131	
	PF	37.00		8450 ± 130	8973 ± 131	
	PF	40.00		8700 ± 110	9289 ± 111	
	PF	43.00		9760 ± 130	10603 ± 131	

Core	Material Dated	Depth (cm)	Non-¹⁴C AMS Control Point (yr BP)	¹⁴C AMS dates		Revised Age Model
				Radiocarbon Age ± error (yr BP)	Calendar age ± error (cal yr BP)	
	PF	48.00		10120 ± 150	11032 ± 151	
	PF	57.00		11990 ± 200	13401 ± 201	
	PF	65.00		12120 ± 180	13532 ± 181	
	PF	75.00		14800 ± 260	17433 ± 260	
	PF	85.00		17170 ± 270	20159 ± 270	
	PF	95.00		18500 ± 270	21835 ± 270	
	PF	105.00		20900 ± 310	24625 ± 310	
	PF	115.00		21630 ± 320	25450 ± 320	
	PF	125.00		26190 ± 600	29878 ± 600	
	PF	135.00		27060 ± 470	30707 ± 470	
MD 95-2043	PF	14.00		1980 ± 60	1469 ± 62	SS
	PF	54.00		3216 ± 37	2944 ± 40	
	PF	96.00		4275 ± 41	4314 ± 44	
	PF	178.00		5652 ± 42	5984 ± 45	
	PF	238.00		6870 ± 50	7336 ± 52	
	PF	298.00		8530 ± 47	9088 ± 49	
	PF	348.00		9200 ± 60	9911 ± 62	
	PF	418.00		9970 ± 50	10872 ± 52	
	PF	487.00		10560 ± 60	11687 ± 62	
	PF	512.00		10750 ± 60	12083 ± 62	
	PF	588.00		11590 ± 60	13010 ± 62	
	PF	595.00		11880 ± 80	13293 ± 81	
	PF	682.00		12790 ± 90	14362 ± 91	
	PF	708.00		13100 ± 90	14990 ± 91	
	PF	758.00		14350 ± 110	16821 ± 111	
	PF	802.00		15440 ± 90	18202 ± 91	
	PF	858.00		18260 ± 120	21551 ± 121	
	PF	30.50		3535 ± 30	3360 ± 34	

Core	Material Dated	Depth (cm)	Non-^{14}C AMS Control Point (yr BP)	^{14}C AMS dates		Revised Age Model
				Radiocarbon Age ± error (yr BP)	Calendar age ± error (cal yr BP)	
	PF	46.50		4830 ± 50	5036 ± 52	
	PF	160.50		10830 ± 35	12231 ± 38	
	PF	210.50		12010 ± 70	13401 ± 72	
	PF	280.50		12370 ± 35	13785 ± 38	
	PF	340.50		13025 ± 35	14904 ± 38	
	PF	370.50		13295 ± 45	15291 ± 47	
	PF	435.50		14010 ± 90	16321 ± 91	
	PF	499.50		14700 ± 80	17335 ± 81	
	PF	579.50		16330 ± 110	19140 ± 111	
	PF	691.50		17820 ± 45	20937 ± 47	
	PF	748.50		18400 ± 130	21723 ± 131	
	PF	880.50		20750 ± 150	24379 ± 151	
MD04-2797CQ	PF	0.00		1105 ± 20	622 ± 25	SS
	PF	200.00		7465 ± 30	7875 ± 34	
	PF	330.00		8965 ± 30	9548 ± 34	
	PF	470.00		12605 ± 40	14031 ± 43	
	PF	511.00		13800 ± 100	16041 ± 101	
	PF	610.00		15590 ± 50	18391 ± 52	
MD99-2343	PF	28		790 ± 40	374 ± 43	SS
	PF	118		3390 ± 50	3183 ± 52	
	PF	238		6210 ± 50	6584 ± 52	
	PF	604		14550 ± 110	17130 ± 111	
MNB 3 (5, 10)	Z2 Tephra	40.00	3570			No
	PF	75.00		5040 ± 40	5341 ± 43	
	BZ: Ia/Ib boundary	78.00	5100			
	End S1	128.00	6700			
	PF	125.00		7840 ± 40	8252 ± 43	
	Interruption of S1	142.00	8200			

Core	Material Dated	Depth (cm)	Non-¹⁴C AMS Control Point (yr BP)	Radiocarbon Age ± error (yr BP)	Calendar age ± error (cal yr BP)	Revised Age Model
	PF	157.00		9030 ± 60	9637 ± 62	
	Start S1	161.00	9600			
	BZ: II/Ic boundary	175.00	11600			
	PF	220.00		14100 ± 200	16468 ± 201	
	BZ: III/II boundary	260.00	16100			
	PF	318.00		16610 ± 80	19485 ± 81	
	PF	387.00		19860 ± 80	23357 ± 81	
ODP 964A	PF	2.50		1250 ± 30	730 ± 34	SS
	PF	9.50		2360 ± 30	1915 ± 34	
	PF	65.50		13050 ± 60	14928 ± 62	
	PF	87.50		17730 ± 80	20822 ± 81	
ODP 969A	PF	6.50		3340 ± 30	3113 ± 34	SS
	PF	25.50		7420 ± 30	7829 ± 34	
	PF	34.50		9700 ± 40	10534 ± 43	
	PF	58.50		15240 ± 50	17977 ± 52	
ODP 973A	PF	2.50		1390 ± 30	876 ± 34	L
	PF	46.50		3370 ± 30	3156 ± 34	
	PF	102.50		14450 ± 50	16984 ± 52	
ODP 975B	PF	9.00		2455 ± 30	2029 ± 34	SS
	PF	51.00		7070 ± 40	7504 ± 43	
	PF	91.00		13330 ± 60	15355 ± 62	
	PF	131.00		15870 ± 80	18677 ± 81	
	PF	190.00		19460 ± 110	22867 ± 111	
ODP 977 (11)	PF	20.00			1159	L
	PF	60.00			4220	
	BS: HE1 (MD95-2043)	295.20	15207			
	BS: HE2 (MD95-2043)	415.00	23403			
P4 (12)	BS	87.00	6900			L
	BS	135.00	9000			

| Core | Material Dated | Depth (cm) | Non-^{14}C AMS Control Point (yr BP) | ^{14}C AMS dates | | Revised Age Model |
				Radiocarbon Age ± error (yr BP)	Calendar age ± error (cal yr BP)	
	BS	145.00	9800			
	BS	240.00	14600			
SK-1	PF	143.50		3810 ± 100	3687 ± 101	SS
	PF	284.00		6580 ± 70	7033 ± 72	
	PF	524.00		9640 ± 80	10449 ± 81	
	PF	690.00		13430 ± 130	15511 ± 131	
SU81-07	δ18O	11.00	3473			L
	δ18O	51.00	4717			
	δ18O	111.00	9147			
	δ18O	151.00	12585			
	δ18O	161.00	13341			
	δ18O	191.00	14598			
	δ18O	211.00	15952			
	δ18O	291.00	19003			
T87/2/20G (13)	PF	21.00		11680 ± -	13087 ± 201	L
	PF	38.00		15640 ± -	18420 ± 201	
	PF	71.00		26100 ± -	29812 ± 201	
T87/2/27G (14)	BZ: I/II boundary (I)	12.00	9600			L
	PF	70.00		29800 ± 700	33336 ± 700	
	PF	86.50		35100 ± 1400	38994 ± 1400	
TR172-22	O2 Isotope Stage 1/2 boundary	40.00	11000			L
TRI171-15 (7)	T-IB	90	10000			L
	T-IA	190	13000			
	BS: Stage 1/2 boundary (G. inflata)	240	15000			
Z1 (5)	PF	37.00		9170 ± 80	9857 ± 81	No
	PF	61.00		11570 ± 40	12990 ± 43	
	PF	94.00		14230 ± 50	16640 ± 52	
75KS5 (15)	Unknown	11.00		5621 ± 56		L
		30.00		12133 ± 203		

Core	Material Dated	Depth (cm)	Non-14C AMS Control Point	14C AMS dates		Revised Age Model
				Radiocarbon Age ± error	Calendar age ± error	
			(yr BP)	(yr BP)	(cal yr BP)	
		90.00		26701 ± 1872		
75KS76 (15)	Unknown	15.00		3810 ± 363		L
		29.00		7429 ± 1034		
		46.00		15050 ± 680		
		55.00		20937 ± 1263		

List of control points used for revised chronology and age models. Material used for control points: BF = Benthic foraminifera; BS = Biostratigraphic Correlation; EZ = Ecozone Correlation; F = Foraminifera (type not specified) MOL = Mollusc; δ18O = δ18O Correlation; PF = Planktonic foraminifera; PT = Pteropods. (I) = Biostratigraphic events interpolated from figures in the original publication. S1 = Sapropel 1 start and end dates used, as specified in the original publication. MIS = Marine isotope stage. 14C AMS dates with reported errors were recalibrated using Calib v.7.0.2, utilising the Marine13 calibration curve and with an average ΔR value of 58 ± 15 14C yrs for the Mediterranean Sea (Reimer and McCormac, 2002; Faivre et al., 2015; Stuiver et al., 2017). Revised Age Model: L = Linear interpolation; SS = Smooth spline (0.3) weighted interpolation.

Notes: (1) Depth & Age values obtained from Figs. 5 & 6 (Capotondi et al., 1989); (2) "Planktonic Foraminiferal Assemblage Zone" boundaries defined by (Principato, 2003). The original Age Model for BC06 used interpolated AMS 14C dates from AD91-7 (Giunta et al., 2003); (3) BS79-33 (Sbaffi et al., 2001); $U_{37}^{k\prime}$ SST record of MD95-2043 (Cacho et al., 1999); (4) Ecozones as defined by Capotondi et al. (1999); (5) No sample depths provided, so no revised Age Model; (6) Ecozones as defined by Capotondi et al. (1999) and Sbaffi et al. (2001); (7) TIA and TIB as defined by Ruddiman and McIntyre (1981); Stage 1/2 boundary defined by the absence of G. inflata (Muerdter and Kennett, 1983/84); (8) Biozonation defined as "glacial" (Zone III), "transitional" (Zone II) and "postglacial" (Zone I) (Jorissen et al., 1993); (9) MD 04-2797 CQ (Rouis-Zargouni et al., 2010); (10) Biozonation as defined by Casford et al. (2002); (11) HE = event terminations in the N. pachyderma curve of MD95-2043 (Cacho et al., 1999); (12) Biostratigraphically correlated to IN68 Adriatic cores of Jorissen et al. (1993); (13) No AMS error reported, therefore a ±200 yr error was applied when recalibrating the AMS dates; (14) Zonal boundary I/II as defined by Jorissen et al. (1993); (15) Pangaea® comment: corrected for reservoir age. Therefore, AMS ages not recalibrated.

298

b) Age quality and number of samples per chronozone

Site Name	YD 11550-12800 (±50) cal ky BP		BA 12800-14700 (±50) cal ky BP		HS1 14700-17100 (±50) cal ky BP	
	AQ	No. of samples	AQ	No. of samples	AQ	No. of samples
AC 85-4	4	4	4	6	4	8
AEG-19	1	1	2	2	2	2
AEG-20	2	1	2	1	3	1
AEG-22					3	1
AEG-3					3	1
AEG-4	4	1	4	1	4	1
AEG-5			2	1		
BC 02	4	1				
BC 06	4	3	4	4	4	5
BC 07	4	2	4	3	4	3
BC 15	2	2	2	3	2	3
BS 78-12	1	2	2	4	2	3
BS 79-22	3	7	3	16	3	12
BS 79-33	2	5	2	6	3	10
BS 79-37	1	4	2	6	2	7
BS 79-38	3	14	4	19	3	15
C 40	3	2	3	3	3	7
C 69	2	4	2	2	1	2
CEUTA10PC08	2	8	1	12	1	27
Chain61-19	4	3	4	6	4	9
CS72-37	3	1	2	3	2	3
GNS 84-c106	2	12	1	19	2	10
IN 68-21	2	1	2	3	1	3
IN 68-28	4	2	4	1	4	2
IN 68-29	4	1	4	2	4	3
IN 68-3	2	3	2	3	1	7
IN 68-38	4	1	4	2	4	2
IN 68-5	2	3	1	5	1	11
IN 68-7	3	1	3	2	2	2
IN 68-9	2	4	2	7	1	3
KET80-03	2	2	1	3	1	3
KET80-19	2	3	2	5	3	5
KET80-39	3	2	2	4	2	4
KS 310	2	2	1	3	2	4
LC 07	4	1	4	1	4	2
LC 21	2	3	1	3	1	3
LC-31	2	2	1	7	2	6
LynchII-3	4	1				
M40/4 82-2SL	1	39	2	39	1	16
MAR03-02	3	1	3	2	3	3

Site Name	YD 11550-12800 (±50) cal ky BP		BA 12800-14700 (±50) cal ky BP		HS1 14700-17100 (±50) cal ky BP	
	AQ	No. of samples	AQ	No. of samples	AQ	No. of samples
MAR03-03			3	1	3	1
MAR03-25	3	1	3	1	3	2
MAR03-27	3	1	3	1	3	3
MAR03-28	3	1	3	1	3	1
MD 04-2797 CQ	2	5	1	7	1	8
MD 84-641	2	2	1	4	2	2
MD 95-2043	1	10	1	13	1	7
MD 99-2346	1	8	1	35	1	47
MD99-2343	3	5	2	7	2	9
MNB 3	3	28	3	17	2	17
ODP 964A	2	2	2	2	1	2
ODP 969A	2	2	2	3	2	4
ODP 973A	3	1	2	2	1	3
ODP 975B	2	4	2	5	1	8
ODP 977	4	3	4	5	4	4
P4	4	2	4	2	4	4
SK1	2	4	2	4	1	5
SL-11	4	10	4	14	4	10
SL-21	4	4	4	5	4	5
SU81-07	2	2	2	4	2	5
T87/2/20G			2	2	3	2
T87/2/27G			3	1	3	1
TRI171-15	4	2	4	2	4	3
TRI172-22					4	1
Z1	2	9	1	21	1	8
75KS5	2	1	3	1	3	2
75KS76	3	1	3	1		
Total number of samples		257		370		373
Total number of cores per chronozone	60		62		63	

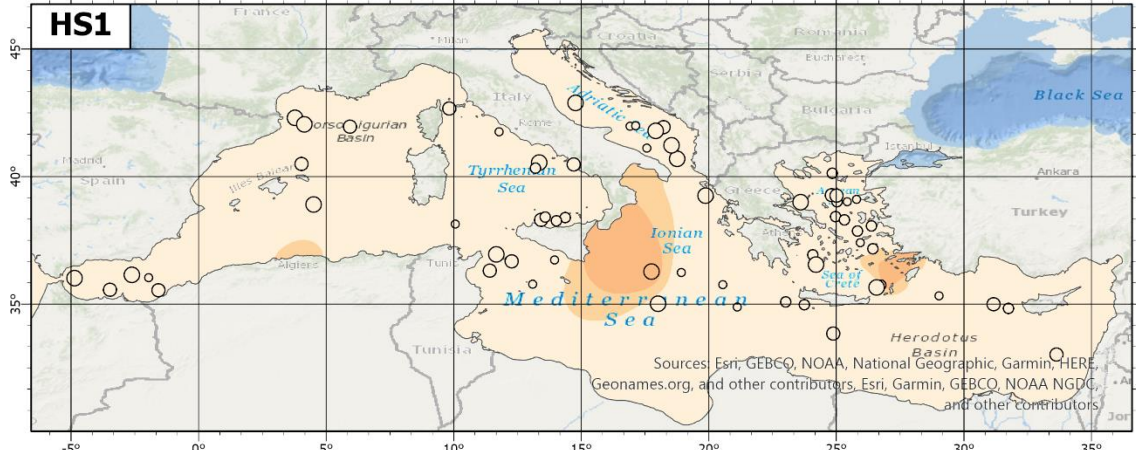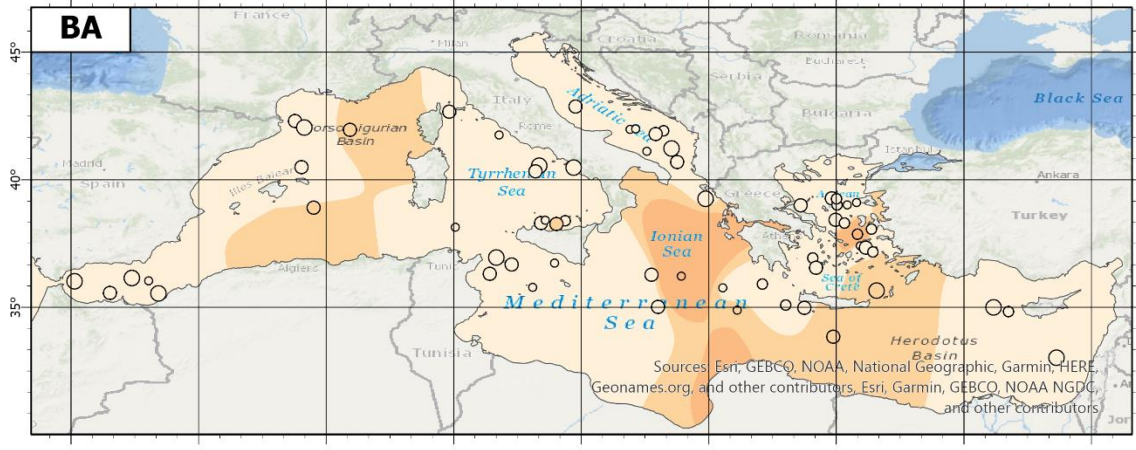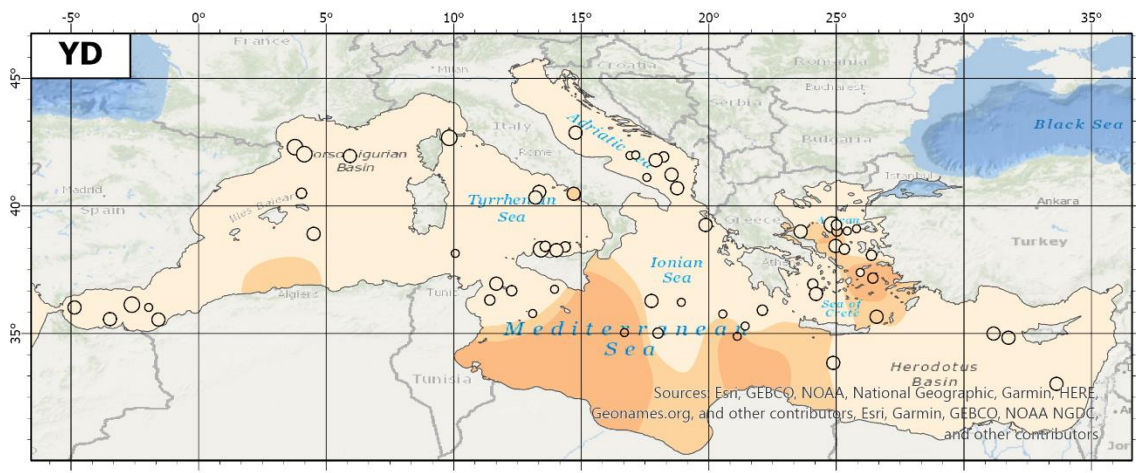*Age quality (AQ) and number of samples per chronozone.*
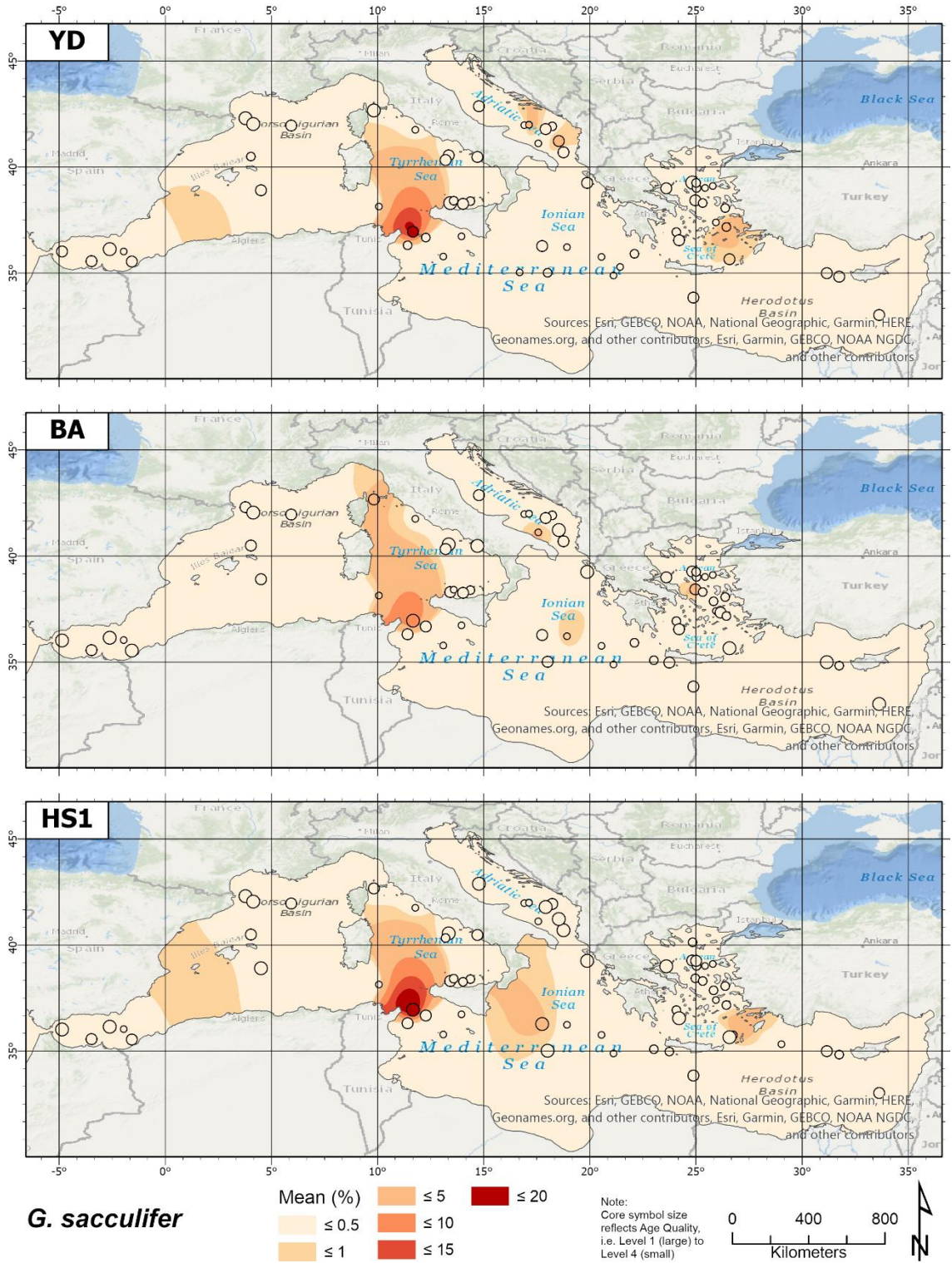
Appendix 2
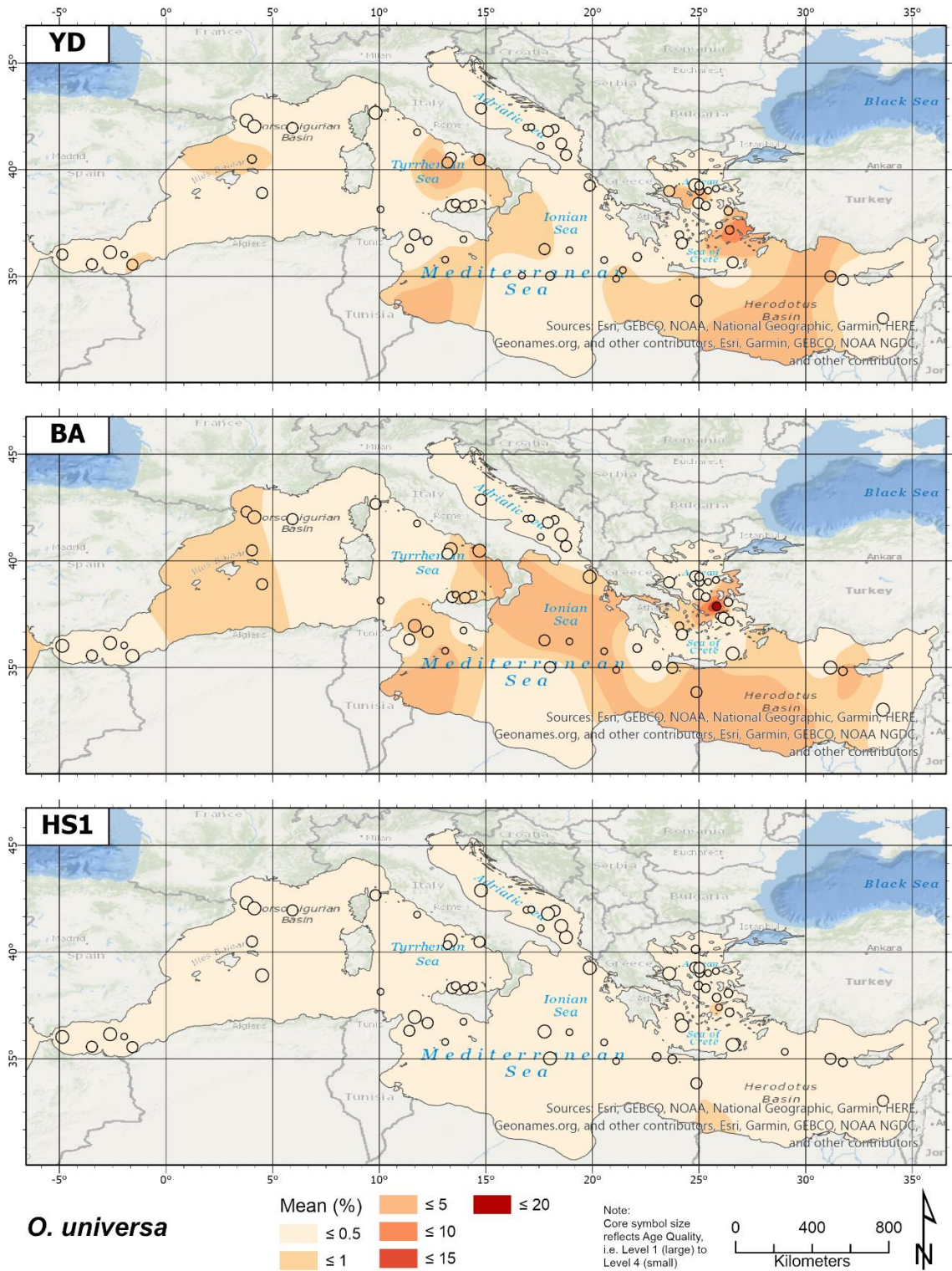
Spatial distribution of O. universa (%) during HS1, BA and YD.

Spatial distribution of G. siphonifera (%) during HS1, BA and YD

Spatial distribution of G. sacculifer (%) during HS1, the BA and YD.

Appendix 3

Ecological preferences of planktonic foraminifera in the western Mediterranean

N. incompta

Although originally defined as a subpolar species when included with *N. pachyderma*, its distribution spans temperate to subtropical waters, though with a preference for cooler waters (Bé and Tolderlund, 1971; Hilbrecht, 1996; Žarić *et al.*, 2005; Kučera, 2007). It is a relatively shallow dwelling non-spinose species, with an ALD ~81m (Rebotim *et al.*, 2017). The highest fluxes and abundances of *N. incompta* coincide with mid-temperature ranges, with medium to high productivity (Žarić *et al.*, 2005). During spring or autumn blooms, *N. incompta* is out competed by the more opportunistic *G. bulloides* and *T. quinqueloba*, but flourishes during later periods of increased stratification and is closely linked to the presence of a DCM (Rohling and Gieskes, 1989; Rohling *et al.*, 1993). Heightened productivity in a DCM is central to the lifecycle of many foraminifera, i.e. as a site of increased food availability, reproduction and for acquiring symbionts. However, this is especially true for *N. incompta*. The DCM assemblage is composed of various species of green algae, chlorophytes, coccolithophores, diatoms and dinoflagellates, which are attracted by the continuous renewing of nutrients from the nutricline below (Rohling and Gieskes, 1989; Latasa *et al.*, 2017). For *N. incompta*, availability, quality and type of food are the principal factors governing its presence in the DCM (Rohling and Gieskes, 1989; Schiebel *et al.*, 2001). When the pycnocline lies below the euphotic zone and no DCM develops, neogloboquadrinids are usually absent (Rohling and Gieskes, 1989). To date only 2 genotypes have been identified, with only the Atlantic Type I of relevance to this study.

G. bulloides

Highly productive environments are characterised by species such as *G. bulloides*, *N. incompta* and *G. glutinata* (Žarić *et al.*, 2005). The opportunistic *G. bulloides* thrives in central upwelling regions, as its respiration in O_2 depleted waters is not limited by the presence of algal symbionts, therefore it can take advantage of increases in algal prey (Bijma *et al.*, 1992; Hilbrecht, 1996). *G. bulloides* has a wide average living depth (ALD) range (~102m), with a preference to inhabit above the thermocline, though it is also found in deeply mixed waters ≤200m, especially during spring storms (Schiebel *et al.*, 1997; Rebotim *et al.*, 2017).

In the Mediterranean, *G. bulloides* has a depth range between the mixed layer to deeper levels (50-200m) (Pujol and Vergnaud Grazzini, 1995). Its distribution in the Mediterranean reflects a wide SST tolerance, though it has a notable preference for cooler more eutrophic waters, especially in the western basin (Cifelli, 1974; Thunell, 1978; Pujol and Vergnaud Grazzini, 1995; Mallo *et al.*, 2017). In the modern Gulf of Lion, *G. bulloides* is the dominant species,

especially in sites within the Rhône Delta plume (Rigual-Hernández *et al.*, 2012).

G. ruber plexus

G. ruber white is a shallow dwelling (~56m) tropical to subtropical species, with an optimal SST range from 21.8 to 30.6°C (Bijma *et al.*, 1990; Žarić *et al.*, 2005; Rebotim *et al.*, 2017). Traditionally, *G. ruber* white is commonly used as indicator of warm water oligotrophic conditions. However, it has a greater ability to utilise the nutrition from primary producers that other predatory species, allowing it to expand its habitat from warm stratified oligotrophic waters to eutrophic upwelling regions (Anderson, 1983; Seears *et al.*, 2012; Schiebel and Hemleben, 2017). This is evident within the gyres of the Alboran Sea, as well as in the Arabian Sea, where both *G. ruber* white Types Ib2 and IIa are found (Bárcena *et al.*, 2004; Hernández-Almeida *et al.*, 2011; Seears *et al.*, 2012). In the modern Mediterranean Sea, a number of tropical to transitional *G. ruber* white genotypes have been identified, including *G. ruber* pink, Types Ia, IIa and IIb (Darling and Wade, 2008; Aurahs *et al.*, 2009; Aurahs *et al.*, 2011; André *et al.*, 2014). Indeed, the Type IIa cluster has been reclassified as *G. elongatus* and has two subtypes (IIa1 and IIa2), which form two distinct stable populations that exclusively inhabit the western (Type IIa1) and eastern (Type IIa2) Mediterranean basins (Aurahs *et al.*, 2009). Ecological, seasonal and depth habitat variations have been recognised within these *G. ruber* plexus genotypes, e.g. *G. elongatus* inhabits higher productivity shallow waters (Numberger *et al.*, 2009).

G. ruber white is one of the most abundant foraminifera species in the modern Mediterranean Sea, dominating much of the eastern basin, though it decreases in the western basin, especially towards the north-western basin (Cifelli, 1974; Thunell, 1978; Pujol and Vergnaud Grazzini, 1995; Mallo *et al.*, 2017). Within the modern Gulf of Lion, *G. ruber* white forms part of the shallow water (<50m) summer to early autumn assemblage in strongly stratified waters, along with *O. universa*, *G. siphonifera*, *G. ruber* pink and *G. sacculifer* (which is absent in the pre-Holocene record), and *G. truncatulinoides* at depth (Pujol and Vergnaud Grazzini, 1995; Rigual-Hernández *et al.*, 2012).

The modern distribution of *G. ruber* pink is closely linked to SST (i.e. it has a preference for warmer SST) and it has a stable shallow ALD (Bé and Tolderlund, 1971; Žarić *et al.*, 2005; Kučera, 2007; Rebotim *et al.*, 2017). It is regarded a "summer species" in comparison to the more ubiquitous *G. ruber* white (Salmon *et al.*, 2015; Schiebel and Hemleben, 2017). *G. ruber* pink forms only a minor component of the modern Gulf of Lion assemblage, though is common late summer species in the eastern basin (Pujol and Vergnaud Grazzini, 1995; Rigual-Hernández *et al.*, 2012).

T. quinqueloba

T. quinqueloba is a small species typical in cold water species, typical of summer polar to sub-polar waters and the spring bloom in temperate waters (optimal SST of <12°C), though it is tolerant of higher SST tropical/subtropical waters (Bé and Tolderlund, 1971; Schiebel and Hemleben, 2005; Darling *et al.*, 2017; Schiebel and Hemleben, 2017). It has facultative chrysophycophyte symbionts and in the past, was described primarily as a shallow water species that was restricted mainly to the photic zone (Hemleben *et al.*, 1989; Rohling *et al.*, 1993). However, more recent studies calculated an ALD of ~144m (typical ALD range of 70 to 180m) and its depth habitat is not restricted to specific SST or density ranges (Rebotim *et al.*, 2017). It is usually associated with chlorophyll redistribution, high primary production, food (diatom) availability and it can demonstrate opportunistic behaviours similar to *G. bulloides* in upwelling regions (Sautter and Thunell, 1991; Conan and Brummer, 2000; Schiebel *et al.*, 2001; Schiebel and Hemleben, 2017). It is tolerant to low salinities and has been linked to enhanced riverine nutrient input in both high or low turbidity and highly productive waters (Rohling *et al.*, 1993; Ortiz *et al.*, 1995; Retailleau *et al.*, 2012). In the Bay of Biscay, it flourished in shallow waters during periods of heightened productivity associated with nutrient rich river discharged into oligotrophic summer waters (Retailleau *et al.*, 2011; Retailleau *et al.*, 2012). It was inferred that *T. quinqueloba* was better adapted to thrive in these eutrophic low salinity waters due to the potential presence of facultative chrysophycophyte symbionts (Retailleau *et al.*, 2011).

T. quinqueloba is rare in the modern Mediterranean Sea, though it occurs in greater abundances in the Alboran Sea and northern regions of the Gulf of Lion, Tyrrhenian and Aegean Seas. Its distribution in modern Mediterranean surface sediments is similar to that of *G. bulloides* (Thunell, 1978). Its presence is coincident with cool (<15°C) deeply mixed waters, gyres, areas of deep and intermediate water formation, and within the LIW current (Cifelli, 1974; Thunell, 1978; Pujol and Vergnaud Grazzini, 1995; Bárcena *et al.*, 2004; Hernández-Almeida *et al.*, 2011; Rigual-Hernández *et al.*, 2012).

O. universa

O. universa is a cosmopolitan species found in tropical to temperate waters, with a variable feeding strategy, transitioning from herbivorous as a juvenile to predominantly carnivorous in adulthood (Hemleben *et al.*, 1989). Its governing factors primarily are SST and food, and it has as stable depth preference (ALD ~79m) (Rebotim *et al.*, 2017; Schiebel and Hemleben, 2017). *O. universa* is common in the southern western basin, with a decreased presence in the late summer waters of the north-west basin (Thunell, 1978; Pujol and Vergnaud Grazzini, 1989; Mallo *et al.*, 2017). However, some variability is seen in the Gulf of Lion, with peaks of *O. universa* at the end of the spring in higher productivity sites and in late summer/autumn in lower productivity sites (Rigual-Hernández *et al.*, 2012). In addition, during the 1997-1998 El Niño

event, autumn SST were anomalously high and winds were weakened, inhibiting deep winter mixing in the Gulf of Lion, allowing *O. universa* to flourish (Rigual-Hernández *et al.*, 2012). Genetic analysis has identified the Mediterranean Type III genotype, associated with upwelling and nutrient-rich mixed layer, particularly in the western basin (de Vargas *et al.*, 1999; Mallo *et al.*, 2017; Schiebel and Hemleben, 2017).

G. inflata

G. inflata is a transitional species and has a wide tolerance to SST variations, ranging from subtropical to subpolar waters, though it has a preference for cooler waters (<20°C) (Bé and Tolderlund, 1971; Bé and Hutson, 1977; Hemleben *et al.*, 1989). It feeds on both chrysophytes and diatoms, and is indicative of intermediate trophic levels (Hemleben *et al.*, 1989; Van Leeuwen, 1989). It is a deep dwelling species with an ALD of ~104m, though calcification occurs throughout the year between 20-500m (van Raden *et al.*, 2011; Rebotim *et al.*, 2017). *G. inflata* has two genotypes, though Type I is only relevant for this region (Morard *et al.*, 2011). In the modern western Mediterranean, *G. inflata* is a key winter species (Thunell, 1978; Pujol and Vergnaud Grazzini, 1995; Rohling *et al.*, 2004; Rigual-Hernández *et al.*, 2012). It thrives in many different environments, such as a deep mixed layer associated with a deep pycnocline, where temperatures within the eutrophic zone are cool and homogenous, areas of high food abundance such as within the Rhône Delta plume, within the MAW in the Alboran Sea and along the N. African coast, or on the fringes of upwelling areas (Van Leeuwen, 1989; Rohling *et al.*, 1993; Pujol and Vergnaud Grazzini, 1995; Bárcena *et al.*, 2001; Bárcena *et al.*, 2004; Rigual-Hernández *et al.*, 2012). During bloom events, the opportunistic *G. bulloides* is quicker to respond to the initial high productivity, whereas *G. inflata* flourishes later in the spring (Bárcena *et al.*, 2004).

G. scitula

Originally classified by Bé (1977) as a polar / subpolar species, its distribution is much more extensive and it is typical of intensely mixed eutrophic temperate waters, especially during the spring bloom (Itou *et al.*, 2001; Chapman, 2010; Schiebel and Hemleben, 2017). It has a broad SST tolerance but has a preference to cooler waters, especially when found in association with Neogloboquadrina species and *T. quinqueloba* (Thunell, 1978; Rohling *et al.*, 1993). It is been suggested that *G. scitula* feeds on settling fine particulate organic matter that does not need to be fresh, implying it is an opportunistic species (Itou *et al.*, 2001; Schiebel and Hemleben, 2005, 2017). Despite being a deeper dwelling species, it has been observed within low salinity neritic waters (<20m) adjacent to a river mouth (Retailleau *et al.*, 2011). It was assumed that it was transported up from deeper offshore waters as a result of upwelling and flourished due to the high food availability.

G. glutinata

G. glutinata is a ubiquitous species, abundant from tropical to temperate waters, slowly decreasing in subpolar waters (Hemleben *et al.*, 1989; Kučera, 2007; Schiebel and Hemleben, 2017). It has a wide SST tolerance and variable depth habitat, ranging from shallow to the deep mixed waters above the thermocline and has the shallowest ALD (78.6m) of all non-spinose eutrophic species (Bé and Tolderlund, 1971; Thunell and Reynolds, 1984; Hilbrecht, 1996; Rebotim *et al.*, 2017). Their diet consists mainly of fresh prey, particularly diatoms, though it periodically utilises facultative chrysophytes symbionts (Hemleben *et al.*, 1989). *G. glutinata* is known to feed on diatoms (Hemleben *et al.*, 1989) and is found frequently on the margins of productive zones (Bé and Hutson, 1977). As shallow eutrophic species, they respond to deep mixing events, such as upwelling, eddies, storms and monsoons (Schiebel *et al.*, 1995; Conan and Brummer, 2000; Schiebel and Hemleben, 2000; Schiebel *et al.*, 2001; Retailleau *et al.*, 2010). Hilbrecht (1996) noted *G. bulloides* and *G. glutinata* have different feeding strategies in upwelling regions and the spatial and temporal distribution of these species may be related to the phytoplankton bloom succession of dinoflagellates to diatoms. Studies in the Panama Basin determined that *G. glutinata* has a bi-modal seasonal flux pattern, peaking in shallow mixed waters with a deep thermocline in the summer, then again during high productivity and upwelling events during the spring bloom, when nutrients are entrained into surface waters (Thunell and Reynolds, 1984). Only four genotypes have been identified, with Type I and III located in the nearby subtropical North Atlantic (Ujiie and Lipps, 2009; André *et al.*, 2014). However, with such a broad geographic distribution and tolerances, it is believed that more cryptic species have yet to be identified (André *et al.*, 2014).

G. truncatulinoides

G. truncatulinoides is a large distinctive morphospecies, with both dextral and sinistral coiling varieties. *G. truncatulinoides* inhabits tropical/ subtropical waters in the northern hemisphere, but also extends to polar Antarctic waters in the southern hemisphere (Bé and Tolderlund, 1971; Schiebel and Hemleben, 2017). It has the deepest depth habit of all modern planktonic foraminifera, which is governed by its annual reproductive cycle, ontogeny, food requirements and it calcifies its test at the top of the thermocline (Lohmann and Schweitzer, 1990; Schiebel and Hemleben, 2017). Reproduction occurs at depth, then enhanced vertical mixing is required to transport juveniles up to shallow productive surface waters in the late winter; during the summer it descends to significant depths (>1000m) (Lohmann and Schweitzer, 1990; Schiebel and Hemleben, 2017). It has a variable algal diet, consuming green algae, chrysophytes or diatoms, depending on which is available (Hemleben *et al.*, 1989). In general, SST, along with seasonality and mixed layer depth are the key ecological variables that govern its distribution (Waterson *et al.*, 2017). Genetic analysis of *G. truncatulinoides* has identified four genotypes,

with the subtropical Type II the only variety that displays both coiling varieties and it is found both in the central North Atlantic and the Mediterranean Sea (de Vargas *et al.*, 2001; Darling and Wade, 2008; André *et al.*, 2014). Within Type II, the two coiling varieties have different ecological preferences. Sinistral individuals require a deeper thermocline to complete its life cycle, and correlates with periods of deep winter convection and vertical mixing, and are most abundant between 200 to 600m (Bé, 1977; Lohmann and Schweitzer, 1990; Schiebel *et al.*, 2002a; Darling and Wade, 2008; Ujiié *et al.*, 2010). In contrast, dextral varieties are indicative of a weakly stratified water column and a shallow thermocline, and are more abundant within 100 to 200m (Bé, 1977; Lohmann and Schweitzer, 1990; Schiebel *et al.*, 2002a; Darling and Wade, 2008; Ujiié *et al.*, 2010).

In the modern Mediterranean Sea, *G. truncatulinoides* sinistral is a key minor species, with <1% of the population composed of the dextral variety (Thunell, 1978; Pujol and Vergnaud Grazzini, 1995; Rigual-Hernández *et al.*, 2012). It is most abundant during winter months in the western basin during periods of deep mixing, and at sub-thermocline depths in the summer (Pujol and Vergnaud Grazzini, 1995). In the Mediterranean, winter convection and vertical mixing are the primary factors fulfilling its life cycle requirements, followed by SST and food availability (Pujol and Vergnaud Grazzini, 1995). *G. truncatulinoides* was absent from the Mallo *et al.* (2017) survey, as the sampling depth of the summer plankton tow was too shallow to record *G. truncatulinoides*, who would have descended deeper waters at the time. In the Gulf of Lion, *G. truncatulinoides* sinistral are present throughout the year, in particular during the winter deep mixing events and are the dominant non-spinose species during the summer, at depths (>500m) (Pujol and Vergnaud Grazzini, 1995; Rigual-Hernández *et al.*, 2012).

SPRUDTS

In many studies, seven generally low frequency spinose species, with an optimum SST preference of >20°C, have been grouped together into what is known as the SPRUDTS group (*G. **s**iphonifera*, *H. **p**elagica*, *G. **r**ubescens*, *O. **u**niversa*, *B. **d**igitata*, *G. **t**enella* and *G. **s**acculifer*) (Rohling *et al.*, 1993). Although many of these species have differing habitat ranges and ecological preferences, they are frequently grouped together in cluster analyses and have been inferred to indicate warm subtropical water conditions in palaeoenvironmental studies, especially when they co-occur with *G. ruber* (Rohling *et al.*, 1993). Some of the more prevalent SPRUDTS species in the western Mediterranean are discussed below.

G. rubescens

Although there are few ecological studies focusing on this species, *G. rubescens* has been used to mark the end of the summer monsoon in the northeaster Indian Ocean, when nutrients in surface waters were depleted (Conan and Brummer, 2000). It has a variable depth habitat from

surface to subsurface, deepening with increasing mixed layer temperature (Rebotim *et al.*, 2017). In the modern Mediterranean, its abundance is low throughout the year (<1%), and predominantly occurs in the central and eastern Mediterranean, along the North African coast and in the Alboran Sea (Pujol and Vergnaud Grazzini, 1995). It was not reported in the modern Gulf of Lion (Rigual-Hernández *et al.*, 2012).

G. siphonifera

G. siphonifera is a deeper dwelling (~84m) tropical to transitional species, traditionally associated with warm stratified waters with an optimum temperature range >20°C (Žarić *et al.*, 2005; Rebotim *et al.*, 2017; Schiebel and Hemleben, 2017). However, to-date it has four genotypes, with two ecological variable genotypes of interest in the Mediterranean, i.e. the cosmopolitan Type IIa (+ 6 subtypes) associated to a mesotrophic DCM, and Type IIb is associated with higher productivity and upwelling (de Vargas *et al.*, 2002; Darling and Wade, 2008). *G. siphonifera* has a similar distribution to the cosmopolitan *O. universa* in surface sediment studies in the Mediterranean, varying in abundance from 1 to 10% within the eastern basin, the Alboran and Balearics Seas (Thunell, 1978). In addition, their distribution varied seasonally and spatially in surface water surveys across the two basins. Pujol and Vergnaud Grazzini (1995) reported greater abundances in the eastern basin during the winter, whereas in the summer it had greater abundance in the western basin and was replaced by *G. ruber* white in the eastern basin (Cifelli, 1974; Mallo *et al.*, 2017).

B. digitata

This is a poorly studied, rare subsurface dwelling spinose species that is regionally more common in the Mediterranean that elsewhere globally (Hemleben *et al.*, 1989). In studies of modern sediments and plankton tows, it only forms part of the incoming subtropical assemblage in the Alboran Sea and <1% in the Gulf of Lion (Cifelli, 1974; Rigual-Hernández *et al.*, 2012). It is believed to thrive in higher nutrient availability, following a phytoplankton bloom (Schiebel and Hemleben, 2017).